

Bridge Security Design Manual



U.S. Department
of Transportation

**Federal Highway
Administration**

Technical Report Documentation Page

1. Report No. FHWA-HIF-17-032	2. Government Accession No.	3. Recipient Catalog No.	
4. Title and Subtitle Bridge Security Design Manual		5. Report Date June 2017	
		6. Performing Organization Code	
7. Author(s) Carrie Davis, PE; Eric Sammarco, PhD, PE; Eric Williamson, PhD, PE		8. Performing Organization Report No.	
9. Performing Organization Name and Address HDR Engineering and Protection Engineering Consultants		10. Work Unit No. (TRAIS)	
		11. Contract or Grant No. DTFH6114D00049/5009	
12. Sponsoring Agency Name and Address Federal Highway Administration 1200 New Jersey Ave. SE Washington, DC 20590		13. Type of Report and Period Covered	
		14. Sponsoring Agency Code	
15. Supplementary Notes			
16. Abstract <p>The Bridge Security Design Manual provides information for structural engineers, planners, owners and others to incorporate effective strategies in bridge projects and make highway systems resilient against terrorist threats. These threats have been a growing concern in the U.S. since the 9/11 attacks. While previous infrastructure security research and practice have focused primarily on buildings, the limited bridge-specific design guidance suggests that bridges can be better protected against common loadings these terrorist threats can impart to bridge components. "The primary objective of this bridge security design manual is to present state-of-the-art guidance on bridge-specific security planning, extreme loading phenomenology and characterization, and protective design strategies to be used by the highway bridge community in terrorist threat vulnerability assessments of existing bridges, resilient design of new bridge construction, and emergency planning efforts."</p> <p>The manual covers a broad range of topics, including security planning, material performance, blast phenomenology, mechanics of structural elements, dynamic response of structures, protective design guidance and example designs for several component types (such as concrete towers), and the use of the software tool, Anti-terrorism Planner for Bridges (ATP-Bridge). It is intended to be a resource for broad audiences to better understand bridge security and a reference tool for designers to build protection into bridges and enable the highway systems they connect to function at a high level under a variety of threats. It makes use of the latest technology and research, including the ATP-Bridge tool.</p>			
17. Key Words Bridge security; security planning; security design; blast phenomenology; anti-terrorism planning; AT-Planner for Bridges; protective design; extreme loading; vulnerability assessment; resilient design.		18. Distribution Statement	
19. Security Classification (of this report) Unclassified	20. Security Classification (of this page) Unclassified	21. No. of pages 291	22. Price

TABLE OF CONTENTS

Foreword	1
1.0 Introduction.....	3
1.1 History of Terrorist Events Involving Transportation Infrastructure	4
1.2 Risk Management and Security Planning for Highway Bridges.....	7
1.3 Bridge Design for Terrorist Events	7
1.4 Recent Advances in Transportation Infrastructure Security	9
1.5 Anti-Terrorist Planner for Bridges (ATP-Bridge) Software	11
1.6 Chapter Summary.....	12
2.0 Security Planning for Highway Bridges	13
2.1 Threat Mitigation Strategies.....	14
2.1.1 Planning and Coordination Measures	15
2.1.2 Information Control Measures.....	15
2.1.3 Site Layout Measures.....	15
2.1.4 Access Control/Deterrent Measures	16
2.1.5 Deception Measures.....	17
2.2 Project Coordination	18
2.3 Additional Publically Available Bridge Security Guidance	19
2.4 Chapter Summary.....	19
3.0 Materials Performance	20
3.1 Explosives	20
3.1.1 High Explosives	21
3.1.2 Types of Explosive Charges	21
3.1.3 TNT Equivalency.....	22
3.1.4 Charge Shape	24
3.2 Reinforced Concrete.....	25
3.2.1 Effect of Strain Rate on Material Response.....	25
3.2.2 Strength Values for Design.....	28
3.2.3 Rate-Dependent Constitutive Models.....	29
3.2.4 Thermal Effects.....	31
3.3 Structural Steel	35
3.3.1 Effects of Strain Rate on Material Response	36
3.3.2 Strength Values for Design.....	37
3.3.3 Rate-Dependent Constitutive Models	38

3.3.4	Thermal Effects.....	40
3.4	Chapter Summary.....	45
4.0	Blast Phenomenology	47
4.1	Types of Explosions	48
4.2	Shock Waves in Air.....	50
4.3	Far-Field Behavior of Shock Waves	50
4.3.1	Spherical Free-Air Burst.....	52
4.3.2	Spherical Air Burst	52
4.3.3	Hemispherical Surface Burst	53
4.4	Near-field Behavior of Shock Waves.....	53
4.5	Shock Wave Interaction with Bridge Components	57
4.6	Blast Load Computation.....	62
4.6.1	Blast Load Scaling	63
4.6.2	Empirical Methods.....	65
4.6.3	Ray Tracing Methods.....	66
4.6.4	Numerical Methods.....	68
4.7	Chapter Summary.....	69
5.0	Mechanics of Structural Elements	70
5.1	Conventional Reinforced Concrete Elements	70
5.1.1	Spall and Breach	70
5.1.2	Direct Shear Response	72
5.1.3	Flexural Response.....	76
5.1.4	Tension Membrane Response	79
5.1.5	Compression Membrane Response.....	80
5.2	Prestressed and High-Performance Concrete Elements	81
5.2.1	Prestressed Concrete	81
5.2.2	High-Performance Concrete	82
5.2.3	Fiber-Reinforced Concrete.....	86
5.3	Structural Steel Elements	90
5.3.1	Local Breach	90
5.3.2	Flexural Response.....	90
5.3.3	Local and Global Buckling	92
5.3.4	Shear Response	92
5.3.5	Tension Membrane Response	93

5.4	High-Strength Steel Cables	94
5.5	Chapter Summary.....	94
6.0	Dynamic Response of Structures	95
6.1	Dynamic Analysis Process	96
6.2	Performance Criteria	99
6.3	Pressure-Impulse (P-I) Diagrams	101
6.4	Single-Degree-of-Freedom (SDOF) Analysis.....	104
6.4.1	Equivalent SDOF System Properties	106
6.4.2	Blast Loads for Equivalent SDOF Systems	109
6.4.3	Resistance Functions.....	111
6.5	Multi-Degree-of-Freedom (MDOF) Systems and Finite Element Analysis	114
6.6	Chapter Summary.....	116
7.0	Protective Design Guidance for Reinforced Concrete Columns	118
7.1	Design Loads.....	118
7.1.1	Blast Loads.....	118
7.1.2	Other Loading Considerations	123
7.2	Failure Modes and Performance Criteria	125
7.3	Design Strategies and Detailing Recommendations	127
7.4	Recommended Design Procedure	128
7.4.1	Boundary Conditions	129
7.4.2	Analysis Approach.....	130
7.4.3	Structural Design	130
7.5	ATP-Bridge Design Examples	130
7.6	Overview of Threat Mitigation Retrofit Strategies	142
7.7	Chapter Summary.....	143
8.0	Protective Design Guidance for Steel Cellular Towers	144
8.1	Design Loads.....	145
8.1.1	Blast Loads.....	146
8.1.2	Other Loading Considerations	149
8.2	Failure Modes and Performance Criteria	150
8.3	Design Strategies and Detailing Recommendations	153
8.4	Recommended Design Procedure	154
8.4.1	Boundary Conditions	154
8.4.2	Analysis Approach.....	155

8.4.3	Structural Design	156
8.5	ATP-Bridge Design Example.....	156
8.6	Overview of Threat Mitigation Retrofit Strategies	163
8.7	Chapter Summary.....	165
9.0	Protective Design Guidance for Reinforced Concrete Towers.....	167
9.1	Design Threats.....	168
9.1.1	Blast Loads.....	169
9.1.2	Other Loading Considerations	172
9.2	Failure Modes and Performance Criteria	172
9.3	Design Strategies and Detailing Recommendations	174
9.4	Recommended Design Procedure	178
9.4.1	Boundary Conditions	179
9.4.2	Analysis Approach.....	180
9.4.3	Structural Design	182
9.5	ATP-Bridge Design Examples	184
9.6	Overview of Threat Mitigation Retrofit Strategies	192
9.7	Chapter Summary.....	193
10.0	Protective Design Guidance for High-Strength Steel Cables	194
10.1	Cable Types	195
10.2	Design Loads	197
10.2.1	Explosive Threats.....	197
10.2.2	Kinetic Energy Penetrators	199
10.2.3	Cutting Threats.....	201
10.2.4	Other Loading Considerations	204
10.3	Failure Modes and Performance Criteria.....	204
10.4	Design Strategies and Detailing Recommendations.....	205
10.5	Recommended Design Procedures	207
10.5.1	ATP-Bridge for Cable Vulnerability	207
10.5.2	Numerical Simulations for Cable and Cable Component Vulnerability	209
10.5.3	Bridge Performance Assessment	211
10.6	ATP-Bridge Design Examples	212
10.6.1	Linear Shaped Charge against Stay Cable	213
10.6.2	Block Charge against Steel Cable.....	214
10.6.3	Diamond Charge against Steel Cable	216

10.7	Overview of Threat Mitigation Retrofit Strategies.....	218
10.8	Chapter Summary	219
11.0	Protective Design Guidance For Other Bridge Components.....	220
11.1	Flexural Members.....	220
11.1.1	Member Types	220
11.1.2	Design Loads	222
11.1.3	Failure Modes and Performance Criteria.....	222
11.1.4	Design Considerations	223
11.2	Bridge Decks	224
11.2.1	Deck Types	224
11.2.2	Design Loads	224
11.2.3	Failure Modes and Performance Criteria.....	225
11.2.4	Design Considerations	225
11.3	Design Considerations for Other Components.....	225
11.3.1	Bridge Bearings	226
11.3.2	Abutments and Riprap Walls.....	226
11.3.3	Bridges over Navigable Waterways.....	227
11.3.4	Horizontally Curved Bridges	227
11.3.5	Truss Bridges	227
11.3.6	Built-Up and Laced Members.....	228
11.3.7	Proprietary Protection Methods	229
11.4	Future Research Needs	229
11.5	Chapter Summary	230
12.0	Anti-Terrorist Planner for Bridges (ATP-Bridge) Software.....	231
12.1	Software Overview	232
12.2	Software Operation.....	233
12.3	Overview of Analysis Methodology.....	240
12.3.1	Blast Load Computation	241
12.3.2	Dynamic Response Algorithm for Reinforced Concrete Columns.....	242
12.3.3	Dynamic Response Algorithm for Steel Cellular Tower Panels	243
12.3.4	Dynamic Response Algorithm for Reinforced Concrete Tower Panels	243
12.3.5	Dynamic Response Algorithm for High-Strength Steel Cables	244
12.4	ATP-Bridge Design Examples	245
12.4.1	Reinforced Concrete Bridge Columns	245

12.4.2	Steel Cellular Bridge Towers.....	257
12.4.3	Reinforced Concrete Bridge Towers	264
12.4.4	High-Strength Steel Cables.....	272
12.5	Chapter Summary	277
References	278

LIST OF FIGURES

Figure 1.1 Histogram of Documented Worldwide Terrorist Attacks against Transportation Systems [8]	5
Figure 1.2 Terrorist Attack Statistics between 1980 and 2006 Involving Highway Bridges Located in Industrialized Nations [17, 18]	6
Figure 1.3 Illustration of Blast-Damaged Bridges, (a) Bridge Deck Breach Due to Above-Deck Detonation [19], (b) Catastrophic Failure of Bent Columns Due to Below-Deck Detonation [20].....	8
Figure 1.4 Illustration of Airblast Complexities from a Below-Deck Detonation [21].....	9
Figure 3.1 Explosive Materials Classification Illustration [45].....	20
Figure 3.2 Experimental Results Showing Increased Yield Stress with Increased Strain Rate for Tension-Loaded Steel Reinforcing Bars [55]: (a) Results for Nominal Grade 60 Steel, (b) Effect of Static Yield Strength on Strain-Rate Sensitivity	26
Figure 3.3 Experimental Results Showing Increased Concrete Compressive and Tensile Strength with Increased Strain Rate [54]	27
Figure 3.4 Illustration of Chemical and Physical Changes to Concretes as Temperatures Increase [61] ($1^{\circ}\text{C} = 33.8^{\circ}\text{F}$)	32
Figure 3.5 Model for Uniaxial Compressive Stress-Strain Characteristics of Siliceous (conservative for calcareous) Concretes at Temperature θ [62, 63]	33
Figure 3.6 Typical Uniaxial Stress-Strain Behavior of Structural Steels [65].....	35
Figure 3.7 Illustration of Strain-Rate Effects on Stress-Strain Behavior of Typical Structural Steels [50].....	36
Figure 3.8 Experimental Strain Rate Data for Mild and High-Tensile Steel (1-MPa = 145.04-psi) [69].....	40
Figure 3.9 Simplified Uniaxial Stress-Strain Model for Carbon Steels at Temperature, θ , at or above 400°C (752°F) [61].....	41
Figure 3.10 Complex Uniaxial Stress-Strain Model for Carbon Steels at Temperature, θ , less than 400°C (752°F) [61].....	42
Figure 3.11 Graphical Depiction of Strength and Modulus Reduction Factors for Carbon Steels at Temperature θ [61] ($1^{\circ}\text{C} = 33.8^{\circ}\text{F}$)	42
Figure 3.12 Graphical Depiction of Reduction Factors for Strength and Modulus of Cold-Worked Steel Reinforcement and Strength of Bolts and Welds at Temperature θ [61] ($1^{\circ}\text{C} = 33.8^{\circ}\text{F}$)	44
Figure 4.1 Influence of Standoff to Height Ratio on Blast Load Resulting from Spherical Surface Burst: (a) Far-Field Detonation, (b) Near-Field Detonation [18]	49
Figure 4.2 Illustrating Damage Potential for Different Types of Explosions (images adapted from blast tests supporting [24]): (a) Near-Field Explosions Typically Promote Flexural Response in “Heavier” Bridge Components, (b) Near-Contact Explosions Can Cause Localized Material Damage and Deformation, (c) Contact Charges Produce Extensive Localized Material Damage	50
Figure 4.3 Overpressure History for Ideal Far-Field Shock Wave [18]	51
Figure 4.4 Far-Field External Detonation Scenarios: (a) Spherical Free-Air Burst, (b) Spherical Air Burst, (c) Hemispherical Ground Burst [18]	52
Figure 4.5 Comparison of Normally Reflected and Side-On Pressure-Time Histories [18]	54
Figure 4.6 Schematic of Regular Oblique Reflection of Planar Shock Wave [18]	55

Figure 4.7 Schematic of Mach Reflection Evolution [5].....	56
Figure 4.8 Empirical Reflection Coefficient Curves as a Function of Angle of Incidence [50].....	56
Figure 4.9 Vortex Formation around Convex Corner [76].....	57
Figure 4.10 Schematic of Planar Shock Front Interaction with Building Structure [18]	58
Figure 4.11 Simplified Linear Representation of the Effect of Clearing on Pressure-Time History.....	59
Figure 4.12 Effect of Section Shape on Physical Standoff and Angle of Incidence [18].....	61
Figure 4.13 Effect of Charge Shape on Initial Shock Front Geometry [18].....	62
Figure 4.14 Graphical Depiction of Hopkinson-Cranz Cube-Root Blast Scaling Concept [18].....	64
Figure 4.15 Positive Phase Shock Wave Parameters for a Spherical TNT Explosion in Free Air at Sea Level [18].....	66
Figure 4.16 Illustration of Typical Ray Path Model Utilizing Image Source Concept for a First-Order Reflection [18]	67
Figure 5.1 Spall and Breach Behavior of Blast-Loaded RC Panels (adapted from [85]): (a) Spall Damage, (b) Crater and Spall Damage, (c) Section Breach.....	72
Figure 5.2 Blast Pulse Definitions and Damage Contour Plots at Incipient Failure for Case A and Case B Finite Element Simulations [18]	74
Figure 5.3 RC Cross-Section Showing Diagonal Rebar Resisting Direct Shear [86]	76
Figure 5.4 Idealized Resistance-Deflection Curve for Fixed-Fixed Flexural Member Exhibiting Tension Membrane Action [18].....	80
Figure 5.5 Forces Developing During Compression Membrane Response [86].....	81
Figure 5.6 Unconfined Compressive Stress-Strain Relationship of Concretes having Different Strengths [88]	84
Figure 5.7 Illustrating Confinement Effect on Ductility of High-Strength Concrete [88]	85
Figure 5.8 Influence of Steel Fiber Volume Fraction on Stress-Strain Behavior of Concrete having 9,000-psi Compressive Strength [88]	87
Figure 5.9 Influence of Steel Fiber Aspect Ratio on Stress-Strain Behavior of Concrete having 9,000-psi Compressive Strength [88].....	87
Figure 5.10 Stress and Strain Distribution across Depth of Singly Reinforced Fibrous Concrete Beam [88]	89
Figure 5.11 Local Breaching Failure of Steel Bridge Tower Test Specimens [93].....	90
Figure 5.12 Theoretical Stress Distribution for Pure Bending at Various Stages of Yielding: (a) Elastic, (b) Elastoplastic, (c) Plastic [50]	91
Figure 5.13 Typical Moment-Curvature Relationships for Steel Plates and Beams [86].....	91
Figure 6.1 Illustration of Local Response versus Global Response [18].....	96
Figure 6.2 Illustration of Structural Response Regimes on Elastic Response Spectrum for Right-Triangular Pulse Load.....	102
Figure 6.3 Analytically Derived Normalized P-I Diagrams for Three Different Pulse Loads.....	103
Figure 6.4 Schematic of Bounding Iso-Damage Curve Considering Multiple Component Modes of Response	104
Figure 6.5 Transformation of Continuous System to Equivalent SDOF System [18].....	105
Figure 6.6 Right-Triangular Blast Pulse for Equivalent SDOF Dynamic Analysis	111
Figure 6.7 Schematic of Equivalent SDOF Flexural Resistance Function [18]	112

Figure 6.8 Qualitative Direct Shear Resistance Function for Reinforced Concrete Flexural Member [18]	113
Figure 6.9 Experimental Development of Resistance Function for CFS Stud [101].....	113
Figure 6.10 Illustration of MDOF Analysis Approaches, (a) Advanced Single-Component Frame Analysis [102], (b) 3-D Finite Element Simulation [33]	115
Figure 7.1 Effect of Section Shape on Physical Standoff and Angle of Incidence [18].....	119
Figure 7.2 Blast Load Characterization for Reinforced Concrete Column Subjected to Close-In Detonation: (a) Overpressure and Specific Impulse Histories, (b) Variability in Overpressure Distribution with Time [18]	121
Figure 7.3 Effect of Charge Orientation and Point of Initiation on Blast Load Severity [18].....	122
Figure 7.4 Reflected Pressures due to the Ground, Deck, and Abutment [104].....	123
Figure 7.5 Ground Crater in Front of Khobar Towers (1996)	124
Figure 7.6 (a) Spall Damage to Concrete Column Sides and Cratering Damage to Front Face [24], and (b) Breach Damage [107].....	125
Figure 7.7 Dynamic Shear Response of Half-Scale RC Bridge Column Specimens Subjected to Small-Standoff Bulk Explosive Detonations [24]	126
Figure 7.8 Shear-Dominated Behavior of Quarter-Scale RC Bridge Column Specimens Subjected to Standoff Detonations [25]: (a) Direct Shear Failure at Column Base, (b) Dynamic Shear Behavior	127
Figure 7.9 Design Example 7.1 Elevation	131
Figure 7.10 Design Example 7.1 Details	131
Figure 7.11 Design Example 7.1 Sample Column Geometry Input	132
Figure 7.12 Design Example 7.1 Sample Load Input.....	133
Figure 7.13 Design Example 7.1 Results for 36-in. Diameter Column.....	134
Figure 7.14 Design Example 7.1 Results for 60-in. Diameter Column.....	134
Figure 7.15 Design Example 7.1 Effects of Concrete Strength on Column Response – 3,000 psi Concrete	135
Figure 7.16 Design Example 7.1 Effects of Concrete Strength on Column Response: (a) 6,000 psi Concrete, (b) 10,000 psi Concrete.....	136
Figure 7.17 Design Example 7.1 Effects of Concrete Cover on Column Response: (a) 1.5 in. Cover, (b) 3 in. Cover	137
Figure 7.18 Design Example 7.1 Effects of Type and Amount of Transverse Reinforcement on Column Response: (a) #4 hoops at 12 in. OC typical and 6 in. OC within end regions, (b) #6 spiral at 4 in. OC	137
Figure 7.19 Design Example 7.1 Effects of Amount of Longitudinal Reinforcement on Column Response: (a) 8 #8 evenly spaced, (b) 10 #8 evenly spaced	138
Figure 7.20 Design Example 7.1 Optimized Design: (a) Column Input, (b) Results	139
Figure 7.21 Design Example 7.2 Elevation	140
Figure 7.22 Design Example 7.2 Details	140
Figure 7.23 Design Example 7.2 Local Damage Results for 6-ft Standoff Distance	141
Figure 7.24 Design Example 7.2 Local Damage Results for 7-ft Standoff Distance	141
Figure 7.25 Design Example 7.2 Results for 8-ft Standoff Distance.....	142
Figure 8.1 Illustrative Details of Example Steel Cellular Bridge Tower.....	144
Figure 8.2 Truck Located Close to Structural Components of Steel Bridge [118].....	146
Figure 8.3 Access to Steel Cellular Tower [119].....	147

Figure 8.4 Detonation Sequence for Series 2 Test [113] (a) A Few Micro-Seconds after Detonation, (b) Approximately 1 Millisecond after Detonation.....	149
Figure 8.5 Specimen Geometry for Series 1 Experimental Testing Program from Pooled-Fund Study on Steel Cellular Towers [113]	151
Figure 8.6 Varied Damage Levels from Series 1 Tests [113].....	151
Figure 8.7 Varied Damage Levels from Series 2 Tests [113].....	152
Figure 8.8 Sample Steel Panel Geometry Input.....	157
Figure 8.9 Illustration Showing Cell Depth Corresponding to (a) 40-in. and (b) 50-in.	157
Figure 8.10 Geometry of Vertical and Horizontal Stiffening Angles.....	158
Figure 8.11 Example Threat Definition for Steel Cellular Tower	159
Figure 8.12 Isometric Views (a) In Front of and (b) Behind the Panel Being Analyzed	159
Figure 8.13 Analysis Results Showing Some Tearing at Edge of Panel for Baseline Threat	160
Figure 8.14 Iso-Damage Plot for Baseline Example	161
Figure 8.15 Global Failure of Front Panel due to Charge of 2,000-lbs TNT	161
Figure 8.16 Modified Front Panel with 70-ksi Steel and 3-in. Thickness	162
Figure 8.17 Localized Breach in Baseline Design.....	163
Figure 8.18 Recommended Retrofit Option [113].....	165
Figure 9.1 Illustrating Public Accessibility to Cable-Stayed Bridge Towers (photo from [123]).....	167
Figure 9.2 Illustrating Presence of Service-Level Axial Stress and Orthotropic Steel Reinforcing Configurations in Typical Cable-Stayed Bridge Towers (photo from [124]).....	168
Figure 9.3 Emphasizing Public Accessibility to Cable-Stayed Bridge Towers [125].....	169
Figure 9.4 Illustration of Hypothetical Two-Cell RC Tower Leg Subject to Explosive Charges Placed On/Off the Tower Leg's Plan Centerline	171
Figure 9.5 Post-Test Images of Close-In Blast Test against Scaled RC Tower Panel Specimen Showing Significant Breach Damage [127].....	173
Figure 9.6 Collapse of Cable-Stayed Bridge due to Close-In Detonation near RC Tower Base (adapted from [129])	174
Figure 9.7 Illustrating Steel Reinforcement Buckling in Reinforced Concrete Panels Following Localized Concrete Damage [132].....	175
Figure 9.8 Illustrating Component-Level Buckling of Reinforced Concrete Panels Following Extensive Concrete Damage [132].....	177
Figure 9.9 Post-Test Image of Hardened RC Tower Specimen Back Face.....	177
Figure 9.10 Images of Hardened RC Tower Specimen Steel Reinforcing Cage.....	178
Figure 9.11 Part of a High-Fidelity Computational RC Tower Leg Model [18].....	182
Figure 9.12 Schematic Illustration of Component-Level Flexural and Direct Shear Response of RC Tower Panel, Section View of Single-Cell Tower Leg [18].....	183
Figure 9.13 Example RC Tower Section Dimensions	184
Figure 9.14 Steel Reinforcement Details and Material Properties for Blast-Loaded Panel of Example RC Tower	185
Figure 9.15 Explosive Threat Definition for Example RC Tower.....	186
Figure 9.16 ATP-Bridge 3-Dimensional Graphics Display of Example RC Tower	186
Figure 9.17 Spall and Breach Damage of Baseline RC Tower Panel Design	187

Figure 9.18 Effect of (left) Increasing Transverse Reinforcing Bar Size and (right) Increasing Concrete Strength on Material-Level Damage.....	188
Figure 9.19 Effect of Increasing Sustained Axial Compressive Stress on Local Damage	189
Figure 9.20 ATP-Bridge Analysis Results for RC Tower Panel having Increased Section Thickness	190
Figure 9.21 Illustrating Material-Level Spall Damage in ATP-Bridge 3-Dimensional Graphics Window	191
Figure 9.22 Illustrating Component-Level Peak Dynamic Response in ATP-Bridge 3-Dimensional Graphics Window	191
Figure 9.23 Illustrating Recommended RC Tower Panel Retrofit, Section View [128]	193
Figure 10.1 Cable-Stayed Bridge [133]	194
Figure 10.2 Suspension Bridge [134]	194
Figure 10.3 Typical Single Strand and 27-Strand Stay Cable Sections [135]	196
Figure 10.4 (left to right) San Francisco–Oakland Bay Bridge [136]; Overall and Close-Up View of Golden Gate Bridge Main Suspension Cable [137].....	196
Figure 10.5 Examples of Hanger Cables in Suspension Bridges (left: [138]; right: [139])	197
Figure 10.6 Notional Example of Bulk Explosive Threat on Cable-Stayed Bridge [140]	198
Figure 10.7 Numerical Models of Block Charge Threat; Placed on Cable (left) and with Standoff (right) [141]	198
Figure 10.8 Diamond Charge Geometry [135]	199
Figure 10.9 Diamond Charge Model with 31-Strand Cable [135]	199
Figure 10.10 Examples of Cable Failure Due to Diamond Charge; Left: Failure of 25% of Strands; Right: Complete Failure of Cable [135]	199
Figure 10.11 Shaped Charge Geometry and Action [142]	200
Figure 10.12 Schematic of Explosively Formed Penetrator [143]	201
Figure 10.13 Schematic of Flyer Plate.....	201
Figure 10.14 Cross Section Exothermic Torch [144]	202
Figure 10.15 Exothermic Torch in Use [145]	202
Figure 10.16 Plasma Cutter [146]	203
Figure 10.17 Gasoline Powered Cut-Off Saw	203
Figure 10.18 Metal-Clad Linear Shaped Charge (left: [147]) and Flexible Shaped Charge (right: [148]).....	204
Figure 10.19 Flexible Linear Shaped Charge about Pipe Circumference, Before Detonation and After Detonation [149]	204
Figure 10.20 Eulerian Mesh and Materials (Air = Blue, Explosive = Red) Surrounding the Lagrangian Mesh of a Multi-Strand Cable Element (Black) [151]	211
Figure 10.21 Example of Numerical Model of Undamaged Cable-Stayed Bridge [153]	213
Figure 10.22 Cable and Flexible Linear Shaped Charge Input Screens	213
Figure 10.23 Analysis Results for 13-Strand Stay Cable Subjected to 200-gr/ft (left) and 400-gr/ft (right) Flexible Linear Shaped Charges.....	214
Figure 10.24 Cable and 20-lb TNT Block Charge Input Screens.....	215
Figure 10.25 Analysis Results for 31-Strand Stay Cable Subjected to 20-lb TNT Block Charge with 4-in. OD (left) and 8-in. OD (right)	216
Figure 10.26 Cable and 3-lb Diamond Charge Input Screens	217
Figure 10.27 Analysis Results for 19-Strand Stay Cable with 4-in. OD (left) and 31-Strand Stay Cable with 8-in. OD (right) Subjected to 3-lb C-4 Diamond Charge	217

Figure 11.1 Confinement Effects at Abutment [21]	226
Figure 11.2 Example of Steel Laced Column [157]	228
Figure 12.1 ATP-Bridge Software	231
Figure 12.2 Schematic of ATP-Bridge Project Organization	232
Figure 12.3 ATP-Bridge Interactive Help Utility	233
Figure 12.4 ATP-Bridge General Project Information Form	234
Figure 12.5 ATP-Bridge Main Form	234
Figure 12.6 Example ATP-Bridge Component Definition Form for a Reinforced Concrete Bridge Column.....	235
Figure 12.7 New Threat Scenario Association Form.....	236
Figure 12.8 Example ATP-Bridge Threat Definition Form for a Reinforced Concrete Bridge Column.....	236
Figure 12.9 ATP-Bridge Main Form with One Bridge Component and One New Threat Scenario that Has Not Been Analyzed.....	237
Figure 12.10 ATP-Bridge Component Analysis Form.....	237
Figure 12.11 ATP-Bridge Main Form with One Bridge Component and One Threat Scenario that Has Been Analyzed.....	238
Figure 12.12 Example ATP-Bridge Results Form for RC Bridge Column.....	239
Figure 12.13 ATP-Bridge Main Form Showing RC Column Peak Flexural Response in 3- D Graphics Window	240
Figure 12.14 RC Column Design Example 1 Elevation	246
Figure 12.15 RC Column Design Example 1 Details	246
Figure 12.16 RC Column Design Example 1 Sample Column Geometry Input.....	247
Figure 12.17 RC Column Design Example 1 Sample Load Input.....	248
Figure 12.18 RC Column Design Example 1 Results for 36-in. Diameter Column.....	249
Figure 12.19 RC Column Design Example 1 Results for 60-in. Diameter Column.....	249
Figure 12.20 RC Column Design Example 1 Effects of Concrete Strength on Column Response – 3,000 psi Concrete	250
Figure 12.21 RC Column Design Example 1 Effects of Concrete Strength on Column Response: (a) 6,000 psi Concrete, (b) 10,000 psi Concrete.....	251
Figure 12.22 RC Column Design Example 1 Effects of Concrete Cover on Column Response: (a) 1.5 in. Cover, (b) 3 in. Cover	252
Figure 12.23 RC Column Design Example 1 Effects of Type and Amount of Transverse Reinforcement on Column Response: (a) #4 hoops at 12 in. OC typical and 6 in. OC within end regions, (b) #6 spiral at 4 in. OC	252
Figure 12.24 RC Column Design Example 1 Effects of Amount of Longitudinal Reinforcement on Column Response: (a) 8 #8 evenly spaced, (b) 10 #8 evenly spaced.....	253
Figure 12.25 RC Column Design Example 1 Optimized Design: (a) Column Input, (b) Results.....	254
Figure 12.26 RC Column Design Example 2 Elevation	255
Figure 12.27 RC Column Design Example 2 Details	255
Figure 12.28 RC Column Design Example 2 Local Damage Results for 6-ft Standoff Distance.....	256
Figure 12.29 RC Column Design Example 2 Local Damage Results for 7-ft Standoff Distance.....	256

Figure 12.30 RC Column Design Example 2 Results for 8-ft Standoff Distance	257
Figure 12.31 Sample Steel Panel Geometry Input.....	258
Figure 12.32 Illustration Showing Cell Depth Corresponding to (a) 40-in. and (b) 50-in.	259
Figure 12.33 Geometry of Vertical and Horizontal Stiffening Angles.....	260
Figure 12.34 Example Threat Definition for Steel Cellular Tower	260
Figure 12.35 Isometric Views (a) In Front of and (b) Behind the Panel Being Analyzed	261
Figure 12.36 Analysis Results Showing Some Tearing at Edge of Panel for Baseline Threat	261
Figure 12.37 Iso-Damage Plot for Baseline Example	262
Figure 12.38 Global Failure of Front Panel due to Charge of 2,000-lbs TNT	262
Figure 12.39 Modified Front Panel with 70-ksi Steel and 3-in. Thickness	263
Figure 12.40 Localized Breach in Baseline Design.....	264
Figure 12.41 Example RC Tower Section Dimensions	265
Figure 12.42 Steel Reinforcement Details and Material Properties for Blast-Loaded Panel of Example RC Tower	265
Figure 12.43 Explosive Threat Definition for Example RC Tower.....	266
Figure 12.44 ATP-Bridge 3-Dimensional Graphics Display of Example RC Tower	266
Figure 12.45 Material-Level Spall and Breach Damage of Baseline RC Tower Panel Design	267
Figure 12.46 Effect of (left) Increasing Transverse Reinforcing Bar Size and (right) Increasing Concrete Strength on Material-Level Damage.....	268
Figure 12.47 Effect of Increasing Sustained Axial Compressive Stress on Material-Level Damage	269
Figure 12.48 ATP-Bridge Analysis Results for RC Tower Panel having Increased Section Thickness	270
Figure 12.49 Illustrating Material-Level Spall Damage in ATP-Bridge 3-Dimensional Graphics Window	271
Figure 12.50 Illustrating Component-Level Peak Dynamic Response in ATP-Bridge 3- Dimensional Graphics Window	271
Figure 12.51 Example of Numerical Model of Undamaged Cable-Stayed Bridge [153]	272
Figure 12.52 Cable and Flexible Linear Shaped Charge Input Screens	273
Figure 12.53 Analysis Results for 13-Strand Stay Cable Subjected to 200-gr/ft (left) and 400-gr/ft (right) Flexible Linear Shaped Charges.....	273
Figure 12.54 Cable and 20-lb TNT Block Charge Input Screens.....	274
Figure 12.55 Analysis Results for 31-Strand Stay Cable Subjected to 20-lb TNT Block Charge with 4-in. OD (left) and 8-in. OD (right)	275
Figure 12.56 Cable and 3-lb Diamond Charge Input Screens	276
Figure 12.57 Analysis Results for 19-Strand Stay Cable with 4-in. OD (left) and 31- Strand Stay Cable with 8-in. OD (right) Subjected to 3-lb C-4 Diamond Charge	276

LIST OF TABLES

Table 3.1 TNT Equivalences (data from [46, 49]).....	24
Table 3.2 Reinforced Concrete Constant Dynamic Increase Factors (adapted from [50]).....	28
Table 3.3 Compressive Strength Reduction Factor, Strain at Ultimate Stress, and Ultimate Strain for Normal-Weight and Lightweight Concretes at Temperature θ [62, 63].....	33
Table 3.4 Dynamic Increase Factors (DIFs) for Yield Strength of Various Structural Steels (adapted from [50])	37
Table 3.5 Dynamic Increase Factors (DIFs) for Ultimate Strength of Various Structural Steels (adapted from [50])	37
Table 3.6 Empirical Cowper-Symonds Equation Coefficients for Various Metals (adapted from [68]).....	39
Table 3.7 Reduction Factors for Hot-Rolled Carbon Steels at Temperature θ , Relative to an Ambient Temperature of 20°C (68°F) [61]	43
Table 3.8 Reduction Factors for Cold-Worked Steel Reinforcement, Bolts, and Welds at Temperature θ [61]	44
Table 5.1 Values for constants in Equation (5-2) (adapted from PDC-TR 06-01 [86])	75
Table 6.1 Example of System Performance Criteria for Blast-Resistant Design (adapted from [74]).....	100
Table 6.2 Example of Relationship between System Performance Criteria and Component Damage for Blast-Resistant Design (adapted from [74]).....	100
Table 6.3 Equivalent SDOF Transformation Factors for Simply Supported, One-Way Spanning Flexural Elements (adapted from [94]).....	108
Table 6.4 Equivalent SDOF Transformation Factors for Fixed-Fixed, One-Way Spanning Flexural Elements (adapted from [94]).....	108
Table 6.5 Equivalent SDOF Transformation Factors for Propped Cantilever, One-Way Spanning Flexural Elements (adapted from [94]).....	109

FOREWORD

The protection of buildings against the effects of explosions, man-made and accidental, has been a national interest for years. For nearly half a century, the U.S. Government has invested in research and development efforts focused on wartime defense scenarios involving nuclear events and high-explosive detonations, as well as other threats. In addition, the heavy industrial sector has long been concerned with damage and injury mitigation from accidental explosions occurring at petrochemical facilities. Over the last decade or so, with the rise in international and domestic terrorist activities, major concerns have been raised regarding the state-of-security of the nation's infrastructure.

While previous infrastructure security research and practice have focused primarily on building structures, recent worldwide statistics indicate a trend of increasing attacks against public transportation assets, with highway infrastructure being among the most frequently targeted. This statistical observation agrees well with the numerous threats received by U.S. Government authorities against various public highway bridges since the tragic domestic terrorist attacks of September 11, 2001. Public highway bridges are highly accessible, and, unlike typical building structures, they often lack the level of structural redundancy and exterior envelope protection needed to adequately withstand the extensive localized damage likely to result from a nearby explosion. Furthermore, the limited amount of bridge-specific protective design guidance in today's engineering guidelines and specifications suggests that the nation's existing highway bridges can be better protected against large-scale terrorist attacks and anti-terrorist/force protection (ATFP) concepts are not being incorporated into new highway bridge construction. Furthermore, as evidenced by recent non-terrorist-related bridge collapses around the nation, the sudden failure of a highway bridge located on a major transportation corridor has the potential to cause significant economic loss, human casualties, and societal distress.

The primary objective of this bridge security design manual is to present state-of-the-art guidance on bridge-specific security planning, extreme loading phenomenology and characterization, and protective design strategies to be used by the highway bridge community in terrorist threat vulnerability assessments of existing bridges, resilient design of new bridge construction, and emergency planning efforts. When compared to the amount of knowledge and formal guidance that currently exists for security and protective design of critical building structures, bridge security in the U.S. is in a relative stage of infancy. As such, bridge security will continue to be an active area of research and development for years to come, and this manual will be updated and expanded accordingly to remain a comprehensive, state-of-the-art reference for the highway bridge community.

A companion software program called Anti-Terrorist Planner for Bridges (ATP-Bridge) accompanies this bridge security design manual and will also be updated and expanded as bridge security knowledge and technology continue to develop and mature. In summary, ATP-Bridge is a practical design-level tool capable of predicting the response and incurred damage of critical bridge components subjected to a variety of explosive threat scenarios. The software is user-friendly, expedient, and enables the highway bridge community to implement essential blast-resistant analysis and design strategies without having to solely rely on time-consuming, costly, and complex resources such as physical testing or high-fidelity computational modeling. Applications and use of ATP-Bridge are discussed throughout many chapters of this manual.

The major limitation of this manual is simply the current bridge security state-of-practice. The content of this manual includes the most up-to-date discussions, guidance, and references on bridge security planning, extreme loading phenomenology and characterization, and protective design strategies for highway bridges. Much of what is presented herein is directly informed from recent bridge security research and experimental testing, and, where information is lacking, the need for additional research and development is emphasized.

In general, this manual is intended to be used by appropriate personnel within and associated with the highway bridge community, including, but not limited to, bridge engineers, vulnerability assessment personnel, and emergency planning and response professionals. The level of detail provided within this manual varies from topic to topic, with the general assumption that readers will possess basic knowledge of infrastructure security and engineering principles. It should be emphasized, however, that the level of knowledge required to read this manual is not the same thing as the level of knowledge required to carry out some of the recommended analysis and design procedures provided herein. The authors have made clear to the reader where recommended analysis and/or design procedures demand extensive knowledge and expertise in certain technical areas (e.g., high-fidelity finite element analysis). This bridge security design manual is currently in its first publication state (i.e., Revision 0).

1.0 INTRODUCTION

The protection of buildings against the effects of explosions, man-made and accidental, has been a national interest for years. For nearly half a century, the United States (U.S.) Government has invested in research and development efforts focused on wartime defense scenarios involving nuclear events and high-explosive detonations, as well as other threats. In addition, the heavy industrial sector has long been concerned with damage and injury mitigation from accidental explosions occurring at petrochemical facilities. Over the last decade or so, with the rise in international and domestic terrorist activities, major concerns have been raised regarding the state-of-security of the nation's infrastructure.

While previous infrastructure security research and practice have focused primarily on building structures, recent worldwide statistics indicate a trend of increasing attacks against public transportation assets, with highway infrastructure being among the most frequently targeted. In 1998, highway infrastructure was reportedly *the most* frequently attacked transportation target worldwide [1]. This statistical observation agrees well with the numerous threats received by U.S. Government authorities against various public highway bridges since the tragic domestic terrorist attacks of September 11, 2001. Public highway bridges are highly accessible, and, unlike typical building structures, they often lack the level of structural redundancy and exterior envelope protection needed to adequately withstand the extensive localized damage likely to result from a nearby explosion. Furthermore, the limited amount of bridge-specific protective design guidance in today's engineering guidelines and specifications suggests that the nation's existing highway bridges can be better protected against large-scale terrorist attacks and anti-terrorist/force protection (ATFP) concepts are not being incorporated into new highway bridge construction. As evidenced by recent non-terrorist-related bridge collapses [2, 3, 4, 5], the sudden failure of a highway bridge located on a major transportation corridor has the potential to cause significant economic loss, human casualties, and societal distress.

From a national defense perspective, the U.S. military relies heavily on the public highway system for moving military equipment and personnel from military installations to various seaports and airports around the country. The Strategic Highway Network (STRAHNET) system of public highways forms a key component of U.S. strategic defense policy, providing access, continuity, and emergency transport of personnel and equipment in times of peace and war. The 61,000-mile system comprises approximately 45,400 miles of Interstate and defense highways and 15,600 miles of other important public highways [1]. The collapse of a major STRAHNET highway bridge could seriously hinder the U.S. military's ability to mobilize resources and expeditiously respond to a domestic or international defense situation.

The recent trend of increasing worldwide attacks and identified vulnerabilities associated with public highway bridges highlight the need for security enhancement of existing and future bridges. However, implementing an across-the-board terrorist threat mitigation effort for the entire U.S. highway bridge inventory and instituting a nationwide integration of protective design guidance into the design of new bridges are monumental endeavors demanding a prohibitive amount of time and resources. As such, security enhancement must be approached in a strategic manner that allows for the most efficient use of available resources. Realizing that the risk of an attack and the severity of the consequences associated with an attack are likely to vary among the bridges in the U.S. highway inventory, ATFP retrofits of existing bridges must be

prioritized. Additionally, because typical bridge engineers often lack a thorough understanding of advanced structural dynamics and protective design fundamentals, bridge-specific protective analysis and design concepts must be available in practical form and disseminated in a clear and understandable manner. Significant research over the past decade has led to several important advancements in the areas of vulnerability assessment and risk-based prioritization methods, component-level blast load characterization and dynamic response analysis procedures, and blast mitigation techniques; however, little has been done to synthesize the state-of-the-art. An essential next step towards enhanced resiliency of the nation's public highway bridges is to begin transitioning novel bridge security technology to appropriate personnel within and associated with the bridge engineering community. The major goal of this manual is to facilitate the technology transfer process by providing comprehensive bridge security guidance and supplemental references for existing highway bridges and new highway bridge construction. While other security-related threats such as intentional vehicle/vessel impact, mass fires, and cutting threats will be discussed throughout this manual, primary focus is given to various types of high-explosive threats.

This chapter begins with a review of past terrorist events involving transportation infrastructure. The topic of bridge-specific risk management and security planning is then discussed followed by an introduction to bridge design for terrorist events. A review of recent advances in transportation infrastructure security follows, after which an introduction to the Anti-Terrorist Planner for Bridges (ATP-Bridge) software is provided.

1.1 History of Terrorist Events Involving Transportation Infrastructure

A large-scale terrorist attack against a major U.S. highway bridge was thought highly unlikely a little more than a decade ago. Construction drawings and design details for major transportation infrastructure were available to the public, and major bridge design codes lacked provisions addressing protective design. The domestic terrorist attacks of September 11, 2001 mark a tragic and unforgettable day in U.S. history. These terrorist-related events resulted in numerous fatalities, gross economic loss, and a nationwide pandemic of fear and anxiety. While the events of September 11, 2001 opened the eyes of many Americans to the true potential of domestic and international terrorist organizations, the reality is that such groups have been active across the globe for decades. Between 1990 and 2000, the Bureau of Alcohol, Tobacco, and Firearms reports that more than 2,500 criminal bombings occurred per year in the U.S. alone [6]. Latest reports out of Washington D.C. on intelligence and security officials around the world claim a growing pool of terrorists and corruption that is beginning to overwhelm security and intelligence tracking capabilities [7]. A particularly concerning trend in recently documented terrorist activity is the increase in attacks on worldwide public surface transportation infrastructure. As can be seen in Figure 1.1, the number of documented terrorist attacks against these types of targets increased from less than 70 attacks in 1998 to nearly 400 attacks in 2015. Per the U.S. State Department, the number of violent attacks against transportation targets increased from 20 percent of all violent attacks in 1991 to nearly 40 percent in 1998 [6].



Figure 1.1 Histogram of Documented Worldwide Terrorist Attacks against Transportation Systems [8]

As of the first quarter of 2010, the Mineta Transportation Institute (MTI) documented 1,633 worldwide terrorist attacks against public surface transportation infrastructure—161 of which specifically targeted highway infrastructure. Moreover, 82 of the documented highway infrastructure attacks involved explosives and/or incendiaries. Although the 1977 explosion on the Route 1 Bridge in Florida Homestead and Key West is the only U.S. highway infrastructure *attack* currently documented in MTI’s database, intelligence gathered from captured terrorists and threats received by U.S. authorities suggest that the potential for a future attack is high.

In February of 1982, police discovered approximately 40 lbs of a powerful liquid explosive left in a parked car beneath the Bay Bridge on the San Francisco side [9]. In June of 1993, police arrested nine Muslim fundamentalists who were planning to blow up the George Washington Bridge as well as the Holland and Lincoln Tunnels in New York. Just one month later in July of 1993, an Islamic Jihadist caller warned that an extremist group had planted explosives on all bridges leading to Canada on the Niagara Frontier [9]. In May of 2000, an Al Qaeda training manual was captured in Manchester, England during a police investigation of a home belonging to an alleged member of Al Qaeda. The captured training manual contained goals that included missions for gathering information about the enemy and for blasting and destroying bridges leading into and out of major cities [10]. In a similar vein, as a Caltrans-funded Bay Area Security Enhancement Project neared completion in 2003, a captured Al Qaeda leader revealed that a bridge in San Francisco or San Mateo was on a list of possible targets for the terrorist network [10]. In May of 2003, a naturalized U.S. citizen living in Columbus, Ohio was arrested for conspiring to commit a terrorist act that involved severing the main suspension cables of the Brooklyn Bridge with blow torches [11]. In June of 2003, Mohammed Rauf, an Al Qaeda operative, was arrested for plotting to destroy the Brooklyn Bridge. While in custody, Rauf also admitted to conspiring to pinpoint targets for simultaneous terrorist attacks on New York City and Washington [12]. Less than a year later in April of 2004, the U.S. Coast Guard received notification of a bomb discovery on the Bay St. Louis Bridge in Mississippi. The bridge operator

who submitted the notification discovered a package secured to a main bridge girder with bungee cords. The package was later opened and found to contain a plastic container that housed a brown box with wires sticking out of it [13]. New York City was once again terrorized with a bomb threat to the Brooklyn Bridge in October 2010. During this incident, authorities discovered a flashlight connected with copper wiring along with two suspicious packages lying on each side of the bridge deck [14]. On May 2, 2011, the day after Osama bin Laden was killed by U.S. Navy SEALs, the Coronado Bridge near San Diego, California was temporarily shut down after a suspicious object resembling a pipe bomb was found on the bridge deck. The bridge was later re-opened after authorities identified the object as inert military ordinance [15]. In April of 2012, five men were apprehended for plotting to “blow up” a highway bridge just south of Cleveland, Ohio. The men were arrested after leaving two toolboxes at the base of the bridge that contained inert C-4 explosive purchased from an undercover FBI agent days earlier [16].

Despite the long list of threats against signature highway bridges in the U.S., it should be emphasized that worldwide historical data suggest that terrorists tend to attack typical, non-iconic transportation infrastructure with the greatest frequency. In the context of this manual, an iconic bridge refers to a one-of-a-kind structure exhibiting a unique design (e.g., true or tied arch, cable-stayed, or suspension) that compliments the surrounding landscape and carries a significance to the local community. Between 1980 and 2006, the MTI database includes 53 terrorist attacks that specifically targeted public highway bridges, 20 of which occurred in industrialized nations [17]. Of the 53 worldwide bridge attacks, 58-percent involved non-iconic structures. Furthermore, of the 20 bridge attacks occurring in industrialized nations, 35-percent involved non-iconic structures. These statistics are further illustrated in Figure 1.2 for the 20 bridge attacks occurring in the U.S., Europe, and Australia.

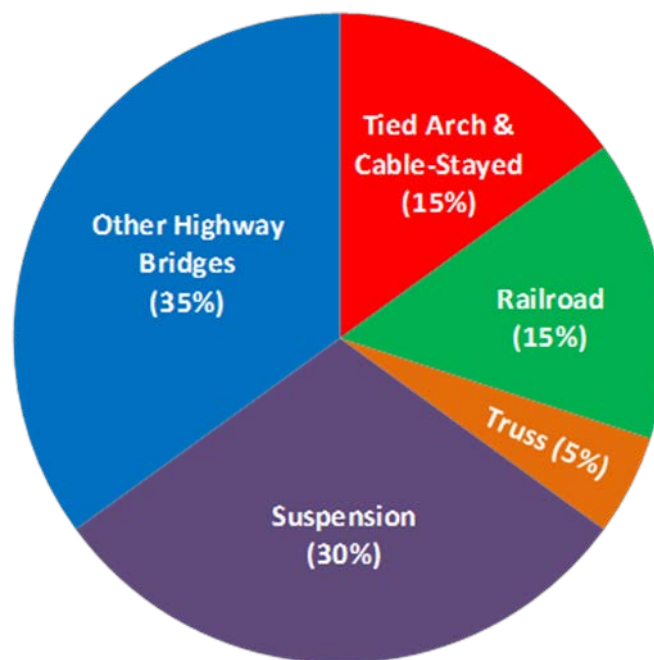


Figure 1.2 Terrorist Attack Statistics between 1980 and 2006 Involving Highway Bridges Located in Industrialized Nations [17, 18]

1.2 Risk Management and Security Planning for Highway Bridges

An essential aspect of security planning and risk management for our nation's transportation infrastructure is identifying the degree to which threat mitigation measures may be needed for a given transportation asset. For the case of highway bridges, some may require a significant degree of threat mitigation, while others may not require any. To make such a determination, an assessment of bridge importance and vulnerability is needed. The assessment should include factors such as social/economic impact of bridge loss, significance in terms of defense/security of a region, state, and/or the entire nation, average daily traffic, average daily truck traffic, distance to the nearest detour, and symbolic importance.

Other important aspects of security planning and risk management for highway bridges include, but are not limited to, credible threat determination and the identification of threat mitigation strategies that are feasible and most prudent for a given highway bridge. Effective threat mitigation strategies can take many forms, such as planning and coordination measures, information control measures, site layout measures, access control and deterrent measures, and deception measures. It is also important for bridge owners and engineers to understand that bridge security should not be considered in isolation, rather measures should be integrated at the outset of a project and regarded as a key component of the entire design process. In a similar vein, while coordination among the members of a project team is always important, the significance can be greater for bridge security than for other hazards.

Risk management and security planning for highway bridges, though currently not standardized and still very much a work in progress, will play a vital role in enhancing the security and resilience of our nation's transportation sector in the coming years. Chapter 2 of this manual is dedicated to the topic of security planning for highway bridges and offers additional discussion and guidance as well as relevant state-of-the-practice references.

1.3 Bridge Design for Terrorist Events

From a terrorist attack point of view, bridges possess several unique characteristics relative to building structures. Bridges are rarely if ever constructed with an exterior façade or structural envelope. Thus, main structural components of a bridge are directly exposed to the environment rendering them vulnerable to direct loading from an explosive threat and relatively easy access by terrorist personnel or vehicles. The ability to impose physical standoff—that is, the distance between a threat and a target—through deterrent systems such as barriers, bollards, or landscaping, or through controlled access points, can be limited or even unachievable in certain situations. Buildings generally have more structural members than bridges and therefore inherently possess greater structural continuity and redundancy than a typical highway bridge. Consequently, bridges have comparatively less ability to withstand extensive localized damage, especially when extensive damage occurs to a critical substructure element such as a bridge pier (Figure 1.3).



Figure 1.3 Illustration of Blast-Damaged Bridges, (left) Bridge Deck Breach Due to Above-Deck Detonation [19], (right) Catastrophic Failure of Bent Columns Due to Below-Deck Detonation [20]

The fact that most highway bridges are directly exposed to the environment, coupled with the difficulties associated with imposing physical standoff, greatly increases their vulnerability to severe, close-in threats; whether from bulk explosives, a contact charge, vehicle impact, or a precision cutting threat. These severe, close-in threats can give rise to unique material and component-level behavioral aspects and failure mechanisms that are not typically encountered in conventional bridge design and can have a major influence on structural member performance and capacity. For example, an acutely blast-loaded structural member undergoes a complex dynamic response evolution that begins with local material-level response adjacent to the explosive charge and transitions to component-level response as the entire structural member is set in motion. Early-time material damage, such as local spall/breach damage for concrete material or local denting/breach damage for steel material, can significantly influence later-time component response and thus represents a unique dynamic coupling phenomenon that is rarely (if ever) considered in conventional design. A lucid discussion on high-explosive materials and the dynamic performance of typical construction materials is provided in Chapter 3 of this manual. In addition, Chapter 5 is devoted to the discussion of unique behavior aspects and structural mechanics of blast-loaded bridge components. The concept of dynamic response evolution as it pertains to blast-loaded members is also touched upon in the beginning of Chapter 6.

Another unique characteristic of highway bridges is the exceptionally complex airblast environment that can be generated during a close-in explosive attack. Take, for example, a below-deck detonation as shown in Figure 1.4. The geometry of a typical highway bridge can consist of multiple shock wave reflecting surfaces and partially vented cells. Interaction of the incident and multiple reflected shock waves can result in complex spatial and temporal variations in the resulting blast loads acting on nearby structural members. In addition, partially vented cells—such as between the underside of a bridge deck and two adjacent bridge girders—can lead to exacerbated overpressure stagnation and ultimately greater blast loads on affected structural members.

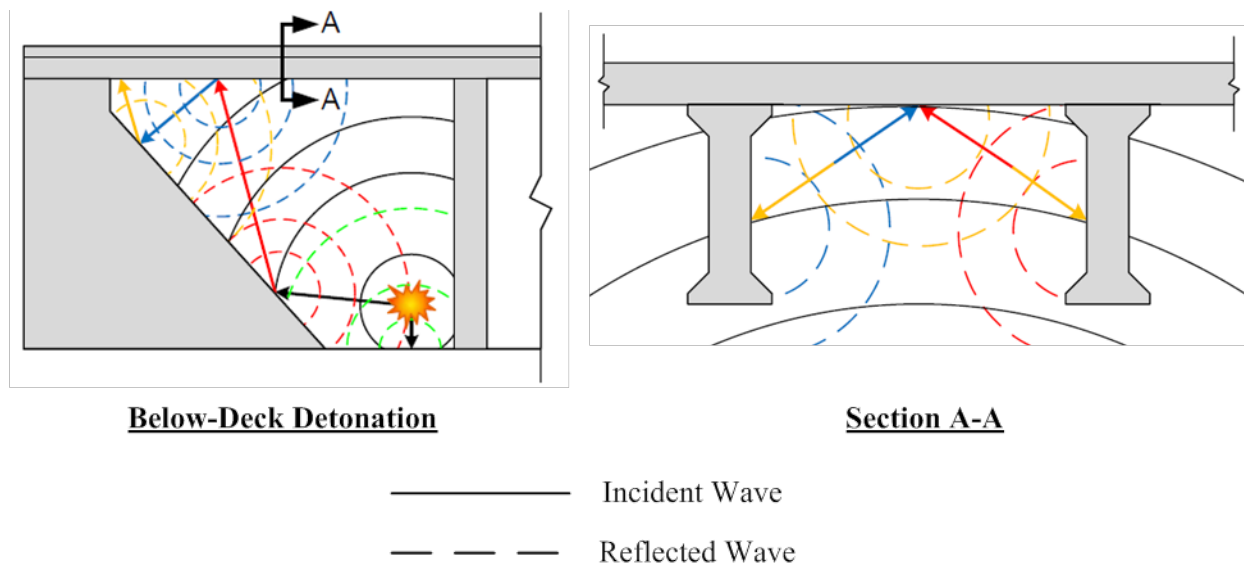


Figure 1.4 Illustration of Airblast Complexities from a Below-Deck Detonation [21]

Adding to the complexity of the airblast environment near a highway bridge is the slender nature of many structural members; a bridge column being a prime example. As is discussed in more detail in Section 1.4 and Chapter 4 of this manual, slender members tend to benefit from enhanced clearing and wrap-around pressure effects once engulfed by the shock flow from a high-explosive detonation. The slender member disrupts the shock flow causing highly turbulent behavior along its leeward face. During this process, positive pressures develop along the member's leeward face, which partially negate incident-face reflected pressures and ultimately reduce the net blast load imparted to the slender member. Due to the various blast load complexities associated with highway bridges, many of the state-of-the-practice blast load characterization methods commonly employed for building structures cannot be used directly to calculate blast loads for highway bridges.

A chief objective of this bridge security design manual is to educate the reader on the unique facets of physical security and protective design for highway bridges. As was noted throughout this section, Chapters 3 through 5 focus on material-level performance, blast load phenomenology, and component-level behavioral aspects, respectively. Discussion and guidance on various dynamic analysis approaches are provided in Chapter 6, and Chapters 7 through 11 apply the knowledge, techniques, and guidance offered in the previous chapters to specific protective design strategies for various structural components of a highway bridge. In addition, this bridge security design manual is intended to act as a perpetual springboard from which state-of-the-art advances in bridge security can be transitioned from research to practice. Chapters 7 through 11 do not represent an exhaustive list of all critical structural members comprising our nation's highway bridge inventory, rather they represent the current state of knowledge and highlight the need for future research and development. Some examples of recent advances in bridge security are provided in the following section.

1.4 Recent Advances in Transportation Infrastructure Security

While recent government funding has gone to support the development of risk-based prioritization and vulnerability assessment procedures [22, 23], various government agencies and

other organizations have also funded research to extend the knowledge in blast load characterization, structural response to blast loads, and blast threat mitigation retrofits. For example, researchers at the University of Texas at Austin recently conducted an experimental test program with the main objective to develop a national standard for the blast-resistant design of highway bridge columns [24]. Funded by the National Cooperative Highway Research Program (NCHRP), the research involved large-scale blast tests in two phases. The first phase focused on characterizing the behavior of shock waves near slender structural components, such as bridge columns, and the second phase focused on the response of half-scale reinforced concrete column specimens subjected to small standoff and near-contact detonations. The Phase 1 results provided significant insight into blast load characterization for slender structural components, and the Phase 2 tests yielded information for developing design criteria for blast-resistant columns. Researchers at the State University of New York (SUNY) at Buffalo were funded by the Federal Highway Administration (FHWA) to investigate how seismically designed bridge columns perform during a blast event [25, 26]. Two test series were conducted, and the test matrices consisted of quarter-scale column specimens having different permutations of steel reinforcement detailing and steel jacketing. Additional experiments have undertaken blast testing of other critical bridge components, including prestressed concrete girders [27], structural steel bridge towers [28, 29], reinforced concrete bridge towers [30], and main stay and suspension cables [31].

Given the complexity and high cost associated with experimental blast testing, researchers have also used computational simulation tools to better understand the effects of blast on the structural performance of critical highway bridge components. For instance, researchers at the U.S. Army Engineer Research and Development Center (ERDC) used three different blast load prediction tools, each offering a different level of fidelity and associated computational expense, to estimate the transient overpressures delivered to the components of a typical highway bridge from a below-deck detonation [32]. The findings indicated that drastically different blast loads can be predicted depending on the load characterization methodology. During the NCHRP-funded highway bridge column project, researchers from the University of Texas at Austin conducted a series of computational fluid dynamics and nonlinear finite element analyses to further investigate the Phase 1 and Phase 2 experimental blast tests [33]. The simulation results confirmed that slender structural components experience a reduced net blast load due to enhanced clearing and wrap-around pressure effects. Researchers at SUNY Buffalo carried out a similar computational study with the chief objective of investigating the behavior of shock waves near exposed structural steel wide-flange sections [34]. Their conclusion of a net reduction in the blast load due to enhanced clearing and wrap-around pressure effects closely aligned with that from the NCHRP bridge column research. Computational research from the University of California at Berkeley investigating the effects of above-deck detonations on the performance of cable-stayed and suspension bridge decks led to the concept of a frangible deck panel designed to fail early to vent blast loads the structure would otherwise be required to resist [35].

While not an exhaustive list, the experimental and computational research programs highlight the fact that the state-of-the-art in bridge-specific protective design has only begun to mature over the past decade. Nonetheless, the experimental results and findings from these research programs largely remain fragmented throughout the academic community and open literature. A chief objective of this bridge security design manual is to synthesize the state-of-the-art and present it

in a practical and applied form for immediate use by the bridge engineering community, highway bridge vulnerability assessment professionals, and emergency planning personnel.

1.5 Anti-Terrorist Planner for Bridges (ATP-Bridge) Software

While international terrorist organizations have been active across the globe for decades, attacks against public surface transportation infrastructure (as pointed out in Section 1.1) have been a growing concern. Considerable research has been carried out in the area of bridge security over the past decade. Important advancements have been made in the areas of vulnerability assessment and risk-based prioritization methods, component-level blast load characterization and dynamic response analysis procedures, and blast threat mitigation techniques. Although much research is still needed, it is important to begin transferring these state-of-the-art protective design concepts and methodologies to the appropriate users within the bridge engineering community, including vulnerability assessment and emergency planning personnel. An essential next step in enhancing the security of public highway bridges is to synthesize this newly developed protective design technology into an expedient and user-friendly engineering tool capable of facilitating effective anti-terrorist/force protection (ATFP) retrofits of current bridges, safe designs of new bridges, as well as assessment and emergency planning efforts. Such a tool would enable practicing bridge engineers to implement essential blast-resistant analysis and design strategies without having to rely on time-consuming, costly, and complex resources such as physical testing or high-fidelity computational modeling. Anti-Terrorist Planner for Bridges (ATP-Bridge) has been developed to specifically address these highway infrastructure security issues and, more generally, to help facilitate the implementation of research findings into current practice. This software was collaboratively developed by The University of Texas at Austin and Protection Engineering Consultants, LLC, with sponsorship from the U.S. Department of Homeland Security and technical direction from the U.S. Army Engineer Research and Development Center (ERDC).

ATP-Bridge is a practical engineering-level software program capable of predicting the response and incurred damage of critical bridge components subjected to a variety of explosive threat scenarios. ATP-Bridge features flexible software architecture designed to be continuously informed and updated with state-of-the-art research and intuitive, user-friendly functionality that aligns with practice. The software relies on fast-running computational algorithms that have been verified and validated against available experimental data. ATP-Bridge is intended to be utilized primarily by bridge engineers and vulnerability assessment personnel, but it can also be used by emergency responders and law enforcement professionals to help quantify the likelihood of a major transportation disruption resulting from a postulated malicious attack. This information can then be used to support emergency planning decisions such as critical resource allocation.

The current version of ATP-Bridge (Version 3) encompasses component response models for reinforced concrete (RC) bridge columns, steel suspension bridge tower panels, RC bridge tower panels, and high-strength steel cables. Regarding threat scenarios, the software can consider contact and near-contact high-explosive charges, standoff detonations from bulk high-explosive threats, and various thermal, mechanical, and explosive cutting threats. Numerous design examples utilizing the ATP-Bridge software are provided throughout this manual in the component-specific design chapters and Chapter 12. Also provided in Chapter 12 is additional

background and technical discussion regarding ATP-Bridge software architecture, analysis capabilities, and applications.

1.6 Chapter Summary

This chapter began with an examination of worldwide historical data and past events (both successful and thwarted) related to highway bridge attacks. The need for enhanced bridge security and dissemination of bridge-specific protective design strategies to the bridge engineering community was highlighted. An introduction to risk management and security planning for highway bridges was provided as a lead-in to Chapter 2 of this manual.

In this chapter, an introductory discussion on bridge design for terrorist events was also provided. The discussion addressed the many unique features of highway bridges that make them particularly vulnerable to malicious attacks; arguably the most critical feature being public accessibility. Recent advances in transportation infrastructure security was also covered in this chapter, and a brief overview of the ATP-Bridge software—an engineering-level tool for component-level vulnerability assessment and protective design of critical bridge components; a companion tool to this manual—was provided.

In Chapter 2, the topic of security planning for highway bridges will be addressed in more detail. The chapter will cover various threat mitigation strategies for highway bridges, security-related project coordination issues, and references to additional publicly available bridge security guidance will be provided.

2.0 SECURITY PLANNING FOR HIGHWAY BRIDGES

Compared to other hazards, the protective design of structures to resist terrorist threats is a relatively new field. Research to date has focused primarily on buildings, with limited attention paid to bridges. Since the terrorist attacks of September 11, 2001, interest in protecting bridges and other transportation assets has become a pressing issue of national importance. The U.S. Department of Homeland Security identifies transportation as a critical sector for our nation. An essential aspect of security planning is identifying the degree to which protective measures may be needed for a given project. Thus, some bridges may require a significant degree of protection, while others may not require any. To make such a determination, an assessment of bridge importance and vulnerability is needed.

Although a variety of approaches have been proposed in the research literature [22, 23, 36], there is no nationally accepted procedure currently followed by different state Department of Transportations (DOTs) for assessing the importance and vulnerability of bridges and other transportation assets. At present, bridge owners must establish their own methodology for assessing the importance of a bridge so that available funds to enhance transportation infrastructure security can best be prioritized. Factors that are common to many of the proposed procedures include:

- Social/economic impact of bridge loss
- Role played by bridge in defense/security of region/state/nation
- Average daily traffic
- Average daily truck traffic
- Distance to nearest detour
- Symbolic importance

Some work has been carried out to assist bridge owners and transportation planners in the development of a consistent framework for developing effective security practices and security plans. One such tool recently developed by the Transportation Security Agency (TSA) of the Department of Homeland Security (DHS) is known as the Transportation Security Template and Assessment Review Toolkit (T-START) [37]. This web-based software is composed of five separate security guidance modules that address highway transportation security. To use this tool, it is necessary to register an account with the TSA.

Before developing a plan to enhance bridge security, bridge owners should first understand the potential threats acting against a bridge as well as the terrorists' goals and tactics. There are numerous combinations of explosive devices, cutting devices, impact vehicles, and specific attack locations to consider.

The goal of security planning for highway bridges is to develop economical, unobtrusive, and effective methods to mitigate the risk of terrorist attacks against critical bridges to an acceptable level. Acceptable risks are defined as the hazards a risk manager (e.g., bridge owner) is willing to

accept considering available resources, the residual probability of an attack, and the potential consequences after the implementation of countermeasures. It is impossible to design all bridges to withstand all possible combinations of terrorist attacks that may occur [38]. There are simply too many combinations. Terrorists are unpredictable, and the specific threats they pose are uncertain. Additionally, unlike other threats such as violent acts of nature, terrorists can adapt to mitigation and security measures. Thus, it is important to determine the most likely tactics from the terrorists' perspective and reduce the number of possible combinations of attacks that need to be considered for the purposes of design. It is also important to recognize that not all threats can be mitigated to such a degree that there will be no resulting damage. Because bridges are open to the travelling public, potential threats can be severe. A large enough truck bomb located close enough to a critical structural component will cause extensive damage. Accordingly, the goal of security planning is to reduce risk to an acceptable level, realizing that it cannot be completely eliminated. This situation for bridges differs considerably from that of critical buildings in which protected perimeters can be established to keep standoff distances large enough to ensure that such buildings will survive an attack. This type of protection would defeat the purpose of constructing a bridge with open access to vehicular traffic, and it is therefore necessary to accept some level of risk. The level of risk acceptance will depend upon the importance of the bridge, available resources, and other factors described in this chapter.

It is important for bridge owners to understand that security measures should not be considered in isolation. Rather, bridge security should be taken as a component of the entire design process, which considers all necessary load cases and combinations. For example, some state DOTs have developed procedures to assess bridge importance to assist in prioritizing seismic rehabilitation efforts. These procedures established for assessing bridge importance should be used in conjunction with security considerations. For owners and engineers interested in learning more about bridge security strategies and risk reduction, a list of references is provided at the end of the chapter. The *AASHTO Bridge Security Guidelines* [36] can be consulted to identify a range of possible threats, attack modes, and vulnerabilities for different bridge components and bridge systems.

Unlike design for natural disasters, which has been part of engineering practice for many years, design for security is an emerging field. While significant research has advanced the field over the past 15 years, research findings have not been readily implemented into everyday design practice. Aside from the uncertainty associated with designing for such events, computing the loads and structural response, even when the design threat is known, can be a challenge. For blast events, the load a structure must resist is highly dependent upon the size, shape, and orientation of the charge relative to the component of interest. It is also highly dependent upon the distance between the target and the explosive (known as the *standoff distance*), and several other factors. The physics of explosions and how these events create loads on bridge components is discussed in detail in Chapter 4 of this manual.

2.1 Threat Mitigation Strategies

Various threat mitigation strategies or countermeasures can be used to address general or specific threats to bridges. These measures include planning and coordination, sensitive information control, site layout, access control, deception, and structural hardening. They can be used to displace the threat to less attractive targets, increase the likelihood of terrorists being detected

and identified, keep casualties to a minimum, improve emergency response time, increase public confidence, improve structural response, or a combination of these events. The following strategies are based on work reported by Williamson and Winget [38]. The intent of the following discussion is to identify major areas of concern and steps that can be taken to address these concerns. The list is not intended to address every conceivable issue that may develop when considering bridge security on a given project. Thus, the items addressed provide a good starting point from which owners, planners, emergency response personnel, and engineers can initiate a dialogue to best meet the needs of a specific project.

2.1.1 Planning and Coordination Measures

- Updating the emergency operations plan/crisis management plan to include response and recovery to a terrorist threat involving a bridge
- Communication and coordination with local, state, and federal law enforcement agencies to obtain terrorism intelligence, training, and technical support
- Regular drills, tabletop exercises, and full-scale simulations to test response procedures, communication, and coordination
- Planning additional redundancy in the transportation system through alternate routes, traffic management, modified lane usage, etc.
- Planning for prompt debris removal and repairs to ensure rapid restoration of services and restore public confidence in the transportation infrastructure
- Developing a training plan for maintenance personnel to be observant of surroundings and capable of dealing with suspicious objects

2.1.2 Information Control Measures

- Establish “need-to-know basis” procedures for the release of vulnerabilities, security measures, emergency response plans, or structural details for specific bridges. Because most state DOTs lack the capability to classify documents like the Department of Defense (e.g., Secret or Top Secret), an alternate designation of “Sensitive Security Information” (SSI) should be considered [39].
- Review and sanitize websites for potential information that may be beneficial to terrorists. Removal of data from websites, however, must be balanced with the need for information sharing. For example, information about a specific bridge can be very useful for identifying weaknesses and planning an attack, while general design guidelines usually provide information of limited value to potential terrorists.

2.1.3 Site Layout Measures

- Improved lighting with emergency backup, combined with the elimination of hiding spaces that can be used to prepare explosive charges
- Clearing overgrown vegetation to improve lines of sight to critical areas

- Using creative landscaping with regular maintenance to increase vehicular standoff distance to important structural components
- Elimination of access to critical areas such as beneath the deck, within the enclosed space of a box girder or tower, maintenance rooms, etc.
- Elimination of parking spaces beneath bridges
- Providing pass-through gates in concrete median barriers to enable rerouting of traffic and access for emergency vehicles
- Planning redundancy in individual future bridges, such as using two adjacent two-lane bridges as opposed to one four-lane bridge
- Avoiding architectural features that magnify blast effects, such as recesses or offsets in structural members or unnecessary confined areas

2.1.4 Access Control/Deterrent Measures

- Police patrol, surveillance, and guards
- Keyed or keyless entry systems on access panels, tower entrances, and maintenance areas
- Exterior and interior intrusion detection systems (boundary penetration sensors, volumetric motion sensors, and point sensors)
- CCTV placed where it cannot be easily damaged or avoided, while providing coverage of critical areas to monitor activity, detect suspicious actions, and identify suspects. For full effectiveness, CCTV must be coordinated with the ability of law enforcement to respond quickly when necessary. CCTV, by itself, will have limited effectiveness in deterring would-be terrorists (as evidenced by the attackers in the London subway in 2005 and at the Boston Marathon in 2013).
- Incorporate a high level of identification procedures and verification of credentials for maintenance personnel
- Deny/limit access to critical structural elements (i.e., providing fencing or other protection around cable anchors, restricting access to box girders and cable towers, etc.) and inspection platforms
- Physical barriers to protect critical structural components
- Physical barriers to control or limit access to a bridge when credible threats have been identified (used in conjunction with random vehicle searches)
- Rapid removal of abandoned vehicles
- No-fly zones around critical bridges (including drones or other unmanned aircraft)
- Emergency telephones to report incidents or suspicious activity

- Use of an advanced warning system, including warning signs, lights, horns, and pop-up barricades to restrict access after span failure or other potentially hazardous situation

2.1.5 Deception Measures

- Installing dummy CCTV cameras to augment active cameras when resources are limited
- Parking an abandoned police vehicle nearby
- Posting intrusion detection signs and warnings

In addition to the above lists, structural hardening can also be used to achieve enhanced levels of protection (discussed in Chapters 7-11 of this manual). Costs will vary by bridge type, size, and location, but generally the planning and information control procedures will provide the most significant improvement for minimal additional cost. Site layout and access control will typically provide the next most cost effective solutions, respectively, and structural hardening will normally be the most expensive unless it is accomplished during the design stage. There has been much debate regarding the cost effectiveness of the countermeasures described above relative to structural hardening. In most cases, the initial costs for structural hardening will be greater than those needed for the items given in the previous lists. However, it is important that bridge owners consider lifetime costs when deciding what countermeasures to implement. For example, the initial costs to install CCTV cameras may be less than increasing the size and strength of all critical bridge columns, but the CCTV cameras require monitoring, maintenance, and possible replacement over the same time period that columns would require little follow-on costs after initial construction. Further, CCTV cameras are only effective for bridge security when the information collected is used effectively to coordinate law enforcement and emergency response personnel. Cameras, by themselves, are ineffective at protecting a bridge because they require active monitoring. Strengthening columns is a form of passive protection. Once they are built, they will provide the capacity needed to resist the design-basis threat without any need for long-term monitoring (other than what is already done during routine bridge inspections). Thus, when evaluating the lists above, it is essential to consider the long-term costs over the life of a bridge, the level of coordination with other agencies, hiring and training of personnel to properly operate equipment, etc.

In general, an approach that combines active and passive measures is likely to offer the best solution. With this approach, columns can be strengthened, but not to the degree that would be required if other passive measures were not in place. Thus, when integrated with a CCTV camera system that can detect large trucks with a payload greater than a specific value, a combination of limited monitoring and a modest degree of structural hardening can produce a solution that utilizes the best features of all countermeasure approaches. Other factors to consider include achieving a balance in the visibility of the measures between high visibility to provide deterrence and reassure public confidence, and transparent measures to preserve the architectural and environmental appearance. In addition, the degree of user tolerance for the increased security due to changes in convenience and accessibility, contribution to other threats such as reduced crime, and increased resistance to accidents or natural disasters should also be considered.

2.2 Project Coordination

While coordination among the members of a project team is always important, the significance can be greater for bridge security than for other hazards. To meet design challenges associated with areas of high seismicity, flooding, or other natural disasters, planners and engineers can work together on site planning and overall design to find the best solution available within the project constraints. Thus, if soil conditions are poor at one location, or if channel flow rates or restrictions at a given location are problematic, it may be possible to find an alternate location that reduces these challenges and reduces the structural design demands. Although project constraints may not always permit the optimal structural design solution, coordination can improve the options available. Unlike natural hazards, bridge security requires structures to be protected against intentional man-made acts. Such threats can and have changed with time, and historical data cannot produce the same level of confidence for selecting a design-basis threat like it can for natural hazards. Further, once the planning stage of a project involving natural hazards is complete, the engineering design can proceed independently. At that stage of a project, no amount of additional transportation planning will affect the seismicity at a given site. Protective design of bridges, however, requires coordination throughout the design and operation of bridges. Depending upon the location, average daily traffic, access to critical locations, and other factors, the design-basis threat used to size and detail bridge components can change. For example, if truck traffic is controlled on a given bridge, it might be possible to consider a smaller blast event than would need to be considered if truck traffic is not controlled.

In general, decisions made by different members of the project team can have significant impacts on other groups tasked with ensuring bridge security. Some structural details may make police surveillance difficult. The placement of cameras and other devices may affect bridge aesthetics and other design considerations. Because of these various factors, it is essential that bridge security issues be addressed as soon as possible for a given project. It is also essential that all members of the project team, including law enforcement, military, and emergency response personnel, be present during the early stages of a project. Such coordination will ensure the best possible outcome. If decisions such as design-basis threat, access control, use of supplemental surveillance equipment, and other factors are coordinated among the various members of the project team early and frequently, the costs for bridge security can be kept low. In fact, past research shows that detailing columns for a high level of blast resistance costs about the same as would be required to detail a column for high seismic resistance. When bridge security decisions are not coordinated from the outset, it may be necessary to modify various design parameters, invest in long-term surveillance, or implement structural retrofits. These types of solutions can be very expensive, in terms of actual dollars and in terms of indirect costs associated with delays in progress needed to solve problems that could have been most effectively implemented at the outset of project. For unique or novel bridge systems, owners may wish to consider verification of certain design decisions through a coordinated testing program. A similar approach is used in the building industry when new systems are proposed for seismic-resistant design. Even if testing is not deemed necessary, it is essential that design for bridge security involve frequent and detailed coordination of all the various groups involved with the initial design as well as the long-term maintenance and operation of a given bridge.

2.3 Additional Publicly Available Bridge Security Guidance

Additional guidance on bridge-specific security strategies and risk reduction may be found in the following documents: The Blue Ribbon Panel on Bridge and Tunnel Security (2003) [10], Jenkins (2001) [40], Abramson (1999) [41].

Though not specific to bridges, FEMA has published a series of reports that provide valuable information on risk management to mitigate potential terrorist attacks including FEMA 426 (2003) [42] and FEMA 452 (2005) [43]. Unified Facilities Criteria (UFC) 4-020-01 [44] is a publically available U.S. Department of Defense publication addressing facilities planning that also has guidance that may be relevant for bridges.

2.4 Chapter Summary

This chapter provided an introduction and overview to the topic of security planning for highway bridges. The main goal of security planning is to develop economical, unobtrusive, and effective methods to mitigate the risk of terrorist attacks against critical bridges to an acceptable level. Various threat mitigation strategies for highway bridges were also discussed. A mitigation approach that combines active and passive measures will likely offer the best solution. In addition, the discussion on security-related project coordination issues highlighted the importance of early coordination with the entire project team. Bridge security should be taken as a component of the entire design process. A list of references to additional publicly available bridge security guidance was also provided.

The next chapter focuses on the material-level behavior and performance of high-explosive materials and typical construction materials subjected to extreme loading events. More specifically, Chapter 3 discusses the unique behavioral aspects of explosive materials and performance of reinforced concrete and structural steel under high-rate dynamic loading and sustained thermal loading conditions.

3.0 MATERIALS PERFORMANCE

The performance of materials in a blast environment has a significant effect on the overall outcome. This is true for both the energetic material(s) comprising the explosive source and the construction materials comprising the blast-loaded structure. For the case of a structure, material performance can drive component-level and system-level response. For the case of explosives, material performance translates to explosive efficiency and ultimately relative threat severity.

This chapter discusses the performance of explosive materials and the performance of reinforced concrete and structural steel under high-rate dynamic loading and sustained thermal loading conditions.

3.1 Explosives

Defined in simple terms, an explosion is a sudden physical or chemical change to the state of a mass resulting in energy release and associated particle motion. Explosion effects can include air blast, thermal radiation, cratering, fragmentation, and ground shock. Explosions can be classified into the following broad categories: natural, physical, electrical, nuclear, and chemical. Although nuclear explosions are, in general, significantly more destructive than chemical explosions, weapons using chemical explosions pose the most probable threat to major U.S. transportation infrastructure. A chemical explosion results from a sequence of exothermic chemical reactions between a fuel and an oxidant – commonly referred to as combustion. Strictly speaking, when the chemical reaction progresses at subsonic speeds the combustion process is termed *deflagration*, and when the reaction progresses at supersonic speeds the combustion process is termed *detonation*. Detonations produce the most destructive explosive effects and are most often associated with high explosive materials. For more discussion on explosive effects of detonations, refer to Chapter 4 of this manual. A general classification of explosive materials is presented in Figure 3.1 after Zukas and Walters [45].

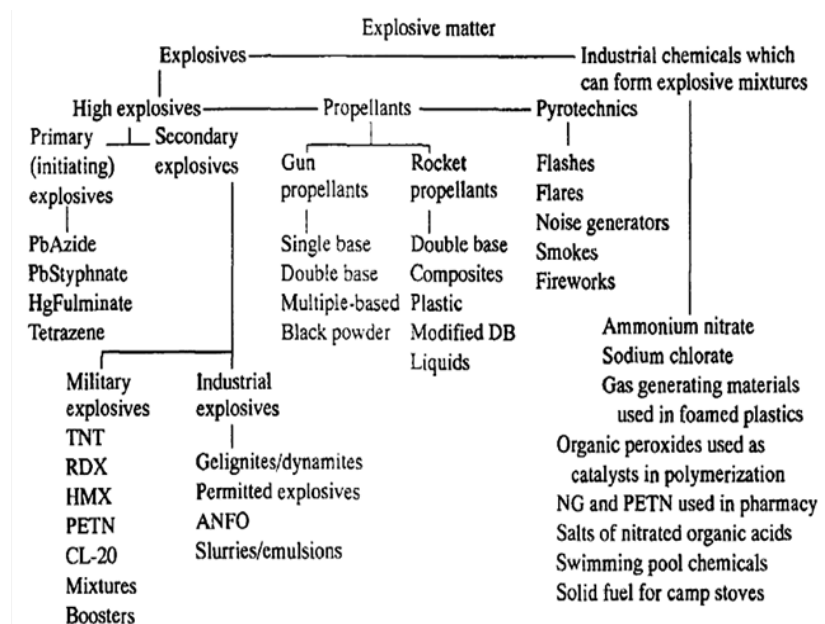


Figure 3.1 Explosive Materials Classification Illustration [45]

3.1.1 High Explosives

Detonations are most often facilitated by high explosives, whereas low explosives tend to deflagrate. It should be noted, however, that providing confining pressure under the proper conditions may cause a low explosive to detonate [46]. Based on stability and ease of ignition, high explosives can be categorized into three general groups: primary, secondary, and tertiary. Primary high explosives, sometimes termed initiators, primers, or catalysts, are relatively unstable energetic materials having a high sensitivity to stimuli such as heat, shock, electricity, and electromagnetic radiation. Spark, flame, or impact easily ignites primary high explosives, and are very likely to detonate. Examples of primary high explosives include lead azide, lead picrate, lead styphnate, diazodinitrophenol (DDNP), *m*-nitrophenyldiazonium perchlorate, tetracene, nitrogen sulfide (N₄S₄), copper acetylide, mercury fulminate, fulminating gold, nitrosoguanidine, and potassium chlorate with red phosphorus (P₄) [45].

Secondary high explosives, although still very volatile materials, are less likely to be readily initiated by spark or impact, thus lending themselves well to industrial and/or military applications. Examples of secondary high explosives include nitroglycerine, TNT, nitrocellulose, nitromethane, cyclotrimethylene trinitramine (RDX), dynamite, and pentaerithrytol tetranitrate (PETN). Volatile secondary high explosives are frequently used as boosters to help reinforce the detonation wave from the detonator (primary high explosive) into the main explosive charge.

Tertiary explosives, sometimes referred to as blasting agents, are very insensitive to input stimuli. Consequently, practical quantities of primary explosive alone cannot reliably detonate them. Tertiary explosives often require intermediate secondary explosive boosters along with a primer to be reliably detonated. An example of a tertiary explosive is ANFO. The explosive content of a given weapon is typically proportioned as follows: (a) a very small quantity of primer, usually less than one gram, (b) the booster weight is typically about a pound to a few pounds, and (c) the bulk of the weapon's explosive content, the relatively insensitive main charge, may constitute over 99 percent of the total explosive material weight [47].

3.1.2 Types of Explosive Charges

Explosives can be delivered and used in bulk form, such as bare or cased explosives. Explosives can also be delivered and used in a form where the effects from detonation are highly directed, such as shaped charges or kinetic energy penetrators.

Bare explosives would be the most typical when delivered as an improvised device. This could be something like ammonium nitrate and fuel oil (ANFO) delivered in barrels inside of a truck that could then be parked in a vulnerable spot near a highway bridge. Primary effects from bare explosives are shock-induced blast pressure and impulse from the detonation.

Cased weapons are typically military in nature and include things like air-to-surface bombs where the high-explosive material is contained and in contact with a heavy metal container. However, a cased weapon could also be an improvised device such as a fire extinguisher packed with explosives. Cased weapons produce small high-velocity (primary) fragments that may need to be considered in the analysis of bridge components, in addition to the shock-induced blast pressure and impulse. Depending on their mass, impacting primary fragments from a cased weapon can deliver additional impulse to nearby bridge components beyond the shock-induced

impulse. Primary fragments also represent a local penetration threat, particularly to steel elements, as well as an additional human injury threat.

Shaped charges can come in two general forms: conical or linear. A conical shaped charge consists of cylindrical blocks of high-explosive in one end of the device which, upon detonation, directs the cone linear material into a narrow jet. Conical shaped charges are primarily used for boring holes in materials such as metal, masonry, or concrete. Conical shaped charges could be used to bore holes through bridge roadways or bridge piers. Once a hole is bored with the conical shaped charge, it could be packed with explosives and detonated to cause additional damage to a bridge component. Owing to confinement effects, this secondary, packed charge would cause greater damage to a targeted bridge component than would occur from the detonation of a bare explosive at some standoff. Linear shaped charges employ the same principal of directing a steel liner via detonation energy focusing, but, rather than boring a hole, linear shaped charges are typically used to cut materials such as steel plate or cables. Linear shaped charges (rigid and flexible varieties) are discussed in more detail in Chapter 10 of this manual, as they can be used quite effectively to sever cable components of long-span bridges.

Kinetic energy penetrators (KEP) are comprised of metal plates backed by high-explosive material. Upon detonation, the metal plate is explosively driven into a target. The metal plate is stable during flight and usually impacts a target at several hundred feet per second. These types of explosive devices are typically used to breach concrete and steel shapes and could be deployed against critical structural components of a highway bridge. KEP threats are also discussed in more detail in Chapter 10 of this manual.

3.1.3 TNT Equivalency

Extensive research has been conducted previously on free-field shock wave behavior as well as the interaction of propagating shock waves with planar reflecting surfaces. Many of these past research programs utilized bare, spherical TNT explosive charges for generating shock waves. Many of the state-of-the-practice blast load characterization techniques make use of empirical data compiled from these extensive research efforts. As such, the concept of an equivalent TNT charge weight was developed to allow for reasonable extrapolation of the TNT-based empirical data to bulk explosive threat scenarios involving explosives other than TNT.

An equivalent TNT charge weight is the weight of TNT required to produce a selected shock wave parameter of a magnitude equal to that produced by a unit weight of the explosive charge in question. The equivalent TNT charge weight for a given explosive is equal to the actual weight multiplied by the *TNT equivalency factor* for that explosive. TNT equivalency factors for a wide range of high explosives have been developed through testing, where incident peak pressure and impulse were measured over a range of scaled standoff distances (for more information on the term *scaled standoff*, refer to Chapter 4 of this manual). In general, equivalency factors for a given explosive can vary with scaled standoff or whether they are based on comparison of peak pressure or impulse. Single TNT equivalency factors based on either incident peak pressure or impulse have been generated by averaging over the range of scaled standoff distances and peak pressures considered during testing. In using averaged TNT equivalency factors, they are only considered valid for the pressure ranges over which they were averaged. In general, averaged equivalent TNT charge weights apply to moderate- or large-standoff scenarios and not to relatively close-in detonations. Furthermore, it should be realized

that they most likely do not represent the actual charge geometry, physical standoff, and/or local atmospheric conditions of the specific threat scenario being considered. Effects from the detonation of a given explosive charge vary as a function of many parameters such as physical standoff, charge geometry (more so in the near-field), charge configuration, the packing or manufacturing quality of the charge, the location of detonation initiation within the charge, and local atmospheric conditions. Accordingly, these averaged equivalency factors should be taken as approximations. Table 3.1 provides a limited collection of publicly available averaged TNT equivalences. The U.S. Department of Defense [48] maintain a more exhaustive collection of averaged TNT equivalences.

When blast test data do not exist for an explosive, comparative values of heats of detonation for TNT and the explosive in question can be used to approximate TNT equivalence [46, 49, 50]. Equation (3-1) provides the calculation necessary to approximate an equivalent TNT charge weight based on heats of detonation.

$$W = \left(\frac{Q_{EXP}}{Q_{TNT}} \right) W_{EXP} \quad (3-1)$$

where:

W = equivalent TNT charge weight

Q_{EXP} = heat of detonation of explosive in question

Q_{TNT} = heat of detonation of TNT

W_{EXP} = charge weight of explosive in question

Theoretical heats of detonation for various explosives, along with equivalent TNT charge weights, can be found in Appendix A of U.S. Department of Energy (1992) *A Manual for the Prediction of Blast and Fragment Loadings on Structures* [51]. In addition, measured heats of detonation for various explosives can be found in U.S. Department of Defense (1984) *Military Explosives* [52].

Table 3.1 TNT Equivalences (data from [46, 49])

Explosive	Avg. TNT Equiv. Factors		Pressure Range¹ (psi)
	Pressure	Impulse	
TNT	1.00	1.00	Standard
ANFO (94/6)	0.82	-	1 – 100
Comp. A-3	1.09	1.076	5 – 50
Comp. B	1.11	0.98	5 – 50
	1.20	1.30	100 – 1,000
Comp. C-4	1.37	1.19	10 – 100
Cyclotol (70/30)	1.14	1.09	5 – 50
HBX-1	1.17	1.16	5 – 20
HBX-3	1.14	0.97	5 – 25
H-6	1.38	1.15	5 – 100
Minol II	1.20	1.11	3 – 20
PBX-9404	1.13	-	5 – 30
	1.70	1.20	100 – 1,000
PBX-9010	1.29	-	5 – 30
PETN	1.27	-	5 – 100
Pentolite (50/50)	1.42	1.00	5 – 100
	1.38	1.14	5 – 600
	1.50	1.00	100 – 1,000
Picratol	0.90	0.93	-
Tetryl	1.07	-	3 – 20
TNETB	1.36	1.10	5 – 100
TRITONAL	1.07	0.96	5 – 100

Note 1: 1 kPa = 6.89 psi

3.1.4 Charge Shape

Charge shape can have a significant effect on resulting blast loads for relatively close-in detonation scenarios—that is, an explosion that takes place relatively close to a target—and the significance of this effect diminishes as the distance between the explosive charge and target of interest increases. Close in to a detonating charge, charge shape largely influences the initial shock front geometry [46]. As will be discussed in Chapter 4, shock front geometry forms the basis for blast scaling laws and is ultimately what dictates the spatial and temporal characteristics of resulting blast loads.

Not only is charge shape an important characteristic for bulk explosive charges, but it also plays an important role in smaller precision explosive charges and devices. For example, the use of moldable and liquid explosive compositions permits charge shaping (and hence shock wave control) to focus blast energy for the specific purpose of cutting and breaching. As is discussed in Chapter 10 of this manual, linear shaped charges and diamond charges pose a significant

cutting threat to main cable elements of long-span bridges. These types of charges are placed in contact with and wrapped around the circumference of a cable element prior to detonation. As another example, military personnel and law enforcement tactical units routinely utilize certain types of precision contact charges to effectively breach through an obstruction and quickly gain access to a target.

3.2 Reinforced Concrete

Reinforced concrete is inherently a complex construction material. The concrete matrix itself comprises a nonhomogeneous mixture of cement, fine aggregate, and coarse aggregate and is well-known to exhibit pressure-sensitive mechanical properties. Deformed steel bars are placed within the concrete matrix during casting to allow for chemical and mechanical bonding as the concrete hardens. The dissimilar material properties of steel and concrete further complicate the behavior of reinforced concrete.

When subjected to extreme loading, reinforced concrete tends to behave differently than under conventional structural design conditions. Under high rates of loading, such as during a blast event, reinforced concrete can temporarily sustain dynamic stresses well more than its static strength. In addition, thermal loading can influence the behavior of reinforced concrete. The following subsections discuss the performance of reinforced concrete under high-rate and thermal loading conditions, and guidance on design material-level strength values for such loading conditions is provided.

3.2.1 Effect of Strain Rate on Material Response

Figure 3.2 presents experimental results illustrating the effect of strain rate on the behavior of tension-loaded steel reinforcing bars. Data for nominal Grade 60 steel shown in Figure 3.2 (on left) reveal a typical threshold strain rate of approximately 2 sec^{-1} , beyond which drastic yield strength enhancement ensues. Figure 3.2 (on right) highlights the fact that lower grade steels tend to realize larger yield strength enhancement than higher grade steels. In general, typical strain-rate effects on the behavior of structural steel include an increase in yield strength; an increase in ultimate strength, albeit smaller than for yield strength; and a slight reduction in the elongation at rupture (i.e., decreased material-level ductility) [53]. The elastic modulus is not as strain-rate sensitive as strength; therefore, the strain rate can easily be converted to a stress rate because the modulus is often assumed to be constant with strain rate [54].

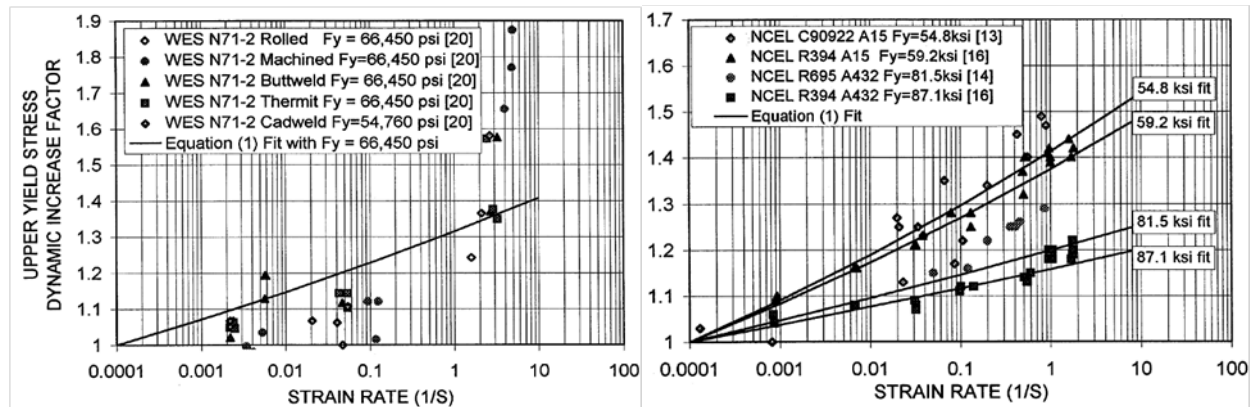


Figure 3.2 Experimental Results Showing Increased Yield Stress with Increased Strain Rate for Tension-Loaded Steel Reinforcing Bars [55]: (left) Results for Nominal Grade 60 Steel, (right) Effect of Static Yield Strength on Strain-Rate Sensitivity

Figure 3.3 presents experimental data for tension-loaded and compression-loaded concrete at different strain rates. Like steel, strain-rate effects on concrete response include increased strength and decreased material-level ductility. However, unlike steel, experimental results suggest that concrete's elastic modulus increases slightly with increasing strain rate [50]. This finding is consistent with experimental data showing the dependence of elastic modulus on unconfined compressive strength. In comparing the curves shown in Figure 3.2 and Figure 3.3, an important observation can be made. The tension-loaded steel and concrete curves show a similar strain-rate threshold of approximately 2-sec^{-1} , whereas the strain-rate threshold for compression-loaded concrete is an order of magnitude greater at approximately 30-sec^{-1} . In terms of governing failure modes, tension-loaded steel and concrete ultimately fail due to unstable crack propagation and subsequent fracture, while compression-loaded concrete ultimately crushes. Most of the data supporting material sensitivity to high-rate loading are purely experimental, and therefore the physical cause is not completely understood. Nonetheless, several hypotheses linking strain-rate threshold to material response modes have been proposed.

Some researchers believe that, for materials whose failure is likely governed by brittle fracture (e.g., concrete in tension), a limited crack velocity phenomenon is the primary cause of rate-dependent strength enhancement. If an attempt is made to force the crack to propagate at velocities greater than the limiting crack velocity then fracture will not occur, allowing local stresses to exceed the material's "static" strength [54]. Similarly, for ductile metals that exhibit plastic deformation by way of molecular dislocation motion, a similar limiting dislocation velocity is believed to occur.

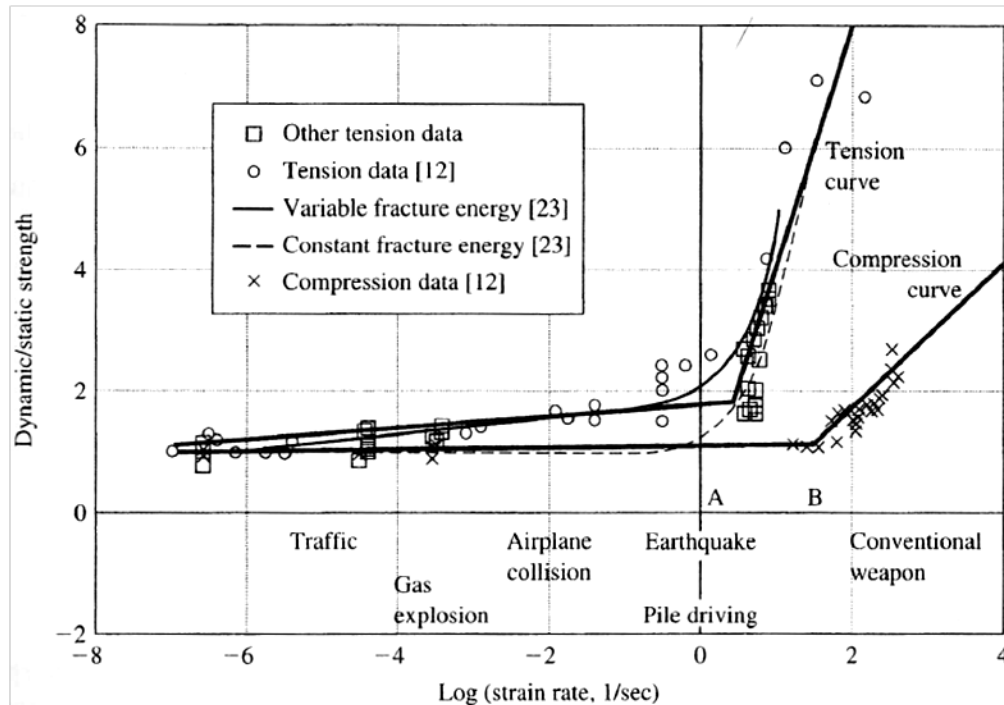


Figure 3.3 Experimental Results Showing Increased Concrete Compressive and Tensile Strength with Increased Strain Rate [54]

For compression-loaded concrete, a phenomenon known as inertial confinement is often suggested as the main cause for the apparent strength increase. It is well known that concrete is a pressure-dependent material. Consider an unconfined compression test of a cylindrical concrete specimen. If the load is applied quasi-statically, the lateral surface of the cylindrical specimen is free to expand due to Poisson's effect, and the specimen essentially remains in a state of uniaxial stress. However, if the same test is performed under high-rate dynamic loading, a delay in the radial expansion occurs while the material is accelerated in the longitudinal direction. The delay in the lateral surface reaching a static equilibrium position (i.e., zero radial stress) results in an effective confining pressure on the lateral surface of the specimen, hence the term inertial confinement [56].

Some researchers argue that, because concrete crushing is a result of extensive micro-cracking, strength enhancement of compression-loaded concrete is a result of a limited crack velocity and not of inertial confinement. Despite the inability of the structural engineering community to reach a consensus on the origin of material sensitivity to strain rate, the evidence of such a phenomenon is clearly discernible in experimental results. Thus, empirically based constant dynamic increase factors (DIFs) and strain-rate-dependent DIF equations have been developed for use in the analysis and design of structural components subjected to high-rate loading such as airblast.

A simple and conservative approach to including strain-rate effects in the analysis and design of blast-loaded structural components is to modify key material properties using empirically-based constant DIFs. Table 3.2 presents DIFs for reinforced concrete and steel reinforcing bars that have been recommended by the U.S. Department of Defense [50]. These DIFs are categorized into modes of structural response and strain-rate levels based on data and observations from

experimental tests. The values given in Table 3.2 for flexure assume a strain rate of 0.10-sec^{-1} and 0.30-sec^{-1} for both steel reinforcing bars and concrete in the low-pressure (far design) and high-pressure (close-in design) ranges, respectively. For reinforced concrete members in compression, the corresponding strain rates are 0.02-sec^{-1} and 0.05-sec^{-1} , respectively [50]. Compression members (i.e., columns) are associated with smaller DIFs than flexural members because dynamic effects of the blast load are most often filtered through supported members (i.e., beams, girders, and slabs) during load transfer. These filtered pressure histories tend to have longer rise times, resulting in lower strain rates. Moreover, DIFs for shear and bond are smaller than those for flexure and compression to prevent brittle failure and to account for uncertainties in the design process for such modes of response [53]. It can also be noted that, for the far and close-in design ranges denoted in Table 3.2, the threshold in terms of scaled standoff is typically taken as 3 (refer to Chapter 4 for more on the term *scaled standoff*).

Table 3.2 Reinforced Concrete Constant Dynamic Increase Factors (adapted from [50])

Response Mode	Low Pressure Region (far design range)			High Pressure Region (close-in design range)		
	Reinforcing Bars		Concrete Compr. Str.	Reinforcing Bars		Concrete Compr. Str.
	Yield	Tensile		Yield	Tensile	
Flexure	1.17	1.05	1.19	1.23	1.05	1.25
Diagonal Tension	1.00	-	1.00	1.10	1.00	1.00
Direct Shear	1.10	1.00	1.10	1.10	1.00	1.10
Bond	1.17	1.05	1.00	1.23	1.05	1.00
Compression	1.10	-	1.12	1.13	-	1.16

3.2.2 Strength Values for Design

Independent from strain-rate effects, concrete and reinforcing steel typically exhibit actual static strength larger than the minimum (nominal) specified design values. In blast-resistant design, this is typically accounted for by using a static increase factor (SIF), which is defined as the ratio of the actual static strength to the specified minimum design value. Numerous mill test reports indicate that the actual static yield strength for Grade 60 reinforcing steel is typically at least 10-percent greater than the minimum specified yield strength of 60-ksi [50]. Similarly, test data indicate that the in-situ 28-day concrete compressive strength of concrete exceeds the specified minimum design strength by 10-percent or more. Based on these data, an SIF of 1.1 is typically used for the static yield strength of reinforcing steel, f_y , and the concrete compressive strength, f'_c , of concrete. If static strength test data are available for a specific application, test values can be used in lieu of nominal values. In this case, a SIF value of 1.0 would be used along with actual static strengths determined from the test data.

For purposes of blast-resistant design using simplified single-degree-of-freedom (SDOF) dynamic analysis methods, the dynamic strength of concrete and reinforcing steel is calculated as show in Equations (3-2) and (3-3), respectively.

$$f'_{dc} = f'_c (SIF)(DIF) \quad (3-2)$$

where:

f'_{dc} = concrete dynamic compressive strength

f'_c = concrete minimum specified compression strength

SIF = static increase factor

DIF = dynamic increase factor (see Table 3.2)

$$f_{dy} = f_y (SIF)(DIF) \quad (3-3)$$

where:

f_{dy} = dynamic yield strength

f_y = static yield strength

For blast-resistant design of prestressed components, SIF and DIF values of 1.0 are typically used for the effective strength of prestressing steel strands.

3.2.3 Rate-Dependent Constitutive Models

While constant DIFs are simplistic and conservative, they do not represent the true, variable dependence on strain rate and they can occasionally produce overly conservative designs. A refined approach to the inclusion of strain-rate effects in the analysis of blast-loaded structural components is to utilize a rate-dependent constitutive model that makes use of an empirically based DIF expression.

Many researchers have proposed strain-rate-dependent DIF expressions for steel reinforcing bars and structural steel shapes. For instance, Malvar (1998) [55] established the empirical DIF expression given in Equation (3-4) which can be used to determine yield and ultimate strength time-dependent DIFs for steel reinforcing bars of a specified static yield strength.

$$DIF = \left(\frac{\dot{\epsilon}}{10^{-4}} \right)^\alpha \quad (3-4)$$

where:

$\alpha = 0.074 - 0.040(f_y/60)$ [DIF for yield strength]

$\alpha = 0.019 - 0.009(f_y/60)$ [DIF for ultimate strength]

f_y = static yield strength [ksi]

$\dot{\epsilon}$ = strain rate as a function of time [sec^{-1}]

The development of strain-rate-dependent DIF expressions for the tensile and compressive strength of concrete has also found interest among various researchers. One of the most well-known DIF expressions for concrete tensile strength is that proposed by Malvar and Ross (1998) [57] and given in Equation (3-5). For strain-rate-dependent concrete compressive strength enhancement, the Comité Euro-International de Béton [58] recommends the empirical DIF expression presented in Equation (3-6). It can be observed that Equations (3-5) and (3-6) are consistent with the data presented in Figure 3.3, where the breaks in the expressions closely match the strain-rate thresholds.

These expressions are well suited for explicit use in engineering-level dynamic analysis models that track strain history. While they also lend themselves well to the integration with complex constitutive models for use in high-fidelity finite element analyses, results from recent computational research suggest that explicitly accounting for concrete compressive strength enhancement in a first-principles computational model can lead to an over-prediction of dynamic compressive strength. Depending on the type of concrete constitutive model and finite element technique employed, inertial confinement effects may already be inherently captured in the computations without the need for explicit integration of a time-dependent DIF relationship [56].

$$\begin{aligned} DIF &= \left(\frac{\dot{\epsilon}_{mr}}{10^{-6}} \right)^{\delta_{mr}} & \text{for } \dot{\epsilon}_{mr} \leq 1 \text{ sec}^{-1} \\ &= \beta \left(\frac{\dot{\epsilon}_{mr}}{10^{-6}} \right)^{\frac{1}{3}} & \text{for } \dot{\epsilon}_{mr} > 1 \text{ sec}^{-1} \end{aligned} \quad (3-5)$$

where:

$\dot{\epsilon}_{mr}$ = strain rate as a function of time in the range of 10^{-6} to $160 \text{ [sec}^{-1}\text{]}$

$$\delta_{mr} = 1 / (1 + 8 f'_c / 1,450)$$

f'_c = static unconfined compressive strength of concrete [psi]

$$\log \beta = 6\delta_{mr} - 2$$

$$\begin{aligned} DIF &= \left(\frac{\dot{\epsilon}_{ceb}}{30 \times 10^{-6}} \right)^{1.026\delta_{ceb}} & \text{for } \dot{\epsilon}_{ceb} \leq 30 \text{ sec}^{-1} \\ &= \gamma \left(\frac{\dot{\epsilon}_{ceb}}{30 \times 10^{-6}} \right)^{\frac{1}{3}} & \text{for } \dot{\epsilon}_{ceb} > 30 \text{ sec}^{-1} \end{aligned} \quad (3-6)$$

where:

$\dot{\epsilon}_{ceb}$ = strain rate as a function of time in the range of 30×10^{-6} to $300 \text{ [sec}^{-1}\text{]}$

$$\delta_{ceb} = 1 / (5 + 9 f'_c / 1,450)$$

$$\log \gamma = 6.156\delta_{ceb} - 2$$

Concrete is known for exhibiting undesirably low tensile strengths—roughly ten percent of its compressive strength [59]. Concrete cracks when its tensile capacity is exhausted, and the true physics of such brittle, discrete behavior is not well represented in common finite element formulations. In subscribing to the limiting crack velocity hypothesis, the onset and time-dependent behavior of local mesh discontinuities (i.e., physical discontinuities between adjacent finite elements) must be accommodated to capture tensile-stress-induced strength enhancement. While most (if not all) commercial finite element analysis codes lack the ability to adaptively consider this level of complexity, they are likely capable of calculating strain rate throughout a dynamic analysis. As such, the explicit inclusion of an empirical DIF expression for concrete tensile strength is often warranted in finite element simulations.

Conversely, concrete's pressure dependency—the cornerstone of the inertial confinement hypothesis—is often accounted for in finite element simulations using a complex plasticity-based constitutive model. Researchers who subscribe to the concept of inertial confinement argue that the explicit inclusion of an empirical DIF expression for concrete compressive strength is redundant and incorrect because the increase in apparent compressive strength is already captured by the pressure-dependent constitutive model. For example, researchers at the University of Missouri, Kansas City simulated concrete cylinder compression tests performed at different strain rates using three different pressure-dependent concrete constitutive models [60]. For each constitutive model, the simulation was conducted with and without explicit use of strain-rate-dependent DIFs. The numerical results support the claim that enhanced concrete compressive strengths can be realized at high load rates without explicitly accounting for strain rate effects in computational simulations involving a pressure-dependent concrete constitutive model. Schwer (2009) [56] derived numerically-based DIFs from finite element simulations of confined and unconfined concrete compression tests using a pressure-dependent concrete material model that did not explicitly include strain rate effects. Schwer's results were found to closely align with experimental results from Split Hopkins Pressure Bar (unconfined) and confined concrete compression tests.

3.2.4 Thermal Effects

Adequate data are not available to support design guidance on thermal effects for concrete materials subjected to close-in blast loads. However, heat transfer from the fireball of an explosion is not likely to be a major issue on the performance of reinforced concrete structural components due to the transient nature of the thermal load.

Sustained thermal loading from fire or other heat sources can, however, potentially affect the mechanical properties of concrete. For example, the ignition of a fuel truck near a highway bridge could pose a sustained thermal loading threat. In general, concrete loses strength as temperature increases. This strength loss is due to changes in the various constituents that make up typical concretes (e.g., coarse/fine aggregates, cementitious materials, water, and other admixtures). The chemical and physical changes to typical concrete with increasing temperature are graphically illustrated in Figure 3.4.

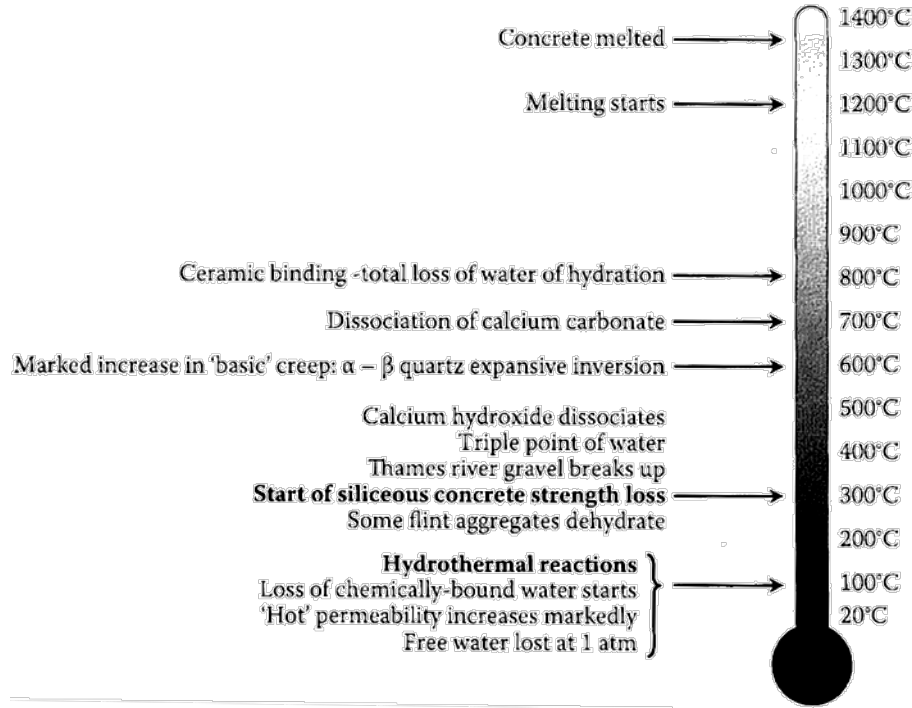


Figure 3.4 Illustration of Chemical and Physical Changes to Concretes as Temperatures Increase [61] (1°C = 33.8 °F)

Concrete compressive behavior at different temperatures will differ from that at room temperature. Eurocodes EN 1992-1-2 [62] and EN 1994-1-2 [63] provide a simplified uniaxial compression stress-strain model for concrete at varying sustained temperatures. This equation represents nonlinear behavior up to the maximum compressive strength as is reproduced in Equation (3-7). Post-peak concrete softening behavior is typically represented with a linearly descending branch as schematically illustrated in Figure 3.5. In addition, Table 3.3 provides concrete compressive strength reduction factors, strain at ultimate stress, and ultimate strain values for normal-weight and lightweight concretes (LWC) at varying temperatures for use in design.

$$\sigma_{c,\theta} = f_{c,\theta} \left[\frac{3 \left(\frac{\varepsilon_{c,\theta}}{\varepsilon_{cu,\theta}} \right)}{2 + \left(\frac{\varepsilon_{c,\theta}}{\varepsilon_{cu,\theta}} \right)^3} \right] \quad (3-7)$$

where:

$\sigma_{c,\theta}$ = concrete stress at strain value $\varepsilon_{c,\theta}$

$f_{c,\theta}$ = maximum concrete compressive stress

$\varepsilon_{cu,\theta}$ = concrete strain at maximum compressive stress, $f_{c,\theta}$

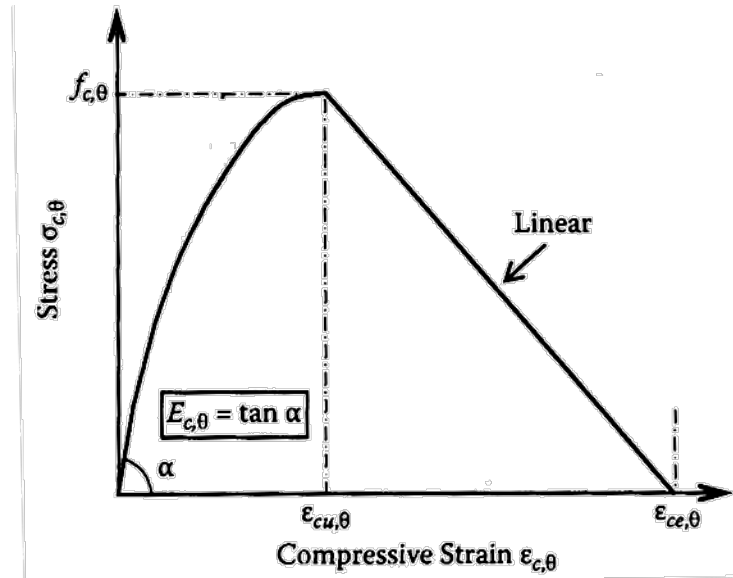


Figure 3.5 Model for Uniaxial Compressive Stress-Strain Characteristics of Siliceous (conservative for calcareous) Concretes at Temperature θ [62, 63]

Table 3.3 Compressive Strength Reduction Factor, Strain at Ultimate Stress, and Ultimate Strain for Normal-Weight and Lightweight Concretes at Temperature θ [62, 63]

Concrete temperature, (°C)	Compressive strength			Strain	
	(NWC) EN 1992-1-2 and EN 1994-1-2	(NWC) EN 1992-1-2	(LWC)	at ultimate stress	at zero stress
	Siliceous $k_{c\theta} = f_{c\theta} / f_c$	Calcareous $k_{c\theta} = f_{c\theta} / f_c$	$k_{c\theta} = f_{c\theta} / f_c$	$\epsilon_{cu\theta}$	$\epsilon_{ce\theta}$
20	1	1	1	0.0025	0.0200
100	1	1	1	0.0040	0.0220
200	0.95	0.97	1	0.0055	0.0250
300	0.85	0.91	1	0.0070	0.0270
400	0.75	0.85	0.88	0.0100	0.0300
500	0.60	0.74	0.76	0.0150	0.0325
600	0.45	0.60	0.64	0.0250	0.0350
700	0.30	0.43	0.52	0.0250	0.0375
800	0.15	0.27	0.40	0.0250	0.0400
900	0.08	0.15	0.28	0.0250	0.0425
1000	0.04	0.06	0.16	0.0250	0.0450
1100	0.01	0.02	0.04	0.0250	0.0475
1200	0	0	0	-	-

Note: 1°C = 33.8°F

While tensile strength of concrete is commonly neglected in design, there are similar relationships for temperature-dependent behavior of concrete in tension given in EN 1992-1-1 [62]. In addition, EN 1994-1-2 [63] provides guidance on post-cooling concrete strength that accounts for damage to the internal concrete microstructure due to heating.

Supplementary Discussion on Component-Level Thermal Effects

Due to (a) the relatively massive size of typical concrete members, (b) the low thermal conductivity of concrete, and (c) the movement of water within the concrete matrix during heating, temperature distribution in concrete elements tends to be complex and non-uniform. Thus, simplified methods have been developed to approximate structural concrete member behavior under sustained thermal loading.

A simplified method commonly used for design is referred to as the *500°C Isotherm Method* [61]. This method assumes that concrete at temperatures exceeding 500°C (932 °F) have zero strength and concrete under this temperature threshold retains full load-bearing capacity and stiffness properties. A reinforced concrete member analysis using this method would consist of the following steps:

1. Obtain 500°C (932 °F) isotherm profile in the member cross-section by performing a thermal analysis for the design thermal load
2. Calculate reduced section dimensions neglecting all concrete beyond the 500°C (932 °F) isotherm
3. Determine the temperature at the center of gravity of each steel reinforcing bar and calculate temperature-dependent material properties for each reinforcing bar (refer to Section 3.3.4 of this manual for temperature-dependent steel properties)
4. Calculate the flexural resistance of the reduced concrete section using standard analysis assumptions (e.g., ACI 318 Flexural Strength)
5. Compare the design load in fire to the calculated reinforced concrete section resistance determined in Step 4

Finally, under sustained thermal loading, spalling of concrete can also occur. Explosive spalling, where concrete is forcefully ejected from a section, is unlikely to occur when the concrete moisture content is less than 3-percent by weight. However, non-explosive spalling can occur in any situation wherein concrete is directly exposed to fire. Non-explosive spalling occurs when stress levels in a load-bearing reinforced concrete member exceed the thermally reduced concrete strength (this would initiate in cover concrete and propagate inward toward the center of the section). Fire-induced concrete spalling can be resisted by providing surface-level steel reinforcement; either welded-wire mesh or closely spaced bars (e.g., 4-in. on center) are typically adequate.

In addition to the fire-related texts and documents referenced throughout this section, Andrew Buchanan's *Structural Design for Fire Safety* [64] text is recommended as an additional

reference for more details regarding materials performance (and structural design) under sustained thermal loads.

3.3 Structural Steel

Metals are generally homogeneous in nature and possess significant strength and ductility characteristics when compared to concrete. There exist many different types of metals that are used in various applications across multiple industries. The most prominent metal construction materials comprising typical highway bridges are carbon and alloy steels.

Typical uniaxial engineering stress-strain behavior of carbon and alloy steels is illustrated in Figure 3.6 and can be generally categorized into three distinct response regimes: linear response up to the material's nominal yield strength, some degree of constant-stress plastic straining (often referred to as the *yield plateau*), and nonlinear post-yield response involving strain hardening up to the material's nominal ultimate strength followed by strain softening that ensues until tensile rupture occurs at the material's maximum elongation. The post-yield regime for typical carbon steels tends to be essentially parabolic in shape. The steel strain-hardens up to ultimate strength at around 18- to 20-percent elongation, followed by strain-softening to tensile rupture. It can also be seen that as strength increases—which is typically associated with an increase in the material's carbon content—material-level ductility decreases and the proportional limit and yield plateau become less well-defined.

When subjected to extreme loading, carbon and alloy steels tend to behave differently than under conventional structural design conditions. Under high rates of loading, such as during a blast event, carbon and alloy steels can temporarily sustain dynamic stresses well more than their static strength. In addition, thermal loading can influence the behavior of carbon and alloy steels. The following subsections discuss the performance of typical structural steels under high-rate and thermal loading conditions, and guidance on design material-level strength values for such loading conditions is provided.

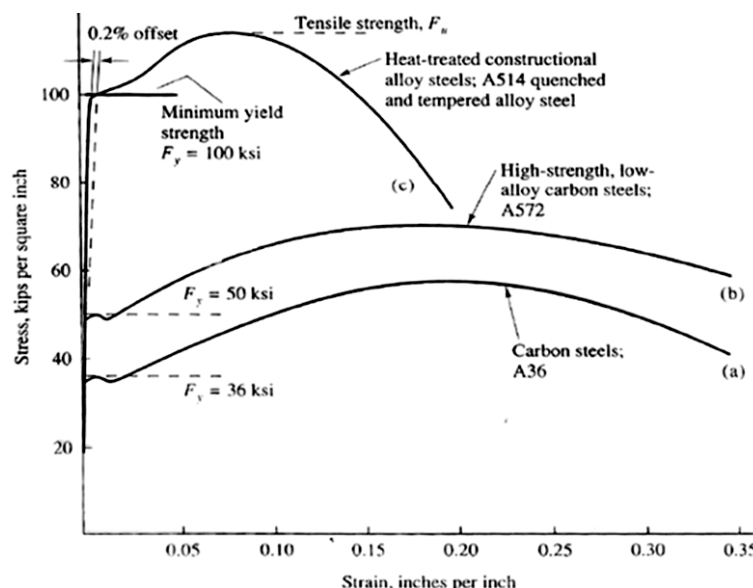


Figure 3.6 Typical Uniaxial Stress-Strain Behavior of Structural Steels [65]

3.3.1 Effects of Strain Rate on Material Response

The effects of high-rate loading on the mechanical behavior of various structural steels have been extensively studied and experimentally observed over the years [46, 48, 50, 53]. Under rapidly applied loads, the rate of strain within the material increases causing a transient change to the material's mechanical properties. Considering the mechanical properties under static loading as a basis, the effects of increasing strain rates are illustrated in Figure 3.7 and can be summarized as: a substantial increase in nominal yield strength, a comparatively less substantial increase in nominal ultimate strength, and a slight reduction in maximum elongation (i.e., a loss in material-level ductility). Unlike concrete, experimental data have shown that the modulus of elasticity for structural steels remains essentially insensitive to strain rate.

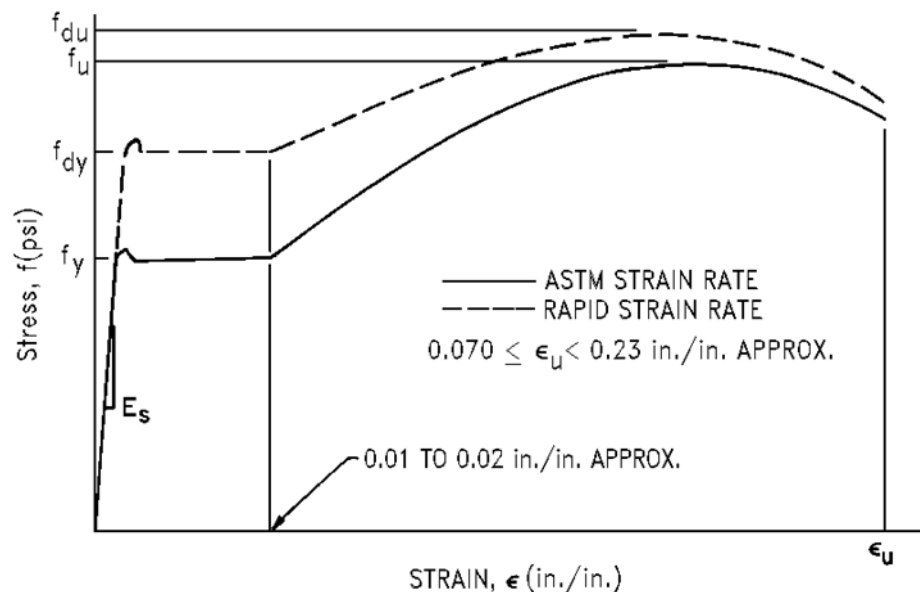


Figure 3.7 Illustration of Strain-Rate Effects on Stress-Strain Behavior of Typical Structural Steels [50]

A simple and conservative approach to including strain-rate effects in the analysis and design of blast-loaded structural components is to modify key material properties using empirically-based constant DIFs. Table 3.4 presents yield strength DIFs for various grades of structural steel that have been recommended by the U.S. Department of Defense [50]. These DIFs are categorized into modes of structural response and strain-rate levels based on data and observations from experimental tests. Structural members loaded in axial tension or compression (e.g., a steel column) are associated with smaller yield strength DIFs than flexural members because dynamic effects of the blast load are most often filtered through supported members (i.e., beams, girders, and slabs) during load transfer. These filtered pressure histories tend to have longer rise times, resulting in lower strain rates. It can also be noted that, for the far and close-in design ranges denoted in Table 3.4, the threshold in terms of scaled standoff is typically taken as 3 (refer to Chapter 4 for more on the term *scaled standoff*).

State-of-the-practice blast-resistant design procedures for structural steel members typically aim to limit member response such that excessive deflections do not occur during a design event—that is, deflections associated with extensive material-level plastic strains well into the strain-

hardening regime of response (refer to Chapter 6 for more on component-level performance criteria). However, situations do arise where excessive deflections must be accommodated, either for a new design or retrofit of an existing structure. In this case, the dynamic ultimate strength of the structural steel should be considered.

Table 3.5 lists experimentally derived ultimate strength DIFs for various structural steels as recommended by the U.S. Department of Defense [50]. Unlike the DIFs for yield strength, these recommended values do not differentiate between low-pressure and high-pressure load levels. It can also be noted that these ultimate strength DIFs are relatively close to unity when compared to the yield strength DIFs. Structural members subjected to blast loads that sustain strains associated with the ultimate strength of the material likely do so near the stage of maximum displacement, where the velocity and thus strain rate are close to or equal to zero [53]. Therefore, a conservative design approach would be to simply set the ultimate strength DIF equal to unity.

Table 3.4 Dynamic Increase Factors (DIFs) for Yield Strength of Various Structural Steels (adapted from [50])

ASTM Grade	Flexure		Axial	
	Low Pressure (Far Design) ($\dot{\epsilon} = 0.10 \text{ sec}^{-1}$)	High Pressure (Close-in Design) ($\dot{\epsilon} = 0.30 \text{ sec}^{-1}$)	Low Pressure (Far Design) ($\dot{\epsilon} = 0.02 \text{ sec}^{-1}$)	High Pressure (Close-in Design) ($\dot{\epsilon} = 0.05 \text{ sec}^{-1}$)
A36 (Gr. 36)	1.29	1.36	1.19	1.24
A588 (Gr. 50)	1.19	1.24	1.12	1.15
A514 (Gr. 100)	1.09	1.12	1.05	1.07

Table 3.5 Dynamic Increase Factors (DIFs) for Ultimate Strength of Various Structural Steels (adapted from [50])

ASTM Grade	DIF
A36 (Gr. 36)	1.10
A588 (Gr. 50)	1.05
A514 (Gr. 100)	1.00

3.3.2 Strength Values for Design

The average yield strength for structural steels having a specified minimum yield strength of 50-ksi or less is generally higher than the specified minimum. Therefore, it is recommended that the minimum design yield strength, as specified by the applicable materials specification (e.g., ASTM), be increased by 10-percent. This is considered in blast-resistant design by multiplying the minimum specified yield strength by a static increase factor (SIF) value of 1.1. This SIF increase should not be applied to high-strength steels (specified minimum yield strength greater than 50-ksi), as available data suggest SIFs less than or equal to 5-percent. Less discrepancy exists between the minimum and average yield strength of higher strength steels because better

quality control is often exercised during the manufacturing process of these more expensive steels (somewhat like A615 versus A706 steel for deformed reinforcing bar manufacturing).

The dynamic yield strength for structural steel in blast-resistant design includes the static increase factor (SIF) and dynamic increase factor (DIF) and is calculated as shown in Equation (3-8). The dynamic ultimate strength is calculated in a similar manner, but using an appropriate ultimate strength DIF.

$$f_{dy} = f_y (SIF)(DIF) \quad (3-8)$$

where:

f_{dy} = dynamic yield strength

f_y = static yield strength

SIF = static increase factor

DIF = dynamic increase factor (see Table 3.4)

3.3.3 Rate-Dependent Constitutive Models

While constant DIFs are simplistic and conservative, they do not represent the true, variable dependence on strain rate and they can occasionally produce overly conservative designs. A refined approach to the inclusion of strain-rate effects in the analysis of blast-loaded structural components is to utilize a rate-dependent constitutive model that makes use of an empirically based DIF expression.

Johnson and Cook's [66] strain-rate sensitive plasticity model is often employed in finite element simulations as a rate-dependent constitutive model for ductile metals, and the model's flow stress rule is given in Equation (3-9). The bracketed term in Equation (3-9) incorporates the yield strength DIF in a logarithmic manner. This constitutive model is particularly useful because its empirical correlation coefficients allow for the model to be calibrated to specific material data.

$$\sigma_y = \left(A + B \bar{\epsilon}_p^n \right) \left[1 + c \ln \left(\frac{\dot{\bar{\epsilon}}}{\dot{\bar{\epsilon}}_o} \right) \right] \quad (3-9)$$

where:

A, B, c, n = empirical correlation constants

$\bar{\epsilon}_p^n$ = effective plastic strain as a function of time

$\dot{\bar{\epsilon}}$ = effective strain rate as a function of time

$\dot{\bar{\epsilon}}_o$ = reference strain rate

σ_y = yield strength

Another widely used DIF expression for the yield strength of structural steel is that proposed by Cowper and Symonds [67] and given in Equation (3-10). Rather than a logarithmic dependence of yield strength on strain rate, Cowper and Symonds proposed an exponential dependence. As with the Johnson-Cook flow stress rule, the Cowper-Symonds expression can be calibrated to specific material data.

$$DIF = 1 + \left(\frac{\dot{\epsilon}_{cs}}{c} \right)^{1/p} \quad (3-10)$$

where:

c, p = empirical correlation coefficients

$\dot{\epsilon}_{cs}$ = strain rate as a function of time

Cowper-Symonds calibration constants for various metals, which have been proposed by several researchers based on experimental findings, are presented in Table 3.6. As an example, some of the basis data are presented in Figure 3.8. In reviewing Figure 3.8, it can be noted that, in general, strain-rate effects on yield strength decrease with increasing steel strength. This trend is consistent with that observed for steel reinforcing bars in Section 3.2.1 of this manual.

Table 3.6 Empirical Cowper-Symonds Equation Coefficients for Various Metals (adapted from [68])

Material	c (sec ⁻¹)	p	Reference
Mild Steel	40.4	5	Cowper and Symonds (1957)
	7.39	4.67	Schneider and Jones (2004)
	114	5.56	Hsu and Jones (2004a)
High-Tensile Steel	3,200	5	Paik and Chung (1999)
Aluminum Alloy	6,500	4	Bodner and Symonds (1962)
	9.39×10^{10}	9.55	Hsu and Jones (2004b)
α -Titanium (Ti 50A)	120	9	Symonds and Chon (1974)
Stainless Steel 304	100	10	Forrestal and Sagartz (1978)

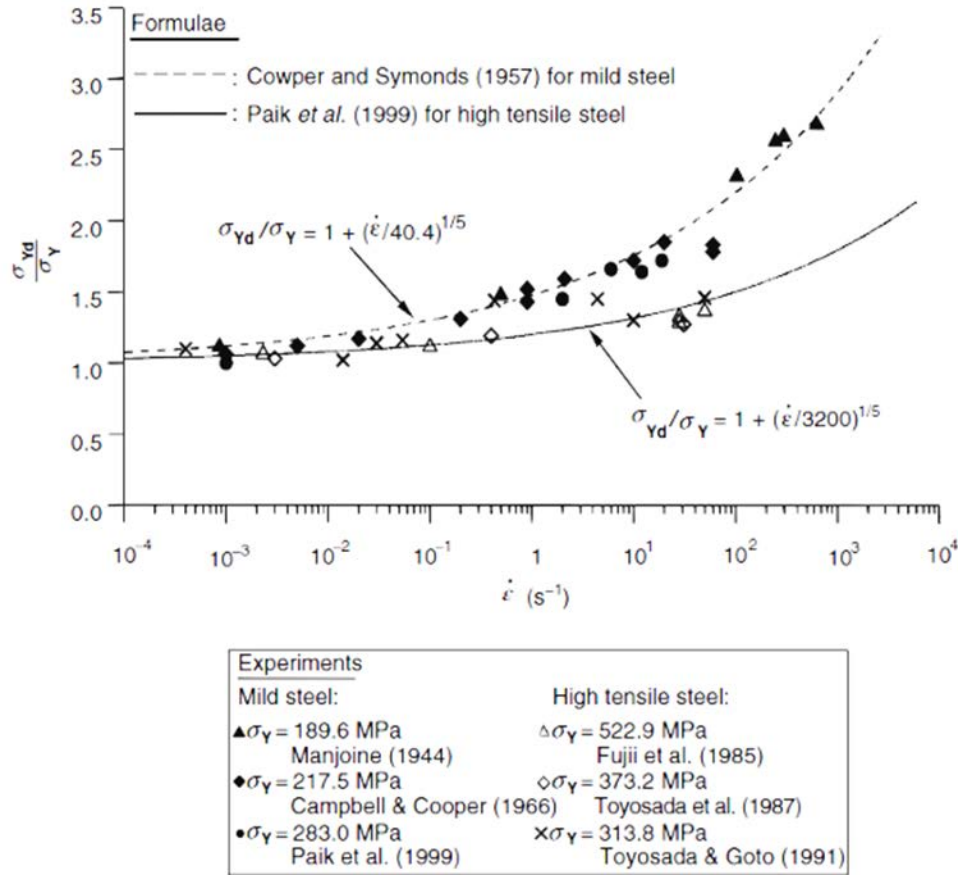


Figure 3.8 Experimental Strain Rate Data for Mild and High-Tensile Steel (1-MPa = 145.04-psi) [69]

3.3.4 Thermal Effects

Adequate data is not available to support design guidance on thermal effects for structural steels subjected to close-in blast loads. However, heat transfer from the fireball of an explosion is not likely to be a major issue on the performance of structural steel components due to the transient nature of the thermal load.

Sustained thermal loading from fire or other heat source can, however, potentially affect the mechanical properties of structural steels. For example, the ignition of a fuel truck near a highway bridge could pose a sustained thermal loading threat. For structural purposes, the degradation of strength associated with sustained thermal loading of steel is typically much more significant than the associated degradation in a structural member's stiffness. Eurocode EN 1993-1-2 [70] provides a simplified symmetric stress-strain curve for carbon steels at various temperatures, θ . The simplified stress-strain curve incorporates a curvilinear range between pre- and post-yield behavior and conservatively considers the effect of creep on yield strength without specifying heating rates. This model is based on the lower bound of transient test results and, because strain-hardening has been shown to be insignificant above temperatures of approximately 400°C (752°F), conservatively assumes perfectly plastic post-yield behavior. The

simplified curve is graphically depicted in Figure 3.9 and is constructed of the following four ranges:

1. A linear range from zero to the proportionality limit stress, $f_{p,\theta}$. The slope of this range, $E_{a,\theta}$, is referred to as the temperature-dependent elastic modulus of steel and degrades with increasing temperature.
2. An elliptical curvilinear range tangent to both the linear-elastic curve and the horizontal line at the yield point where the strain is equal to 2-percent and the stress is equal to the temperature-dependent yield strength, $f_{y,\theta}$, which also degrades with increasing temperature.
3. A constant stress range between strains of 2-percent and 15-percent (an assumed perfectly plastic post-yield response).
4. A linearly descending branch that goes from the temperature-dependent yield plateau to zero stress over the strain range of 15-percent to 20-percent.

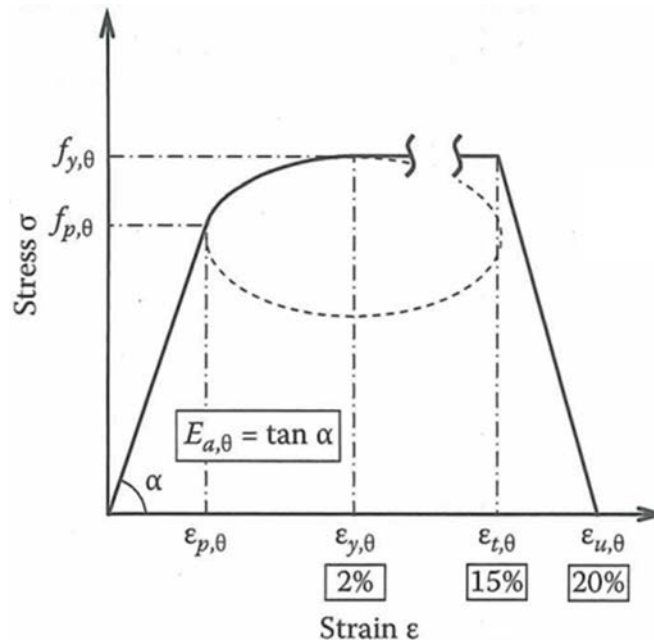


Figure 3.9 Simplified Uniaxial Stress-Strain Model for Carbon Steels at Temperature, θ , at or above 400°C (752°F) [61]

A more complex uniaxial stress-strain representation for thermally loaded structural steels exists for temperatures below 400°C (752°F) that accounts for strain hardening. This model is shown in Figure 3.10 and includes an additional strain-hardening range between 2-percent and 4-percent strain that linearly increases the stress to $1.25f_{y,\theta}$. Equations for this stress-strain curve approximation are provided below. While easily derived, equations describing the various branches of the simplified and complex stress-strain models can be found in Eurocode EN 1993-1-2 [70].

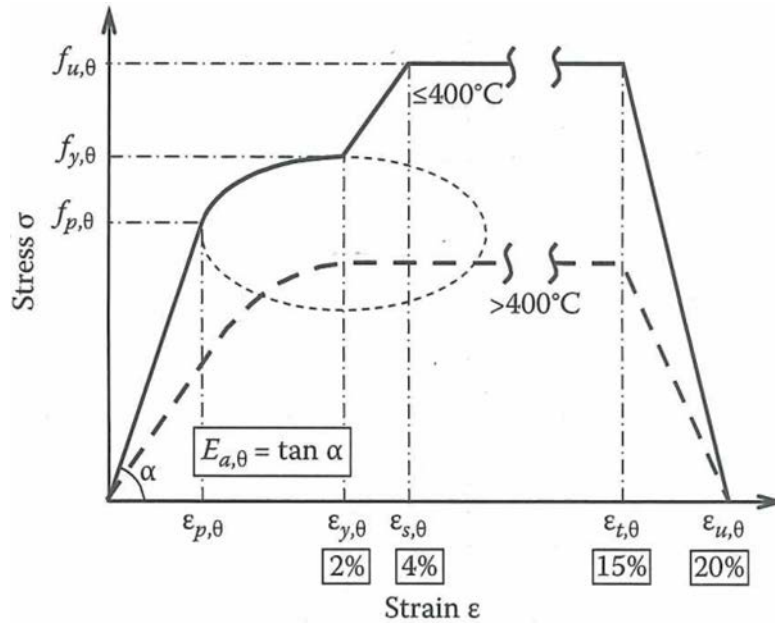


Figure 3.10 Complex Uniaxial Stress-Strain Model for Carbon Steels at Temperature, θ , less than 400°C (752°F) [61]

For simplified design calculations not requiring the full stress-strain response of thermally loaded structural steel, material-level reduction factors from Eurocode EN 1993-1-2 [70] can be used to modify room temperature material properties to account for degradation due sustained thermal loading. Reduction factors for yield strength, proportionality limit stress, and elastic modulus are graphically depicted in Figure 3.11 and tabulated in Table 3.7.

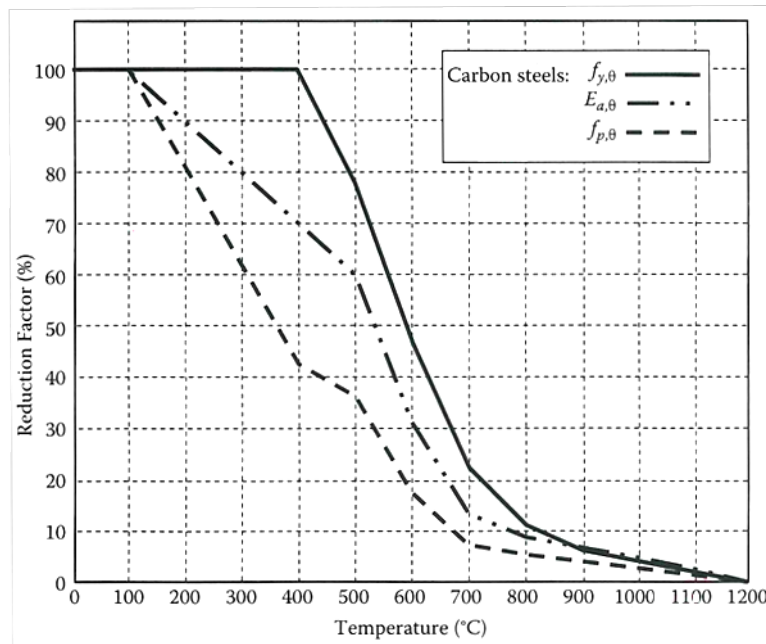


Figure 3.11 Graphical Depiction of Strength and Modulus Reduction Factors for Carbon Steels at Temperature θ [61] (1°C = 33.8°F)

Table 3.7 Reduction Factors for Hot-Rolled Carbon Steels at Temperature θ , Relative to an Ambient Temperature of 20°C (68°F) [61]

Steel temperature θ (°C)	Yield Strength $K_{y\theta} = f_{y\theta} / f_y$	Proportional limit $K_{p\theta} = f_{p\theta} / f_y$	Elastic Modulus $K_{E\theta} = f_{o\theta} / f_o$
20	1.000	1.000	1.000
100	1.000	1.000	1.000
200	1.000	0.807	0.900
300	1.000	0.613	0.800
400	1.000	0.420	0.700
500	0.780	0.360	0.600
600	0.470	0.180	0.310
700	0.230	0.075	0.130
800	0.110	0.050	0.090
900	0.060	0.0375	0.0675
1000	0.040	0.0250	0.0450
1100	0.020	0.0125	0.0225
1200	0.000	0.0000	0.0000

Certain structural elements such as reinforcing bars are cold worked to increase their strength at ambient temperatures. Fastener elements like structural bolts are hardened using heat treatment techniques. For these types of elements, sustained heating causes greater strength loss than for normal carbon steel components. Similarly, due to rapid cooling of welds from their molten state during welding, residual stresses develop in the weld metal and the region of the welded member(s) adjacent to the weld. These residual stresses result in locally hardened steel. During prolonged heating in a fire, welded regions can undergo phase changes resulting in more rapid property degradation with temperature than normal carbon steel. Reduction factors taken from Eurocodes EN 1993-1-2 [70] and EN 1994-1-2 [63] for strength and modulus of elasticity of bolts, welds, and reinforcing steel (rebar) are graphically depicted in Figure 3.12 and tabulated in Table 3.8.

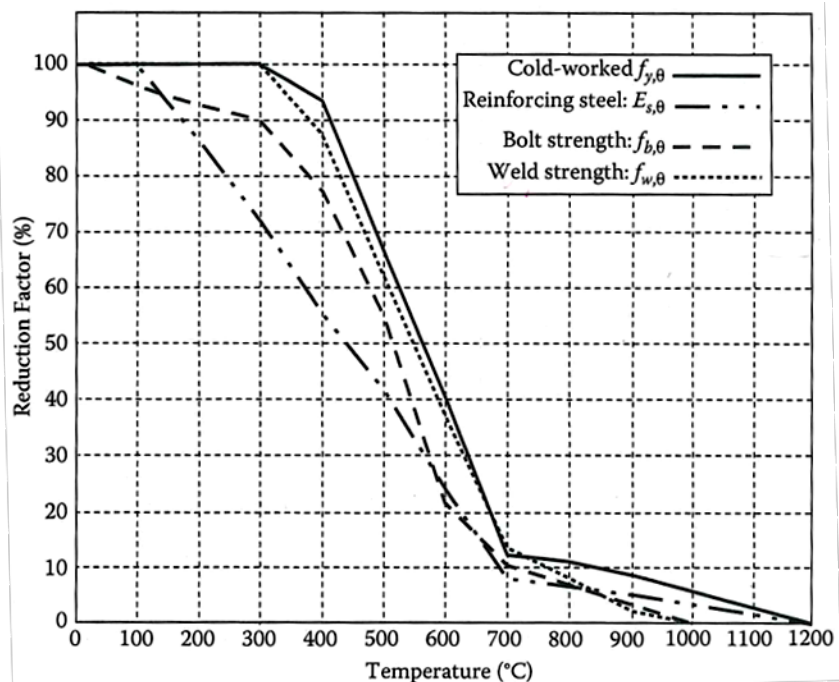


Figure 3.12 Graphical Depiction of Reduction Factors for Strength and Modulus of Cold-Worked Steel Reinforcement and Strength of Bolts and Welds at Temperature θ [61] ($1^{\circ}\text{C} = 33.8^{\circ}\text{F}$)

Table 3.8 Reduction Factors for Cold-Worked Steel Reinforcement, Bolts, and Welds at Temperature θ [61]

Steel temperature θ ($^{\circ}\text{C}$)	Cold-worked reinforcement			STRENGTH	
	Yield Strength	Proportional limit	Elastic Modulus	Bolts	Welds
	$k_{y\theta}$	$k_{p\theta}$	$K_{E\theta}$	$k_{b\theta}$	$k_{w\theta}$
20	1.000	1.000	1.000	1.000	1.000
100	1.000	0.960	1.000	0.968	1.000
150	-	-	-	0.952	1.000
200	1.000	0.920	0.870	0.935	1.000
300	1.000	0.810	0.720	0.903	1.000
400	0.940	0.630	0.560	0.775	0.876
500	0.670	0.440	0.400	0.550	0.627
600	0.400	0.260	0.240	0.220	0.378
700	0.120	0.080	0.080	0.100	0.130
800	0.110	0.060	0.060	0.067	0.074
900	0.080	0.050	0.050	0.033	0.018
1000	0.050	0.030	0.030	0.000	0.000
1100	0.030	0.020	0.020	-	-
1200	0	0	0	-	-

Supplementary Discussion on Component- and System-Level Thermal Effects

Steel is an excellent conductor of heat and typical steel sections are relatively thin. Thus, it is commonly assumed that uniform temperatures exist in thermally loaded steel members. Thus, simple heat transfer analysis methods can be used to approximate temperatures in thermally loaded steel members with reasonable accuracy for design. Once the temperature of the section is known from a heat transfer analysis, the previously summarized reduction factors and/or stress-strain curves can be used to evaluate the ability of a thermally loaded structural steel member to sustain a certain design load. This design approach determines member resistance in the strength domain and compares to demand (i.e., analogous to the LRFD methodology for conventional design).

Because uniform temperature is a typical assumption for steel members, the design problem can also be approached by first identifying design loads then determining the critical temperature at which a section will fail under the design loads. For this design approach, the member can be evaluated for a known temperature or fireproofing measures can be incorporated to ensure the member does not achieve temperatures more than the calculated critical temperature.

Also, due to the slender nature of typical steel sections, additional consideration should be given to buckling limit states. Specifically, due to reductions in elastic modulus and yield strength, local and global buckling capacities will change under sustained thermal loading.

From a system-level perspective, it is important to be cognizant of potential global effects of thermal loading on sub-systems and the structure. Consideration should be given to thermal movement of members and the effects of that movement on structural connections. It is also important to understand that thermal movement will occur in the heating and cooling phases of thermally loaded structures. This thermal movement can unseat connections, give rise to excessive forces in connector elements, distort geometry causing large displacement effects, and have other deleterious effects on the structural system. A robust design should consider the potential for these issues and accommodate them through detailing and choosing appropriate safety factors for design.

In addition to the fire-related texts and documents referenced throughout this section, Andrew Buchanan's *Structural Design for Fire Safety* [64] text is recommended as an additional reference for more details regarding materials performance (and structural design) under sustained thermal loads.

3.4 Chapter Summary

A keen understanding of material-level behavior and performance is critical to the accurate characterization of loads and calculation of structural response to postulated extreme loading events. This chapter began with an overview of chemical explosions with emphasis on high-explosive detonations. Performance of high-explosive materials was discussed along with an overview of different explosive charge types, equivalency factors for non-TNT explosive compositions, and charge shape effects.

Material-level performance of reinforced concrete and metal construction materials was also discussed in this chapter. Given the focus on extreme loading throughout this manual, attention

was paid to unique behavioral aspects of these construction materials when subjected to high-rate loading and sustained thermal loading. Guidance was provided on how to account for high-rate and thermal load effects on key material parameters such as yield strength, ultimate strength, and elastic modulus for purposes of design-level calculations. An introduction to more sophisticated approaches for addressing high-rate and thermal load effects on material performance was also provided for the intended use with high-fidelity finite element analysis techniques.

The next chapter builds upon the performance of high-explosive materials by addressing the effects of a high-explosive detonation on nearby structures. More specifically, Chapter 4 discusses blast phenomenology, shock wave behavior, and introduces various approaches for characterizing blast loads on structural bridge components.

4.0 BLAST PHENOMENOLOGY

A chemical explosion results from a sequence of exothermic chemical reactions between a fuel and an oxidant—commonly referred to as combustion. In general, a fuel is a material that can be readily utilized to generate energy. Fuels can exist in a solid, liquid, or gaseous state, and they are typically made up of organic chemical compounds consisting of various permutations of carbon, hydrogen, nitrogen, sulfur, and oxygen atoms. An oxidant is a reactive and highly electron-negative chemical entity that desires to reach a stable energy state by gaining valence electrons through covalent or ionic bonding with atoms of other chemical entities. Oxygen happens to be a powerful and abundant oxidizing agent, and thus plays a major role in combustion. It should be noted that not all combustion reactions result in a destructive chemical explosion. Rather, most daily processes that utilize combustion as a means to generate useable energy render relatively benign explosive effects. For example, gasoline is the hydrocarbon fuel used to create non-destructive chemical explosions that drive the pistons of internal combustion engines in most automobiles.

Although proven to be a safe means of generating useable energy, combustion can also be employed in a destructive manner to create chemical explosions with the intent of inflicting physical damage and human injury. All combustion reactions involve an oxidation process that progresses from the point of initiation at a rate that depends on various parameters such as pressure, temperature, specific properties of the reactants, mixture properties, and so on [46]. Given the many parameters that characterize a specific combustion reaction, the explosiveness of its effects is largely a function of the chemical reaction rate. If the reaction rate increases, the burning process becomes increasingly violent and may result in the generation of a pressure wave, either in, or emanating from, the reactant. In the limit, the combustion may become so rapid that the pressure pulse ahead of the reaction front, which becomes steeper and steeper as the rate of pressurization increases, suddenly assuming a step condition, generating a shock wave [45]. Strictly speaking, when the chemical reaction zone progresses at subsonic speeds, the combustion process is termed *deflagration*, and, when the reaction zone progresses at supersonic speeds, the combustion process is termed *detonation*. Slow burning deflagrations release energy in the form of thermal radiation and can be associated with controlled flame generation. Faster burning deflagrations are more violent in nature and, in addition to the release of thermal radiation, may produce a pressure wave in the surrounding medium due to the rapidly expanding gas products. Faster burning deflagrations that produce explosive effects are generally associated with low-explosive materials such as propellants and pyrotechnics. Under the right fuel-air conditions, explosive deflagrations can also occur due to the ignition of a flammable vapor cloud.

Detonations produce the most destructive explosive effects and are most often associated with high-explosive materials. The chemical reaction zone of a detonation propagates through the reactants at speeds ranging from 22,000-ft/sec to 28,000-ft/sec for most high-explosive materials, and pressures immediately behind the reaction front can range from 2,700-ksi to 4,900-ksi [50]. Many high-explosive compositions are inherently oxygen deficient, and the detonation process takes place too quickly for the primary reaction to utilize oxygen from the surrounding air. Consequently, only a fraction of the available chemical energy is released during the initial detonation. Of the total energy available for complete combustion of an explosive, only about one-third is produced by the detonation [71]. Additional energy is released in a slower secondary

combustion (or afterburn) process as the detonation products mix with air and burn. As with explosive deflagrations, detonations release energy in the form of thermal radiation and air blast; however, the characteristics of the air blast produced by a detonation (i.e., shock wave) differ from those of a deflagration. From a bridge security and protective design perspective, the effects of an impinging shock wave on critical bridge components are of chief concern. Therefore, this chapter is dedicated to developing an understanding of shock wave physics, the interaction of shock waves with critical bridge components, and quantifying shock-induced blast loads on critical bridge components.

This chapter discusses the effects of deliberately placed chemical explosives intended to damage or fail critical bridge components. While many other accidental (man-made) explosions could be considered, the loads considered herein are those that would be generated by typically man-portable or vehicle-borne high explosive charges.

This chapter begins with an overview of the different types of shock-inducing explosions that are particularly relevant to bridges. A discussion on far-field and near-field shock wave behavior follows, after which an overview of shock wave interaction with typical bridge components is provided. This chapter ends with the presentation of various methods for quantifying shock-induced blast loads on bridge components.

4.1 Types of Explosions

Bridge components are necessarily robust and are not easily damaged through impact or explosion. Therefore, substantial blast damage to bridge components will most often result from high-explosive detonations taking place in the near field—that is, a detonation that takes place in contact with or close to a bridge component. However, far-field events can generate damage in bridge components with larger cross-section exposure, such as deep girders, walls, decks, and steel or concrete box elements. Figure 4.1(a) illustrates the general explosive-to-target geometry for the far-field regime. In this load scenario, a point source approximation is generally valid for the explosive charge and the bridge component is essentially subjected to spatially uniform blast loads that tend to generate damage through flexural, diagonal tension (i.e., beam shear), or punching shear mechanisms. Near-field events will also produce significant damage in larger exposure components, but pressures and impulses in the near field will generally be large enough to generate damage in “heavier” components such as piers and bents as illustrated in Figure 4.2(a). These near-field loads, as graphically illustrated in Figure 4.1(b), are more complex than those from a far-field detonation because they are spatially non-uniform and vary temporally (i.e., different shock wave arrival times along height of bridge component). Near-contact or contact explosions can cause significant damage to robust bridge elements such as piers. Figure 4.2(b) and (c) illustrate the local damage generated by near-contact and contact detonations, respectively.

The following sections discuss the parameters associated with blast loads generated in the far-field, in the near-field, and in the near-contact regimes.

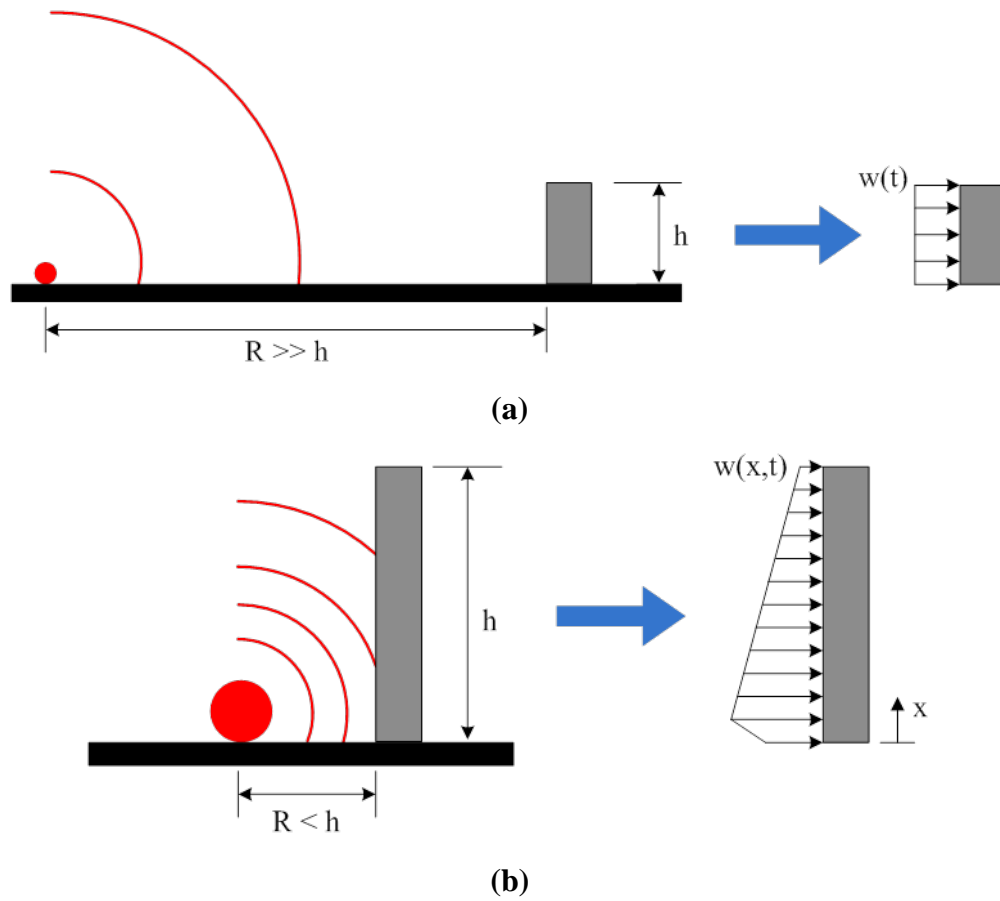


Figure 4.1 Influence of Standoff to Height Ratio on Blast Load Resulting from Spherical Surface Burst: (a) Far-Field Detonation, (b) Near-Field Detonation [18]

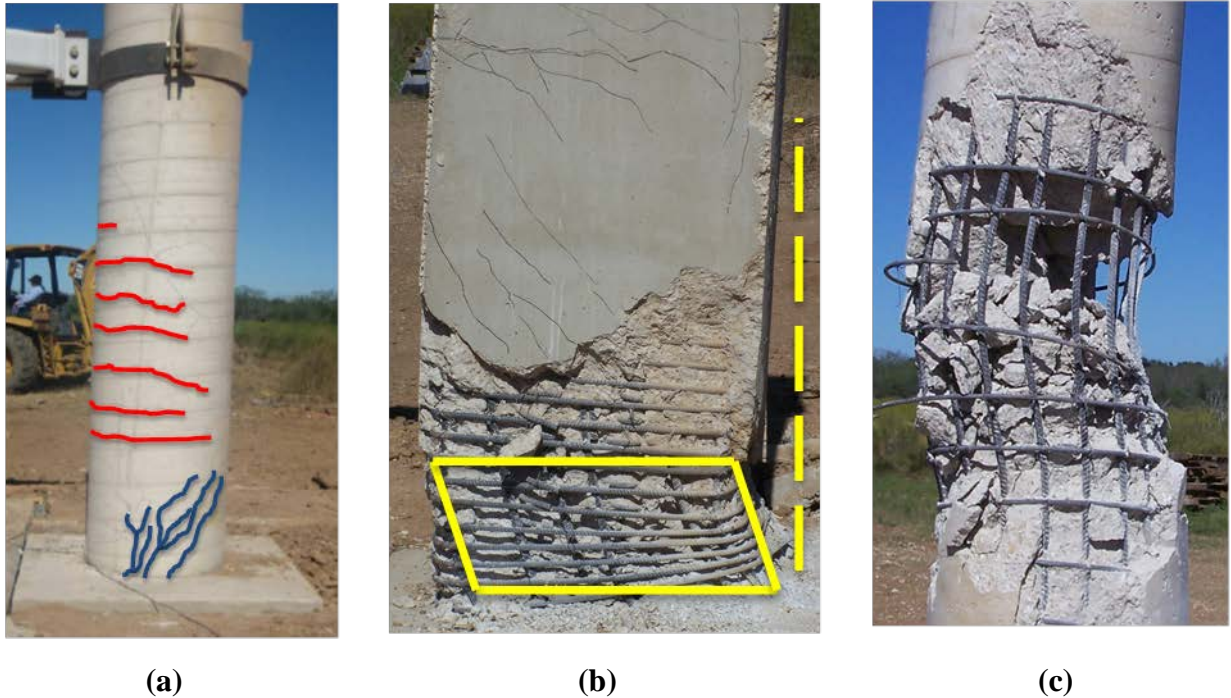


Figure 4.2 Illustrating Damage Potential for Different Types of Explosions (images adapted from blast tests supporting [24]): (a) Near-Field Explosions Typically Promote Flexural Response in “Heavier” Bridge Components, (b) Near-Contact Explosions Can Cause Localized Material Damage and Deformation, (c) Contact Charges Produce Extensive Localized Material Damage

4.2 Shock Waves in Air

The blast effects of an explosion are in the form of a shock wave composed of a high intensity shock front which expands outward from the surface of the explosive into the surrounding air. As the wave expands, it decays in strength, lengthens in duration, and decreases in velocity. Spherical divergence causes this phenomenon as well as by the fact that the chemical reaction is completed, except for some afterburning associated with the hot explosion products mixing with the surrounding atmosphere.

The shock front impinges on structures located within its path and then the shock pressures engulf the entire structure. The magnitude and distribution of the blast loads on the structure arising from these pressures are a function of the following factors: (1) explosive properties, namely type of explosive material, energy output (high- or low-order detonation), and weight of explosive; (2) the location of the detonation relative to structures upon which the shock impinges; and (3) the magnitude and reinforcement of the pressure by its interaction with the ground, or the structure itself. The following sections will address factors (2) and (3); location and interaction of the shock wave with structures. Factor (1) was addressed in Chapter 3 of this manual.

4.3 Far-Field Behavior of Shock Waves

Far-field shock wave behavior pertains to a propagating shock wave that is far from any local obstructions such as a nearby structure that would otherwise disrupt the shock flow and

temporarily alter the wave's behavior. The presence of obstructions significantly influences the local behavior of shock waves.

Figure 4.3 illustrates the overpressure history of an ideal far-field shock wave, where the vertical axis represents incident overpressure (i.e., gauge pressure relative to ambient atmospheric pressure) and the horizontal axis represents time after detonation. Incident overpressure is often referred to as side-on overpressure. An ideal far-field shock wave can be characterized as a nearly instantaneous rise in pressure followed by a rapid decay with time. The time of arrival, t_a , represents the time after detonation at which the shock front encounters a point in space. Upon arrival, a steep rise in pressure up to the peak side-on pressure, P_{so} , occurs followed by a rapid time-dependent decay. The duration of pressure decay to steady-state ambient condition is on the order of milliseconds, and it is often decomposed into a positive phase duration, t_{pos} , and a negative phase duration, t_{neg} . Over-expansion of the gaseous detonation products gives rise to an explosive dilatational wave (i.e., rarefaction wave) that forms and propagates behind the shock front, thus creating the sub-atmospheric or negative phase of the overpressure history shown in Figure 4.3. An additional parameter that is of great importance to the dynamic response analysis of blast-loaded bridge components is the positive phase specific impulse, i_{pos} , which is defined as the area under the positive phase portion of the overpressure history curve.

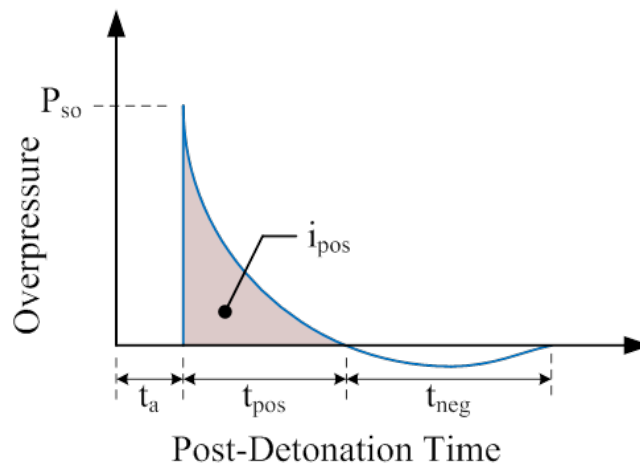


Figure 4.3 Overpressure History for Ideal Far-Field Shock Wave [18]

When a high-explosive charge detonates in the far-field (i.e., relatively far removed from a target of interest) the assumptions of a point source and spherical shock front geometry are typically valid. In this case, the external detonation scenario generally falls into one of three categories: spherical free-air burst, spherical air burst, or hemispherical ground burst [50]. These far-field external detonation scenarios are graphically depicted in Figure 4.4. State-of-the-practice empirical blast load calculation methods for external far-field detonations are introduced in Section 4.6, and additional information can be found in UFC 3-340-02 *Structures to Resist the Effects of Accidental Explosions* [50].

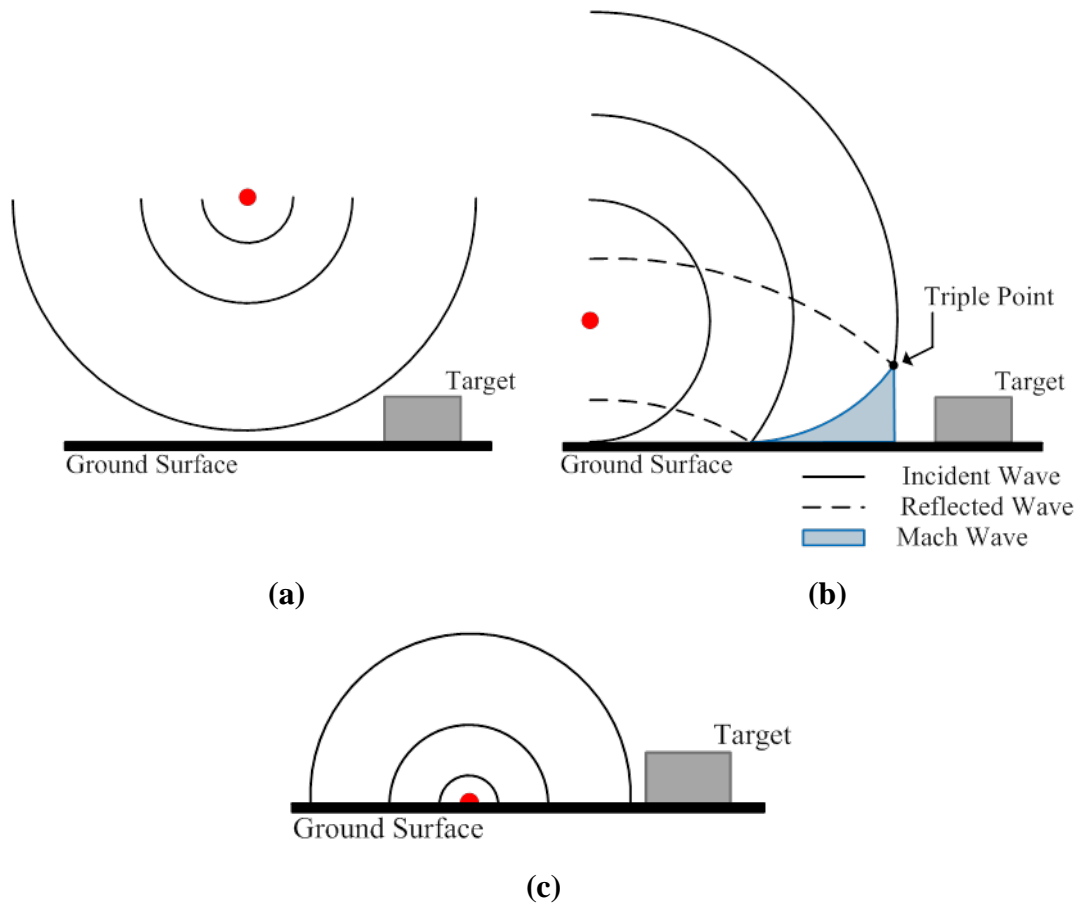


Figure 4.4 Far-Field External Detonation Scenarios: (a) Spherical Free-Air Burst, (b) Spherical Air Burst, (c) Hemispherical Ground Burst [18]

4.3.1 Spherical Free-Air Burst

A spherical free-air burst represents a scenario wherein the explosive charge detonates high enough above the ground surface that the incident shock front reaches the target of interest prior to the ground surface. The significance of this external far-field detonation scenario is the fact that the incident shock front does not get reinforced by a reflected shock wave prior to its interaction with the target, thus delivering comparatively less severe blast loads with respect to an air burst or hemispherical ground burst.

A spherical free-air burst is most often associated with military applications involving air-to-surface exploding ordnance. Accordingly, a free-air burst is not a likely terrorist attack scenario for a highway bridge.

4.3.2 Spherical Air Burst

A spherical air burst is similar to a free-air burst in that the explosion initiates above the ground surface. However, in this case, the height of burst is such that the incident shock wave reflects off the ground surface prior to engaging the target of interest; one example is the detonation of a bomb that is concealed in a thin-walled truck trailer. When a critical angle of incidence between

the incident shock wave and reflecting surface (in this case, the ground surface) occurs, a Mach front is generated.

The *triple point*, which is graphically depicted in Figure 4.4(b), is defined as the intersection between the incident, reflected, and Mach waves. Below the triple point, the Mach front can be taken as spatially uniform with a peak overpressure and positive phase specific impulse greater than those of either the incident or reflected waves. Above the triple point, the airblast environment is more complex. As is illustrated in Figure 4.4b, incident and reflected shock waves continue to propagate outward, each exhibiting different spatial and temporal characteristics. The geometry of the reflected wave front is not quite spherical due to the ground reflection, and it is propagating faster than the incident wave as it travels through the already heated air behind the incident shock front. Consequently, the ratio of triple point height to target height at the target standoff becomes an important parameter for calculating blast loads due to an external far-field air burst. For more detailed information on the shock physics of an external far-field air burst, the reader is encouraged to consult UFC 3-340-02 *Structures to Resist the Effects of Accidental Explosions* [50].

4.3.3 Hemispherical Surface Burst

A hemispherical surface burst represents an external far-field explosion involving an explosive charge that detonates at or very near the ground surface. In this case, the incident shock wave is almost immediately enhanced by ground surface reflection. As is illustrated in Figure 4.4(c), the reflected shock wave then propagates away from the explosive source in a hemispherical geometry until it encounters the target of interest or some other reflecting surface.

For an ideal, perfectly rigid ground surface, the effective load amplification is 2. However ground cratering beneath the charge typically occurs thus absorbing some of the blast energy. Owing to this cratering effect, the effective load amplification is 1.8 is considered a more realistic value than 2 [49].

4.4 Near-field Behavior of Shock Waves

Near-field shock wave behavior pertains to a propagating shock wave whose characteristics are temporarily altered due to the presence of and interaction with a local flow obstruction. The local obstruction is typically of finite geometry such as a building or bridge component.

Impedance is a material property that can be simply defined in this context as the product of mass density and compression wave speed. If a shock wave encounters an interface between two media of different impedances, in this case air and a rigid, planar surface of infinite extent, then a reflected wave is generated. The peak pressure and impulse of the reflected wave are greater than the corresponding incident values because of the pressure enhancement caused by arresting flow behind the reflected shock wave [49]. Figure 4.5 illustrates the difference between a side-on and normally reflected (i.e., the shock front normal is perpendicular to the reflecting surface) pressure history, where the enhanced peak pressure and positive phase specific impulse of the normally reflected wave are apparent. Researchers [72, 73] suggest that the upper limit on peak reflected pressure enhancement can be as much as 12 times greater than side-on pressure. In addition to a normal reflection, shock waves can undergo a regular oblique reflection and a Mach reflection.

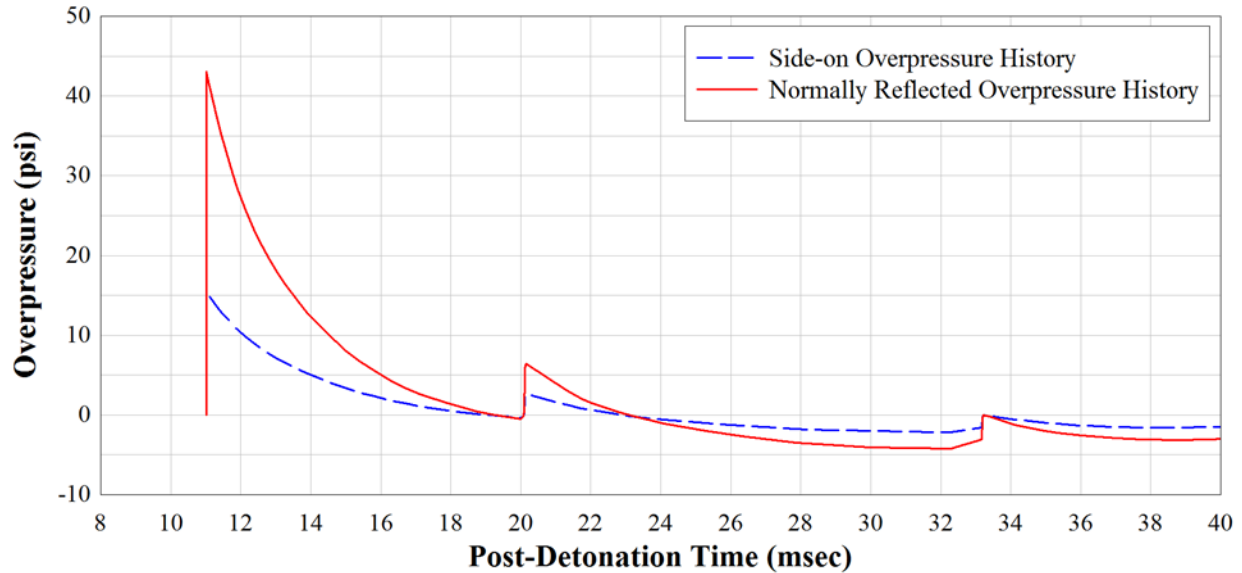


Figure 4.5 Comparison of Normally Reflected and Side-On Pressure-Time Histories [18]

A regular oblique reflection can occur when a shock front strikes a reflecting surface at some angle of incidence, q_i , as shown schematically in Figure 4.6. Unlike the case of a typical acoustic wave, the angle of reflection, q_r , will not be the same as the angle of incidence. In fact, the angle of reflection has been shown to be a monotonically increasing function of the angle of incidence. The difference in the angles of incidence and reflection is chiefly due to the transient state of the air adjacent to the reflecting surface. For a given incident shock strength, there exists a critical angle of incidence, q_{crit} , above which a regular oblique reflection cannot occur [71]. Baker [72] and Mays and Smith [73] go on to explain that when this situation occurs the reflected shock wave catches up and coalesces with the incident shock wave to form a highly reinforced third shock wave—termed a Mach wave after Ernst Mach, who proposed this phenomenon back in 1877.

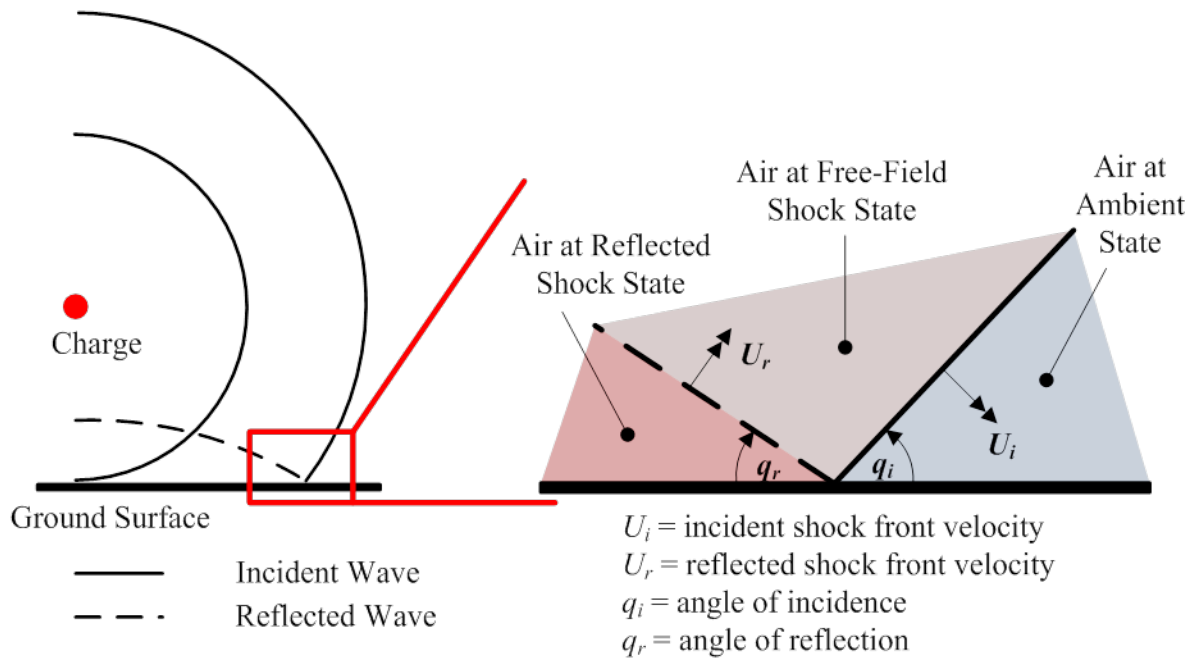


Figure 4.6 Schematic of Regular Oblique Reflection of Planar Shock Wave [18]

Once a Mach wave is formed, it grows rapidly and tends to quickly overtake the initial two-shock system. The junction between the incident, reflected, and Mach fronts is termed the triple point. Furthermore, the nearly vertical Mach wave front is typically referred to as the Mach stem. A schematic illustrating the evolution of a Mach reflection is given in Figure 4.7 for a realistic threat scenario involving a spherical charge that is detonated above a reflecting surface. In reviewing Figure 4.7, it can be seen that (a) the shape of the incident shock front is spherical, whereas the shape of the reflected shock front is not, and (b) regular oblique reflections take place until the critical angle of incidence is achieved. Over the years, experiments have been conducted and data compiled by the U.S. Government to derive empirical curves that relate the reflected pressure coefficient (P_r / P_{so}) to the angle of incidence for several different shock strengths. The resulting set of empirical curves is provided in Figure 4.8. The transition from a regular oblique reflection to a Mach reflection is clearly discernible by the peculiar humps in the various curves of Figure 4.8. In practice, these empirical reflection coefficient curves are often used to account for reflection effects as part of empirical blast load characterization procedures [53, 74, 75].

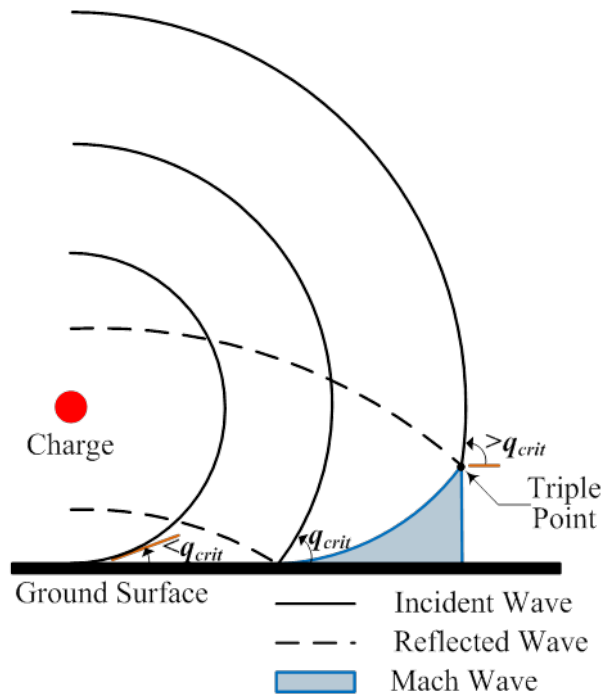


Figure 4.7 Schematic of Mach Reflection Evolution [5]

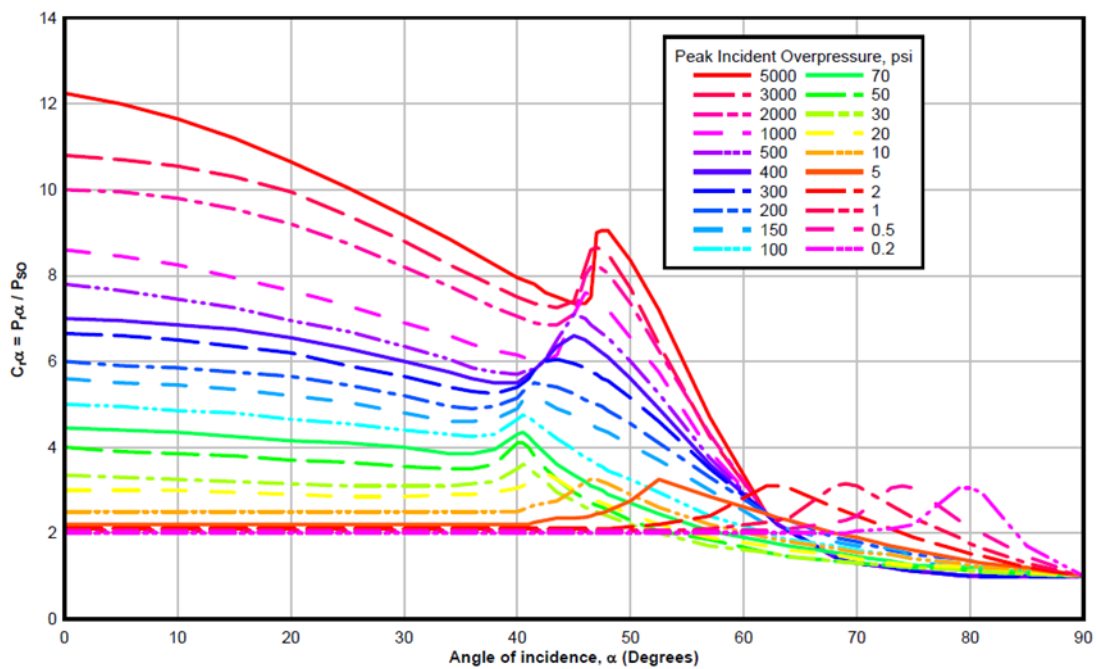


Figure 4.8 Empirical Reflection Coefficient Curves as a Function of Angle of Incidence [50]

4.5 Shock Wave Interaction with Bridge Components

The fluid-structure interaction between a propagating shock wave and a local obstruction, such as a building or bridge, gives rise to a highly complex and transient environment. Structural components not oriented parallel to the shock wave's propagation direction will act as a reflecting surface for the impinging shock wave. As the shock wave passes over the structure, turbulent flow and vortex generation occur near convex corners. Figure 4.9 shows a screen capture of a high-fidelity computational fluid dynamics simulation, where vortex formation occurs as the shock front diffracts around a convex corner of an obstruction. In addition, drag forces are imparted to the structure due to trailing gas particles that have been set in motion by the shock wave. Gas particles move at the particle velocity, which is lower than the shock wave velocity. The particle velocity is associated with dynamic pressure, which is caused by the “wind” generated from the blast shock front [46]. A schematic of this fluid-structure interaction process is illustrated in Figure 4.10 for a threat scenario involving a bulk explosive detonation that occurs far enough away from the target such that the assumption of a planar shock front is valid.

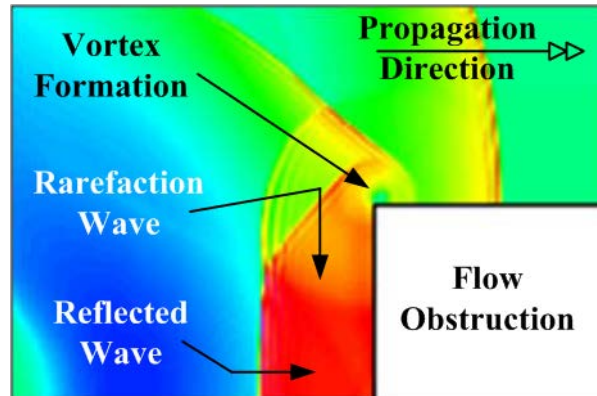


Figure 4.9 Vortex Formation around Convex Corner [76]

The left image in Figure 4.10 represents the time at which the shock front first strikes the front face of the target. The front face pressure is decomposed in the image to include a stagnation pressure, P_{stag} , and a reflected pressure, P_r . The stagnation pressure is the sum of the side-on pressure and the drag pressure from the trailing gas particles. In general, the drag pressure is defined as the product of the dynamic wind pressure and a drag coefficient. The dynamic wind pressure depends on the side-on pressure of the shock wave, and the drag coefficient depends on the shape of the obstruction and (to a lesser extent) the peak dynamic wind pressure. Open-frame structures and small buildings, where a shock wave will produce quick envelopment, are most sensitive to dynamic wind pressures [53]. For the case of a rectangular structure's windward wall, the drag coefficient is taken as unity [50, 75]. The right image of Figure 4.10 is a snapshot later in time when the shock front has progressed over a portion of the target. Side face pressures, P_{side} , are now present in addition to front face pressures. The side face pressure represents the sum of the side-on pressure and the drag pressure, where now the drag pressure is negative in sense (i.e., acting away from the target surface) and a fraction of the full dynamic wind pressure in magnitude. A table of drag coefficients is provided in [50] as a function of peak dynamic wind pressure to be used for roof and side wall pressure calculations. For rectangular buildings, the drag coefficient may be conservatively taken as -0.40 for side walls, leeward walls,

and roofs [75]. The side pressures are shown to decrease with distance away from the target front face because the side-on pressure decreases with increasing distance from an explosive source. It should also be noted that the spatial distribution of the front face reflected pressure is shown to change as the shock front traverses over the target, alluding to the presence of a phenomenon commonly referred to as *clearing*.

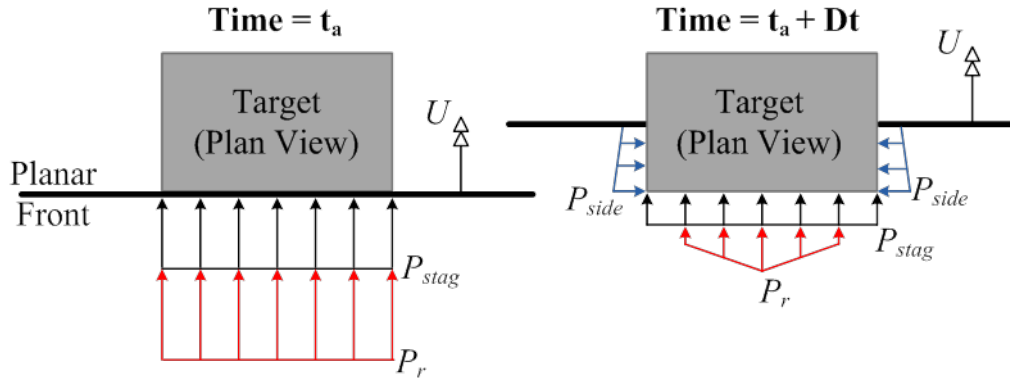


Figure 4.10 Schematic of Planar Shock Front Interaction with Building Structure [18]

Clearing is a process in which reflected pressure seeks relief toward lower pressure regions, and it occurs when a shock wave strikes a reflecting surface having “finite” in-plane dimensions. Clearing starts from the free edges of a finite reflecting surface where an initial pressure differential exists between the reflected pressure acting on the edge of the target and the adjacent side-on pressure in the free air. The free-edge reflected pressure expands outward toward the lower side-on pressure, ultimately resulting in a reduced free-edge pressure equal to the stagnation pressure (illustrated in the right image of Figure 4.10). This clearing process propagates toward the center of the reflecting surface in the form of a dilatational (or rarefaction) wave. Clearing is a time-dependent process that may or may not have a significant influence on the resulting blast load imparted to a target surface. The time it takes for the reflected pressure at a specific point on a planar reflecting surface to be completely relieved to the stagnation pressure can be estimated per the three-transits-to-the-edge expression shown in Equation (4-1) [48]. If the clearing time is greater than the positive phase duration of the reflected pressure pulse, clearing will have a negligible effect on the pressure-time history at the point of interest on the reflecting surface.

$$t_c = \frac{3S}{U} \quad (4-1)$$

where:

S = shortest distance from the point of interest to a free edge

U = shock front velocity

Figure 4.11 provides a graphical representation of the clearing effect on the reflected pressure pulse for a given point of interest. Figure 4.11 illustrates a simplified linear representation that is often adopted in empirical blast load characterization procedures [53, 75], where clearing time is calculated using the three-transits-to-the-edge approach. In Figure 4.11, the solid red line represents the fully reflected pressure history that would occur in the absence of clearing, and the

solid black line represents the stagnation pressure history. The dashed bi-linear curve depicts the effect of clearing on the reflected pressure history at the point of interest. However, overpressure decays exponentially and clearing does not always initiate instantaneously. Because rarefaction waves initiate at free edges of a target surface and propagate inward, the onset and significance of clearing is highly dependent on the specific point of interest on a target surface.

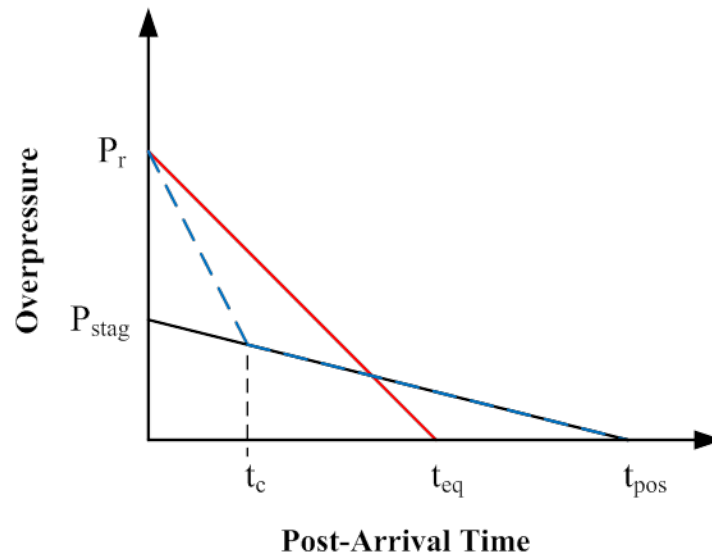


Figure 4.11 Simplified Linear Representation of the Effect of Clearing on Pressure-Time History

In reviewing Figure 4.11, the following conclusions can be made about the effect of clearing on reflected pressure-time histories:

- The magnitude of the peak reflected pressure attained upon shock front arrival is not affected by the presence of clearing
- Clearing acts to reduce the positive phase specific impulse (i.e., reduces the area under the positive phase portion of the pressure-time history curve)
- The onset and influence of clearing is highly dependent on the specific location of interest on a target surface

The three-transits-to-the-edge concept adequately captures the clearing phenomenon and consequent reflected impulse reduction exhibited by planar reflecting surfaces of typical building structures. However, results from recent research suggest that such a concept alone is not adequate for predicting reflected impulse reduction of blast-loaded slender structural components such as exposed girders and columns. In addition to the short clearing time due to the relatively small width of the structural component's blast-loaded face, overpressure tends to build up along the component's leeward face as it quickly becomes engulfed by the shock flow. If the leeward face overpressure develops prior to the end of the front face reflected pressure's positive phase, the structural component realizes a net reduction in the transversely applied blast load. Thus, the leeward face overpressure partially nullifies the front face reflected pressure, resulting in a net blast load reduction. Further complexities associated with slender structural components of

circular cross section—a prevalent shape for reinforced concrete bridge columns—are the difficulty in defining a “free edge” from a clearing perspective and the variable angle of incidence and physical standoff around the circumference of the circular section. Although a unified impulse reduction theory has yet to be put forth in the open literature, various researchers have acknowledged and/or observed the complex shock flow behavior experienced by slender structural components.

As part of a large research effort for the National Cooperative Highway Research Program [24] to develop blast-resistant design provisions for reinforced concrete bridge columns, a detailed experimental and computational study was conducted [33] aimed at characterizing the behavior of shock waves in the vicinity of slender, non-responding structural components of square and circular cross sections. In that, clearing and wrap-around pressure effects were found to contribute to a reduction in the applied blast load; however, it was also observed that (a) the impulse reduction factor depends on the ratio of physical standoff to section width (or diameter in the case of a circular section), and (b) given a circular column with a diameter equal to the width of a square column, the circular column tends to experience a lower net blast load. The findings are graphically summarized in Figure 4.12 and are further described in Chapter 7 of this manual.

The pressure distributions on the square and circular sections represent a snapshot in time, where the solid-arrow pressure distributions are the clearing-affected reflected pressures, the dash-arrow pressure distributions are the leeward face overpressures due to shock flow engulfment, and the hollow-arrow pressure distributions are the incident pressures. The point of interest where the angle of incidence and reflection are shown on both sections is located at the same horizontal distance away from the charge center of gravity (CG). For the specified point of interest, the angle of incidence and physical standoff are both greater for the circular section than the square section. In fact, this is the case for every point along the front half of the circular section’s circumference except for the point directly in front of the charge CG where the section experiences a normal reflection. While the difference in physical standoff is inconsequential for large-standoff threat scenarios, it can have a significant influence on the blast load resulting from a small-standoff detonation—a likely threat scenario for a reinforced concrete bridge column.

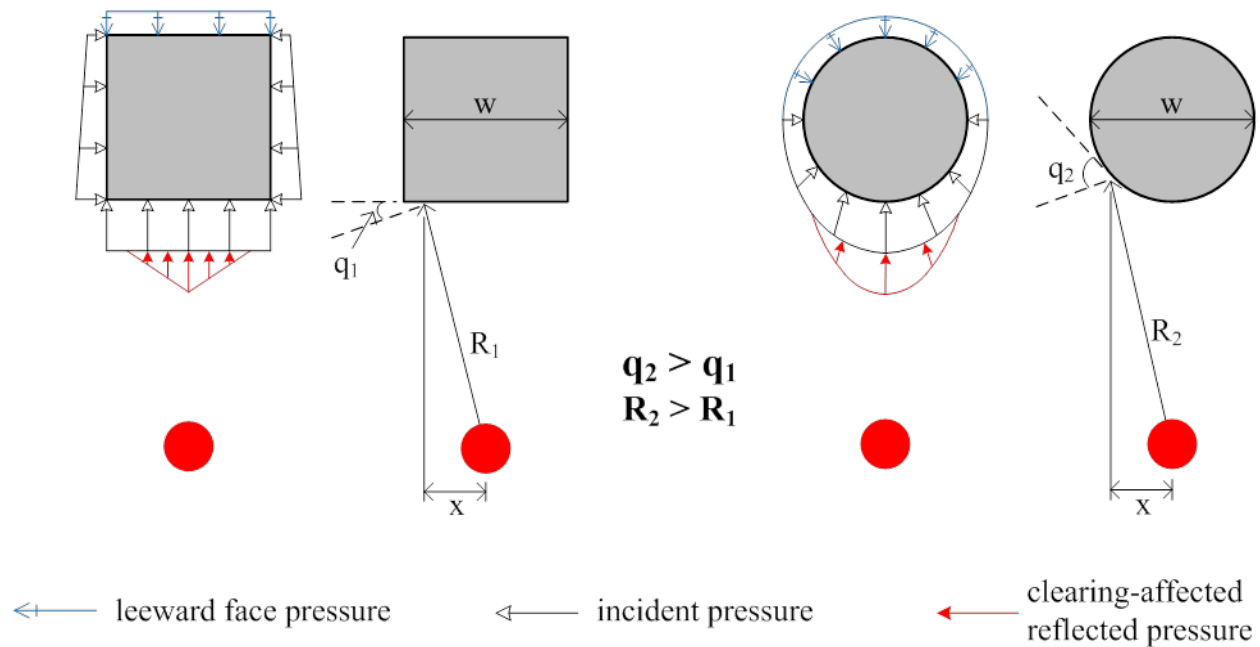


Figure 4.12 Effect of Section Shape on Physical Standoff and Angle of Incidence [18]

The second implication associated with the assumption of an explosive point source and uniform blast load distribution deals with the effect of charge shape on the shock front geometry. Charge shape can have a significant effect on resulting blast loads for relatively close-in detonation scenarios—that is, an explosion that takes place relatively close to a target—and the significance of this effect diminishes as the distance between the explosive charge and target of interest increases. Close in to a detonating charge, the initial shock front geometry is largely influenced by charge shape [46]. As is discussed in Section 4.6.1, shock front geometry forms the basis for blast scaling laws and is ultimately what dictates the spatial and temporal characteristics of resulting blast loads.

The shock wave associated with a high-explosive detonation is initially driven by the forceful expansion of gases. These gases are bi-products of the supersonic combustion reaction that progresses through the explosive material. Hence, the manner in which the gaseous bi-products expand outward is largely a function of charge shape. Once the shock wave disengages from the gaseous bi-products and begins to propagate in a free and stable manner, the shock front transitions to a nearly spherical geometry as it continues to radiate outward from the explosive source. This phenomenon is illustrated in Figure 4.13 for the far-field detonation of a bare, cylindrical explosive charge placed on the ground with its longitudinal axis oriented perpendicular to the ground surface.

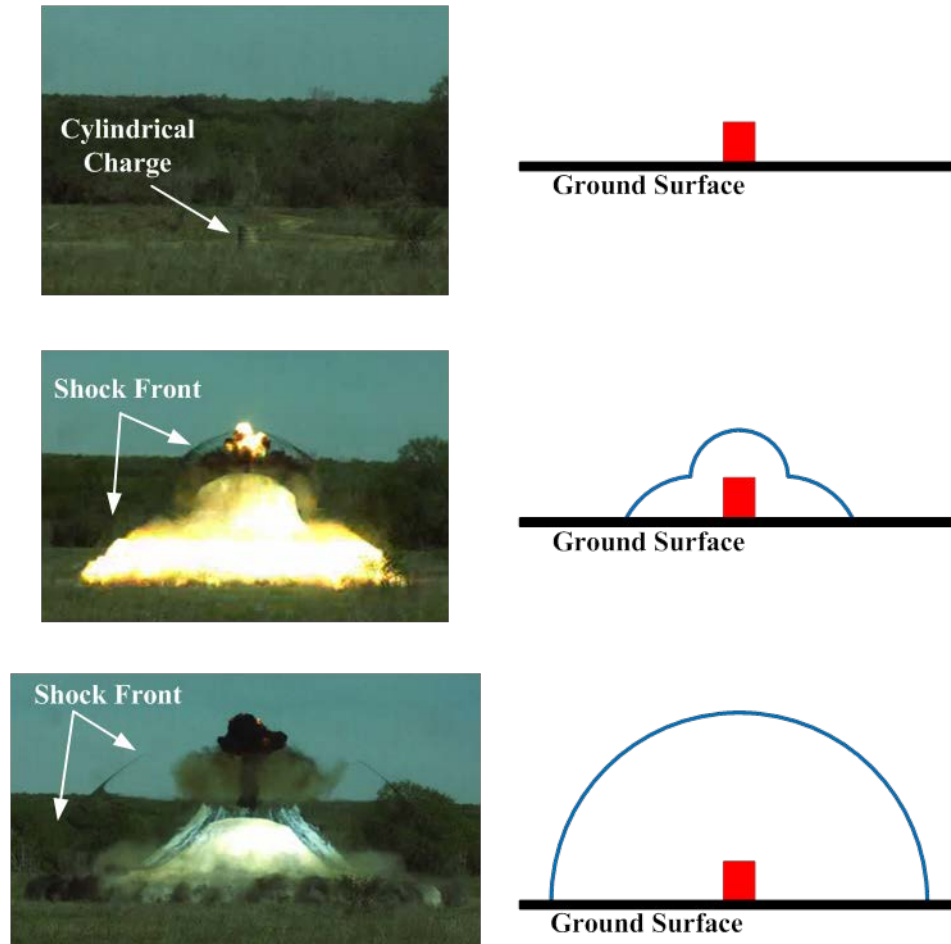


Figure 4.13 Effect of Charge Shape on Initial Shock Front Geometry [18]

A final topic of interest concerns loads caused by fragments. In general, fragments are pieces of matter that get propelled through the air during a detonation event. Fragments can be particles produced by the airblast via destruction and disintegration of nearby objects, or they can be pieces of the explosive casing. When a fragment strikes a target, it imparts an impulse that is additive to that delivered by the shock wave. The magnitude of the additional impulse is a function of the fragment's mass and velocity upon impact. While seemingly simple in theory, it often proves difficult to quantify such loading because fragments are typically irregular in nature and hard to predict a priori [49]. Furthermore, typical casings for terrorist weapons (i.e., vehicle parts, sheet metal, and plastic) are not massive, especially relative to cased military weapons. As such, although they still pose a serious risk of injury to nearby personnel, fragment loads are usually negligible for the performance assessment of critical bridge components subjected to terrorist threat scenarios involving bulk explosives.

4.6 Blast Load Computation

In general, blast load characterization procedures accept threat and target parameters as input. The output can range in complexity from individual blast load parameters, such as peak reflected overpressure and specific impulse, to detailed pressure-time histories defined at various locations over multiple target surfaces. In increasing complexity, blast load characterization procedures

can be broadly classified into three categories: empirical chart-based methods, semi-empirical ray-tracing methods, and high-fidelity computational fluid dynamics (CFD) methods. Each category possesses certain limits of applicability as well as strengths and weaknesses regarding accuracy, complexity, and computational expedience. Therefore, the decision to employ a blast load characterization procedure should be based on many factors including the nature of the threat scenario and target, the amount of time and computing power available, the competency of the analyst, the level of fidelity required, and the type of dynamic response analysis for which the loads are being developed.

4.6.1 Blast Load Scaling

Before discussing each category of computational tools in greater detail, it is necessary to first review the important concept of blast scaling. In addition to its vital role in empirical chart-based blast load characterization procedures, blast scaling can be used to predict shock wave properties from large-scale explosions based on results from experimental blast tests of much smaller scale. The cube-root scaling law, first formulated by Hopkinson [77] and independently re-derived by Cranz [78] is perhaps the most well-known and widely used blast scaling law. This law states that self-similar blast waves are produced at identical scaled distances when two explosive charges of similar geometry and of the same explosive, but of different sizes, are detonated in the same atmosphere. In employing this law, it is customary to make use of the dimensional scaled distance parameter Z as described mathematically in Equation (4-2). A graphical representation of cube-root scaling is provided in Figure 4.14.

$$Z = \lambda R = \frac{R}{W^{1/3}} \quad (4-2)$$

where:

Z = scaled standoff

λ = scale factor = $1/W^{1/3}$ (specific to “cube-root” scaling method)

W = explosive charge weight

R = physical standoff

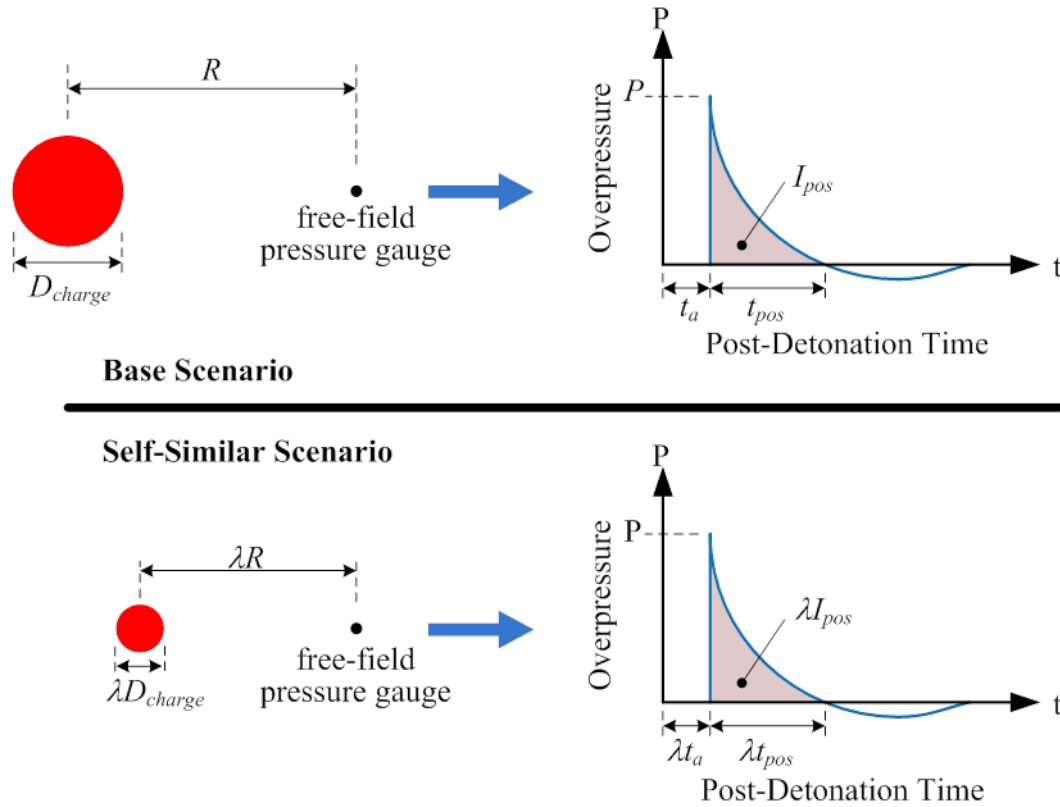


Figure 4.14 Graphical Depiction of Hopkinson-Cranz Cube-Root Blast Scaling Concept [18]

In Figure 4.14, the base scenario, comprising an explosive charge of characteristic dimension D located at a physical standoff R from a far-field pressure gauge, produces a far-field pressure-time history of peak pressure P , time of arrival t_a , positive phase duration t_{pos} , and positive phase specific impulse I_{pos} . The self-similar scenario, consisting of an explosive charge of scaled characteristic dimension λD located at a scaled standoff of λR from a far-field pressure gauge, produces a pressure-time history of similar form as that from the base scenario. The peak overpressure of the self-similar pressure-time history is identical to that of the base scenario; however, the time and impulse values are scaled. The following hypothetical situation further illustrates the concept of cube-root scaling. Consider a threat scenario involving an explosive charge of weight W_1 and physical standoff R_1 from some far-field pressure gauge that produces a measured peak overpressure of magnitude P_1 . The cube-root scaling law states that, for a second threat scenario involving identical atmospheric conditions and a similar explosive charge of weight W_2 , a measured peak overpressure of magnitude P_1 will be achieved at the same far-field pressure gauge if the charge is located at a physical standoff of R_2 as shown mathematically in Equation (4-3).

$$\frac{R_2}{R_1} = \left(\frac{W_2}{W_1} \right)^{1/3} \quad (4-3)$$

In general, for cube-root scaling, pressure and velocity quantities between two self-similar pressure-time histories remain unchanged at homologous times; whereas, time of arrival, duration, impulse, and distance quantities are scaled. The driving principle behind cube-root scaling is that the magnitudes of the various shock wave parameters are proportional to the specific energy (i.e., energy per unit volume) released during a detonation. The volume of a sphere is proportional to the cube of its radius; thus, for a shock front of spherical geometry, the scale factor contains a cube root—hence the term “cube-root scaling.” Results from past experimental blast tests have confirmed the cube-root blast scaling law for charge weights ranging from a few pounds up to several thousand pounds [72]. Because cube-root scaling is based on a spherical shock front, it should be emphasized that it is only valid for bulk explosive threat scenarios where either the point source approximation holds or a truly spherical explosive charge exists. Cube-root scaling should be employed with extreme caution when considering threat scenarios involving a close-in detonation, where the charge shape dictates the initial shock front geometry. For example, for a close-in explosive line or cylindrical charge, square-root scaling should be used because the energy will propagate with the expanding cylindrical shock front [46].

4.6.2 Empirical Methods

Kingery and Bulmash (K-B) [79] developed high-order polynomial curve fits to empirical data relating various shock wave parameters to scaled standoff for idealized spherical TNT free air bursts and hemispherical TNT surface bursts. The empirical data utilized during the least-squares polynomial curve fit analyses were compiled from various sources that included charge weights ranging from less than 2.2-lb [1-kg] to over 881,848-lb [400,000-kg]. Hopkinson-Cranz and Sachs scaling laws were employed to scale all shock wave parameters to one kilogram mass at standard atmospheric sea level conditions. Results from the curve fit analysis are shown in Figure 4.15 for the case of a spherical TNT free air burst.

The K-B graphs—often referred to as the spaghetti charts due to their highly nonlinear nature—and the empirically-based reflection coefficient graph provided in Figure 4.8 form much of the basis for what is arguably the most utilized state-of-the-practice empirical blast load characterization procedure for threat scenarios involving external detonations. The source document for this methodology currently exists as a culmination of empirically-based blast effects and structural design guidance from the U.S. Army, Navy, and Air Force. The title of the document is the Unified Facilities Criteria (UFC) 3-340-02, *Structures to Resist the Effects of Accidental Explosions* [50].

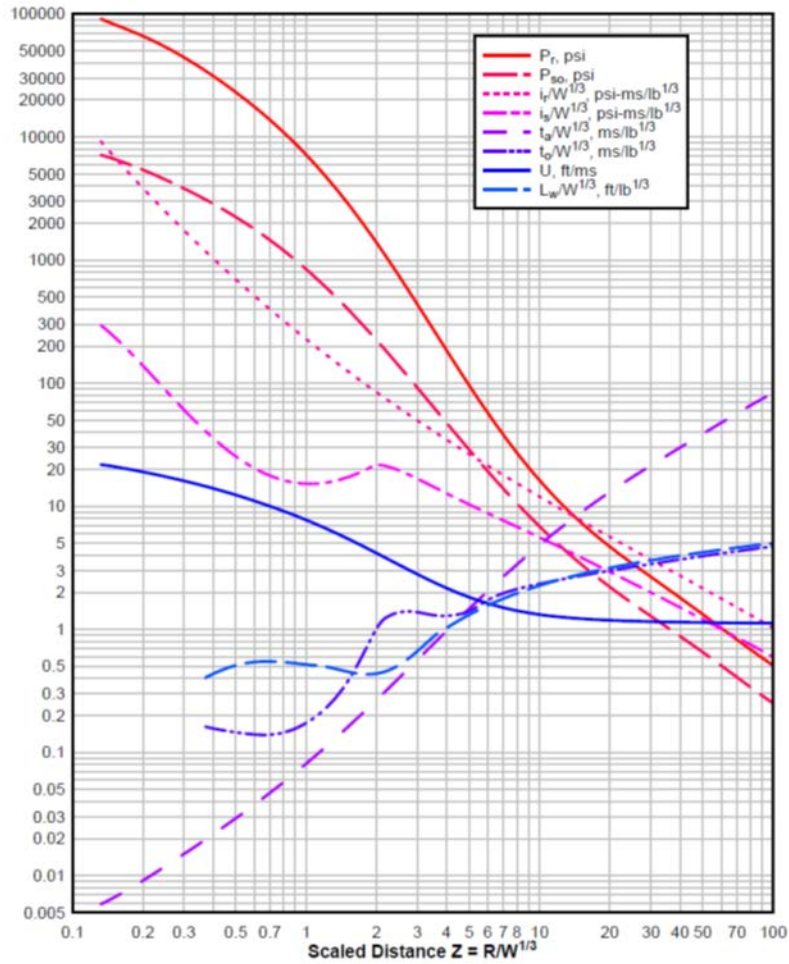


Figure 4.15 Positive Phase Shock Wave Parameters for a Spherical TNT Explosion in Free Air at Sea Level [18]

4.6.3 Ray Tracing Methods

Ray-tracing algorithms were developed to provide a more accurate representation of the airblast environment arising from complex target geometries than can be achieved by purely empirical methods. A few examples of threat scenarios warranting the use of ray-tracing algorithms include internal detonations, external detonations in urban environments, and external detonations beneath a bridge deck. Blast load characterization tools that make use of these algorithms have been primarily developed by defense-related agencies, thus many of them are restricted in use to the U.S. Government and its contractors [53]. Ray-tracing algorithms typically comprise a ray path model, a free-air explosive source model, and a shock addition model.

Ray path models subscribe to the same physical law that governs specular reflections in optics, where the angle of reflection equals the angle of incidence. Such a simplification yields a unique ray path for a given order of reflection and POI on a target surface, and it lends itself well to the use of the image source concept [80]. In applying the image source concept, the effect of a reflecting surface is represented by a second explosive source of the same yield and at the same

standoff as the original explosive source, but located on the opposite side of the reflecting surface. In other words, the reflecting surface is replaced by a symmetric image of the actual explosive source. Physical and image source representations of first-order reflection is illustrated in Figure 4.16. In Figure 4.16, the reflected airblast environment at POI 1 due to a spherical explosive source located at a standoff of R_1 and horizontal offset of X is shown. In the image source analogy, the left wall is removed from the problem and Image 1, a second spherical explosive source (i.e., an image source), is introduced at an identical standoff of R_1 and horizontal offset of X units to the left of POI 1. Free-air blast parameters at POI 1 are then independently calculated for the original and image sources using a free-air explosive source model. Finally, the uncoupled, free-air blast parameters for the two sources are combined using a nonlinear shock addition model to yield reflected blast parameters at POI 1. A first-order reflection is the most straightforward application of the image source concept; however, it can be extended to higher orders of wave reflections.

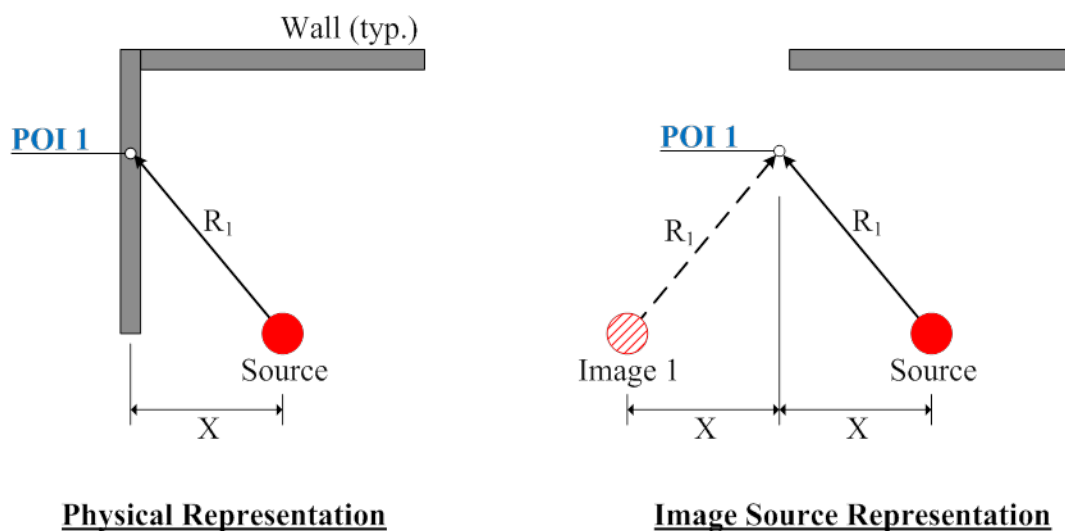


Figure 4.16 Illustration of Typical Ray Path Model Utilizing Image Source Concept for a First-Order Reflection [18]

One of the most well-known and versatile ray-tracing codes in practice is BlastX [81]. The code is owned and maintained by the U.S. Army Engineer Research and Development Center, and its use is restricted to U.S. Government agencies and its contractors. BlastX is a fast-running, engineering-level code that is capable of accurately predicting shock and gas environments resulting from internal or external detonations. The code's ray path model follows a hybrid approach, where low-order reflections are treated with a Mach reflection model and high-order reflections involving relatively low "incident" pressures are treated with image sources. BlastX contains an empirical K-B free-air explosive source model and an extensive collection of tabular source models for a wide variety of military and fertilizer-based explosive compositions. The tabular source models include spherical and hemispherical charges, cylindrical charges of various length-to-diameter ratios (either center or end-detonated), and several 3-D truck bomb configurations [81]. In addition, the code contains an empirically-based clearing model to account for the effect of rarefaction waves arising from finite reflecting surfaces as well as a shock diffraction model to predict the behavior of shock waves around convex corners [76]. Nonlinear shock addition rules are used to combine multiple shock waves at a point of interest.

Most importantly, the code has been extensively validated with experimental data gathered from live blast tests involving internal and external detonations [82]. Given its computational expedience, extensive validation, and ability to handle complex threat scenarios, BlastX was deemed well suited for inclusion in the ATP-Bridge software as its baseline blast load driver. Accordingly, part of the ATP-Bridge software development effort involved extensive collaboration with the U.S. Army Engineer Research and Development Center to devise a specially tailored dynamic link library file designed to programmatically employ BlastX to characterize blast loads on various bridge components. The ATP-Bridge blast load driver is further discussed in Chapter 12 of this manual.

4.6.4 Numerical Methods

Shock propagation through air is a challenging specialization of compressible fluid flow, and the Navier-Stokes partial differential equation (PDE) for compressible flow of Newtonian fluids provides the mathematical basis for which to describe such a phenomenon. The Navier-Stokes PDE formulation is based on the combination of the mass, momentum, and energy conservation laws with an equation of state that relates pressure, temperature, and density [83]. Fluid flow problems governed by the Navier-Stokes PDE can be reduced and solved in an approximate manner using numerical solution techniques. The family of codes utilizing this approach in Eulerian and Lagrangian mesh formulations is called computational fluid dynamics or CFD.

Blast modeling using high-fidelity CFD codes offers enhanced solution resolution relative to empirical and ray-tracing blast load characterization methods. Detailed Arbitrary Lagrangian Eulerian (ALE) simulations are able to capture diffraction and drag phenomena, clearing effects, pressure stagnation in partially vented regions of a structure, the effects of multiple reflections and gas bi-product build-up during internal detonations, as well as many other complicated aspects of shock wave behavior. Ray et al. [84] clearly demonstrated the benefits of sophisticated CFD simulations, where they utilized SHAMRC to analyze a below-deck detonation of a bulk explosive beneath a typical prestressed concrete girder bridge. The analysis was able to capture pressure stagnation near the bridge abutments as well as blast flow channeling between the girders, causing pressure “hot spots” in local regions beneath the bridge deck. While the detailed simulation provided significant insight into shock wave behavior beneath a typical girder bridge, it should be noted that the SHAMRC analysis required a Compaq SC45 super computer with multiple processors running in a parallel architecture. Sophisticated CFD simulations are computationally expensive, and they require considerable modeling expertise. As highlighted previously, the accuracy of an Eulerian or ALE simulation can be heavily influenced by the geometry and general construction of the mesh(s). In addition, careful attention must be paid to the modeling of explosive materials. An accurate CFD simulation for an explosive composition and charge shape requires input for equations of state for the reacted and unreacted phases of the explosive, input for a time-dependent detonation model such as ignition and growth, and input for an afterburn model [81]. In deciding whether to employ a high-fidelity CFD code for the purposes of blast load characterization, the availability of adequate computational resources and modeling expertise, as well as the need for exceptionally detailed load information, should be considered along with the benefits afforded by such an analysis approach.

4.7 Chapter Summary

This chapter introduced blast loads in air produced by high explosives, with an emphasis on the complexities of near-field effects on bridge structures subjected to these explosions. Methods for calculation of key blast parameters required for subsequent structural analysis has also been provided.

While this chapter focused on the type and severity of transient loads that can be delivered to bridge components from explosions, Chapter 5 is dedicated to the structural mechanics that govern the dynamic response of bridge components subjected to these transient blast loads.

5.0 MECHANICS OF STRUCTURAL ELEMENTS

Blast loaded structural components can exhibit unique modes of response that are not typically considered in conventional design. Some of these unique modes of response are a result of the high-intensity, short-duration nature of the blast load, effect of shock wave propagation within the component, the effect of high strain rates on material properties, and effects of boundary conditions for components undergoing relatively extensive plastic deformation. This chapter discusses basic concepts of the mechanics of different modes of response (e.g. spall and breach, flexure, direct shear, and membrane) for different types of structural elements.

5.1 Conventional Reinforced Concrete Elements

5.1.1 *Spall and Breach*

When a force is applied to a structural component, stress waves within the component material are generated regardless of the rate of load application. These compression and shear stress waves propagate through the component material until they encounter an interface of different density (i.e., an impedance mismatch), which could be bounding faces of the component cross-section, embedded steel reinforcing bars (in the case of reinforced concrete), a boundary condition, etc. When an interface is encountered, the stress waves undergo a reflection process. Over time, these successive stress wave reflections within the component material culminate in component-level response (e.g., flexure). In the case of a “static” load, the stress waves cease once the structural component reaches a state of static equilibrium. For structural components subject to static or low-rate dynamic loads, such as gravity and wind loads, the effects of individual stress wave transits on material-level response tend to be relatively benign and thus are almost always neglected in design. Static and low-rate dynamic loads are associated with relatively long rise times to peak magnitude and characteristic durations that are several orders of magnitude larger than individual stress wave transit times (e.g., compression wave speed within component material). Such load characteristics allow for stress and deformation fields throughout a structural component to develop in a relatively slow manner. In contrast, blast load characteristics include extremely short rise time to peak magnitude and durations on the order of milliseconds. The intense and highly transient nature of shock-induced blast loads demand an appreciation for the difference between the propagation speed of the disturbance (i.e., shock wave speed) and that of the imposed deformation (i.e., particle velocity of target material).

When a shock wave strikes a target, initial stress waves within the target material propagate at hypersonic speeds—that is, faster than the sound speed of the target material. However, the speed at which the target material deforms due to the hypersonic shock wave disturbance is slower. The difference between the shock wave speed and particle velocity of the target material can be attributed to inertial effects. Material at rest will move, but not instantly. It may need to overcome its own inertia, or it may need to wait until neighboring material move and constraints on its own motion are freed—this phenomenon was first discussed in the context of concrete inertial confinement under high strain rates in Chapter 3 of this manual. Therefore, initial hypersonic stress waves deliver peak blast pressure and impulse to loaded material faster than it can deform and distribute the effects throughout the entire structural component. As the initial stress waves encounter interfaces of differing impedance, wave reflections and refractions occur, resulting in energy dissipation and decreasing wave speed until the sound speed of the material is eventually reached. These early-time individual wave transit effects can cause severe localized

material damage that may, in turn, influence ensuing component-level response and/or reduce the component's capacity to resist residual loads.

Past experimental research has been conducted to provide further insight into the early-time material behavior of blast-loaded structural components. For example, Marchand and Plenge (1998) [85] utilized experimental results from blast tests of reinforced concrete panels having symmetrical reinforcing steel layouts and varying concrete thicknesses to develop empirical expressions for the prediction of local concrete spall and breach damage. Panel specimens, having large in-plane dimensions relative to their thickness dimension, provide useful target geometry for studying the effects of individual wave transits on early-time material response. Because the wave transit time from the center of the panel's front face to a lateral bounding surface is much greater than that from the center of the panel's front face to its back face (i.e., through-thickness direction), the panel geometry essentially mimics an early-time state of uniaxial strain. Such a strain state distills out most of the complex multi-dimensional wave propagation effects and allows for a clear distinction among local spall, crater, and breach damage. Local spall damage can be described as tensile-stress-induced concrete failure precipitated by wave reflections off non-incident bounding surfaces of the concrete section. When a shock wave strikes an RC panel, a compressive body wave propagates through the thickness of the panel and reflects off its back face. To satisfy equilibrium and kinematic compatibility requirements at the back face, the reflected wave must be tensile in nature. If the tensile stress at the back face of the specimen exceeds the dynamic tensile strength of the concrete, then it fails and spalls off. Local cratering on the blast face occurs when an impinging shock front induces incident-face compressive stresses more than the concrete's dynamic compressive strength, causing the concrete to crush. Complete section breach occurs if the local zones of spall and crater damage overlap within the concrete section. Figure 5.1 provides post-test pictures from a sample of the specimens comprising Marchand and Plenges' experimental database. Figure 5.1a shows a specimen that exhibited back-face spall damage while sustaining no front-face damage. Figure 5.1b shows a specimen that sustained front-face cratering and back-face spall damage, and Figure 5.1c illustrates a complete section breach.

UFC 3-340-02 [50] provides empirical threshold spall and breach curves that can be used to predict concrete spalling or breaching based on the charge weight (cased or bare), standoff, concrete thickness and concrete dynamic compressive strength. These curves are based on many spall tests, including the test program referenced above.

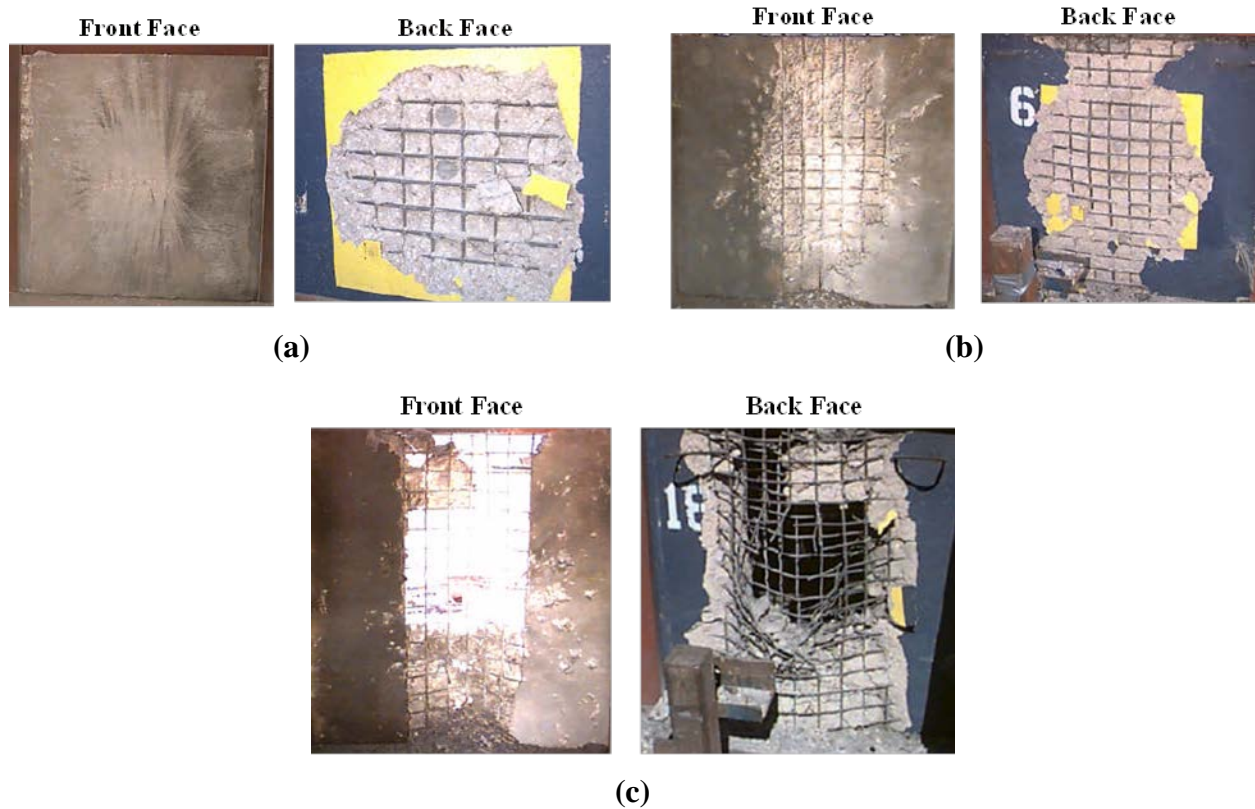


Figure 5.1 Spall and Breach Behavior of Blast-Loaded RC Panels (adapted from [85]): (a) Spall Damage, (b) Crater and Spall Damage, (c) Section Breach

5.1.2 Direct Shear Response

Direct shear response is unique to rapidly loaded structural members and can be characterized by extensive shear deformation that initiates early in time at discrete slip planes near support locations or concentrated loads and is accompanied by little to no curvature along the length of the loaded member. In addition, the discrete slip planes tend to be oriented parallel to the direction of loading and can ultimately lead to brittle localized failure very early in the response of a loaded structural member. A description of this response mode is given by Krauthammer (2008) [46] as: *“For instance, when a slab is supported on walls, supported areas of the slab are restricted from moving with the severe load, while the unsupported areas will be accelerated in the load direction. This very quick relative motion between the supported and unsupported parts of the slab will induce a sharp stress discontinuity at the slab–wall interfaces that can fail the slab along vertical failure planes.”*

As part of an extensive research effort to develop a better understanding of direct shear behavior, Sammarco (2014) [18] devised a hypothetical reinforced concrete (RC) column having typical section and material properties and computationally subjected it to two different blast loads. Both blast loads were taken to be spatially uniform along the column height, but they exhibited different temporal characteristics. As shown in the top of Figure 5.2, the Case A blast pulse was right-triangular in shape with a peak pressure of 100-psi, a specific impulse of 4,200 psi-msec, and a pulse duration of 84-msec. The Case B blast pulse was also right-triangular in shape, but the peak pressure and pulse duration were modified to 3,000-psi and 2.8-msec, respectively, to

deliver a larger peak pressure while still maintaining a specific impulse of 4,200 psi-msec. RC column damage contours at incipient failure for both blast load cases are presented in the bottom of Figure 5.2. In reviewing Figure 5.2, the two different blast loads promoted significantly different modes of structural response. The Case A simulation involved typical flexural response, which is evidenced by the mid-span flexural cracks and concrete compression damage accompanied by diagonal shear cracks near the supports. The Case A simulation ultimately resulted in a flexural-shear failure accompanied by significant curvature along the length of the RC column. Failure initiated at an approximate post-detonation time of 10-msec. In the context of this manual, the term *flexural-shear failure*—often referred to as beam shear failure or diagonal tension failure—represents the traditional mode of shear failure exhibited by flexural members loaded “statically.” Flexural-shear failure involves shear forces derived from the change in moment along the length of the flexural member, and it is typically associated with inclined concrete cracks due to dominating principal tensile stresses.

The Case B simulation resulted in a noticeably different structural response mode and subsequent component failure. In Figure 5.2, the Case B damage contours reveal highly localized material damage near the supports and little to no curvature along the length of the RC column. Back-face spall damage can also be observed due to exceedingly high early-time tensile stresses derived from back-face shock wave reflections. In addition, horizontally oriented (i.e., parallel to blast load direction), discrete slip planes formed near the RC column supports. Ultimately, a direct shear failure was observed at an approximate post-detonation time of 0.57-msec. Examination of stress component histories at the locations of the direct shear failure also revealed that, unlike the Case A flexural-shear response that was governed by principal tensile stress, the Case B early-time direct shear response was governed by the maximum shear stress component.

As part of this study, Sammarco also investigated the hypothetical RC column scenario from modal and frequency domain perspectives. Overall conclusions from this research effort were as follows:

- Direct shear behavior is not related to (and precedes) flexural behavior
- Early-time shear dominance always occurs due to a high-frequency, multi-modal phenomenon; however, whether it results in a direct shear failure depends on the direct shear capacity of the structural component and the high-frequency energy content of the blast pulse
- All other things being equal, the likelihood of direct shear failure increases with increasing peak blast pressure and decreasing pulse duration; both of which increase high-frequency energy content

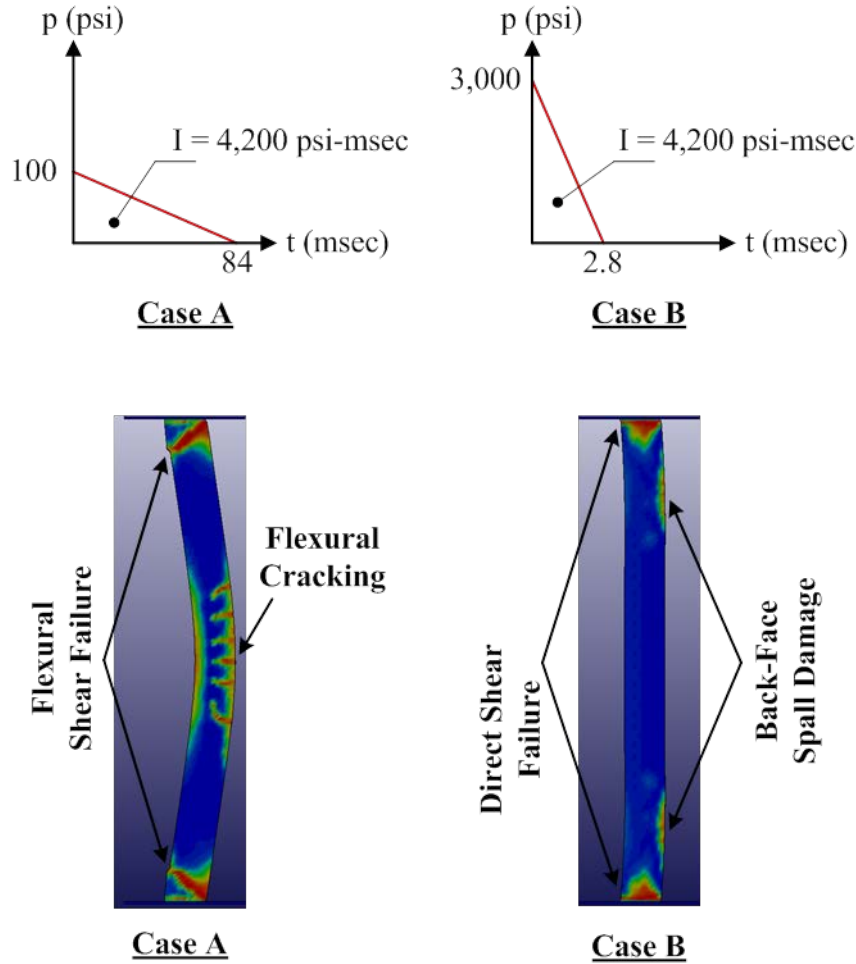


Figure 5.2 Blast Pulse Definitions and Damage Contour Plots at Incipient Failure for Case A and Case B Finite Element Simulations [18]

For design, direct shear failure is prevented by ensuring an RC component possesses adequate direct shear strength through a combination of concrete shear friction and dowel action provided by steel reinforcing bars that cross the potential direct shear slip planes—often termed *shear friction reinforcement*. The direct shear capacity for a monolithic concrete joint can be calculated as shown in Equation (5-1) from PDC-TR 06-01 [86].

$$V_{dc} = 0.16 f'_{dc} d \quad (5-1)$$

where:

V_{dc} = concrete dynamic direct shear capacity (per unit width)

f'_{dc} = concrete dynamic compressive strength (see Chapter 3)

d = effective depth (distance from extreme compression fiber to centroid of tension reinforcement)

If the concrete dynamic direct shear capacity is insufficient, or when the section is in axial tension, shear friction reinforcement is required such that the combined direct shear capacity of concrete and shear reinforcement is larger than the direct shear demand. The direct shear strength at the support when the concrete strength is combined with direct shear strength provided by reinforcing steel across the joint is given by Equation (5-2) from PDC-TR 06-01 [86]. The direct shear capacity of concrete with shear friction reinforcement depends on the type of joint between the component and the support, as indicated in Table 5.1. The shear friction reinforcement area is perpendicular to the failure plane for direct shear shown in Figure 5.3. Since direct shear occurs before significant flexural response, UFC 3-340-01 [48] allows all reinforcement crossing the direct shear crack plane to be included as shear friction reinforcement except bars resisting net tension in the component. This includes flexural bars that are developed past the support. Usually the flexural steel and concrete provide sufficient direct shear resistance. In the cases where they do not, diagonal bars may also be used as shown in Figure 5.3, where only the area of these bars acting parallel to the span (i.e. perpendicular to the direct shear failure plane) is included as A_{vf} in Equation (5-2).

$$V_{dc} = K_1 f'_{dc} d + K_2 (N_c + A_{vf} f_{dy}) \leq K_3 f'_{dc} d \quad (5-2)$$

where:

N_c = applied static axial load force per unit width (positive for compression, negative for tension)

A_{vf} = area of shear friction reinforcement per unit width

f_{dy} = dynamic yield strength (see Chapter 3)

K_i = see Table 5.1

See Equation (5-1) for definition of other terms.

Table 5.1 Values for constants in Equation (5-2) (adapted from PDC-TR 06-01 [86])

Case	K ₁	K ₂	K ₃
Monolithic concrete at joint	0.14	1.2	0.6
Cleaned and roughened joint (to 5mm)	0.12	1.1	0.6
Cleaned unroughened joint	0	1.0	0.4

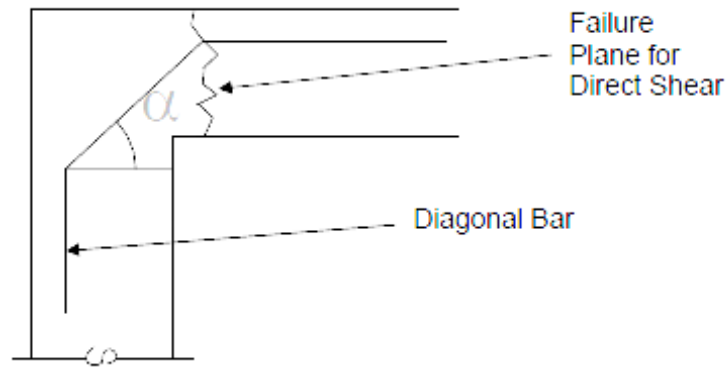


Figure 5.3 RC Cross-Section Showing Diagonal Rebar Resisting Direct Shear [86]

5.1.3 Flexural Response

Most reinforced concrete components subject to far-range blast loading respond primarily in a flexural response mode. A blast loaded component responding in flexural response mode will initially develop resistance that increases approximately linearly with the deflection, until yielding of reinforcement or concrete crushing (depending on the steel reinforcement ratio) initiates at localized regions of the component. The resistance is typically assumed to have the same spatial distribution (e.g., uniformly distributed or concentrated) as the blast load. The yielding regions within a blast-loaded component are known as plastic hinge regions. Once one or more plastic hinge regions develop in the component, depending on the boundary conditions, the resistance reaches the ultimate flexural resistance value and it becomes approximately constant with increasing deflection. For a statically determinate component (e.g. simply supported or cantilever beam or one-way slab), the ultimate flexural resistance is reached at the formation of a single plastic hinge region. For a statically indeterminate component (e.g. simple-fixed or fixed-fixed beam or slab), the ultimate flexural resistance will occur when two or more plastic hinge regions develop in the component.

Reinforced concrete components with relatively high reinforcement ratio may develop concrete crushing at the plastic hinge regions at a deflection corresponding to approximately 2 degrees of support rotation (at a mid-span deflection of approximately $L/60$). For singly reinforced components with high tensile reinforcement ratio, this may result in a sudden significant reduction of the resistance or component failure. However, for components with equal amounts of compression and tension reinforcement, and sufficient confinement provided by shear reinforcement (stirrups), the resistance can continue beyond 2 degrees support rotation with no or slight loss of capacity by transferring of the flexural compressive force to the compression reinforcement. Depending on the type and amount of shear reinforcement (stirrups) and steel reinforcement ratio, reinforced concrete components may not lose their structural integrity until reaching support rotations between 6 and 12 degrees [50].

The value of the ultimate flexural resistance is a function of the ultimate dynamic moment capacity of the component at the location of the plastic hinges. For purposes of simplified blast analysis or design, the ultimate dynamic moment capacity of reinforced concrete component can be calculated using equations from conventional design code provisions with dynamic material strength properties for the concrete and reinforcing steel (including strain rate effects – as

discussed in Chapter 3) in lieu of static strength values. The ultimate dynamic moment capacity of a reinforced concrete beam or slab can be calculated as shown in Equation (5-3). As discussed in the above paragraph, when the support rotation exceeds 2 degrees, crushing of the compression face concrete can occur and the compressive force in the section must be carried by the compression face reinforcement. The moment capacity at this stage can be calculated based on a moment arm equal to the distance between the compression and tension steel and the lesser of the steel areas at each face as shown in Equation (5-4).

$$M_{du} = A_s f_{dy} \left(d - \frac{A_s f_{dy}}{1.7 f'_{dc}} \right) \quad (5-3)$$

where:

M_{du} = ultimate dynamic moment capacity per unit width

A_s = area of tension steel reinforcement per unit width

f_{dy} = dynamic yield strength (see Chapter 3)

f'_{dc} = concrete dynamic compressive strength (see Chapter 3)

d = effective depth (distance from extreme compression fiber to centroid tension reinforcement)

$$M'_{du} = A'_s f_{dy} d_c \quad (5-4)$$

where:

M'_{du} = ultimate dynamic moment capacity per unit width for crushed concrete section

A'_s = lesser of the top or bottom face reinforcing steel area per unit width

f_{dy} = dynamic yield strength (see Chapter 3)

d_c = distance between top and bottom steel reinforcement

For more refined analysis and high-fidelity models, the moment capacities are usually calculated using fiber-section models where the bending moment in the section is calculated by integration of the stress in each fiber, which follows material stress-strain constitutive models for concrete and steel reinforcement. Procedures and equations to determine the flexural stiffness, ultimate dynamic moment capacity and flexural resistance for different types of reinforced concrete components are well established and provided in several references [50, 53, 86].

To develop flexural resistance, the component must be able to develop sufficient shear capacity. The internal shear forces that develop through the component during the dynamic response correspond to the internal shear forces that result from the flexural resistance at a given

deflection applied to the component as a static load. The shear force and reactions at supports that result from the flexural resistance applied to the component as a static load are referred to as equivalent static shear force and equivalent static reactions, respectively. Due to the brittle nature of shear failure, blast loaded components should always be designed such that the shear capacity at any location of the component is always larger than the equivalent static shear force based on the ultimate flexural resistance. Similarly, connections and supports must also be designed with a capacity larger than the equivalent static reactions.

Shear capacity is typically evaluated at “critical sections” or sections of maximum shear (usually near the supports) for each type of components (e.g. beams, slabs), based on conventional static design code provisions. The location of the critical section also depends on the type of loading and whether the component induces compression or tension at the supports. For instance, the critical section for a uniformly loaded beam, when the supports are put in compression, is located at a distance d from the face of the support. When the supports are put in tension, the critical section is at the face of the supports.

The shear capacity can be provided by a combination of concrete diagonal shear capacity and shear reinforcement. Like the ultimate dynamic moment capacity, the dynamic diagonal shear capacity provided by concrete and shear reinforcement can be calculated using equations from conventional design code provisions with dynamic material strength properties for the concrete and reinforcing steel (including strain rate effects – as discussed in Chapter 3). The dynamic shear strength of concrete beams or slabs subject to shear and flexure without significant axial load can be calculated as shown in Equation (5-5). Similar equations for circular sections (e.g. columns) can be used in the same manner. The dynamic increase factor or DIF (see Chapter 3) for the concrete compressive strength in Equation (5-5) should be based on the effect of strain rate on the concrete splitting tension. The DIF for concrete splitting tension is very sensitive to strain rate and can increase significantly at high strain rates. However, for simplicity, the DIF for concrete in compression is typically used in Equation (5-5) in lieu of the DIF for splitting tension for blast design purposes.

$$V_c = K_u \sqrt{f'_{dc}} d \quad (5-5)$$

where:

V_c = concrete dynamic diagonal shear strength per unit width (for flexure without axial load)

f'_{dc} = concrete dynamic compressive strength (see Chapter 3) (MPa or psi)

d = effective depth of flexural reinforcing steel

K_u = constant depending on units
= 2 (English) or 0.167 (Metric)

When the equivalent static shear force exceeds the diagonal shear capacity of concrete, the additional shear capacity is provided by shear reinforcement. The shear capacity provided by the typical case of shear reinforcement perpendicular to the span direction can be calculated as

shown in Equation (5-6). The shear reinforcement included in the calculation of shear capacity must be closed tie stirrups for beams and columns or single leg stirrups for slabs. Interior single leg stirrups can also be used in beams if additional shear reinforcement is needed. Closed ties must be closed with 135° bends. Single leg stirrups must enclose the tension steel bars with a 135° bend and the compression steel bars with a 90-deg bend, as a minimum. For shear reinforcement to be effective, the maximum stirrup spacing s along the span must be such that each 45° crack will be intercepted by at least one stirrup.

$$V_s = \frac{A_v}{s} f_{dy} d \quad (5-6)$$

where:

V_s = shear force capacity per unit width provided by shear reinforcement

A_v = total area of stirrups within the stirrup spacing s

s = stirrups spacing in the direction parallel to the longitudinal reinforcement ($d/2$ maximum)

f_{dy} = dynamic yield strength (see Chapter 3)

d = effective depth of flexural reinforcing steel

5.1.4 Tension Membrane Response

Tension membrane (catenary) response can occur in reinforced concrete components at relatively large transverse deflections when the supports can provide in-plane restraint and can resist the in-plane and transverse forces induced by tension membrane action. The in-plane restraint at the supports causes tension force in the component as transverse deflection increases. If the in-plane restraint at the supports is rigid, tension membrane can develop early in the response. However, the in-plane restraint is usually not fully rigid and the resistance provided by tension membrane at small transverse deflections is relatively low compared to the resistance provided by flexural response. However, at relatively large transverse deflections, tension membrane response can provide significant transverse load resistance. Figure 5.4 illustrates an idealized resistance-deflection curve for a hypothetical fixed-fixed flexural member with tension membrane response. Analytical methods to determine the tension membrane resistance-deflection curve for single-degree-of-freedom (SDOF) analysis of reinforced concrete components can be found in UFC 3-340-02 [50] and PDC-TR 06-01 [86].

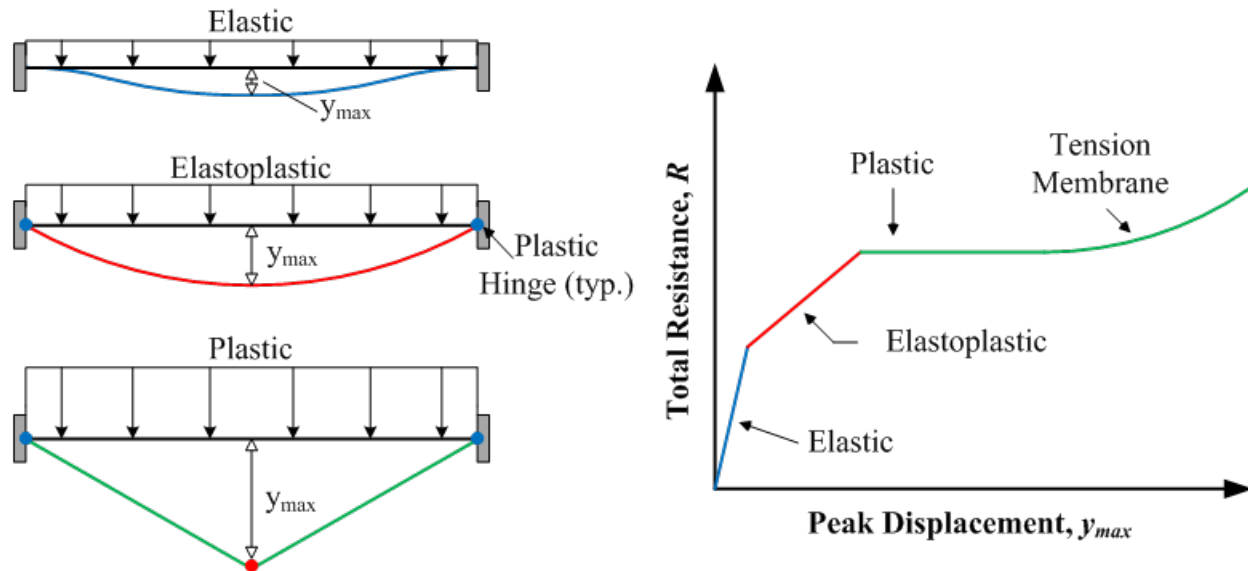


Figure 5.4 Idealized Resistance-Deflection Curve for Fixed-Fixed Flexural Member Exhibiting Tension Membrane Action [18]

The maximum resistance that can be provided by tension membrane is limited by the capacity of the supports to resist the large in-plane forces in the structural component and by the in-plane tension capacity of the structural element. The in-plane tension forces in reinforced concrete components are resisted by the longitudinal steel reinforcement. Therefore, to develop tension membrane action, the longitudinal steel reinforcement must be continuous and have proper anchorage into the supports. Splices and anchorage must be properly designed and detailed to be able to develop the tensile strength of the longitudinal reinforcement.

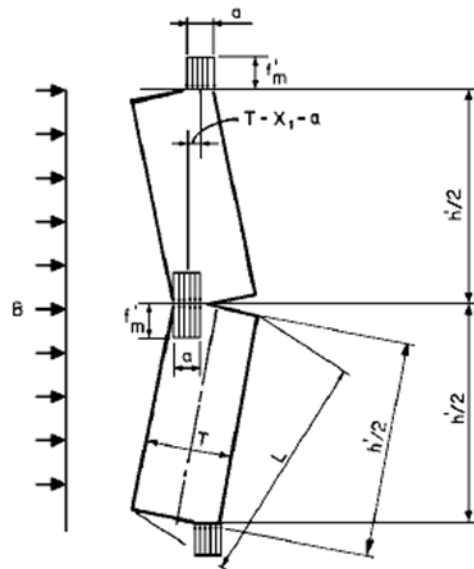
Two-way slabs supported on four edges, and with aspect ratio between 0.5 and 2, may not require external in-plane restraint at the supports to develop resistance through tension membrane action. This type of component can develop a “compression ring” around its boundary that may provide sufficient in-plane restraint to develop tension membrane resistance [50].

5.1.5 Compression Membrane Response

Compression membrane response can occur in reinforced concrete components with rigid supports at both ends of the span. Compression membrane can cause an increased ultimate resistance above the ultimate flexural resistance. Compression membrane response occurs at relatively low deflections, which are less than the component thickness.

The supports must provide in-plane restraint to outward movement such that rotation of the component cross section at the supports generates compressive bearing stresses between the rigid boundary and the unloaded face of the component. These in-plane bearing forces at the supports form resisting couples with the bearing forces from the compression block at the loaded face of the component at the plastic hinge region near mid-span. As deflection increases, crushing of concrete occurs at these locations. The forces developed during compression membrane response are illustrated in Figure 5.5 [86]. These force couples shown in Figure 5.5 provide resistance to lateral load in addition to resistance from flexural response. The maximum compression forces that can develop are limited by the crushing strength of the concrete component and the

boundary elements. While the crushing area (and compression membrane force) increases as deflection increases, the moment arm (distance between the lines of action of the compression forces) decreases as deflection increases. The moment arm (and the resisting force couple) decreases to zero at a deflection approximately equal to the component thickness, when the compression membrane forces at the supports and mid-span become aligned.



*Resisting moment = $f'_m a(T - x_1 - a)$, where x_1 = midspan deflection
 f'_m represents material crushing strength*

Figure 5.5 Forces Developing During Compression Membrane Response [86]

Significant compression membrane resistance typically develops in relatively thick components. In addition, compression membrane is very sensitive to support flexibility (i.e. much more so than tension membrane) [86] and therefore it can only develop in components with relatively rigid supports. Analytical methods to determine the compression membrane resistance-deflection curve for SDOF analysis of reinforced concrete components can be found in UFC 3-340-02 [50] and PDC-TR 06-01 [86].

5.2 Prestressed and High-Performance Concrete Elements

5.2.1 Prestressed Concrete

Typical prestressing steel strands used in precast concrete members are Grade 250 or Grade 270, which have a minimum specified ultimate tensile strength, f_{pu} , of 250-ksi or 270-ksi, respectively. This type of high-strength steel does not exhibit a well-defined yield point and, instead, exhibits a gradual continuous yielding with a curved stress-strain relationship until the ultimate strength is reached [50]. ASTM specifies the yield stress f_{py} as the stress at 1-percent elongation, which ranges between 80 to 90 percent of the ultimate strength, f_{pu} . The ultimate dynamic moment capacity of prestressed concrete components is calculated based on an *effective strength* (or *average stress*) of the prestressing steel, f_{ps} , as shown in Equation (5-7) from UFC 3-340-02 [50].

$$M_{du} = A_{ps}f_{ps}\left(d_p - \frac{a}{2}\right) + A_s f_{dy}\left(d - \frac{a}{2}\right)$$

$$a = \frac{(A_{ps}f_{ps} + A_s f_{dy})}{0.85f'_c b}$$
(5-7)

where:

M_{du} = ultimate dynamic moment capacity

A_{ps} = area of prestressed reinforcement

A_s = area of conventional (non-prestressed) reinforcement

f_{ps} = average stress in the prestressed reinforcement at ultimate load

d_p = distance from extreme compression fiber to centroid of prestressed reinforcement

[other parameters as defined in Equations (5-3) and (5-4)]

Equation (5-7) is applicable for rectangular prestressed cross sections or a flanged section where the thickness of the compression flange is greater than or equal to the depth of the equivalent rectangular stress block. The most accurate way to determine the prestressed reinforcement average stress at ultimate load, f_{ps} , in Equation (5-7) is by trial-and-error stress-strain compatibility analysis. In lieu of such a detailed analysis, UFC 3-340-02 [50] provides simplified design equations for the calculation of f_{ps} for members with bonded and unbonded prestressing tendons.

Prestressed member usually remain almost entirely in compression under conventional service loads. Therefore, for conventional design, design code provisions generally allow higher concrete shear stresses for prestressed concrete members than for conventional reinforced concrete elements. However, for blast loading, the effect of prestressing is essentially lost at ultimate loads. Therefore, for purposes of blast design, concrete shear strength of prestressed members is typically calculated in the same manner as conventional reinforced concrete [50, 86].

5.2.2 High-Performance Concrete

In general, the term *high-performance concrete* (HPC) has taken on multiple different definitions within the structural engineering community. For instance, the Federal Highway Administration defines HPC as “concrete that has been designed to be more durable and, if necessary, stronger than conventional concrete.” And, the American Concrete Institute defines HPC as “concrete meeting special combinations of performance and uniformity requirements that cannot always be achieved routinely using conventional constituents and normal mixing, placing, and curing practices.” Regardless of the formal definition, HPC is typically utilized in industry when optimized performance characteristics, such as high workability, high fluidity, minimum or negligible permeability, and enhanced durability, are required.

Strictly speaking, HPC can either be normal-strength or high-strength in nature. Though, high-strength concrete is often (perhaps wrongly) classified as high-performance concrete due solely to its enhanced strength characteristics. The classification of a concrete as normal-strength or high-strength is somewhat subjective. The American Concrete Institute has attempted to rid this subjectivity by putting forth the definition of normal-strength concrete as any concrete that has a cylinder compressive strength not exceeding 6,000-psi, and concretes with cylinder compressive strengths more than 6,000-psi are considered high-strength. High-strength concrete applications—it's common to see concrete compressive strengths about 20,000-psi and higher—are increasing, especially with high-rise building structures and long-span bridges. Primary advantages of using high-strength, high-performance concrete include, but are not limited to, reduction in member sizes leading to reduced self-weight and superimposed dead loads, longer bridge spans with fewer beams, reduction in the number of supports and supporting foundations due to span increases, superior long-term service performance and durability, reduction in creep and shrinkage, and reduction in maintenance and repair costs. The mechanics of structural elements comprised of HPC are largely identical to those comprised of conventional concrete. Additionally, from a protective design perspective, the high-strength characteristic is of prime interest. Accordingly, the remainder of this section focuses specifically on important material-level aspects of high-strength concrete. For additional information on high-strength concrete beyond what is presented herein, the interested reader is encouraged to review ACI 363R-10 *Report on High-Strength Concrete* [87] developed by American Concrete Institute Technical Committee 363 on high-strength concrete.

Figure 5.6 shows unconfined compressive stress-strain responses of various concretes having different ultimate compressive strengths. Three noteworthy trends can be observed: 1) the elastic modulus (i.e., initial slope of stress-strain curve) increases with increased compressive strength, 2) the compressive strain at ultimate strength increases slightly with increased compressive strength, and 3) the ultimate compressive strain at failure (i.e., material-level ductility) decreases with increased compressive strength. For normal-weight concrete (unit weight of approximately 145-lb/ft³) with a static unconfined compressive strength in the range of 6,000- to 12,000-psi, elastic modulus and modulus of rupture can be approximated with Equation (5-8) and Equation (5-9), respectively [88]. For higher-strength concrete (> 12,000-psi), laboratory testing should be performed to ascertain these material parameters directly.

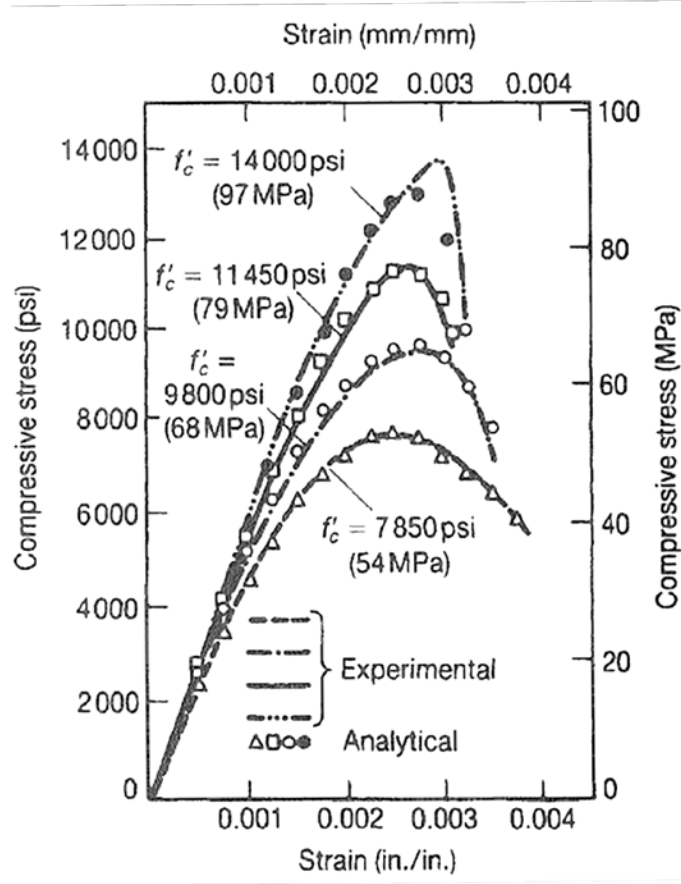


Figure 5.6 Unconfined Compressive Stress-Strain Relationship of Concretes having Different Strengths [88]

$$E_c = \left(40,000\sqrt{f'_c} + 1.0 \times 10^6 \right) \left(\frac{w_c}{145} \right)^{1.5} \quad (5-8)$$

$$f_r = 11.7\sqrt{f'_c} \quad (5-9)$$

where:

f'_c = static unconfined compressive strength [psi]

w_c = unit weight of concrete [lb/ft³]

E_c = elastic modulus [psi]

f_r = modulus of rupture [psi]

The reduction in ductility with increased compressive strength is of concern for protective design applications, as the ability maintain load-carrying capacity under large inelastic deformations is critical for extreme loading situations. Material-level ductility of high-strength concrete can be enhanced in two primary ways: by providing confinement or introducing steel or synthetic fibers to the concrete matrix. The beneficial effects of providing confinement to concrete is well-known, often implemented in practice for even normal-strength concrete, and is illustrated in Figure 5.7. An increase in ductility due to confinement is the result of the triaxial state of stress, which can raise the axial compressive stress by one or more orders of magnitude, depending on the magnitude of lateral confining stress [88]. Passive confinement is typically provided in reinforced concrete members using steel spiral reinforcement or rectangular ties. The presence of the spiral or tie reinforcement acts to enclose the main longitudinal reinforcement to form with the enclosed core a confined concrete area subjected to triaxial stress. Spiral reinforcement has shown to be more effective in confining the core concrete than closed tie reinforcement; nonetheless, they both result in increased material-level ductility. Given the exceptional brittleness of high-strength concrete as illustrated in Figure 5.6, the need to consider confinement reinforcement during structural design becomes critically important. The use of steel or synthetic fibers in the concrete matrix is a second viable option for increasing material-level ductility in high-strength concretes, and this option is discussed in Section 5.2.3.

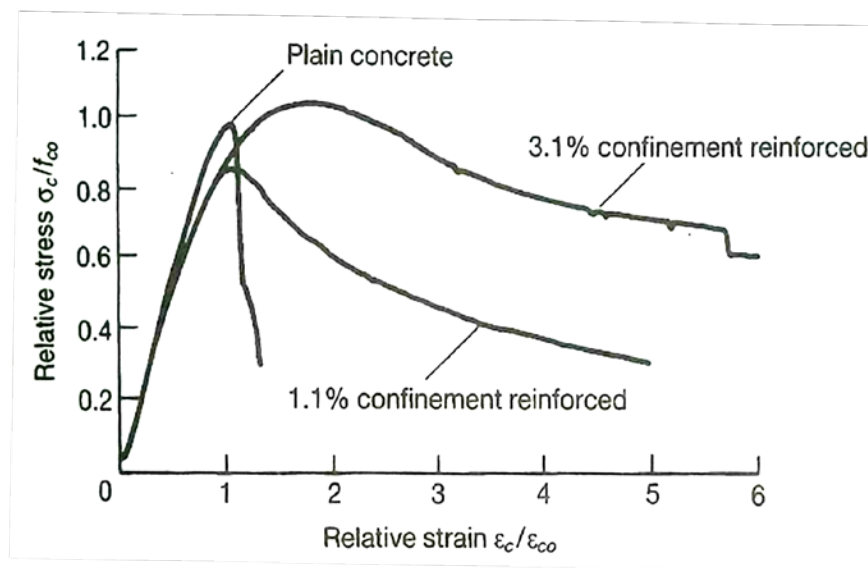


Figure 5.7 Illustrating Confinement Effect on Ductility of High-Strength Concrete [88]

Also of incredible importance in the context of protective design for extreme loading is the effect of load rate on the behavior of high-strength concrete. It was shown in Chapter 3 of this manual that high strain rates in many different construction materials (including concrete) can result in temporary strength gains that should be accounted for when designing for blast effects.

Unfortunately, relatively little information exists in the open literature on high-rate dynamic behavior of high-performance/high-strength concretes. At the time this publication was written, the U.S. Army Engineer Research and Development Center was in the final stages of finishing the draft report *Material Specifications for Attack Countermeasures on Bridges: Advanced Cementitious Materials for Blast Protection* [89] for the Federal Highway Administration. A primary objective of this report was to compile existing dynamic property data, including

compressive strength, tensile strength, elastic modulus, and energy absorption, for six proprietary and research HPCs. Specifically, the report addresses Lafarge's Ductal® products, Densit ApS products, The University of Kassel's B4Q/B5Q mixes, Ultra-HPC-based composites developed at Nanjing University and Southeast University, and multi-scale fiber-reinforced concrete technology developed by the Laboratoire Central des Ponts et Chaussées in Paris, France. Once the final version of this report is generated and made available, it will be the best-known reference for determining dynamic properties of high-strength concretes.

5.2.3 Fiber-Reinforced Concrete

As was mentioned in the previous section, the addition of small fibers in high-performance/high-strength concretes is often done to increase the ductility and overall energy absorbing capacity of the concrete. The addition of small, randomly distributed, discontinuous fibers in concrete significantly aids in arresting the development and propagation of micro-cracks that develop in the concrete matrix upon load application. There exist a variety of commercially available fibers, such as those made from steel, graphite, polypropylene, or glass. Only steel fibers will be specifically addressed herein. It should also be emphasized that fibers should be used in addition to and not in lieu of conventional steel reinforcement.

From a mixing and placing perspective, working with fiber-reinforced concrete can be a bit more difficult than concrete without fibers. Steel fiber contents more than about 2-percent by volume can create difficulties in producing a uniform mix. In addition, it is recommended that maximum aggregate size be limited to 3/8-in. During concrete placing, fibrous concrete often requires more extensive vibrating than nonfibrous concrete. Additional guidance for specifying, proportioning, mixing, placing, and finishing fibrous concrete can be found in ACI Report 544.3R [90].

Per Nawy [88], the following main factors influence the mechanical properties of fiber-reinforced concrete:

- 1) Type of fiber (i.e., the fiber material and its shape)
- 2) Fiber aspect ratio, l/d_f (i.e., the ratio of fiber length-to-diameter)
- 3) Amount of fiber provided in the concrete mix as percentage of total volume
- 4) Fiber spacing
- 5) Concrete Strength
- 6) Size, shape, and preparation of the structural member

The fiber length itself is an important characteristic, as there exists a "critical length" below which a pull-out limit state of the fiber governs and above which a more desirable ductile yield-to-fracture failure sequence of the fiber governs. The influence of fiber volume fraction on the compressive stress-strain response of concrete having a strength of 9,000-psi and a constant fiber length-to-diameter ratio is illustrated in Figure 5.8. Note that the presence of the fibers has little to no influence on the concrete compressive strength but shows significant influence on the post-peak response of the concrete. The increase in ultimate compressive strain and the decrease in slope of the post-peak portion of the curves shown in Figure 5.8 result in increased ductility and energy absorbing capacity of the concrete. Similar trends can be observed in Figure 5.9 for a constant fiber volume fraction and variable fiber length-to-diameter ratio, except the increase in

the latter shows a slight influence (an increase) in compressive strength. The positive effects of fiber-reinforced concrete are all beneficial from a protective design perspective. An increase in material-level ductility and energy absorbing capacity both translate to increased resistance to impact damage (e.g., [91]), as well as blast-induced damage (e.g., [92]).

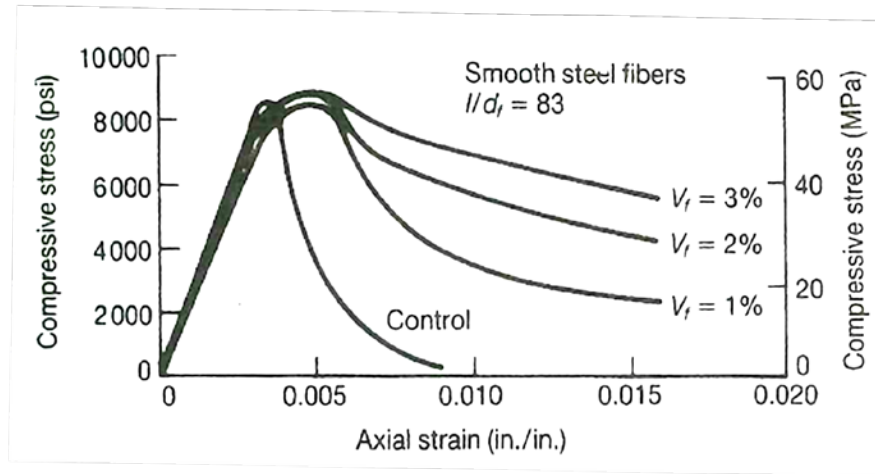


Figure 5.8 Influence of Steel Fiber Volume Fraction on Stress-Strain Behavior of Concrete having 9,000-psi Compressive Strength [88]

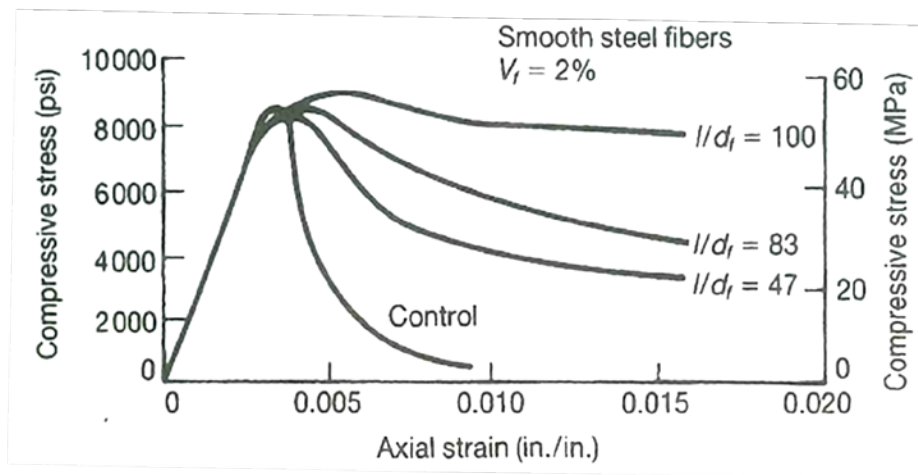


Figure 5.9 Influence of Steel Fiber Aspect Ratio on Stress-Strain Behavior of Concrete having 9,000-psi Compressive Strength [88]

From a structural mechanics perspective, flexural and shear stress calculations for fiber-reinforced concrete differ from those typically used for conventional reinforced concrete due to the presence of the discrete, randomly placed fibers throughout the concrete. For instance, ACI Committee 544 on steel fiber-reinforced concrete [90] derived equations for peak bending stress at first cracking and at ultimate strength for concrete flexural members having only fiber reinforcement (i.e., no rebar), which are provided in Equation (5-10) and Equation (5-11), respectively. ACI Committee 544 [90] also put forth Equation (5-12) for the average sectional shear strength of a concrete flexural member reinforced with steel fibers and without steel rebar.

$$\sigma_f = 0.843 f_r V_m + 425 V_f \frac{l}{d_f} \quad (5-10)$$

$$\sigma_{cu} = 0.97 f_r V_m + 494 V_f \frac{l}{d_f} \quad (5-11)$$

$$v_{cf} = \frac{2}{3} f_t' \left(\frac{d}{a} \right)^{1/4} \quad (5-12)$$

where:

f_r = plane concrete modulus of rupture [psi]

V_m = volume fraction of concrete = $1 - V_f$

V_f = volume fraction of fibers = $1 - V_m$

l/d_f = length-to-diameter ratio of fibers

σ_f = peak bending stress at first cracking of fibrous concrete flexural element [psi]

σ_{cu} = peak bending stress at ultimate strength of fibrous concrete flexural element [psi]

f_t' = tensile splitting strength of plane concrete [psi]

d = effective depth of section [in.]

a = shear span = distance from the point of concentrated load application to the face of the support, or the clear span of the flexural member in the case of a distributed load [in.]

v_{cf} = average shear strength of steel fiber-reinforced concrete flexural member with no rebar [psi]

When a fiber-reinforced concrete flexural member is also reinforced with conventional steel reinforcement, the flexural capacity of such a section must be calculated differently than is done for nonfibrous reinforced concrete flexural members, too. Figure 5.10 shows a rectangular, singly reinforced fibrous concrete section with associated stress and strain distribution diagrams that can be used to visualize force and moment equilibrium at the flexural strength limit state. Familiar to conventional reinforced concrete design are the equivalent rectangular compressive stress block (i.e., the Whitney Stress Block), linear strain distribution over the section height, and the concentrated tensile force from the steel reinforcing bars. The primary difference for a fiber-reinforced section is the presence of an equivalent rectangular tensile stress block in the tensile zone of the concrete; an additional tensile component that must be equilibrated by concrete compression. The equation for the flexural capacity of a fiber-reinforced concrete flexural member with steel rebar is given in Equation (5-13) based on moment equilibrium from Figure 5.10.

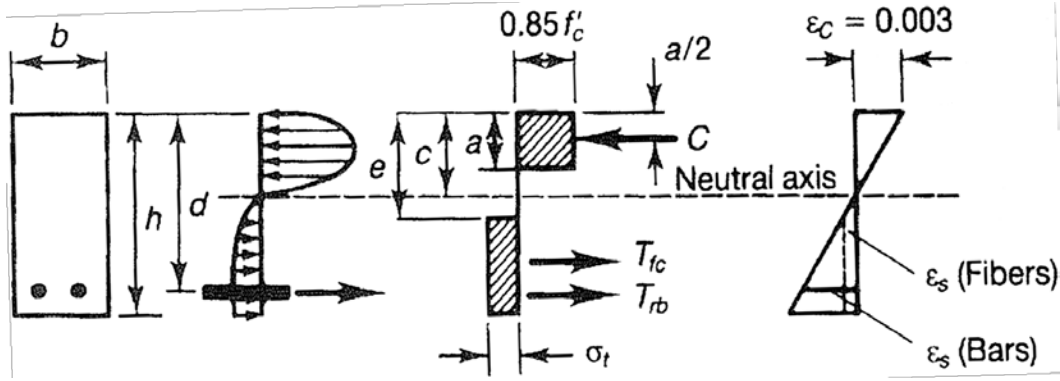


Figure 5.10 Stress and Strain Distribution across Depth of Singly Reinforced Fibrous Concrete Beam [88]

$$M_n = A_s f_y \left(d - \frac{a}{2} \right) + \sigma_t b (h - e) \left(\frac{h}{2} + \frac{e}{2} - \frac{a}{2} \right) \quad (5-13)$$

$$\sigma_t = \frac{1.12l}{d_f \rho_f F_{bc}}$$

where:

l = steel fiber length

d_f = steel fiber diameter

ρ_f = volume percentage of steel fibers

F_{bc} = bond efficiency of steel fibers depending on their characteristics; varies from 1.0 to 1.2

a = depth of equivalent rectangular compressive stress block

b = width of flexural member

c = depth to neutral axis of section

d = effective depth of flexural member, measured to centroid of main tensile reinforcement

e = distance from extreme compression fiber of section to top of tensile stress block of fibrous concrete

σ_t = tensile yield stress in the fiber

5.3 Structural Steel Elements

5.3.1 Local Breach

Local breach in stiffened steel plate elements (e.g. plate components of built-up members such as steel cellular towers) may occur due to contact or near-contact denotations. This type of local failure is controlled by early-time transverse shear failure, as opposed to other more ductile modes of response (e.g., flexure). Figure 5.11 shows examples of local breaching on built-up steel plate structures subject to close-in detonations from an FHWA-sponsored test series [93].



Figure 5.11 Local Breaching Failure of Steel Bridge Tower Test Specimens [93]

Algorithms for evaluating local breaching in steel plate components are available [93]. These procedures are generally based on energy equilibrium, where the energy imparted by the detonation on the breaching area of steel plate is equated to the energy required to fail the plate area in shear. The procedures utilize an interactive process where the breaching area (or “plug”) is varied until the applied energy equals the energy required to breach [93]. The effects of this type of local response mode are of interest for cellular steel towers and are further discussed in Chapter 8.

5.3.2 Flexural Response

Most steel components subject to far-range blast loading respond primarily in flexure. Steel components develop their ultimate flexural resistance through yielding over plastic hinge regions at locations of maximum bending stress. Once one or more plastic hinge regions develop in the component, depending on the boundary conditions, the resistance reaches the ultimate flexural resistance value and it becomes approximately constant with increasing deflection. For a statically determinate component (e.g. simply supported or cantilever beam), the ultimate flexural resistance is reached at the formation of a single plastic hinge region. For a statically indeterminate component (e.g. fixed-fixed beam or plate), the ultimate flexural resistance will occur when two or more plastic hinge regions develop in the component.

Provided that a structural steel component can develop its full flexural capacity, if other local failure modes do not occur, the maximum resistance is a function of the boundary conditions and the ultimate dynamic moment capacity at the plastic hinge regions. Equations for the calculation

of the ultimate dynamic moment capacity and ultimate flexural resistance for different types of structural steel components and boundary conditions are provided in numerous blast design references (e.g. [50, 75, 86]). In general, the dynamic moment capacity of structural steel components can be calculated following equations from conventional design code provisions (e.g. AASHTO or AISC specifications) and using the dynamic yield strength of the steel material (including static and dynamic increase factors, as discussed in Chapter 3) in lieu of the static yield strength. In addition, the transition from elastic yielding to fully plastic yielding should be considered in the calculation of the moment capacity. Figure 5.12 shows a theoretical transition of stress distribution across a cross section of a steel beam at different stages of plastic hinge deformation. Figure 5.13, as taken from PDC-TR 06-01 [86], shows a representative moment-curvature relationship for a simply supported steel beam and plate.

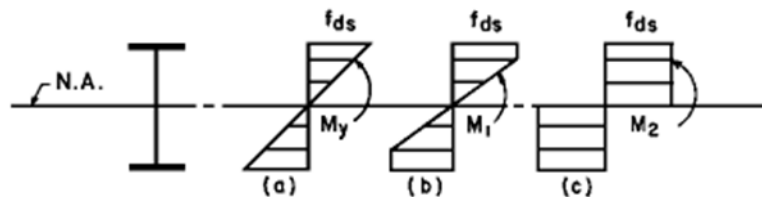


Figure 5.12 Theoretical Stress Distribution for Pure Bending at Various Stages of Yielding:
(a) Elastic, (b) Elastoplastic, (c) Plastic [50]

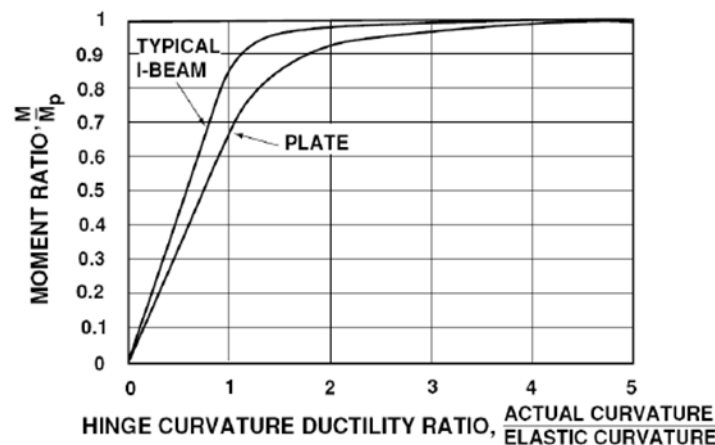


Figure 5.13 Typical Moment-Curvature Relationships for Steel Plates and Beams [86]

As shown in the figure, steel plates generally develop their full plastic moment capacity at a higher curvature ductility ratio than steel beams. UFC 3-340-02 [50] utilizes Equation (5-14) for the calculation of the dynamic moment capacity for compact fully-braced beams and plates based on the average between the elastic section modulus and the plastic section modulus, or the plastic section modulus, depending on the ductility ratio at maximum response. For blast design purposes, the calculation of the dynamic moment capacity for steel beams and plates can be simplified by using the full plastic section modulus for beams and the average between the elastic and plastic section modulus for plates.

$$\begin{aligned}
M_{du} &= f_{dy} \left(\frac{S + Z}{2} \right) && \text{for } \mu \leq 3 \text{ for beams; } 7 \text{ for plates} \\
M_{du} &= f_{dy} Z && \text{for } \mu > 3 \text{ for beams; } 7 \text{ for plates}
\end{aligned}
\tag{5-14}$$

where:

M_{du} = ultimate dynamic moment capacity

S = elastic section modulus

Z = plastic section modulus

μ = ductility ratio

5.3.3 Local and Global Buckling

In general, plate components can usually sustain larger deformation and are less susceptible to effects of global and local buckling on the ultimate flexural capacity than structural steel shapes. For structural steel members to attain full plastic moment capacity and thus exhibit substantial ductility, elements of the cross-section must meet minimum thickness requirements (i.e., a measure of cross-section compactness) to prevent local buckling. For example, certain cross-section width-to-thickness ratios must meet plastic design requirements per conventional design code provisions such as the AASHTO or AISC specifications. Although such provisions are applicable for static loading, due to the relatively short duration of the loads and lateral inertial effects against local buckling, the use of static load criteria for dynamic loading of relatively short durations is considered appropriate for blast design.

In addition, for members that are not fully braced laterally, compression flange unbraced length must be considered in the calculation of the dynamic moment capacity. Blast design guidelines such as UFC 3-340-02 [50] and PDC-TR 06-01 [86] provide equations for lateral bracing requirements and for including the effect of lateral bracing on the dynamic moment capacity of structural steel members.

Furthermore, webs of structural steel members with concentrated loads along a short length of flange (e.g. members providing a point support to other blast loaded members) may be subject to large compressive stresses at the web that may cause local yielding followed by web crippling. Stiffeners bearing against flanges and fastened to the web are usually employed to prevent local instabilities associated with the application of concentrated forces to structural steel shapes [50].

5.3.4 Shear Response

The dynamic shear strength of steel components is given by Equation (5-15). For steel plates and structural shape members where web slenderness (h/t ratio) does not control shear strength per conventional design code provisions, the dynamic yield strength in shear, f_{dv} , in Equation (5-15) is given by $0.55f_{dy}$, where f_{dy} is the dynamic yield strength (see Chapter 3). For members where web slenderness, as defined by the web height to thickness (h/t) ratio, control the shear strength, shear capacity is controlled by instability of the web due to shear stress resulting in elastic or inelastic web buckling, depending on the slenderness of the web. In this case, shear strength equations from conventional design code provisions (e.g. AASHTO or AISC Specifications) can

be used for blast design purposes by substituting the steel dynamic yield strength in lieu of the minimum static yield strength.

$$V_{du} = f_{dy} A_w \quad (5-15)$$

where:

V_{du} = dynamic shear capacity

f_{dy} = dynamic yield strength in shear

A_w = shear area of component (e.g. web area of I-shaped members)

Shear forces are of significance in plastic design primarily because of their possible influence on the plastic moment capacity of a steel member. I-shaped steel sections carry flexural tension and compression forces due to bending moment predominantly in the flanges while shear stresses are carried predominantly through the web. Thus, the plastic moment capacity of I-shaped sections is not generally affected by shear stresses at the web (provided these are below the dynamic yield strength in shear). However, in the case of steel plates or built-up sections, where the web is relied upon to carry a significant portion of the bending moment stresses, the effect of shear stresses on the available moment capacity may be significant. Equation (5-16) from UFC 3-340-02 [50], describes the effect of shear on the available bending moment capacity for steel plates. As it can be observed from Equation (5-16), when shear demand does not exceed 55-percent of the dynamic shear capacity, the effect of shear on the dynamic moment capacity is less than 10-percent and is typically ignored for blast design purposes [50, 86].

$$\frac{M}{M_{du}} = 1 - \left(\frac{V}{V_{du}} \right)^4 \quad (5-16)$$

where:

M = moment capacity including effect of shear force, V

M_{du} = dynamic moment capacity in the absence of shear

V = shear force

V_{du} = dynamic shear capacity in the absence of bending moment calculated

5.3.5 Tension Membrane Response

Tension membrane response can potentially increase the resistance of steel components at relatively large deflections. However, due to the large tension membrane forces that can be generated in the component, tension membrane response for structural steel components is typically limited by the strength of their connections or the in-plane restraint capacity of their supports. In most cases, the amount of in-plane restraint and connection capacity for structural steel components is not sufficient to develop significant tension membrane resistance relative to the flexural resistance of these components. For this reason, significant tension membrane can

usually be achieved only in steel plates or relatively small hot-rolled steel sections (e.g. channels or angles) that are welded or bolted to relatively rigid in-plane supports [86].

5.4 High-Strength Steel Cables

Due to the relatively small presented area of high-strength steel cables, and due to associated clearing and wrap-around effects, blast pressure is generally not a concern for these types of components. The main concern associated with explosives threats for high-strength steel cables is local damage due to impact of high-velocity primary fragments or failure due to loss of individual strands and wires overloaded in shear due to localized shock loads from contact or near-contact charges. Unlike other structural elements, there are no performance criteria for cables that are based on structural response variables such as maximum displacement or rotations. High-fidelity finite element models or other analytical procedures must be employed using the failure criteria for the constituent materials to evaluate the response and performance of this type of component. Performance, failure modes, and protective design strategies for high-strength steel cables are discussed in detail in Chapter 10.

5.5 Chapter Summary

This chapter focused on the structural mechanics governing various modes of response exhibited by blast-loaded bridge components. These response modes included those typically encountered during conventional design (e.g., flexural response) as well as unique modes of response, such as direct shear, local breaching, and post-yield plastic behavior (e.g., tension and compression membrane) modes of response.

In Chapter 6, information and techniques developed in Chapters 3 through 5 are applied in presenting various methods for performing dynamic analysis of blast-loaded bridge components. Component-level performance criteria for blast-loaded bridge components are also addressed.

6.0 DYNAMIC RESPONSE OF STRUCTURES

This chapter provides general guidance on the dynamic analysis process for blast-loaded bridge components and introduces the concept of performance criteria as it relates to building and bridge structures. A comparison between buildings and bridges is drawn to highlight that the bridge security community has not progressed as far as the building security community with the development of a robust performance-based framework for protective design. This chapter also provides detailed descriptions of three specific dynamic analysis methodologies: pressure-impulse diagrams, equivalent single-degree-of-freedom models, and multi-degree-of-freedom models. Guidance on the applicability of each analysis methodology is also provided. The remainder of this section introduces the topic of dynamic structural response with emphasis on the unique aspects that arise when dealing specifically with blast loads.

When a shock wave from a high-explosive detonation strikes a structural component, it imparts an intense pressure pulse having an almost instantaneous rise time and a duration that is typically on the order of milliseconds. Such a loading scenario is a drastic departure from the common static and low-rate dynamic (e.g., wind and seismic) loads that are routinely considered in structural engineering practice. The application time of static loads and the duration of low-rate dynamic loads are typically orders of magnitude larger than stress wave transit times within a structural component, thus leading to the perception of nearly immediate global component response upon load application. The perceived immediate global response is the result of countless stress wave reflections occurring throughout a structural component.

Consider a cantilevered rod subjected to a static axial load at its free end. Regardless of the load rate or magnitude of the applied load, stress waves must travel back and forth from the free end to the fixed end at the sound speed of the rod material until a steady-state condition—static equilibrium in this case—is eventually achieved. From a strictly physical point of view, a structural component must undergo a transient state of response before steady-state behavior can be achieved. Thus, static loads are quasi-static in nature. In general, the effects of individual stress waves from static and low-rate dynamic loads tend to have a negligible effect on structural response, and they are rarely considered in the analysis and design of structural components. Furthermore, structural response to transversely applied static loads is normally governed by flexural deformations, and the response to low-rate dynamic loads is often driven by the component's lowest harmonics which are also flexurally dominated. Results from experimental and computational research on short-duration load effects [24, 18, 25] reveal several unique behavioral aspects that greatly differ from loads typically considered in design and have the potential to govern a component's response and failure capacity.

Unlike structural components subjected to static or low-rate dynamic loads, a blast-loaded structural component undergoes a complex response evolution involving early-time local material response followed by global component response. An illustrative sketch depicting this local-to-global response evolution is provided in Figure 6.1. Local response refers to early-time material behavior that occurs prior to the time in which the entire component is set in motion, and it is chiefly driven by the effects of the impinging shock wave as it propagates through the component material and interacts with cross-sectional free surfaces. Examples of early-time material damage include local denting or breaching of steel components and spalling or breaching of concrete components. Conversely, global response refers to dynamic modes of

response, such as flexure and direct shear, which engage the entire component and depend on characteristics such as boundary conditions, stiffness, mass, and blast pulse duration. In performing a dynamic analysis of a blast-loaded bridge component, it is important that these unique behavioral aspects be considered.

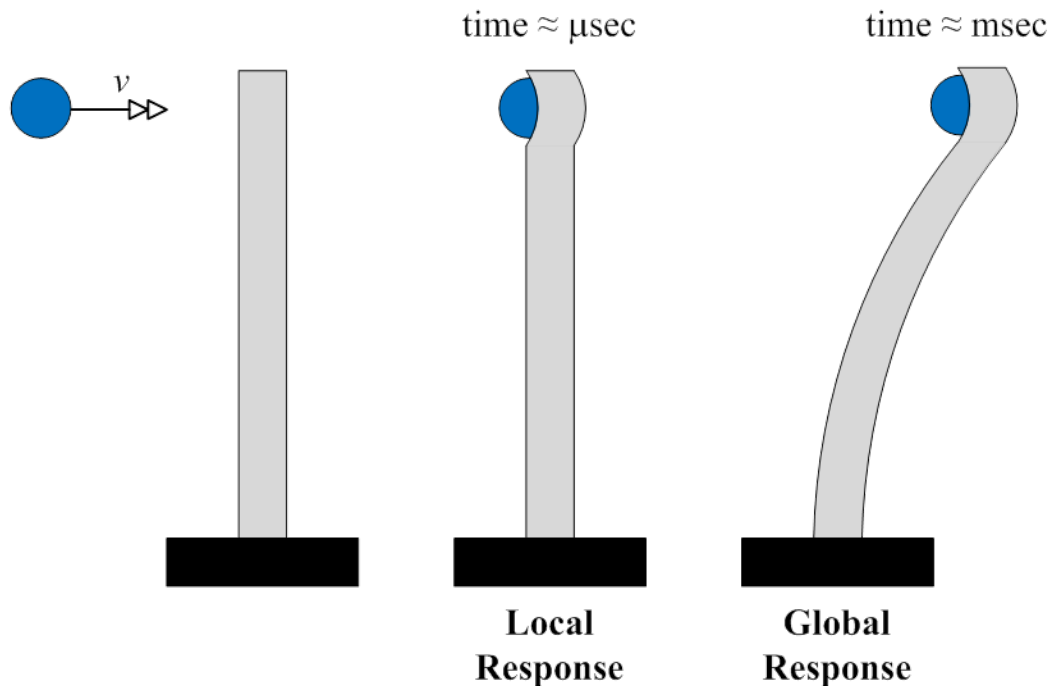


Figure 6.1 Illustration of Local Response versus Global Response [18]

6.1 Dynamic Analysis Process

For situations requiring dynamic analysis, several important factors should be considered during the analysis process. The dynamic analysis process is a critical step in the overall protective design of a bridge structure. Dynamic analysis results serve as input to detailed structural design, and thus have a direct effect on design quality and adequacy. In determining what type of dynamic analysis to conduct, careful consideration should be given to the nature of a given explosive threat and the type of analysis output needed for subsequent design activities. In addition, care must be taken to ensure that blast loads are accurately represented and governing response modes and failure mechanisms of a given target can be adequately captured with the chosen dynamic analysis method. Characterizing the explosive threat should be the first step in the dynamic analysis process. Threat characterization should identify critical information such as explosive composition, charge shape, charge size, standoff distance from a given target, as well as the location and geometry of potential shock wave reflecting surfaces. Once a given threat has been characterized, a determination can be made as to the most appropriate method for representing blast loads during a dynamic analysis. Various methods for calculating blast loads are presented and discussed in Section 6.4.2 and Chapter 4 of this manual. Factors to consider when determining the most appropriate method for calculating blast loads on bridge components include, but are not limited to:

- Standoff distance—that is, the distance between the explosive charge (typically taken from the charge centroid) and target of interest
 - For relatively large standoff distances, point source and planar shock front assumptions may be appropriate.
 - For relatively small standoff distances, consideration should be given to the effects of charge shape and configuration on the time- and position-dependent characteristics of the shock front and resulting blast loads.
- Geometry of target and surrounding environment
 - For relatively slender targets such as bridge columns, overpressure clearing (refer to Chapter 4 for more discussion on phenomenon of clearing) and wrap-around or engulfment effects on net blast loads should be considered.
 - If a target and nearby structural elements or obstructions geometrically represent a complex airblast environment comprised of multiple reflecting surfaces and/or areas for overpressure stagnation (e.g., beneath a bridge deck or near an abutment), then advanced blast load calculations using either a ray-tracing or computational fluid dynamics approach may be necessary.
- Frangibility of nearby structural elements or obstructions
 - If structural elements or obstructions adjacent to a target are determined to be frangible, the potential for overpressure venting should be considered. An example might be an above-deck detonation near a bridge tower, where early-time breach of the bridge deck may allow for overpressure venting and a consequent reduction in net blast loads delivered to the bridge tower.

Once a given threat has been characterized, an appropriate dynamic analysis method must be chosen. For straight-forward blast loads and initial assessments, P-I diagrams are an appropriate tool. By and large, the most common dynamic analysis method for blast-resistant design is component nonlinear dynamic analysis using an equivalent single-degree-of-freedom (SDOF) model. The equivalent SDOF modeling approach reduces a continuous system having distributed mass and stiffness properties to a lumped mass and stiffness definition by assuming a dominant mode of structural response and employing the principle of virtual displacements. Direct output from an equivalent SDOF dynamic analysis includes histories of peak response quantities such as displacement, velocity, and acceleration. Dynamic support reaction histories can also be inferred from the SDOF analysis. A thorough description of the equivalent SDOF modeling approach is provided in Section 6.4, including derivation, intended uses, limitations, as well as tables of input parameters for commonly encountered idealized structural components. For certain situations, a more sophisticated multi-degree-of-freedom (MDOF) dynamic analysis approach may be warranted.

Unlike an equivalent SDOF analysis, an MDOF analysis includes multiple displacement degrees-of-freedom and can refer to either a (loosely) coupled system of SDOF systems, a frame-type

computational model, or a three-dimensional finite element model. Compared to an equivalent SDOF model, an MDOF nonlinear dynamic analysis offers the major advantages of better blast load representation, the ability to capture response coupling between multiple structural components, the ability to capture coupled fluid-structure interaction between an impinging shock wave and target of interest, higher resolution response output, and the ability to capture material damage. However, an MDOF nonlinear dynamic analysis is also significantly more time consuming, complex, and resource intensive than an equivalent SDOF dynamic analysis. A thorough description of the MDOF modeling approach is provided in Section 6.5, including a comparison of frame-type versus three-dimensional finite element models, practical uses, and limitations. Factors to consider when determining the most appropriate dynamic analysis method include, but are not limited to:

- Explosive threat severity
 - For explosive threats likely to cause significant early-time material damage to a target of interest, the equivalent SDOF analysis approach is not recommended. With the equivalent SDOF analysis approach, it is difficult to predict early-time material damage and consider the effect of material damage on component dynamic response (e.g., locally reduced section capacity, modification to a component's dynamic response characteristics, and reduction in component stability).
- Governing failure mechanisms and mode(s) of structural response
 - To successfully use an equivalent SDOF model to perform a component nonlinear dynamic analysis, the governing failure mechanisms and mode(s) of structural response must be identified *a priori*, and they must be quantifiable in terms of a (non)linear force-displacement resistance function (refer to Section 6.4.3 for a discussion on resistance functions).
- Response coupling
 - For structural assemblages consisting of members having fundamental natural periods of vibration that differ by less than a factor of two, it is recommended that member response coupling be considered during the dynamic analysis [94]. Accordingly, in such a situation, an MDOF dynamic analysis approach is recommended.
- Computing resources and technical expertise
 - To perform a nonlinear dynamic analysis using a sophisticated three-dimensional finite element model, considerable computational resources and technical expertise are needed. From a resources perspective, detailed finite element analyses are typically conducted on high-performance computing platforms having a large amount of random access memory (RAM), hard drive space, and the capability of facilitating parallel computations using multiple computing cores. From a technical expertise perspective, specialized skills are

required to define an appropriate computational model, including: the selection of appropriate element formulations, the generation of an appropriate finite element mesh, the definition of appropriate constitutive models, the definition of appropriate contact algorithms (especially for a fully-coupled analysis involving fluid-structure interaction), and the interpretation of finite element results.

6.2 Performance Criteria

Performance criteria is an important yet broad term that can range from system structural performance objectives (or acceptable damage levels) to component response limits. For building structures, the use of performance criteria in extreme loading design procedures is typical. For example, in the case of seismic design, the current state-of-the-practice is to produce a design that satisfies a relationship between building performance level and earthquake ground motion intensity as put forth by the Building Seismic Safety Council [95] and subsequently adopted by ASCE 7-10 *Minimum Design Loads for Buildings and Other Structures*. The performance levels defined by the Building Seismic Safety Council—operational, immediate occupancy, life safety, and collapse prevention—correspond to specific system damage states and associated component response limits. In addition, the ground motion intensity levels represent earthquake events of varying severity in terms of recurrence interval. Based on the occupancy category and design-basis earthquake event for a given building, a target performance level can be identified for design. In practice, performance criteria for seismic design are currently enforced implicitly within building codes. This enforcement is achieved by prescribing an equivalent linear analysis methodology based on the Equal Displacement concept, enforcing over-strength factors for critical elements, and requiring ductile detailing commensurate with anticipated component response for a target building performance level—a prescriptive design approach. True performance-based seismic design is beginning to gain traction in the industry, particularly for high-rise building structures, but is far from commonplace.

Blast-resistant design of building structures also incorporates performance criteria, but in a more explicit manner than state-of-the-practice seismic design procedures. For example, Table 6.1 and Table 6.2 describe typical system performance criteria (or building levels of protection) and component damage states, respectively, to be utilized during blast-resistant design of buildings [74]. Note that Table 6.2 relates component damage to system performance criteria. The U.S. Army Corps of Engineers source document [74] goes on to prescribe specific component response limits for different levels of protection and various construction materials. The component response limits are given in terms of displacement ductility and rotation limits and are directly related to the component damage states of Table 6.2. The typical blast-resistant design process includes nonlinear dynamic analysis of individual components to explicitly compare peak dynamic response with specified component response limits. To achieve a target level of protection for a building, all structural components must be shown to dynamically perform within the specified component response limits. Though blast-resistant building design generally takes a more explicit approach to incorporating performance criteria than seismic-resistant design of buildings, it should be emphasized that both design procedures maintain a relationship between system and component performance.

Table 6.1 Example of System Performance Criteria for Blast-Resistant Design (adapted from [74])

Building Level of Protection	Descriptions of Potential Overall Structural Damage
Below AT Standards ^{1,2}	Severe Damage – Progressive collapse likely. Space in and around damaged area is unusable.
Very Low	Heavy Damage – Onset of structural collapse. Progressive collapse is unlikely. Space in and around damaged area is unusable.
Low	Unrepairable Damage – Progressive collapse will not occur. Space in and around damaged area is unusable.
Medium	Repairable Damage – Space in and around damaged area can be used and is fully functional after cleanup and repairs.
High	Superficial Damage – No permanent deformations. The facility is immediately operable.

Note 1: AT = Anti-Terrorism

Note 2: This is not a level of protection, and should never be a design goal. It only defines a realm of more severe structural response, and may provide useful information in some cases.

Table 6.2 Example of Relationship between System Performance Criteria and Component Damage for Blast-Resistant Design (adapted from [74])

Building Level of Protection	Component Damage		
	<i>Primary Components</i>	<i>Secondary Components</i>	<i>Non-Structural Components</i>
Below AT Standards ¹	Hazardous	Blowout	Blowout
Very Low	Heavy	Hazardous	Hazardous
Low	Moderate	Heavy	Heavy
Medium	Superficial	Moderate	Moderate
High	Superficial	Superficial	Superficial

Note 1: AT = Anti-Terrorism

The concept of performance criteria for blast-loaded bridges is not nearly as well defined as those for buildings. While component response limits and/or damage levels have been proposed for certain bridge components based on experimental and computational research, there currently exists a major knowledge gap in relating component damage to system-level bridge performance. In certain situations, building component response limits have been used as a starting point for defining appropriate bridge component limits, but, in general, it should be emphasized that building component response limits do not translate directly to bridge structures. Consequently, a comprehensive performance-based design framework for blast-loaded bridges currently does not exist. As the bridge security community generates and gathers additional data from future research programs and event reconnaissance efforts, the development of a comprehensive performance-based protective design framework for bridge structures will begin to mature. Throughout the component-specific design chapters of this bridge security design manual, proposed component response limits and/or damage levels are provided as available.

6.3 Pressure-Impulse (P-I) Diagrams

For conceptual design activities and expedient threat assessments, pressure-impulse (P-I) diagrams, which are plots that relate combinations of peak pressure and applied impulse to specific component peak response quantities or damage states (sometimes referred to as iso-damage curves), are an economical and time-efficient tool. However, P-I diagrams yield little quantitative dynamic response information and therefore are not well suited to support detailed protective design or rigorous threat assessments. This section focuses on the derivation and application of P-I diagrams.

It is well known from the theory of structural dynamics that a distinct relationship exists between the fundamental natural period of a structural element and the duration of a pulse-like forcing function. In the protective design community, this relationship is interpreted as three distinct structural response regimes: impulsive, dynamic, and quasi-static. In the impulsive regime, the ratio of load duration to the fundamental period of a structural component is small (e.g., $t_d < 0.25T_n$), which gives rise to a scenario wherein the load is applied and removed before the structural component exhibits any appreciable deformation. Impulsive loads can be treated as an initial velocity condition based on the relationship between impulse and momentum. The response of a structural component subjected to an impulsive load is largely driven by applied impulse and is essentially independent of peak overpressure or blast pulse shape. In the quasi-static regime of response, the ratio of pulse duration to the fundamental period of a structural component is large (e.g., $t_d > 10T_n$), which often gives rise to a scenario wherein the magnitude of the applied load exhibits minimum decay prior to the time at which the loaded structural component attains its peak flexural displacement. Peak overpressure and structural stiffness drive quasi-static response, and load duration and mass have minimal to no influence on structural response. The dynamic regime of response, often referred to as the transition region, represents scenarios wherein the pulse duration and natural period are of similar magnitude (e.g., $10T_n > t_d > 0.25T_n$). Structural response in the dynamic regime is relatively complex and can be influenced by peak overpressure, applied impulse, load duration, and mass. These distinct response regimes can be graphically identified via an elastic response spectrum.

Figure 6.2 shows an elastic displacement response spectrum for a right-triangular pulse load. The vertical axis of the response spectrum represents the ratio of peak dynamic displacement, x_{max} , to peak static displacement, (P_{max} / K) , where P_{max} is the magnitude of the pulse load and K is the stiffness of a structural component. The horizontal axis represents the ratio of pulse duration, t_d , to the fundamental natural period of a structural component, T_n . Note that, for ratios of pulse duration to natural period less than or equal to 0.01, the corresponding peak displacement ratios are constant and near zero. This range of duration-to-period ratios represents the impulsive response regime. For duration-to-period ratios greater than or equal to 10 in Figure 6.2, the peak displacement ratios are again constant at values nearing 2. This range of duration-to-period ratios represents the quasi-static response regime. For duration-to-period ratios between 0.01 and 10, the variation in peak displacement ratio is significant. This range of duration-to-period ratios represents the dynamic response regime, where the influence of load characteristics and dynamic response characteristics on peak displacement is graphically emphasized. By re-casting an elastic response spectrum using different horizontal- and vertical-axis values, the same information concerning the response of a structural component to a pulse-type load can be represented in a different way.

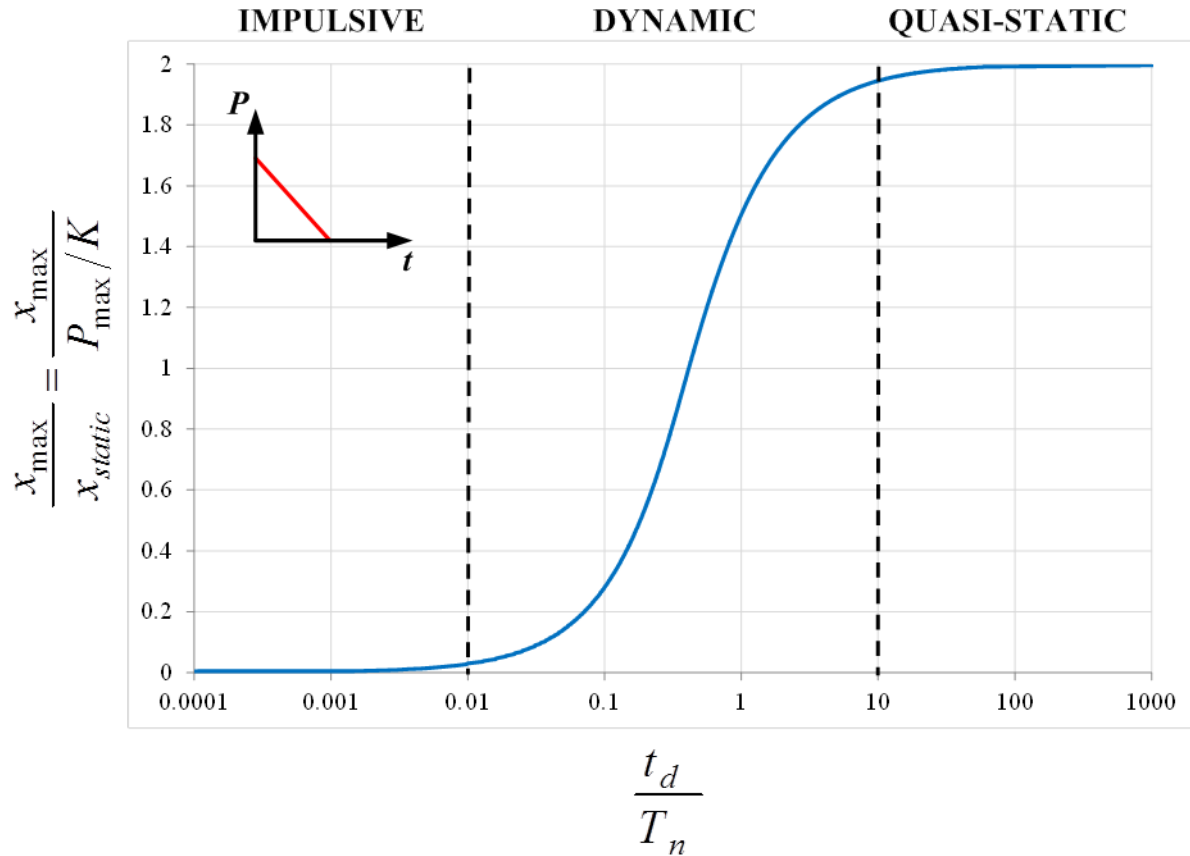


Figure 6.2 Illustration of Structural Response Regimes on Elastic Response Spectrum for Right-Triangular Pulse Load

Figure 6.3 illustrates analytically derived normalized P-I diagrams for three different pulse shapes: a rectangular pulse, a right-triangular pulse, and an exponentially decaying pulse. In Figure 6.3, vertical-axis values represent normalized peak pulse magnitude and are mathematically equal to the reciprocal of the Figure 6.2 vertical-axis values. Horizontal-axis values represent normalized applied impulse values, where M is the total mass of a structural component. Note that the curves in Figure 6.3 exhibit asymptotic behavior in the impulsive and quasi-static response regimes and variable behavior in the dynamic response regime (the curve elbows), as was also noted in the elastic displacement response spectrum of Figure 6.2. Though Figure 6.2 and Figure 6.3 represent the same type of load and structural component data, their practical use is quite different.

Elastic response spectra are typically used in earthquake engineering applications, where peak dynamic response is desired for a given excitation and structural system, component, or modal property. P-I diagrams are widely used in the protective design community for preliminary component design and damage assessment purposes. Given a structural component and target kinematic response criterion (e.g., peak dynamic displacement) or damage level, combinations of load magnitude and applied impulse that will cause a structural component to reach a target kinematic response or damage level can be determined. Thus, P-I diagrams are often referred to as iso-damage curves. In effect, a P-I curve defines the threshold above which a specified performance criterion or damage level will be exceeded. Once specific P-I combinations are determined from a P-I diagram, they can then be related to specific bulk explosive threats. While

Figure 6.3 presents analytically derived P-I diagrams in a normalized form, they can also be generated computationally or experimentally and in pure load magnitude versus applied impulse form. A practical Excel-based tool that is commonly used to computationally develop P-I diagrams is called the Single-Degree-of-Freedom Blast Effects Design Spreadsheet (SBEDS) [96]. SBEDS can be downloaded from the U.S. Army Corps of Engineers' Protective Design Center website by U.S. Government employees and their contractors. Numerous P-I curves corresponding to different target kinematic response values or damage levels can be plotted on the same graph for rapid assessment purposes. In addition, P-I curves corresponding to different modes of structural response (e.g., flexure and direct shear) can be plotted on the same graph and enveloped to produce a bounding iso-damage curve. Such is illustrated schematically in Figure 6.4.

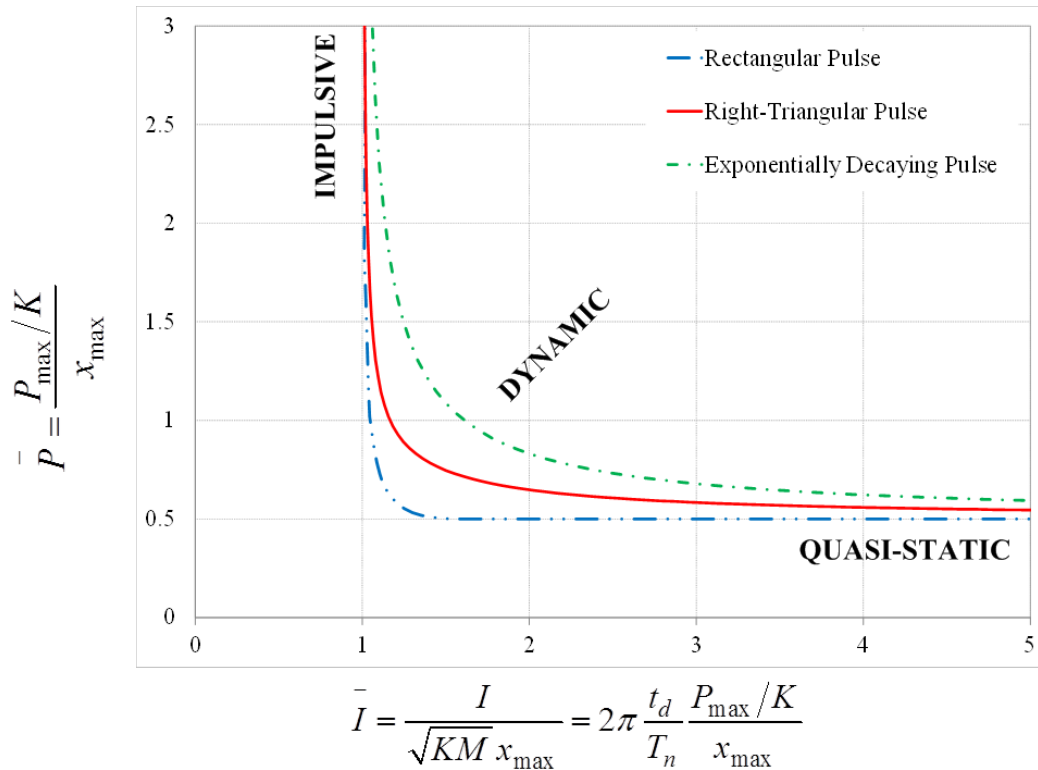


Figure 6.3 Analytically Derived Normalized P-I Diagrams for Three Different Pulse Loads

As mentioned previously, P-I diagrams are most effective for preliminary component design and damage assessment activities. Given a specified bulk explosive threat, P-I diagrams can be used to quickly determine an expected level of damage for a structural component or to determine a preliminary structural component size that meets a specified response limit or damage level. Alternatively, given a structural component and target performance criterion, acceptable standoff distances and/or explosive charge weights can be back-calculated from critical pressure-impulse combinations. Back-calculation can be done using blast effects tools such as ConWEP [97] and SBEDS [96] or the Kingery-Bulmash blast parameter charts (often referred to as the spaghetti charts) in UFC 3-340-02 [50].

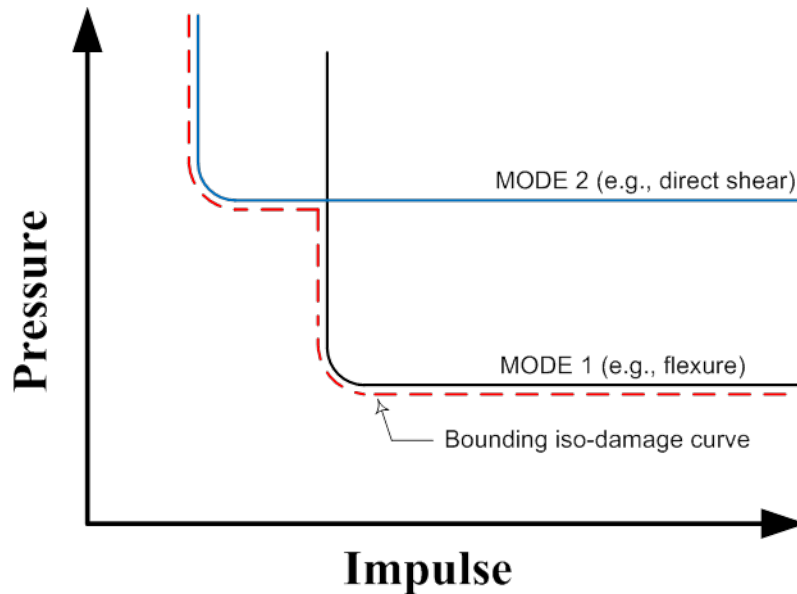


Figure 6.4 Schematic of Bounding Iso-Damage Curve Considering Multiple Component Modes of Response

6.4 Single-Degree-of-Freedom (SDOF) Analysis

Most structural elements are continuous in nature. They possess distributed stiffness and mass properties, comprising an infinite number of displacement degrees of freedom. The dynamic response of continuous systems to an externally applied load can be mathematically described by partial differential equations, the solution to which can be approximated with numerical solution techniques such as finite elements. Finite element numerical solution techniques require considerable expertise, knowledge of base materials, and computational resources. An alternative approach to approximating the dynamic response of continuous systems that has found much use by practitioners in the protective design community is the application of equivalent single-degree-of-freedom (SDOF) models [46, 50, 54, 75, 94].

Given a continuous system with known stiffness and mass properties, a well-defined external load, and a dominant mode of component response, a normalized displaced shape (often referred to as a shape function) is assumed and the principle of virtual displacements employed to derive a work-equivalent SDOF system. As shown in Figure 6.5, the transformation of a continuous system to an equivalent SDOF system reduces the governing partial differential equation to a semi-discrete ordinary differential equation that only depends on time. The equivalent stiffness, K^* , mass, M^* , and applied load, P^* , parameters for the equivalent SDOF system are determined by equating internal work, kinetic energy, and external work of the two systems, respectively. These calculations are given in Equations (6-1) through (6-3) for the continuous system shown in Figure 6.5 (for full derivations, see for instance [54, 94, 98, 99]). Once the equation of motion for the equivalent SDOF system has been formulated, it can be readily solved using an implicit or explicit numerical time integration method. The implicit Newmark-Beta Method and explicit Central Difference Method are perhaps the most widely used numerical time integration techniques, and they can be found in many introductory structural dynamics texts [54, 94, 98, 99].

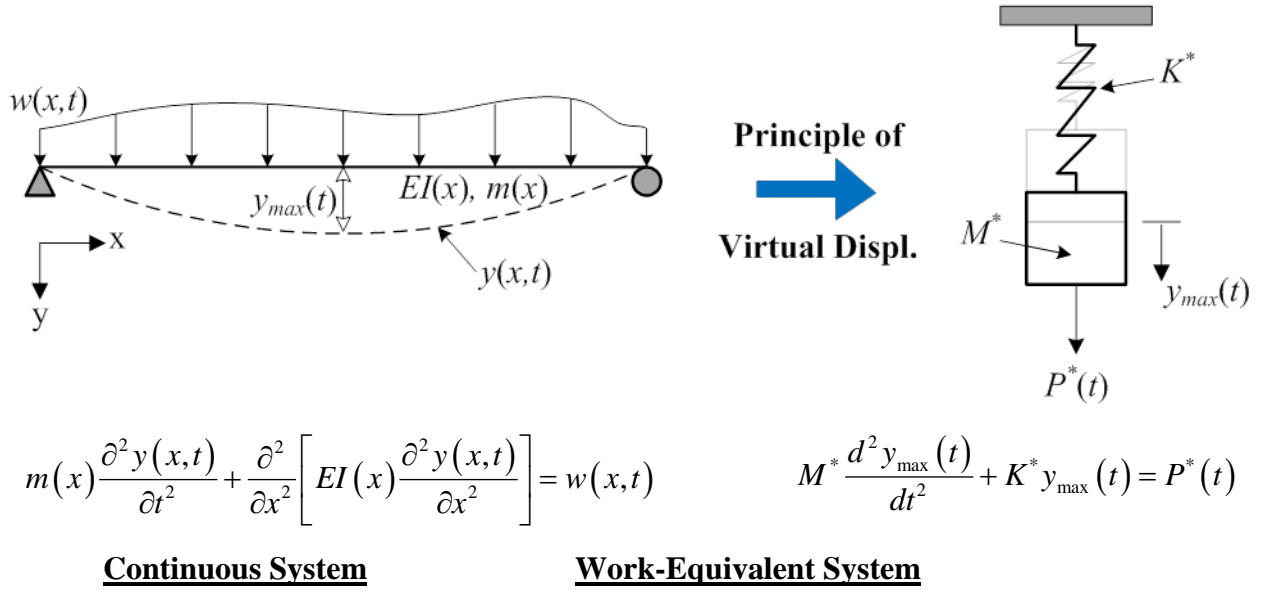


Figure 6.5 Transformation of Continuous System to Equivalent SDOF System [18]

$$K^* = \int_0^L EI(x) \left[\frac{d^2}{dx^2} \psi(x) \right]^2 dx \quad (6-1)$$

$$M^* = \int_0^L m(x) \psi^2(x) dx \quad (6-2)$$

$$P^*(t) = \int_0^L w(x,t) \psi(x) dx \quad (6-3)$$

where:

$EI(x)$ = continuous system's distributed flexural rigidity

$m(x)$ = continuous system's distributed mass

$w(x,t)$ = continuous system's time-dependent, distributed load

$\psi(x) = y(x,t)/y_{\max}(t)$ = normalized displacement field (i.e., shape function)

x = distance along the length of continuous system

L = total length of continuous system

K^* = equivalent SDOF system stiffness

M^* = equivalent SDOF system mass

$P^*(t)$ = equivalent SDOF time-dependent load

The equivalent SDOF model is relatively fast-running, requires modest computational resources, and can predict the peak response of a continuous system with reasonable accuracy. As such, the equivalent SDOF analysis method is by and large the state-of-the-practice for predicting component blast response. The equivalent SDOF method is well suited for situations involving planar shock waves (i.e., uniform blast loads) and structural components undergoing a well-characterized, dominant mode of response. For situations involving blast loads from close-in detonations and/or structural components undergoing complex response (e.g., extensive early-time material damage, coupled response modes), a modified SDOF approach or multi-degree-of-freedom (MDOF) analysis may be warranted.

6.4.1 Equivalent SDOF System Properties

The transformation of a continuous system to a work-equivalent SDOF system—sometimes referred to as a *generalized* SDOF system—is covered in most structural dynamics texts, where application is typically relegated to the elastic range of response [98, 99]. For an elastically responding continuous system, Equation (6-1) can be easily evaluated for use in the ordinary differential equation given in Figure 6.5 for an equivalent SDOF system. However, for continuous systems exhibiting significant material nonlinearity, as is often the case for blast-loaded structural components, determination of the equivalent stiffness parameter becomes challenging. The blast community mitigates this issue by re-casting the governing ordinary differential equation to allow for the direct use of a resistance function that relates total system resistance (i.e., the SDOF system restoring force) to peak displacement [50, 54, 75, 94]. Representing the product of SDOF system stiffness and displacement by a nonlinear resistance function is prudent and arguably necessary for conducting a dynamic analysis of a blast-loaded structural component that exhibits nonlinear behavior. The re-casted equation of motion for an equivalent SDOF system is presented in what follows, and resistance functions are discussed in greater detail in Section 6.4.3.

In deriving the re-casted form of the ordinary differential equation governing the dynamic response of equivalent SDOF systems, the classical form given in Figure 6.5 is first re-expressed as shown in Equation (6-4). Mass and load transformation factors are then introduced as shown in Equations (6-5) and (6-6), respectively. Stiffness, K , is defined in terms of the continuous system's load distribution, and it is numerically equal to the total load of the same distribution that would cause a unit deflection at the point where the deflection is equal to that of the equivalent system (y_{\max} in the case of Figure 6.5). Consequently, the stiffness transformation factor must always equal the load transformation factor [54, 94]. With this relationship in mind, Equation (6-4) can be rewritten as shown in Equation (6-7). Dividing both sides of Equation (6-7) by the load transformation factor and representing the internal resistance as a function of displacement (i.e., a resistance function) yields the final form given in Equation (6-8). This re-casted equation of motion for an equivalent SDOF system is extremely useful. The total system mass is the only parameter in need of transformation, and the SDOF resistance and load functions can be defined directly from the continuous system. Also, the use of a resistance function provides a convenient way to incorporate constitutive and geometric nonlinearity, as well as complex component response modes, into the dynamic analysis. Tabulated equivalent system properties for commonly encountered idealized one-way spanning structural elements are presented in Table 6.3 through Table 6.5. Tabulated equivalent system properties for commonly encountered idealized two-way spanning structural elements can be found in UFC 3-340-02 [50].

$$\left(\frac{M^*}{M_{tot}} M_{tot} \right) \frac{d^2 y_{\max}(t)}{dt^2} + \left(\frac{K^*}{K} K \right) y_{\max}(t) = \frac{P^*(t)}{P_{tot}(t)} P_{tot}(t) \quad (6-4)$$

$$\beta_M = \frac{M^*}{M_{tot}} \quad (6-5)$$

$$\beta_L = \frac{P^*(t)}{P_{tot}(t)} = \frac{K^*}{K} \quad (6-6)$$

$$\beta_M M_{tot} \frac{d^2 y_{\max}(t)}{dt^2} + \beta_L K y_{\max}(t) = \beta_L P_{tot}(t) \quad (6-7)$$

$$\beta_{LM} M_{tot} \frac{d^2 y_{\max}(t)}{dt^2} + R[y_{\max}(t)] = P_{tot}(t) \quad (6-8)$$

where:

M_{tot} = continuous system's total mass

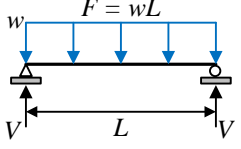
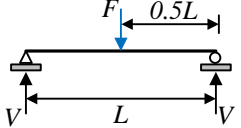
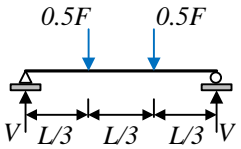
K = continuous system's total load required to cause a unit displacement at the y_{\max} location

$P_{tot}(t)$ = continuous system's total applied load

$\beta_{LM} = \beta_M / \beta_L$ = load-mass transformation factor

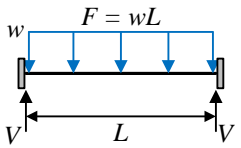
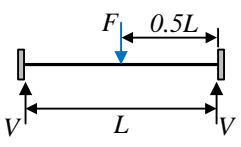
$R[y_{\max}(t)]$ = resistance function

Table 6.3 Equivalent SDOF Transformation Factors for Simply Supported, One-Way Spanning Flexural Elements (adapted from [94])

Loading Diagram	Response Regime	Load-Mass Factor ¹ , β_{LM}	Maximum Resistance, R_u	Stiffness Coeff., k	Dynamic Reaction, V
	Elastic	0.78	$\frac{8M_p}{L}$	$\frac{384EI}{5L^3}$	$0.39R + 0.11F$
	Plastic	0.66	$\frac{8M_p}{L}$	0	$0.38R_u + 0.12F$
	Elastic	0.49	$\frac{4M_p}{L}$	$\frac{48EI}{L^3}$	$0.78R - 0.28F$
	Plastic	0.33	$\frac{4M_p}{L}$	0	$0.75R_u - 0.25F$
	Elastic	0.60	$\frac{6M_p}{L}$	$\frac{56.4EI}{L^3}$	$0.62R - 0.12F$
	Plastic	0.56	$\frac{6M_p}{L}$	0	$0.52R_u - 0.02F$

Note 1: The provided load-mass factors assume uniformly distributed mass

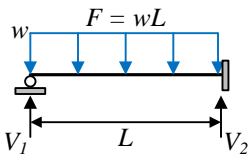
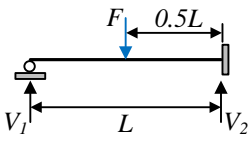
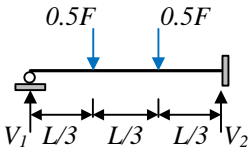
Table 6.4 Equivalent SDOF Transformation Factors for Fixed-Fixed, One-Way Spanning Flexural Elements (adapted from [94])

Loading Diagram	Response Regime	Load-Mass Factor ¹ , β_{LM}	Maximum Resistance ² , R_u	Stiffness Coeff., k	Dynamic Reaction, V
	Elastic	0.77	$\frac{12M_p^s}{L}$	$\frac{384EI}{L^3}$	$0.36R + 0.14F$
	Elastic-Plastic	0.78	$\frac{8}{L}(M_p^s + M_p^m)$	$\frac{384EI}{5L^3}$	$0.39R + 0.11F$
	Plastic	0.66	$\frac{8}{L}(M_p^s + M_p^m)$	0	$0.38R_u + 0.12F$
	Elastic	0.37	$\frac{4}{L}(M_p^s + M_p^m)$	$\frac{192EI}{L^3}$	$0.71R - 0.21F$
	Plastic	0.33	$\frac{4}{L}(M_p^s + M_p^m)$	0	$0.75R_u - 0.25F$

Note 1: The provided load-mass factors assume uniformly distributed mass

Note 2: M_p^s = ultimate moment capacity at support; M_p^m = ultimate moment capacity at mid-span

Table 6.5 Equivalent SDOF Transformation Factors for Propped Cantilever, One-Way Spanning Flexural Elements (adapted from [94])

Loading Diagram	Response Regime	Load-Mass Factor ¹ , β_{LM}	Maximum Resistance ² , R_u	Stiffness Coeff., k	Dynamic Reaction, V
	Elastic	0.78	$\frac{8M_p^s}{L}$	$\frac{185EI}{L^3}$	$V_1 = 0.26R + 0.12F$ $V_2 = 0.43R + 0.19F$
	Elastic-Plastic	0.78	$\frac{4}{L}(M_p^s + 2M_p^m)$	$\frac{384EI}{5L^3}$	$V = 0.39R + 0.11F \pm \frac{M_p^s}{L}$
	Plastic	0.66	$\frac{4}{L}(M_p^s + 2M_p^m)$	0	$V = 0.38R_u + 0.12F \pm \frac{M_p^s}{L}$
	Elastic	0.43	$\frac{16M_p^s}{3L}$	$\frac{107EI}{L^3}$	$V_1 = 0.54R + 0.14F$ $V_2 = 0.25R + 0.07F$
	Elastic-Plastic	0.49	$\frac{2}{L}(M_p^s + 2M_p^m)$	$\frac{48EI}{L^3}$	$V = 0.78R - 0.28F \pm \frac{M_p^s}{L}$
	Plastic	0.33	$\frac{2}{L}(M_p^s + 2M_p^m)$	0	$V = 0.75R_u - 0.25F \pm \frac{M_p^s}{L}$
	Elastic	0.55	$\frac{6M_p^s}{L}$	$\frac{132EI}{L^3}$	$V_1 = 0.17R + 0.17F$ $V_2 = 0.33R + 0.33F$
	Elastic-Plastic	0.60	$\frac{2}{L}(M_p^s + 3M_p^m)$	$\frac{56EI}{L^3}$	$V = 0.62R - 0.12F \pm \frac{M_p^s}{L}$
	Plastic	0.56	$\frac{2}{L}(M_p^s + 3M_p^m)$	0	$V = 0.52R_u - 0.02F \pm \frac{M_p^s}{L}$

Note 1: The provided load-mass factors assume uniformly distributed mass

Note 2: M_p^s = ultimate moment capacity at support; M_p^m = ultimate moment capacity at mid-span

6.4.2 Blast Loads for Equivalent SDOF Systems

Given an explosive charge weight and standoff distance, pressure and impulse data must first be calculated for a bridge component of interest. This can be done in several ways with corresponding levels of fidelity. The simplest and lowest fidelity approach is to use empirical data relating scaled standoff for an equivalent TNT charge weight to various blast effects parameters [50] to calculate pressure and impulse data over the blast-loaded surface of a bridge component. Alternatively, a ray-tracing algorithm, such as Bridge Explosive Loading (BEL) [100], can be utilized to generate pressure histories over the incident surface of a bridge component. Ray-tracing algorithms offer an increased level of fidelity in calculating blast loads by explicitly considering threat details such as explosive composition, charge shape, and reflecting surface geometry. The most rigorous and highest fidelity approach to calculating blast loads is to perform a computational fluid dynamics (CFD) simulation. A CFD simulation can capture the detonation event and ensuing fluid-structure interaction between the impinging shock wave and a bridge component of interest. Depending on whether a coupled or uncoupled CFD simulation is desired, the target could be represented as either non-responding (i.e., rigid) or deformable. Like the ray-tracing approach, reflected pressure histories can be obtained from a CFD simulation. However, unlike the ray-tracing approach, the CFD approach is capable of explicitly capturing complex shock flow phenomena such as overpressure stagnation and

clearing, diffraction, drag, and flow engulfment, all of which can have a significant influence on net blast loads—especially for slender structural components such as beams and columns. While the CFD approach offers the highest level of fidelity in calculating blast loads, it is also the most time-consuming and complex approach.

Once pressure and impulse data have been calculated for a given explosive threat and bridge component of interest, spatial and temporal simplifications to the load data are typically made to yield a single, representative load pulse to be used as the forcing function for an equivalent SDOF dynamic analysis. Various simplification procedures have been put forth for specific bridge components [18, 33, 34], and the most commonly used approach for an impulsively driven structural element—that is, a structural element having a fundamental natural period that is at least 5π times larger than the blast pulse duration [46]—is presented below.

The procedure for developing a representative right-triangular blast pulse for use in an equivalent SDOF dynamic analysis begins by calculating equivalent uniform specific impulse and reflected pressure values, as shown in Equations (6-9) and (6-10). These equivalent uniform load parameters maintain external work equivalency with the actual spatially varying load parameters, and they conveniently permit the use of a shape function (and load-mass factors) based on a structural component's flexural response under the action of a uniformly distributed load. It should be noted that for planar slab-type elements, reflected pressure/impulse distributions and the flexural shape function would be known in terms of two spatial coordinates. Therefore, Equations (6-9) and (6-10) would contain area integrals. Next, a pulse duration is calculated such that the equivalent uniform specific impulse is preserved. This is done by setting the magnitude of a hypothetical right-triangular pressure pulse equal to the equivalent uniform reflected pressure and solving for the pulse duration that sets the integral of the pressure pulse equal to the equivalent uniform specific impulse. The resulting equation for an impulse-preserved right-triangular pulse duration is provided in Equation (6-11). Finally, the magnitude of the right-triangular blast pulse is calculated by multiplying the equivalent uniform reflected pressure by the length and width of a target's blast-loaded face, as shown in Equation (6-12). The resulting blast pulse, to be used as the forcing function in an equivalent SDOF dynamic analysis, is graphically depicted in Figure 6.6.

$$I_{eq} = \frac{\int_0^L I_{peak}(x) \psi(x) dx}{\int_0^L \psi(x) dx} \quad (6-9)$$

$$P_{eq} = \frac{\int_0^L P_{peak}(x) \psi(x) dx}{\int_0^L \psi(x) dx} \quad (6-10)$$

$$t_d = \frac{2I_{eq}}{P_{eq}} \quad (6-11)$$

$$F_{max} = P_{eq} b L \quad (6-12)$$

where:

$I_{peak}(x)$ = distribution of peak specific impulse along component length

$P_{peak}(x)$ = distribution of peak reflected pressure along component length

$\psi(x) = y(x,t)/y_{max}(t)$ = normalized displacement field (i.e., shape function)

P_{eq} = equivalent uniform reflected pressure

I_{eq} = equivalent uniform specific impulse

t_d = duration of right-triangular blast pulse (see Figure 6.6)

F_{max} = peak total load of right-triangular blast pulse (see Figure 6.6)

b = width of structural component's blast-loaded face

L = length of structural component's blast-loaded face

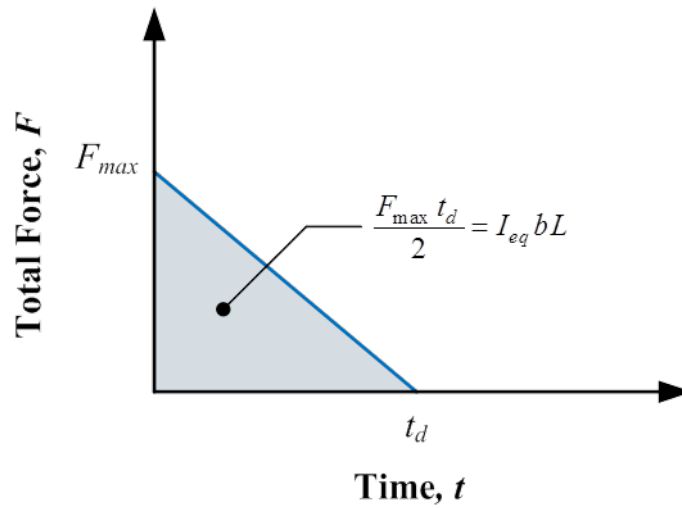


Figure 6.6 Right-Triangular Blast Pulse for Equivalent SDOF Dynamic Analysis

6.4.3 Resistance Functions

As mentioned in Section 3.1.1, the use of a resistance function to describe the restoring force of an equivalent SDOF system provides a convenient way to incorporate constitutive and geometric nonlinearity, as well as complex component response modes, into a dynamic analysis. Figure 6.7 illustrates this feature for the familiar case of a fixed-fixed flexural member designed to develop its full flexural capacity and subjected to a uniformly distributed load. The resistance function can capture the different types of responses of flexural members, including the development of plastic hinges and tension membrane response. Tension membrane response is a large-deformation mode of response that can be engaged typically after the flexural response and it involves cable- or fabric-like behavior dominated by axial tension forces. It should be noted that there is no well validated approach for including tension membrane response in a resistance-

deflection relationship due to a number of variables affecting tension membrane that are difficult to understand and control, even under test conditions.

Because the deflected shape of the flexural member changes with the development of plastic hinges, a unique shape function and load-mass transformation factor are required for each stage of response. Tables of load-mass factors and resistance function control points for a variety of idealized continuous systems were provided in Section 3.1.1. Figure 6.8 provides another qualitative example of the ability to capture complex component behavior with a resistance function. Figure 6.8 represents the evolution of direct shear response, from peak shear strength to post-peak residual capacity due to kinking of longitudinal steel reinforcement. For complex continuous systems not covered in these tables, load-mass factors and resistance functions can be derived computationally or experimentally.

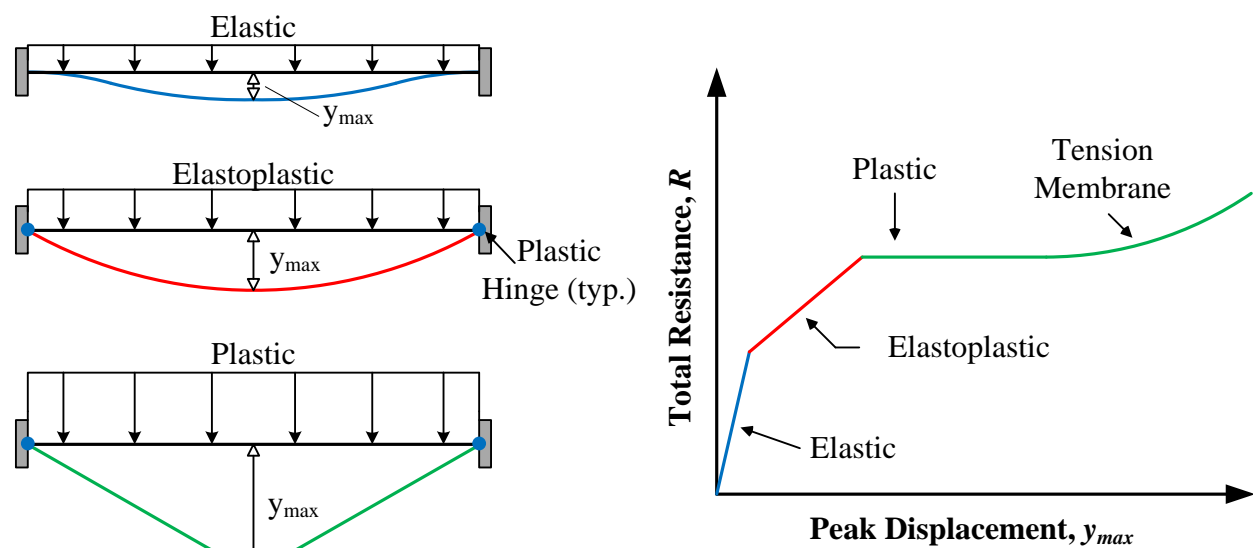


Figure 6.7 Schematic of Equivalent SDOF Flexural Resistance Function [18]

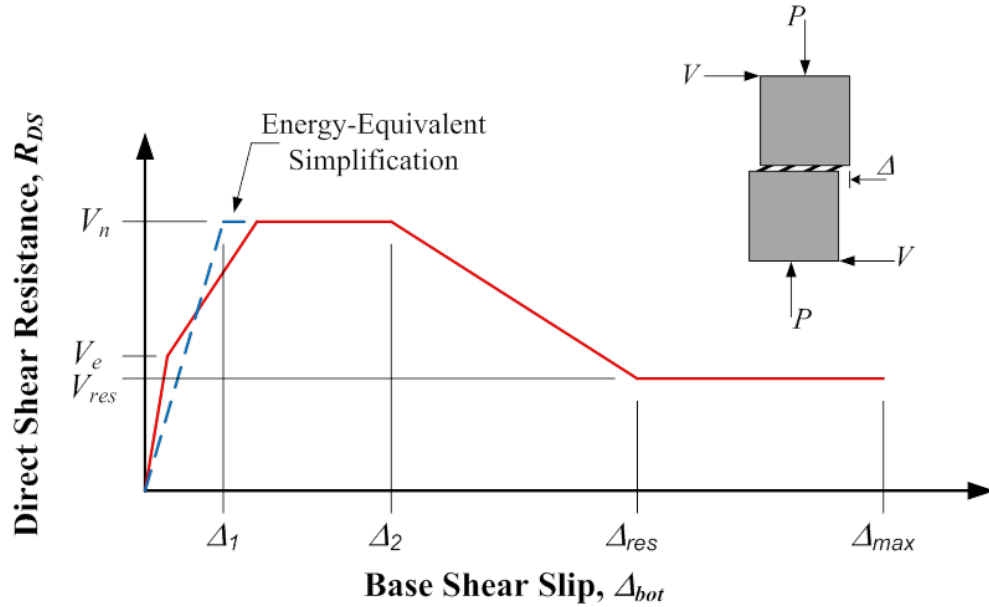


Figure 6.8 Qualitative Direct Shear Resistance Function for Reinforced Concrete Flexural Member [18]

Figure 6.9 illustrates the experimental development of a resistance function for a cold-formed steel stud. The load tree testing apparatus aims to simulate a uniformly distributed load. During the test, structural steel bracing elements were placed along the length of the stud to prevent a premature buckling failure. Bracing against global buckling permitted the stud to reach the tension membrane regime of response, shown in the Figure 6.9 plot.

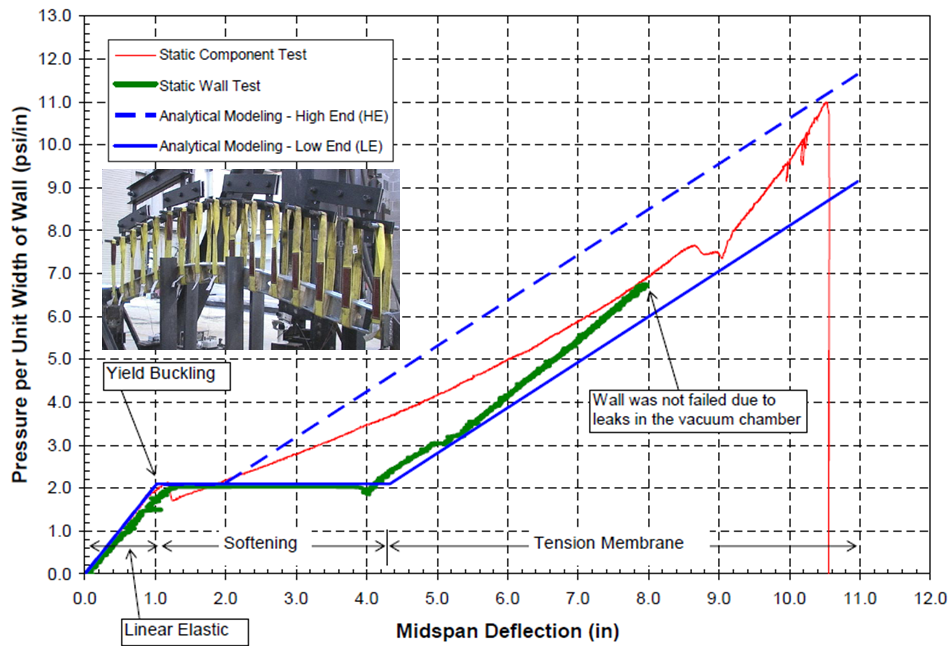


Figure 6.9 Experimental Development of Resistance Function for CFS Stud [101]

6.5 Multi-Degree-of-Freedom (MDOF) Systems and Finite Element Analysis

The equivalent SDOF analysis approach described in Section 6.4 is highly advantageous for design activities because it is computationally expedient, relatively simple to conduct, and focuses on the types of peak response quantities that typical performance-based, component design provisions consider. Nonetheless, such an analysis approach has limited applicability. Equivalent SDOF models are not capable of computing detailed force and deformation response quantities throughout a structural component's entire computational domain. In addition, an a priori knowledge of the component's dominate response mode(s) must be known to postulate realistic shape functions and formulate an appropriate resistance function. For situations involving complex multi-modal component behavior, response coupling between multiple components, complex load definitions, and/or severe localized response (e.g., spall and/or breach damage), it may be necessary to employ a multi-degree-of-freedom (MDOF) analysis approach.

MDOF analysis approaches can range in complexity from two-dimensional frame analyses to rigorous three-dimensional finite element simulations. Frame analyses offer the ability to idealize a structural component as an assemblage of line elements encompassing multiple displacement degrees of freedom, thus allowing for multi-modal response. In addition, an MDOF frame model can comprise structural systems, which enables the interaction among individual responses of multiple members (i.e., response coupling) to be captured computationally. This feature can be particularly important for situations involving structural assemblages consisting of members having fundamental natural periods of vibration that differ by less than a factor of two [94]. Material nonlinearity is typically addressed using lumped plasticity (i.e., plastic hinges), the onset of which is handled via yield criteria on the stress resultant level. Geometric nonlinearity can be incorporated into the analysis by implementing a tangent stiffness matrix (P- δ effect) and enforcing incremental equilibrium on the deformed configuration of the structure or structural component (P- Δ effect). Blast loads are introduced as force histories applied to nodal locations throughout the computational domain. As such, MDOF frame analyses uncouple structural response from blast load history. There exist several commercially available frame analysis programs capable of conducting a nonlinear dynamic analysis. While MDOF frame models offer additional analysis capabilities beyond that of equivalent SDOF models, they still lack the level of resolution afforded by sophisticated three-dimensional finite element simulations.

The difference in solution resolution between MDOF frame models and three-dimensional finite element simulations are qualitatively illustrated in Figure 6.10. Figure 6.10a is an illustration of an advanced single-component MDOF frame analysis for blast-loaded reinforced concrete building columns [102], and Figure 6.10b compares the response prediction of a blast-loaded reinforced concrete bridge column using a high-fidelity finite element model with that observed during the actual blast test [33]. Unlike MDOF frame models, sophisticated three-dimensional finite element models discretize the entire geometry of a structural component. Such a computational domain allows for stress and strain histories to be tracked at essentially any material point within the structural component. This level of resolution captures three-dimensional aspects of component response, and it permits a detailed representation of damage evolution. Early-time stress wave transits within the computational domain can lead to localized material failure (i.e., spall and/or breach damage), and the effects of early-time material damage on component response can be captured. Unlike MDOF frame models where plastic hinging is typically lumped at a single nodal location, high-fidelity finite element models well

accommodate the spread of plasticity and consequent onset of finite length plastic hinges. In addition to increased resolution from a behavioral point of view, three-dimensional finite element models offer greater flexibility in blast load definition.

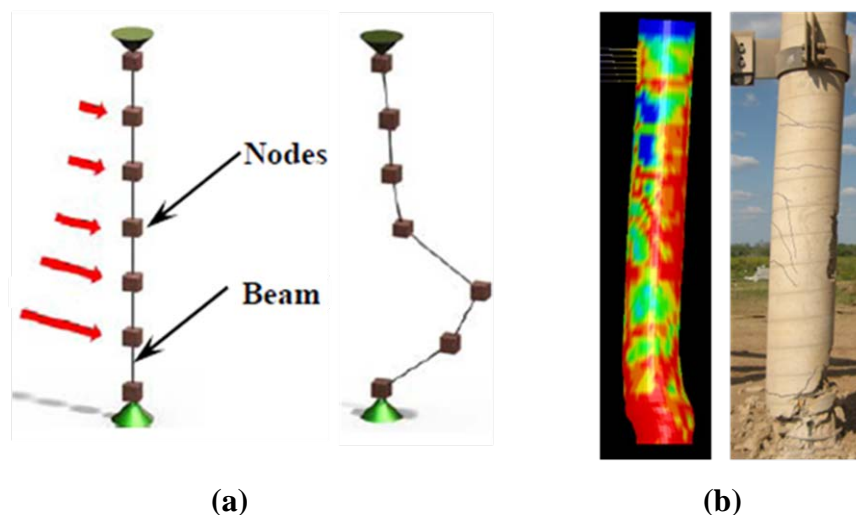


Figure 6.10 Illustration of MDOF Analysis Approaches, (a) Advanced Single-Component Frame Analysis [102], (b) 3-D Finite Element Simulation [33]

Traditional finite element simulations of structural members typically consist of a purely Lagrangian mesh—that is, field variables are related to spatial coordinates and material points are tied to and move with the computational domain—wherein pre-defined load histories are employed. The development of load histories can be done via any of the load characterization techniques described in Section 6.4.2 or Chapter 4 of this manual. Such an analysis approach is termed *uncoupled* because the interaction between the blast load and structural component is neglected (i.e., loads are determined independently and used as input to the response analysis). The most rigorous and complex approach to simulating the response of blast-loaded structural components is to conduct what is typically referred to as a *coupled* analysis. A coupled analysis involves the simulation of the impinging shock wave and structural component. A purely Eulerian mesh—that is, material “flows” through a fixed computational domain—can be implemented for such an analysis, where the explosive material, air, and structural component are all modeled as “fluids.” However, aside from uncoupled CFD blast load characterization as previously described in Section 6.4.2, a purely Eulerian mesh description is only useful when considering extreme loading scenarios involving contact or near-contact detonations. Under these loading conditions, component response can be viewed as hydrodynamic in nature, where inertia initially governs the process and material strength is a second-order effect [103]. For such loading scenarios, the primary interest from a dynamic analysis point of view is to predict the extent and severity of local material damage incurred by a structural component. A purely Eulerian mesh description should not be used to computationally investigate component response of a structural element.

For threat scenarios involving a bulk explosive charge at some appreciable standoff from a target of interest, a coupled analysis requires utilization of a multi-physics modeling approach that comprises Lagrangian and Eulerian mesh descriptions. In general, including fluid flow (i.e., Eulerian shock wave propagation) and solid mechanics (i.e., Lagrangian structural response) in a

single computational model is challenging. Careful attention must be paid to the definition of appropriate contact algorithms and interface mesh descriptions to accurately facilitate fluid-structure interaction between the impinging shock wave and structural component of interest.

Three-dimensional finite element simulations offer enhanced solution resolution relative to equivalent SDOF models and MDOF frame analyses; however, this benefit comes at the expense of increased complexity and resource demand. Constructing an appropriate finite element mesh requires an experienced analyst. Mesh geometry, directionality, and density, as well as element formulation, can all have a significant influence on the fidelity of computed results. For coupled analyses, considerable care must be exercised in defining appropriate coupling algorithms and interface mesh descriptions to handle the interaction of the blast load with the structural component. Regarding material response, sophisticated constitutive models with empirically calibrated parameters are often required. In developing an appropriate constitutive model, strain-rate effects should also be considered. From a computational resource point of view, it should be noted that standard laptops with factory hardware are generally not capable of handling detailed finite element simulations. Parallel processing is commonplace with large and/or coupled simulations, and an exceptionally large amount of random access memory (RAM) is often required. Pre- and post-processing large finite element simulations can also be challenging. While being able to track stress and strain histories at any material point within the computational domain may be a desired feature, it also creates an exorbitant amount of output that must be stored, post-processed, and correctly interpreted. A large amount of output often requires extremely large hard drive space and a long time to post-process. From a design point of view, sophisticated finite element analyses can be more of a hindrance than an aid. Design information such as section kinetics (forces and moments) and kinematics (displacements and rotations) are not standard outputs. Finally, and perhaps most importantly, it should be emphasized that three-dimensional finite element analyses are not justified for situations where the load input or threat information is not well defined. “It is a waste of time to employ methods having precision much greater than that of the input of the analysis [94].”

6.6 Chapter Summary

Dynamic analysis is a critical step in the overall protective design of a bridge structure. Dynamic analysis results serve as input to detailed structural design, and thus have a direct effect on design quality and adequacy. This chapter began with a brief introduction to structural dynamics with emphasis on the unique load and structural response aspects associated with airblast loading from a high-explosive detonation. A rigorous dynamic analysis process was recommended in Section 6.1, along with a list of various influential factors that should be considered during the process. A discussion on performance criteria was given in Section 6.2, during which a comparison was made between buildings and bridges to highlight the relative infancy of performance-based design for the latter. The derivation and application of pressure-impulse diagrams was provided in Section 6.3. The single-degree-of-freedom dynamic analysis approach was introduced in Section 6.4, including: the derivation and application of equivalent SDOF systems, tables of equivalent SDOF system properties for commonly encountered structural components, the treatment of blast loads for equivalent SDOF systems, and the derivation and application of resistance functions. The equivalent SDOF analysis approach is by and large the current state-of-the-practice for blast-resistant design and thus was covered in the greatest detail. Multi-degree-of-freedom dynamic analysis approaches were discussed in Section 6.5, with

emphasis on practical application, technical and computational resource requirements, and limitations.

Unique dynamic analysis aspects specific to bridge components are addressed in the component-specific design chapters of this manual, as well as the use of ATP-Bridge to perform a dynamic analysis of bridge components. Protective design strategies specific to reinforced concrete bridge columns are discussed in the next chapter.

7.0 PROTECTIVE DESIGN GUIDANCE FOR REINFORCED CONCRETE COLUMNS

Bridge columns subjected to blast loads and other terrorist threats demonstrate a wide range of response modes depending upon the severity of the threat. Less severe threats can often be mitigated with limited protective design measures and often lead to a response governed by flexure and diagonal tension shear, with limited localized damage. Under severe threats associated with large quantities of explosive near or contact with a column, localized behavior at discrete sections governs response. Under such conditions, failure modes specific to high intensity, short duration loading must be considered. These response modes include localized spall and breach at a cross-section and direct shear at the column supports (primarily the base). Such behavior is usually not of concern under typical loading conditions. Additional details regarding the response of blast-loaded columns are described subsequently in this chapter.

7.1 Design Loads

Threats of primary concern in the protective design of reinforced concrete bridge columns are due to the detonation of high explosives in close proximity. These loads can cause extremely large pressures and impulses, leading to column damage and potentially failure. Other threats of concern include fragment loading associated with the detonation of an explosive, intentional ramming by high-speed vehicles, linear shape charges and other types of contact charges that produce highly localized damage, and standoff weapons such as flyer plates or rocket propelled grenades (RPGs). Intentionally set fires may also be a concern. Additional details describing these loads and threats are provided in the following subsections.

7.1.1 Blast Loads

When blast loads act on bridge columns, careful consideration must be given to the variation in pressure that develops along the height of the column and how this variation in intensity changes with time. Further, the shape of a column and the way pressures act on a given cross-section must also be considered. For example, the interaction of blast overpressures on a round column is notably different than a square or rectangular column. Unlike wind loads that cause negative pressures to develop on the leeward side, blast overpressures are larger than atmospheric pressure and therefore give rise to positive pressures acting around the perimeter of any given cross-section. Thus, the pressures that rapidly engulf a typical blast-loaded bridge column must be accounted for when determining the loading history as a function of time and location.

For massive structural components such as typical reinforced concrete bridge columns, structural response has been shown to depend strongly upon applied impulse rather than peak overpressure. As such, of greatest concern when predicting loads acting on bridge columns is the area under the pressure history (i.e., impulse) rather than the value of overpressure at any one specific time.

Various researchers have proposed load modification factors on impulse to account for the differences between round and rectangular cross-sections. Several researchers have proposed constant reduction values ranging from 0.8 [104] to 0.85 [26]. Shi et al. [105] performed a series of computational fluid dynamics simulations to investigate shock wave behavior near rectangular and circular columns. During the study, it was found that leeward face overpressures tend to develop quicker for circular columns because their smooth circumference minimizes flow

separation as the shock wave diffracts around the section. In addition, it was found that rectangular column width (normal to the shock propagation direction) has more influence on the resulting blast load than column depth. The wider the rectangular section, the more drastic the flow separation and the longer it takes to generate leeward face overpressures. As part of a large research effort for the National Cooperative Highway Research Program [24] to develop blast-resistant design provisions for reinforced concrete bridge columns, Williams [33] conducted a detailed experimental and computational study characterizing the behavior of shock waves near slender structural components of square and circular cross sections. During Williams' study, clearing and wrap-around pressure effects were found to contribute to a reduction in the applied blast load; however, it was also observed that (a) the impulse reduction factor depends on the ratio of physical standoff to section width (or diameter in the case of a circular section), and (b) given a circular column with a diameter equal to the width of a square column, the circular column tends to experience a lower net blast load. Williams' findings are graphically summarized in Figure 7.1.

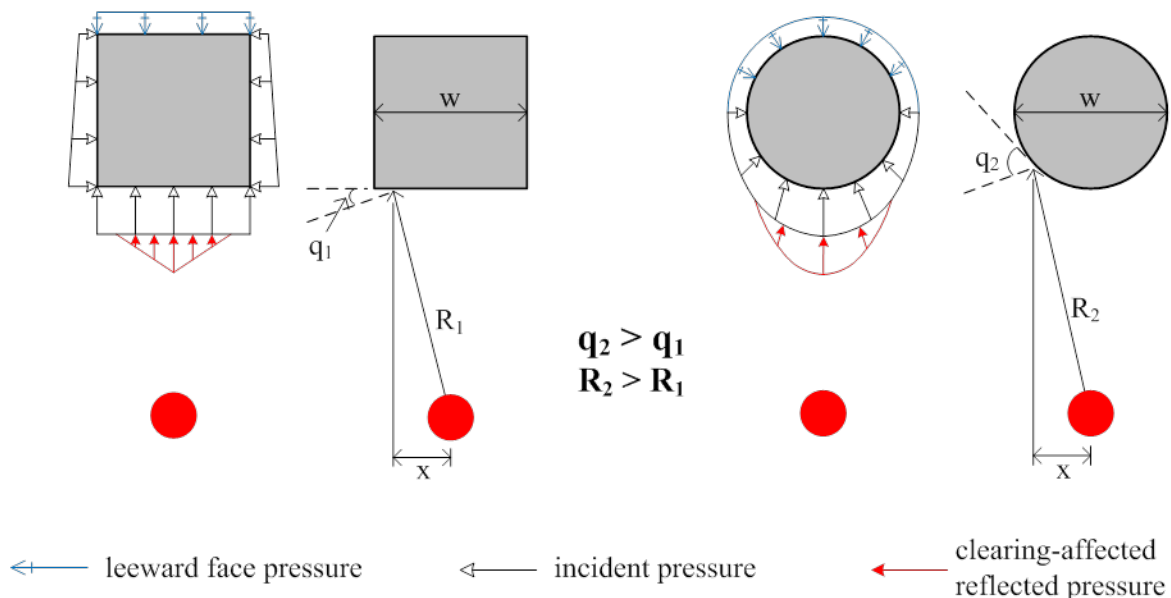


Figure 7.1 Effect of Section Shape on Physical Standoff and Angle of Incidence [18]

The pressure distributions on the square and circular sections represent a snapshot in time, where the solid-arrow pressure distributions are the clearing-affected reflected pressures, the dash-arrow pressure distributions are the leeward face overpressures due to shock flow engulfment, and the hollow-arrow pressure distributions are the incident pressures. The point of interest where the angle of incidence and reflection are shown on both sections is located at the same horizontal distance away from the charge center of gravity (CG). For the specified point of interest, the angle of incidence and physical standoff are both greater for the circular section than the square section, which is true for every point along the front half of the circular section's circumference except for the point directly in front of the charge CG where the section experiences a normal reflection. While the difference in physical standoff is inconsequential for large-standoff threat scenarios, it can have a significant influence on the blast load resulting from a small-standoff detonation—a likely threat scenario for a reinforced concrete bridge column. Another contributing factor to the lower net blast load experienced by the circular section could

potentially be the minimized flow separation and hence quicker leeward face overpressure generation afforded by its smooth geometry, as pointed out previously by Shi et al. [105]. It should also be mentioned that the circular section in Figure 7.1 inscribes the square section, implying that the circular section has less material than the square section. Consequently, the circular section provides less inertial resistance to a blast load than the square section, perhaps marginalizing the difference in net blast load between the two section geometries. In fact, while Williams [33] demonstrated that even though circular columns must resist less load than the same sized square columns, they also have less overall resistance. Thus, the overall damage experienced by the two different cross-sections varied by threat scenario. Sometimes, the square columns performed better even though they had to sustain a higher load. These results suggest that it is difficult to establish general conclusions on the response of blast-loaded components and analyses must be conducted to fully understand the response of a column to a specific threat.

Based on the results of Williams' study, empirical impulse reduction expressions for square and circular sections were proposed, and they are given in Equations (7-1) and (7-2) respectively. These expressions represent a lower bound, and hence conservative estimate of impulse reduction based on the available data. Furthermore, the proposed expressions are valid for (R/D) ratios less than 4.5.

$$\zeta_s = 0.013 \frac{R}{D} + 0.49 \quad (7-1)$$

$$\zeta_c = 0.019 \frac{R}{D} + 0.39 \quad (7-2)$$

where:

ζ_s = impulse reduction factor for square sections

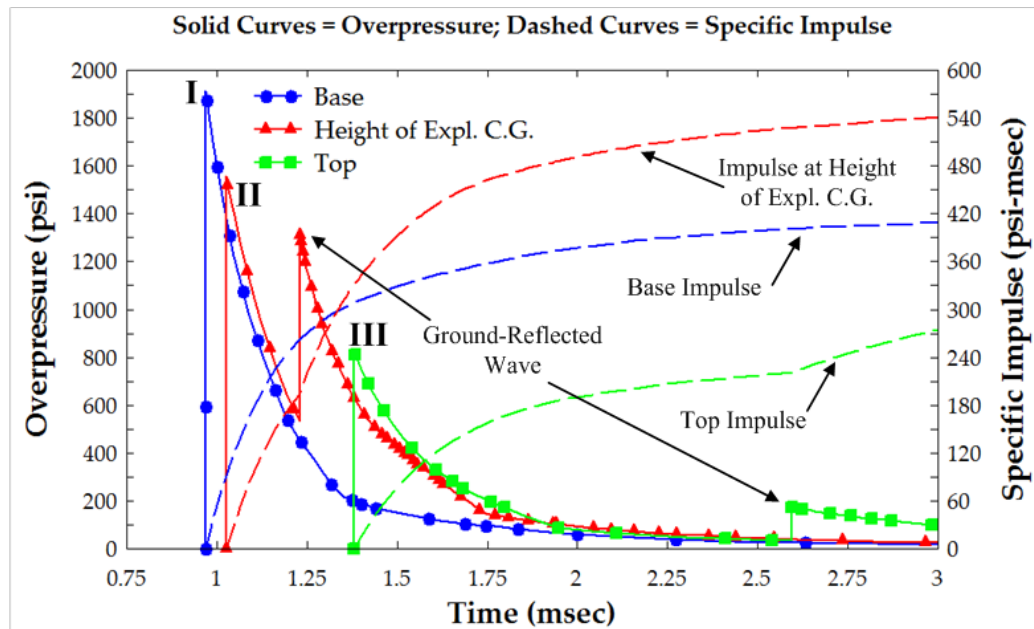
ζ_c = impulse reduction factor for circular sections

R = physical standoff distance [ft]

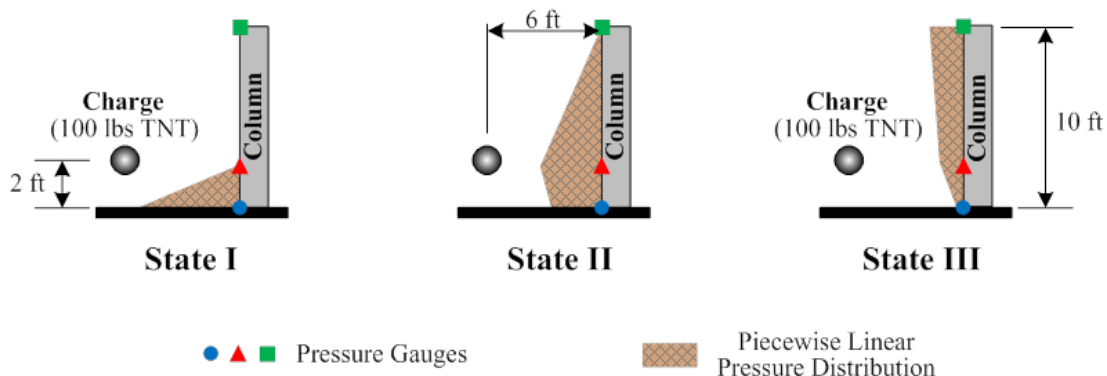
D = section diameter or edge width facing load [ft]

In cases where standoff distance is large, blast pressures are reasonably approximated as being uniform over the structure or component being analyzed. In cases of close-in detonations, which are important threat scenarios for bridge columns that are easily accessible, the variation in pressure with time and column position becomes an important consideration for accurately computing loads [33]. Figure 7.2 shows a close-in detonation of a spherical charge acting against a column. In the graph shown in Figure 7.2a, the solid curves with symbols represent pressure histories, and the dashed curves represent specific-impulse histories. The different curve symbols in Figure 7.2a correspond to different locations along the column height, as indicated in the graph legend as well as in Figure 7.2b. Perhaps the most apparent observation that can be made from the graph of Figure 7.2a is that, unlike the case of a planar shock front, the overpressure and specific impulse histories vary along the column height. Regarding spatial load variation, the peak overpressure occurs at the column base, whereas the peak specific impulse occurs at the elevation of the charge CG. Both peak load quantities are well in excess of those delivered to the top of the column. Upon closer inspection of the Figure 7.2a pressure history curve at the height

of the charge CG, two overpressure peaks occur. As indicated in the graph, the second peak can be attributed to the trailing ground-reflected shock wave that results from a regular oblique reflection. Because the charge is in such close proximity to the column, the critical angle of incidence is never achieved. Consequently, the incident and ground-reflected shock waves never coalesce to form a Mach stem, and the two waves strike the column at different times. This near-field reflection behavior is also manifested in the pressure history at the top of the column (i.e., the solid curve with square symbols in the graph of Figure 7.2a).



(a)



(b)

Figure 7.2 Blast Load Characterization for Reinforced Concrete Column Subjected to Close-In Detonation: (a) Overpressure and Specific Impulse Histories, (b) Variability in Overpressure Distribution with Time [18]

The three elevation sketches in Figure 7.2b emphasize the transient nature of a close-in detonation. The three blast load states depicted in the three elevation sketches correspond to the roman numerals in Figure 7.2a. The roman numerals identify snapshots in time where the three

pressure gauges experience their peak overpressure. In Figure 7.2b, the hatched areas represent piecewise linear approximations to the spatial distribution of overpressure acting along the column height. Note that over a time interval of roughly two milliseconds, the spatial distribution of overpressure exhibits significant variation. For the given threat scenario, the assumption of a uniform spatial distribution of applied overpressure or specific impulse would result in a poor representation of the true blast load.

For close-in explosions typical of the threats against bridge columns, charge shape could be important because it defines the shock front geometry [46] and hence the pressure and loading history. An example of this effect for a cylindrical charge oriented with its longitudinal axis normal to the ground surface was presented in Chapter 4 of this manual. Aside from charge shape, the charge orientation, and the point of initiation (i.e., center-detonated, end-detonated, etc.), as illustrated in Figure 7.3, can also strongly influence the loads acting against a bridge column. For instance, a cylindrical charge oriented with its longitudinal axis normal to the ground surface and top-detonated presents more surface area of explosive material to the target, but the detonation wave progresses toward the ground surface. Whereas, a cylindrical charge oriented with its longitudinal axis parallel to the ground surface and initiated at the end farthest from the target presents comparatively less explosive surface area but drives the detonation wave toward the target. Close-in to a target, these two detonation scenarios would deliver notably different blast loads to a nearby target.

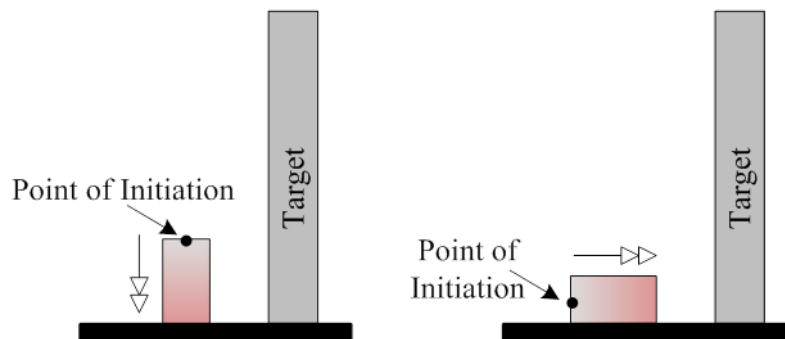


Figure 7.3 Effect of Charge Orientation and Point of Initiation on Blast Load Severity [18]

For threat scenarios involving detonations underneath a bridge, prediction of the loads acting on a column are complicated by reflections off the ground, the deck, and potentially abutments. Figure 7.4 shows a schematic of a scenario in which a charge is detonated above the ground near an abutment. The importance of reflected pressures that develop strongly depends upon the specific geometry of the threat under consideration and varies significantly based on distance to an abutment, column height, explosive charge weight, and height of burst. While not always true, reflections from abutments and decks tend to be phased in time such that the most critical column section (typically at the same height as the charge CG) has been fully loaded before shock reflections can potentially influence performance. Thus, in many cases, the complications with shock reflection can be ignored or approximated because they play a limited role in affecting column response at the critical cross-section. Of course, this simplification does not hold in all cases, and engineering judgment and/or detailed analyses are needed to determine its importance. An initial assessment of performance can be made by computing the time of arrival of peak overpressure at various locations.

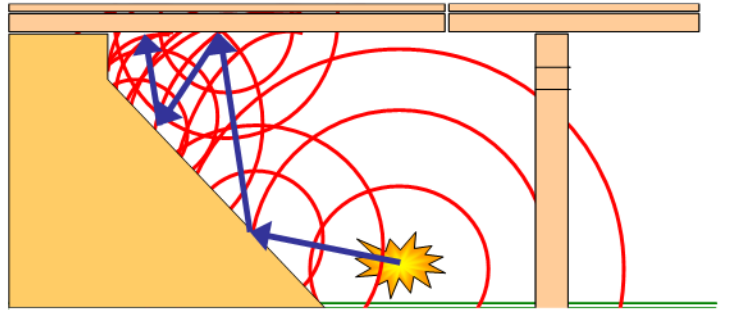


Figure 7.4 Reflected Pressures due to the Ground, Deck, and Abutment [104]

To accurately compute blast loads, it is possible to use simplified chart methods or blast load simulation software specifically developed for this purpose. Within ATP-Bridge, blast loads are computed using a modified version of the BLASTX [106] ray-tracing software as an internal dynamic link library within the program (i.e., this happens automatically without the user needing to specify such an analysis). Users can select the explosive composition (e.g., TNT, C-4, etc.), position, and orientation. In addition, as part of the ATP-Bridge output, users can review computed overpressure histories at twenty different locations along the height of a column. While it is possible to account for important features of close-in explosions in an approximate manner using chart-based procedures, the time and effort needed to do so would be excessive. Furthermore, chart-based methods are not readily able to account for reflections from an abutment, the deck, etc., which make their use in computing blast loads impractical. Therefore, engineers are encouraged to utilize blast load simulation software to accurately compute the loads acting on a bridge column. The most important factors that affect the loads acting on bridge columns due to close-in explosions (e.g., charge weight, explosive type, structure geometry, explosive shape, explosive orientation, deck reflections, clearing, flow engulfment, etc.) are all included in the load prediction procedure used by ATP-Bridge.

7.1.2 Other Loading Considerations

Aside from pressure loads resulting from the detonation of an explosive, bridge columns can also be subjected to several other potential loads associated with a terrorist threat, including fragment loads, vehicle impact, ground cratering, and fire. In general, fragments are pieces of matter that get propelled through the air during a detonation event. Fragments can be particles produced by the airblast during the breakup of nearby objects, or they can be pieces of an explosive casing. When a fragment strikes a target, it imparts an impulse that is additive to that delivered by the shock wave. The magnitude of the additional impulse is a function of the fragment's mass and impact velocity. While seemingly simple in theory, it often proves difficult to quantify such loading because fragments are typically irregular in shape and have a distribution that is difficult to predict [49]. Furthermore, typical casings for terrorist weapons (i.e., vehicle parts, sheet metal, and plastic) are not massive, especially relative to cased military weapons [49]. As such, although they still pose a serious risk of human injury to nearby personnel, fragment loads are typically deemed negligible for the performance assessment of critical bridge components subjected to terrorist threat scenarios involving bulk explosives.

Vehicles used in a malevolent attack can be assumed to be travelling at a velocity that exceeds typical designs for accidental impact. Nonetheless, for highway bridge columns, vehicle speed can usually be controlled through simple sitework measures including ditches, medians, and

bollards or other protective measures. In some cases, however, site conditions do not permit such options, and bridge columns must be designed to withstand direct impact from vehicles. In general, the impact force is a function of the size and speed of the vehicle hitting the bridge. The impact force of a vehicle may be computed using principals of dynamics, which consider the mass, velocity, energy absorption, and deceleration of the vehicle on impact. As crashworthiness criteria have become more demanding over the years (e.g., AASHTO MASH), designs to mitigate vehicle impact have improved. As such, the threat of intentional vehicle collision is expected to be largely mitigated by following required design provisions, though special consideration should still be given to assessing the loads from such a scenario when the situation warrants it.

Ground cratering occurs when soil is ejected from the ground surface due to large pressure loads that may be attributed to an above-ground or shallow-buried explosive. The extent of ground cratering is highly dependent upon charge location, charge weight, and soil conditions. Figure 7.5 shows an 85-foot wide and 35-foot deep ground crater that developed because of the large truck bomb that was set off in front of Khobar Towers in 1996. The development of ground craters can strongly influence the survivability of a bridge column to blast. Except for cases of very weak soil or buried charges, loads from explosives acting directly against a column are of greatest importance. Expressed differently, blasts large enough to cause the ground crater seen at Khobar Towers would be sufficient on their own to cause column failure without ground cratering being of concern. In the Khobar Towers incident, severe building damage occurred despite it being located approximately 72 feet from the truck bomb. If ground cratering is felt to be a special design consideration, ground crater sizes can be estimated using the CONWEP software [97].



Figure 7.5 Ground Crater in Front of Khobar Towers (1996)

Intentional fires may also be of concern, but this threat takes sufficient exposure time to cause damage. In the time it takes for a fire to damage a reinforced concrete bridge column, motorists can evacuate the area. Engineered explosives such as linear shaped charges or other hand-emplaced charges could also be a threat scenario of interest. Given the typical massive size of reinforced concrete bridge columns or the large number of smaller columns that may appear at a given pier, coupled with the highly localized damage these types of threats cause, the primary concern is the loss of section integrity that may occur at a critical location such as a splice region or near the ends. Provided steps are taken to locate critical regions away from places that are

easily accessible, the localized damage associated with hand-emplaced charges, RPGs, linear shape charges, etc. can be readily mitigated.

7.2 Failure Modes and Performance Criteria

Reinforced concrete bridge columns subjected to blast loads can experience several different failure modes depending upon the specific details associated with the threat scenario under consideration. For cases where reasonable standoff distances can be established, explosive charge weights are small, or improvised explosives are not highly energetic, RC bridge columns will respond primarily in flexure. This mode of response is often termed as a “global” response mode because the entire length of the member is engaged in the response, and the section properties and support conditions play an important role in the behavior exhibited. Blast damage for this range of response can lead to the development of flexural cracking, and it can also cause diagonal tension shear cracks that are attributed to the sectional shear associated with flexure.

As loading becomes more severe, other failure modes start to dominate behavior. First, localized spall and breach damage becomes noticeable. This type of damage is associated with stress wave propagation through a given cross-section and is essentially independent of the member support conditions. Second, a mode of failure that is unique to blast-loaded structural components in this threat regime involves highly localized damage near the end regions of a column. For threat scenarios involving vehicle-borne improvised explosive devices (VBIEDs), based on typical column heights and heights of burst associated with trucks and other vehicles, the critical location is primarily the column base.

The terms *spall*, *cratering or crushing*, and *breach* are often used in conjunction with localized sectional damage. Spall is defined as tensile-stress-induced concrete failure caused by stress wave reflections off the side and back faces of a concrete section. Cratering is a compressive-stress-induced concrete failure caused on the front face, and breach occurs when local zones of spalling and cratering meet to produce a through-thickness concrete failure. Figure 7.6 shows pictures of these types of local damage. Column parameters that are most influential in preventing local damage include column diameter and concrete strength.

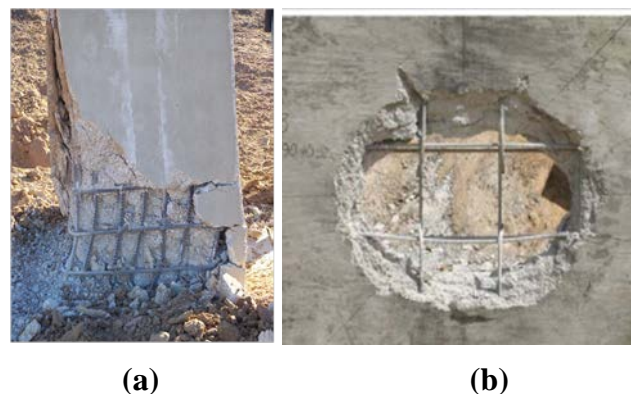


Figure 7.6 (a) Spall Damage to Concrete Column Sides and Cratering Damage to Front Face [24], and (b) Breach Damage [107]

Researchers from the University of Texas at Austin (UT-Austin) conducted an extensive research program with a main objective of developing protective design guidance for blast-loaded RC bridge columns [24, 33, 108]. Part of the program involved subjecting half-scale RC column

specimens to small-standoff bulk explosive detonations. Post-test photos of three blast-damaged column specimens are shown in Figure 7.7. These columns exhibited extensive early-time spall damage followed by discrete slip and/or distributed shear deformation near the column base. This complex, shear-dominated response evolution is collectively termed *dynamic shear behavior*. Researchers from the State University of New York (SUNY) at Buffalo observed similar shear-dominated behavior during an experimental blast test program aimed at investigating multi-hazard design strategies for RC bridge columns [25]. Figure 7.8a shows a SUNY Buffalo test specimen that exhibited a direct shear failure at the column base due to excessively high early-time shear forces. Similar behavior has been observed for building columns directly exposed to blast [109]. The dissertation by Sammarco [18] provides a detailed discussion of this phenomenon and the factors that contribute to its development.

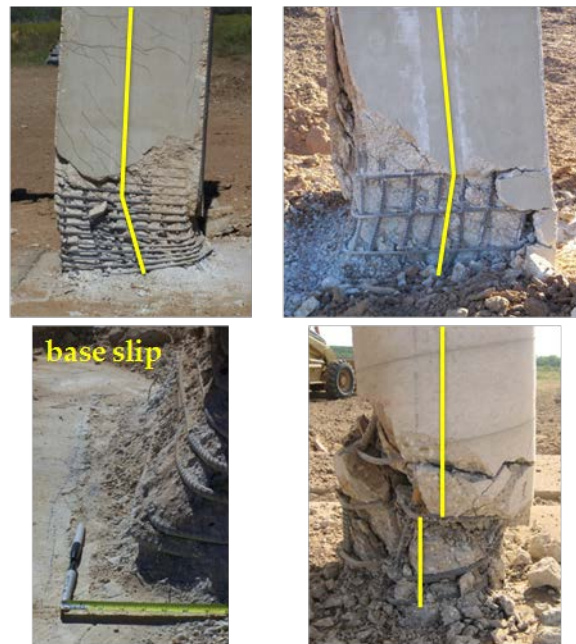


Figure 7.7 Dynamic Shear Response of Half-Scale RC Bridge Column Specimens Subjected to Small-Standoff Bulk Explosive Detonations [24]



Figure 7.8 Shear-Dominated Behavior of Quarter-Scale RC Bridge Column Specimens Subjected to Standoff Detonations [25]: (a) Direct Shear Failure at Column Base, (b) Dynamic Shear Behavior

Performance criteria used to assess the behavior of RC columns subjected to blast loads is based on deformation and ductility. Because of the severe and infrequent nature of blast loads, RC columns are permitted to undergo damage in mitigating blast effects. Localized spall and breach is permitted, as is inelastic material behavior through plastic hinging. Based on the research findings documented in NCHRP 645 [24], different design categories have been established for bridge columns depending upon the design-basis threat. These categories are identified in the NCHRP 645 report [24] and further clarified in the AASHTO *Bridge Security Guidelines* [36]. In the most severe design category (Category C), columns must follow specified detailing requirements to ensure ductile behavior. Further, the maximum plastic hinge rotation must remain less than 10 degrees, and the maximum permissible displacement ductility is 15. For Category C columns, these component-level response limits must be confirmed with a nonlinear dynamic analysis. For columns that fall into less severe design categories, no special blast analysis must be performed, though special detailing may be needed if the threat is moderate (Category B). Readers should consult the above-referenced documents for additional information.

7.3 Design Strategies and Detailing Recommendations

Referring to the AASHTO *Bridge Security Guidelines* [36], design of RC columns to resist blast loads can be placed in one of three categories depending upon the severity of the threat. In Category A, which is the least severe category, no special blast-resistant design requirements are required. In Category B, columns are required to include improved detailing, but no threat-specific analyses are needed. The enhanced detailing is adequate to mitigate threats of this severity. In the most demanding Category C designs, columns are required to utilize blast-specific detailing, which requires 50% more transverse steel than would be used for seismic-

resistant designs. In addition, blast-specific analyses must be conducted using nonlinear structural dynamics. Equivalent linear, static analysis methods are not acceptable.

There is wide agreement that a sound and practical design strategy incorporates the *four D's*: (1) Deter, (2) Deny, (3) Detect, and (4) Defend. The basis for this framework is to implement the most cost-effective mitigation strategies to protect RC bridge columns from blast loads. Because columns subjected to small or moderate threats do not require enhanced blast protection, structural design in this category is straightforward. Nonetheless, consideration must be given to the measures needed to ensure this design category and the costs of these measures. For example, increasing standoff and column protection will reduce the loads a bridge column may need to resist, but the costs for additional real estate, bollards, etc. may cost more than enhanced structural detailing. Further, maintenance costs may also increase if special devices or other features for maintaining standoff are installed. Ultimately, the most cost-effective solution should be sought. Readers are referred to the AASHTO *Bridge Security Guidelines* [36] for an extensive list of techniques that can be used to achieve the four D's of protective design.

For structural modifications, the following recommendations are relevant to the design of RC bridge columns:

- Provide enough shear resistance to develop the full flexural capacity of the RC column, thus precluding a non-ductile, shear-dominated mode of failure (i.e., capacity design approach)
- Increase redundancy by providing multiple load paths. This includes, but is not limited to, decreasing spacing of longitudinal girders and stringers, decreasing deck beam spacing, etc.
- When detailing discrete hoop or tie transverse reinforcement, use “blast hooks” consisting of bars with a 135-degree hook and a tail length equal to the greater of 20 bar diameters or 10 inches.
- Avoid the use of splices in critical (e.g., at the column base) or easily accessible locations.
- Ensure ductile response under large deformations.

Additional detailing guidance for each Design Category can be found in the AASHTO *Bridge Security Guidelines* [36].

7.4 Recommended Design Procedure

For RC bridge columns that fall into blast protection design category A or B, no special analysis for blast is required. For Category A columns, the design is based on all applicable load cases ignoring blast. For Category B columns, enhanced detailing requirements are necessary. The detailing requirements are consistent with seismic detailing and are not expected to negatively influence performance for other applicable load cases. As such, it is recommended that Category B columns be designed as they typically would be for the expected design loads. Then, as a final step, enhanced detailing should be provided.

Category C columns require a nonlinear dynamic structural response calculation to ensure all applicable component-level response limits are met. While this design category addresses the most severe loads designers will need to consider, the column is permitted to undergo large inelastic deformations, and blast will often not control the design. Accordingly, it is recommended that a Category C column first be designed based on all other applicable loads the column in question will need to resist. Then, once a preliminary design has been developed, performance of the column can be evaluated using ATP-Bridge. Detailed examples of the ATP-Bridge software are provided in Section 7.5 of this chapter and throughout this manual. The use of ATP-Bridge is not required, though nonlinear dynamic analysis that accounts for plastic hinging, strain-rate effects, and other aspects of structural response under blast must be included. The use of ATP-Bridge is the simplest and most direct way of assessing the response of Category C columns.

7.4.1 *Boundary Conditions*

Because of the highly-localized nature of blast loads, structural response to these loads tends also to be localized to individual components. While overall system behavior is important in having the ability to redistribute loads from damaged components, this effect typically takes place later in time after component response to blast has already taken place. As such, columns can reasonably be analyzed and designed for blast by treating them as individual elements.

Boundary conditions to use at the column ends will depend upon details of the column-to-foundation and column-to-superstructure connections. In many cases, the column base at the foundation can be assumed as fixed because of the heavy footings or pile caps that are often used in highway construction. The boundary conditions for the top of the column can be idealized based upon the orientation of the charge relative to the column axis and based on the column-to-superstructure connection details. Because bridge girders are stiff axially, it is reasonable to assume no translation occurs along the span of a bridge, though translation may occur perpendicularly to it. A deep cap beam may prevent rotation and allow for the development of bending moment at the column top, while other details may not. ATP-Bridge allows the use of idealized support conditions (free, roller, pin, and fixed) as well as partial restraints that can be specified through translational and rotational elastic springs. Ultimately, engineering judgment is needed to assign specific boundary conditions for a specific threat scenario. Bridge engineers, however, are familiar with making such assumptions for other design loads, and this knowledge can be readily applied to the case of blast loads.

Because acceptable performance under blast is based on deformation and ductility, it is suggested that less rigid support conditions be considered when there is uncertainty with the model to use for the actual case. Less restraint will lead to larger displacements than when greater restraint is specified, so this approach is often the most conservative. Nonetheless, engineers should consider upper-bound and lower-bound cases, particularly when there is uncertainty regarding the boundary conditions, to ensure the final design satisfies all applicable limits. As such, this may require performing one analysis assuming a fixed condition at the upper column support and another analysis assuming a roller condition. Because ATP-Bridge can perform these analyses quickly on a PC, this evaluation can be rapidly completed to ensure the column under consideration will perform within the expected bounds.

7.4.2 Analysis Approach

Only columns in Design Category C require analysis for a specific blast threat scenario. Analyses for this category must consider dynamic structural response, nonlinear structural response, strain-rate effects, and localized damage. Such analyses cannot be readily accomplished using hand-based solution techniques. These analysis requirements are supported by the ATP-Bridge software and require little prior experience by program users to effectively employ this analysis approach. If ATP-Bridge is not used, it is recommended that analyses be conducted with computer software having the features described above. Advanced frame analysis software that allows a column to be analyzed using multiple frame elements is one option, and nonlinear finite element software is another option. When using either of these options, special care should be taken to accurately define the load as a function of time and position over the entire column height. The applied loads should account for suitable reductions based on column cross-section shape (see Section 7.1.1). Due to the difficulty in accurately defining loads, appropriate nonlinear material models, damage-dependent response, and other aspects of behavior under blast, it is recommended that only very experienced engineers pursue this option. In addition, it is highly recommended that validation studies be conducted prior to applying general analysis techniques to a new design. While this approach may be reasonable and appropriate for unique designs or for bridges deemed to have a high likelihood of being attacked, it is expected that the vast majority of designs can be accurately determined through the use of ATP-Bridge.

7.4.3 Structural Design

A common perception is that designing bridge columns to resist blast will result in large cost increases. When blast is considered as part of the design for a new bridge, the increase in costs for the vast majority of cases is expected to be small. Structural design to mitigate blast requires the use of additional transverse reinforcing steel to ensure ductile behavior, and it may also require additional flexural steel and/or an increase in column size depending upon the design-basis threat. Nonetheless, if these design modifications to typical designs are established at the outset of new projects, the increase in costs is relatively small. For retrofit of existing bridges, structural mitigation techniques can be expensive. This issue is discussed further in Section 7.5.

The general structural design procedure for designing RC bridge columns for blast requires first establishing the design-basis threat, then determining the appropriate design category based on the severity of the threat, and finally providing the necessary detailing. As described previously, only columns in Design Category C require nonlinear dynamic analysis under the predicted blast loads. Then, like design for any other load, iterations may be needed to meet the performance criteria. Detailed examples showing this process are provided in the next section.

7.5 ATP-Bridge Design Examples

The following design examples aim to illustrate the design process for reinforced concrete highway bridge columns subjected to blast loads. Each design example utilizes the ATP-Bridge software presented in Chapter 12 combined with the design guidance presented in Chapter 7. Standard column designs, boundary conditions, and material properties were selected for the design examples, based upon design examples found in NCHRP Technical Report 645 [24].

Design Example 1

The following design example considers the response of a reinforced concrete bridge column for a relatively large threat. Evaluate the column, designed for a non-seismic region, for the given close-in blast load. If the column is insufficient, redesign the column to meet all applicable design checks. Refer to Figure 7.9 for threat details and Figure 7.10 for column design details. Use ATP-Bridge to perform the analysis and design. Figure 7.11 provides a sample of the required column geometry inputs to setup the design example in ATP-Bridge. A sample of the required load inputs for ATP-Bridge is provided in Figure 7.12.

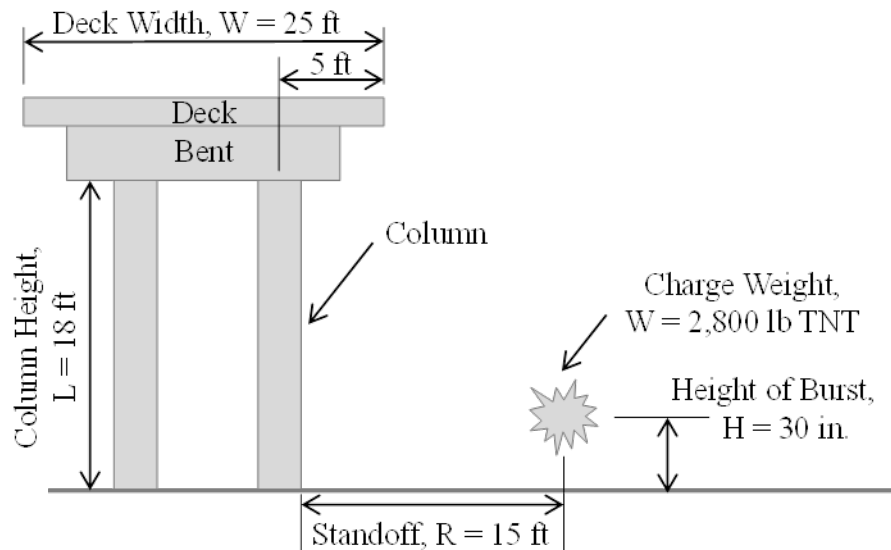


Figure 7.9 Design Example 7.1 Elevation

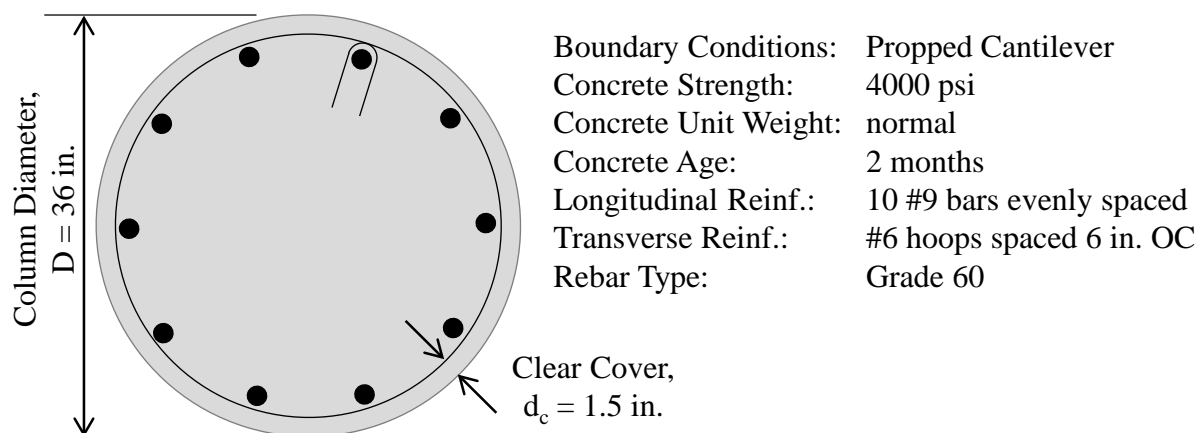


Figure 7.10 Design Example 7.1 Details

Geometry Supports Material Advanced

Section
Elevation

90 Deg

180 Deg

0 Deg

270 Deg

Global Dimension Transverse Rebar Longitudinal Rebar

Overall Geometry

Height: 18 ft

End Region Length: 2 ft

Diameter: 36 in

Global Dimension Transverse Rebar Longitudinal Rebar

Spacing & Clear Cover

End Region Spacing: 6 in

Interior Region Spacing: 6 in

Cover: 1.5 in

Type & Size

Type: Hoops

Bar Size: # 6

Diameter: 0.75 in

Figure 7.11 Design Example 7.1 Sample Column Geometry Input

The screenshot shows the 'Static Load' tab in the ATP-Bridge software. The top panel is a 2D coordinate system with a red circle (explosive charge) at (15, 0) and a white circle (column) at (0, 0). The bottom panel contains the following input fields:

Explosive Info.	
Charge Weight:	2800 lbs
Charge Diameter:	44.95 in
Shape:	Spherical
Orientation:	Vertical
Type:	TNT (density 1.63 g/cc based on 64 kg)

Distances	
Distance X:	15 ft
Distance Y:	0 in
Direction Z:	30 in

Deck Geometry	
Deck Width (+X)	60 in
Deck Width (-X)	240 in
Deck Width (+Y)	150 in
Deck Width (-Y)	150 in

Figure 7.12 Design Example 7.1 Sample Load Input

In response to the given threat of 2,800 lb of TNT at a 15-ft standoff distance, the 36-in. diameter column suffers a breach failure near the threat location (see Figure 7.13). The initial column design is insufficient for the given blast load due local breaching failure, therefore the column must be redesigned. Several design variables can be adjusted including column diameter, concrete strength, concrete cover, transverse reinforcement, and longitudinal reinforcement. Span and boundary conditions are assumed to be constant. In the following section, each variable is adjusted to illustrate the positive and negative attributes of each possible solution.

Column diameter is evaluated first. Increasing the column diameter from 36 in. to 60 in. for a threat of 2,800 lb of TNT at a standoff distance of 15 ft eliminates breaching and spalling damage (see Figure 7.14). Because the local damage checks in ATP-Bridge are satisfied, dynamic shear and flexural response of the column are then checked. As shown in Figure 7.14, the peak displacement is 0.6 in. and the maximum support rotation is 0.89 degrees. NCHRP Technical Report 645 [24] recommends a plastic rotation limit of 1.0 degree, which is satisfied. Therefore, this portion of the design example illustrates the benefit of increasing the column diameter to prevent breach of a concrete bridge column subjected to blast loads.

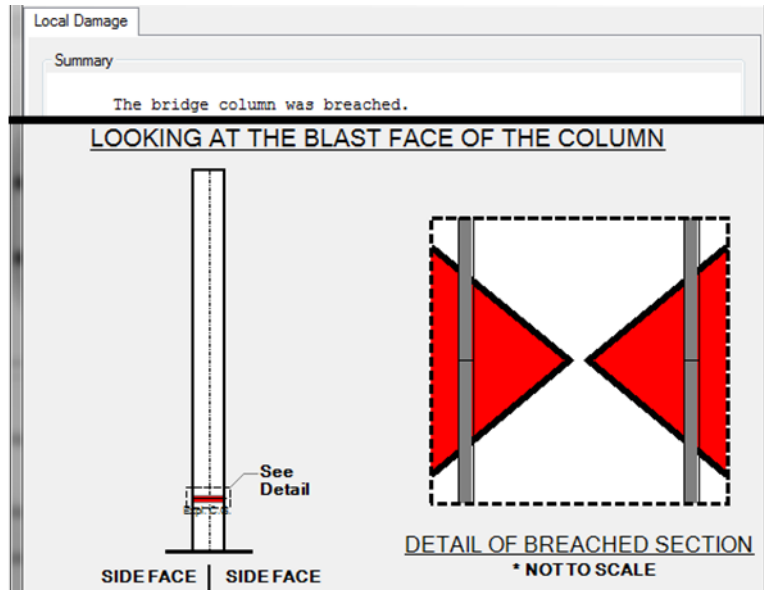


Figure 7.13 Design Example 7.1 Results for 36-in. Diameter Column

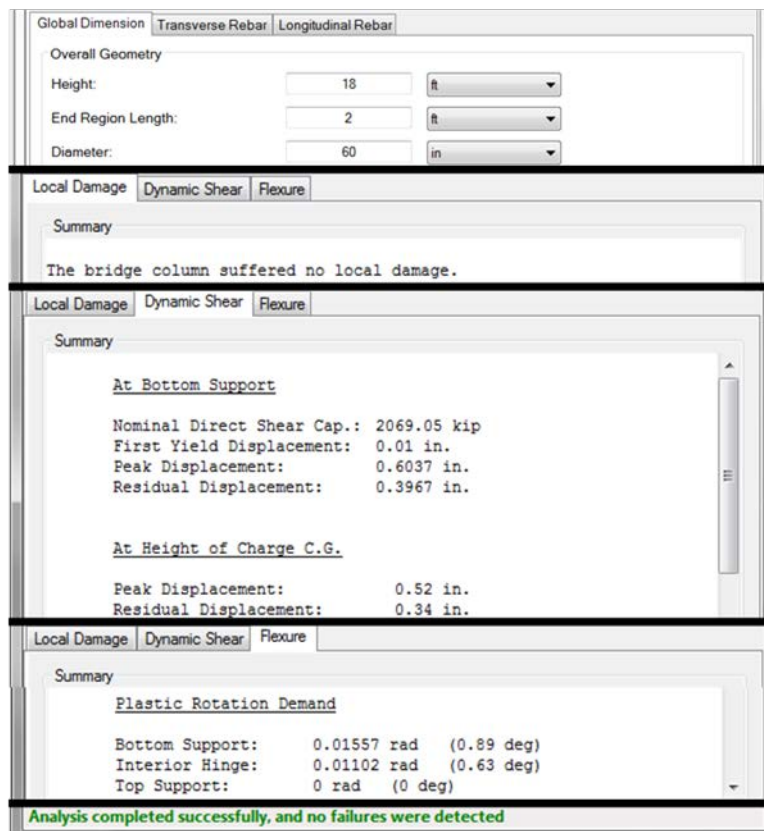


Figure 7.14 Design Example 7.1 Results for 60-in. Diameter Column

If the column diameter is reduced to 36 in. (consistent with the initial design), adjusting any other variable (concrete strength, concrete cover, transverse reinforcement, and longitudinal reinforcement) results in a breached column section. Therefore, the most influential variable in preventing a breach failure is column diameter; however, other factors can be optimized after

column diameter is increased. Each of the following variables will be adjusted (one by one): concrete strength, thickness of concrete cover, amount and type of transverse reinforcement, and amount of longitudinal reinforcement. After the influence of each variable on column response is discussed, an optimized column design is presented.

Concrete strength is evaluated next. The 60-in. diameter column design assumed a concrete strength of 4,000 psi. Varying the concrete strength from 3,000 psi to 10,000 psi for a threat of 2,800 lb of TNT at a standoff distance of 15 ft changes the column response significantly. The 60-in. column design with a 3,000 psi concrete strength now fails the local damage checks in ATP-Bridge due to excessive concrete spall damage on the rear and side faces of the column (see Figure 7.15). Increasing the concrete strength to 6,000 psi eliminates spall damage of the 60-in. diameter column (see Figure 7.16a). Because the local damage checks in ATP-Bridge are satisfied, dynamic shear and flexural response of the column are then checked. As shown in Figure 7.15b, the peak displacement for the 6,000 psi concrete strength, 60-in. diameter column design is 0.52 in., a reduction in displacement of 13% compared to the 4,000 psi concrete strength, 60-in. diameter column design. Lastly, increasing the concrete strength to 10,000 psi (see Figure 7.16b) results in a dynamic direct shear failure (i.e., longitudinal rebar ruptures due to excessive shear slip at the column base). Therefore, high-strength concrete does not help to optimize this column design.

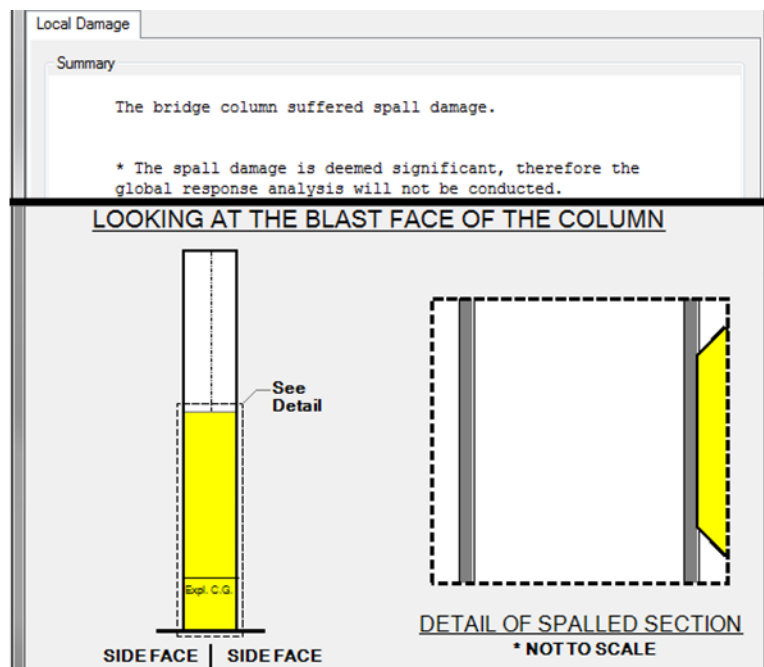


Figure 7.15 Design Example 7.1 Effects of Concrete Strength on Column Response – 3,000 psi Concrete

Concrete cover is evaluated next. The 60-in. diameter column design assumed a 1.5-in. thick concrete cover (see results in Figure 7.17a). Increasing the concrete cover by 50% from 1.5 in. to 3 in. for a threat of 2,800 lb of TNT at a standoff distance of 15 ft reduces the peak column displacement slightly by 6% (see Figure 7.17b). Therefore, additional concrete cover provides minimal improvement to column design optimization.

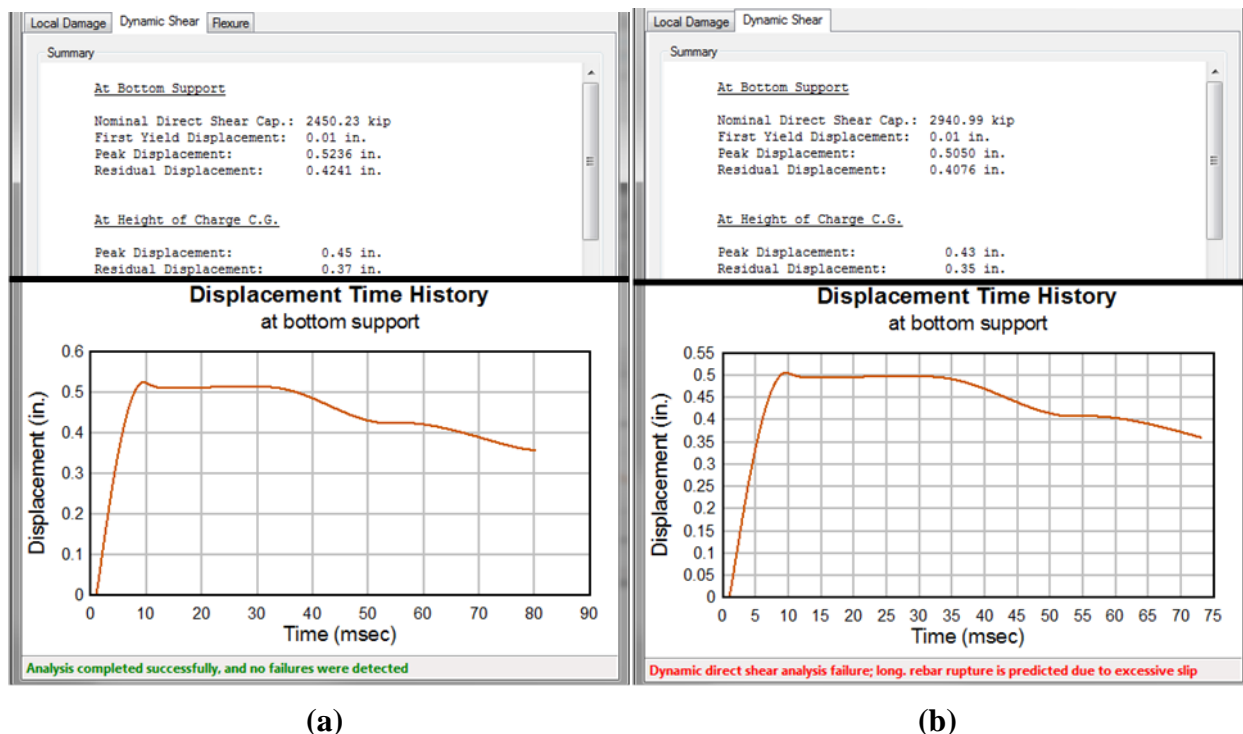
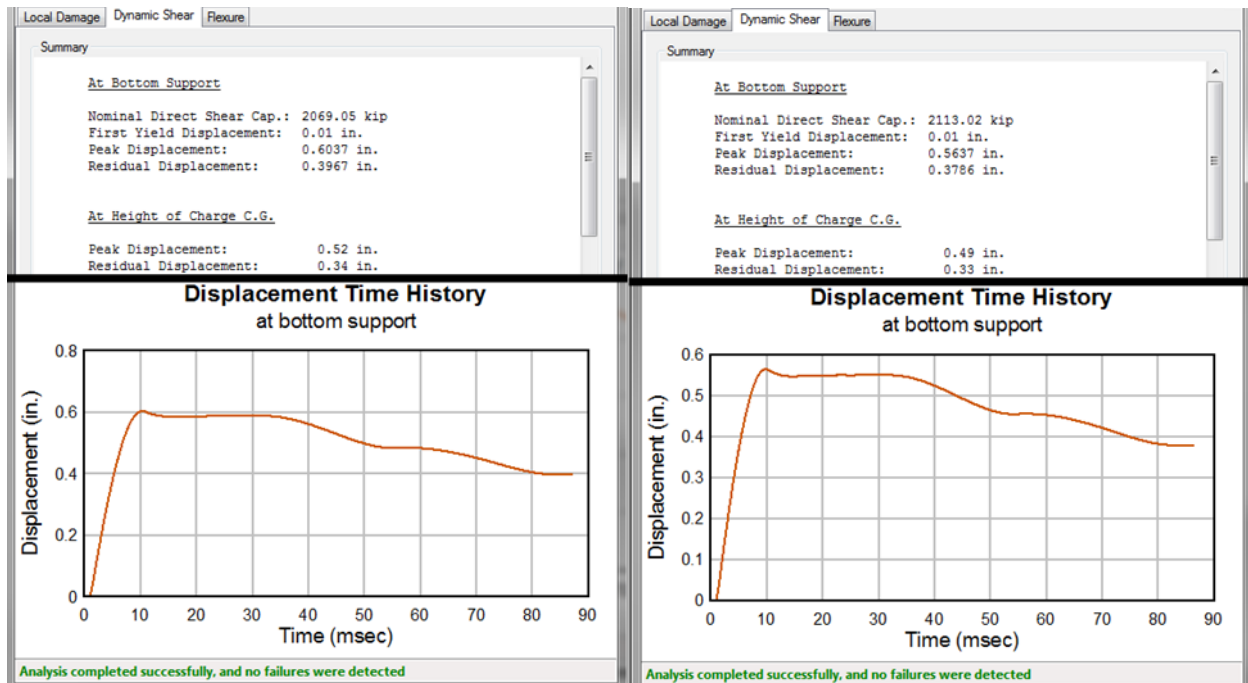


Figure 7.16 Design Example 7.1 Effects of Concrete Strength on Column Response: (a) 6,000 psi Concrete, (b) 10,000 psi Concrete

The amount and type of transverse reinforcement is evaluated next. The 60-in. diameter column design assumed #6 hoops at 6 in. on center (OC) along the full column height (see results in Figure 7.14). Optimizing hoop size and spacing to #4 hoops at 12 in. OC typical and 6 in. OC within the 3-ft long end regions for a threat of 2,800 lb at a standoff distance of 15 ft results in a sufficient column design with minimal change in column response (see Figure 7.18a).

Additionally, increasing the transverse reinforcement to #6 spiral at 4 in. OC along the full column height results in a sufficient column design with minimal change in column response (see Figure 7.18b). Therefore, transverse reinforcement can be optimized for blast loads once local damage requirements are met.

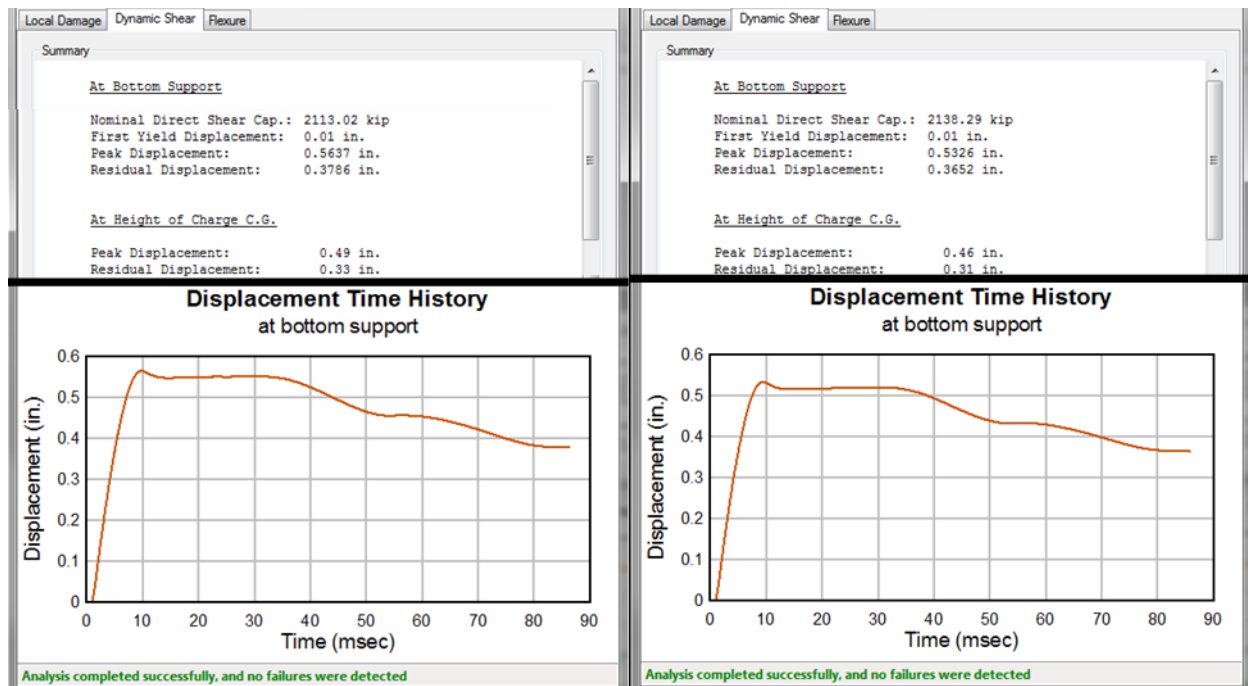
The amount of longitudinal reinforcement is evaluated next. The 60-in. diameter column design assumed 10 #9 bars evenly spaced around the circumference of the circular column section (see results in Figure 7.14). Reducing the longitudinal reinforcement to 8 #8 bars evenly spaced for a threat of 2,800 lb of TNT at a standoff distance of 15 ft results in a sufficient column design for local damage and shear. However, as shown in Figure 7.19a, the maximum support rotation is 1.24 degrees, which is greater than the 1.0-degree plastic rotation limit recommended in the NCHRP Technical Report 645 [24]. Therefore, additional longitudinal reinforcement is required. Increasing the longitudinal reinforcement to 10 #8 rebar evenly spaced results in a sufficient column design with a maximum support rotation of 1.0 degree (see Figure 7.19b). Therefore, longitudinal reinforcement can also be optimized for blast loads once local damage requirements are met.



(a)

(b)

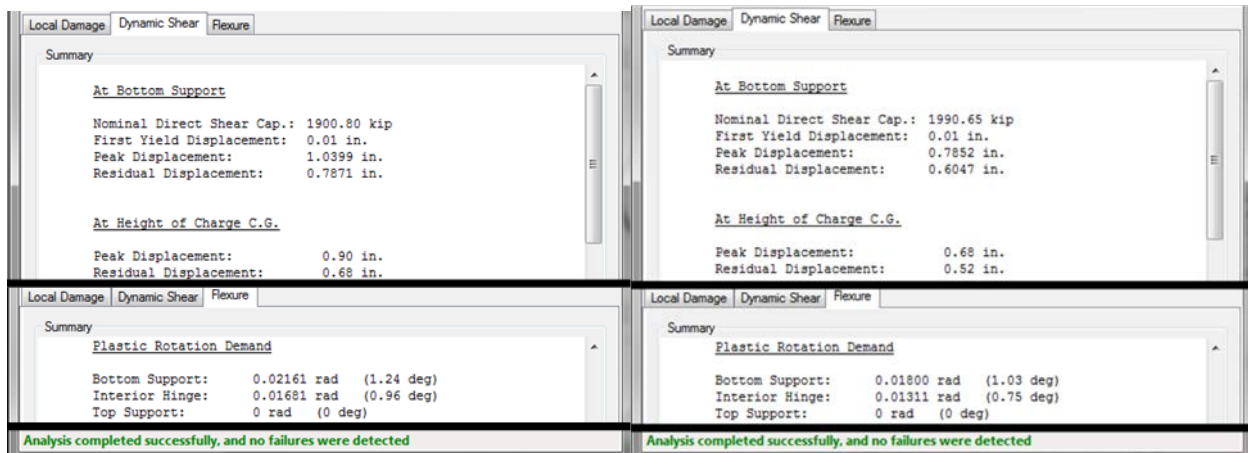
Figure 7.17 Design Example 7.1 Effects of Concrete Cover on Column Response: (a) 1.5 in. Cover, (b) 3 in. Cover



(a)

(b)

Figure 7.18 Design Example 7.1 Effects of Type and Amount of Transverse Reinforcement on Column Response: (a) #4 hoops at 12 in. OC typical and 6 in. OC within end regions, (b) #6 spiral at 4 in. OC



(a) (b)

Figure 7.19 Design Example 7.1 Effects of Amount of Longitudinal Reinforcement on Column Response: (a) 8 #8 evenly spaced, (b) 10 #8 evenly spaced

Lastly, using the lessons learned from adjusting each variable, the initial 60-in. diameter column design is optimized. The initial 60-in. diameter column design included 4,000 psi concrete reinforced with 10 #9 longitudinal bars evenly spaced and #6 hoops at 6 in. OC along the full column height and having 1.5 in. of concrete cover. As shown in Figure 7.14, the column design subjected to a threat of 2,800 lb of TNT at a standoff distance of 15 ft results in a peak displacement of 0.52 in. and a maximum support rotation of 0.89 degrees.

The optimized column design includes a 60-in. diameter column comprised of 5,000 psi concrete reinforced with 10 #8 longitudinal bars evenly spaced and #4 hoops at 12 in. OC typical and 6 in. OC within the 3 ft long end regions (see Figure 7.20a). The optimized column design subjected to a threat of 2,800 lb of TNT at a standoff distance of 15 ft results in a sufficient column design for local damage, dynamic shear, and flexure. As shown in Figure 7.20b, the peak displacement is 0.76 in., and the maximum support rotation is 1.0 degrees—equivalent to the 1.0-degree plastic rotation limit recommended in the NCHRP Technical Report 645 [24]. Therefore, multiple column designs are adequate for the given threat.

(a) Column Input

Geometry | Supports | Material | Advanced

5000 psi Concrete

Global Dimension | Transverse Rebar | Longitudinal Rebar

Overall Geometry

Height: 18 ft

End Region Length: 3 ft

Diameter: 60 in

Global Dimension | Transverse Rebar | Longitudinal Rebar

Spacing & Clear Cover

End Region Spacing: 6 in

Interior Region Spacing: 12 in

Cover: 2 in

Type & Size

Type: Hoops

Bar Size: #4

Diameter: 0.5 in

Global Dimension | Transverse Rebar | Longitudinal Rebar

Add Row | Delete Rows | Equal Distr.

Rows	Bar Size	Diameter	Location	Units
8	#8	1	252.00	Degrees
9	#8	1	288.00	Degrees
10	#8	1	324.00	Degrees

(b) Results

Local Damage | Dynamic Shear | Flexure

Summary

At Bottom Support

Nominal Direct Shear Cap.: 2167.75 kip

First Yield Displacement: 0.01 in.

Peak Displacement: 0.7565 in.

Residual Displacement: 0.5838 in.

At Height of Charge C.G.

Peak Displacement: 0.65 in.

Residual Displacement: 0.50 in.

Local Damage | Dynamic Shear | Flexure

Summary

Plastic Rotation Demand

Bottom Support: 0.01788 rad (1.02 deg)

Interior Hinge: 0.01315 rad (0.75 deg)

Analysis completed successfully, and no failures were detected

(a) (b)

Figure 7.20 Design Example 7.1 Optimized Design: (a) Column Input, (b) Results

This comprehensive design example illustrated an insufficient initial column design for the given threat. ATP-Bridge was used to evaluate the initial column design for blast loads and adjust different design variables to provide adequate solutions. While multiple solutions are possible, the best solution depends on the flexibility of design parameters for each unique bridge design.

Design Example 2

The following design example considers the response of a reinforced concrete highway bridge column for a smaller threat than was investigated in Design Example 1.

Evaluate the column, designed for a non-seismic region, for the given close-in blast load. If the column is insufficient, determine the amount of additional standoff required to meet all applicable design checks. Assume that this is an existing bridge and in this case providing adequate standoff distance is preferred over a column retrofit. Refer to Figure 7.21 for threat details and Figure 7.22 for column design details. Use ATP-Bridge to perform the analysis and design.

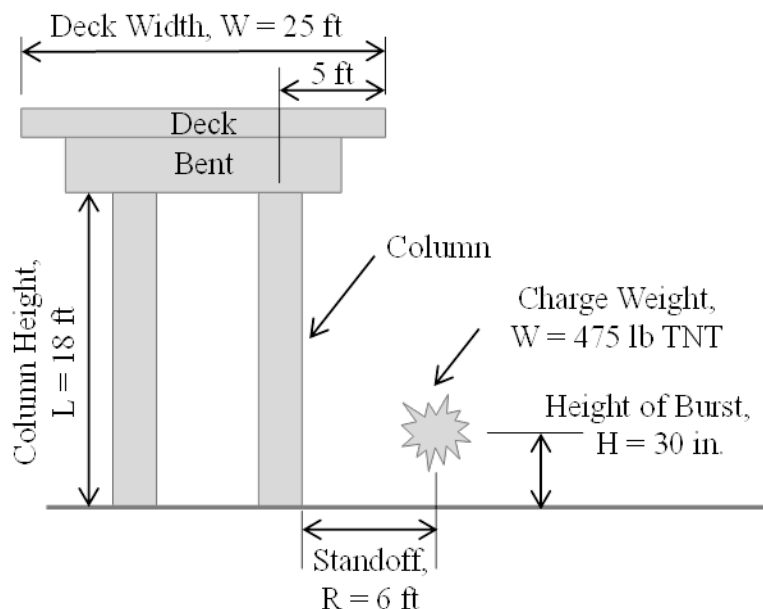


Figure 7.21 Design Example 7.2 Elevation

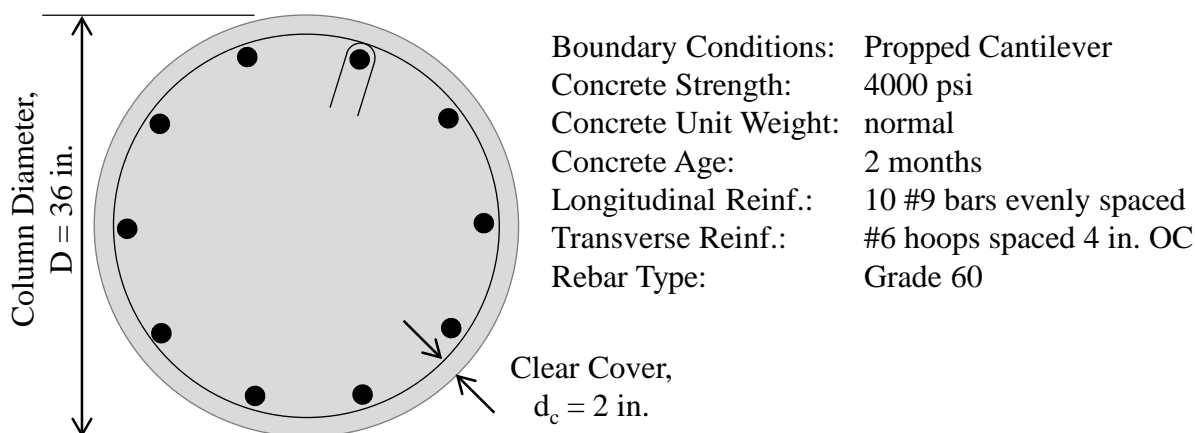


Figure 7.22 Design Example 7.2 Details

In response to the given threat of 475 lb of TNT at a 6-ft standoff distance, the 36-in. diameter column suffers a breach failure near the threat location (see Figure 7.23). Therefore, additional standoff distance is required to adequately protect the column.

Increasing the standoff distance from 6 ft to 7 ft for a threat of 475 lb of TNT eliminates breaching of the 36-in. diameter column. However, the column experiences concrete spall damage on the rear and side faces of the column (see Figure 7.24). Because the local damage checks in ATP-Bridge are satisfied, dynamic shear and flexural response of the column are then evaluated. The peak displacement is 10.75 in. and the maximum support rotation is 0.64 degrees. NCHRP Technical Report 645 [24] recommends a plastic rotation limit of 1 degree, which is satisfied. In summary, this design example illustrates the benefit additional standoff distance alone has on the design of a blast-loaded reinforced concrete bridge column.

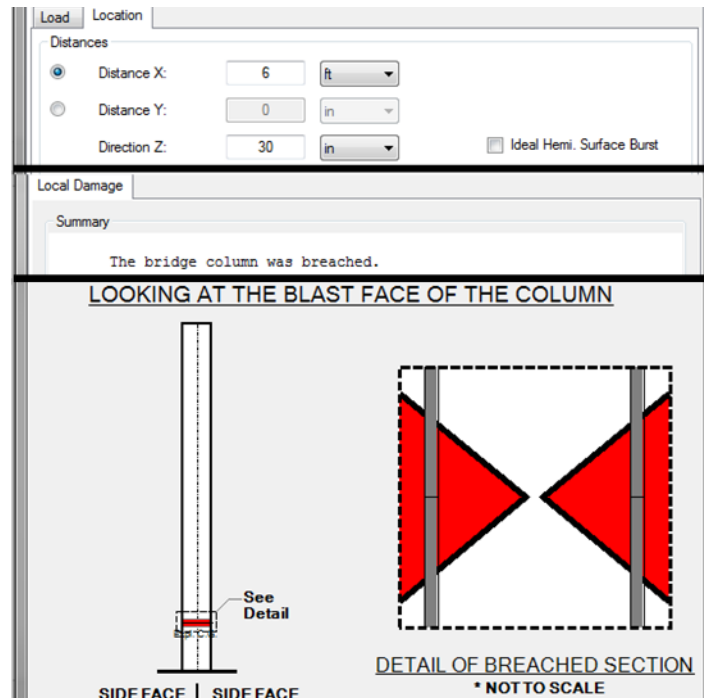


Figure 7.23 Design Example 7.2 Local Damage Results for 6-ft Standoff Distance

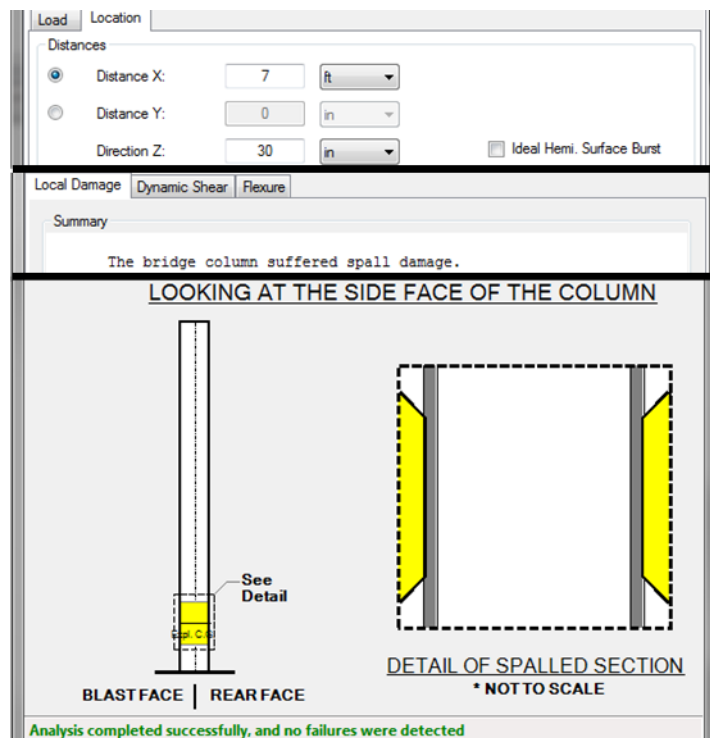


Figure 7.24 Design Example 7.2 Local Damage Results for 7-ft Standoff Distance

Determine the amount of additional standoff distance required to prevent spall damage. Increasing the standoff distance from 6 ft to 8 ft for a threat of 475 lb of TNT eliminates

breaching and spall of the 36-in. diameter column (see Figure 7.25). Because the local damage checks in ATP-Bridge are satisfied, dynamic shear and flexural response of the column are then evaluated. As shown in Figure 7.25, the peak displacement is 0.28 in. and the maximum support rotation is 0.46 degrees. NCHRP Technical Report 645 [24] recommends a plastic rotation limit of 1 degree, which is satisfied. In summary, this design example illustrates the benefit additional standoff distance alone has on the design of a blast-loaded reinforced concrete bridge column.

The screenshot displays the ATP-Bridge software interface with the following sections:

- Load Location**
 - Distances:
 - Distance X: 8 ft
 - Distance Y: 0 in
 - Direction Z: 30 in
 - ☐ Ideal Hemi. Surface Burst
- Local Damage** (Dynamic Shear | Flexure)
 - Summary: The bridge column suffered no local damage.
- Local Damage** (Dynamic Shear | Flexure)
 - Summary:
 - At Bottom Support
 - Nominal Direct Shear Cap.: 1082.55 kip
 - First Yield Displacement: 0.01 in.
 - Peak Displacement: 0.2788 in.
 - Residual Displacement: 0.1347 in.
 - At Height of Charge C.G.
 - Peak Displacement: 0.24 in.
 - Residual Displacement: 0.12 in.
- Local Damage** (Dynamic Shear | Flexure)
 - Summary:
 - Plastic Rotation Demand
 - Bottom Support: 0.00809 rad (0.46 deg)
 - Interior Hinge: 0.00057 rad (0.03 deg)
 - Top Support: 0 rad (0 deg)
- Analysis completed successfully, and no failures were detected**

Figure 7.25 Design Example 7.2 Results for 8-ft Standoff Distance

7.6 Overview of Threat Mitigation Retrofit Strategies

Threat mitigation strategies to improve the survivability of existing RC bridge columns subjected to terrorist threats can be divided into non-structural and structural modifications. Because blast loads can be drastically reduced with standoff, and because the range of possible threats to be considered can be reduced with access control measures, one retrofit strategy is to create standoff using landscaping, berms, bollards, etc. to reduce the maximum blast load a column would be required to withstand. Other methods of access control, such as fencing, can also be used to limit the ability of a potential terrorist to easily get near a critical column. The range of non-structural mitigation measures is vast, but aesthetics, bridge maintenance, and other factors also must be considered when using this approach. Accordingly, all potential non-structural retrofit measures should be thoroughly vetted with appropriate personnel to ensure factors other than security are adequately addressed prior to implementation.

Structural research specifically targeting the retrofit of existing RC bridge columns to withstand a range of terrorist threats has been limited. The most promising structural retrofits involve the use of column jacketing [110]. The primary options for jacket materials are fiber-reinforced polymer (FRP) or steel, though proprietary materials such as Hardwire® [111] have also been considered. In the work by Crawford et al. [110], the authors demonstrate the effectiveness of using steel and FRP jackets in mitigating blast damage to RC columns. In their test program, the researchers showed that the jacketed columns could survive a small standoff threat (10 ft) while the unjacketed columns were not. One limitation of this research is that it primarily focused on building columns, which have different support conditions, member connectivity, and structural configurations than typical bridge columns. In addition, this research did not address the issue of direct shear at the column base, which is known to be a dominant failure mode for blast-loaded RC bridge columns. Typically, when FRP or steel jackets are used in retrofitting RC columns for improved resistance to seismic events, a gap is left at the base of the column to ensure the improved capacity would not place excessive demands on the foundation, which is difficult and expensive to retrofit. This gap, however, presents a potential vulnerability in mitigating direct shear damage due to a close-in detonation. To overcome this problem, Fouché, et al. [112] developed a special base clamping system that provides improved capacity to direct shear at the base. While this system does require post-installing anchors into a footing or cap beam, the procedure is minimally invasive. The benefit it provides in mitigating direct shear failures is an important attribute that makes this approach better than the jacketing methods that have been used previously to retrofit columns for improved resistance to earthquake damage. Furthermore, the steel jacket is believed to provide better fire and impact resistance than FRP jackets, suggesting that this approach be considered prior to other options.

7.7 Chapter Summary

In this chapter, protective design guidance for blast-loaded reinforced concrete bridge columns was provided. An overview of relevant design loads/threats was provided with specific focus on explosive threats and associated blast loads. Failure modes and performance criteria specific to blast-loaded reinforced concrete bridge columns was also discussed. Design strategies and detailing recommendations based on recent experimental research (NCHRP Report 645) was presented, along with a recommended protective design procedure for blast-loaded reinforced concrete bridge columns. Two design examples using the ATP-Bridge software were illustrated, and this chapter ended with a discussion on some specific threat mitigation retrofit techniques.

Chapter 8 switches focus to protective design guidance for steel cellular towers. Such towers are typically associated with suspension bridges, some of the oldest long-span bridges in the U.S. highway bridge inventory.

8.0 PROTECTIVE DESIGN GUIDANCE FOR STEEL CELLULAR TOWERS

Steel cellular towers are used as the primary gravity-load carrying components on many suspension bridges. The cross-section of these towers consists of inter-connected plates, angles, and stiffeners arranged in a manner that creates a large number of individual cells. A schematic view of such a cross-section is given in Figure 8.1.

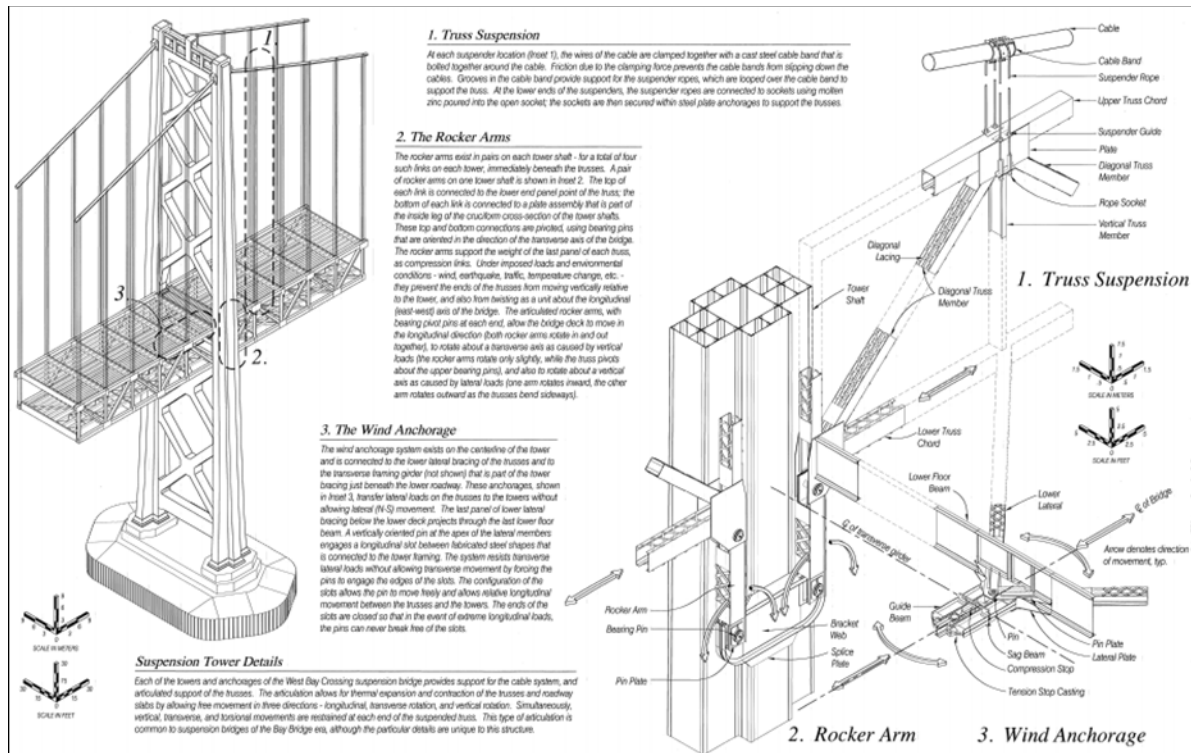


Figure 8.1 Illustrative Details of Example Steel Cellular Bridge Tower

Because such towers are often close to the road and pedestrian access, they can potentially be subjected to contact or near-contact charges of varying quantities. Access to the interior of a steel cellular tower is also a concern.

Owing to the unique features associated with these structural components, limited general information exists regarding how steel cellular towers are analyzed and designed (even for traditional loads). A thorough review of the research literature indicates the design of steel cellular towers is not thoroughly documented or described. Discussions with bridge design firms specializing in long-span bridges confirms this lack of information on the design of a “typical” steel cellular tower. Further, because the current preference for long-span bridges in the U.S. is for cable-stayed bridges using towers constructed of reinforced concrete, there are very few new steel cellular towers either currently under construction or recently built. Accordingly, the primary concern with steel cellular towers is protecting existing critical infrastructure. To do so, it is necessary to understand the geometry and design of these existing steel cellular towers and how these features impact the loads these structures might face and the manner in which they can respond.

The only comprehensive study on the response of steel cellular towers, which included large-scale testing and detailed computational simulation, is “Validation of Numerical Modeling and Analysis of Steel Bridge Towers Subjected to Blast Loading.” This research was organized as a large pooled-fund study (TPF 5(110)) coordinated by the Federal Highway Administration. Experimental testing was carried out by researchers at the Engineer Research and Development Center (ERDC) of the U.S. Army Corps of Engineers (USACE). There are few papers in the research literature that focus on the protective design of suspension bridges. Available papers do not take a detailed look at the cellular tower response, nor are they validated with experimental test data. Thus, given the current state of knowledge and availability of relevant information, the material in this chapter is largely based on the results of the pooled-fund study mentioned previously.

The pooled-fund study consisted of four different test series (Series 1-4) and detailed computational modeling. Series 1 focused on the front plate of steel cellular towers, Series 2 considered a cellular geometry more complex than Series 1 that represented the complete first cell of a steel suspension bridge tower. Series 3 focused on localized response and retrofit options and utilized a simple test setup focusing on the response of individual plates. Series 4, the final test series, served to validate the findings from the computational studies and three prior test series. Thus, it had the most complex setup of any of the tests and was configured to be three cells wide by three cells deep. Series 3 and 4 were conducted at a reduced scale relative to Series 1 and 2 for economical and logistical reasons.

The intent of this chapter is to include important information from this research program to give readers a good understanding of the potential loads and corresponding response of steel cellular towers subjected to large blast threats. Information from the pooled-fund study has been augmented by other relevant information found in the research literature or based on the experience of the authors. For additional details, readers are highly encouraged to review the reports from the pooled-fund study [113, 114, 115, 116, 117].

8.1 Design Loads

The protective design of steel cellular towers must consider a range of threats. Because of the limited standoff that exists on many bridges with these types of towers, a primary concern is the mitigation of blast loads due to a VBIED (Figure 8.2). While multiple VBIEDs acting simultaneously is possible, this threat scenario is assumed to have a low likelihood of occurrence due to the coordination needed to conduct such a sophisticated attack and because of potential space constraints that may prevent multiple trucks from being positioned around a tower. Consideration must also be given to scenarios involving hand-emplaced explosive devices, ranging from unsophisticated bulk explosive charges in a backpack to more sophisticated cutting charges. Additional threats include mechanical cutting devices, thermal devices, and intentional fire. While cutting devices may require considerable time on target to inflict significant damage, even slight damage may be of concern due to the challenges associated with repairing such a critical component in the overall structural system of a suspension bridge. Additional details for different types of threats are provided in the following subsections. It should be noted, however, that the focus of this chapter is on protective design modifications for blast loading, which was the primary focus of the pooled-fund study mentioned previously [113].



Figure 8.2 Truck Located Close to Structural Components of Steel Bridge [118]

8.1.1 Blast Loads

Blast loads acting against steel cellular towers can result from a large truck IED (Figure 8.2) located near a tower, or blast loads can be due to hand-emplaced devices that are man-portable (Figure 8.3). An issue of significant importance is that many older bridges with steel cellular towers are configured in such a way that standoff distances between a truck and the tower can be quite small. As discussed previously in Chapter 4, increasing standoff distance is an extremely effective way to mitigate blast effects. Doubling the distance between an explosive and target requires that the charge size be increased by a factor of eight to achieve the same peak pressure because of the cubic relationship between these variables (see Chapter 4). When standoffs are limited, blast load intensities have the potential to be quite large. Thus, the biggest challenge in designing steel cellular towers to resist blast effects is the potentially severe load magnitudes that need to be resisted.

If access to the interior of a steel cellular tower cannot be controlled, it is possible to detonate man-portable charges within the interior of a tower. Because of the confinement effects associated with this scenario, peak blast pressures and impulses can become quite high despite the limited quantity of explosives (relative to a truck IED) that can be introduced to the interior of a tower. Furthermore, predicting the loads associated with such a scenario is complicated and requires specialized software to produce a reasonable answer. Because of the unique geometry of existing steel cellular towers, and because of the complications associated with predicting loads and response for an internal blast threat, a simplified general analysis and design procedure does not currently exist. Because this capability is not included within ATP-Bridge, it is not considered further in this manual. In situations where such a scenario is of concern, it is

recommended that consultants with appropriate expertise be retained to help conduct the necessary analyses and design calculations.



Figure 8.3 Access to Steel Cellular Tower [119]

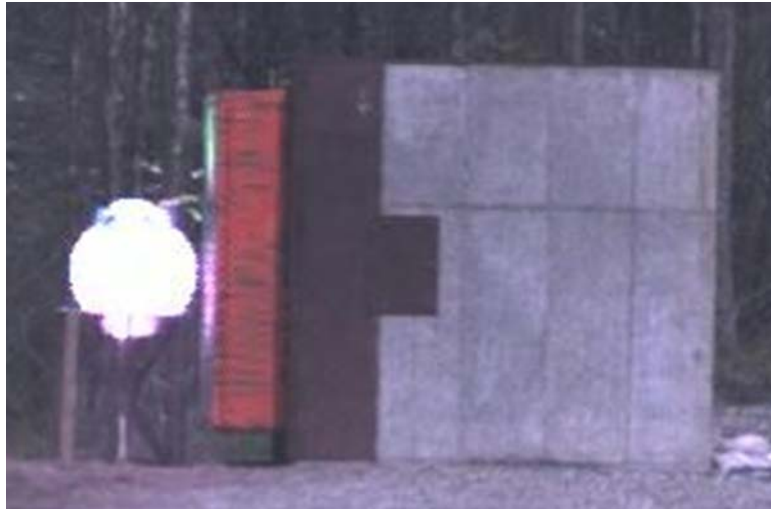
In plan view, the location of a truck relative to the centerline of a tower may create a very complicated loading case. For a truck positioned immediately next to a tower where the point of detonation is aligned with the tower centerline, the loads on the front face will be approximately uniform across the tower width at a given height above the deck, though the intensity will diminish with height. While the standoff and angle of incidence will vary some across the tower width, it is reasonable and conservative to consider the tower to provide a reflecting surface that is approximately 90-degrees to the direction of blast wave travel. In cases of complex tower geometries, including setbacks, reentrant corners, and other such features, it may be necessary to conduct sophisticated airblast analyses that account for these features. Such analyses are not currently available within ATP-Bridge. Loads on the sides of the tower will generally be of much lower intensity than the front face and will include only side-on pressures. In addition, the load on the sides will be phased in time so that it is not uniform across the entire width of the side like it approximately is on the front. Further, the load intensity is changing with time and position so that the sides of the tower furthest from the source of detonation will need to resist a smaller load than the portion near the front. While in some cases it may be necessary to account for this variation, it will likely be acceptable in most scenarios to simply assume the side-face loading has the same peak magnitude as the leading edge. In some cases where the load variation is significant (e.g., wide towers), it is advisable to compute loads over the side faces using groups or zones of cells, where the load over a given zone or group is uniform, though the load in one zone or group can differ from an adjacent zone or group. Whether the loading is considered uniform across the entire side face will be scenario specific. For threats of interest and typical tower geometries, it is reasonable to assume the entire side face is loaded at the same time. For the conditions assumed with the point of detonation perfectly aligned with the tower centerline, the total net load acting on the tower will be maximized as the entire width of the front face will be exposed to a reflected pressure. Predicting the blast load on the front face at the most highly loaded elevation (typically at the height of burst) is of primary importance for this case. Because

of this, the experimental and computational research program carried out for the pooled-fund study on steel suspension bridge towers focused on this scenario [113].

In cases where the center of detonation of the explosive threat is not aligned with the centerline of the tower, particularly in cases where the center of detonation may be close to the corner of a tower, the prediction of loads and response becomes much more complicated. Under such a scenario, both the tower front face and side face will be exposed to reflected pressures. The specific geometry of the case being considered will significantly affect the computed results. The angle of incidence, and hence the reflection coefficient, will change along the front and side faces. Relative to the case where a truck is perfectly aligned with the tower centerline, the load intensity will vary across the width of both the side and front faces. The load intensity will be greatest at the point closest to the center of detonation and will diminish as the distance from the explosive increases. Because the damage resulting from these load cases is expected to be unsymmetrical over the cross-section of a tower, these threats can often be the most critical. To date, research exploring this scenario has been limited, and simplified methods for predicting loads and response are not currently available. Therefore, if such cases are of concern, the use of high-fidelity finite element analyses by personnel with appropriate experience and expertise should be used. A scenario of this type is not currently available within ATP-Bridge.

Hand-emplaced explosives must be man-portable and will be of a much smaller size than a truck bomb. Nonetheless, this threat still requires consideration because these explosives have the potential of being placed in contact with a steel cellular tower (or within the interior of a tower if appropriate access control is not established). Though small, contact charges have the potential to cause localized failure and breach of the tower perimeter. In the pooled-fund study previously conducted, project researchers and bridge owners considered damage to be tolerable if it was limited to just the front row of cells and did not propagate into neighboring cells [113]. This level of damage, however, may not be tolerable for other cases in which towers are small or composed of relatively few cells. Therefore, bridge owners should establish acceptable levels of damage, based on the geometry, material properties, and other details of the specific bridge being evaluated. In general, determining the amount of damage to cause collapse can be useful in establishing acceptable response limits. Because surveillance and police patrols can help minimize the likelihood of hand-emplaced threats, this scenario is not considered as critical as the large VBIED threat in most cases.

Large, near-contact detonations can produce large fireballs (see Figure 8.4), raising the question as to whether heat transfer from a VBIED is of concern. Fragments may also be of concern. Because the duration of loading is so short, Walker, et al. (2011) [113] indicate there is insufficient time for significant heat transfer to occur, even for thin steel components. Computational studies further support this conclusion. Fragments associated with VBIEDs have been shown in recent studies to not be of significant concern because of their small size and because they are highly dispersed at a variety of oblique angles of impact [120].



(a)



(b)

Figure 8.4 Detonation Sequence for Series 2 Test [113] (a) A Few Micro-Seconds after Detonation, (b) Approximately 1 Millisecond after Detonation

8.1.2 Other Loading Considerations

Because steel cellular towers are built up from steel plates of varying thicknesses, it is possible that mechanical or thermal cutting devices can be used to inflict damage. While such methods of attack may require significant time on target to induce appreciable damage, even slight damage may be of concern due to the challenges associated with repairing such a critical component in the overall structural system of a suspension bridge. Intentional fires are also of concern given that steel without fire protection can lose capacity in a short period of time. Although the threat of intentional ramming by a truck or other vehicle (including ship or barge) cannot be ignored, the geometry of most bridges with steel cellular towers, coupled with existing protection measures to reduce the effects of an accidental impact from a vehicle or boat, make this mode of attack less attractive than other modes. Nonetheless, even though the methods of attack

addressed in this subsection are expected to be less likely than those associated with a VBIED, these threats should not be ignored.

8.2 Failure Modes and Performance Criteria

Steel cellular towers may be vulnerable to severe blast and other threats described in the preceding section. Under large, close-in threats, steel towers may experience severe localized damage including breach of a panel, leading to the development of steel fragments. These fragments are often referred to as secondary debris because they form as a result of blast damage to the target and are not part of the enclosure (casing) containing the explosive, which create primary fragments or debris. Secondary fragments from the front face may in turn impact and damage other cells within the cross-section of a tower. In general, secondary fragments are of much greater concern than primary fragments associated with a VBEID threat. Per Walker, et al. (2011) [113],

Being vehicle-borne, a VBIED can obviously produce a large amount of high-velocity [primary] metal fragments as it is blown apart. Having the combined effects of high mass and velocity, these fragments can potentially impart structural loadings higher than that from just airblast alone. However, recent studies [8] showed that the fragments from a VBIED are of sufficiently small size and are so highly dispersed that they in fact do not significantly affect the damage to a structure. Damage resulting from an actual fragment-producing VBIED and the equivalent amount of un-cased explosives were found to be approximately the same. Thus, [primary] fragment loadings from the vehicle bomb are often neglected in structural vulnerability studies.

In the pooled-fund study on steel cellular towers, project researchers evaluated performance over a wide range of threats. For small threats, tower response will remain elastic. As threat size increases, steel components will experience yielding, leading to permanent plastic deformations. Depending on the specific design details of a given tower, it is possible (and perhaps likely) that connections will yield and fail before the front plates reach their full capacity. Nonetheless, the only detailed data that currently exist are for cases where the front plates are the most critical components. Thus, the current discussion focuses on the front plates of a tower, but engineers should also consider the response of supporting stiffeners, connections, and diaphragms. Such details are included in the examples presented at the end of this chapter. For severe threats, the front plate of a tower will rupture, becoming a secondary fragment that will load other steel plates in its flight path. In the pooled-fund research program, tearing of the front plate typically initiated along vertical stiffeners located at the edges of a panel. Initiation along the vertical edges was most likely attributed to the specific geometry associated with the specimens being tested. Nonetheless, these specimens were representative of a typical steel suspension bridge tower and are therefore taken to be indicative of how other steel cellular towers may respond. It is important to note this discussion refers to the original, un-retrofitted geometry in which the aspect ratio of the front panel was approximately 4.3:1, indicating the response was primarily one-way with the largest shear forces acting along the vertical edges. Figure 8.5 shows the geometry of the specimens used in the Series 1 testing program. Figure 8.6 and Figure 8.7 show ranges of response associated with the first two test series in the pooled fund study. In these figures, the quantity “X” refers to a relative charge weight. The actual charge weight is not given

for security reasons. To get a sense of what the value “X” represents, the overall goal of the research effort was to mitigate a threat of 5X acting at a standoff of 4 ft. in a full-scale scenario.

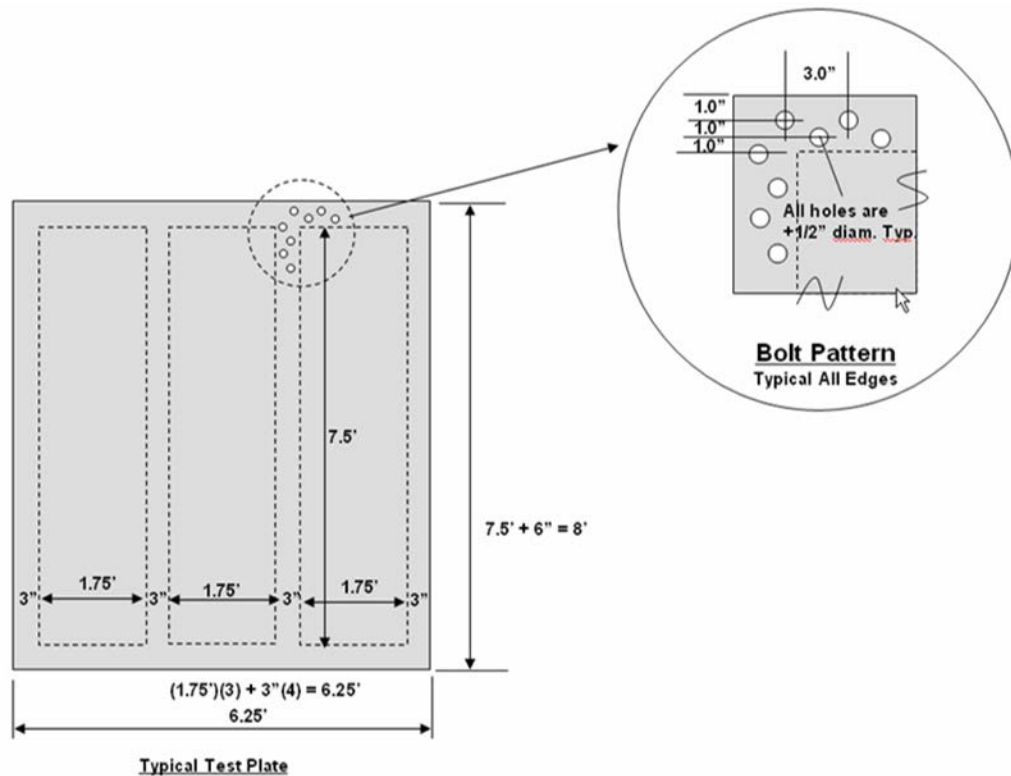


Figure 8.5 Specimen Geometry for Series 1 Experimental Testing Program from Pooled-Fund Study on Steel Cellular Towers [113]

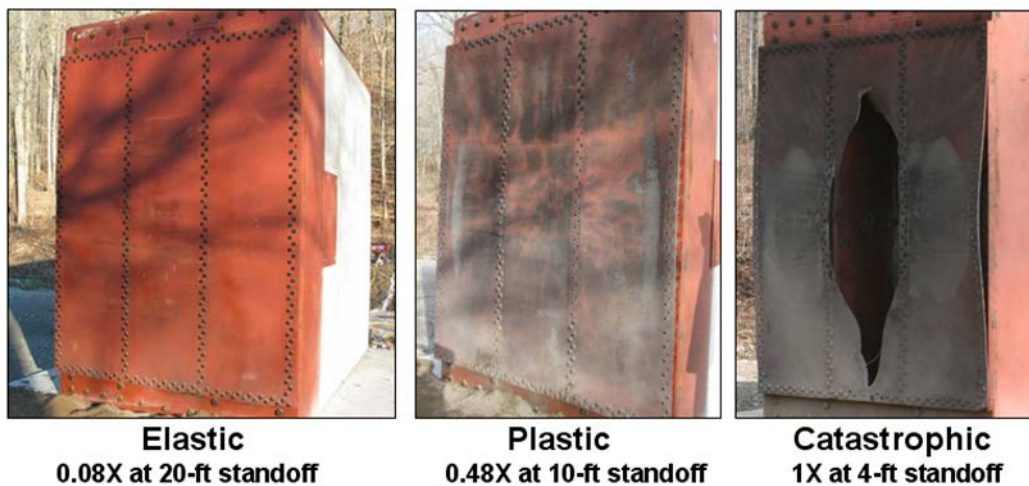


Figure 8.6 Varied Damage Levels from Series 1 Tests [113]

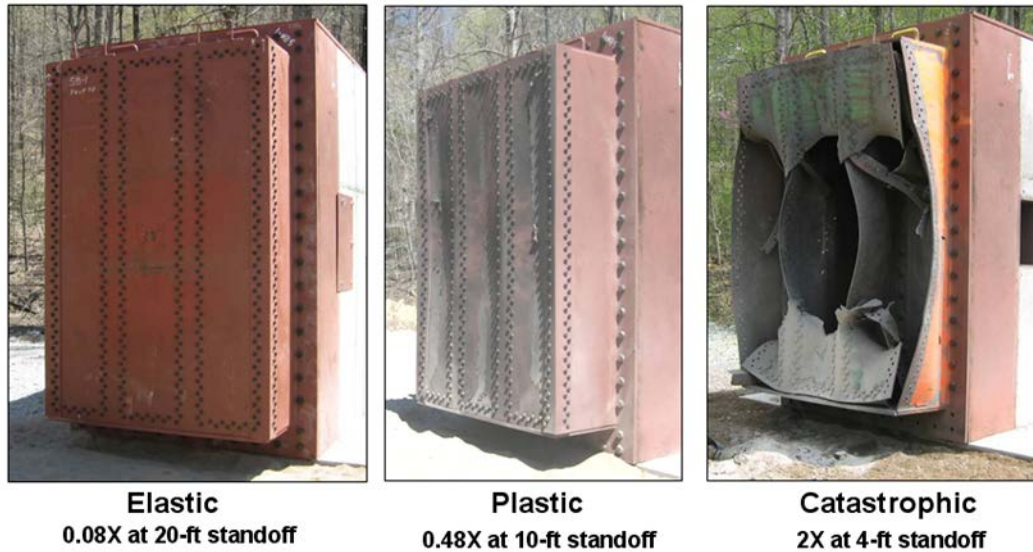


Figure 8.7 Varied Damage Levels from Series 2 Tests [113]

The test results demonstrated how the threat severity affected the size and distribution of fragments that would form in the case of “Catastrophic” response as depicted in the figures above. At the initial threshold when steel plate rupture occurred, plates would first begin to fail along the vertical edges as indicated previously. Eventually, at the threshold of fragment formation, the plate velocity would be large enough to tear away from the top and bottom edges after rupturing along the sides. In this initial range of fragment formation, approximately one-half of the front plate would typically turn into a large fragment while the other half of the plate would fold back onto itself without tearing away. With increasing load severity, the front plate would tear into two distinct halves, with each half forming into fragments. In the pooled fund study, Walker, et al. (2011) [113] note that both halves of the plate “flew away at a velocity of 1,893 ft/s. After the test, these fragments were found about 300 ft. behind the target.” As threat severity increased further, the front plate would tear into many smaller fragments that could typically not be found after testing. Although the fragments for the most severely loaded cases were smaller than those for less severe threats, the velocities were considerably larger (estimated by Walker, et al. [113] to be greater than 3,000 ft/s). As such, the kinetic energy these fragments would impart to cells behind them was a significant threat. To evaluate this hypothesis, a test was set up with three plates arranged, one behind the other, and spaced 1 ft. apart in the scaled test. Under the most severe threat (5X), all three plates failed. In this test, the first plate ruptured, flying into the second, which then failed, flying into the third plate. The third plate also failed, demonstrating the severity of this threat and the need to be concerned about fragment loadings on interior tower cells associated with failed plates from perimeter cells.

Because of the threat associated with flying fragments from failed portions of a steel cellular tower and the possibility of this damage propagating into adjacent cells, establishing acceptable performance requires a consideration of the effect of localized damage on overall structural integrity. Although the tests conducted for the pooled-fund study did not directly assess the possibility of progressive collapse, project researchers and other participants concluded that many towers could withstand the failure of the first row of cells without leading to bridge failure [113]. Per Walker, et al. (2011) [113], “Upon discussion with the Pooled Fund Participants, it was concluded that in most cases, the bridges could survive the loss of the front row of cells

without suffering progressive collapse. Thus, the front row of cells was considered as a sacrificial zone.” The acceptable level of damage used in the pooled-fund study, however, may not be appropriate in all cases, especially for small towers that have few cells. For these towers, the performance criteria may require that no localized failure occurs. Because of the difficulty associated with predicting response from airblast and the possible formation of “flyer plate” fragments that could impact neighboring cells, ATP-Bridge takes a conservative approach and simply indicates when breach of the front plate occurs. While this limit by itself is more restrictive than the recommendation given in the pooled-fund study, it is considered reasonable given the uncertainties associated with different cellular tower geometries that may be encountered in practice. Moreover, the hypothesis that the first row of cells can be considered as sacrificial has not been validated experimentally, further suggesting that the conservative approach adopted within ATP-Bridge is appropriate. Example analyses conducted using ATP-Bridge are provided later in this chapter. For some bridges, it may be appropriate to consider the global response of a tower using computational tools that are more sophisticated than ATP-Bridge. These tools can ensure a damaged tower can support the loads acting on it without collapsing. Such an approach can help eliminate the inherent conservatism in the response limits recommended above, though it will require analysts with appropriate expertise for conducting high-fidelity simulations.

8.3 Design Strategies and Detailing Recommendations

Steel cellular towers have lost favor as a preferred structural system for long-span bridges. Even among suspension bridges where steel cellular towers were once the primary choice for tower construction, many countries around the world have utilized concrete towers. In the United States, the vast majority of suspension bridges using steel cellular towers were constructed between the 1920s and early 1970s [121]. Today, concrete towers on cable-stayed bridges appear to be the most popular structural system to bridge over long spans. Many of the longest bridges being constructed today are located in other countries, most notably China (though Denmark has also produced some notable long-span bridges). Because of the lack of emphasis on the design of new long-span bridges using steel cellular towers for the primary gravity-load carrying component, the focus on design and detailing should be aimed at protecting existing infrastructure, which is covered in Section 8.6. In cases where new steel cellular towers may be utilized, attention should be given to providing some standoff protection between the tower and roadway. While this design strategy is challenging given that it may lead to higher costs, the investment may be worthwhile to reduce the maximum credible threat and the degree of hardening that must be provided. Structural hardening should be focused on the portion of the tower near the level of the deck. Because of the rapid dissipation of blast loads, the upper portions of a tower will likely require minimal, if any, protection. It is important to note that, even for “traditional” loads including Dead, Live, Wind, and Seismic, the design of steel cellular towers and long-span bridges in general requires advanced skills and knowledge not found in typical design offices. Such bridges are normally designed by consulting firms specializing in these types of structures. Likewise, for the case of protective design against potential terrorist threats, it is recommended that firms specializing in this field be employed to carry out the design. The unique features and design challenges associated with these bridges is such that simplified analysis and design procedures are usually not adequate. Nonetheless, simplified analyses of portions of a tower may reveal important aspects of behavior. This approach to

assessing localized damage and not the entire tower response forms the basis of ATP-Bridge (described in further detail in Section 8.5 and Chapter 12 of this manual).

While costs need to be evaluated, it is recommended that detailing of steel cellular towers consider using modern high-strength, high-ductility alloys that were not available in the past when many of the suspension bridges in the U.S. were built. For example, in the pooled-fund study introduced in the previous sections, one of the retrofits that showed good performance was constructed using ASTM A709 Grade 70 steel [113]. There are now steels having a yield strength in the 100-ksi range that also show good ductility. Detailing the geometry of how the steel plates within a tower are configured requires a balance between strength and stiffness. Reducing the span of individual plates and promoting two-way action through the arrangement of stiffeners and diaphragms, in general, improves overall performance to blast loads. Nonetheless, attention must be given to providing an overly stiff plate that has limited shear strength along its edges and can become a fragment that flies into other plates. Novel approaches may utilize details such as employing slotted holes or energy-absorbing bolts, venting, and frangible (controlled failure with alternative load paths) surfaces. Because these approaches have not been validated experimentally, however, caution must be exercised when establishing the overall design and detailing needed to construct a blast-resistant steel cellular tower. More research is needed to better understand how such towers behave under large blast loads, though this research may not be as high of a priority as other structural systems given the limited number of steel cellular towers currently being built in the U.S.

8.4 Recommended Design Procedure

For the case of blast-loaded steel cellular towers, the recommended design procedure included within this manual should be regarded as a preliminary approach. Using ATP-Bridge to evaluate potential vulnerabilities and performance is recommended. Such analyses within ATP-Bridge can allow designers to determine acceptable plate thicknesses and other details to mitigate the design-basis threat, and it can help with preliminary cost estimates. While this level of analysis may be adequate in some scenarios, it is expected and recommended that detailed finite element analyses be carried out for the proposed final design to ensure localized damage predicted in ATP-Bridge does not propagate into adjacent cells. Furthermore, detailed finite element models are needed to evaluate overall tower integrity and resistance to progressive collapse. ATP-Bridge is only able to predict the response of the front plate of the blast-loaded cells.

8.4.1 Boundary Conditions

In a steel cellular tower, the built-up configuration of the plates establishes the boundary conditions for analysis. Based on parametric FEA studies conducted when developing ATP-Bridge, analyses of interior cells (i.e., cells not on the perimeter of a tower face) showed that the arrangement of stiffeners and diaphragms typically allow the response of steel panels to be computed individually. Thus, for the range of parameters considered, there was not significant coupling between one panel and the next based on the how the stiffeners and diaphragms were arranged. For example, in Figure 8.5, the response of the center panel can be reasonably approximated without direct consideration of the panels to the left and right. The damage shown in Figure 8.6 suggests this hypothesis is reasonable. In cases where catastrophic damage does not occur and panels experience plastic deformation without failing, a simplifying assumption would be to model a panel as though it were simply supported around its perimeter, which would allow

rotations at the edges to occur (thereby increasing computed displacements) and would produce a higher demand at the center of the plate than if the edges were fully clamped. A more realistic assumption would be to model the plate as being supported by flexible elements (like a beam on an elastic foundation), where the relative stiffness of the stiffeners and diaphragms supporting a panel are accounted for in the analyses.

For high intensity loads where failures can be highly localized, the effect of boundary conditions on predicted response is not as significant as when a panel remains intact because of the nature in which shock waves propagate through the plate material [45]. Research on breach of stiffened steel panels is limited. In the development of ATP-Bridge, the work of Jones (1976) [122] was used to develop computational models that can account for localized plate failure when the rupture of a plate may also involve a stiffener or possibly wrap around a stiffener. For complete details of this approach, see Puryear, et al. (2013) [93]. As Figure 8.6 and Figure 8.7 show, plate failure typically occurs in a manner where the stiffener plays a limited role other than providing shear restraints at the edge of a panel. Thus, modeling a panel as being simply supported may be adequate for estimating localized failure if the extent of damage extends to the panel perimeter. In ATP-Bridge, users specify diaphragm spacing and cross-sectional dimensions of angles supporting the front plate of a steel cellular tower. These analyses consider the relative strength and stiffness of the edge supports relative to the panel and have been validated against the data collected in the pooled-fund study on steel cellular towers.

8.4.2 Analysis Approach

For designers wishing to understand the potential for damage and possible breaching of the front plate of a steel cellular tower, ATP-Bridge is a useful tool. ATP-Bridge has limitations, however, in that it does not consider overall tower response when localized damage occurs, nor does it attempt to model the propagation of damage into the plates of neighboring cells when rupture of the front panel occurs and forms a fragment that may fly into the interior of a steel cellular tower. Thus, ATP-Bridge focuses on predicting the local damage to the most heavily loaded cell within a steel cellular tower.

The analysis approach recommended for design is to use ATP-Bridge as a first step to evaluate the extent of localized damage that may occur for a given threat scenario. Because ATP-Bridge has been validated against the limited test data that currently exist, this prediction of initial damage should be reasonable. If the extent of predicted damage is tolerable (e.g., localized failure does not occur), this analysis step may be the only one required to evaluate steel cellular tower response to a postulated terrorist threat. If the extent of damage is more severe, however, it is recommended that high fidelity finite element analyses be conducted to evaluate the likelihood of damage propagation resulting from the formation of “flyer plates” from the front face of the tower and to evaluate overall tower integrity and the potential for progressive collapse. Even with this approach, a great deal of caution should be exercised when evaluating the computed results. Using one of the most advanced analysis approaches currently available in which coupled blast and structural response were considered, researchers on the pooled-fund study were initially surprised by the under-prediction of damage in the Series 4 tests that considered a 3×3 cell arrangement [113]. This area of behavior and response is not well understood, and the available test data are limited. Thus, extreme care should be used when evaluating the performance of a steel cellular tower subjected to high intensity blast loads. Only highly

qualified individuals with extensive experience using advanced simulation software should be used to conduct such studies.

8.4.3 Structural Design

Design of steel cellular towers, as mentioned previously, requires engineers with specialized knowledge and experience, even for traditional loads. Thus, structural design for blast and other postulated threats is but one aspect of the overall design that must be considered. Because solutions for improving response to blast, such as increasing structural mass to improve inertial resistance, might make the design unsuitable for seismic demands the tower may face, design for blast cannot be done independently. Using the guidelines given in the previous subsections, engineers can specifically evaluate steel cellular tower response subjected to large blast loads. Overall design, however, must be coordinated with other experts that have appropriate experience because many aspects of design are case dependent.

8.5 ATP-Bridge Design Example

The following design example shows the predicted behavior of the front panel of a steel cellular tower. Rather than providing multiple examples, a single baseline scenario is shown along with a description of how the response changes for modifications to the threat and design parameters. Also discussed are measures that can be taken if the threat becomes too severe. Such analyses fit within the overall design process for the front panel of steel cellular towers subjected to blast loads as described in the previous section. Each design example utilizes the ATP-Bridge software, which is presented in detail in Chapter 12.

In this example, the baseline threat is assumed to act against the front panel of a steel cellular tower with dimensions representative of those found on existing suspension bridges. The material properties are selected to be consistent with ASTM A36 steel as used in the pooled-fund test program, but users can specify other properties if they so desire.

The panel considered for the baseline case is 140-in. tall by 40-in. wide and is assumed to be 2-in. thick. The basic user interface for specifying the overall panel geometry is shown in Figure 8.8. At the top of the figure below the component name, the panel geometry and material properties are listed. By selecting the “Material” tab just below this text box, users can specify values for other types of steel. Near the bottom of this form is where users specify the overall dimensions and thickness of a front panel plate. Users also specify the diaphragm geometry, which informs ATP-Bridge of the total depth of a front cell on the tower. A cross-sectional view of the tower for a 40-in. and a 50-in. diaphragm is shown in Figure 8.9 for illustrative purposes. In the baseline case, a 40-in. cell depth is assumed.

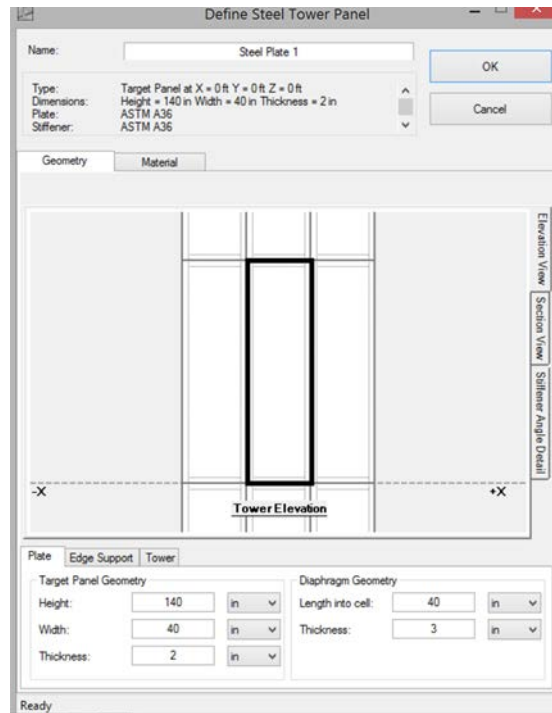
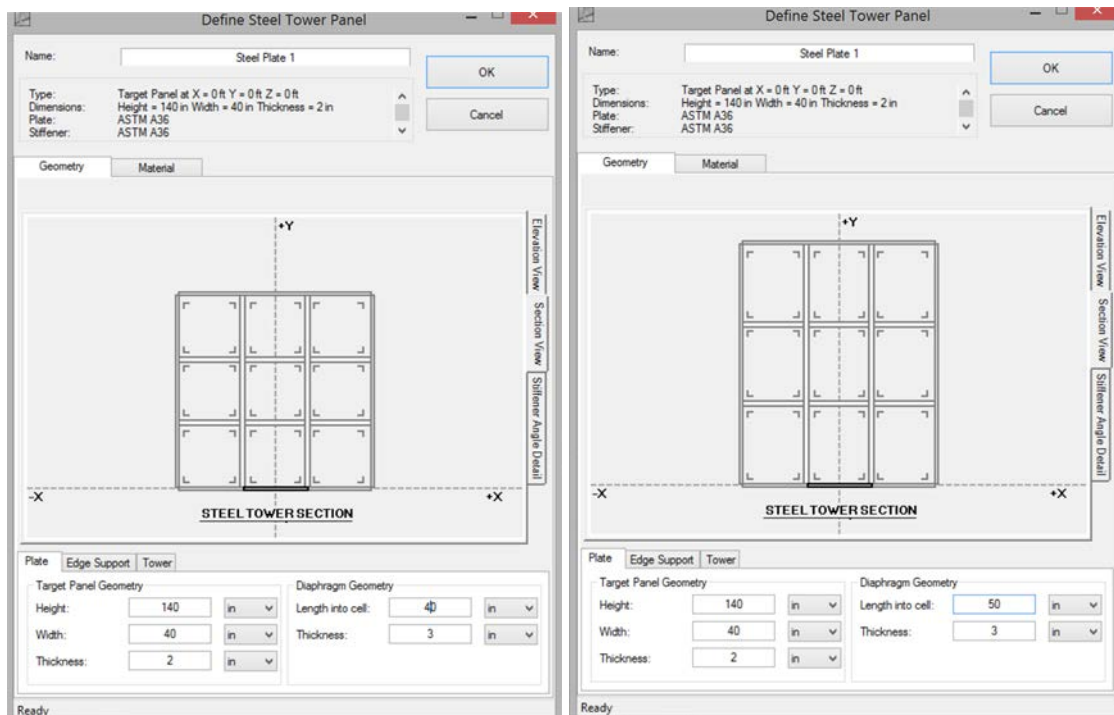


Figure 8.8 Sample Steel Panel Geometry Input



(a)

(b)

Figure 8.9 Illustration Showing Cell Depth Corresponding to (a) 40-in. and (b) 50-in.

The stiffener angles supporting the front face of the cellular tower are assumed to have a leg in contact with the front panel that is 4-in. wide and 0.5-in. thick. This leg of the stiffening angle affects the transverse stiffness of the panel being analyzed. Because the other leg of the angle is fastened to a plate perpendicular to the front panel and effectively extends the depth of the cell, it is not necessary to provide a specific value for the leg dimension because it has little influence on the computed structural response. This simplification is based on the results of parametric FEA studies. Figure 8.10 shows the geometry for the stiffening angles used in this example. The “Tower” tab within the bottom portion of the form simply gives the location of the panel relative to the overall tower dimensions for the purposes of predicting blast loads. While the focus of the response calculations is on a single panel, the specific tower dimensions influence the pressure history a panel will experience based on the effects of how reflected pressures develop and how clearing occurs (see Chapter 4 for additional details on the phenomenology of blast loads). For this example, the tower is assumed to be 30-ft. wide, and the panel being analyzed is directly in the middle.

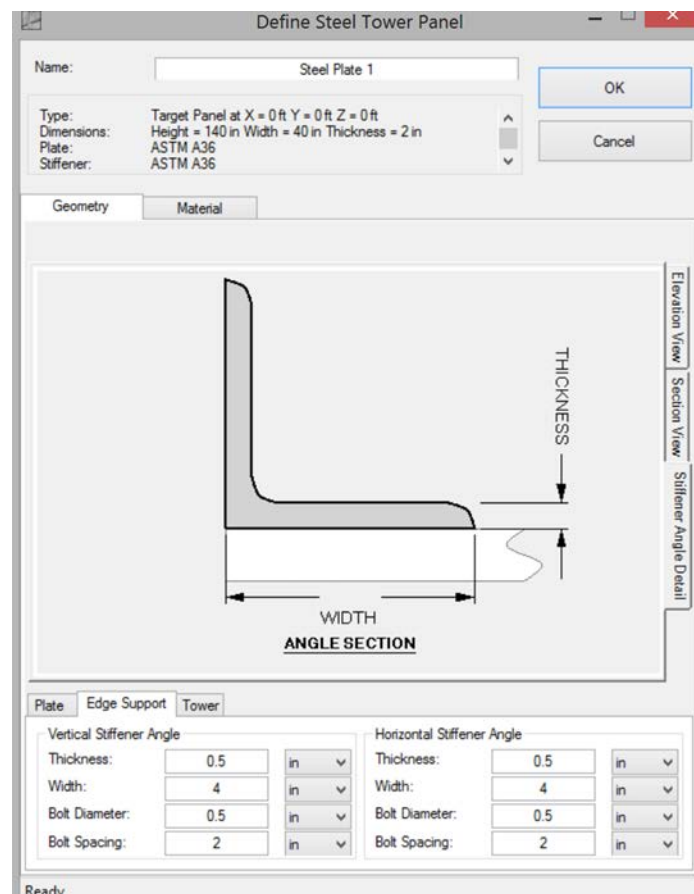


Figure 8.10 Geometry of Vertical and Horizontal Stiffening Angles

The initial threat considered for this scenario is a charge of 1000 lbs. of TNT at a distance of 5 ft. from the front panel. The charge is assumed to be elevated off the deck at a height of 70 in. as shown in the example threat definition given in Figure 8.11.

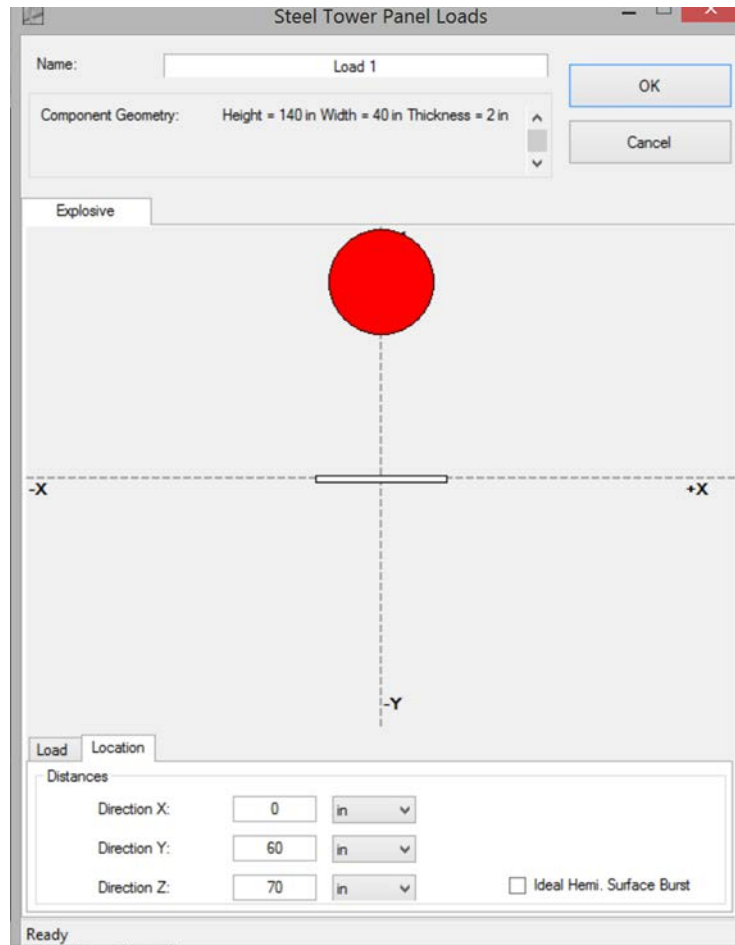


Figure 8.11 Example Threat Definition for Steel Cellular Tower

Once the threat and panel properties are specified, an analysis of the response can be conducted. In addition, ATP-Bridge allows the user to view the panel and threat in its 3D viewer so users can ensure consistency with their input. Two different views of the panel and charge for this scenario are shown in Figure 8.12.

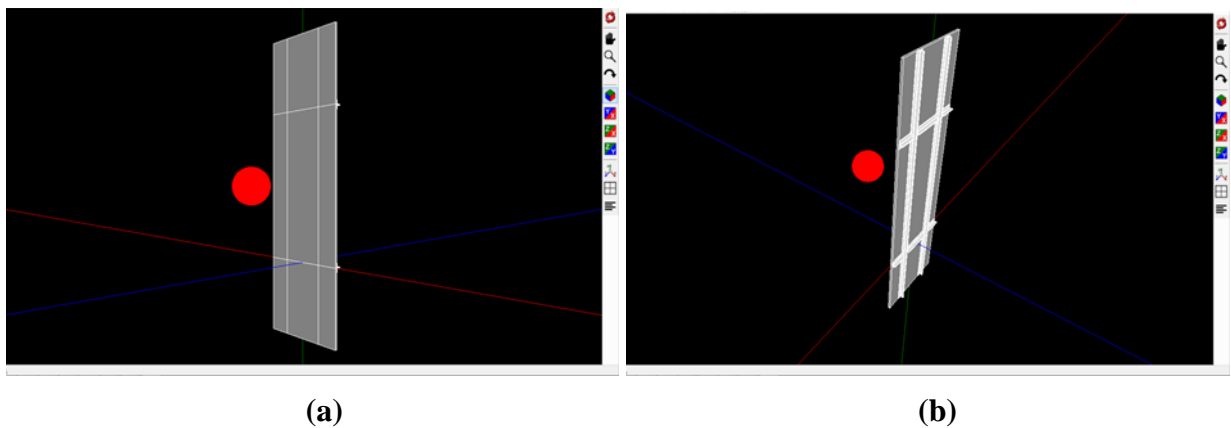


Figure 8.12 Isometric Views (a) In Front of and (b) Behind the Panel Being Analyzed

For this threat, no local damage is predicted, though some partial tearing along the plate edges is expected. Results from this analysis are shown in Figure 8.13.

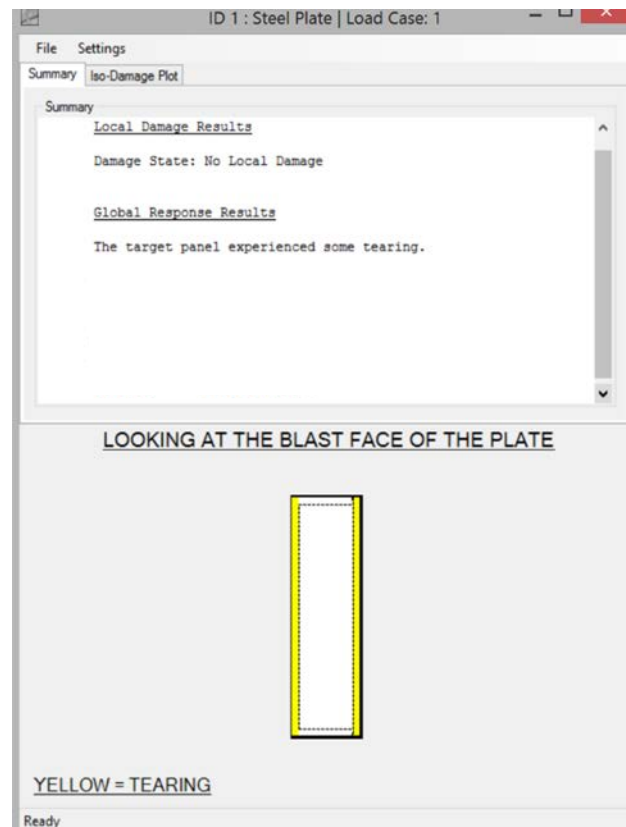


Figure 8.13 Analysis Results Showing Some Tearing at Edge of Panel for Baseline Threat

ATP-Bridge has a unique capability for analyzing the response of steel panels within cellular towers by generating what is known as an “iso-damage” curve as shown in the tab near the top of the form in Figure 8.13. This plot provides curves that show when the threshold associated with different failure modes is reached. For the baseline threat, the predicted iso-damage plot is shown in Figure 8.14. As this figure indicates, the standoff and charge size associated with the onset of tearing, global failure, and local breach can be readily identified. Within ATP-Bridge, “global failure” is the term used to indicate failure of the panel along its perimeter to become a flyer plate. While this type of failure does not necessarily mean global collapse of the steel tower under consideration, the acceptable damage within ATP-Bridge is assumed to be limited to this case. Knowledge of the thresholds associated with different limit states as shown in the iso-damage plot is quite helpful in studying response and evaluating potential design modifications. For example, in this case, the graph indicates that the charge must be quite close (approximately 1.3 ft.) to the target for local breach to control. At larger standoffs, the onset of tearing will control. This plot also indicates that a charge weight greater than approximately 1500 lbs. of TNT will cause global failure of the front plate before local breach will occur (where the edges of the panel remain intact but a localized failure within the boundary of the panel occurs). To verify this understanding, the threat acting against the baseline panel is increased to 2000 lbs. TNT. Results for this analysis are provided in Figure 8.15. As expected, global failure controls the response.

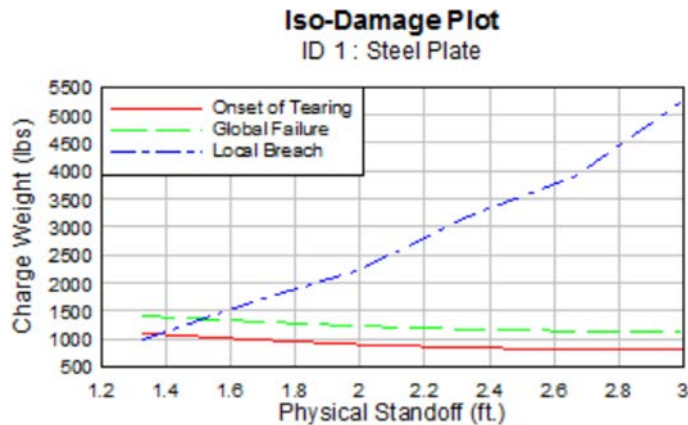


Figure 8.14 Iso-Damage Plot for Baseline Example

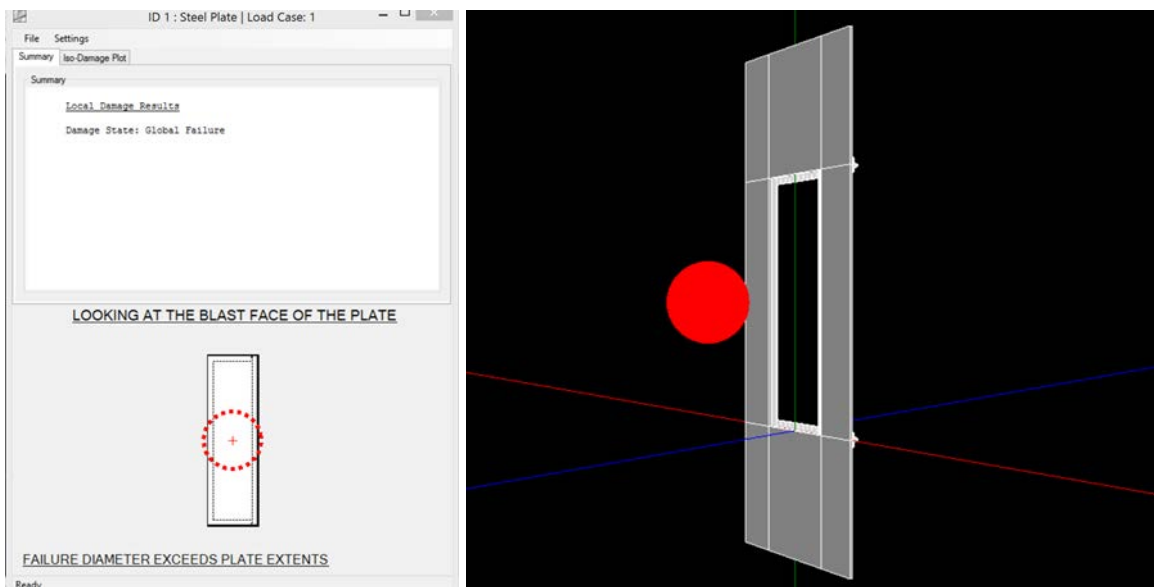


Figure 8.15 Global Failure of Front Panel due to Charge of 2,000-lbs TNT

To mitigate this more severe threat of 2000 lbs. TNT relative to the baseline threat of 1000 lbs. TNT, several options can be considered. The strength of the steel can be increased, the thickness of the front plate could be increased, and the geometry of the front panel dimensions could be adjusted using additional stiffeners. Connection failure must also be considered for any of these potential retrofits. Increasing the capacity of the front plate so that it can survive will result in large forces being transferred to stiffener and diaphragm components. Currently, ATP-Bridge assumes failure will occur in the front plate and does not directly check the supporting components. Such a check can be conducted with detailed FEA models after ATP-Bridge is used to help identify initial plate properties capable of surviving the design-basis threat. For the present example, the only change that is considered is doubling the thickness of the front plate to 4 in. Although an increase to a 3-in. plate and 3.5-in. plate were considered, these modifications did not prevent global failure of the plate. In Walker, et al. (2011) [113], a combined approach is recommended where several options are used in combination. For example, for this case, it is possible to increase the steel strength to 70-ksi and use a front plate that has a thickness of 3 in. With this combination of design changes, the front panel survives the 2000-lb. threat with no

local or global damage, and the peak deflection is predicted to be 6.35 in. (Figure 8.16). Of course, in a retrofit situation it would not be possible to change the material strength of the entire front panel, but the retrofit material could be made of higher strength steel than the tower. Additional information on retrofits is provided in the next section.

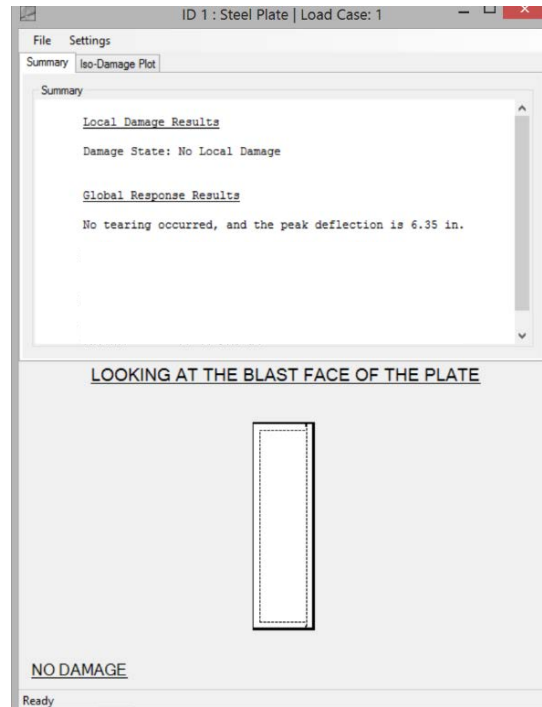


Figure 8.16 Modified Front Panel with 70-ksi Steel and 3-in. Thickness

Finally, to illustrate the possibility of local breaching and an associated threat for the original baseline design, consider a new charge of 500 lbs. TNT placed at 1.25 ft. (16 in.) from the front panel. As expected from the iso-damage plot, this case produces localized breach failure with a predicted breach diameter of 32.5 in. Results for this case are shown in Figure 8.17.

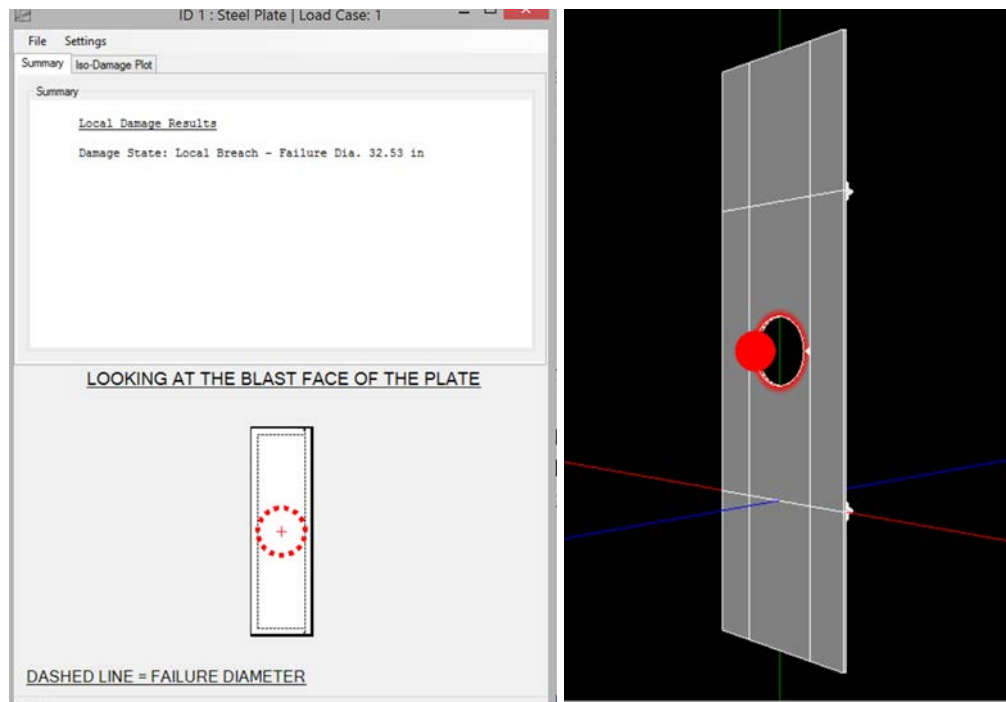


Figure 8.17 Localized Breach in Baseline Design

8.6 Overview of Threat Mitigation Retrofit Strategies

Retrofitting steel suspension bridge towers to withstand severe close-in blast threats was a primary focus of pooled-fund study TPF 5(1190) “Validation of Numerical Modeling and Analysis of Steel Bridge Towers Subjected to Blast Loading.” In fact, much of the individual reports in 2011 by Walker, et al. [113, 114, 115, 116, 117] go into extensive detail regarding the various retrofit options considered. Readers interested in this information are highly encouraged to review these reports. In this section, a summary of the work completed, along with recommendations for effective retrofit approaches, is provided.

As indicated by Walker, et al. (2011) [113], all retrofits, to be effective, “must somehow reduce the applied force, and/or it must increase the structural resistance, and/or it must increase the mass and thus the inertial resistance. Keeping these basics in mind, the myriad of structural hardening schemes can be grouped into several basic categories.” In many cases, it may not be easy to independently adjust the mass and stiffness of a retrofit since the addition of any component tends to affect both properties. In the pooled fund study, Walker et al. (2011) [113] report “The benefits of adding combined mass and resistance were clearly demonstrated in Series 2, where a retrofitted model was constructed and tested at several different levels of explosive loading.” The retrofit used a built-up front plate (i.e., added mass and resistance) and added internal diaphragms to shorten the unsupported length of the towers, which shortened the panel span length and gave an aspect ratio expected to engage 2-way response (i.e., added resistance). The specimen with this retrofit did perform much better than the original specimen, but it also suffered localized damage that raised concerns because of the high-speed fragment that was produced. As indicated by Walker, et al. (2011) [113], “This test result was the first to highlight the conflicting challenges of mitigating these near-contact detonations. If the structure is over-stiffened, it will not have sufficient strain capacity to absorb the kinetic energy that remains

beyond that absorbed through inertial resistance. A delicate balance must be achieved between stiffening/strengthening and ductility.”

Other “exotic” high-strength, light-weight materials were considered during the test program (e.g., carbon, Dyneema, and others), but these materials performed poorly because they did not provide sufficient strength and had such a low weight they did not improve inertial resistance. In general, project researchers found concrete and steel to offer the best options for potential retrofits. Various techniques for filling the cells of steel cellular towers were considered, including fills made from concrete, sand, or water. This evaluation was conducted computationally. None of the options considered proved to be a workable solution due to practical reasons and performance issues. For example, filling the cells clearly makes inspection difficult if not impossible. The fills considered also led to high shear demands on the tower that could not be withstood due to the large transfer of forces from the fill material to the steel tower components.

Sacrificial shields were considered as part of the test program where the shield was intended to add mass to increase inertial resistance but provide limited strength so large force demands would not be transferred to steel tower components that could not resist such high forces. The sacrificial shields considered consisted of a concrete panel mounted to the front of a steel cellular tower specimen. Results from the test program showed that, while the sacrificial shield concept is sound, practical space limitations and other logistical factors constrained the size of a panel that could be used. In the end, the benefit of the shields tested was negligible because “residual kinetic energy of the sacrificial concrete slab overwhelmed the resistance (strain capacity) of the responding steel plate” [113]. Further, placing a sacrificial shield in front of a tower effectively creates a smaller standoff than would otherwise exist. Thus, the large blast pressures would cause these shields to fail and place high load demands on the components behind them that they were supposed to protect. Eventually, for steel cellular towers considered in this previous study [113], the sacrificial shield concept was not found to be effective. Nonetheless, future research on this topic is recommended to evaluate overall tower response and propagation of damage from exterior cells to interior cells for different shielding options.

Structural shields, which add mass and strength, were also considered. According to Walker, et al. (2011) [113], “The great challenge in this case is to design a structural shield of sufficient mass and strength that all of the explosive energy is effectively depleted by the shield before reaching the protected tower walls.” Because of limited standoff distances and the associated available space within which a structural retrofit can be constructed, coupled with practical considerations related to available plate thicknesses and material strengths, pooled-fund project researchers concluded that completely mitigating that largest magnitude threat considered would require the first row of cells to experience damage to help dissipate the energy of the loading. Thus, the first row of cells was considered sacrificial [113]. Again, this level of damage may not be permissible in all cases. The retrofit option of the structural shield, among the wide variety of options considered, was the best alternative. Per Walker, et al. (2011) [113]:

While many other configurations were considered, that shown in [Figure 8.18] was found to be optimal in terms of minimum steel thickness requirements and damage containment to the front row of cells only. The configuration utilizes a 3.5-in.-thick (full-scale) HPS Grade 70 steel C-shaped structural shield. The side “wings” that

form the C-shape offer multiple benefits, i.e., they stiffen the shield to induce a stiffer 2-way response, but not so stiff that local shearing occurs. They serve as side supports for the front portion of the shield and help transfer more of the reaction loads to the upper and lower diaphragm sections that should have more inherent strength to resist these reactions. Also, they offer the added benefit of protection of the side walls in case the VBIED is detonated near a tower edge. In addition to the C-shaped shield, Grade 70 diaphragms (7/8-in. thick) are added in the rearward cells at 1/4-points between the existing diaphragms.

While the actual damage experienced by steel cellular towers was greater than predicted by state-of-the-art coupled analyses using the DYSMAS code, the overall behavior was still quite good and better than the performance achieved with other retrofit options.

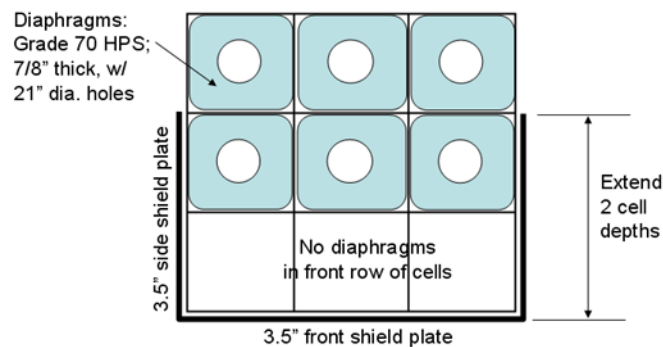


Figure 8.18 Recommended Retrofit Option [113]

The last retrofit option considered in the test program included a “catcher beam” to arrest the fragments that would be expected to develop for the design-basis threat when the front plates fail. In this arrangement, the first row of cells is left unmodified (i.e., not strengthened) and are permitted to fail because they are considered sacrificial. Per Walker, et al. (2011) [113], the catcher beam concept relies on “placement of a structural beam with sufficient mass and strength behind the fragmenting plate to catch the plate and arrest its motion. The catcher beam absorbs the kinetic energy of the fragment(s) through inertia and internal strain.” While the catcher beam concept was effective at slowing or preventing the propagation of fragments, the protected structure must still be able to absorb the imparted energy. Thus, the catcher beam essentially redirects the energy of the flying fragments to other parts of the structure. This concept can be successful, but there exist significant challenges in its implementation. Further study of this approach is warranted.

While many of the tested retrofits performed well, no single retrofit provided the desired level of protection that was set as an objective for the pooled-fund study. Thus, Walker, et al. (2011) [113] highly recommend combining retrofit concepts to produce a solution with the desired performance, such as shielding and additional diaphragms.

8.7 Chapter Summary

In this chapter, challenges associated with the design and retrofit of steel cellular towers were presented. Because steel cellular towers are no longer a favored structural system used in constructing long-span bridges in the U.S., emphasis should be on protecting existing

infrastructure composed of these types of components. Because this structural system is used in some of the most heavily traveled bridges in the U.S., it is critical that protective design strategies be developed to protect such bridges from potential terrorist attacks. What makes protecting these components extremely challenging is the small standoff distances that are normally present on the bridges where steel cellular towers are found.

In this chapter, failure modes and overall behavior of blast-loaded steel cellular towers were presented. A detailed example using ATP-Bridge was provided. The chapter concluded with a description of possible retrofit techniques that can be used to mitigate damage to steel cellular towers subjected to close-in detonations, and the most effective retrofit from past testing was described. In the next chapter, protective design of reinforced concrete towers is presented. These types of structural components are highly favored today when designing and constructing long-span bridges, particularly cable-stayed bridges. Thus, the information in the next chapter is highly relevant for the design of new bridges and the protection of existing bridges constructed using reinforced concrete towers.

9.0 PROTECTIVE DESIGN GUIDANCE FOR REINFORCED CONCRETE TOWERS

Reinforced concrete (RC) bridge towers are particularly important to the structural stability of a cable-stayed bridge. RC bridge towers transmit gravity loads from the bridge deck to the foundation, and they often play an essential role in the lateral force resisting system of a cable-stayed bridge. While local damage to the bridge deck and/or supporting bridge girders is undesirable, redundancy and ductility will often allow for internal forces to redistribute when damage occurs to these components, thus allowing an alternate load path to be realized and global stability maintained. Conversely, extensive damage to an RC bridge tower carries great potential for partial or total collapse of a bridge.

From a security perspective, RC bridge towers are particularly vulnerable to attack due to their public accessibility. Figure 9.1 illustrates their accessibility by vehicles and personnel; a similar security challenge that also exists for steel suspension bridge towers and that was discussed in Chapter 8 of this manual. Because RC bridge towers are often close to the road and pedestrian access, they can potentially be subjected to relatively severe and close-in threats such as hand-emplaced explosives or vehicle-borne improvised explosive devices (VBIED). As can be seen in Figure 9.1, accessibility of the main stayed cables is also a major security concern and is addressed in detail in Chapter 10 of this manual. Access to the interior of an RC bridge tower is also a concern.



Figure 9.1 Illustrating Public Accessibility to Cable-Stayed Bridge Towers (photo from [123])

The panels of RC bridge towers, while seemingly like typical RC walls and slabs, possess unique characteristics that must be considered when assessing their performance to blast loads. As is shown in Figure 9.2, the deck of a cable-stayed bridge is supported by inclined, high-strength steel cables that are anchored to the bridge tower and deck. The cables deliver a vertical force component to the bridge tower, which, in turn, induces an axial compressive stress in the tower panels. To carry this service-level axial stress, the tower panels are normally designed to have an orthotropic steel reinforcement layout, where the larger bars are oriented in the vertical direction as shown in Figure 9.2. Adding to their complexity is the fact that RC bridge tower panels are not isolated. Tower sections generally are comprised of one or more monolithic boxes with horizontal diaphragms discretely spaced along the tower height.

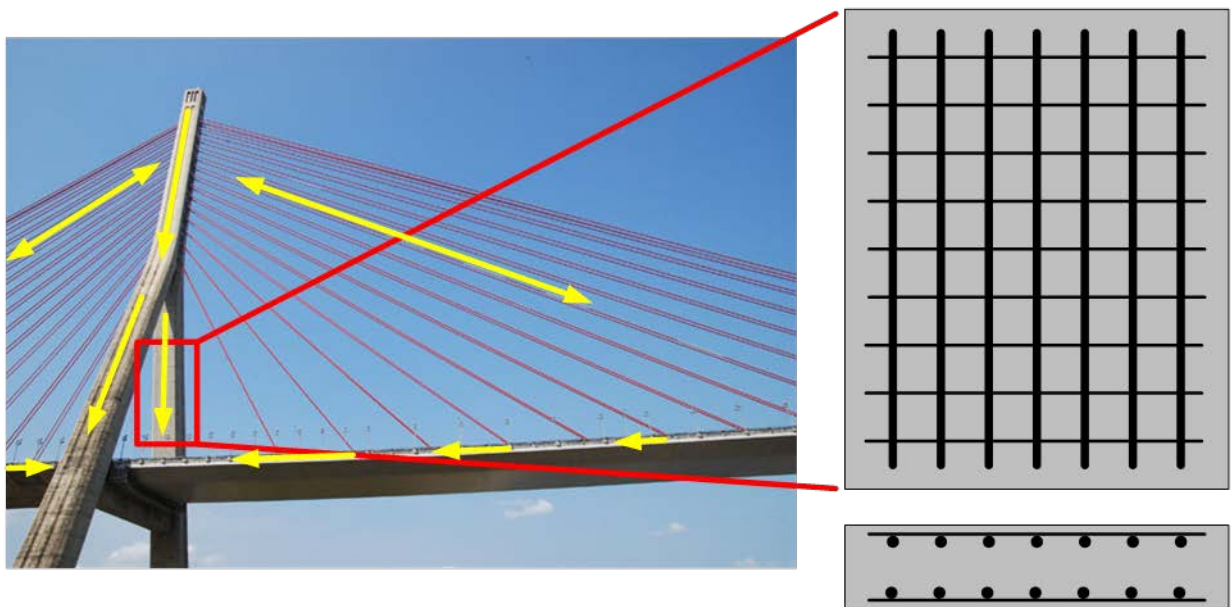


Figure 9.2 Illustrating Presence of Service-Level Axial Stress and Orthotropic Steel Reinforcing Configurations in Typical Cable-Stayed Bridge Towers (photo from [124])

9.1 Design Threats

Like steel cellular towers from Chapter 8 of this manual, the protective design of RC bridge towers must consider a range of threats. Because of the limited standoff that exists on many bridges with these types of towers (Figure 9.3), a primary concern is the mitigation of blast loads due to a VBIED. In addition, consideration must be given to scenarios involving hand-emplaced explosive devices, ranging from unsophisticated bulk explosive charges in a backpack to more sophisticated breaching charges. The potential for an intentional fire or vehicular/vessel impact also exists; though, as will be discussed in Section 9.1.2, consequences from these threats are likely to be less severe than from the close-in detonation of a high-explosive charge. As such, the focus of this chapter is on protective design modifications for blast loading.



Figure 9.3 Emphasizing Public Accessibility to Cable-Stayed Bridge Towers [125]

9.1.1 Blast Loads

Blast loads acting against RC bridge towers can result from a VBIED located near a tower, or blast loads can be due to hand-emplaced devices that are man-portable. The possibility of multiple VBIEDs being detonated around a tower certainly exists; however, the cost to protect against successive attacks is high relative to the likelihood of a sophisticated aggressor carrying out such an attack. An issue of significant importance is the proximity of these types of towers to the bridge deck (i.e., pedestrian walkways and roadway). Owing to this proximity issue, the ability of a terrorist to place many high-explosives very close to an RC bridge tower exists and is a realistic and concerning scenario. Chapter 4 discussed how increasing standoff is the most effective way to mitigate blast effects. Doubling the distance between an explosive and target requires that the charge size be increased by a factor of eight to achieve the same peak pressure because of the cubic relationship between these variables (see Chapter 4). When standoffs are limited, blast load intensities have the potential to be quite large. Thus, the biggest challenge in designing RC bridge towers to resist blast effects is the potentially severe load magnitudes that need to be resisted.

Many RC bridge towers are designed to accommodate an access hatch/door at deck level, to facilitate interior inspection of the tower. If access to the interior of the tower cannot be controlled, it is possible to detonate man-portable charges within the interior of a tower. Because of the blast pressure confinement effects associated with this scenario, peak blast impulses can become quite high despite the limited quantity of explosives (relative to a VBIED) that can be introduced to the interior of a tower. Predicting blast loads for such an explosion scenario would require specialized analysis techniques capable accounting for shock-induced pressures and gas pressures, as well as the multiple shock wave reflections that would take place within the interior of an RC tower. Ray-tracing tools and computational fluid dynamics codes (see Chapter 4) could both be viable analysis options. It should also be mentioned that the current version of ATP-Bridge (Chapter 12) does not address explosive threats interior to an RC tower.

Like steel cellular towers, the plan location of an explosives-laden truck relative to the centerline of an RC tower may create a very complicated blast load case. For a truck positioned immediately next to a tower, where the point of detonation is aligned with the tower centerline (Charge 1 in Figure 9.4), blast loads on the incident face of the tower leg will not be uniform across the tower width at a given height above the deck, until some distance above the explosive. The standoff and angle of incidence will be variable across the tower leg's reflecting face; however, in many cases, it is reasonable and conservative to consider a normally reflecting planar shock wave. Loads on the sides of the tower leg will be of lower intensity than the reflecting face. It is typically acceptable in most scenarios to simply assume the side-face loading has a peak magnitude equal to that experienced by the tower leg's leading edge (i.e., the corner joining the side-on and reflecting faces). Whether the loading is considered uniform across the entire side face may be scenario specific. For the conditions assumed with the point of detonation perfectly aligned with the tower leg's plan centerline, the total net load acting on the tower leg will be greatest as the entire width of the front face will be exposed to reflected pressure. For this threat scenario, predicting the reflected blast load at the height of burst is of primary importance.

In cases where an explosive threat's point of detonation is not aligned with the plan centerline of the tower leg (Charge 2 in Figure 9.4), particularly in cases where the point of detonation may be close to the corner of a tower, the prediction of loads and response becomes much more complicated. In such a scenario, the tower leg's front face and side face will be exposed to blast loads at an incidence angle. The specific geometry of the case being considered will significantly affect the computed loads and response. The angle of incidence, and hence the reflection coefficient, will change along the faces in line-of-sight of the explosive. Relative to the case where a truck is perfectly aligned with the tower leg's plan centerline, the load intensity will vary across the width of the side and front faces. The load intensity will be greatest at the point closest to the center of detonation (i.e., shortest standoff) and will diminish as the distance from the explosive increases.

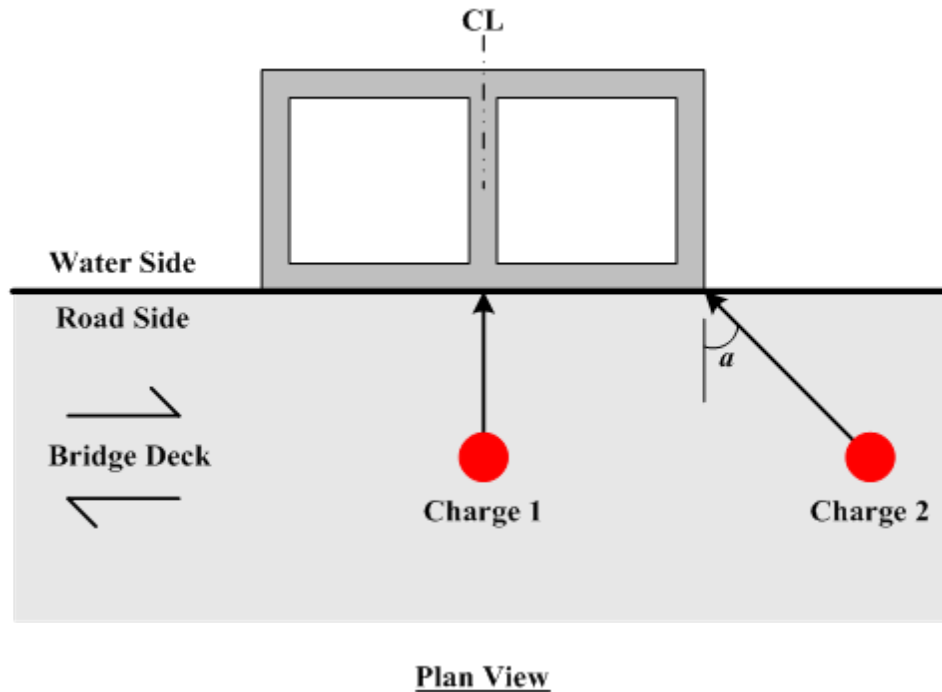


Figure 9.4 Illustration of Hypothetical Two-Cell RC Tower Leg Subject to Explosive Charges Placed On/Off the Tower Leg's Plan Centerline

In both the centerline-detonated and off-center detonated explosive threat scenarios discussed in the previous paragraphs, additional blast load complexity exists due to the angled geometry of typical RC tower legs (e.g., A-frame construction such as shown in Figure 9.2). A shock wave's angle of incidence along the height of an angled RC tower leg varies in such a way as to promote comparatively more severe blast loads than would be experienced by a straight tower leg (e.g., H-frame construction).

In addition to airblast effects, large close-in detonations can produce extensive fireballs near the target thus raising the question as to whether heat transfer from a VBIED is of concern. As was discussed in Chapter 3 of this manual, thermal effects from the fireball of a detonation are typically not a concern because the transient nature of the event typically allows insufficient time for significant heat transfer to occur. Depending on the type of large explosive threat, fragments may also be of concern—particularly for explosives contained in robust and/or heavy casing material or designed specifically to throw fragments/plates. In a recent study by Kersul (2000) [120], it was concluded that fragments associated with VBIEDs tend not to be of significant concern because of their small size and because they are so highly dispersed during the explosion.

Hand-emplaced explosives must be man-portable and accordingly of much smaller size than a truck bomb. Nonetheless, this threat still requires consideration because these explosives can be placed directly in contact with an RC tower. Though small, these contact charges have the potential to cause localized failure and breach of the tower perimeter. Furthermore, if an RC tower leg is attacked with multiple hand-emplaced contact charges, local breach damage could become significant enough to compromise the gravity-load carrying ability of the tower and ultimately precipitate partial or global bridge collapse. Because surveillance and police patrols

can help minimize the likelihood of multiple hand-emplaced threats, the hand-emplaced threat is not considered as critical as the large VBIED threat.

9.1.2 Other Loading Considerations

Thermal effects from a sustained fire (e.g., ignition of a tanker truck on or near a bridge) can pose a threat to the structural integrity of reinforced concrete members. For instance, PTI DC45.1-12 *Recommendations for Stay-Cable Design, Testing, and Installation* [126] defines a hydrocarbon pool fire and puts forth thermal effects requirements for stay cables and anchorages. Sustained thermal loading can degrade concrete material properties, cause spall damage, and distort geometry during the post-event cooling process producing (potentially large) displacement-based forces to develop in structural members. Additional discussion regarding thermal effects on the performance of reinforced concrete members is provided in Chapter 3 of this manual.

Although the threat of intentional ramming by a ground-based vehicle or maritime vessel cannot be ignored, the geometry of most long-span bridges comprising RC towers, coupled with existing protection measures to reduce the effects of an accidental impact from a vehicle or maritime vessel, make this mode of attack less attractive than others.

While the non-explosive threats discussed in this subsection are generally expected to be either less likely or less severe than an explosive attack involving a VBIED or precision contact charge, these threats should always be considered. It is not inconceivable that certain bridge-specific details or site features may give rise to exceptionally heightened vulnerability to these non-explosive threats.

9.2 Failure Modes and Performance Criteria

Given the size and massiveness of typical RC bridge towers, system-level tower response and associated damage is not of primary concern with respect to a close-in explosive threat. Rather, extensive localized damage to one or multiple panels of an RC tower leg that, in turn, precipitates gross loss in gravity-load carrying capacity and/or partial or total bridge collapse is the primary failure mode of interest.

Chiarito et al. at the U.S. Army Engineer Research and Development Center (ERDC) recently carried out a multi-series experimental test program where they subjected scaled RC tower panel specimens to close-in explosive charges [127, 128]. Figure 9.5 presents a few post-test images from a Series 1 test [127] that highlight the severity of breach damage that can be sustained by a blast-loaded RC tower panel. During their Series 1 “baseline vulnerability” tests, this type of extensive breach damage was observed for most all specimens. In addition, the generation of high-velocity secondary fragments comprised of rubblized concrete was observed during many of the tests. While additional research is needed to quantify the vulnerability of leeward tower panels to secondary fragment effects, the ERDC research team postulates generally low vulnerability.



Figure 9.5 Post-Test Images of Close-In Blast Test against Scaled RC Tower Panel Specimen Showing Significant Breach Damage [127]

Tang and Hao (2010) [129, 130] conducted numerical simulations of a representative cable-stayed bridge subjected to close-in bulk explosive detonations to ascertain whether extensive localized damage to critical structural components could precipitate collapse of the bridge. Their analysis approach consisted of two steps. The first step involved simulation of a detonation event to predict localized damage to the targeted structural component. The second step involved removing damaged portions of the targeted structural component from the computational model and performing a progressive collapse analysis considering appropriate service loads. Results from their computational study revealed that collapse of the bridge was likely when extensive blast-induced damage occurred to an RC pier or tower; however, collapse was not likely due to extensive blast-induced damage to the deck of a main or back span. Figure 9.6 shows an image of Tang and Hao's computational model 16-sec into a collapse analysis following extensive blast-induced damage to the base of an RC tower. The cable-stayed bridge ultimately suffered total collapse during this scenario. At 16-sec into the collapse analysis, lateral deflections in the two RC towers were observed to be about 65-ft while peak vertical deflections in the main span exceeded 100-ft. As can be seen in Figure 9.6, shear failure of the left back-span deck was also observed which subsequently caused the right back-span to be uplifted vertically and eventually fail. Tang and Hao's computational research went on to investigate the effect of charge standoff on localized damage and collapse potential. While this computational study was certainly not exhaustive in terms of postulated explosive threats and cable-stayed bridge geometries/design, it underscored that extensive localized damage to main gravity-load carrying elements of cable-stayed bridges can precipitate partial or total bridge collapse and enforcing standoff (which is often difficult if not impossible for most bridges) can be an extremely effective mitigation measure.

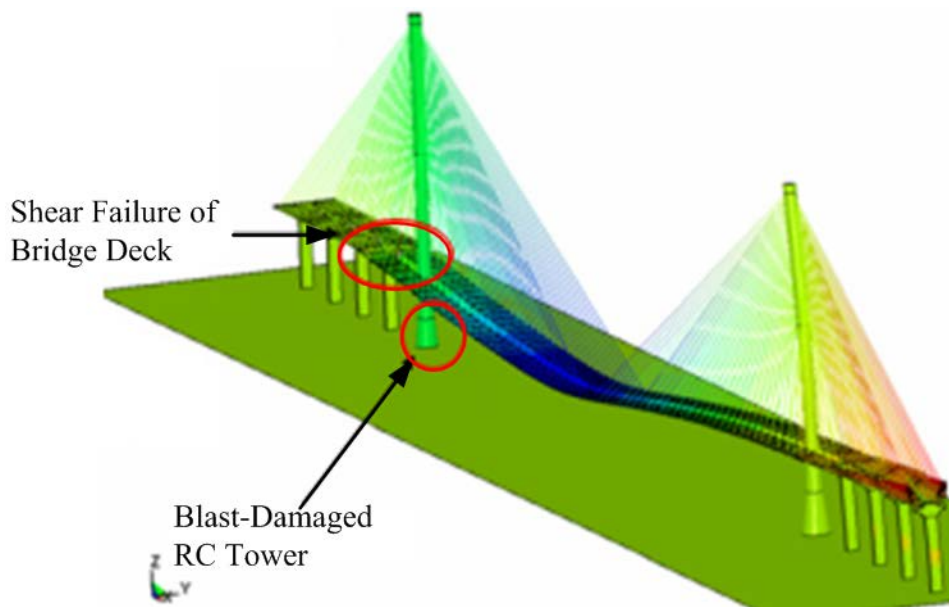


Figure 9.6 Collapse of Cable-Stayed Bridge due to Close-In Detonation near RC Tower Base (adapted from [129])

As was discussed in Chapter 6 of this manual, there currently exist no well-developed or standardized component-level response limits and associated system-level performance criteria for blast-loaded bridges. Such criteria do exist for building structures, but their empirical basis does not extrapolate directly to bridges in all cases. Until additional research can be conducted to establish bridge-specific blast performance criteria, knowledge gained from existing research must be used in conjunction with advanced analysis techniques to ensure a robust RC tower design or retrofit that can provide adequate load carrying capacity following a design-basis extreme loading scenario. Protective design and retrofit strategies, detailing recommendations, and an overall recommended design procedure, all aimed at enhancing the robustness of an RC tower, are provided in the remainder of this chapter. Design examples using the ATP-Bridge software are also provided at the end of the chapter.

9.3 Design Strategies and Detailing Recommendations

As was discussed earlier in this chapter, extensive damage to individual RC tower panels is of primary concern. Because there exist no component-level performance criteria pertaining to specific concrete breach diameter thresholds above which certain RC bridge tower configurations and geometries lose their gravity-load carrying capacity, it is recommended that RC tower panels be designed to prevent breach damage for a given design-basis threat whenever possible. Past research has shown that increasing concrete panel thickness and concrete compressive strength are both effective in increasing the spall and breach capacity of a concrete panel [85] and is typically the most cost-effective method of reducing spall/breach. And, while it will not prevent spall/breach from occurring, increasing the total reinforcement ratio of a concrete panel can decrease the extent of breach damage [85] and decreasing reinforcement spacing may restrain spall. The use of high-performance and fiber-reinforced concretes can also increase an RC tower panel's spall and breach capacity. The use of steel spall plates to retain spalled concrete on the back face of a blast-loaded RC panel can be advantageous in certain applications. The use of steel plates on the front face of an RC panel may also be advisable for

shock attenuation. Given a design-basis explosive threat, ATP-Bridge can be used to design RC tower panels to minimize or prevent spall and breach damage. Although, it should be noted that the current spall/breach algorithm in ATP-Bridge cannot address high-performance or fiber-reinforced concretes.

Even if protective design measures are taken to prevent breach damage for a given design-basis threat, extensive local concrete damage in the forms of front-face or back-face spall can potentially lead to secondary RC panel instabilities. Figure 9.7 shows examples of rebar buckling instabilities following loss of rebar cover. While the particular images of damaged load-bearing RC walls shown in Figure 9.7 were captured during earthquake post-event reconnaissance efforts, the damage and associated limit state are also applicable to close-in detonations against load-bearing RC tower panels. Detailing strategies to prevent local rebar buckling include placing the heavier vertical bars inside of the transverse bars and limiting the unbraced length of vertical bars with smaller transverse bar spacing. Smaller transverse rebar spacing will also promote enhanced concrete core confinement, which, in turn, will increase an RC panel's capacity to resist localized concrete damage and rebar buckling. Whenever possible, rebar splices should be located away from anticipated areas of potential severe blast loads (e.g., near an RC tower base and at/near deck level) and lap splices should be provided with additional lap length. Welded and mechanical bar splices may be used in place of lap splices only if structural response is limited to elastic behavior. Tying separate curtains of vertical rebar together using stirrups in the through-thickness direction can also be done for some limited height of an RC tower panel above the bridge deck. It is recommended that a maximum stirrup spacing of $d_{bar}/5$ be used, with 180-deg hooks at both ends in areas where spall is expected (90-deg hooks may be used in tower faces not exposed to blast and that are not likely to suffer spall damage). In general, seismic detailing provisions of load-bearing RC walls offer many design strategies that would also be beneficial for protective design of RC tower panels (for example, see [131]). The detailing recommendations for blast-loaded RC bridge columns put forth by Williamson et al. in NCHRP Report 645 [24] also serve as helpful and relevant guidance for designing blast-loaded RC tower panels.

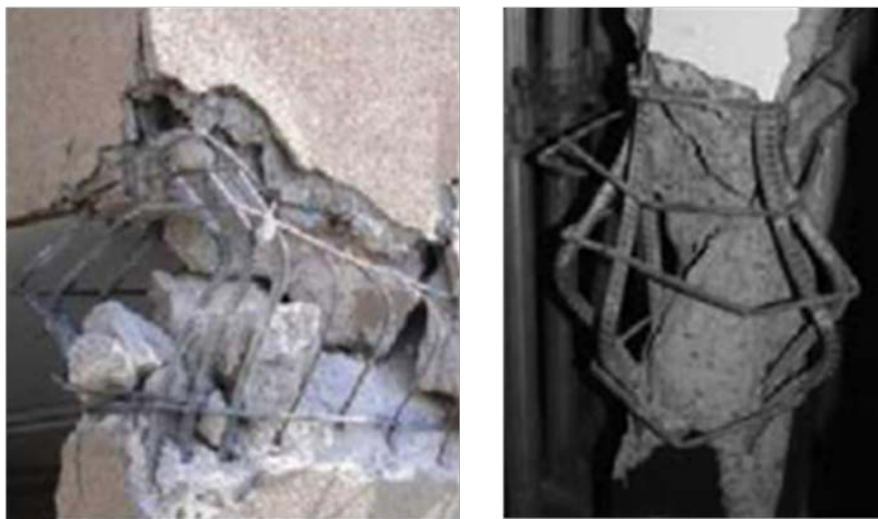


Figure 9.7 Illustrating Steel Reinforcement Buckling in Reinforced Concrete Panels Following Localized Concrete Damage [132]

Because RC bridge towers are subject to sustained service-level axial compressive loads, component-level buckling of an entire RC tower panel is another limit state that must be considered in context of protective design for extreme loading; especially if the potential for extensive material-level concrete damage exists. Figure 9.8 shows examples of RC panel buckling following extensive concrete damage. While the particular images of damaged load-bearing RC walls shown in Figure 9.8 were again captured during earthquake post-event reconnaissance efforts, the damage and associated limit state are certainly applicable to close-in detonations against load-bearing RC tower panels, too. The section geometry and properties of an RC tower panel, panel edge conditions, and location(s) of horizontal diaphragms within the RC tower can all influence the susceptibility of an RC tower panel to component-level buckling. If extensive concrete damage occurs early in time due to a close-in detonation event, the loss of concrete cover and (even worse) loss of concrete core confinement can act to increase an RC tower panel's effective slenderness thus rendering it more susceptible to component-level buckling. Given the difficulties with simulating significant sustained axial compression during and immediately following live blast tests, very little (if any) blast-related experimental data addressing this phenomenon currently exist from which to establish component-level blast performance criteria. "Residual capacity" tests have been performed by some researchers, where blast-damaged specimens are transported to a structural laboratory and quasi-statically loaded in axial compression until failure is observed. While this two-step testing approach certainly yields interesting and useful data, issues related to (a) specimen disturbance during transport and quasi-static test setup and (b) the absence of the coupled, dynamic nature of response that would be experienced by a blast-damaged, load-bearing structural member put to question the validity of two-step residual capacity test data with respect to performance criteria development. As such, the design strategy for preventing component-level buckling of blast-loaded RC tower panels should incorporate the detailing recommendations for ensuring concrete core confinement and local buckling resistance of vertical steel reinforcement and should rely on advanced dynamic analysis techniques capable of simulating the coupled, dynamic nature of a blast-damaged, load-bearing RC tower panel.

In some cases, it is possible that a project-specific design-basis threat is so severe that a conventional reinforced concrete design solution becomes prohibitive. In these cases, the current state-of-the-practice has been to employ extensive hardening strategies such as steel-concrete composite sections (e.g., steel plates with reinforced concrete in between and tied together with steel studs that are welded to the steel plates and embedded in the concrete) over some height of an RC tower. An example of this extensive hardening is shown in Figure 9.9 for a scaled RC tower specimen that was hardened with steel-concrete construction and blast tested on its side. This single scaled blast test was conducted as a proof-of-concept for a specific project. Figure 9.10 shows images of the RC tower specimen's extensive steel reinforcing cage. Heavier bars can be seen on the inside of the lighter, closely spaced transverse bars. In addition, discrete spiral reinforcement can also be seen running longitudinally along the RC tower specimen to provide additional concrete confinement.



Figure 9.8 Illustrating Component-Level Buckling of Reinforced Concrete Panels Following Extensive Concrete Damage [132]

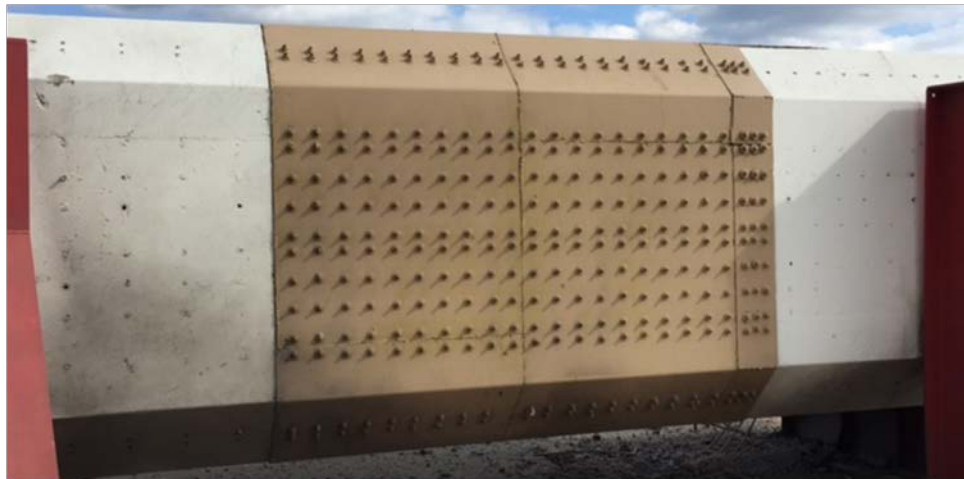


Figure 9.9 Post-Test Image of Hardened RC Tower Specimen Back Face



Figure 9.10 Images of Hardened RC Tower Specimen Steel Reinforcing Cage

9.4 Recommended Design Procedure

The chief protective design objective for blast-loaded RC towers is to mitigate extensive local damage to individual RC tower panels such that gross loss in gravity-load carrying capacity and consequent collapse of the bridge is prevented. To achieve this chief objective, a recommended design procedure consisting of the following steps should be carried out:

- Blast load characterization
- Component-level analysis and design of most severely loaded RC tower panel(s)
- System-level analysis to evaluate potential for collapse of bridge

These steps are further described in the following paragraphs. It should be noted that implicit in this recommended design procedure is the assumption that a computational model of the entire bridge already exists to support conventional design tasks.

Given a specific design-basis explosive threat, the first step in the recommended design procedure is to characterize blast loads on the RC tower of interest. The blast load characterization method should be carefully selected based on the nature of the design-basis explosive threat (e.g., type of explosive composition, charge shape, bare or cased charge, external or internal detonation, charge standoff from RC tower panels, etc.), and Chapter 4 of this manual can be consulted for additional guidance on the selection process.

The next step in the recommended design procedure is to use the existing computational model of the bridge to determine the design axial compressive load carried by the RC tower. Component-level dynamic analysis of the blast-loaded RC tower panels is then conducted to determine adequate panel thicknesses and steel reinforcing layouts to minimize localized damage (spall and breach) and prevent component-level damage/failure. Proper rebar detailing should be followed to ensure that concrete core integrity is maintained in the presence of spall damage. The analysis should consider the sustained axial compressive load carried by the RC tower and

should follow the boundary condition and analysis approach guidance provided in Sections 9.4.1 and 9.4.2, respectively. Component-level dynamic analysis and RC tower panel design iterations should ensue until acceptable RC tower panel blast performance is achieved. At this stage of the protective design process, *acceptable blast performance* should be taken to mean minimal localized damage (spall and breach) and no component-level flexural or direct shear failure. Effects of any component-level damage on system-level bridge response is evaluated in the next step of the design procedure, the results of which may warrant an additional iteration on component-level dynamic analysis and RC panel design.

The final step in the recommended design procedure is to map any incurred RC tower damage from the final component-level dynamic analyses into the existing computational bridge model and perform a dynamic collapse analysis. Extreme care must be taken in interpreting RC tower damage and appropriately representing that damage in the context of a system-level computational model of the entire bridge. No standard procedures or techniques exist for this task and the complexity involved will be highly project-specific. Should the collapse analysis result in partial or total bridge collapse, an additional iteration on RC tower panel design, component-level dynamic analysis, and system-level collapse analysis should be carried out for a redesigned or retrofitted condition. Additional guidance on performing the dynamic collapse analysis is provided in Section 9.4.2.

It should be emphasized that the recommended protective design procedure described in the previous paragraphs require an in-depth knowledge of blast effects, high-rate and large deformation material response, and advanced dynamic analysis and computational modeling. Accordingly, it is recommended that the protective design of RC towers be performed by highly qualified structural engineers with extensive experience in analysis and design for extreme loading.

9.4.1 Boundary Conditions

As is discussed in more detail in Section 9.4.2, it is recommended that component-level dynamic analysis of RC tower panels begins with expedient, moderate-fidelity analysis tools for preliminary analysis. If the geometry or structural component configuration is complex, the standoff is below 1-ft/lb^{1/3} scaled range, or if the preliminary analysis results are in question, high-fidelity finite element analysis of the blast-loaded RC tower should be conducted to obtain detailed information regarding component blast damage. The complex nature of the latter task warrants specific discussion on appropriate structural idealizations, simplifications, and boundary condition definitions in developing the detailed finite element model of an RC tower. While a detailed treatment of finite element formulations, meshing conventions, kinematic constraint/contact definitions, and otherwise is beyond the scope of this manual, the following paragraphs offer some general guidance and issues to be considered. It is recommended that only highly qualified individuals with extensive experience using advanced simulation software perform this detailed finite element modeling task.

The objective of the high-fidelity finite element analysis is to determine with a high level of confidence the extent and severity of local damage likely to be incurred by a blast-loaded RC tower. In addition to generating a high-quality finite element mesh and constitutive representation of the RC tower—both of which are discussed in Section 9.4.2—the definition of appropriate boundary conditions is critical to the accuracy of the nonlinear dynamic analysis.

Appropriate boundary conditions must be defined at any locations along the height of the RC tower where interfacing structural members of the cable-stayed bridge exist. Interfacing members can include, but are not limited to, reinforcement, stay cables, the bridge deck, additional members of the bridge tower (if only a single leg of a bridge tower is being analyzed) and the tower foundation. Boundary conditions can be applied with special computational elements, such as springs or calibrated finite elements, or they can be applied with kinematic constraints such as single-point constraints, constrained nodal rigid bodies, etc. For instance, the presence of interfacing stay cables can be represented with tension-only spring elements and the rigidity of an interfacing bridge deck can be represented with shell elements that have been calibrated (i.e., thickness and elastic properties) from the existing computational model of the entire bridge (the one that has been assumed to exist to support conventional design tasks). If the considered explosive threat is located at deck level, then the flexibility of the RC tower foundation is likely not of primary concern for the analysis; however, a representation of the bridge deck may be needed. In this case, computational nodes at the base of the RC tower section can simply be given a fully or partially fixed kinematic constraint.

Related to boundary conditions is the need to accurately represent the presence of sustained gravity loads in the RC tower prior to simulating a transient blast event. The application of such loads is typically performed during a “preload” stage of the simulation, either statically using an implicit solver or quasi-statically using an explicit solver and special “dynamic relaxation” controls (i.e., one or multiple temporary damping mechanisms). Regardless of the preload technique, it is imperative that the RC tower model reaches a state of static equilibrium under the correct sustained gravity loads prior to performing a subsequent nonlinear dynamic blast analysis. The gravity loads should be held constant throughout the transient phase of the simulation, and a post-event phase of the analysis should also be performed wherein the gravity load remains active on the blast-damaged RC tower to observe whether any structural instabilities precipitate.

9.4.2 Analysis Approach

The recommended protective design procedure for RC towers entails component-level and system-level dynamic analysis. Additional guidance for both analysis tasks is provided in the following paragraphs. Additional general discussion on dynamic analysis methods for blast-loaded bridges can be found in Chapter 6, and additional discussion on the capabilities and use of ATP-Bridge can be found in Chapter 12 of this manual.

Regarding component-level dynamic analysis of RC tower panels, it is recommended that the ATP-Bridge software first be used to establish preliminary panel thickness, concrete compressive strength, and steel reinforcing bar sizes and layout. As is demonstrated and further described in Section 9.5 and Chapter 12 of this manual, respectively, the current version of ATP-Bridge can expediently predict spall and breach damage and peak dynamic response of blast-loaded conventional RC panels comprising a two-cell RC tower leg (see Figure 9.4). Because material-level concrete damage is highly localized and thus essentially independent of panel boundary conditions (edge effects may come into play for localized damage very near the edge of a panel), ATP-Bridge can also be used to assess spall and breach damage of RC tower legs having section geometries other than that depicted in Figure 9.4. However, if the RC tower in question is not of the two-cell rectangular variety, component-level dynamic response (e.g., flexural response)

cannot be evaluated using ATP-Bridge. An example of a potential alternative component-level dynamic analysis tool for preliminary RC panel design would be the U.S. Army Corps of Engineer's Single-Degree-of-Freedom Blast Effects Design Spreadsheets (SBEDS) tool [86]. RC tower panel designs requiring high-performance or fiber-reinforced concretes or significant, non-conventional hardening (e.g., steel-concrete composite construction; see Figure 9.9) also cannot be evaluated using the current version of ATP-Bridge. It should be mentioned, however, that ATP-Bridge future development plans include additional capabilities to address "special" concretes and various non-conventional design and retrofit strategies.

Once a preliminary RC tower panel design is developed using ATP-Bridge, it is recommended that a high-fidelity finite element model of the blast-loaded RC tower be developed for subsequent nonlinear dynamic analysis. The objective of the high-fidelity finite element analysis is to determine with a high level of confidence the extent and severity of local damage likely to be incurred by the blast-loaded RC tower. While a detailed treatment of finite element formulations, meshing conventions, and otherwise is beyond the scope of this manual, the following paragraph offers some general guidance and issues to be considered.

Given the highly-localized nature of a close-in detonation against a massive RC bridge tower, the finite element mesh and material model definitions can be phased in complexity. For example, concrete need only be represented by 3-dimensional brick elements and a complex nonlinear material model for the region of the RC tower nearest the explosive charge where nonlinear behavior and material damage/failure are anticipated. Beyond the height of burst and where the RC tower remains elastic, the reinforced concrete finite element mesh can likely transition to shell and/or beam elements and a simplified material model. Depending on the situation, an elastic material model may be sufficient in the transitioned zone of the model. Alternatively, a simple elastic-plastic model may be helpful in retaining a nominal ability to capture nonlinear behavior in the transition zone. In addition, a simple elastic-plastic model is a relatively inexpensive approach for preliminary investigation of post-event collapse potential, capturing partial plasticity in certain regions of the mesh for load distribution, and even preliminary analysis to identify proper mesh fidelity zones. In the high-damage region of the RC tower, steel reinforcement should be represented explicitly with an appropriate beam element formulation, nonlinear material model, and a coupling algorithm to capture its bonded behavior with the concrete. Outside of the high-damage region of the RC tower, steel reinforcement can likely be represented with the shell/beam elements in a "smeared" manner with a primary focus on capturing the elastic stiffness of the reinforced concrete. A major challenge with this zoned modeling approach is identifying the high-damage region of the RC tower to begin with. Doing so requires some initial trial and error simulations, engineering judgement, and extensive experience with nonlinear computational modeling. An example of part of a high-fidelity computational RC tower model is illustrated in Figure 9.11. Boundary conditions and initial conditions (i.e., sustained gravity loads) of the high-fidelity finite element model should be established and implemented based on guidance provided in Section 9.4.1.

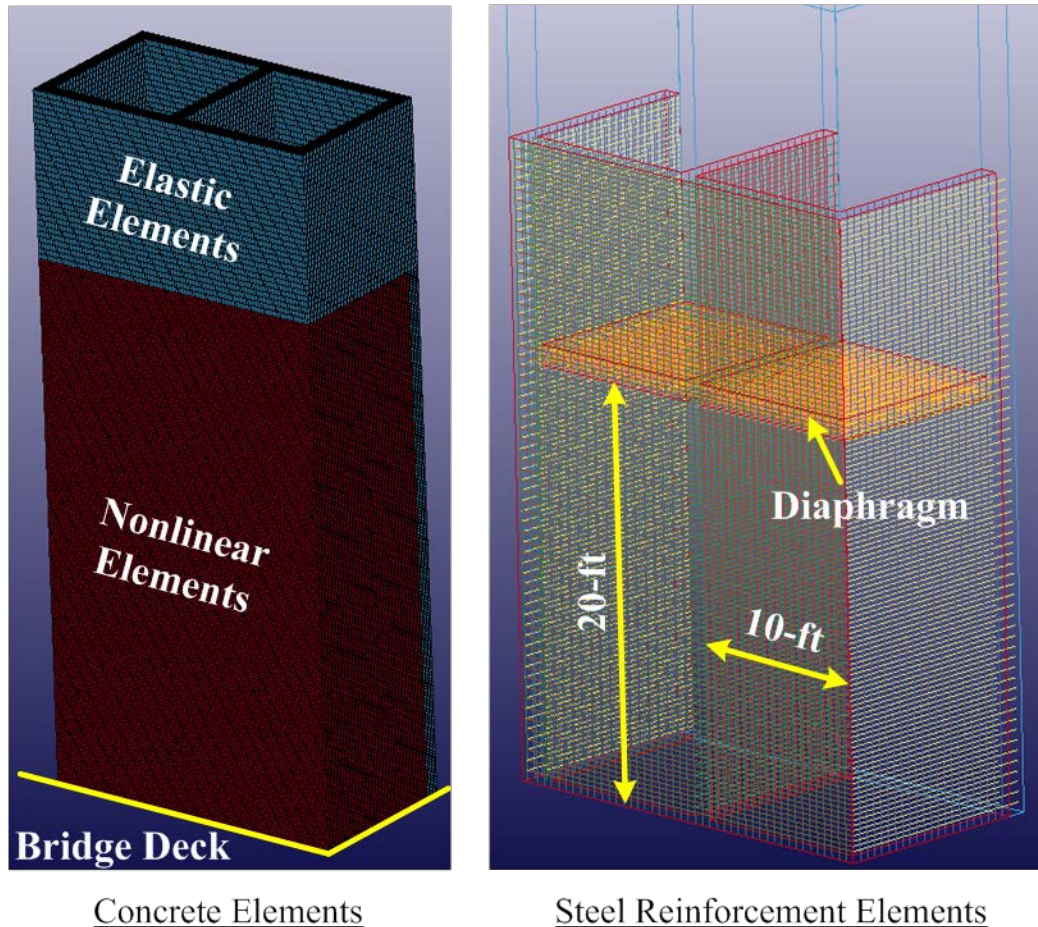


Figure 9.11 Part of a High-Fidelity Computational RC Tower Leg Model [18]

The objective of the system-level progressive collapse analysis is to evaluate whether RC tower damage determined from the component-level analysis will result in partial or total collapse of the bridge. The first step of the system-level collapse analysis is to modify the existing computational model of the bridge to accurately reflect the post-event damaged state of the blast-loaded RC tower. Care must be taken in interpreting RC tower damage and representing that damage in the system-level computational model of the bridge. No standard procedures or techniques exist for this task and the complexity involved will be highly project- and model-specific. The second step of the system-level collapse analysis is to conduct a nonlinear dynamic simulation of the modified computational bridge model. In addition to an accurate representation of blast damage, the bridge model should also include appropriate conventional design loads that are likely to be present during a postulated terrorist attack.

9.4.3 Structural Design

Due to the massiveness of typical cable-stayed bridge towers and the close-in nature of explosive threats likely to be deployed against these types of bridges, extensive damage to individual RC tower panels is of primary concern. Significant localized damage to one or multiple RC tower panels can precipitate gross loss in load carrying capacity and consequent partial or total bridge collapse, and this was illustrated in Section 9.2.

Material-level spall and breach damage, component-level direct shear failure, and component-level flexural failure are the critical failure modes of interest for blast-loaded RC tower panels. Strategies for increasing an RC tower panel's resistance to local spall and breach damage were discussed in Section 9.3, along with detailing recommendations for mitigating potential secondary limit states such as local rebar buckling and component-level buckling that can result from extensive concrete damage. As mentioned previously, the ATP-Bridge software can be used to expediently evaluate the potential for spall and breach damage of conventional RC tower panels and should be used to determine preliminary RC tower panel thickness, concrete compressive strength, and steel reinforcing sizes and layouts.

Figure 9.12 provides schematic illustrations of component-level flexural and direct shear modes of response for an RC tower panel, where the solid red lines denote typical crack patterns and the dashed blue lines denote typical (and exaggerated) deformations associated with each mode of response. RC panel design and detailing guidance for flexural and direct shear modes of response were provided in Chapter 5 of this manual and apply to RC tower panels. It should be reiterated here that blast loads are highly transient in nature, and as such require consideration of strain-rate effects on material response; whether that be in the form of single-valued dynamic increase factors applied to static material properties or strain-rate dependent material models in the context of finite element analysis. Methods to account for strain-rate effects on material response were provided in Chapter 3 of this manual and apply to RC tower panels.

Another important facet of RC towers that must be considered during the structural design of individual tower panels is the presence of sustained axial compression and its effect on the critical modes of response. As was discussed and illustrated in Section 9.3, the presence of sustained axial compression can give rise to secondary instabilities, such as local rebar buckling and component-level buckling, because of significant early-time concrete damage (spall and breach). In addition, and perhaps more familiar to bridge engineers, are the 2nd order P- δ effects associated with component-level flexural response in the presence of axial compression.

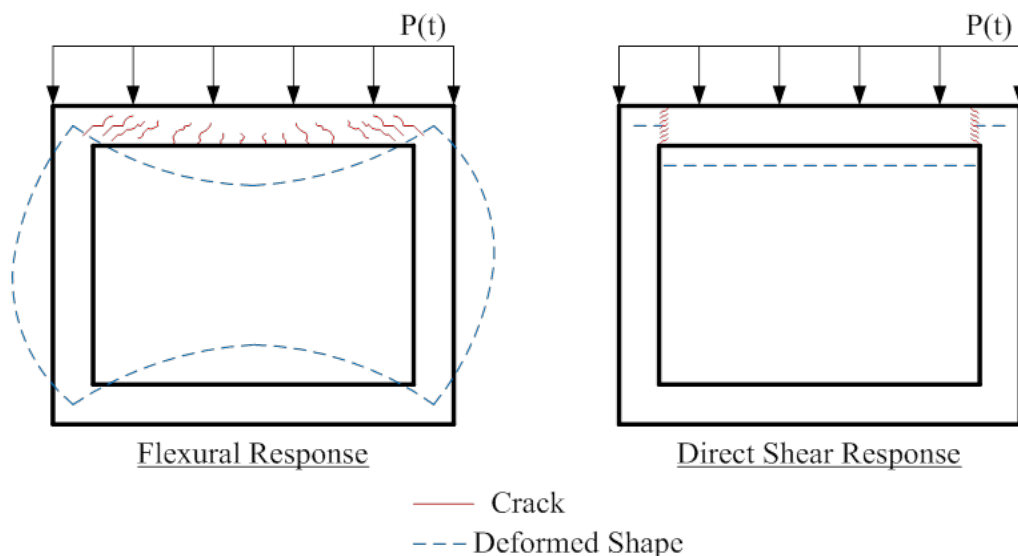


Figure 9.12 Schematic Illustration of Component-Level Flexural and Direct Shear Response of RC Tower Panel, Section View of Single-Cell Tower Leg [18]

9.5 ATP-Bridge Design Examples

In this section, a demonstration on how to use the ATP-Bridge software for preliminary design of an RC tower panel subject to an explosive threat is provided. A baseline scenario is first introduced, after which various problem parameters are modified to illustrate their effect on the blast performance of the example RC tower panel.

The example RC tower has two cells and is rectangular in geometry, as shown in Figure 9.13. The clear distance between front and back RC panels is 144-in., and the clear distance between a side and interior RC panel is also 144-in. All RC panels have a nominal thickness of 12-in. In addition, the vertical distance from the bridge deck to the bottom face of the first horizontal diaphragm is 288-in., and the diaphragm thickness is 12-in. Steel reinforcement details and material properties for the targeted panel are shown in Figure 9.14. The main longitudinal reinforcement consists of #9 bars at 6-in. on-center, and the transverse reinforcement consists of #4 bars at 6-in. on-center. The static unconfined concrete compressive strength is taken as 4,000-psi, and the static yield strength of the steel reinforcement is taken as 60,000-psi.

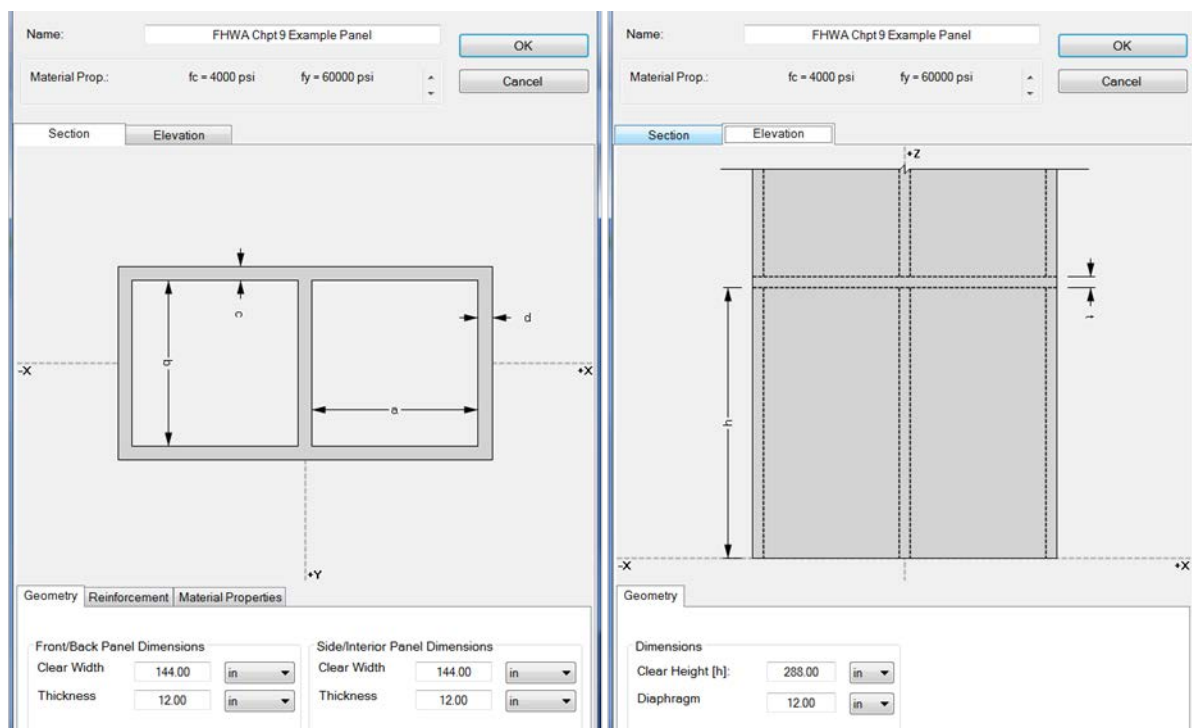


Figure 9.13 Example RC Tower Section Dimensions

Figure 9.14 Steel Reinforcement Details and Material Properties for Blast-Loaded Panel of Example RC Tower

As shown in Figure 9.15, the explosive threat is defined as 1,000-lbs of ammonium nitrate and fuel oil (ANFO) deployed as a cylindrical charge having a length-to-diameter ratio of unity. The charge is placed essentially on the bridge deck, centered with the right-front RC tower panel (the hatched panel in Figure 9.15), and oriented such that its longitudinal axis is perpendicular to the plane of the bridge deck. The charge standoff is set at approximately 60-in. from the exterior face of the targeted RC tower panel. Plan and elevation views of the threat scenario are illustrated in the ATP-Bridge 3-dimensional graphics window in Figure 9.16.

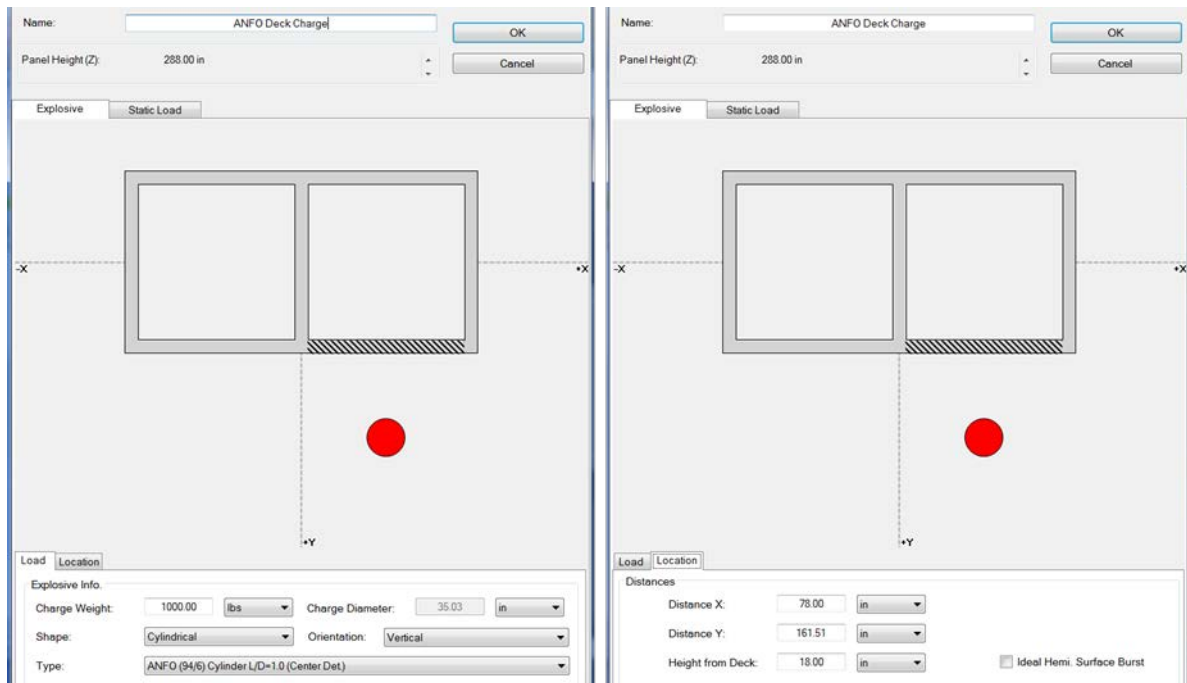


Figure 9.15 Explosive Threat Definition for Example RC Tower

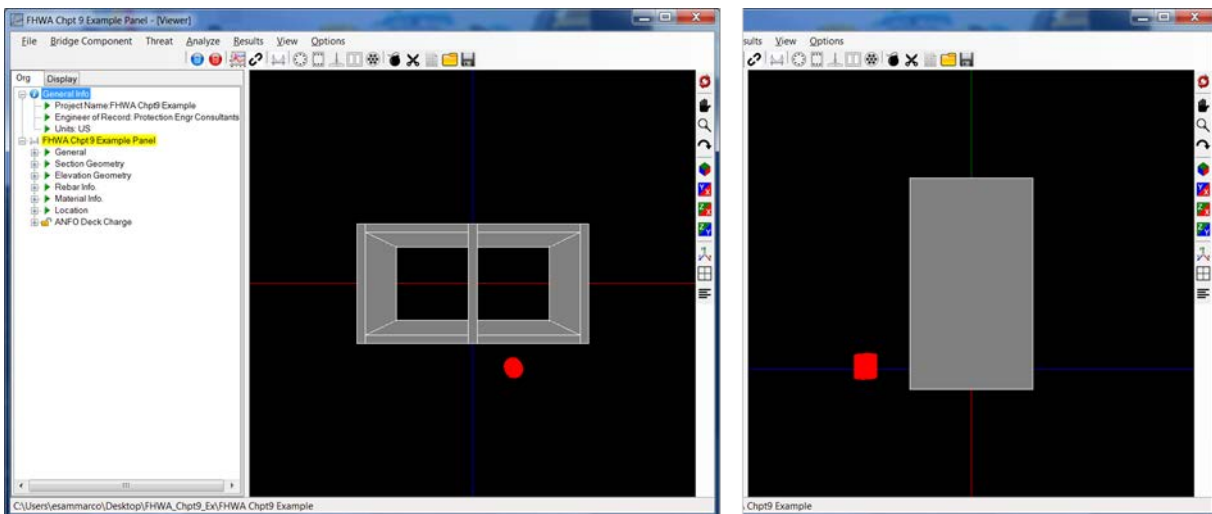


Figure 9.16 ATP-Bridge 3-Dimensional Graphics Display of Example RC Tower

Once the RC tower panel and explosive threat are defined, ATP-Bridge is used to perform an analysis to assess local spall and breach damage and predict peak component blast response. The results of the baseline analysis are presented in Figure 9.17. For this baseline example, ATP-Bridge predicts local breach damage in the form of a 43.5-in. breach hole near the bridge deck. The ATP-Bridge local damage results also provide a spall threshold thickness of 62.60-in. and a breach threshold thickness of 28.36-in. These threshold thicknesses are interpreted as the RC panel thickness below which the stated local damage state will occur. For instance, to prevent breach damage for the given explosive threat and RC tower panel properties, the RC tower panel thickness would need to increase to 28.36-in. It should also be noted that, because local breach

damage was predicted, the ATP-Bridge response algorithm terminated prior to assessing the blast-loaded RC panel's component-level response. This early termination occurs when local breach damage is predicted because (a) it should be taken as an undesirable limit state warranting a design change and (b) because the component-level part of the response algorithm was not developed to account for the effect of early-time breach damage on component response.

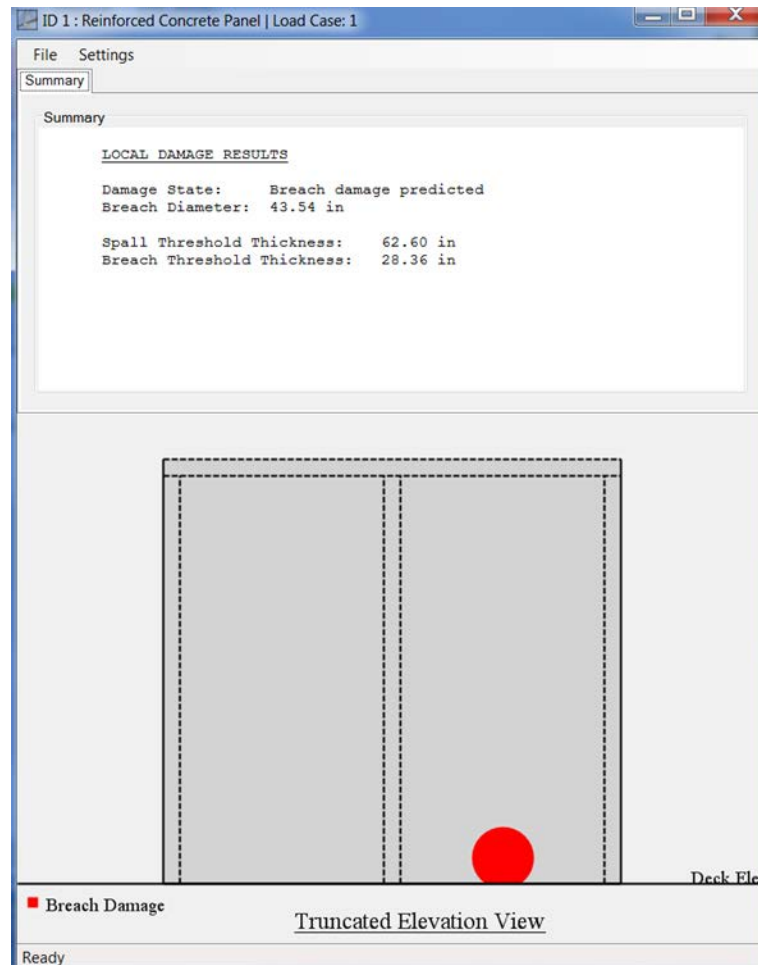


Figure 9.17 Spall and Breach Damage of Baseline RC Tower Panel Design

From the baseline RC tower panel definition, two modifications are now made to illustrate their effect on breach damage. First, the transverse reinforcing bar size in the targeted RC panel is increased to #6 bars. Local damage results for this modification are shown in the left image of Figure 9.18, where the breach diameter decreased from 43.54-in. to 41.96-in. with no change to the predicted damage threshold thicknesses. The second modification involves an increase in the static unconfined concrete compressive strength from 4,000-psi to 6,000-psi. Local damage results for this modification are shown in the right image of Figure 9.18, where it can be seen that (a) the predicted breach diameter increased from 43.54-in. to 46.37-in. and (b) the spall and breach threshold thicknesses both decreased from 62.60-in. and 28.36-in. to 58.90-in. and 26.68-in., respectively.

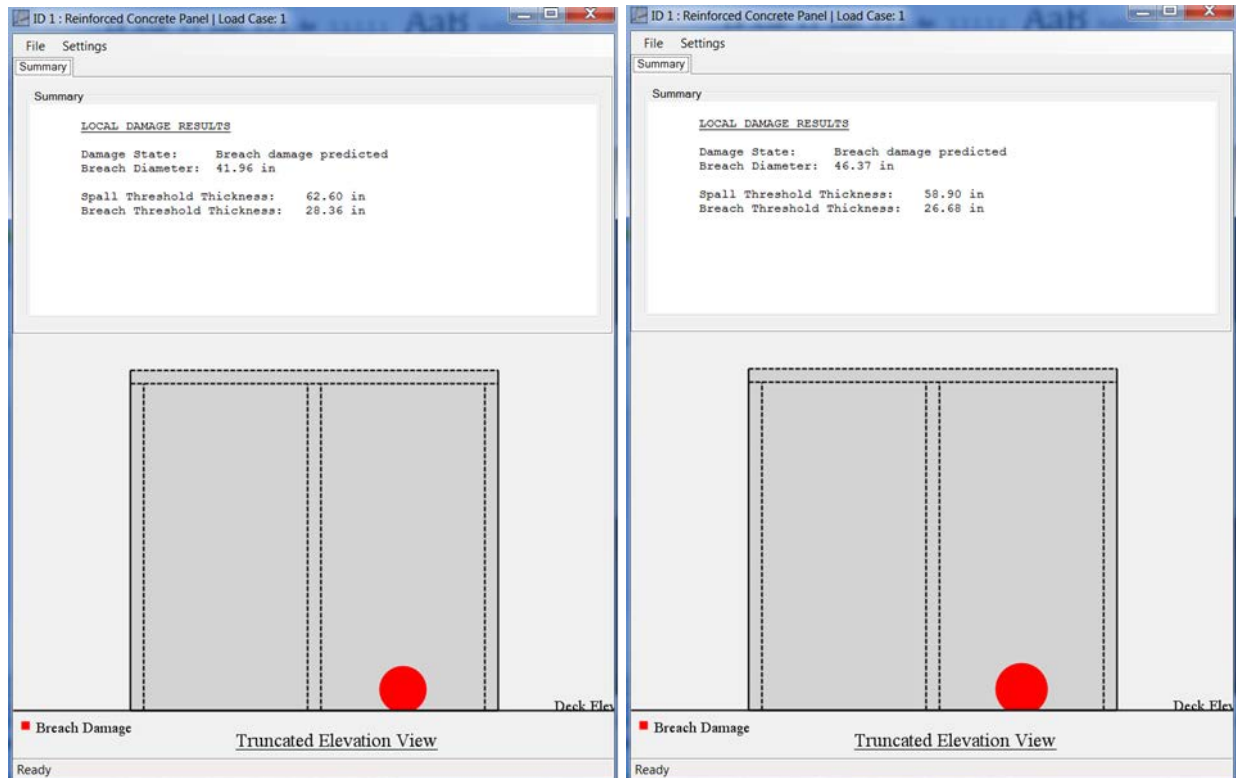


Figure 9.18 Effect of (left) Increasing Transverse Reinforcing Bar Size and (right) Increasing Concrete Strength on Material-Level Damage

In addition to investigating modifications to the RC tower panel section properties, the effect of having sustained axial compressive stress present in the targeted RC tower panel on material-level breach damage is investigated. Specifically, an axial compressive stress of 2,400-psi is introduced, as shown in the left image of Figure 9.19. Local damage results for this modification are shown in the right image of Figure 9.19, where the axial compressive load (which adds 1-dimensional confining stress to the concrete) acts to reduce the extent of breach damage from a diameter of 43.54-in. to 40.07-in. with no change to the predicted damage threshold thicknesses.

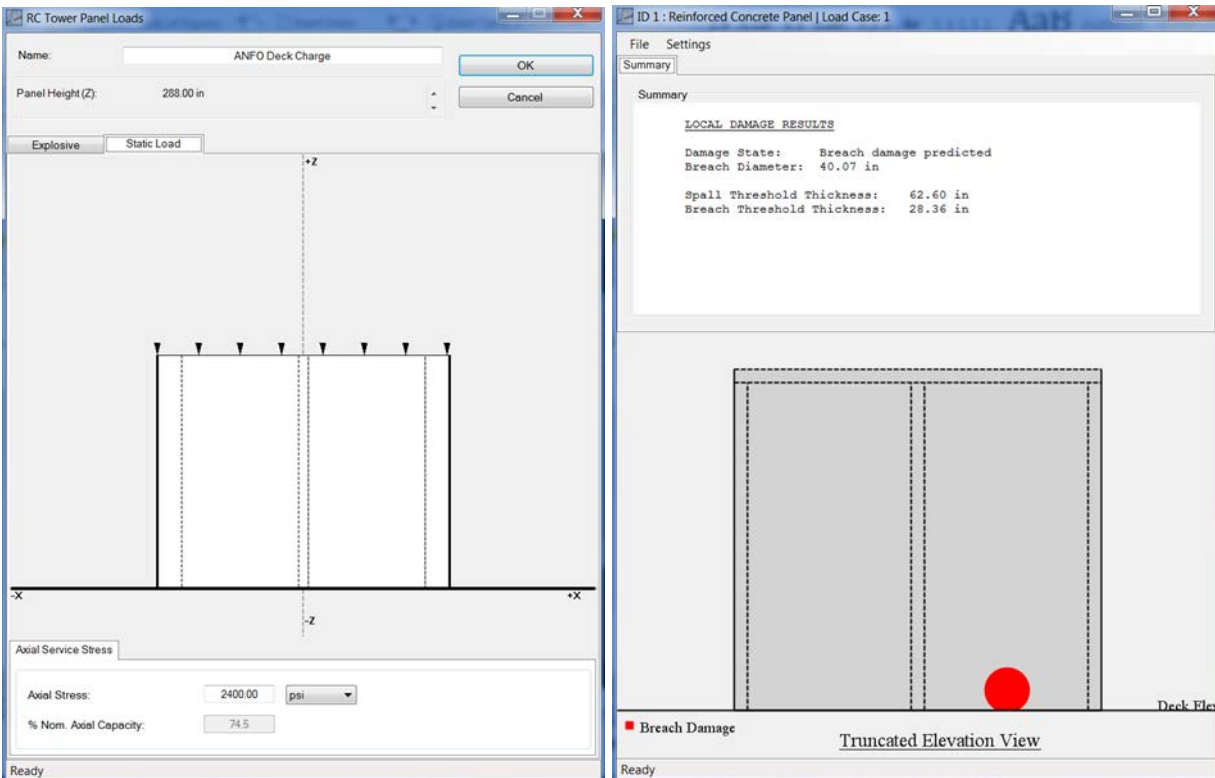


Figure 9.19 Effect of Increasing Sustained Axial Compressive Stress on Local Damage

The last modification to investigate is the effect of increasing the targeted RC tower panel thickness to 30-in., which is above the reported breach threshold thickness. The thicker RC tower panel is then subjected to the same explosive threat, and the results of the analysis are shown in Figure 9.20. The thicker RC tower panel did not breach; however, extensive spall damage (spall diameter of 78-in.) was predicted. Because breach was not predicted in this scenario, ATP-Bridge also performed a component-level dynamic analysis. In Figure 9.20, a peak dynamic displacement of 3.75-in. and a peak dynamic edge rotation of 3-deg were predicted. While component blast response limits for building structures are not entirely applicable for bridges (see Chapter 6 for more discussion on bridge-specific performance criteria), the U.S. Army's recommended single-degree-of-freedom response limits for blast-loaded RC panels [74] are provided in ATP-Bridge. The bottom portion of the ATP-Bridge form in Figure 9.20 presents a table of these response limits, and the blast-loaded RC tower panel is classified per these response limits in the "Summary" box of the ATP-Bridge form shown in Figure 9.20. For instance, based on the component response prediction for this example, the blast-loaded RC tower panel was classified as a heavily damaged component corresponding to a very low level of protection. Predicted component damage for this classification includes significant, unreparable permanent deflections with component failure not likely.

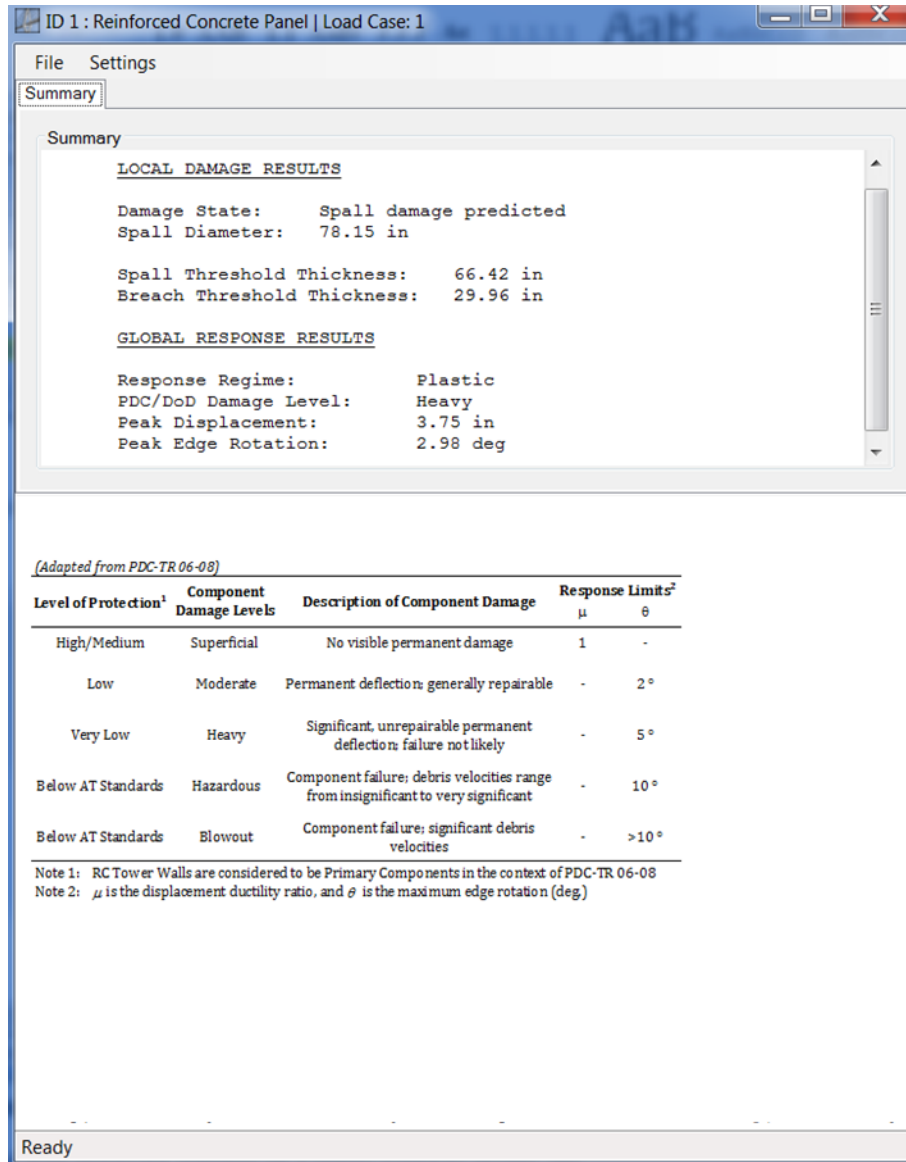


Figure 9.20 ATP-Bridge Analysis Results for RC Tower Panel having Increased Section Thickness

In addition to quantitative results, the ATP-Bridge 3-dimensional graphics utility in the Main Form can be used to qualitatively review dynamic response results. For instance, Figure 9.21 illustrates the 78-in. diameter extent of spall damage that was predicted for the blast-loaded 30-in. thick RC tower panel. In Figure 9.21, an isometric view of the two-cell RC tower leg is shown in the ATP-Bridge 3-dimensional graphics window with spall damage denoted by the yellow contour on the RC tower panel and the ANFO charge denoted by the red cylinder. In addition, Figure 9.22 qualitatively illustrates the predicted peak component-level dynamic response of the blast-loaded RC tower panel. More details on how ATP-Bridge can present dynamic analysis results are given in Chapter 12 of this manual.

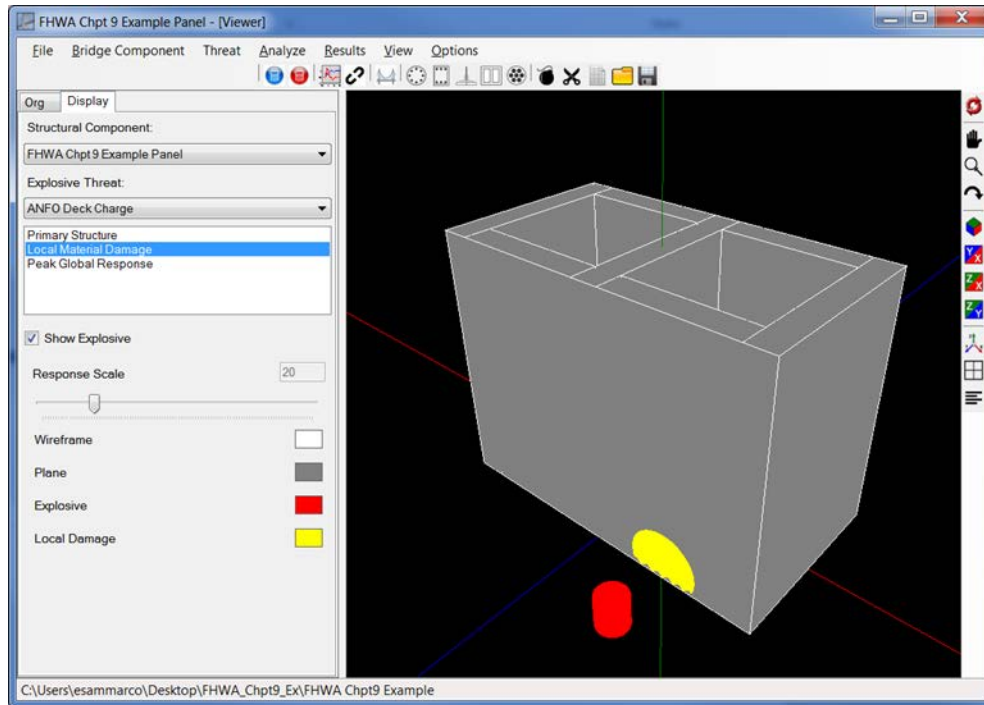


Figure 9.21 Illustrating Material-Level Spall Damage in ATP-Bridge 3-Dimensional Graphics Window

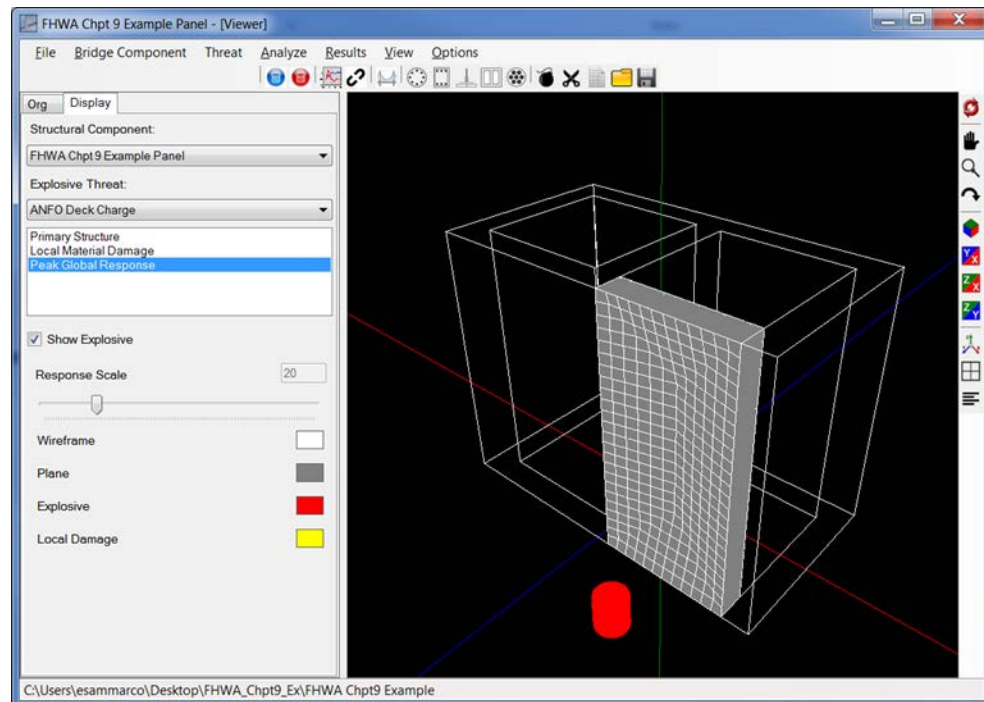


Figure 9.22 Illustrating Component-Level Peak Dynamic Response in ATP-Bridge 3-Dimensional Graphics Window

9.6 Overview of Threat Mitigation Retrofit Strategies

Given the difficulties associated with enforcing standoff on a public highway bridge, the potential exists for an adversary to place a large amount of explosives very close to or in contact with an RC tower panel. This type of explosive threat scenario—a likely design-basis threat for cable-stayed bridges—results in severe blast loads and represents an extremely challenging situation from a threat mitigation retrofit perspective. In addition, very little experimental research focused on the development effective threat mitigation retrofit strategies for close-in detonations against RC towers has been conducted to date. Some structural retrofits that have been put forth to date include different types of spall plates, suppressive shields (i.e., nested shapes), and sacrificial panels placed in front of a protected RC panel. The multi-series experimental test program conducted by Chiarito, Ray, et al. at the U.S. Army Engineer Research and Development Center (ERDC) [127, 128] represents the only well-documented such research program known to the authors.

As part of ERDC’s multi-series experimental test program, they investigated many different RC tower panel mitigation strategies for explosive threats having a scaled standoff less than $1.0\text{-ft/lb}^{1/3}$. The various mitigation strategies employed different tactics, such as:

- Providing additional inertial resistance using a sacrificial concrete panel placed in front of the RC tower panel. The air gap should not be sealed and the sacrificial panel should be placed at least one RC panel thickness away.
- Attempting to reduce the peak shock pressure experienced by the RC tower panel using a 1-Butene polymer “duct seal putty” layer on the blast face of the RC tower panel
- Providing additional strength using high-strength steel plate applied to the blast face of the RC tower panel
- Increasing standoff to the RC tower panel using an array short PVC pipes containing duct seal putty and positioned with their longitudinal axis parallel to the RC tower panel normal and supporting high-strength steel plate nearest the explosive charge
- Providing additional tensile strength using FRP sheets externally applied to the RC tower panel back face
- Creating impedance miss-matches by providing stacked layups consisting of different combinations of steel plate, concrete panel, and air gaps applied to the blast face of the RC tower panel
- Mimicking a typical blast door design by providing through-bolted steel plates on both sides of the RC tower panel

Unfortunately, most of the investigated retrofit strategies still experienced local breach failure to varying degrees of severity. The most promising retrofit strategy was found to be the blast door design, which consisted of steel plates on either side of the RC tower panel and through-bolted together as schematically illustrated in Figure 9.23. Post-test observations of this retrofit strategy included an intact blast-face steel plate with approximately 20 through-bolts missing and in

intact back-face steel plate with permanent local denting of approximately 2 inches. This is the same retrofit strategy that was previously mentioned in Section 9.3 and illustrated in Figure 9.9 as a baseline hardening strategy now used for new construction.



Figure 9.23 Illustrating Recommended RC Tower Panel Retrofit, Section View [128]

A bridge deck fuse system consisting of frangible deck panels near a bridge tower has also been proposed by researchers at the University of California, Berkeley [35]. The concept of the Son-Astaneh Fuse System (SAFS) is to provide sacrificial panels in the bridge deck that are designed to fail and disintegrate early in time once loaded with blast-induced pressures. Disintegration of the sacrificial panels acts to disrupt the shock wave reflection process, permits overpressure venting through the hole in the bridge deck, and ultimately reduces load effects on the adjacent bridge tower. Concept development of the SAFS blast threat mitigation strategy was done computationally, the results of which were favorable. However, to the authors' knowledge, the SAFS concept has yet to be subjected to live blast testing.

While the blast threat mitigation strategies for RC tower panels provide a starting point from which the bridge security community can begin to develop protective design retrofit recommendations, much research and innovation is still needed in this area.

9.7 Chapter Summary

In this chapter, challenges associated with the design and retrofit of RC towers of cable-stayed bridges were presented. Because this structural system is used in some of the most heavily traveled bridges in the U.S., it is critical that protective design strategies be developed to protect such bridges from potential terrorist attacks. What makes protecting RC towers extremely challenging is the small standoff distances that are normally present with cable-stayed bridges.

In this chapter, failure modes and overall behavior of blast-loaded RC towers were presented. An example using ATP-Bridge was provided. The chapter concluded with a description of possible protective design retrofit techniques that can be used to mitigate damage to RC towers subjected to close-in detonations, and the most effective retrofit strategy from past experimental testing was described. In the next chapter, protective design strategies high-strength steel cable components are presented.

10.0 PROTECTIVE DESIGN GUIDANCE FOR HIGH-STRENGTH STEEL CABLES

There are two main types of cable bridges: Cable-stayed and Suspension. Cable-stayed bridges utilize multiple cables to support long bridge spans by tying each cable back to a support tower as shown in Figure 10.1. The size and number of cables varies from bridge to bridge and often varies between each cable on a particular bridge.

Suspension bridges are comprised of two or four main suspension cables that span the length of the bridge as well as suspender or “hanger” cables that connect the main suspension cables to the bridge deck; see Figure 10.2.

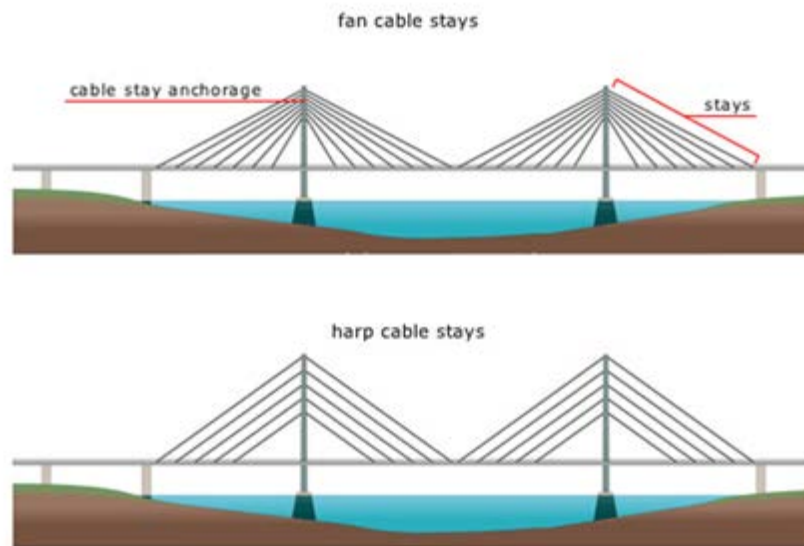


Figure 10.1 Cable-Stayed Bridge [133]

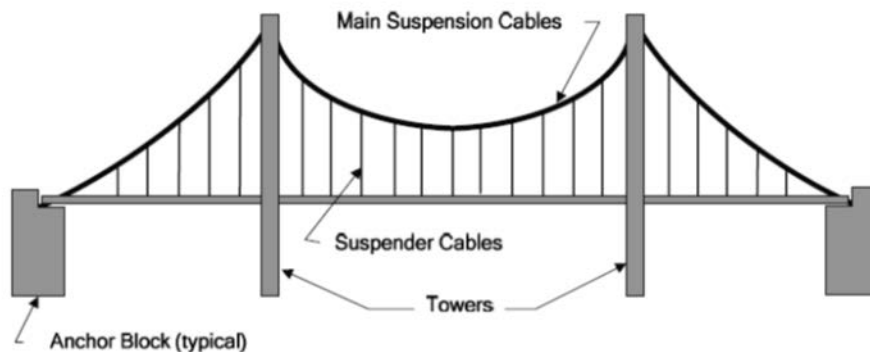


Figure 10.2 Suspension Bridge [134]

Critical components on suspension and cable-stayed bridges are vulnerable to terrorist attacks, due to their easy access. With weight and cost constraints, the geometry of bridges is typically as compact as possible in cross-section and, thus, cables, cable anchors, cable saddles and the supporting towers are in close proximity to the roadway. The vulnerabilities and protective design of steel towers and reinforced concrete towers have been discussed in Chapters 8 and 9, respectively. Protective design guidance for steel cables is presented in this chapter.

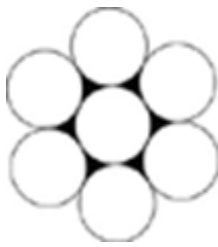
There are several terrorist threats that can be aligned against cables and cable support elements; these include explosives (bulk and shaped), explosive devices (shaped charges and explosively formed projectiles) and cutting tools (torches and saws). Due to the small amount of time required on target to employ these methods, each threat can be considered credible and the most likely threat will be a function of the sophistication and motivation of the attacker. The likelihood of a threat application will be unique to each bridge and a proper threat assessment should be performed by qualified professionals, to define the design basis threats (DBTs); the definition of the DBTs is beyond the scope of this chapter.

Resiliency and redundancy are critical issues for vulnerability of any type of bridge or structure subjected to natural or man-made threats. For suspension and cable-stayed bridges, there is little redundancy if a tower loses its load-carrying capability, as discussed in Chapters 8 and 9. For suspension bridges, there is also little redundancy if the main suspension cables are compromised. However, main suspension cables may vary from a few inches in diameter to 10s of inches in diameter and thus require a significant amount of explosives or an exceptionally large kinetic energy penetrators to cause failure. The hanger cables are easier to damage but there is inherent resiliency due to their large number and low operating stresses, which are typically 30-percent of the Guaranteed Ultimate Tensile Strength (GUTS). The loss of a single stay-cable or hanger is unlikely to cause failure of the bridge as the load will be transferred to adjacent cables which have the capacity to carry the extra load; however, for most cable-stay bridges, the loss of two consecutive cables is not acceptable. Thus, multiple stay-cables or hangers must be destroyed before the bridge is compromised. This is an obvious observation that will be apparent to a motivated attacker. It is not difficult to fail multiple un-protected cables simultaneously. Again, the level of probability is a function of the attacker's motivation and resources, and this risk is best assessed by qualified security professionals. The goal of this chapter is to assess vulnerability and provide guidance on protective design for cables when a credible threat has been identified.

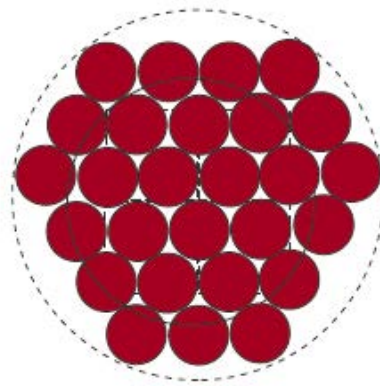
10.1 Cable Types

There are three main types of cables: stay cables, main suspension cables, and hanger cables.

Stay cables are typically formed of several strands which are in turn composed of several high-strength steel wires. A typical strand is 0.6-in. in diameter and made from 7 wires as shown in the left of Figure 10.3. Cable sizes range from 7 strands to 157 strands with most cables consisting of 30 to 40 strands; a 27 strand stay cable is shown in the right of Figure 10.3. While stay cables are typically composed of multiple strands, other geometries have been used, such as individual wires wrapped in a spiral and wires with different cross-sections, locked together to promote load sharing.



7-wire Strand,
0.6-in Diameter



27- Strand Stay Cable



Figure 10.3 Typical Single Strand and 27-Strand Stay Cable Sections [135]

The main suspension cables are typically formed on site by winding thousands of individual wires together using traveling carriages and then compacting the cross-section with hydraulic presses. The cross-sections of two very large main suspension cables are shown in Figure 10.4; note that main suspension bridge cables may be 30% of the diameters shown in Figure 10.4. As mentioned earlier, main suspension cables are generally massive and thus more difficult to compromise.

The suspenders on a suspension bridge are typically between 2.5-in. and 3.5-in. in diameter and can be configured in different ways. One example from a U.S. suspension bridge is shown in the left of Figure 10.5. A wire rope suspender from a commercial vendor is shown in the right of Figure 10.5.

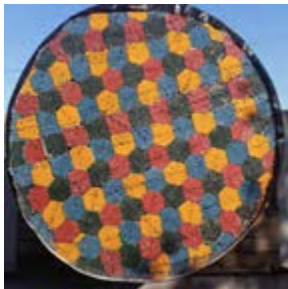
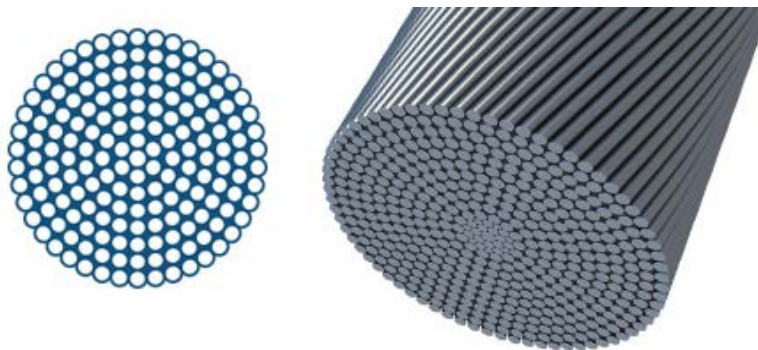


Figure 10.4 (left to right) San Francisco–Oakland Bay Bridge [136]; Overall and Close-Up View of Golden Gate Bridge Main Suspension Cable [137]



Hanger Cable from U.S.
Suspension Bridge



Spiral Wire Hanger Cable

Figure 10.5 Examples of Hanger Cables in Suspension Bridges (left: [138]; right: [139])

10.2 Design Loads

There are many terrorist threat scenarios that are applicable to bridge cables and a full listing is not possible. The most likely threats are organized into three categories: explosives, explosive devices, and cutting, as described in the next three subsections. Other potential threat scenarios are discussed in Section 10.2.4

10.2.1 Explosive Threats

Explosive threats are defined as those that apply shock loads only, with no accompanying fragments or projectiles. There are three main threats of concern.

The bulk explosive threat is composed of a large amount of bare explosive placed at a distance from the cable. Given the small presented area and large mass of a cable, bulk explosives are not a significant threat and unlikely to be successful in damaging a single cable or multiple cables. An adversary is unlikely to use this threat for the sole purpose of attacking the cables, but could use it to damage the bridge deck and towers. It is possible that the overpressure might damage cable anchorages and cable bands in the vicinity, as these have larger presented areas. This threat is shown notionally in Figure 10.6.

Block charges contain smaller amounts of explosive and are placed directly on or near cables. This threat is likely to be used by un-sophisticated attackers who can obtain explosive material but are not knowledgeable in efficient applications. With a sufficient amount of explosive, the cables can be completely severed or some of the strands may fail; in the latter case, the cable may still carry load. A numerical model representation of this threat is shown in Figure 10.7.

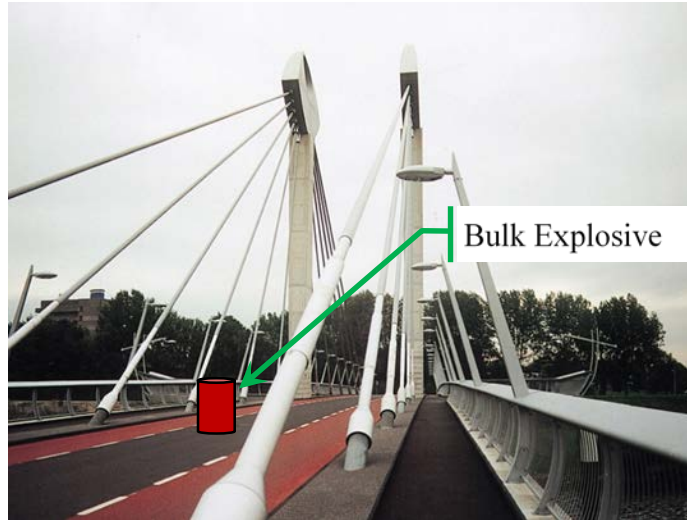


Figure 10.6 Notional Example of Bulk Explosive Threat on Cable-Stayed Bridge [140]

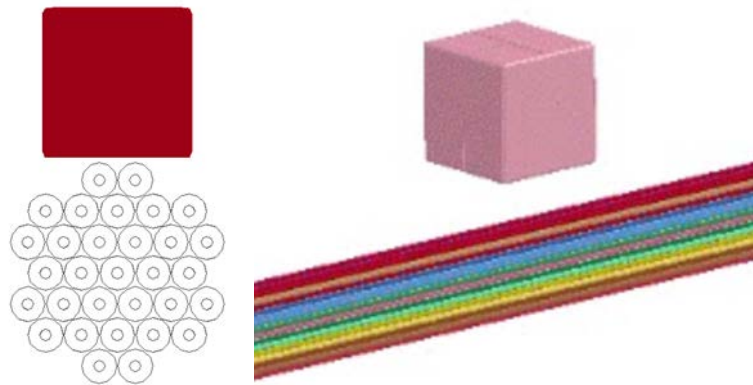


Figure 10.7 Numerical Models of Block Charge Threat; Placed on Cable (left) and with Standoff (right) [141]

The diamond charge is a sophisticated explosive technique that is well-known in the military and demolition communities and is used to focus the shock to create maximum damage. Block C-4 is formed into a diamond shape that is wrapped around the cable; see Figure 10.8 and Figure 10.9. The length of the diamond equals the circumference of the cable and the transverse length is one half of the circumference. The thickness of the diamond charge sheet is adjusted as necessary for the target material and strength. The charge is initiated at the two short-span vertices simultaneously, causing the detonation to propagate from both sides of the diamond toward the center. The collision of the shock produces far more cable damage than a block charge of the same mass. The post-test condition of two specimens subjected to diamond charge attack is shown in Figure 10.10.

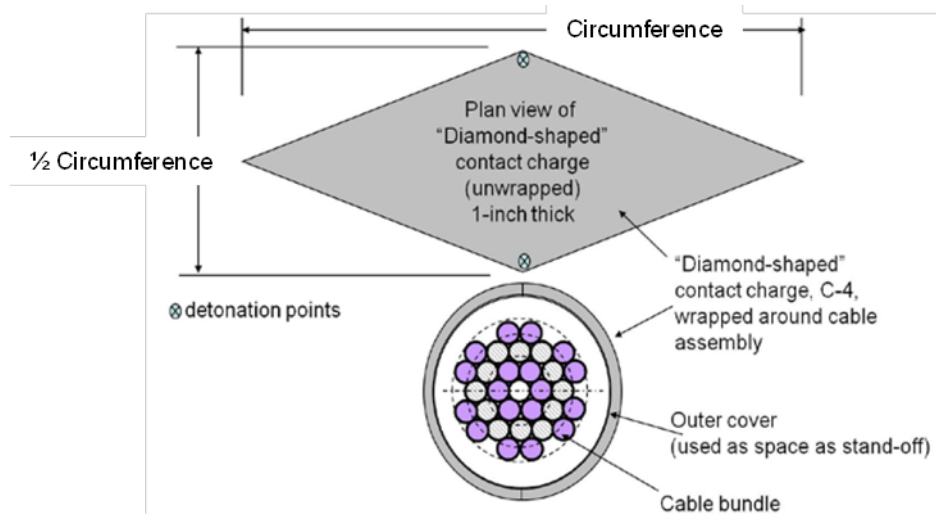


Figure 10.8 Diamond Charge Geometry [135]

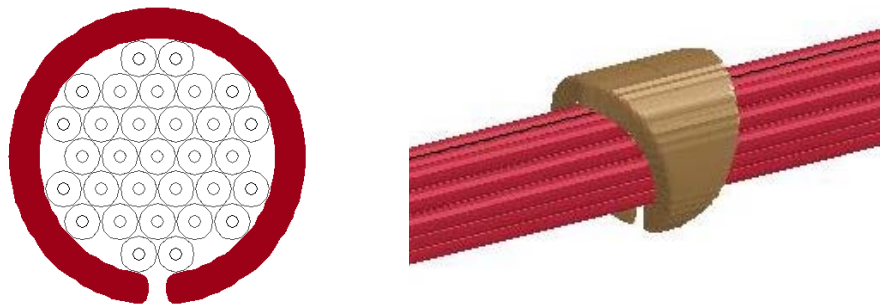


Figure 10.9 Diamond Charge Model with 31-Strand Cable [135]



Figure 10.10 Examples of Cable Failure Due to Diamond Charge; Left: Failure of 25% of Strands; Right: Complete Failure of Cable [135]

10.2.2 Kinetic Energy Penetrators

Kinetic Energy Penetrators (KEPs) are defined as threats that combine explosives with metallic components to create large and fast-moving projectiles. These types of devices are widely used by the military and, while they require some sophistication to fabricate and deploy, they are a common weapon system used by terrorists as well as insurgents in overseas wars. These weapons are capable of defeating armored vehicles and hardened structures and thus any counter-measure

or protective design will necessarily be large and massive, potentially larger and heavier than can be borne by a cable bridge.

There is a spectrum of KEPs and the three basic types are discussed briefly here. As with other terrorist threats against bridge structures, a standard or required design basis threat has not been identified and implemented by the bridge engineering community. A security risk assessment must be performed by qualified personnel to identify a particular KEP threat, after which mitigation methods or protective hardware can be developed.

Shaped charges consist of explosive placed behind a liner that is designed to collapse and create a very high speed molten jet; the liner is typically metallic, although other materials such as glass have been used. The velocity of the jet can range from 10,000- to 30,000-ft/sec and small diameter holes with deep penetration are created in the target. A schematic of a shaped charge is shown in Figure 10.11. Due to the small volume of damage that is created, shaped charges are unlikely to create significant damage in a cable and thus are an unlikely threat. It is noted that the same concept is used in linear shaped charges which can be used to create a long cut in a target face; these are discussed in the next subsection.

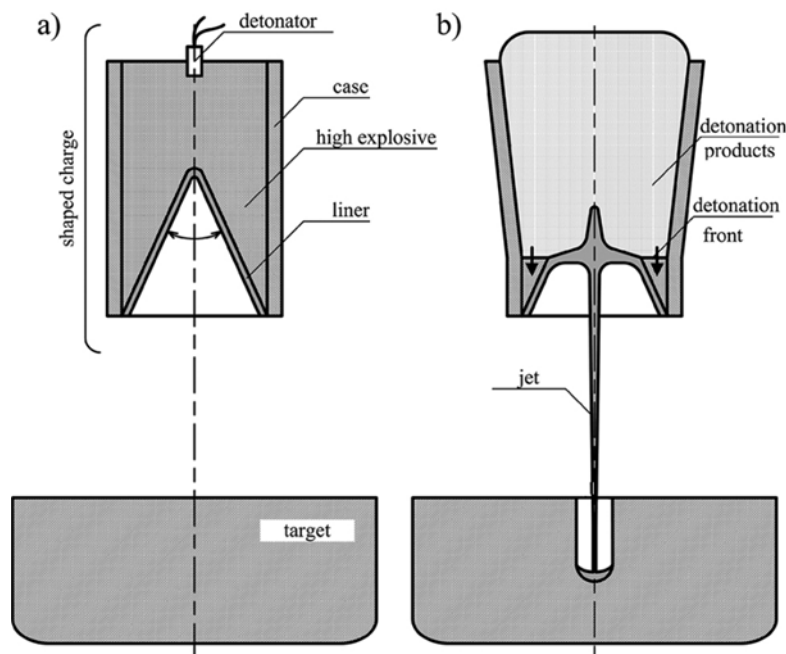


Figure 10.11 Shaped Charge Geometry and Action [142]

Explosively-formed penetrators (EFPs) create bullet-shaped, aerodynamic fragments with a velocity in the range of 5,000- to 10,000-ft/sec. They are composed of explosives placed behind a metallic liner with a shallow curvature (less than for shaped charges). The fragment does not penetrate as far as a shaped charge but the hole is larger. The flight of the fragment is stable and these devices can be aimed at a target from a substantial standoff distance. A schematic of an EFP is shown in Figure 10.12.

A flyer plate consists of explosives placed behind a flat sheet of metal. The flat-plate shape is maintained during the flight and velocities up to 5,000-ft/sec are typical. Since the projectile

shape is not aerodynamic, there is less accuracy and a smaller standoff distance is required to guarantee target engagement. The plate mass and explosive weight can be very large. In comparison to an EFP with the same explosive and projectile mass, these devices create less penetration but the holes are larger. A generic flyer plate is shown Figure 10.13.

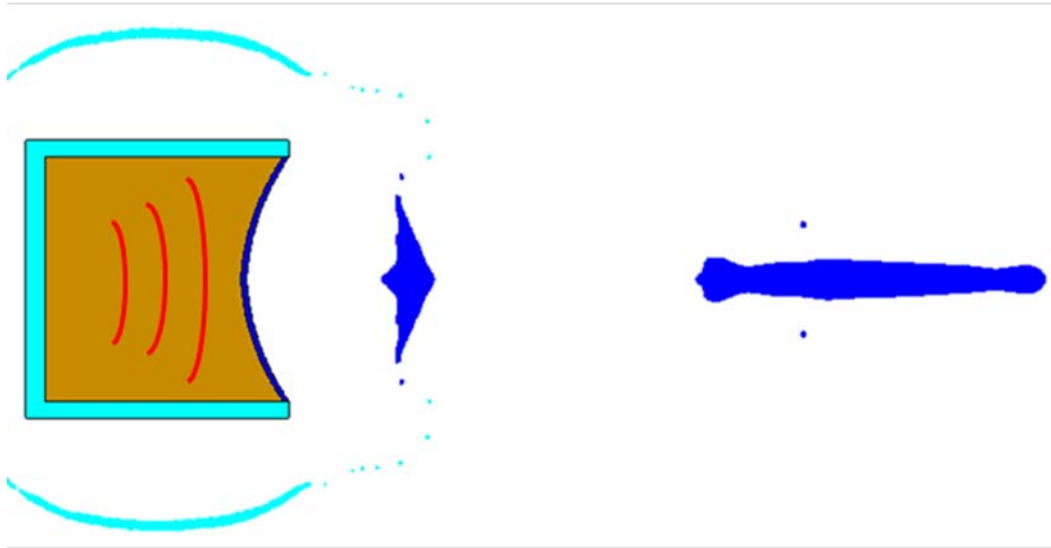


Figure 10.12 Schematic of Explosively Formed Penetrator [143]

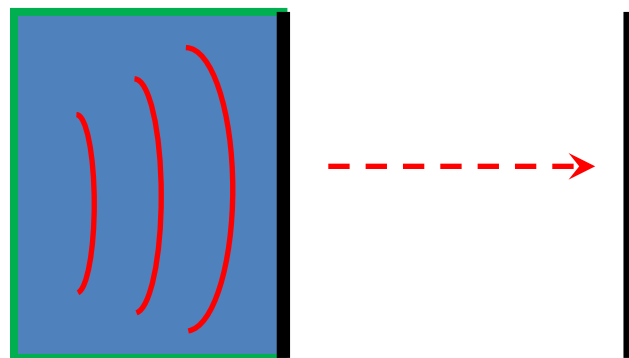


Figure 10.13 Schematic of Flyer Plate

Again, there are a variety of kinetic energy penetrators and the size and effectiveness of each device varies widely. As there is no standard design basis threat for KEPs, a security risk assessment is required to define the threat that is applicable and appropriate for a particular bridge.

10.2.3 Cutting Threats

Cutting threats for cables include thermal devices and mechanical tools.

Thermal threats include oxy-acetylene torch, exothermic torch, and plasma cutter. Oxy-acetylene torches are commonly used in steel fabrication and demolition and burn using a mixture of acetylene gas and oxygen; the equipment is bulky and less likely to be used than an exothermic torch.

The exothermic torch is a cluster of small-diameter rods contained within hollow tubes, as illustrated in Figure 10.14. Pure oxygen is pushed through the tube and supports iron burning on the order of 10,000 °F; this cutting process is illustrated in Figure 10.15.



Figure 10.14 Cross Section Exothermic Torch [144]



Figure 10.15 Exothermic Torch in Use [145]

Plasma torches use a high velocity plasma jet to melt the metal and force the molten metal through the kerf and out beneath the metal. In the plasma cutting process, illustrated in Figure 10.16, an inert gas is forced at a high velocity from the nozzle along with an electrical arc between the nozzle and the base metal. The arc transforms some of the gas into plasma. Plasma torches are capable of cutting faster than oxy-fuel torches, but because the molten metal is forced out through the bottom, the kerf is often larger. A plasma torch is also not able to cut through thicker materials as efficiently as oxy-fuel or exothermic torches because it has to force the molten metal out through the bottom as opposed to the metal being oxidized as in an oxy-fuel cutting process. In addition, a plasma torch requires a power source, making it a less attractive cutting tool.

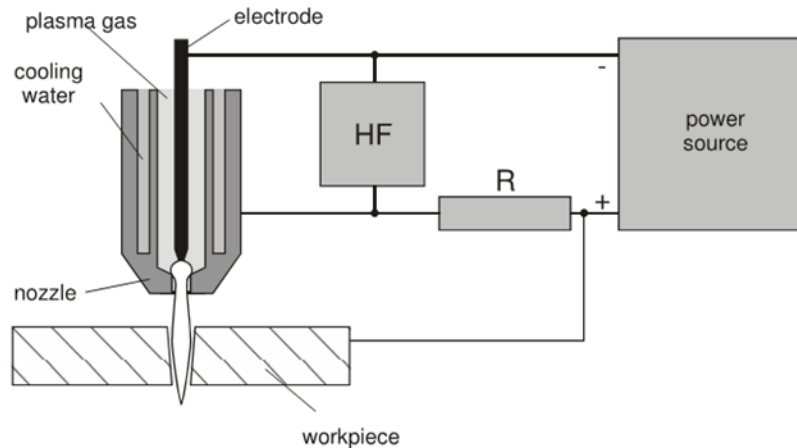


Figure 10.16 Plasma Cutter [146]

Mechanical cutting tools include circular saws and grinders, with the most likely threat to steel cables being a gasoline powered cut-off saw as shown in Figure 10.17. A variety of blade types and sizes for cutting different materials is readily available. Solid abrasive wheels are typically used for cutting most ferrous metals. The cutting rate of the saw is dependent on the material thickness, and the time required to cut a unit cross-sectional area increases nonlinearly with thickness of the material.



Figure 10.17 Gasoline Powered Cut-Off Saw

The LSC threat includes conventional linear shaped charges and flexible linear shaped charges, which are shown in the left and right sides, respectively, of Figure 10.18. Flexible linear shaped charges can be placed on curved surfaces, as shown in Figure 10.19. Linear shaped charges are typically specified by the amount of explosive per length, with grains per foot being the common unit.



Figure 10.18 Metal-Clad Linear Shaped Charge (left: [147]) and Flexible Shaped Charge (right: [148])



Figure 10.19 Flexible Linear Shaped Charge about Pipe Circumference, Before Detonation and After Detonation [149]

10.2.4 Other Loading Considerations

Additional types of threats may be identified during a security risk assessment and must be considered in the design of the bridge, using suitably qualified experts and engineers.

10.3 Failure Modes and Performance Criteria

Local failure can occur due to damage of the strands and wire and loss of anchorage or support at the ends of the cables. Global bridge failure can occur due to the reduced capacity of the damaged cable system.

Cable failure occurs due to loss of the individual strands and wires, which may be cut with an explosive device or cutting tool, or overloaded in shear due to localized shock loads from a block or diamond charge. Cables are not always completely severed in an attack and can provide some residual capacity; thus, there is a range of damage states from undamaged to complete failure. Unlike the design of structural elements in buildings, there are no performance criteria for cables, based on structural response variables, such as maximum displacement or rotation. Numerical methods or analytical procedures must be employed using failure criteria for the constituent materials to determine the level of cable failure. These methods have been used to create

algorithms and associated software for predicting the level of damage and residual capacity for some of the threats described in Section 10.2; this software is presented later in Section 10.6.

Anchorage at the ends of cables may fail in a variety of ways, specific to the particular geometry and materials that are used. A KEP attack on a deck-level anchor may cut some of the cables and the associated shock may dislodge the anchor wedges, freeing the remaining cables. Similarly, a bulk or block explosive could create a shock wave that travels down the cable and anchorage and dislodges the anchor wedges. A sufficiently large bulk explosive charge may damage the deck and supporting structural members to which the anchorage is joined. Cable bands at the top of suspension hanger cables are harder to access, but a diamond or block charge could be placed on the saddle hardware and cause complete or partial failure. There are no established or accepted procedures for predicting anchorage or saddle failure and numerical models or physical testing must be employed on a case-by-case basis, using the design basis threat.

The bridge itself may fail when the cable system and/or deck structure are sufficiently compromised. As mentioned earlier, it is unlikely that a bridge will fail due to the loss of a single stay cable or hanger cable; while bridge collapse due to loss of a single main suspension cable is possible, these cables are large and less likely to be attacked. If a sufficient number of stay cables or hanger cables are destroyed in a coordinated attack with multiple explosive charges, the remaining cables and structure may not be able to carry the loads from the failed cables and, thus, will also fail, resulting in a progression of cable failures until the bridge collapses. In this case, the performance criterion is *prevention of collapse*. Since each bridge is unique, this must be considered on a bridge-by-bridge basis. To assess the performance, given a specific threat scenario, the engineer should determine the number of cables that will fail or be damaged in the attack, the residual capacity of those cables which are not damaged, and should develop a numerical model of the entire bridge structure that incorporates the failed or damaged cables. The analysis should consider dynamic loading of the remaining cables as the load is transferred from the failed cables, as well as the failure of the stiffening girder or truss and the stability of the compression strut or tension tie. This model should be subjected to the service loads existing at the time of the attack and will determine if the damage grows to the point that the bridge collapses.

10.4 Design Strategies and Detailing Recommendations

Bridge cable systems are typically designed first to meet service loads, including dead load, live load, wind loads, etc. If terrorist threats must be considered, it is typically after the cable system has been designed. For new and existing bridges, the designer has a number of strategies that can be employed.

In the first design strategy, the resistance of the overall cable system may be enhanced by increasing the number of cables or their strength or both, assuming that the terrorist threat is successful against some of the cables. The number of lost cables is based on the number of simultaneous attacks that are stipulated in the design basis threat that was developed by the security professional. The increase in the number or strength of the cables is determined by analyzing the re-distribution of the loads from the damaged or failed cables to the rest of the bridge.

Depending on the threat, increasing the standoff between the cable and the threat may be an effective design strategy. The destructive ability of explosive threats greatly decreases with distance from the target. Increased standoff could be accomplished by placing a steel or plastic tube around the cable, from the deck to a height that will be difficult for the terrorist to scale. The tube approach will also decrease the effectiveness of diamond charges unless the explosive weight is increased, which may deter the terrorist from using this tactic. For all cutting threats, a standoff tube will reduce the efficiency of the cutting process, requiring a larger time on target, which also discourages the use of this tactic.

For explosive devices such as kinetic energy penetrators, standoff alone is not sufficient. In this case, additional physical protection is required, using high strength steels, concretes, and other materials, often in large amounts. KEPs are a common military-grade weapon and thus military-grade solutions will be required. The weight and geometry requirements for these protective devices will be large and perhaps prohibitively so.

Hardening is another strategy that works to defeat all three types of threats (explosive, explosive device, and cutting). Hardening may be accomplished with protective structures composed of strong materials, large mass, and effective geometric designs. Hardening can be expensive and the effects of the extra weight on the bridge structure must be considered.

The ends of stay cables are often anchored by spreading the individual strands and placing them into conical ducts in a steel fixture; the cables are placed in tension, friction wedges are inserted, and the tension is reduced. Tests performed by the US Army Engineer Research and Development Center have shown that a shock wave will emanate from the explosive site and travel along the cable to the anchorages and may dislodge the wedges, thus removing the ability of the cable to carry load. There is scant research and data on this failure mechanism and its mitigation, and therefore, design strategies can only be postulated. It may be possible to mechanically lock the wedges into the conical ducts such that they quickly re-engage the cable after the shock relieves the load on the portion of the cable in the duct. Dampers and concentrated masses outside the anchorages may also be used to reduce shock wave transmission.

Anchorages and saddles may also be susceptible to explosive threats (bulk, block, and diamond charge) and explosive device attack (kinetic energy penetrators). In this case, the designs must be modified to resist these loads, by changing the materials, geometry and attachment methods. Anchorages and saddles are relatively complicated structures and no simple design strategies exist. Numerical simulations of the threat scenario against hardened design concepts will be required to identify a design solution.

The last design strategy is based on physical security, by limiting access to the cable system and reducing the time on target, with personnel barriers and with surveillance and rapid response of law enforcement. Designers typically cannot specify or require implementation of this strategy as it is outside their area of responsibility, but they can be an active advocate as part of the design team.

10.5 Recommended Design Procedures

As discussed in the previous section, there are a number of design strategies to defeat terrorist attacks on cable bridges. As there is a limited amount of experimental and numerical model data, government agencies and the bridge engineering community have not developed or officially approved, recommended, or required protective design procedures for bridge components or the overall bridge structure, for any of the aforementioned strategies.

As described and recommended here, the designer or engineer will need to determine the level of damage due to a terrorist attack on individual cables or components, using either ATP-Bridge (described in more detail in Chapter 12 of this manual) or a numerical simulation. ATP-Bridge can be used to predict the vulnerability of the cables, such as the number of failed and damaged cables for various explosive threats, the residual strength of cables that are only damaged and the time to failure for various cutting threats. The results of the ATP-Bridge analysis or the numerical simulations are then inserted into a sufficiently sophisticated numerical model of the entire bridge to assess the potential for collapse.

The two procedures for determining the failed or damaged state of the cable or cable component are ATP-Bridge and numerical simulations and these are described in the following subsections.

10.5.1 ATP-Bridge for Cable Vulnerability

As introduced in previous chapters and discussed in detail in Chapter 12 of this manual, ATP-Bridge is a software tool developed by the US Army Corps of Engineers Engineer Research and Development Center, with funding provided by the Department of Homeland Security [150]. The vulnerability of cables to different terrorist tactics was assessed through evaluation of existing experimental data for some explosive threats, reviews of manufacturer's literature for cutting threats, and numerical simulations to provide synthetic data that supplement test data and to create synthetic data for terrorist tactics with no data.

10.5.1.1 ATP-Bridge Explosive Threats

The development of the ATP-Bridge vulnerability algorithms for explosive threats acting on cables is discussed in [141]. As discussed in Section 10.2, two explosives threats are considered: block explosive and diamond charge. LS-DYNA simulations of block explosives and diamond charges acting against different types and sizes of cables were executed, after verification and calibration of the modeling approach through comparisons with test data developed by ERDC [135]. Different modeling approaches for the wires and strands in the cables were developed and evaluated, including pure Eulerian, solid elements, beam element wires, and beam element strands; the final version included beam elements for the strands with null-shell wrappers and constrained nodal rigid bodies to replicate the contact and motion between the strands. The Arbitrary Lagrangian Eulerian (ALE) methodology was used to replicate the explosive process.

The independent variables in the LS-DYNA simulation matrix included explosive threat (block or diamond charge), standoff, tension (% of GUTS), strand count, and charge weight. Fast running models for the block explosives and diamond charges were created through curve fits with different combinations of the independent variables. For the block explosive vulnerability curve fits, the independent variable was a scaled weight variable that consists of the charge weight, clearing and standoff factor, and the cross-sectional area of the cable. For the diamond

charge, the independent variable was similar to the scaled weight variable of the block charge but the exponent on the charge weight was modified. Curves of remaining cable capacity after attack versus scaled weight were created, for different combinations of cable tension and number of strands. These curves were developed and implemented into the vulnerability algorithm for block explosive charges.

The current ATP-Bridge software may be used to predict the number of intact strands after the detonation of the two explosive threats (block and diamond charge) acting against stay cables with 6 different strand counts (7, 13, 19, 27, 31, and 61) and hanger cables with just one strand count. Nine different explosive materials can be defined, including C-4, Comp B, TNT, Nitromethane and others. Examples of the application of ATP-Bridge can be found in Section 10.6.

10.5.1.2 ATP-Bridge Cutting Threats

The development of the ATP-Bridge vulnerability algorithms for cutting threats acting on cables is discussed in [151]. As discussed in Section 10.2.3, three cutting threats are considered: thermal devices, mechanical tools, and linear shaped charges (LSCs). For thermal devices and mechanical tools, the entire cross-section of the cable can be cut, if an attacker is allowed unlimited time and cutting supplies, and therefore, the estimated time to fail the cable is predicted. For the linear shaped charge, the number of failed strands is predicted.

As discussed in [151], for the thermal tool threats, the time required to cut a cable was determined from published data for cutting rates in steel plate and then converted to an equivalent cutting rate in steel cables, with an adjustment factor to account for the difference in thermal conductivity between a bundle of strands and a monolithic steel plate. To account for the difference between the cable and plate cutting rates, a scaling factor was calculated in [151] using data from [152], where an exothermic torch was used to cut a cable. The factor was found to be 0.078, suggesting the efficiency of cutting a cable is approximately 8% that of cutting a monolithic plate. This factor was applied in the thermal cable algorithm to the oxy-acetylene, exothermic and plasma plate curves. Cable cut times for all cutter types (oxy-acetylene, exothermic and plasma) are reported by the algorithm. For the mechanical tool threats, the time required to cut a 2-in diameter hanger cable was reported in [152]. To estimate cut time for other cross-sectional areas, the shape of the cut time versus cross sectional area curve for the cable was assumed to be the same as for high strength armor steel. A factor of 0.44 was applied to the high strength armor steel curve to match the 2-in diameter hanger cable data point. The resulting curve was used to determine the time to completely cut a cable in ATP-Bridge.

For the linear shaped charge, two configurations are considered in ATP-Bridge: a non-flexible LSC placed on one side of the cable and a flexible LSC wrapped about the circumference of the cable. For the non-flexible LSC, data was available only for penetration into mild steel plate and an effective thickness for the cable was derived as describe in [151]. No data was available for an FLSC on a curved surface and an equivalent thickness was derived from the geometry of the cable and plate. The radius of curvature possible for flexible LSCs as a function of charge weight was obtained from manufacturer data. A curve of radius of curvature versus charge weight was developed and used as a check to insure that the flexible LSC can bend sufficiently for the specified number of strands. For flexible and non-flexible configurations, if the specified number

of strands is less than the minimum number of strands required to prevent complete failure for a particular LSC, severance is reported; otherwise, the cable is reported intact.

Examples of the application of ATP-Bridge can be found in Section 10.6.

10.5.2 Numerical Simulations for Cable and Cable Component Vulnerability

The algorithms for cable vulnerability in ATP-Bridge cover a limited number of scenarios, in terms of threats and cable configurations. ATP-Bridge also does not consider cable components, such as anchors and saddles, which may be susceptible to deliberate attack. Therefore, the engineer or designer may be required to perform numerical simulations to determine the vulnerability for a different cable, cable component, and threat.

Numerical simulations of explosive and explosive devices are complicated and require a significant level of expertise and experience on the part of the modeler. This type of modeling and simulation are often performed for military applications, where close-in detonations and penetrating weapons must be defeated. A bridge design firm should assess the qualifications of their staff to perform these simulations and, if necessary, hire a specialty firm that works in the field of military and terrorist weapons effects.

The finite element modeling of cables and cable components subjected to weapons effects presents some unique challenges; the following subsections present guidance and recommendations that should be considered for this modeling. As appropriate, the discussion addresses modeling of 1) local cable response where failure occurs early and is localized, 2) full cable response where the anchorages and supports at the ends must be considered and 3) cable component response. The unique features of the explosive and explosive device modeling are also highlighted.

10.5.2.1 Extent of Model and Boundary Conditions

All numerical models should be three dimensional, but symmetry can be employed as appropriate to reduce the model execution time and memory requirements.

For close-in explosive charges and explosive devices, local cable damage will occur over the cross-section and in the vicinity of the charge. The finite element model of the cable should extend sufficiently far that reflections from the ends of the cable model will not affect the prediction. Point masses may be used at the end of the cables to represent the anchors or section of cable that is not modeled.

Some threats such as bulk explosives or large block charges might induce a response over the full length of the cable; in this case, the FEM should extend from the anchor at the deck level to the saddle or mount at the suspension cable or tower attachment. Cable anchors are typically massive devices that provide axial restraint to the cable but may also include dampers that act in the directions perpendicular to the cable's long axis. These can have a significant effect on the whiplash motion of the cable due to explosive charges and should be modeled in sufficient detail.

The finite element models of the cable components such as anchors and saddles will be connected to the deck, tower or other supporting structure. For explosive threats such as bulk and block explosives, the finite element model should contain a sufficient extent of this supporting

structure such that the load and stress transferred from the cable component can be sufficiently converted to internal strain energy and kinetic energy of the support structure. The loads and response from explosive devices such as kinetic energy penetrators will be localized and the duration of the event will be short, such that small models of the cable components should be sufficient and the full deck and supporting structure aren't required. It is noted that the modeler must exercise his/her judgment for determining the size and extent of the model in terms of representing the bridge and it is recommended that different boundary conditions and extent of modeling be evaluated to assess the potential effects on the predicted response.

10.5.2.2 Material Modeling

Material modeling is a critical part of successfully modeling explosively loaded structures that undergo large and rapid deformations. Relevant materials include cable steel, structural steel, concrete, and rebar; if protective devices are modeled, the materials could include high performance concrete, ultra-high performance concrete and armor-grade steels. Numerous material models exist and even for a single material, there are many candidate models. The correct choice depends on the physical material, the type of loading, and the rate of loading. The modeler's experience and expertise are perhaps most important for this part of the finite element modeling, in choosing the material model and picking the material constants.

For explosive and explosive device threats, the loading rates and material strain rates can be high and rate effects should be included in the material model formulation. Also, the material models should replicate damage growth and failure intrinsically and the use of ad hoc material erosion criteria should be avoided. The material models should also be able to differentiate between failure in compression, tension, and shear. Finally, the material model performance should be verified through comparisons with test data as much as possible; if such data does not exist, tests should be performed, at the loading rates anticipated and to the level of damage that is expected.

Again, material modeling is a complicated topic and the advice or services of a numerical modeling expert are recommended.

10.5.2.3 Explosive Load Modeling

For the majority of terrorist attack scenarios, the explosive threat should be modeled explicitly with an ALE approach, in which the explosive, air, and any projectile or fragmenting material are represented as Eulerian materials that interact with the cable or cable component, which are modeled as Lagrangian. Semi-empirical loading methods such as the Kingery-Bulmash equations are not appropriate for loading the very small surface of the cable but can be employed for cable components if the explosive is sufficiently far away and the geometry of the component is relatively simple, such that multiple shock reflections aren't created by re-entrant corners, overhangs, and other features of the bridge.

An ALE model for the explosive, air, and projectile can require a large amount of computational time and memory. To minimize these requirements, the extent of the Eulerian domain can be tailored to the particular problem and need not encompass all of the Lagrangian material. In Figure 10.20, the Lagrangian cable is shown in black; the extent of the Eulerian air mesh and explosive mesh are shown in blue and red, respectively. After the detonation occurs and the

shock and explosive byproducts have exited the Eulerian domain, the Eulerian mesh can be removed from the calculation, to further decrease the model's execution time.

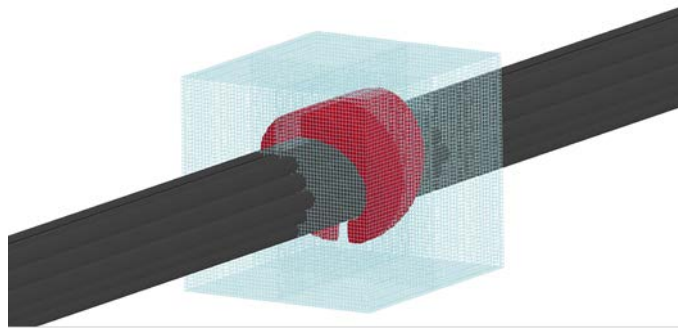


Figure 10.20 Eulerian Mesh and Materials (Air = Blue, Explosive = Red) Surrounding the Lagrangian Mesh of a Multi-Strand Cable Element (Black) [151]

10.5.2.4 Analysis Approach

The finite element software program must be capable of modeling large deformations that occur in a short amount of time. There are a number of suitable, commercially-available codes, such as LS-DYNA, ANSYS, ABAQUS, etc.

Suitable element formulations must be chosen. For explosive and explosive device simulations, solid and shell elements should be fully integrated in areas where large deformations, damage, and failure are expected; reduced integration can be used in the remaining areas. Standard “best-practices” for element geometry (Jacobian, warpage, aspect ratio, skew, etc.) should be followed. The mesh should be fine in the area of the penetrator or the explosive charge and can be coarsened further away. The size of the elements and material type determine the time step and should be chosen carefully to not degrade fidelity of the simulation but also to allow execution in a reasonable amount of clock time. While the best element size varies from problem to problem, 5 to 10-mm is common for the Lagrangian materials. Modeling experience is an important factor in developing a superior mesh, in terms of predictive quality and execution time; re-meshing can be labor intensive and should be minimized if possible.

10.5.2.5 Interpreting Analysis Results

With properly chosen material models and constants, an appropriate mesh, proper extent of the model's boundaries, correct initial conditions, and a robust interface between the Eulerian and Lagrangian materials, the finite element software will generate a large database of kinematic and state variables that can be analyzed, plotted, and queried. Animations from the simulations combined with fringe plots of key state variables can be examined to determine the performance of the cable or cable component. As performance criteria do not exist, the engineer/modeler must apply his/her judgment to determine if the cable or cable component has performed satisfactorily. If not, the design may be revised and the analysis re-run until the performance is satisfactory.

10.5.3 Bridge Performance Assessment

The results of the cable and cable component vulnerability assessments discussed in Section 10.5.1 should be used to develop a numerical model of the entire bridge, that reflects the reduced

capacities; this model would then be analyzed using the service loads expected to be present at the time of the attack. The engineer would assess the additional damage due to the reduced cable and cable component capacities and would determine if the damage is likely to grow and result in complete collapse.

For instance, one of the design basis threats may consist of the simultaneous application and detonation of ten separate 10-lb block charges placed on 10 sequential cables, on one side of the bridge. ATP-Bridge would be used to determine how many strands would remain for each of the 10 cables; multiplying the number of strands by the cross sectional area of the cable will give the remaining cross-sectional area. The numerical model for the bridge would be modified by reducing the cross-sectional area of these 10 cables; the modified model would be exercised with the applied loads and the engineer would determine if collapse is likely. If so, the designer may revise the design if it is a new bridge or he/she may develop a retrofit protective device. This retrofit might consist of adding steel or polymer tubes around the lower (accessible) portion of the cable; the standoff would greatly reduce the effectiveness of the block charge. Alternatively, for a new bridge, the number of cables or their cross-section might be increased.

As another example, the design basis threat may include a 1,000-lb TNT vehicle bomb that is detonated at the elevation of a semi-trailer bed. The bomb would damage the deck and potentially the support structure for the cable anchors. A numerical model of the cable anchor design would be developed and subjected to semi-empirical blast load histories or to an ALE representation of the explosive detonation and propagation. The resulting predicted damage to the cable anchors in the vicinity of the charge would be mapped onto the model for the entire bridge, along with the damage to the deck and the supporting structure. This damaged bridge model would be assessed for service loads and the potential for collapse would be estimated. If the collapse potential was sufficiently large, a new design could be developed or protective structure retrofits could be devised, fabricated and installed.

10.6 ATP-Bridge Design Examples

As discussed earlier, the design of a bridge to withstand a terrorist attack is a three step process. In the first step, the damage or failure of the individual cables or cable components would be assessed, with ATP-Bridge or with a detailed numerical simulation. In the second step, the damaged/failed components would be mapped into a numerical model of the overall bridge to create a new post-attack model; a representative example of a numerical model of an undamaged bridge is shown in Figure 10.21. In the third step, the post-attack bridge model would be subjected to the service loads that exist at the time of attack and the results of the analysis would be used to assess the probability that the damage will grow and the bridge will collapse.

Examples of the first step of the process are presented here, using ATP-Bridge to determine the level of damage and failure.

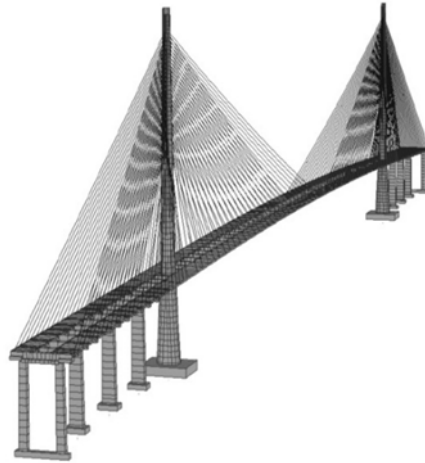


Figure 10.21 Example of Numerical Model of Undamaged Cable-Stayed Bridge [153]

10.6.1 Linear Shaped Charge against Stay Cable

In this example, the design basis threat for a cable-stayed bridge includes 200-gr/ft flexible linear shaped charges that will wrap around the circumference of a 13-strand stay cable.

After starting the ATP-Bridge software, a new project is created and a steel cable is defined as shown in Figure 10.22. The outer diameter of the environmental cover is chosen to be 3-in. The flexible linear shaped charge threat is defined as shown in Figure 10.22. The results of the analysis show that the cable is not severed; see the left side of Figure 10.23.

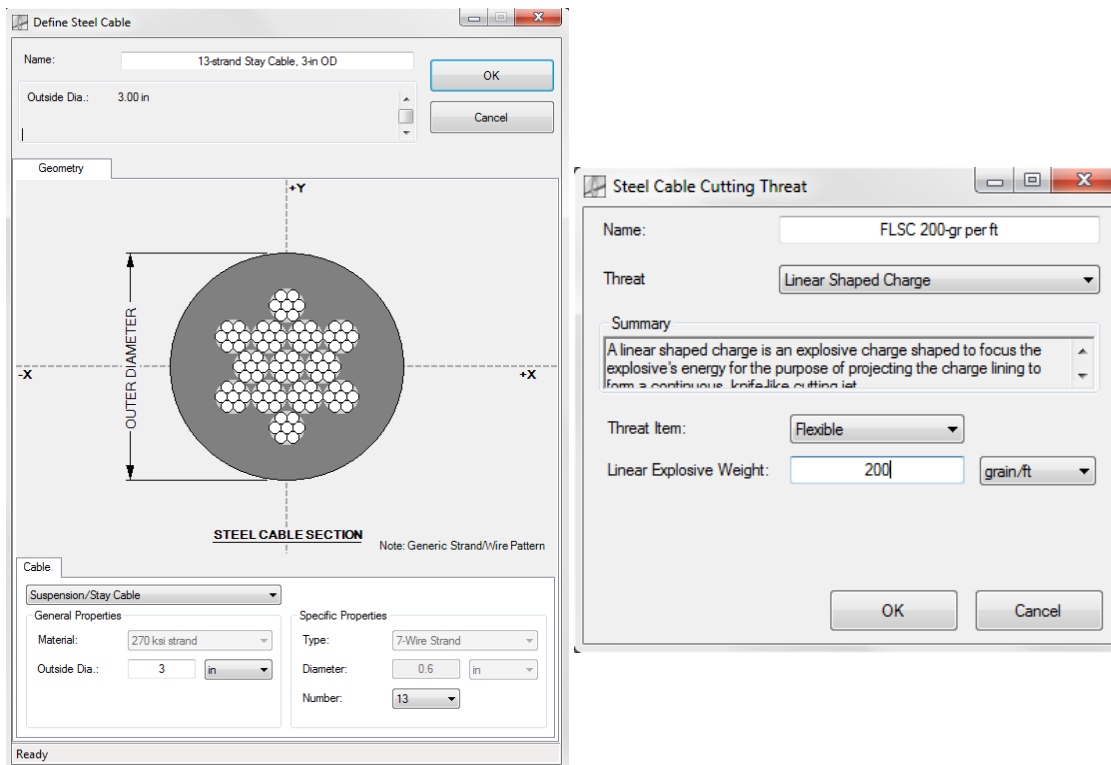


Figure 10.22 Cable and Flexible Linear Shaped Charge Input Screens

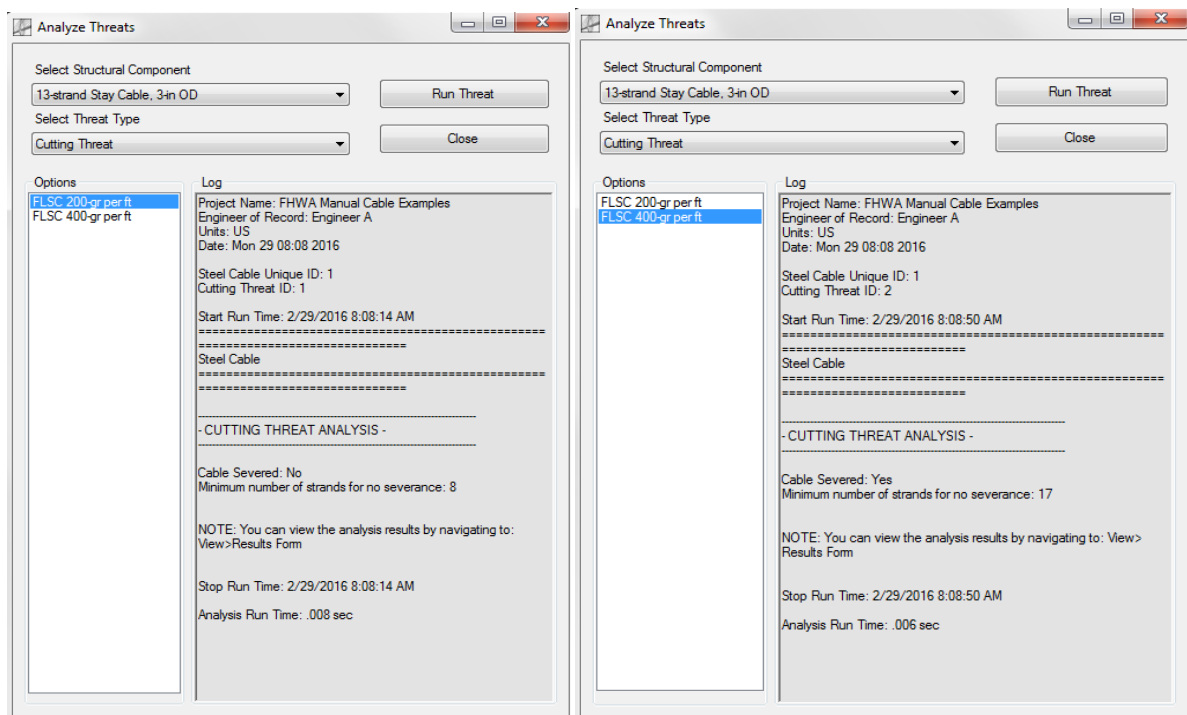


Figure 10.23 Analysis Results for 13-Strand Stay Cable Subjected to 200-gr/ft (left) and 400-gr/ft (right) Flexible Linear Shaped Charges

If the flexible linear shaped charge is increased to 400-gr/ft, the cable is severed, as shown in the right side of Figure 10.23.

Currently, ATP-Bridge only defines severed or non-severed as the final state. In reality, the 200-gr/ft charge will damage the cable to some extent and there will be a reduced capacity; however, current research and available data do not allow the definition of this reduced capacity.

10.6.2 Block Charge against Steel Cable

In this example, the design basis threat for a cable-stayed bridge includes a block of 20-lb TNT placed next to a 31-strand stay cable with a 4-in outer diameter for the environmental cover. The steel cable and the block charge are defined as shown in Figure 10.24. The results of the analysis show that 20 strands of the cable are severed and 11 intact strands remain; see left side of Figure 10.25.

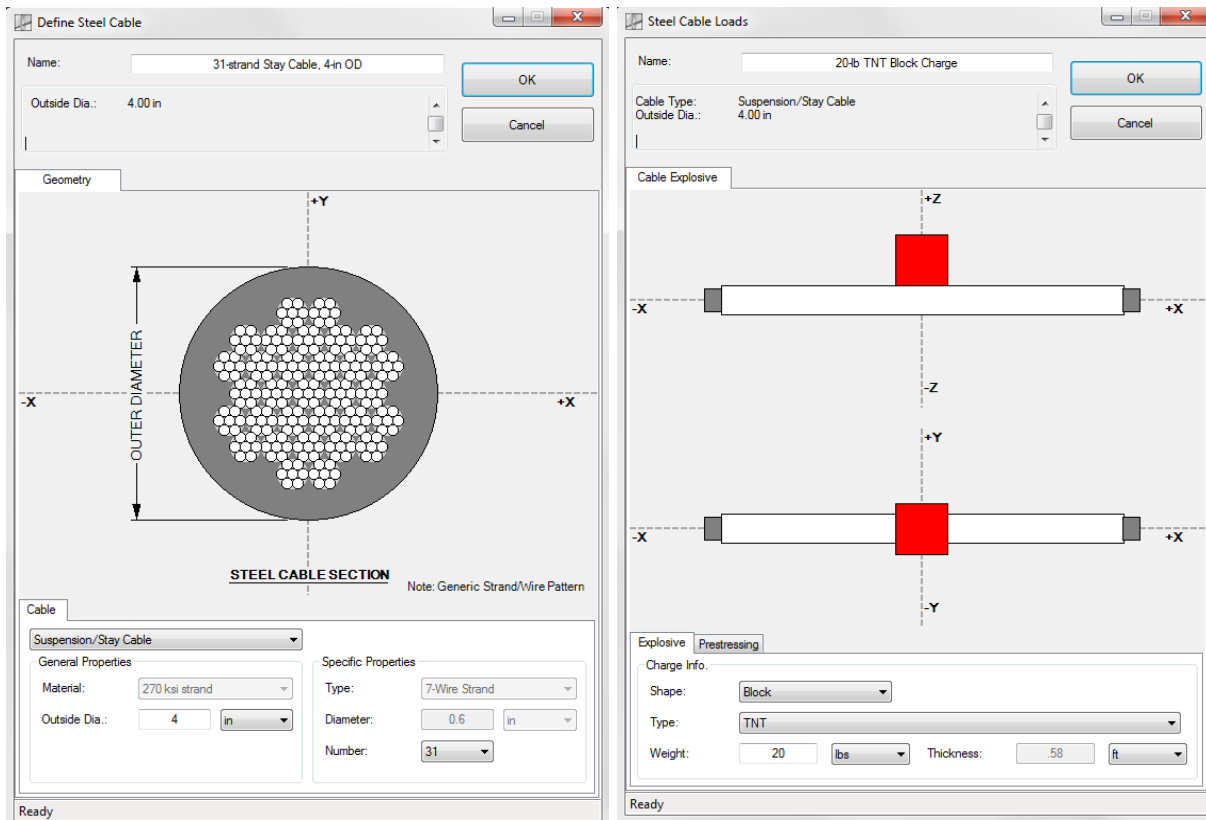


Figure 10.24 Cable and 20-lb TNT Block Charge Input Screens

If the standoff to the 20-lb charge is increased by 2-in. to 4-in (i.e., outer diameter of the environmental cover is increased to 8-in), the number of intact strands increases to 25, as shown in the right side of Figure 10.25.

As mentioned earlier, the engineer would multiply the number of intact strands by the cross-sectional area of each strand and use that to define the cross-sectional area for that cable in the numerical model of the entire (damaged) bridge.

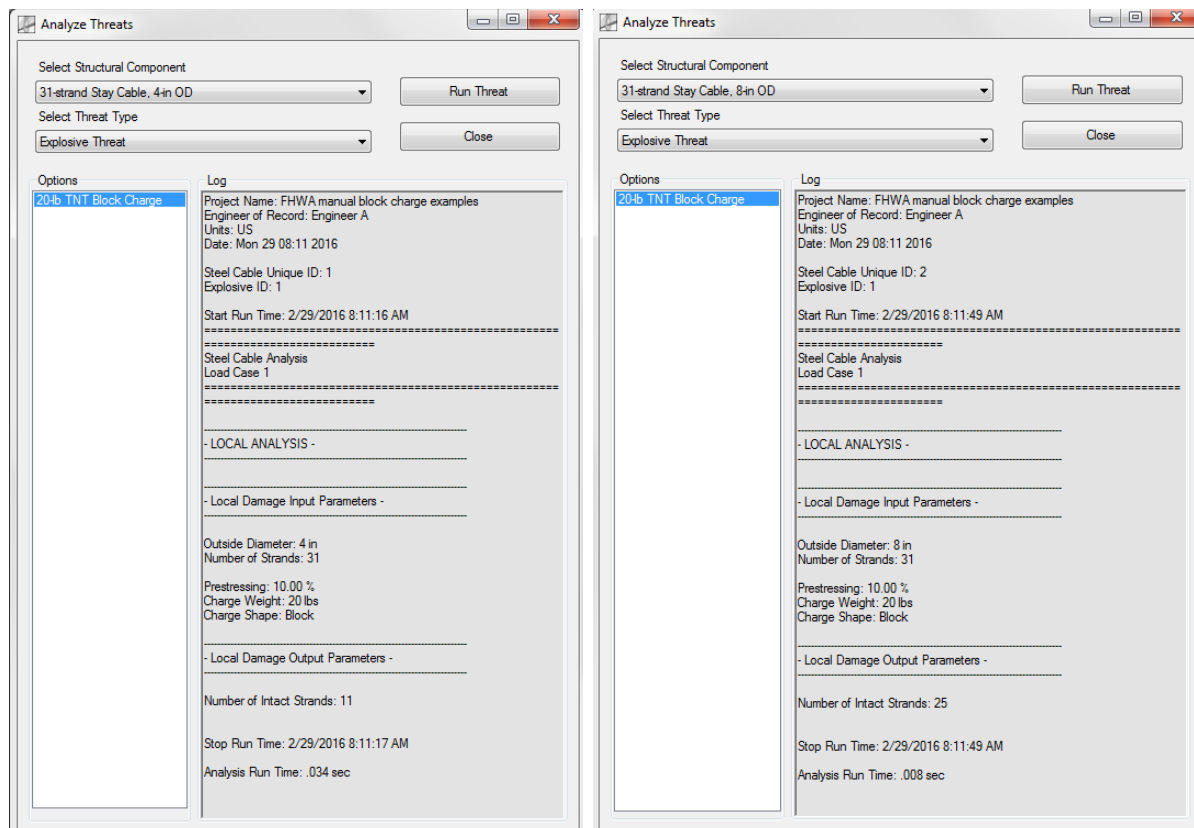


Figure 10.25 Analysis Results for 31-Strand Stay Cable Subjected to 20-lb TNT Block Charge with 4-in. OD (left) and 8-in. OD (right)

10.6.3 Diamond Charge against Steel Cable

In this example, the design basis threat for a cable-stayed bridge includes a 3-lb C-4 diamond charge placed on a 19-strand stay cable with a 4-in outer diameter for the environmental cover. The steel cable and the diamond charge are defined as shown in Figure 10.26. The results of the analysis show that 12 strands of the cable are severed and 7 intact strands remain; see left side of Figure 10.27.

If the number of strands is increased to 31 and the outer diameter is increased by 4-in to 8-in, no strand failure occurs, as shown in the right side of Figure 10.27. As mentioned earlier, the engineer would multiply the number of intact strands by the cross-sectional area of each strand and use that to define the cross-sectional area for that cable in the numerical model of the entire (damaged) bridge.

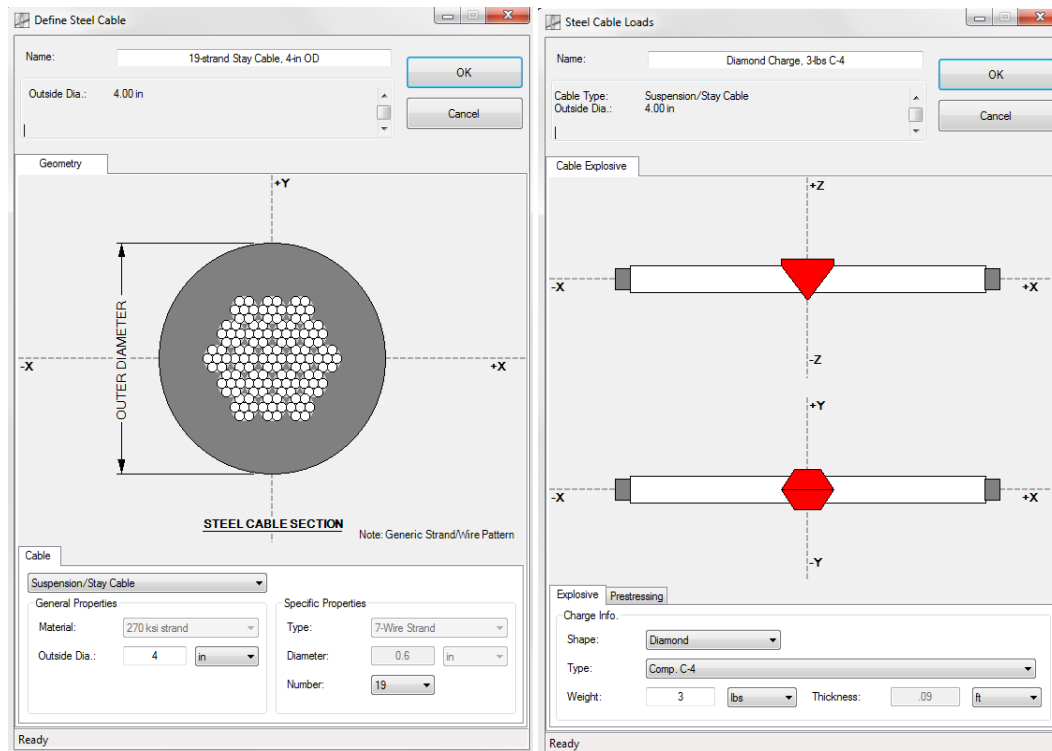


Figure 10.26 Cable and 3-lb Diamond Charge Input Screens

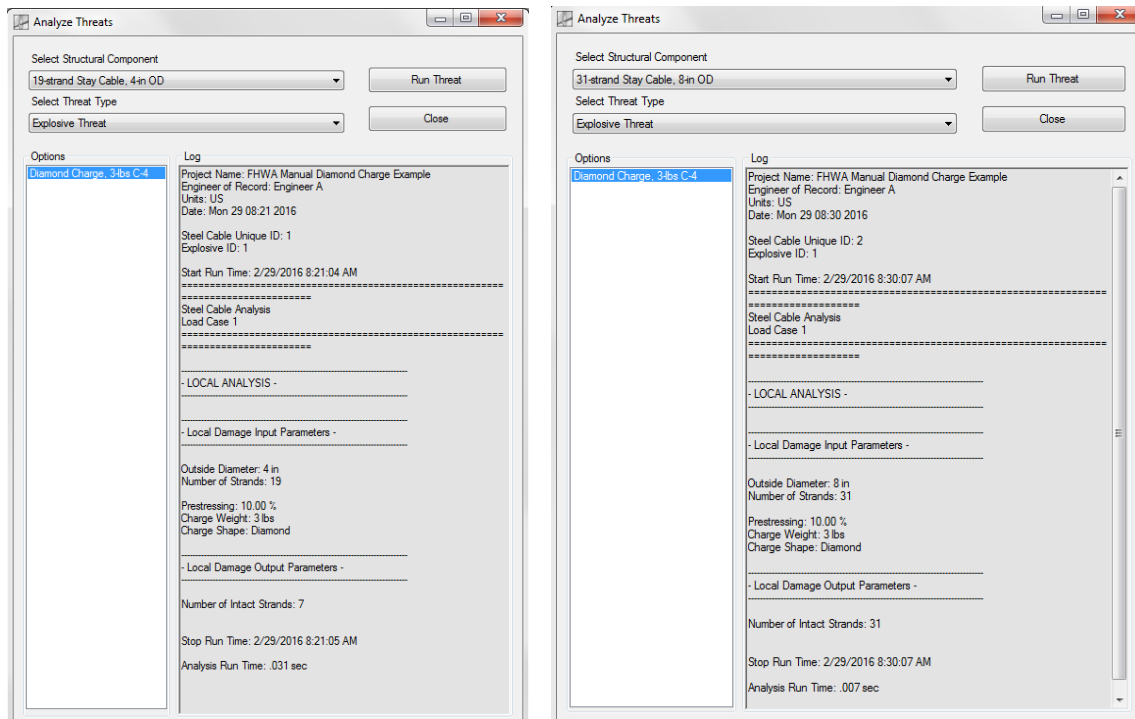


Figure 10.27 Analysis Results for 19-Strand Stay Cable with 4-in. OD (left) and 31-Strand Stay Cable with 8-in. OD (right) Subjected to 3-lb C-4 Diamond Charge

10.7 Overview of Threat Mitigation Retrofit Strategies

As discussed in Chapter 2, detection, delay and response are typical parts of the operational security strategy. Physical mitigation devices and approaches are discussed in this section.

There are a number of retrofit strategies that may be applied to existing cable bridges subjected to potential terrorist attack. It is recognized that existing bridges are unique structures that were designed to meet the service requirements while minimizing three key variables: weight, space, and cost. These variables are not independent and changing one will affect the others. Implementation of retrofit strategies will add weight and require space, and the designers must determine if these additional demands can be met without compromising the function or safety of the bridge.

At the overall bridge level, threat mitigation can be achieved through additional load paths, such as the addition of stay cables and hanger cables. This would require additional anchors and attachments. It may be possible to add additional hangers to suspension bridges but the costs and the closure of traffic lanes could make this impractical. For cable-stayed bridges, the connections at the top of the towers for the converging stay cables are typically packed tightly and the existing space may not be sufficient for additional connections; the additional connections would modify the tower structure in that area, which could reduce strength and ductility. This approach would also increase the dead load on the bridge, due to the additional cables and may affect the aerodynamic loads. However, in principle, adding additional load paths is a viable approach.

At the cable and cable component level, two strategies may be employed: increased standoff and hardening. As demonstrated in the examples in the previous section, increasing the standoff between cables and the block charge and diamond charge threats will decrease the number of strands that are damaged or failed. This may be accomplished by adding tubes around the easily accessible portions of the cables near the bridge deck. The material may be thin walled steel or moderately thick polymers, chosen to resist deliberate removal. A clamshell configuration could be used to place the tubes around the cable, with the hinge section and locking sections designed to resist removal. The ends of the tube would be sealed to prevent water intrusion. This approach could also be used for cable anchors, which tend to be cylindrical and are also near the bridge deck. Given the complex geometry of some cable saddles, implementation of a standoff surface could require the creation of specially formed components that are locked around the saddle hardware. In general, the standoff approach would work well for small explosive threats such as the block charge and diamond charge as well as the cutting threats (mechanical, thermal, and LSC) and would provide some benefit for a large bulk charge on the deck. Standoff will not reduce the vulnerability to explosive devices such as kinetic energy penetrators.

The second strategy for retrofitting cables and cable components is to harden the components by the addition of protective hardware, which also would increase standoff. For cables and some cable components, tubes composed of high strength steel and filled with high performance or ultra-high performance concrete would provide protection against all explosives, explosive devices and cutting threats. Other dense and strong materials and novel geometries could also be employed. However, as noted earlier, if the design basis threat includes kinetic energy penetrators, which are military-grade threats, then the protection will have to perform similar to military armor and will not be light-weight or inexpensive. For existing bridges which have been optimized for weight, the additional weight may not be acceptable; space to place the hardware

may be another issue. In general, the development of protective hardware will require expertise in weapons effects and protective structure design.

Protective systems for bridge cables and cable components have been developed, tested and installed on bridges by commercial companies; information on these products and companies may be found through an internet search. A summary is not provided here as the product designs constantly evolve, there are often proprietary issues that must be resolved, and mention of these products in this manual may be construed as an endorsement. It is also noted that a number of specialized design firms provide protective structure design services that are relevant to the development of retrofit strategies. At the current time, it is recommended that this strategy include strict performance criteria and project testing to verify the effectiveness of the protective measure for the specified threats.

Government agencies have performed research into identifying and evaluating hardening techniques and materials for cables and cable components. The reader is referred to Chiarito et al. 2011 and Ray et al. 2012.

Finally, additional research into new and retrofit hardening strategies is needed, to develop improved designs and materials that reduce the weight demands and costs associated with current devices.

10.8 Chapter Summary

Cable bridges are attractive targets for terrorist attack due to their iconic nature, ease of access to the key structural components, and the perception that redundancy is limited. A number of explosives, kinetic energy penetrators, and cutting threats may be brought to bear against the cables and cable components. For some threats and cables, the vulnerability may be assessed with ATP-Bridge; for other cables and cable components, a detailed numerical simulation of the threat and bridge component must be performed to assess vulnerability. Testing at the material, component and structural level is needed to develop data that supports or verifies the predictions from ATP-B and numerical simulations.

Two design approaches can be followed. In the first, the damaged state of the cables or cable components is assessed, for the particular threat. A model of the damaged bridge is then created by inserting the reduced cable/component capacities into the numerical model of the pristine bridge. The potential for collapse of the entire bridge can be assessed after the damaged bridge model is subjected to the service loads at the time of attack. In the second, variations of the numerical model of the entire bridge are developed by removing different combinations and numbers of cables or cable components; these models are executed and analyzed to determine how many cables or cable components must be lost before the bridge collapses. The relative importance of the cables or cable components is identified and the appropriate level of protective design is determined.

If collapse is indicated, the bridge designer can modify the design to add redundancy to the overall bridge or can modify the cable and cable component design, or can add mitigation methods such as standoff and physical hardening. The final design will balance the service requirements with the protective elements, to achieve a bridge that is safe and minimizes the requirements for cost, weight, and space.

11.0 PROTECTIVE DESIGN GUIDANCE FOR OTHER BRIDGE COMPONENTS

This chapter addresses bridge components that, to date, have not been well studied. Accordingly, these components must be treated in a less detailed manner than the specific bridge components discussed in the previous chapters. The components described in this chapter are divided into categories based on the primary mode of response that must be resisted under normal loading conditions. When appropriate, protective design strategies are recommended, and any relevant research is provided so that readers can find additional information as needed.

11.1 Flexural Members

A flexural member in bridge systems is any structural component that, under normal loading conditions, primarily serves to carry gravity loads acting transversely to the axis of the member. Flexural members resist these gravity loads primarily through bending deformations (though shear deformations can be important in the case of short and deep members).

11.1.1 Member Types

Flexural members include primary girders supporting the bridge deck, but they also include stringers and floor beams that make up the deck system of many bridges. The following terminology is commonly used to describe bridge flexural members: girders (or trusses) span longitudinally between points of support, floor beams span transversely from girder to girder, and stringers span longitudinally from floor beam to floor beam.

Girders come in a variety of shapes and materials including both steel and concrete. Steel girders can come from rolled sections, or they can be built up from flat plates. Cross-sections can be I-shaped or box-shaped. Likewise, concrete can be cast in a variety of shapes using a wide range of compressive strengths. Concrete flexural members can be conventionally reinforced or prestressed. Like steel, concrete can come in solid I-shapes or in box sections. Many bridges throughout the U.S. utilize standard AASHTO girders such as the Type IV girder.

To date, only limited testing has been conducted against flexural members. Cofer et al. (2012) describe two blast tests that were conducted against prestressed concrete bridge girders. One test considered response to a blast originating from underneath the girder, while the other test considered a blast load acting on the top of the girder. A limitation of the test program was that only an individual girder was tested. No composite interaction with a bridge deck was included. Nonetheless, the testing revealed important information regarding the response of flexural members to blast loads. In both scenarios, localized shear deformations were large enough to cause severe damage and overall girder failure. The blast damage locally rubblized concrete, causing loss of section capacity, which eventually led to collapse. Areas away from the point of detonation showed little to no damage from the blast. Thus, an important observation from this test program is that severe localized damage can lead to section loss and overall component failure in a similar manner to what was observed for reinforced concrete bridge columns (see Chapter 7) where localized shear failure occurred at the column base.

A type of flexural member that deserves special consideration is a box girder, whether constructed of steel or concrete. Although the state of stress due to normal gravity loads is much different in a flexural member than an axial member, it is still necessary to develop preliminary

guidance that can be used to aid in the design of box girders. Severe, localized blast damage to these types of members can be informed by the research conducted on the response of steel and concrete towers (see Chapters 8 and 9, respectively). The internal arrangement of plates and stiffeners within a cellular tower is typically much different than the internal bracing system used in steel box girder bridges. Nonetheless, given the absence of directly applicable research, it is recommended that the findings presented in Chapters 8 and 9 be used to help identify critical modes of response.

The book by Bulson (1997) [154] is one of the few references that specifically considers the behavior of bridges in response to blast loads. The book reports that previous terrorist incidents have resulted in damage to bridge decks and truss members. The author points out that there is very little data available pertaining to the response of bridges subjected to explosions. Of the limited data available, much is based on observations made during wartime for bridges subjected to engineered military weapons. Such information is likely not representative of a typical terrorist attack. A major point of relevance to the response of flexural members comes from experiences gained in the demolition of bridges in Bosnia. There, it was learned that reinforced concrete box girder bridges were destroyed mainly by charges placed at deck level.

In the remainder of the chapter discussing the effects of explosions on structures, Bulson [154] suggests a procedure for classifying bridges based on their redundancy, and he provides several simplified methods for estimating residual capacity of blast-damaged bridges. The residual capacity is assumed to be a function of the original live load capacity and the loss of cross-sectional area. In addition, the book stresses the importance that local damage could have on critical members. For example, if prestressed tendons are cut in girders, the overall capacity could be reduced by as much as 50 percent.

Main girders can be constructed using a variety of unique configurations, including trusses and other types of built-up sections. Typically, such unique girders are used on long-span bridges and are not routinely used in everyday design practice. The general guidance for such girders is to understand how localized damage propagates and whether this damage propagation can cause overall bridge failure. Because of the difficulties in developing simplified engineering models that can accurately predict loads and response, analysis of these special types of flexural members will likely require high-fidelity finite element analyses with a fine enough mesh to capture the behavior of interest. Such models will likely only be needed in special cases, and these analyses should only be performed by engineers with suitable experience to do such work.

Aside from girders that act as primary members, many bridge systems include secondary floor beams and other flexural members. These members are typically used to help distribute loads to the girders and to provide bracing. It is recommended that secondary members in bridges be treated similarly to those in buildings. The technical report *Single Degree of Freedom Structural Response Limits for Antiterrorism Design* (PDC-TR-06-08) [74] provides definitions and response limits for secondary members responding to blast loads. In the event designers are interested in damage propagation following an event to assess the likelihood of collapse, UFC 4-023-03 *Design of Buildings to Resist Progressive Collapse* [155] also provides definitions and response limits for primary and secondary members. Secondary members are generally permitted to undergo higher levels of damage than the girders in withstanding the controlling design-basis threat so long as this damage does not control the performance of the girders. For example, if a

secondary beam provides bracing to a primary girder, and the failure of the secondary member would lead to lateral torsional buckling or other failure mode of the girder, the beams would only be permitted to undergo damage to a point where they can still provide bracing to the girders. If secondary members do not serve a critical role and are there simply to aid in distributing gravity loads, beams can undergo damage up to the onset of failure. To determine acceptable deformation limits associated with the response of secondary components, readers are encouraged to consult PDC-TR-06-08 [74] and potentially UFC 4-023-3 [155].

11.1.2 Design Loads

Flexural members may be subjected to large blast loads resulting from either below-deck or above-deck explosions. They may also be subjected to hand-emplaced explosives, shaped charges, or cutting devices. Finally, box-girders may be subjected to internal explosions if access to the inside of the girders cannot be controlled. The use of hand-emplaced explosives, shaped charges, mechanical cutting devices, and similar threats are of greatest concern near abutments where direct access to girders and other flexural members is easiest. While these threats are still possible near the middle of a span, the logistics to implement them is more difficult. Large VBIEDs are of concern near the mid-span and end locations. The number of threat locations that may require consideration will depend upon how access below a bridge is controlled, which is generally project specific. Load combinations for design should follow the AASHTO “Extreme Event II” case. The AASHTO *Bridge Security Guidelines* [36] provides a range of suitable charge weights associated with different types of vehicles. A variety of blast-load scenarios can be efficiently evaluated using the ATP-Bridge software, which is described in detail in Chapter 12.

11.1.3 Failure Modes and Performance Criteria

Failure modes associated with blast-loaded flexural members include global and local cases. Globally, such members can fail in flexure through the formation of a collapse mechanism due to the development of plastic hinges. Adequate bracing or lateral support to allow for a flexural failure can be challenging to achieve in practice, particularly given that blast loads induce dynamic, oscillating behavior where the portion of the section in compression shifts from the top half to the bottom half with time. Diagonal tension (also known as sectional shear) failures and direct shear failures are global failure modes that are also possible. Because of the large mass and flexural capacity of many bridge girders, developing a global failure mode is difficult, though localized failure can propagate and lead to global failure. Localized failure modes of concern include crushing, cratering, and breach of concrete members as well as local buckling and breach (i.e., perforation) of steel members. Localized damage in splice regions can lead to damage propagation and overall member failure. Localized damage can also cause a loss in prestressing force, thereby reducing the overall capacity of a prestressed girder.

Like other blast-loaded bridge components described previously in this manual, recommended performance criteria are based on limiting overall deformations to certain values depending upon the performance level desired. For example, elastic response may be desirable for some bridges deemed to be of critical importance. Less important bridges may be permitted to undergo large deformations. Based on a study to evaluate the redundancy of bridge systems, Liu et al. [156] proposed the maximum girder displacement be limited to 1-percent of the span length. This limit was established so vehicles that might be on a blast-loaded bridge at the time of an attack would

be able to drive to safety, accounting for the discontinuity that develops between the abutment and damaged girder. At larger deformations, Ghosn and Moses indicate that deflections are too great to allow people to drive off a damaged bridge. Nonetheless, it may be suitable in some cases to allow larger deformations than suggested by Liu et al. [156] depending upon the importance of a given bridge.

It is difficult to recommend performance limits associated with localized damage. Such damage is extremely challenging to predict due to highly nonlinear response in which materials such as steel or concrete behave more like a fluid than a solid. Estimates of spall, breach, and perforation damage can be made using the empirical relationships given in UFC 3-340-02 [50]. These empirical relationships will likely be suitable in the vast majority of cases, but it may sometimes be necessary to conduct high-fidelity finite element analyses to better understand the particular conditions for the project of interest. What is most important is that the local damage be used to consider how the overall response is affected. For example, predicting localized breach in a steel girder in the middle of the web may not severely affect the overall response or lead to girder failure. The same damage to the bottom or top flange, however, may lead to collapse. Thus, the specific location and extent of local damage should be evaluated to determine what consequences that damage poses to the overall capacity of the flexural members being analyzed and the system to which it is a part.

11.1.4 Design Considerations

Reinforced concrete and prestressed members generally possess less ductility than steel members, are usually not detailed for load reversals or uplift loading, and the potential loss of cover and strand de-bonding from local blast damage can significantly reduce their capacity. Nonetheless, because many designers rely heavily on prestressed bridges, several protective strategies should be considered that reduce their vulnerability. For example, undraped tendons will not possess a vertical component in the prestressing force, while the vertical force in draped tendons will reduce girder capacity for uplift forces.

Large uplift forces acting on girders and other flexural members are amplified by a pressure buildup (and corresponding increase in impulse) in confined regions. When combined with concrete cratering and spalling, these uplift forces may lead to significantly reduced capacities from a loss of cover, prestress bonding, and composite action with the deck. In addition, the combined actions of flexure, uplift, and a potential loss of seating from local failures may lead to collapse of the girders. Large explosive loads possess the potential for either local or global shear or flexural failure, and local failure of one span may lead to knocking/pulling adjacent girders off their supports. Longer span members are generally more resilient to blast loads because they tend to be more massive, stronger, and more flexible [38].

Flexural members can be designed for large uplift forces using various techniques. For example, providing continuous top and bottom reinforcement in concrete members and adding stiffeners and strengthening lateral bracing on steel members to prevent local buckling before members reach their full plastic capacity can greatly improve girder response to below-deck blast loads. In general, member connections should be designed to allow the connected members to reach their full strength. The general philosophy is to prevent failure from occurring in the connections. Additionally, girders can be restrained with steel cables to reduce the chance of seating loss at the supports. Hinge restrainers can be utilized to hold the superstructure to the columns (similar

in concept to the restrainer systems currently used in seismically active regions). Also, increasing the size of abutment seats and adding hinge seat extensions under expansion joints might reduce the chance of failure.

11.2 Bridge Decks

Bridge decks can be constructed in a variety of ways using a wide range of materials. Aside from providing a surface on which traffic can pass, the bridge deck acts together with the girders and other flexural members to create a bridge's superstructure. Although the behavior of individual parts of the superstructure (such as the girders) is important, what is more important is how the integrated system behaves when loaded. For typical highway bridges, the girders are mechanically joined to the deck at discrete locations using shear studs or deformed bars. The behavior of this composite system should be understood for successful implementation of bridge security design provisions.

11.2.1 Deck Types

Bridge decks can be divided into the following main categories: concrete deck slabs, metal grid decks, orthotropic steel decks, wood decks, and FRP decks. Often, the bridge deck plays the primary role of transferring gravity loads from traffic to the supporting flexural members and is an essential component in the overall behavior of the floor system. In some bridges, however, the deck can be suspended (e.g., suspension bridge) or can carry a significant axial force as part of a compression strut (e.g., cable-stayed bridge). According to the 2014 NBI survey (<https://www.fhwa.dot.gov/bridge/nbi/deck.cfm>), the overwhelming majority (74%) of bridges utilize cast-in-place concrete decks, with precast concrete panel decks a distant second (12%). Given that concrete decks make up more than 85% of bridges in the NBI database, the discussion in this section focuses on these types of bridge decks.

Aside from traditional cast-in-place concrete deck slabs, concrete decks can also be constructed using full-depth or partial-depth precast panels. Some concrete deck slab systems are post-tensioned. Particularly in the case of steel girder bridges, it is possible to use stay-in-place corrugated metal formwork or temporary formwork. Because of the variety of construction methods used in practice, coupled with the extremely limited data available on how such deck systems behave compositely with flexural members under different blast scenarios, the components should be analyzed separately to determine peak deflection and as fully composite to determine reaction forces.

11.2.2 Design Loads

Bridge decks may be subjected to large blast loads resulting from either below-deck or above-deck explosions. While hand-emplaced charges and mechanical cutting devices can also conceivably be used, these threats are not of significant concern for most bridge decks given their large area and overall redundancy. A potential exception, however, must be considered for box-girder bridges. In these types of bridges, the deck plays an important role in providing a closed-section, which is much more resistant to torsional demands than an open cross-section. In cases involving horizontally-curved box-girder bridges, special attention should be given to the loads on the deck and the effect the consequent damage has on overall bridge response. In addition, the possibility of internal blasts using hand-placed charges should be a concern in these

cases because blast load effects are amplified within the enclosed volume of a box-girder (see Chapter 4 regarding how confinement enhances blast loads).

11.2.3 Failure Modes and Performance Criteria

The failure mode of primary concern is localized spall and breach. Such localized failures can occur for either below-deck or above-deck scenarios. Unless the threat in question is large enough to significantly damage the supporting girders, localized deck failure in most cases will not adversely affect overall bridge system performance. In fact, as discussed in more detail in the next section, such localized failure may be beneficial in venting loads and reducing the stresses that need to be resisted by primary flexural members. The main performance criterion is to ensure that the extent of damage to the deck is not so large that it compromises overall system behavior. This is particularly true in cases where the superstructure depends on the deck and girders acting compositely to resist normal design loads.

11.2.4 Design Considerations

For explosions underneath a bridge, the deck will be subjected to uplift forces, which can be significantly amplified by a pressure buildup in the confined regions between the girders and near the abutments. These uplift forces may cause the deck to separate from the girders. For explosions on top of a bridge, the deck will experience increased dynamic loads in addition to the gravity loads. Large explosive loads possess the potential for localized shear or membrane failure of the deck. Depending on the quantity of explosives, deck failures will often be localized between supporting components, such as beams or girders, which may allow confined pressures under the deck to vent. Decks can be designed to resist uplift forces using techniques such as providing continuous top and bottom reinforcement in the slabs. However, in designing for blast scenarios, it is recommended that the deck be considered sacrificial and that efforts be focused on protecting the supporting structure. The deck should only be strengthened when needed for stability or for structural integrity, such as ensuring sufficient torsional strength is provided in curved steel trapezoidal box-girder bridges in the event a portion of the deck is compromised.

11.3 Design Considerations for Other Components

Developing a list of “other” bridge components that have not been addressed in the sections above or previous chapters is a difficult task given the wide range of bridge structural systems, materials, and obstacles that bridges are designed to cross. The same bridge over water has different threats and concerns than if it were a highway interchange over land. Truss bridges have unique challenges that are different than those of other bridge systems. Thus, trying to capture all of these unique aspects of bridge security for the breadth of bridges that make up the infrastructure is not feasible. Accordingly, the aim of this section is to address some specific cases that fall under the larger umbrella of “other components” that have not been previously addressed. The intent is not to provide an exhaustive list. Further complicating this issue is that limited research data exist to demonstrate how these components behave when subjected to blasts or other threats. Therefore, the following list of components and accompanying design recommendations are based on the experience of the authors. Future research, which is presented in the next section, should be conducted to help address the limitations in knowledge presented below.

11.3.1 Bridge Bearings

A primary function of bridge bearings is to accommodate thermal movements of the superstructure relative to the substructure. Different types of bearings (e.g., elastomeric pads, pot bearings, etc.) are used on bridge systems with steel and concrete girders. In most cases, a targeted attack against a bridge bearing is not likely to cause overall bridge collapse unless the damage is so extensive as to severely reduce the capacity of the girder and/or cap beam (or other type of pier) upon which the girders sit. The main challenge with protecting bridge bearings is the fact that they are relatively small and are typically directly exposed. Thus, placement of explosives in contact or in near proximity with a bearing can cause significant damage. Particularly near abutments, it may be relatively easy to access bridge bearings. While damage to a bearing is not likely to cause catastrophic behavior, a major concern is that it is quite difficult and costly to replace a bearing on an existing bridge. For the long-term performance of a bridge, correct functioning of the bridge bearings is important. The primary bridge security design strategy for bridge bearings is access control, making it difficult to get close to the bearings. This may be done with fencing, or it might be done with coordinated monitoring using CCTV cameras and police response, frequent police patrols, etc. Coordinating security with law enforcement personnel has the added benefit of reducing vandalism and other minor crimes.

11.3.2 Abutments and Riprap Walls

Abutments and riprap walls are frequently used in the design of highway bridges. Because of the typical unobstructed access these elements provide to the underside of the superstructure near the ends of a bridge, some thought should be given to access control and monitoring. These components themselves, however, are quite massive and should not be a controlling feature of a bridge security mitigation plan. Any size threat that can severely damage an abutment will also severely damage a bridge, likely to the point of failure. One aspect of behavior that should be considered with these elements is the blast load enhancement effect they can provide near the ends of a bridge. Figure 11.1 shows how the abutment geometry can cause multiple blast load reflections, which can increase the load effects on the substructure and superstructure components near the end of a bridge relative to the mid-span region [104].

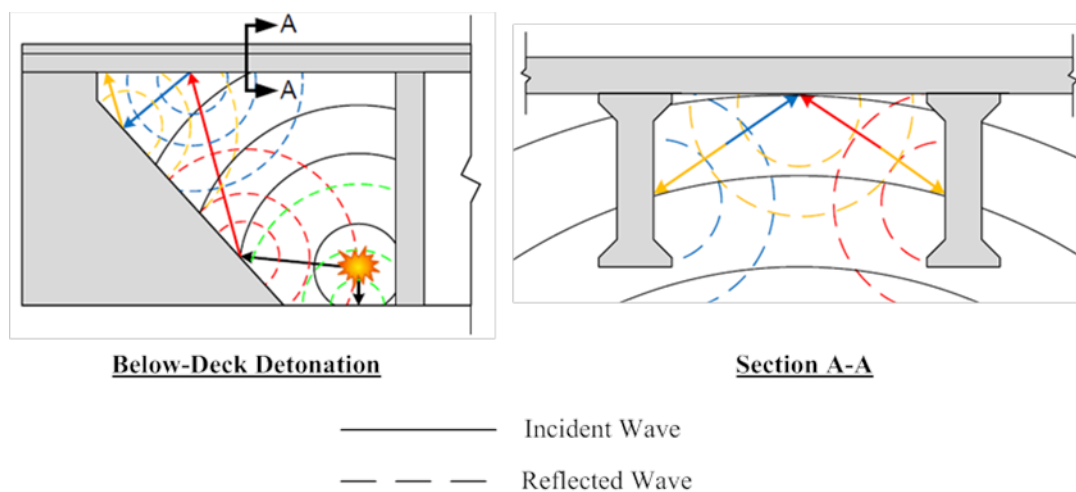


Figure 11.1 Confinement Effects at Abutment [21]

11.3.3 Bridges over Navigable Waterways

Bridges that span over navigable waterways must consider some additional threats that do not require consideration for bridges spanning over land. Because the speed of watercraft on navigable channels is highly dependent upon the channel geometry, bridge pier layout, current, water depth, etc., providing general protective design guidance is not practical. Typically, watercraft will be travelling at a slower speed than trucks or other vehicles travelling over roads, so the potential speed of impact is expected to be less for piers in water than piers founded in soil. Piers in the water can be protected from vehicle impact using dolphins, fenders, rock islands, or other systems. Aside from protecting against impact, pier protective measures provide an effective way to increase standoff from an explosive detonated on a ship or barge. Because barges and barge groups can potentially carry a much larger volume of material than an individual truck over land, attention must be given to how the design-basis explosive threat is determined. Underwater detonations can create a water plume that causes damage from the mass momentum of the fast-moving water being propelled against bridge components. In this case, the shock wave energy is dissipated in getting the water moving. To be effective, the charge must be at an optimum depth, and the bridge needs to be somewhat close to the water [38]. Given the wide range of possible configurations and threat scenarios, critical bridges may require finite element analyses that account for fluid-structure interaction.

11.3.4 Horizontally Curved Bridges

Horizontally curved bridges are commonly used at highway interchanges as direct connectors that allow traffic from one highway to blend directly into another highway. Unlike straight bridges, horizontally curved bridges must resist significant torsional demands due to the eccentricity that exists between the gravity loads and the points of vertical support at the bridge piers. These torsional demands are well understood for dead and live loads. For bridge security, however, the size and placement of a hypothesized blast may place additional torsional demands on a horizontally curved bridge that may not have been originally considered during design. For example, a VBIED acting near the mid-span places additional torsional demands on the bridge superstructure and the loads that are transferred to the piers. Furthermore, oscillatory response of the bridge, or loads acting upward from a below-deck blast, can lead to torsional demands that act opposite to those considered under typical loading conditions. Therefore, while bridge security planning and project team coordination is important to all projects, it may be even more critical in the case of horizontally curved bridges (or other unique bridge systems) because the design can be strongly influenced by how design-basis threats are selected. The primary recommendation for these types of bridges, as with all types, is to ensure the entire project team meets frequently and early to coordinate bridge security planning into the overall design process.

11.3.5 Truss Bridges

For the global response of a truss bridge, depending upon the threat being considered, truss members may be subject to loads that cause stress reversals relative to normal loading conditions. As such, truss elements designed for tension may buckle in compression, and connections at gusset plates may be required to resist forces much different than those due to typical design loads. For above-deck explosions, truss members will experience explosive loading in addition to the gravity loads. These increased loads will most likely be localized near the explosion, and, aside from just acting downward, they possess the potential for inducing

extreme lateral forces on the members themselves. Though steel cutting is difficult without direct contact with an explosive, it could occur with a very large explosion close to cables or truss members. Upper and lower chords of shorter-span trusses are the most vulnerable [38], and their failure could result in total collapse of a bridge. Truss members can be improved by reinforcing connections to ensure members reach their full plastic capacity, using energy absorbing connections, or wrapping or partially shielding truss members near deck level with protective armor to protect against localized damage from blast and fragmentation. While wrapping a member will improve its strength, it may also increase the overall demand on the member because wrapping and shielding will lead to a larger presented area than the member initially had. Accordingly, the increase in strength as well as the corresponding increase in demand both need to be considered when developing a retrofit or strengthening plan.

11.3.6 Built-Up and Laced Members

Rather than using a solid cross-section comprised of one homogeneous piece of material, many bridges (particularly older bridges) utilize built-up and laced members [157]. Figure 11.2 shows an example of such a cross-section. Predicting the loads that a laced member must resist cannot be readily accomplished using the simplified approaches routinely used in practice. Because the cross-section is not solid, there is a complicated environment of shock refraction, reflection, and clearing among the various parts of the built-up member, with blast effects infiltrating to the inside of the cross-section. In their report, Noriega and Crane (2013) [157] adopt a simplified approach in which ConWEP [97] is used to predict blast loads on different portions of the blast-loaded face, but they acknowledge such a method neglects clearing and other important effects. At the conclusion of their report, the authors recommend using “computational fluid dynamics to study the behavior of the air blast as it interacts with the column openings.”



Figure 11.2 Example of Steel Laced Column [157]

11.3.7 Proprietary Protection Methods

Various vendors have advertised the use of special structural systems or materials to mitigate the effects of blast loads and other non-explosive threats acting against structures. A search of the internet will reveal a wide array of different products including cellular materials, advanced composites, ultra-high-strength concrete, and high-strength steels. Many of these products have the potential to be useful in protecting bridges from blast loads and other hazards. Most of these products, however, have not undergone rigorous testing to demonstrate their viability for the severe threats that are often considered for protective design of bridges. Consequently, prior to using or specifying any of the proprietary products that can be found on the market, it is important for engineers to require details of any prior testing to ensure the product(s) will work as desired under the conditions being considered for design. If such testing has not been completed, it is recommended that a rigorous testing program (perhaps as part of the design or construction process) be carried out to ensure the product will perform as advertised. It is also important to note that some protection measures may need to work effectively against more than one threat, e.g., against blast, hand-held cutting devices or tools, and specific fire events.

11.4 Future Research Needs

The protective design of bridges to withstand potential terrorist attacks is a relatively new field. The design of bridges to resist earthquakes dates back many years. The Ministry of the Interior of Japan issued “The Seismic Design of Abutments and Piers” in 1924 [158] following the Great Kanto earthquake of 1923. Since that time, there has been worldwide interest in protecting bridges against earthquakes, and the field has advanced considerably through the efforts of a large number of researchers and designers. In comparison, strong interest in blast-resistant design of bridges developed following the terrorist attacks of September 11, 2001. While significant advancements have been made in the protective design of bridges, much time and research are still needed to mature the field to a level that is similar to seismic-resistant design. Accordingly, the list of research needs is vast and not easily captured in a simple list. The intent of this section is to draw attention to the most significant current research needs. The specific topics requiring attention will necessarily need to be expanded and revised with time.

To date, only a few large-scale experimental testing programs have been carried out to study how different bridge components respond to blast or other impulsive loads. Tests have been conducted against reinforced concrete bridge columns, a single cell of a reinforced concrete cable-stayed bridge tower, steel suspension bridge towers, prestressed concrete girders, and cables. Despite the valuable information these past tests have provided, one drawback is the limited scale of the tests. These past tests have been conducted on structures $\frac{1}{4}$ to $\frac{1}{2}$ scale, and they have been conducted on isolated components. For example, bridge columns have been tested without the presence of a deck or axial loads on the columns. Steel suspension bridge tower tests have only considered a portion of a tower cross-section, and the tests did not include large membrane stresses in the plates to account for the large axial force a suspension bridge tower must withstand. Thus, there is a significant need to conduct blast testing against critical bridge components using boundary and loading conditions that do a better job matching in-service conditions than past testing has.

A major limitation of past testing and current ongoing work is that there is no widely accepted testing protocol for validating the performance of bridge structural components and systems to

resist blast or other terrorist loads. For seismic-resistant design, such protocols exist and are widely accepted. For example, Appendix S of the *AISC Seismic Provisions* provides detailed test requirements and loading histories to demonstrate a specific connection detail meets the requirements to be used in a Special Moment Frame or Intermediate Moment Frame system. ACI also has testing protocols to ensure structural systems or connection details meet the required strength and ductility demands of a given application. Most often, these testing methods are used to demonstrate adequate performance of new systems or connections that have not been previously tested. Likewise, for blast-resistant design, a uniform testing protocol is recommended to ensure current and new structural systems satisfy design requirements.

Finally, very little is known about the residual capacity of blast-damaged bridge components. With the exception of tests completed at ERDC in support of an experimental program carried out by researchers from the University of Connecticut [159], past testing of blast-loaded bridge components has not evaluated residual capacity. As such, the system-wide implications of blast damage are not well understood. For example, if a reinforced concrete cable-stayed bridge tower suffers damage (localized spall, breach, etc.), it is unclear how the entire bridge will behave and whether or not the bridge will be able to carry dead and live loads. If the design objective for extreme blast loads is “Collapse Prevention”, much research is needed to understand how blast damage to one or more critical components affects overall resiliency of a bridge. A fundamental question is whether or not survivors will be able to safely exit a bridge or whether emergency response personnel can access a bridge to help survivors. If a bridge does survive, it then becomes necessary to assess damage and the ability to repair such damage. All of these aspects of bridge security require much attention, and future research should be dedicated to addressing these concerns.

The focus of this section was on giving broad recommendations on future research needs related to protective design of blast-loaded bridges. The recommendations given were not specific to a certain bridge structural system or material type. If specific guidance at this level is of interest, readers are encouraged to consult the references given at the end of this manual. Most of the reports and papers cited in earlier chapters include detailed recommendations for improving performance of specific blast-loaded bridge components. The main point of this section was to emphasize that the field of bridge security is relatively new, especially in comparison to the design of bridges to resist earthquakes. As such, much research is needed to fully understand how blast-loaded bridges behave when subjected to different threat scenarios.

11.5 Chapter Summary

This chapter provided an overview of the protective design of bridge components not explicitly addressed in previous chapters. When available, research results were provided to demonstrate the primary failure modes that should be considered. The chapter also described future research needs, making the case that much time and effort is required to mature the field of protective-design of bridges to a level similar to that of seismic-design of bridges. In the next chapter, the ATP-Bridge software is presented. Although prior chapters used this software to analyze specific examples, the next chapter provides detailed background information on how the software works and the assumptions implicit within each of the analysis algorithms.

12.0 ANTI-TERRORIST PLANNER FOR BRIDGES (ATP-BRIDGE) SOFTWARE

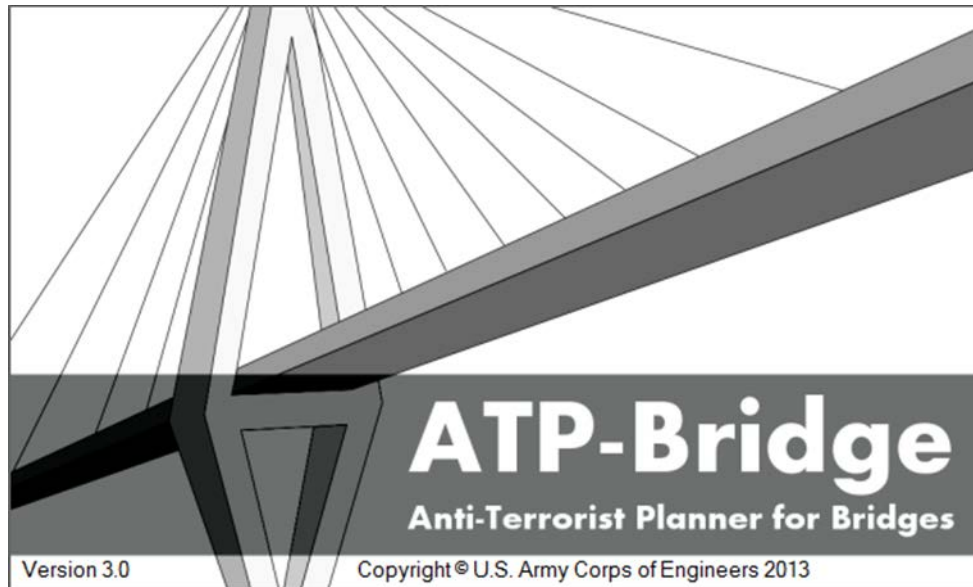


Figure 12.1 ATP-Bridge Software

While international terrorist organizations have been active across the globe for decades, attacks against public surface transportation infrastructure have been a growing concern. As a result, considerable research has been carried out in the area of bridge security over the past decade. Important advancements have been made in the areas of vulnerability assessment and risk-based prioritization methods, component-level blast load characterization, dynamic response analysis procedures, and blast threat mitigation techniques. Although much research is still needed, it is important to begin transferring these state-of-the-art protective design concepts and methodologies to the appropriate users within the bridge community. As such, an essential next step in enhancing the security of public highway bridges is to synthesize this newly developed protective design technology into an expedient and user-friendly engineering tool capable of facilitating effective anti-terrorist/force protection (ATFP) retrofits of current bridges, safe designs of new bridges, as well as emergency planning efforts. Such a tool would enable practicing bridge engineers to implement essential blast-resistant analysis and design strategies without having to rely on time-consuming, costly, and complex resources such as physical testing or high-fidelity computational modeling. Anti-Terrorist Planner for Bridges (ATP-Bridge) has been developed to specifically address these highway infrastructure security issues and, more generally, to help facilitate the implementation of research findings into current practice.

ATP-Bridge, shown in Figure 12.1, is a practical engineering-level software program capable of predicting the response and incurred damage of critical bridge components subjected to a variety of threat scenarios. ATP-Bridge features flexible software architecture designed to be continuously informed and updated with state-of-the-art research and intuitive, user-friendly functionality that aligns with practice. The software relies on fast-running computational algorithms that have been verified and validated against available experimental data. ATP-Bridge is intended to be utilized primarily by bridge engineers and vulnerability assessment personnel, but it can also be used by emergency responders and law enforcement professionals to

help quantify the likelihood of a major transportation disruption as a result of a postulated malicious attack. This information can then be used to support emergency planning decisions such as critical resource allocation.

12.1 Software Overview

ATP-Bridge is an interactive, menu-driven software program designed to operate efficiently on a Personal Computer (PC). In developing the overall program architecture, emphasis was placed on ensuring user-friendliness and computational expedience without compromising the fidelity of analysis results. In the context of ATP-Bridge, computational expedience refers to single-component analysis times on the order of seconds to minutes while operating on a standard PC having factory hardware. The graphical user interface (GUI) was designed to accommodate a global system approach to information handling. In ATP-Bridge, a “project” is associated with an entire bridge structure. Within a given project, users may define and evaluate multiple bridge components. In addition, multiple threat scenarios may be defined for each bridge component. This organizational scheme was adopted to allow for rapid assessment/comparison of multiple bridge components. ATP-Bridge’s project organization scheme is illustrated in Figure 12.2. A lucid description of the software architecture is given by Bui [160].

The current version of ATP-Bridge (Version 3) encompasses component response models for reinforced concrete (RC) bridge columns, steel suspension bridge tower panels, RC bridge tower panels, and high-strength steel cables. With regard to threat scenarios, the software is capable of considering contact and near-contact high-explosive charges, standoff detonations from bulk high-explosive threats, and various thermal, mechanical, and explosive cutting threats.

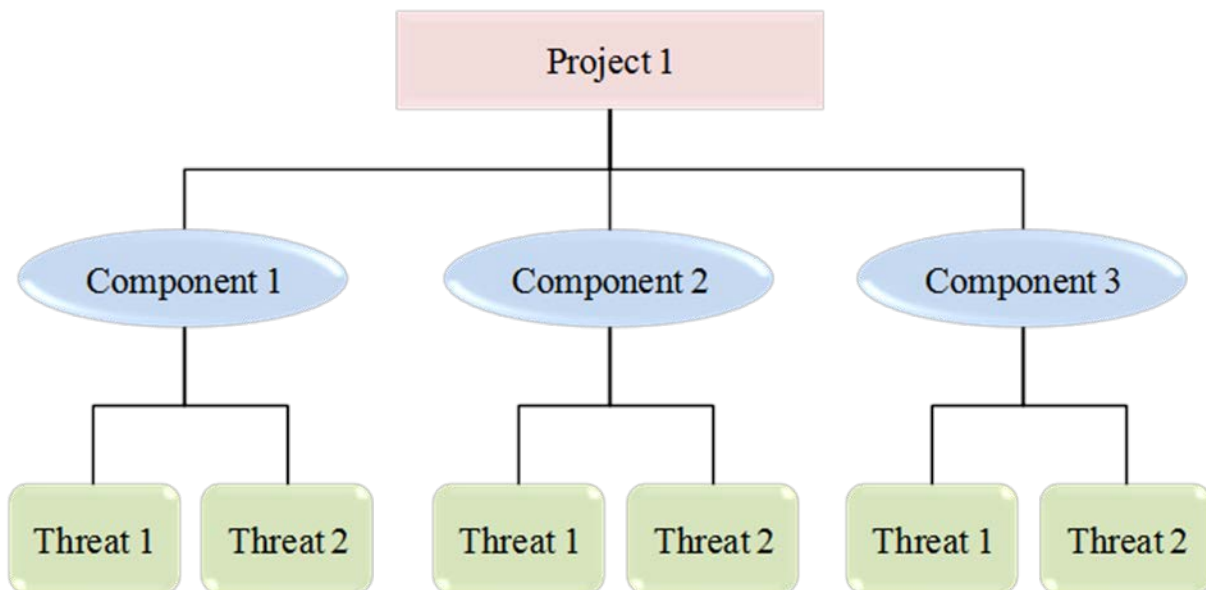


Figure 12.2 Schematic of ATP-Bridge Project Organization

12.2 Software Operation

The ATP-Bridge software was designed to operate efficiently and with an intuitive feel with respect to the typical design process and terminology of a bridge engineer. The software features an interactive help utility that provides a detailed description of all software functionality. From the ATP-Bridge main form, the help utility can be accessed through the Options → Help drop-down selection. The main form page of the ATP-Bridge help utility is illustrated in Figure 12.3. New ATP-Bridge users are encouraged to review the help utility in detail prior to using the software.

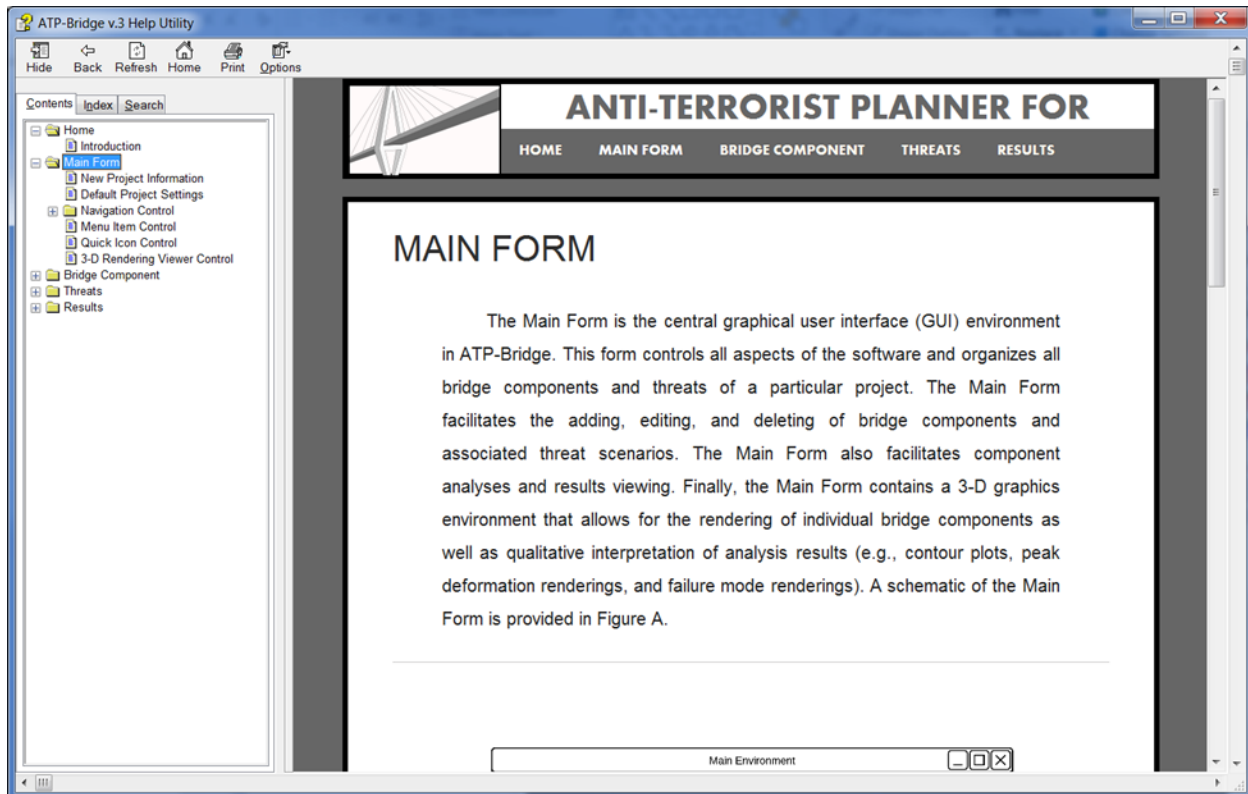
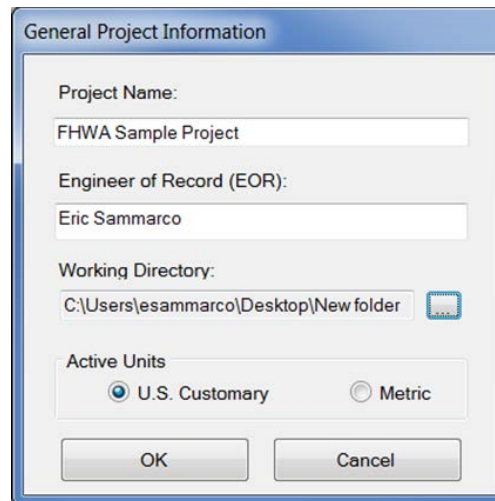


Figure 12.3 ATP-Bridge Interactive Help Utility

As a brief example and supplement to the ATP-Bridge help utility, the remainder of this section steps through the process of evaluating a hypothetical scenario wherein an RC bridge column is subjected to a bulk explosive threat. After launching ATP-Bridge, the first step is to create a new project by either clicking the “new project” quick button or selecting “new project” from the File → New Project drop-down menu. A General Information form appears, as shown in Figure 12.4. The General Information form is where a user can input project-specific information such as project name, engineer of record, and the desired units system. The General Information form is also where a user specifies a working directory to which analysis results are written and the ATP-Bridge project file is saved. Once the General Information form is filled out and the “OK” button is clicked, the ATP-Bridge Main form appears as shown in Figure 12.5. The tree view control is located on the left side of the Main form, and this control is where bridge components and associated threat scenarios are organized for a particular project and accessed. The three-dimensional (3-D) graphics window and associated quick buttons are located on the right side of the Main form. The 3-D graphics window is interactive and allows for qualitative, visual

representations of component-specific analysis results. Most of the program's functionality is controlled by the drop-down menus and quick buttons located across the top of the Main form. In reviewing from left to right the drop-down menu titles, the intuitive general flow of ATP-Bridge can be realized: bridge component definition, threat definition, dynamic response analysis, and presentation of analysis results.



The 'General Project Information' dialog box contains the following fields and controls:

- Project Name:** FHWA Sample Project
- Engineer of Record (EOR):** Eric Sammarco
- Working Directory:** C:\Users\esammarco\Desktop\New folder (with a folder icon button)
- Active Units:** U.S. Customary (selected), Metric
- Buttons:** OK, Cancel

Figure 12.4 ATP-Bridge General Project Information Form

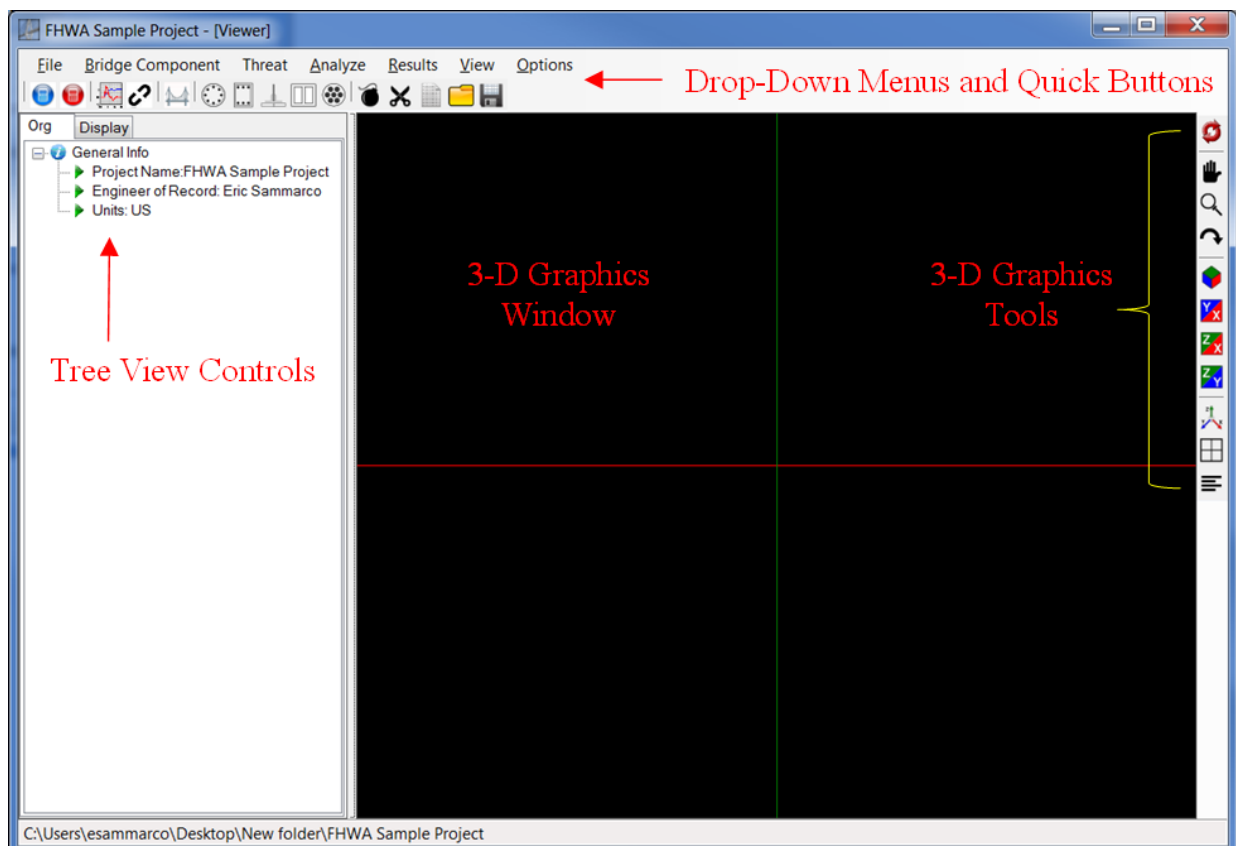


Figure 12.5 ATP-Bridge Main Form

From the top of the Main form, a circular RC bridge column component is defined by first selecting such a component from the “Bridge Component” drop-down menu or associated quick button. Once selected, the circular RC column Component Definition form appears as shown in Figure 12.6. From the Component Definition form, a user navigates the input tabs to define the column name, column and steel reinforcing geometry, support conditions, and material properties. The “Advanced” tab shown in Figure 12.6 deals with concrete spill limits and is described (use and implications) in more detail in the ATP-Bridge help utility. Also, as denoted in Figure 12.6, the RC column component can be viewed in section or elevation from within the Component Definition form. The left and right images of Figure 12.6 illustrate the section and elevation views, respectively. Once all required component information is entered into the Component Definition form, the “OK” button is clicked and the Main Form re-appears with the new bridge component shown in the left-pane tree view control (see Figure 12.5 for tree view control).

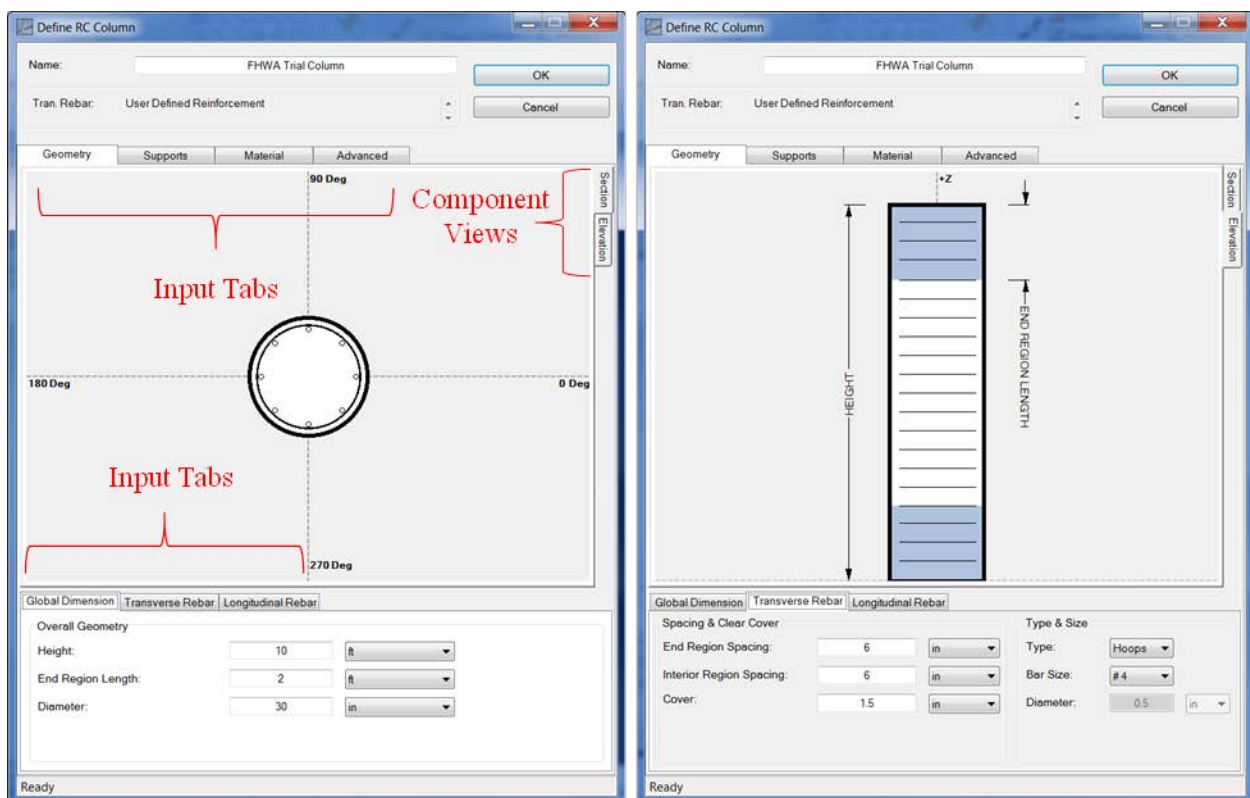


Figure 12.6 Example ATP-Bridge Component Definition Form for a Reinforced Concrete Bridge Column

The next step in the RC column evaluation process is to define the bulk explosive threat scenario. This is done by first initiating a new threat scenario by selecting Threat → New Explosive Threat from the drop-down menu or associated quick button at the top of the Main form. Once done, the New Threat Definition Association form appears as shown in Figure 12.7. The purpose of this form is to associate the new threat scenario with a specific bridge component that has already been defined for the project. In this case, a new explosive threat scenario is to be defined for the previously created circular RC bridge column named “FHWA Trial Column.”

After identifying the appropriate bridge component and clicking “Select,” the Threat Definition form appears as shown in Figure 12.8.

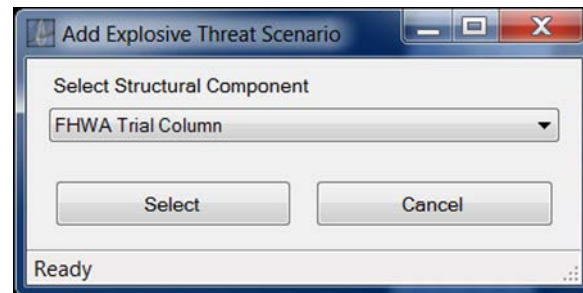


Figure 12.7 New Threat Scenario Association Form

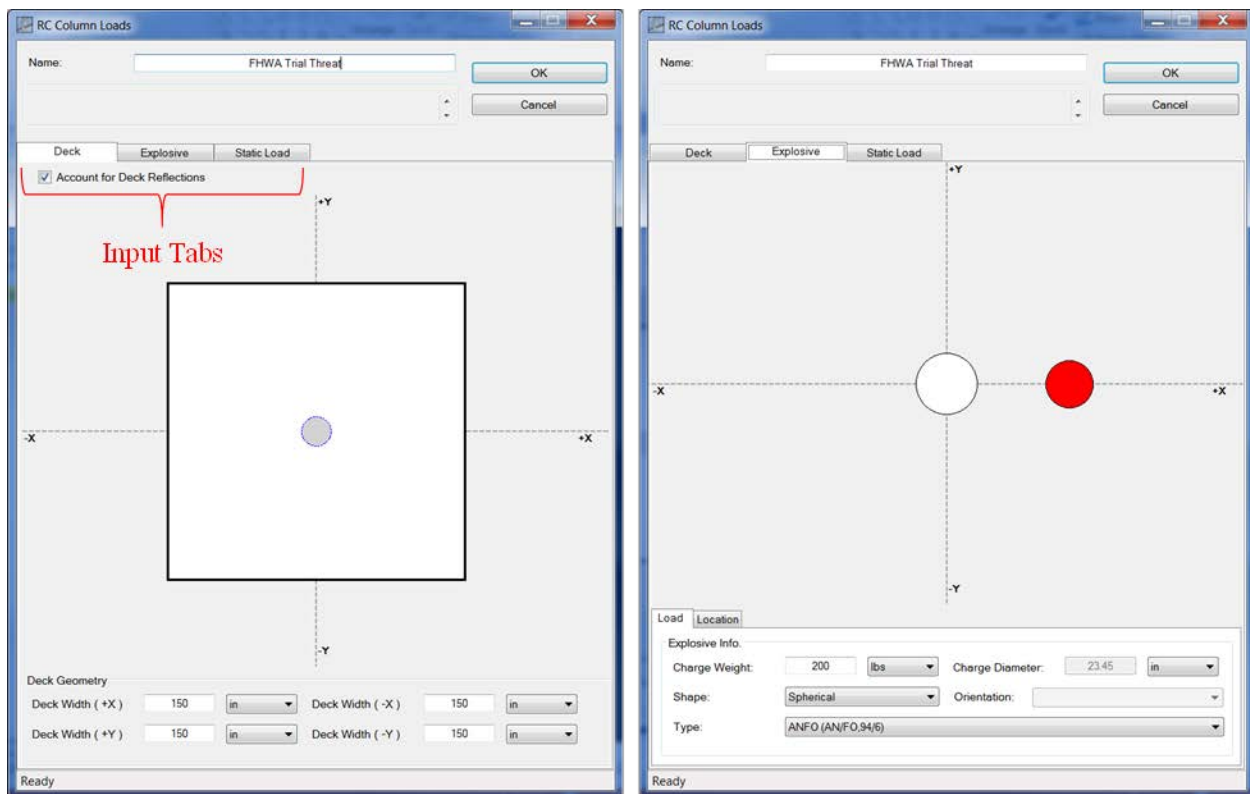


Figure 12.8 Example ATP-Bridge Threat Definition Form for a Reinforced Concrete Bridge Column

From the Threat Definition form, the input tabs are navigated to input various threat-specific information such as bridge deck geometry—important for blast load calculations; a straddle bent column, for instance, may not have a bridge deck directly above it—explosive composition, charge weight, charge shape, charge location, and any static axial loads acting on the RC bridge column. Once all required threat information is entered into the Threat Definition form, the “OK” button is clicked and the Main Form re-appears, as shown in Figure 12.9. The new threat shows up in the left-pane tree view control on the Main form under the associated bridge component and with an open lock icon indicating that it has not been analyzed yet. Note in Figure 12.9 that the defined RC bridge column is displayed in the 3-D graphics window.

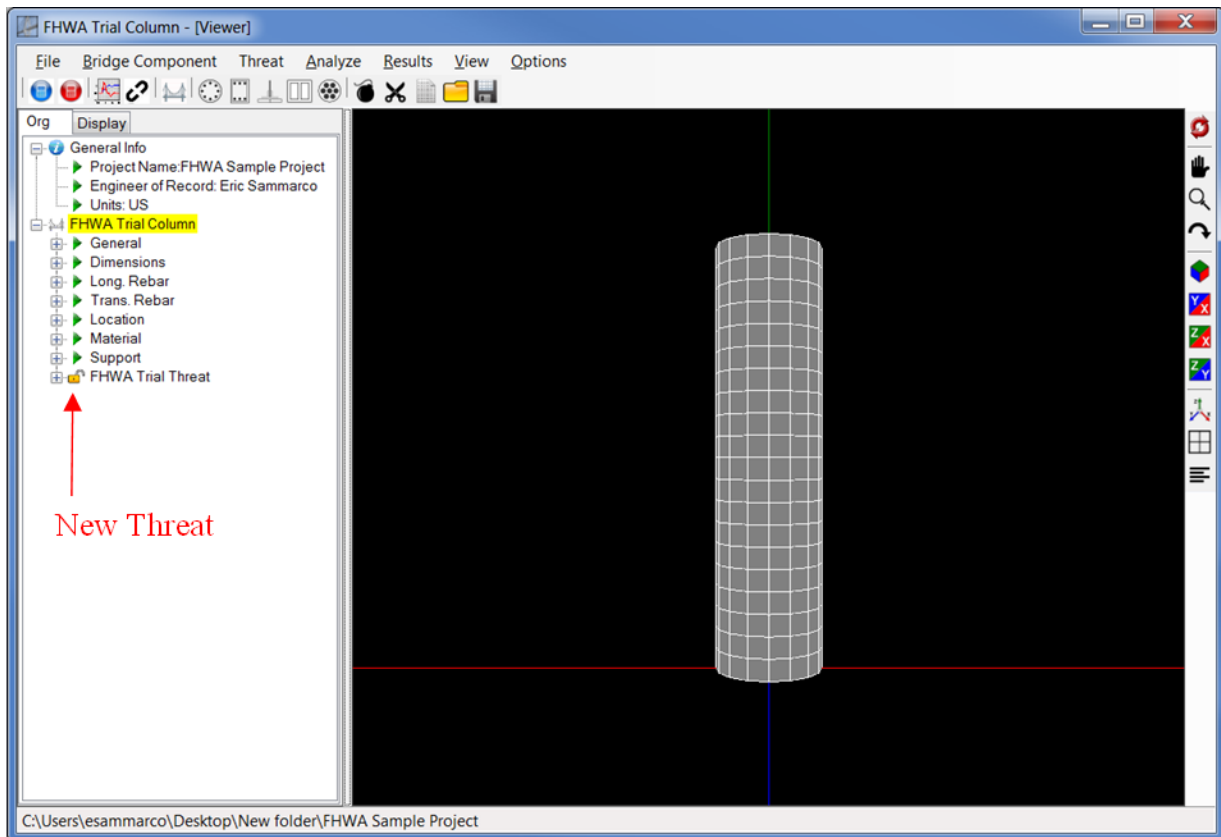


Figure 12.9 ATP-Bridge Main Form with One Bridge Component and One New Threat Scenario that Has Not Been Analyzed

The next step in the evaluation process is to conduct a response analysis for the defined RC bridge column and bulk explosive threat. This is done by first selecting Analyze → Component in the drop-down menu or clicking the associated quick button on the top of the Main form. Once done, the Analysis form will appear as shown in Figure 12.10. The Analysis form indicates which bridge component is being analyzed, and it also contains an analysis log that can be reviewed once the response analysis is complete (a log file is also saved in the specified working directory). The response analysis is initiated by clicking the “Run Threats” button on the Analysis form.

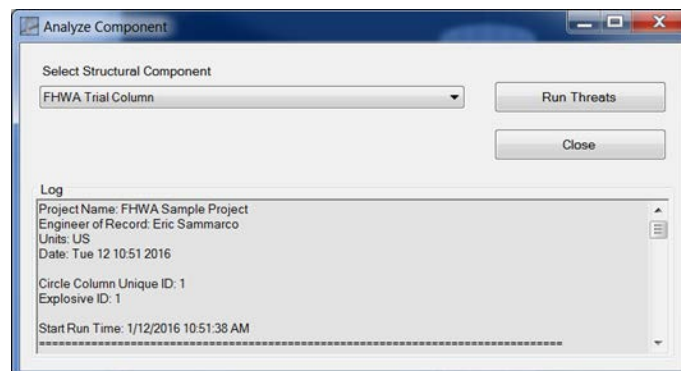


Figure 12.10 ATP-Bridge Component Analysis Form

Once the analysis is complete, the Analysis form is closed by clicking “Close” and the Main form re-appears. In the left-pane tree view control of the Main form, the lock icon next to the analyzed threat will be in the closed position indicating that the threat has been analyzed, as shown in Figure 12.11. Two options exist for reviewing RC column component analysis results: quantitative review via the Results form or qualitative review via the 3-D graphics window.

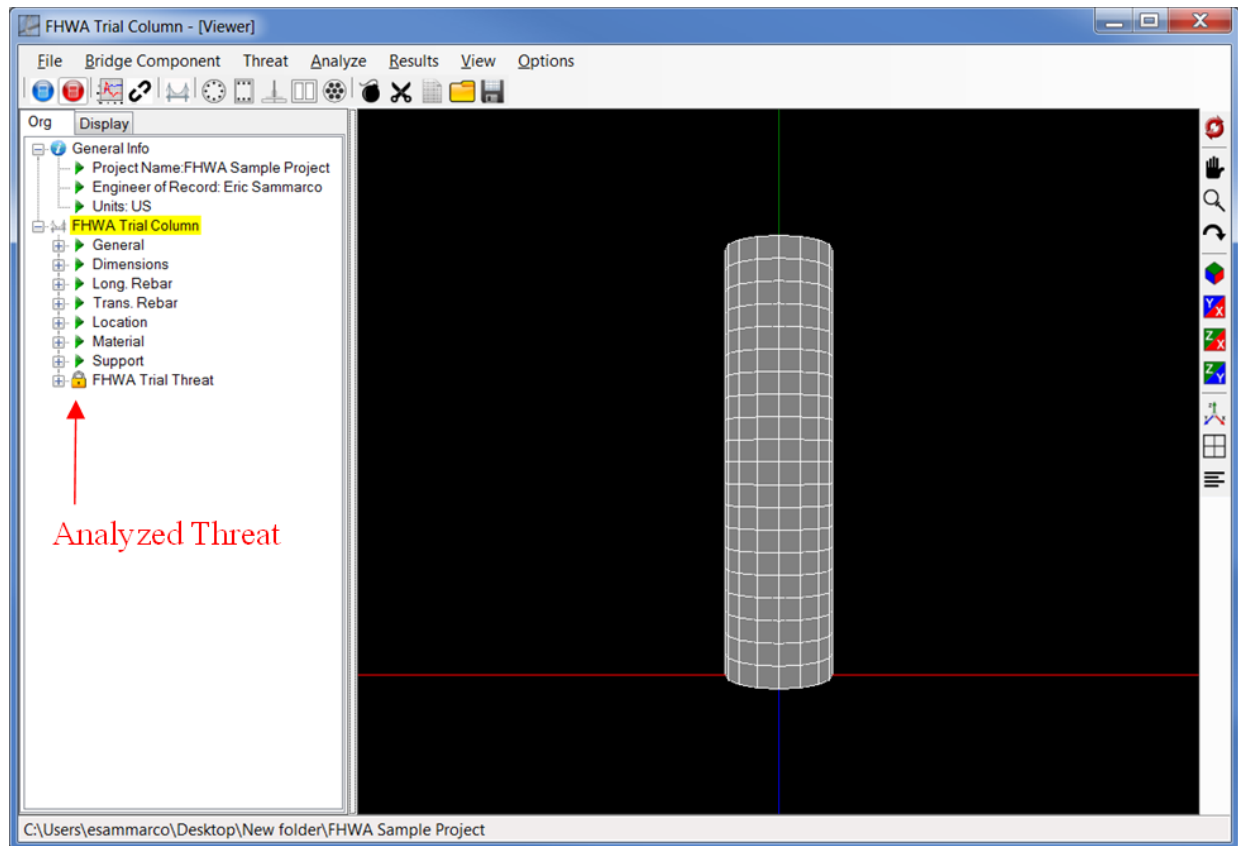


Figure 12.11 ATP-Bridge Main Form with One Bridge Component and One Threat Scenario that Has Been Analyzed

Quantitative results can be accessed by selecting Results → View Explosive Threat Results from the Main form drop-down menu or by clicking the associated quick button on the top of the Main form. The Results form for an RC bridge column is shown in Figure 12.12. As is denoted by the results tabs in the left image of Figure 12.12, RC column analysis results are categorized in early-time local damage (i.e., concrete spall and breach damage), component-level dynamic shear response, and component-level flexural response. For each category of results, summary information is presented in the “Summary” rich text box and various results figures and/or history plots can also be accessed via the drop-down menu in the middle of the Results form. All response history plots that are generated during an analysis are also written to the specified working directory as (*.csv) files. For example, the left image of Figure 12.12 shows that the hypothetical circular RC bridge column suffered no local spall or breach damage, and the right image of Figure 12.12 shows a flexural hysteresis plot of the RC bridge column indicating that the diagonal tension (i.e., traditional beam shear) capacity of the component was exceeded during the response analysis. This result reveals that the hypothetical RC bridge column was not designed for the shear associated with the formation of its dynamic flexural capacity.

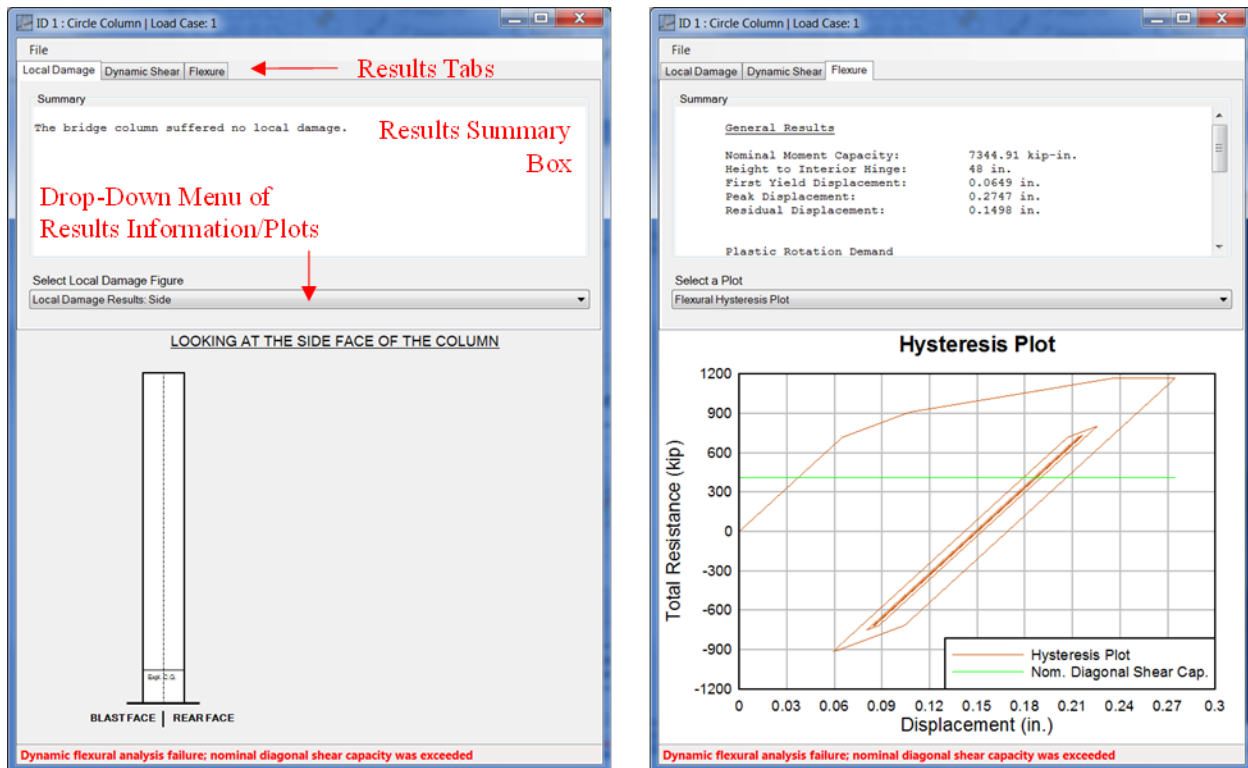


Figure 12.12 Example ATP-Bridge Results Form for RC Bridge Column

Qualitative results can be accessed by toggling the Main form tree view control tab to “Display,” as shown in Figure 12.13. By toggling to the “Display” tab, the left pane of the Main form transforms to a collection of 3-D graphics display options that are consistent with the response analysis results of the selected bridge component (an RC bridge column in this particular case). In general, whichever bridge component is highlighted in the Main form tree view control prior to toggling the tree view control tab to “Display” will be represented in the 3-D graphics window for qualitative results processing. As can be seen from Figure 12.13, RC column local damage, peak flexural response, and peak dynamic shear response results can all be visualized in the 3-D graphics window. In addition, a user can toggle the explosive charge on or off, increase the response scale factor, and toggle various graphics colors from the left pane of the Main form. The 3-D graphics quick buttons, located along the right edge of the Main form, can also be used to modify the view within the 3-D graphics window.

This concludes the example evaluation of a circular RC bridge column subjected to a bulk explosive threat. A detailed explanation of all ATP-Bridge functionality can be found in the ATP-Bridge help utility, which can be accessed by selecting Options → Help from the Main form drop-down menu.

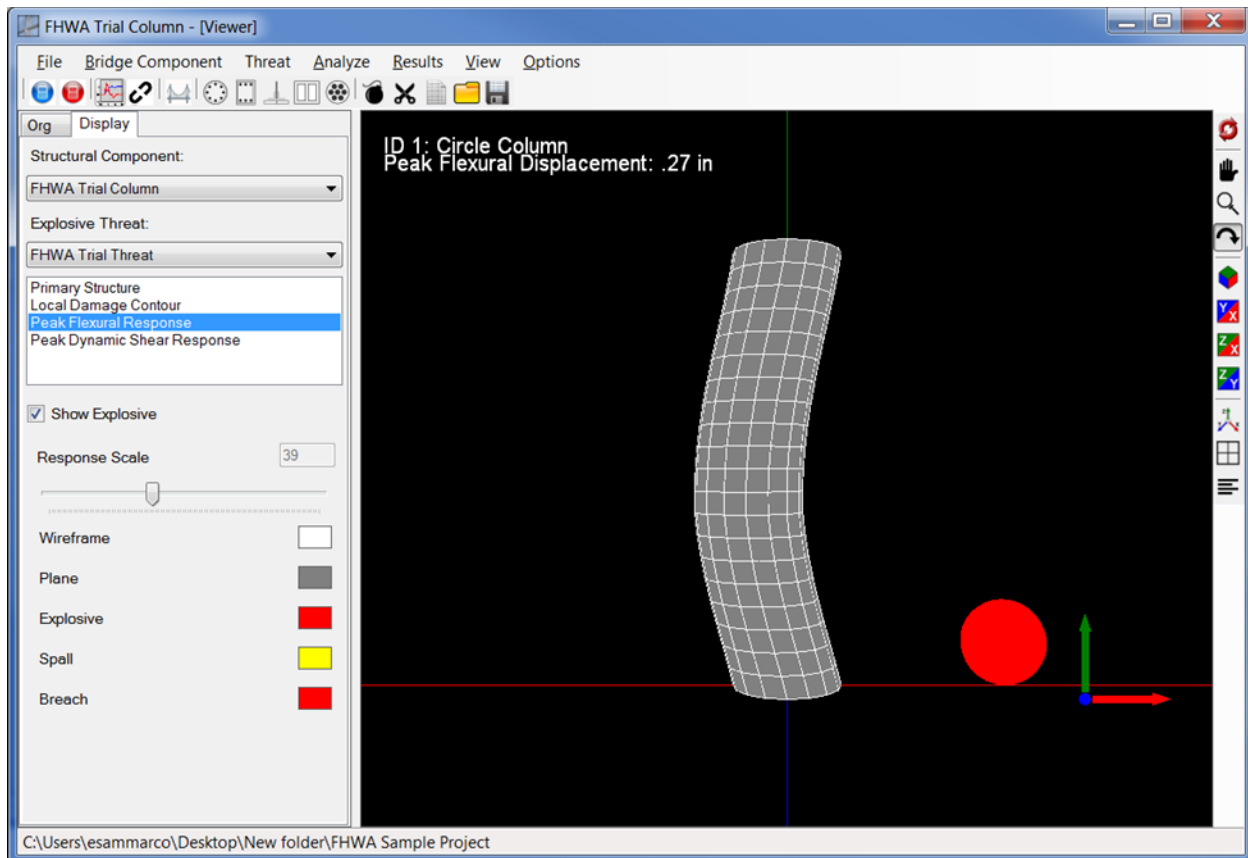


Figure 12.13 ATP-Bridge Main Form Showing RC Column Peak Flexural Response in 3-D Graphics Window

12.3 Overview of Analysis Methodology

A chief objective of the ATP-Bridge software is to provide rapid component-level dynamic response and damage prediction capabilities to allow a user to quickly ascertain the vulnerability of critical bridge components to postulated terrorist attack scenarios. ATP-Bridge is not intended to replace high-fidelity computational modeling tools, but rather to provide an easy-to-use engineering tool that is fast-running yet maintains sufficient assessment- and design-level fidelity. Thus, the ATP-Bridge blast load drivers and component-specific response/damage algorithms have been formulated from classical structural mechanics theory and/or vetted empirical data, distilled down to optimize computational speed and focus solely on governing component-level modes of response and damage mechanisms, and validated against available experimental data.

In general, the ATP-Bridge analysis process is essentially identical for all bridge components. Given a threat scenario, loads are first calculated for a specific bridge component. Once the transient blast loads are characterized for a given threat scenario, the dynamic response is computed for a specific bridge component. While the actual formulation of each response model is highly component-specific, they all incorporate computational algorithms that differentiate between local and global response. Local response is characterized by early-time material behavior that occurs prior to the time at which the entire component is set in motion, and it is

chiefly driven by the effects of the impinging shock wave as it propagates through the component material and interacts with the component section's bounding surfaces. Depending on the component material, local damage may be associated with spall, cratering, tearing, and/or complete section breach. It is this type of behavior and potential damage that the local response analyses aim to capture. Conversely, global response refers to dynamic modes of response that engage the entire component and depend on characteristics such as boundary conditions, stiffness, mass, and blast pulse duration. Failure criteria for global response modes are typically associated with peak plastic deformations; thus, the global response analyses focus on the prediction of critical kinematic response parameters.

The following subsections provide additional detail and references for the ATP-Bridge blast load drivers and all component-specific dynamic response algorithms. These subsections are not intended to be a rigorous methodology manual, but rather an overview containing sufficient information to intelligently operate the ATP-Bridge software. Interested readers are encouraged to review the provided references for more lucid descriptions of the ATP-Bridge computational algorithms.

12.3.1 Blast Load Computation

The ATP-Bridge software makes use of two different approaches for characterizing blast loads on bridge components. The first approach is consistent with the current state-of-the-practice [50], and it utilizes empirical relationships derived from idealized spherical and hemispherical high-explosive detonation scenarios to determine peak reflected pressures and specific impulses delivered to a target of interest—often referred to as the Kingery-Bulmash (KB) equations [79]. The second approach is more rigorous than the former, and it utilizes a modified version of the BlastX software [82]. BlastX is a fast-running, engineering-level code that combines an extensive collection of synthetically generated free-air explosive source models [81] with a physics-based ray tracing algorithm to yield a versatile blast load characterization tool capable of predicting both shock and gas environments resulting from internal or external detonations. BlastX can account for the presence of multiple reflecting surfaces as well as the influence of charge shape and spatial/temporal variation in reflected pressure on the resulting blast load. BlastX also includes shock clearing and diffraction models to account for the behavior of shock waves in the vicinity of complex, finite target geometries.

In postulating likely high-explosive attack scenarios to include in the ATP-Bridge software, attention was paid to past bridge attacks, both successful and thwarted. These past events suggest near-field, above-deck and below-deck threats comprising a wide range of explosive compositions and non-spherical charge shapes. While the KB equations have found much practical use for situations involving far-field detonations and planar target surfaces, their limits of applicability render them marginally useful in ATP-Bridge. The KB equations work well for far-field detonations, where the charge can be taken as a point source that generates a spherical or hemispherical shock front. However, as the physical standoff between the charge and a target of interest decreases, charge shape becomes important (it dictates the initial shock front geometry). The KB equations are not capable of predicting near-field blast loads from non-spherical charges. Moreover, recent research [81, 161] has shown that, for close-in detonations, the KB equations do not adequately predict the extremely high pressures and associated impulses generated near the charge surface. This research also showed that using the KB equations with

constant TNT equivalency factors to predict blast loads from close-in charges of non-TNT explosive compositions does not work well. The free-air explosive source models of BlastX include non-spherical charges, non-TNT explosive compositions, and have been shown to predict the intense airblast environment near the charge surface with reasonable accuracy [82, 81]. Accordingly, ATP-Bridge predominately uses the modified version of the BlastX code to characterize blast loads on bridge components. The KB equations are only used with the empirically-based local damage models for the RC bridge columns and RC cable-stayed bridge tower panels because they were originally calibrated using such a load characterization approach.

12.3.2 Dynamic Response Algorithm for Reinforced Concrete Columns

Predicting the dynamic response of a blast-loaded RC bridge column is challenging. The column's relatively slender, bounded geometry gives rise to a number of behavioral complexities—both with regard to shock wave behavior in the vicinity of the column and early-time, local material behavior—that generally do not exist for the familiar case of a planar-type target such as the exterior surface of a building structure. In addition, the airblast environment from a below-deck bulk explosive detonation—perhaps the most likely threat scenario for an RC bridge column—requires the consideration of multiple reflecting surfaces and the potential for spatial and temporal variations in the reflected pressures during blast load characterization. All of these specific issues were thoroughly addressed in the formulation of the component response model.

The computational algorithm for the local response analysis extends an empirically-based one-dimensional (1-D) wave propagation methodology developed for the prediction of local spall/breach damage of blast-loaded RC panels [85] to account for two-dimensional effects associated with the finite dimensions of a column's cross-section relative to its height. Empirical data from the 1-D spall/breach research were integrated with synthetic data generated from an extensive parametric study using computational fluid dynamics simulations to derive back- and side-face spall and breach threshold curves for blast-loaded RC columns. Given the total applied impulse from a bulk explosive threat, along with various column section parameters, ATP-Bridge can utilize the local damage threshold curves to predict back- and side-face spall/breach damage.

The computational algorithm for the global response analysis employs an enhanced single-degree-of-freedom (SDOF) approach that considers flexural and dynamic shear modes of response. Due to the notably different dynamic characteristics of the two global response modes, it was deemed appropriate to treat them in an uncoupled manner. The flexural response portion of the model is purely mechanics-based. It includes strain-rate-dependent material properties and accounts for material and geometric nonlinearities in predicting peak component displacements and rotations. The dynamic shear portion of the model also includes strain-rate-dependent material properties, and it combines a modified version of an empirical direct shear model [162] with a semi-empirical shear slip distribution model to predict discrete slip and distributed shear behavior. This modeling approach attempts to capture the influence of early-time material damage on the dynamic shear behavior of blast-loaded RC columns. Peak kinematic responses calculated from the flexural and dynamic shear global response analyses can then be compared with project-specific response limits to determine whether component failure occurs.

A detailed presentation of the RC bridge column dynamic response algorithm development and validation is provided by Sammarco [18], and additional details of the RC bridge column local damage algorithm are provided by Puryear et al. [163].

12.3.3 Dynamic Response Algorithm for Steel Cellular Tower Panels

Steel suspension bridge towers are cellular structures consisting of a matrix of interconnected, built-up steel boxes. Cells are typically constructed by fastening plate steel to structural steel angles using either rivets or high-strength steel bolts. The cellular nature of these towers presents many challenges from a blast-resistant analysis/design perspective. For instance, if an exterior cell wall experiences local breach damage or a global tensile rupture failure, the secondary debris will likely be accelerated into interior cell walls at potentially damaging speeds. In addition, the exterior hole may allow for overpressures to infiltrate the tower and load interior surfaces. While such complexities are certainly of concern and should be addressed, the current version of ATP-Bridge focuses primarily on predicting the response of an exterior cell wall to a postulated terrorist threat.

The computational algorithm for the local response analysis utilizes an energy balance concept to predict whether a bulk explosive threat produces an early-time breach hole in the exterior cell wall. In general, a breach occurs if the externally applied energy from the explosive charge exceeds the critical failure energy of the incident steel plate [122]. In determining the critical failure energy, a critical plate velocity is derived based on the assumptions of a rigid-perfectly-plastic system and simultaneous transverse shear failure around the assumed failure diameter. The computational algorithm iterates on failure diameter until the extents of the cell wall are reached. The presence of transverse stiffener plates and their effect on the critical failure energy is considered during the analysis.

The computational algorithm for the global response analysis utilizes a set of empirically derived expressions to characterize the anticipated range of global responses a steel plate component may exhibit when subjected to a bulk explosive threat. The expressions consider elastic flexural response, plastic flexural response, tension membrane response, partial tensile rupture, and global failure by tensile rupture. Synthetic data resulting from an extensive computational parametric study were used to formulate the empirical expressions. Upon completion of a steel tower panel response analysis, ATP-Bridge reports the predicted global response mode, critical kinematic response parameters, and whether local and/or global failure occurs. In addition, ATP-Bridge allows for the generation of an iso-damage plot that may be consulted to quickly relate any combination of explosive charge weight and physical standoff for a given steel plate configuration and explosive material to the considered damage thresholds; namely, local breach damage, the onset of boundary tearing, and global tensile rupture failure.

A detailed presentation of the steel cellular tower panel local damage algorithm is provided by Puryear et al. [163].

12.3.4 Dynamic Response Algorithm for Reinforced Concrete Tower Panels

RC cable-stayed bridge tower panels, while seemingly similar to typical RC walls and slabs, possess unique characteristics that must be considered during the response analysis. The deck of a cable-stayed bridge is supported by inclined stay cables that are anchored to the bridge tower

and deck. The stay cables deliver a vertical force component to the bridge tower, which, in turn, induces an axial compressive stress in the tower panels. To carry this service-level axial stress, the tower panels are typically designed to have an orthotropic steel reinforcement layout, where the larger bars are oriented in the vertical direction. The effects of service-level axial compressive stress and orthotropic rebar configurations on the response of blast-loaded RC tower panels are captured in the local and global analysis models.

As with the RC bridge column component, the focus of the local response analysis for blast-loaded RC cable-stayed bridge tower panels is to predict whether early-time spall and/or breach occurs. The development of the local damage model modifies an empirically-based 1-D wave propagation methodology developed for the prediction of local spall/breach of blast-loaded RC panels [85] to account for the effects of axial pre-compression and orthotropic rebar configurations. Modifications were devised based on synthetic data generated from high-fidelity Arbitrary Lagrangian-Eulerian (ALE) computational simulations. The axial pre-compression was found to reduce material damage in the in-plane dimension parallel to the applied axial load for relatively small applied impulses and associated strain rates. However, as the severity of the threat scenario is increased, the material's inherent resistance to the induced motion—often referred to as inertial resistance—dominates the response, rendering the axial pre-compression essentially negligible. It was also found that the amount of concrete damage remains essentially independent of the reinforcement configuration. The amount of concrete that flows out of the core, however, and thus the residual capacity of the component, does depend on the amount and configuration of reinforcement. The current version of ATP-Bridge does not explicitly address residual capacity, but the ability to do so is certainly of interest for future research and software enhancement.

The development of a global response model for blast-loaded RC cable-stayed bridge tower panels relies on an empirical method. Experimental blast test data involving isolated one-way and two-way RC panels were first used to validate an uncoupled modeling approach. The BlastX code was used to generate blast pressure histories at various locations on the incident face of an RC panel specimen. The blast pressure histories were then mapped to a Lagrangian finite element mesh of the RC panel specimen being analyzed, and a 3-D nonlinear dynamic analysis was conducted. The validated computational modeling approach was then employed in an extensive computational parametric study involving numerical models of full-scale RC bridge tower legs having various panel aspect ratios. Results from the parametric study [18] were then used to derive a fast-running empirical response prediction expression for use in ATP-Bridge.

A detailed presentation of the RC tower panel dynamic response algorithm development and validation is provided by Sammarco [18], and additional details of the RC tower panel local damage algorithm are provided by Puryear et al. [164].

12.3.5 Dynamic Response Algorithm for High-Strength Steel Cables

Main suspension/stay cables and secondary hanger/suspender cables play a major role in the gravity force resisting system of long-span bridges. The failure of one or more cable components could result in local or global instability of such bridges. Consequently, these components are considered to be likely targets for a malevolent bridge attack. For example, in May of 2003, a naturalized U.S. citizen living in Columbus, Ohio was arrested for conspiring to commit a terrorist act that involved using blow torches to sever the main suspension cables of an iconic

New York state highway bridge [11]. The current version of ATP-Bridge is capable of considering block and diamond-shaped contact charge threats as well as thermal, mechanical, and linear shaped charge threats.

The component response models for block and diamond charge threats were developed from synthetic data resulting from ALE computational simulations. Diamond-shaped contact charge simulations were first conducted, and the resulting empirical model was validated against test data from the U.S. Army Engineer Research and Development Center (ERDC) [31]. Once the numerical simulation approach was validated for diamond-shaped contact charges, a similar approach was employed for the development of an empirical response model for block-shaped contact charges.

The component response models for cable cutting threats are empirical in nature and are based on a relatively small experimental dataset. Thus, this topic lends itself well to future experimental research. The current version of ATP-Bridge is capable of considering thermal and mechanical cutting threats as well as linear shaped charge cutting threats. Given geometric and material information of a considered main stay/suspension cable or secondary hanger/suspender cable, the fast-running component response models predict an estimated time it would take to completely sever the target cable. For linear shaped charge threats, the minimum number of strands required to prevent a given cable component from being completely severed is also reported.

A detailed presentation of the bridge cable damage algorithm development and validation is provided by Barsotti et al. [165].

12.4 ATP-Bridge Design Examples

12.4.1 Reinforced Concrete Bridge Columns

The following design examples aim to illustrate the design process for reinforced concrete highway bridge columns subjected to blast loads. Each design example utilizes the ATP-Bridge software combined with the design guidance presented in Chapter 7. Standard column designs, boundary conditions, and material properties were selected for the design examples, based upon design examples found in NCHRP Technical Report 645 [24].

Design Example 1

The following design example considers the response of a reinforced concrete bridge column for a relatively large threat. Evaluate the column, designed for a non-seismic region, for the given close-in blast load. If the column is insufficient, redesign the column to meet all applicable design checks. Refer to Figure 12.14 for threat details and Figure 12.15 for column design details. Use ATP-Bridge to perform the analysis and design. Figure 12.16 provides a sample of the required column geometry inputs to setup the design example in ATP-Bridge. A sample of the required load inputs for ATP-Bridge is provided in Figure 12.17.

Note, the longitudinal rebar placement in Figure 12.16 was determined using the equal distribution option in ATP-Bridge, which evenly spaces the rebar around the circumference. The final longitudinal rebar location (Figure 12.15) is normally unknown, therefore design should

typically consider the worst case orientation (for smallest flexural capacity) with respect to the explosive location.

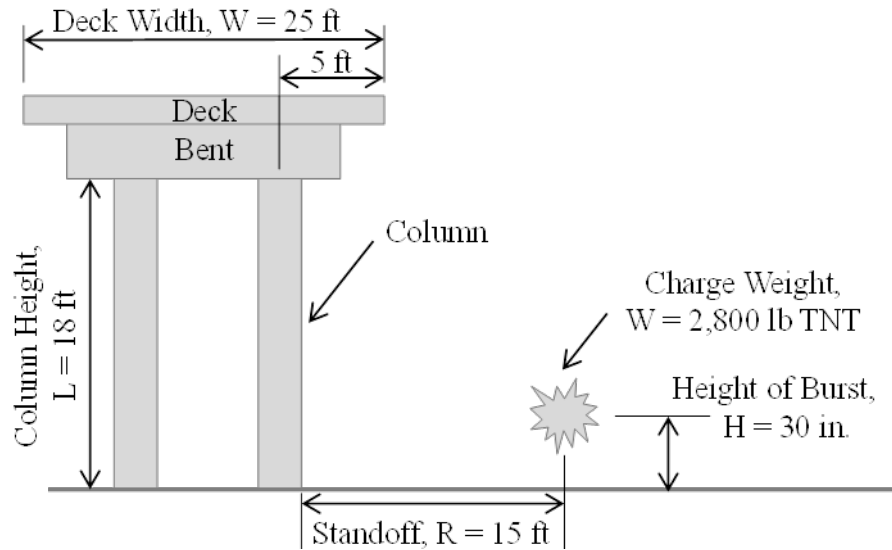


Figure 12.14 RC Column Design Example 1 Elevation

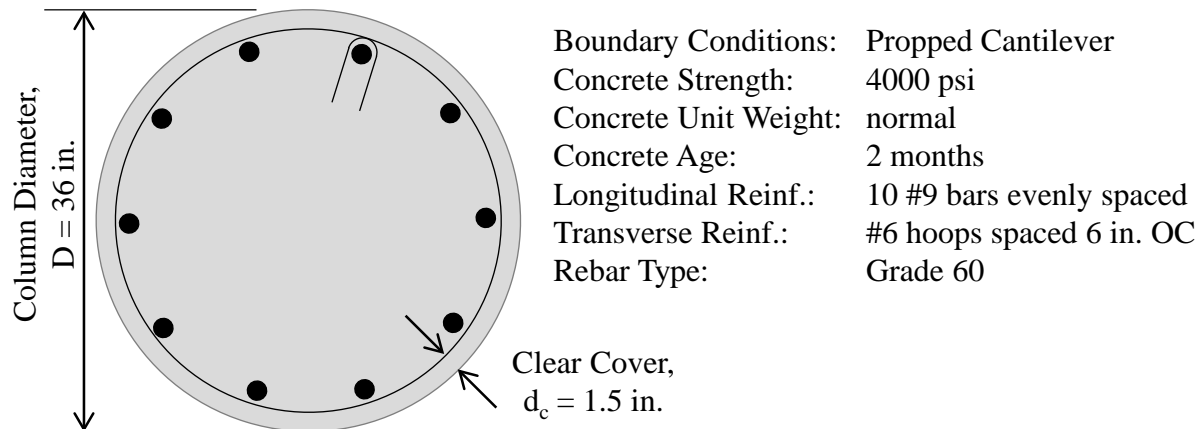


Figure 12.15 RC Column Design Example 1 Details

Geometry Supports Material Advanced

Section
Elevation

90 Deg

180 Deg

0 Deg

270 Deg

Global Dimension Transverse Rebar Longitudinal Rebar

Overall Geometry

Height: 18 ft

End Region Length: 2 ft

Diameter: 36 in

Global Dimension Transverse Rebar Longitudinal Rebar

Spacing & Clear Cover

End Region Spacing: 6 in

Interior Region Spacing: 6 in

Cover: 1.5 in

Type & Size

Type: Hoops

Bar Size: # 6

Diameter: 0.75 in

Figure 12.16 RC Column Design Example 1 Sample Column Geometry Input

The screenshot shows the 'Static Load' tab in the ATP-Bridge software. The top panel is a 2D coordinate system with a red circle (explosive charge) at (15, 0) and a white circle (column) at (0, 0). The bottom panel contains the following input fields:

Explosive Info.	
Charge Weight:	2800 lbs
Charge Diameter:	44.95 in
Shape:	Spherical
Orientation:	Vertical
Type:	TNT (density 1.63 g/cc based on 64 kg)

Distances	
Distance X:	15 ft
Distance Y:	0 in
Direction Z:	30 in

Deck Geometry	
Deck Width (+X)	60 in
Deck Width (-X)	240 in
Deck Width (+Y)	150 in
Deck Width (-Y)	150 in

Figure 12.17 RC Column Design Example 1 Sample Load Input

In response to the given threat of 2,800 lb of TNT at a 15-ft standoff distance, the 36-in. diameter column suffers a breach failure near the threat location (see Figure 12.18). The initial column design is insufficient for the given blast load due to local breaching failure, therefore the column must be redesigned. Several design variables can be adjusted including column diameter, concrete strength, concrete cover, transverse reinforcement, and longitudinal reinforcement. Span and boundary conditions are assumed to be constant. In the following section, each variable is adjusted to illustrate the positive and negative attributes of each possible solution.

Column diameter is evaluated first. Increasing the column diameter from 36 in. to 60 in. for a threat of 2,800 lb of TNT at a standoff distance of 15 ft eliminates breaching and spalling damage (see Figure 12.19). Because the local damage checks in ATP-Bridge are satisfied, dynamic shear and flexural response of the column are then checked. As shown in Figure 12.19, the peak displacement is 0.6 in. and the maximum support rotation is 0.89 degrees. NCHRP Technical Report 645 [24] recommends a plastic rotation limit of 1.0 degree, which is satisfied. Therefore, this portion of the design example illustrates the benefit of increasing the column diameter to prevent breach of a concrete bridge column subjected to blast loads.

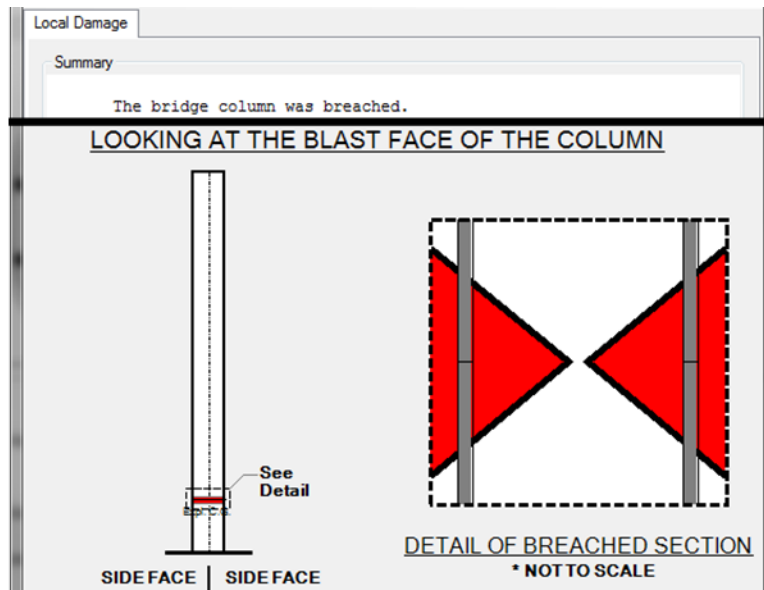


Figure 12.18 RC Column Design Example 1 Results for 36-in. Diameter Column

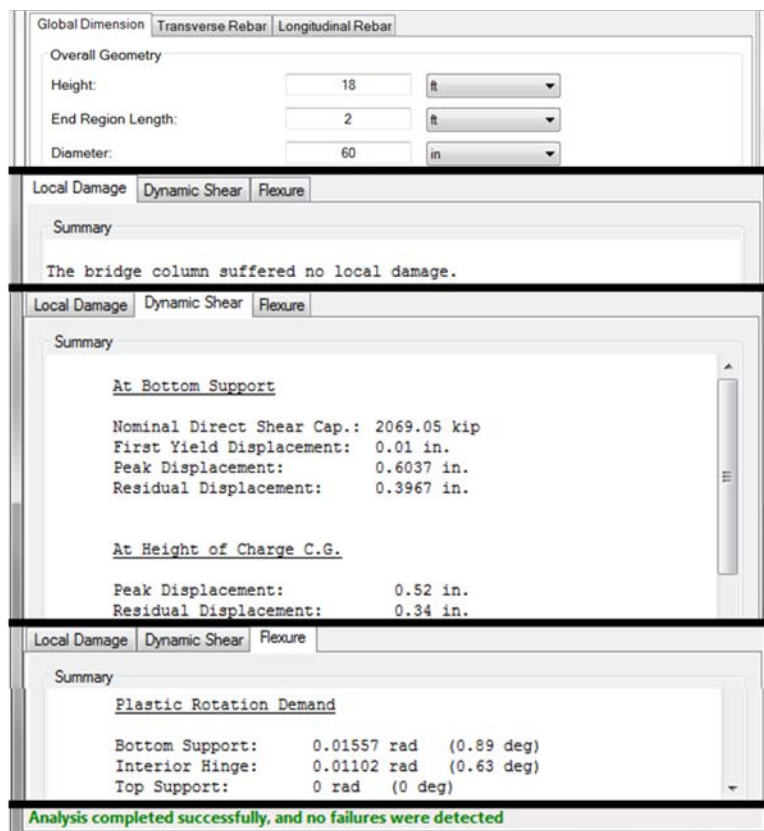


Figure 12.19 RC Column Design Example 1 Results for 60-in. Diameter Column

If the column diameter is reduced to 36 in. (consistent with the initial design), adjusting any other variable (concrete strength, concrete cover, transverse reinforcement, and longitudinal reinforcement) results in a breached column section. Therefore, the most influential variable in preventing a breach failure is column diameter; however, other factors can be optimized after column diameter is increased. Each of the following variables will be adjusted (one by one): concrete strength, thickness of concrete cover, amount and type of transverse reinforcement, and amount of longitudinal reinforcement. After the influence of each variable on column response is discussed, an optimized column design is presented.

Concrete strength is evaluated next. The 60-in. diameter column design assumed a concrete strength of 4,000 psi. Varying the concrete strength from 3,000 psi to 10,000 psi for a threat of 2,800 lb of TNT at a standoff distance of 15 ft changes the column response significantly. The 60-in. column design with a 3,000 psi concrete strength now fails the local damage checks in ATP-Bridge due to excessive concrete spall damage on the rear and side faces of the column (see Figure 12.20). Increasing the concrete strength to 6,000 psi eliminates spall damage of the 60-in. diameter column (see Figure 12.21a). Because the local damage checks in ATP-Bridge are satisfied, dynamic shear and flexural response of the column are then checked. As shown in Figure 12.21a, the peak displacement for the 6,000 psi concrete strength, 60-in. diameter column design is 0.52 in., a reduction in displacement of 13% compared to the 4,000 psi concrete strength, 60-in. diameter column design. Lastly, increasing the concrete strength to 10,000 psi (see Figure 12.21b) results in a dynamic direct shear failure (i.e., longitudinal rebar ruptures due to excessive shear slip at the column base). Therefore, high-strength concrete does not help to optimize this column design.

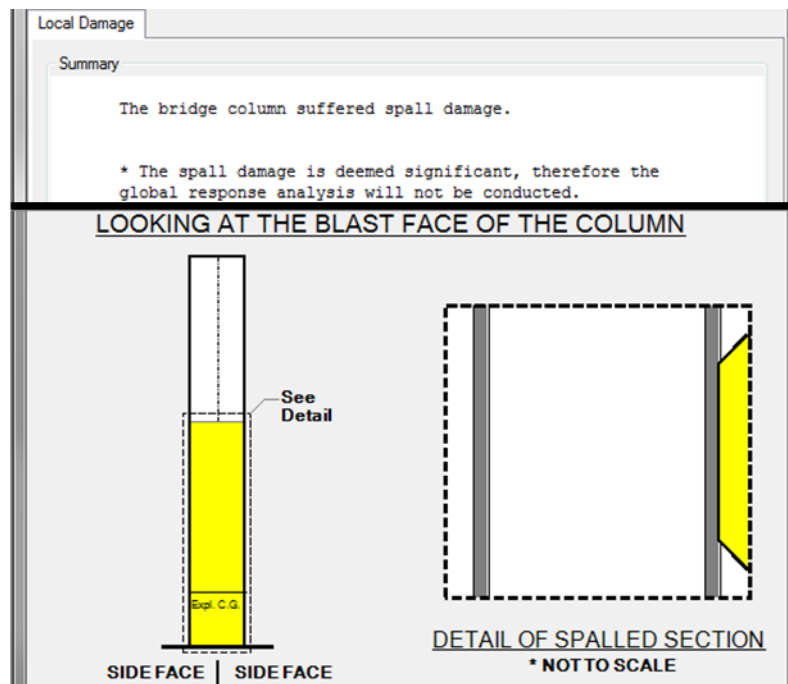


Figure 12.20 RC Column Design Example 1 Effects of Concrete Strength on Column Response – 3,000 psi Concrete

Concrete cover is evaluated next. The 60-in. diameter column design assumed a 1.5-in. thick concrete cover (see results in Figure 12.22a). Increasing the concrete cover by 50% from 1.5 in. to 3 in. for a threat of 2,800 lb of TNT at a standoff distance of 15 ft reduces the peak column displacement by 6% (see Figure 12.22b). Therefore, additional concrete cover provides minimal improvement to column design optimization.

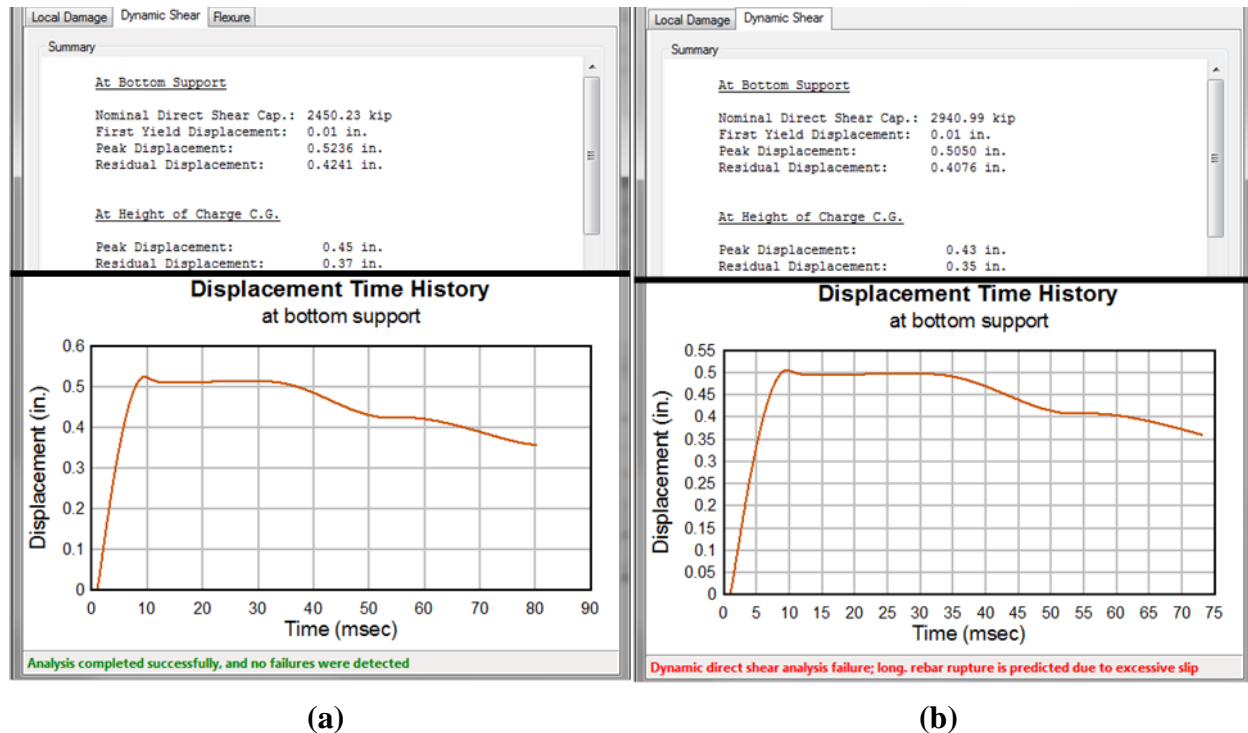


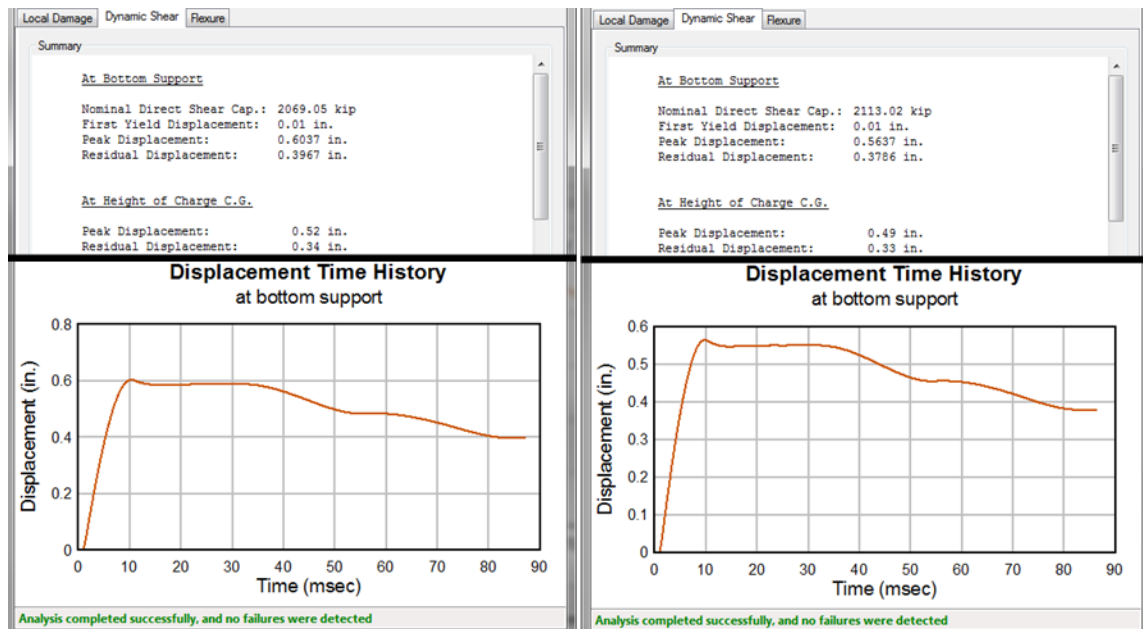
Figure 12.21 RC Column Design Example 1 Effects of Concrete Strength on Column Response: (a) 6,000 psi Concrete, (b) 10,000 psi Concrete

The amount and type of transverse reinforcement is evaluated next. The 60-in. diameter column design assumed #6 hoops at 6 in. on center (OC) along the full column height (see results in Figure 12.19). Optimizing hoop size and spacing to #4 hoops at 12 in. OC typical and 6 in. OC within the 3-ft long end regions for a threat of 2,800 lb at a standoff distance of 15 ft results in a sufficient column design with minimal change in column response (see Figure 12.23a).

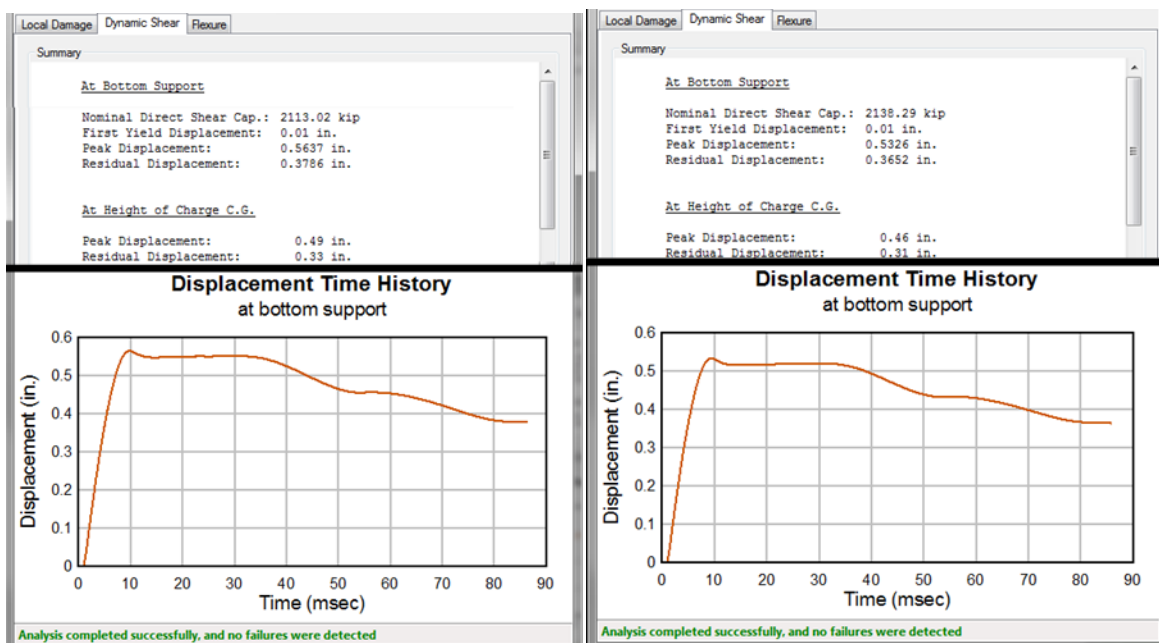
Additionally, increasing the transverse reinforcement to #6 spiral at 4 in. OC along the full column height results in a sufficient column design with minimal change in column response (see Figure 12.23b). Therefore, transverse reinforcement can be optimized for blast loads once local damage requirements are met.

The amount of longitudinal reinforcement is evaluated next. The 60-in. diameter column design assumed 10 #9 bars evenly spaced around the circumference of the circular column section (see results in Figure 12.19). Reducing the longitudinal reinforcement to 8 #8 bars evenly spaced for a threat of 2,800 lb of TNT at a standoff distance of 15 ft results in a sufficient column design for local damage and shear. However, as shown in Figure 12.24a, the maximum support rotation is 1.24 degrees, which is greater than the 1.0 degree plastic rotation limit recommended in the NCHRP Technical Report 645 [24]. Therefore, additional longitudinal reinforcement is required. Increasing the longitudinal reinforcement to 10 #8 rebar evenly spaced results in a sufficient

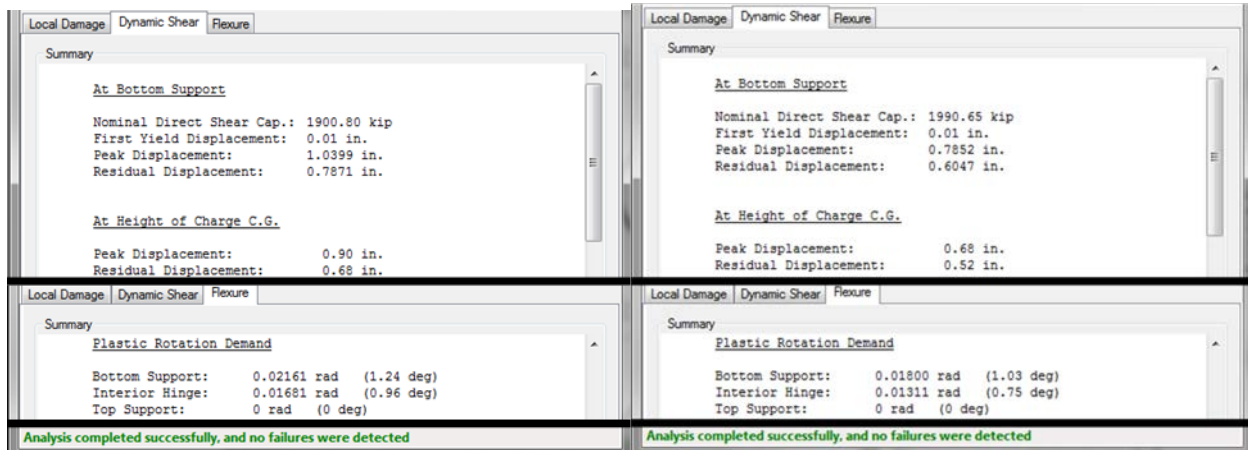
column design with a maximum support rotation of 1.0 degree (see Figure 12.24b). Therefore, longitudinal reinforcement can also be optimized for blast loads once local damage requirements are met.



(a) (b)
Figure 12.22 RC Column Design Example 1 Effects of Concrete Cover on Column Response: (a) 1.5 in. Cover, (b) 3 in. Cover



(a) (b)
Figure 12.23 RC Column Design Example 1 Effects of Type and Amount of Transverse Reinforcement on Column Response: (a) #4 hoops at 12 in. OC typical and 6 in. OC within end regions, (b) #6 spiral at 4 in. OC



(a) (b)

Figure 12.24 RC Column Design Example 1 Effects of Amount of Longitudinal Reinforcement on Column Response: (a) 8 #8 evenly spaced, (b) 10 #8 evenly spaced

Lastly, using the lessons learned from adjusting each variable, the initial 60-in. diameter column design is optimized. The initial 60-in. diameter column design included 4,000 psi concrete reinforced with 10 #9 longitudinal bars evenly spaced and #6 hoops at 6 in. OC along the full column height and having 1.5 in. of concrete cover. As shown in Figure 12.19, the column design subjected to a threat of 2,800 lb of TNT at a standoff distance of 15 ft results in a peak displacement of 0.52 in. and a maximum support rotation of 0.89 degrees.

The optimized column design includes a 60-in. diameter column comprised of 5,000 psi concrete reinforced with 10 #8 longitudinal bars evenly spaced and #4 hoops at 12 in. OC typical and 6 in. OC within the 3 ft long end regions (see Figure 12.25a). The optimized column design subjected to a threat of 2,800 lb of TNT at a standoff distance of 15 ft results in a sufficient column design for local damage, dynamic shear, and flexure. As shown in Figure 12.25b, the peak displacement is 0.76 in., and the maximum support rotation is 1.0 degrees—equivalent to the 1.0 degree plastic rotation limit recommended in the NCHRP Technical Report 645 [24]. Therefore, multiple column designs are adequate for the given threat.

(a) (b)
Figure 12.25 RC Column Design Example 1 Optimized Design: (a) Column Input, (b) Results

This comprehensive design example illustrated an insufficient initial column design for the given threat. ATP-Bridge was used to evaluate the initial column design for blast loads and adjust different design variables to provide adequate solutions. While multiple solutions are possible, the best solution depends on the flexibility of design parameters for each unique bridge design.

Design Example 2

The following design example considers the response of a reinforced concrete highway bridge column for a smaller threat than was investigated in Design Example 1.

Evaluate the column, designed for a non-seismic region, for the given close-in blast load. If the column is insufficient, determine the amount of additional standoff required to meet all applicable design checks. Assume that this is an existing bridge and in this case providing adequate standoff distance is preferred over a column retrofit. Refer to Figure 12.26 for threat details and Figure 12.27 for column design details. Use ATP-Bridge to perform the analysis and design.

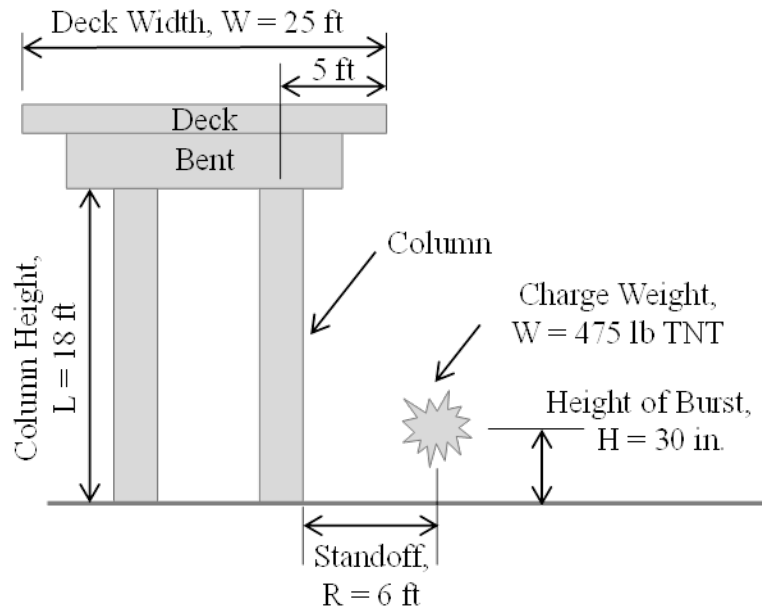


Figure 12.26 RC Column Design Example 2 Elevation

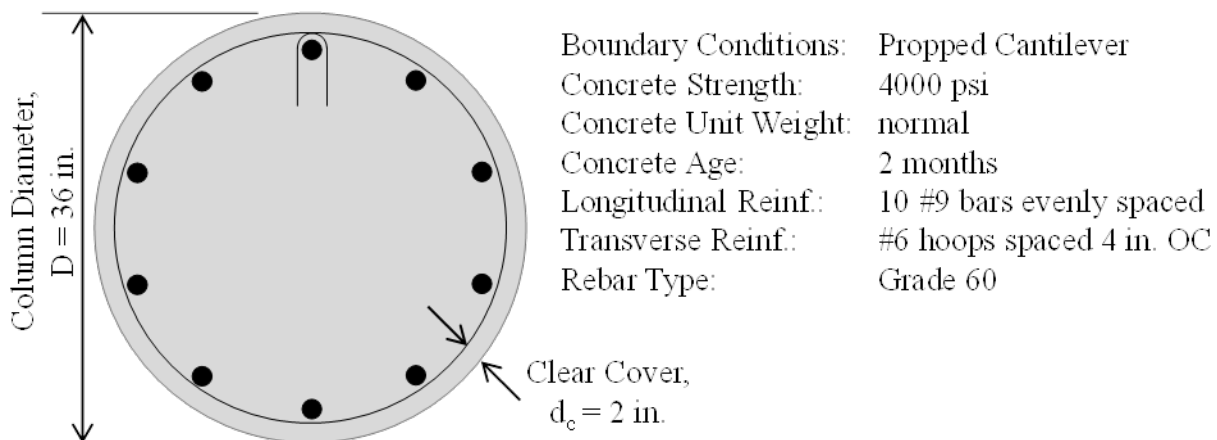


Figure 12.27 RC Column Design Example 2 Details

In response to the given threat of 475 lb of TNT at a 6-ft standoff distance, the 36-in. diameter column suffers a breach failure near the threat location (see Figure 12.28). Therefore, additional standoff distance is required to adequately protect the column.

Increasing the standoff distance from 6 ft to 7 ft for a threat of 475 lb of TNT eliminates breaching of the 36-in. diameter column. However, the column experiences concrete spall damage on the rear and side faces of the column (see Figure 12.29). Because the local damage checks in ATP-Bridge are satisfied, dynamic shear and flexural response of the column are then evaluated. The peak displacement is 10.75 in. and the maximum support rotation is 0.64 degrees. NCHRP Technical Report 645 [24] recommends a plastic rotation limit of 1 degree, which is satisfied. In summary, this design example illustrates the benefit additional standoff distance alone has on the design of a blast-loaded reinforced concrete bridge column.

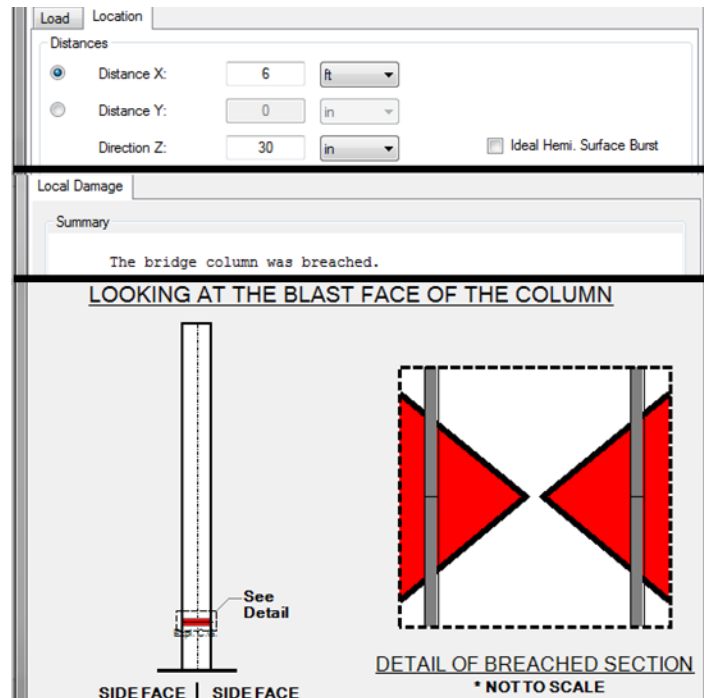


Figure 12.28 RC Column Design Example 2 Local Damage Results for 6-ft Standoff Distance

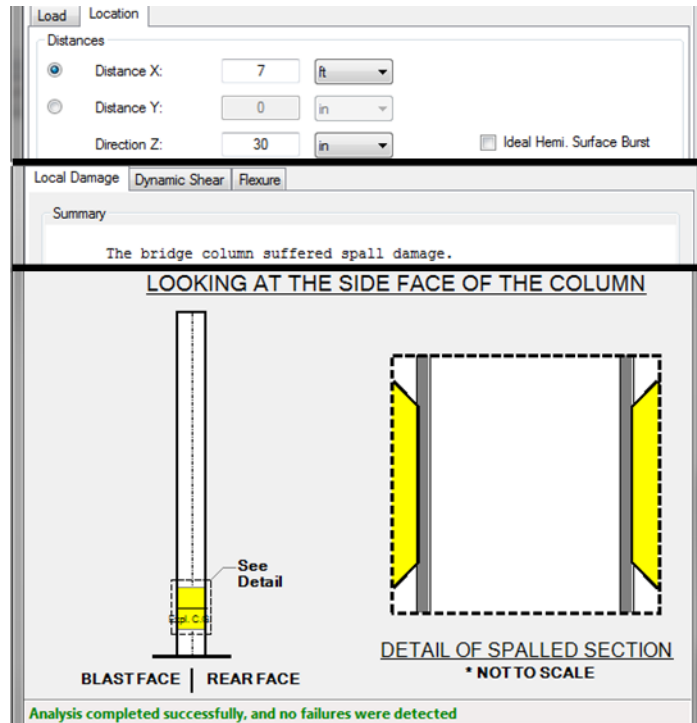


Figure 12.29 RC Column Design Example 2 Local Damage Results for 7-ft Standoff Distance

Determine the amount of additional standoff distance required to prevent spall damage. Increasing the standoff distance from 6 ft to 8 ft for a threat of 475 lb of TNT eliminates breaching and spall of the 36-in. diameter column (see Figure 12.30). Because the local damage checks in ATP-Bridge are satisfied, dynamic shear and flexural response of the column are then evaluated. As shown in Figure 12.30, the peak displacement is 0.28 in. and the maximum support rotation is 0.46 degrees. NCHRP Technical Report 645 [24] recommends a plastic rotation limit of 1 degree, which is satisfied. In summary, this design example illustrates the benefit additional standoff distance alone has on the design of a blast-loaded reinforced concrete bridge column.

The screenshot displays the ATP-Bridge software interface with the following sections:

- Load Location**
 - Distances:
 - Distance X: 8 ft
 - Distance Y: 0 in
 - Direction Z: 30 in
 - ☐ Ideal Hemi. Surface Burst
- Local Damage** (Summary)
 - The bridge column suffered no local damage.
- Dynamic Shear** (Summary)
 - At Bottom Support
 - Nominal Direct Shear Cap.: 1082.55 kip
 - First Yield Displacement: 0.01 in.
 - Peak Displacement: 0.2788 in.
 - Residual Displacement: 0.1347 in.
 - At Height of Charge C.G.
 - Peak Displacement: 0.24 in.
 - Residual Displacement: 0.12 in.
- Flexure** (Summary)
 - Plastic Rotation Demand
 - Bottom Support: 0.00809 rad (0.46 deg)
 - Interior Hinge: 0.00057 rad (0.03 deg)
 - Top Support: 0 rad (0 deg)
- Status Bar:** Analysis completed successfully, and no failures were detected

Figure 12.30 RC Column Design Example 2 Results for 8-ft Standoff Distance

12.4.2 Steel Cellular Bridge Towers

The following design example shows the predicted behavior of the front panel of a steel cellular tower. Rather than providing multiple examples, a single baseline scenario is shown along with a description of how the response changes for modifications to the threat and design parameters. Also discussed are measures that can be taken if the threat becomes too severe. Such analyses fit within the overall design process for the front panel of steel cellular towers subjected to blast loads as described in the previous section. Each design example utilizes the ATP-Bridge software.

In this example, the baseline threat is assumed to act against the front panel of a steel cellular tower with dimensions representative of those found on existing suspension bridges. The steel

properties are assumed to be consistent with ASTM A36 steel as used in the pooled-fund test program, but users are able to specify other properties if they so desire.

The panel considered for the baseline case is 140-in. tall by 40-in. wide and is assumed to be 2-in. thick. The basic user interface for specifying the overall panel geometry is shown in Figure 12.31. At the top of the figure below the component name, the panel geometry and material properties are listed. By selecting the “Material” tab just below this text box, users can specify values for other types of steel. Near the bottom of this form is where users specify the overall dimensions and thickness of a front panel plate. Users also specify the diaphragm geometry, which informs ATP-Bridge of the total depth of a front cell on the tower. A cross-sectional view of the tower for a 40-in. and a 50-in. diaphragm is shown in Figure 12.32 for illustrative purposes. In the baseline case, a 40-in. cell depth is assumed.

Define Steel Tower Panel

Name: Steel Plate 1

Type: Target Panel at X = 0 ft Y = 0 ft Z = 0 ft

Dimensions: Height = 140 in Width = 40 in Thickness = 2 in

Plate: ASTM A36

Stiffener: ASTM A36

OK

Cancel

Geometry

Material

Elevation View

Section View

Stiffener Angle Detail

-X

+X

Tower Elevation

Plate

Edge Support

Tower

Target Panel Geometry

Height: 140 in

Width: 40 in

Thickness: 2 in

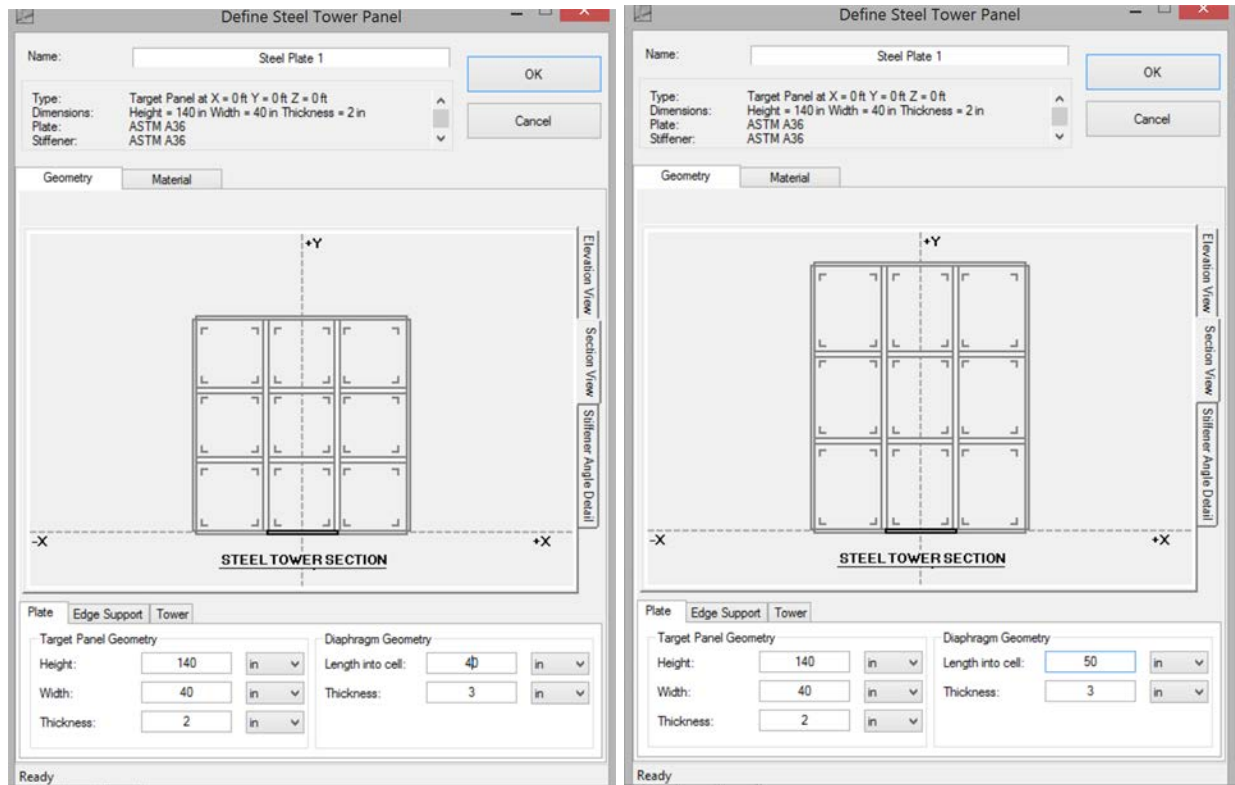
Diaphragm Geometry

Length into cell: 40 in

Thickness: 3 in

Ready

Figure 12.31 Sample Steel Panel Geometry Input



(a)

(b)

Figure 12.32 Illustration Showing Cell Depth Corresponding to (a) 40-in. and (b) 50-in.

The stiffener angles supporting the front panel are assumed to have a leg in contact with the front panel that is 4-in. wide and 0.5-in. thick. Because the other leg of the angle is fastened to a plate perpendicular to the front panel and effectively extends the depth of the cell, it is not necessary to provide a specific value for the leg dimension. Figure 12.33 shows the geometry for the stiffening angles used in this example. The “Tower” tab within the bottom portion of the form simply gives the location of the panel relative to the overall tower dimensions for the purposes of predicting blast loads. While the focus of the response calculations is on a single panel, the actual tower dimensions influence the pressure history a panel will experience based on the effects of how reflected pressures develop and how clearing occurs (see Chapter 4 for additional details on the phenomenology of blast loads). For this example, the tower is assumed to be 30-ft. wide, and the panel being analyzed is directly in the middle, which is what should typically be assumed to develop the worst-case loading scenario.

The initial threat considered for this scenario is a charge of 1000 lbs. of TNT at a distance of 5 ft. from the front panel. The charge is assumed to be elevated off the deck at a height of 70 in. as shown in the example threat definition given in Figure 12.34.

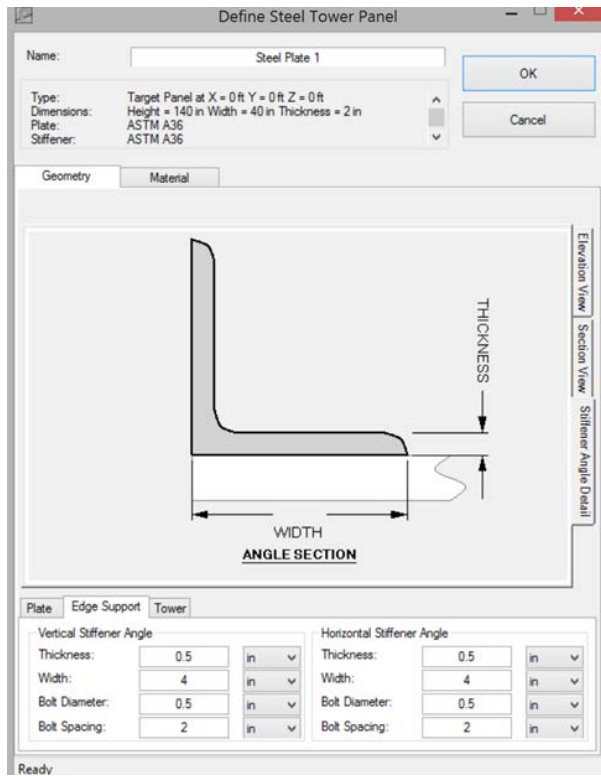


Figure 12.33 Geometry of Vertical and Horizontal Stiffening Angles

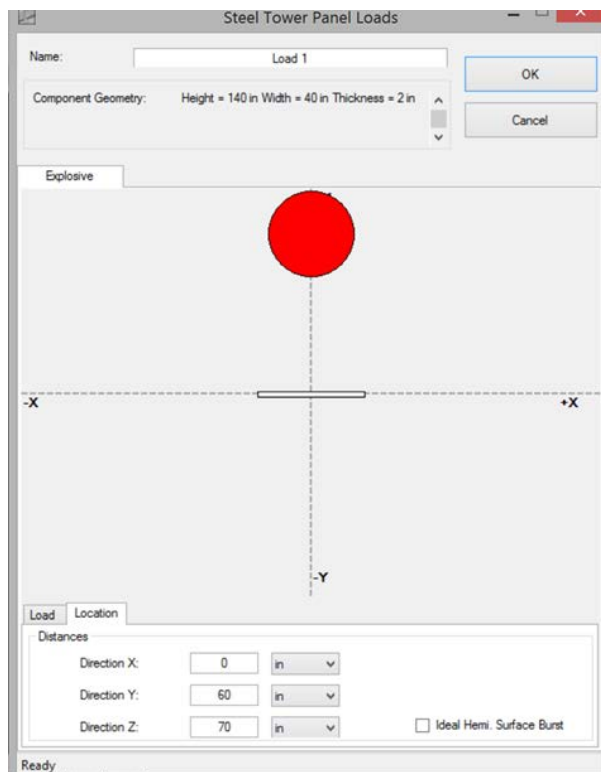


Figure 12.34 Example Threat Definition for Steel Cellular Tower

Once the threat and panel properties are specified, an analysis of the response can be conducted. In addition, ATP-Bridge allows the user to view the panel and threat in its 3D viewer so users can ensure consistency with their input. Two different views of the panel and charge for this scenario are shown in Figure 12.35.

For this threat, no local damage is predicted, though some partial tearing along the plate edges is expected. Results from this analysis are shown in Figure 12.36.

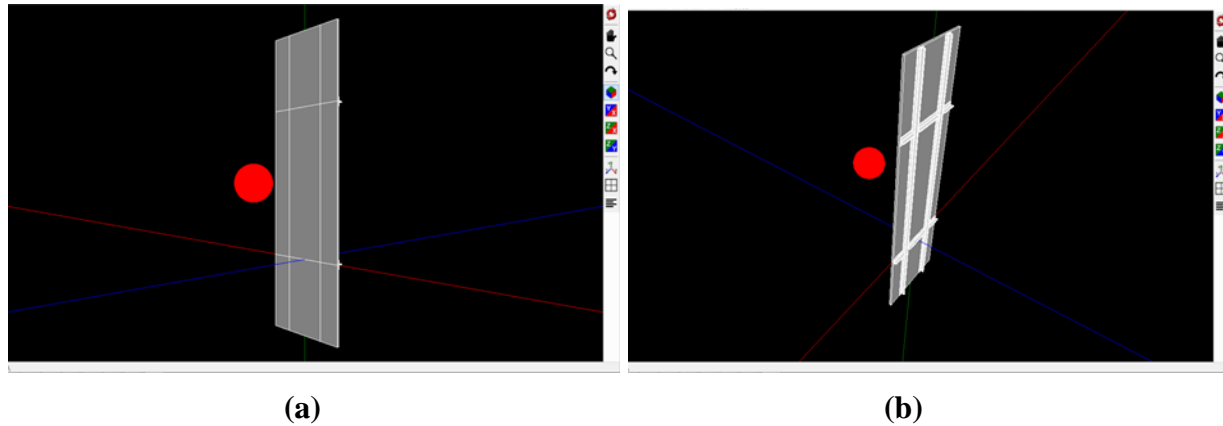


Figure 12.35 Isometric Views (a) In Front of and (b) Behind the Panel Being Analyzed

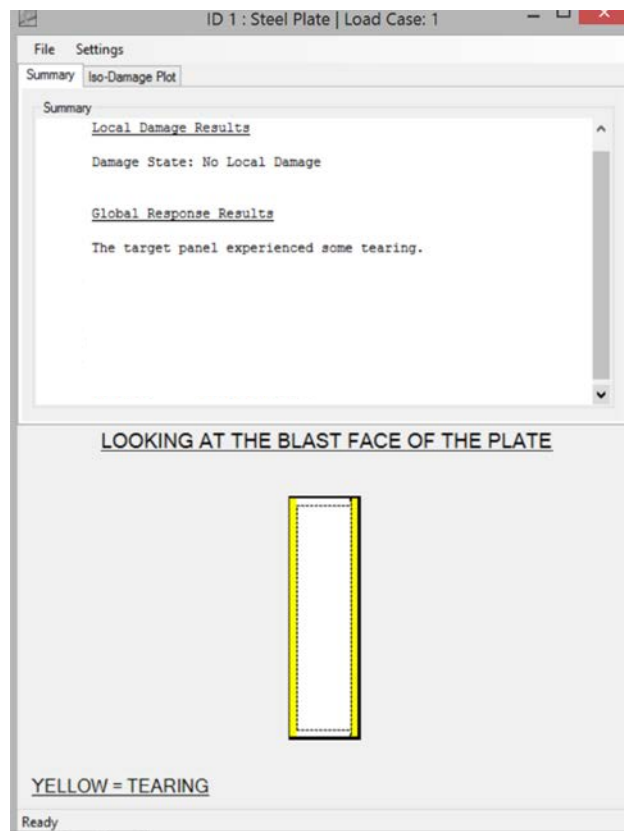


Figure 12.36 Analysis Results Showing Some Tearing at Edge of Panel for Baseline Threat

A unique capability within ATP-Bridge for analyzing the response of steel panels within cellular towers is the ability to generate what is known as an “iso-damage” curve as shown in the tab near the top of the form in Figure 12.36. This plot provides curves that show when the threshold associated with different failure modes is reached. For the baseline threat, the predicted iso-damage plot is shown in Figure 12.37. As this figure indicates, the standoff and charge size associated with the onset of tearing, global failure, and local breach can be readily identified. Such knowledge is quite helpful in studying response and evaluating potential design modifications. For example, in this particular case, the graph indicates that the charge has to be quite close (approximately 1.3 ft.) to the target for local breach to control. At larger standoffs, the onset of tearing will control prior to global failure because the charge weight to induce tearing is smaller than the curve for global failure. What this plot also indicates is that, for the baseline panel considered, a charge weight greater than approximately 1500 lbs. of TNT will cause global failure (i.e., the entire panel fails along its perimeter and becomes a flyer plate) before local breach will occur (where the edges of the panel remain intact but a localized failure within the boundary of the panel occurs). To verify this understanding, the threat acting against the baseline panel is increased to 2000 lbs. TNT. Results for this analysis are provided in Figure 12.38. As expected, global failure controls the response.

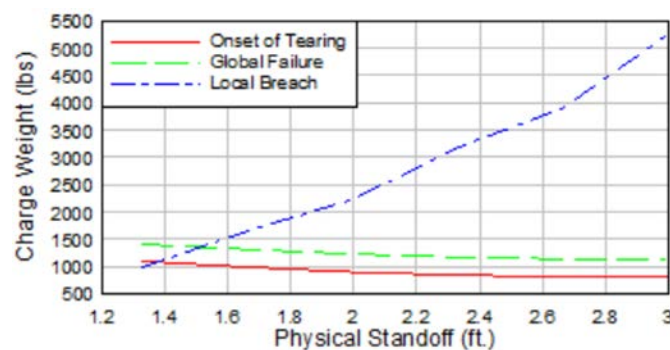


Figure 12.37 Iso-Damage Plot for Baseline Example

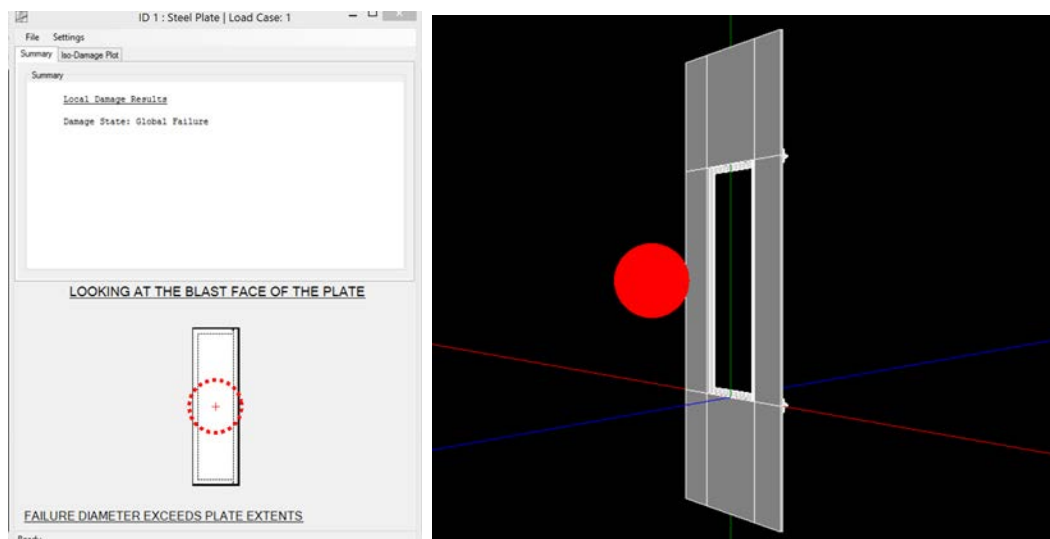


Figure 12.38 Global Failure of Front Panel due to Charge of 2,000-lbs TNT

To mitigate this more severe threat of 2000 lbs. TNT relative to the baseline threat of 1000 lbs. TNT, several options can be considered. The strength of the steel can be increased, the thickness of the front plate could be increased, and the geometry of the front panel dimensions could be adjusted through the use of additional stiffeners. For the present example, the only change that is considered is doubling the thickness of the front plate to 4 in. Although an increase to a 3-in. plate and 3.5-in. plate were considered, these modifications did not prevent global failure of the plate. In Walker, et al. (2011) [113], a combined approach is recommended where several options are used in combination. For example, for this particular case, it is possible to increase the steel strength to 70-ksi and use a front plate that has a thickness of 3 in. With this combination of design changes, the front panel survives the 2000-lb. threat with no local or global damage, and the peak deflection is predicted to be 6.35 in. (Figure 12.39). Of course, in a retrofit situation it would not be possible to change the material strength of the entire front panel, but the retrofit material could be made of higher strength steel than the tower. Additional information on retrofits is provided in the next section.

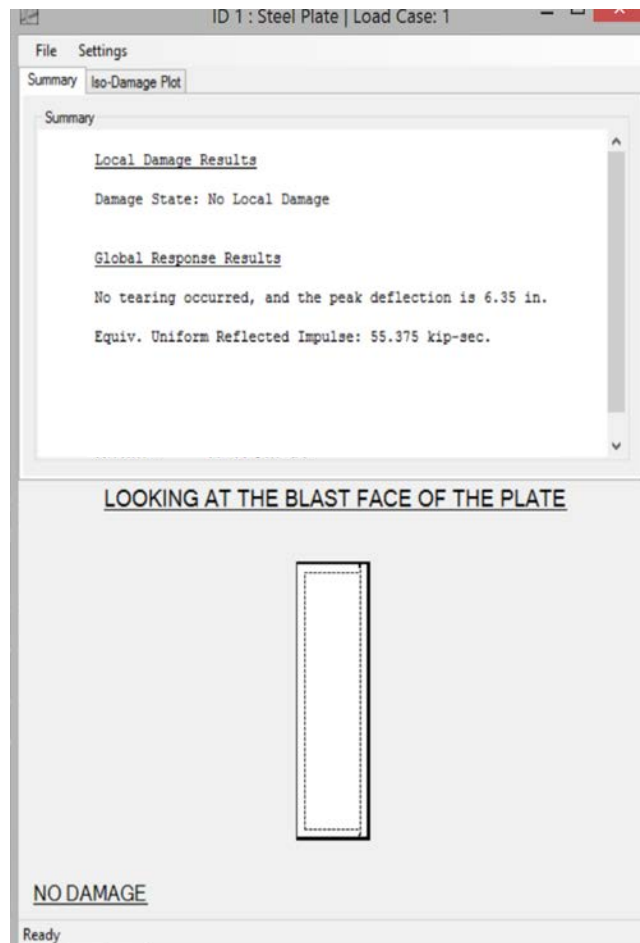


Figure 12.39 Modified Front Panel with 70-ksi Steel and 3-in. Thickness

Finally, to illustrate the possibility of local breaching and an associated threat for the original baseline design, consider a new charge of 500 lbs. TNT placed at 1.25 ft. (16 in.) from the front panel. As expected from the iso-damage plot, this case produces localized breach failure with a predicted breach diameter of 32.5 in. Results for this case are shown in Figure 12.40.

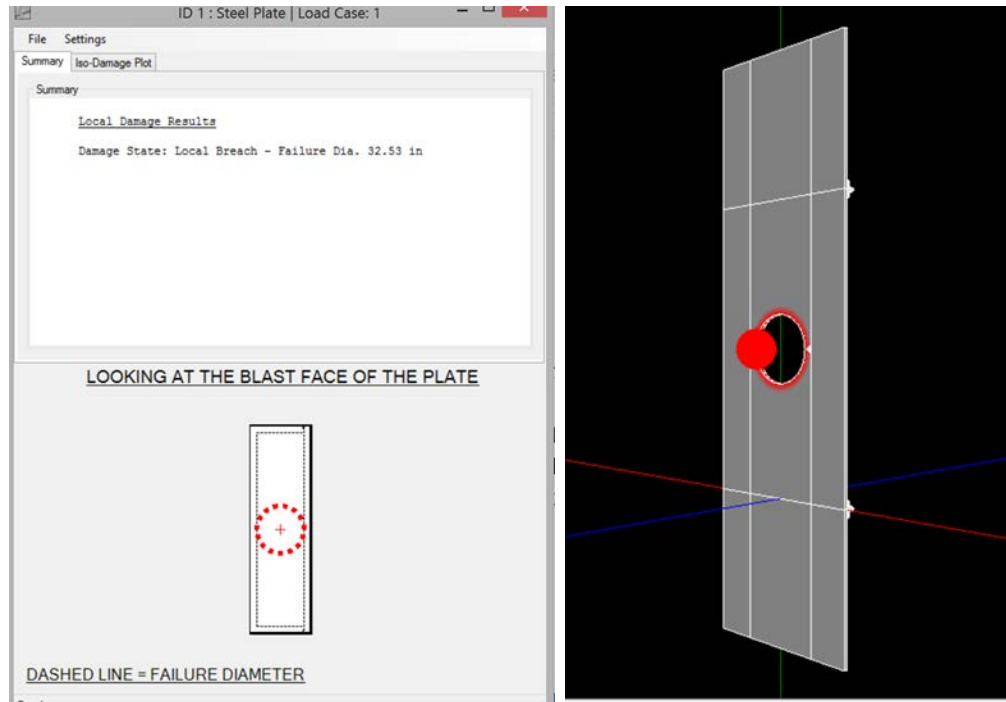


Figure 12.40 Localized Breach in Baseline Design

12.4.3 Reinforced Concrete Bridge Towers

In this section, a demonstration on how to use the ATP-Bridge software for preliminary design of an RC tower panel subject to an explosive threat is provided. A baseline scenario is first introduced, after which various problem parameters are modified to illustrate their effect on the blast performance of the example RC tower panel.

The example RC tower has two cells and is rectangular in geometry, as shown in Figure 12.41. The clear distance between front and back RC panels is 144-in., and the clear distance between a side and interior RC panel is also 144-in. All RC panels have a nominal thickness of 12-in. In addition, the vertical distance from the bridge deck to the bottom face of the first horizontal diaphragm is 288-in., and the diaphragm thickness is 12-in. Steel reinforcement details and material properties for the targeted panel are shown in Figure 12.42. The main longitudinal reinforcement consists of #9 bars at 6-in. on-center, and the transverse reinforcement consists of #4 bars at 6-in. on-center. The static unconfined concrete compressive strength is taken as 4,000-psi, and the static yield strength of the steel reinforcement is taken as 60,000-psi.

Name: FHWA Chpt 9 Example Panel

Material Prop.: $f_c = 4000$ psi $f_y = 60000$ psi

Section | Elevation

Geometry | Reinforcement | Material Properties

Front/Back Panel Dimensions

Clear Width	144.00	in
Thickness	12.00	in

Side/Interior Panel Dimensions

Clear Width	144.00	in
Thickness	12.00	in

Name: FHWA Chpt 9 Example Panel

Material Prop.: $f_c = 4000$ psi $f_y = 60000$ psi

Section | Elevation

Geometry

Dimensions

Clear Height [h]	288.00	in
Diaphragm	12.00	in

Figure 12.41 Example RC Tower Section Dimensions

Name: FHWA Chpt 9 Example Panel

Material Prop.: $f_c = 4000$ psi $f_y = 60000$ psi

Section | Elevation

FRONT PANEL SECTION DETAIL

Geometry | Reinforcement | Material Properties

Longitudinal Reinforcement

Bar Size:	# 9
Spacing [s]:	6.00 in
Effective depth	10.50 in
Rebar Ratio:	0.0317

Transverse Reinforcement

Bar Size:	# 4
Spacing:	6.00 in
Effective depth:	11.31 in
Rebar Ratio:	0.006

Name: FHWA Chpt 9 Example Panel

Material Prop.: $f_c = 4000$ psi $f_y = 60000$ psi

Section | Elevation

FRONT PANEL SECTION DETAIL

Geometry | Reinforcement | Material Properties

Concrete

Compressive	4000.00	psi
-------------	---------	-----

Steel Reinforcement

Yield Strength:	60000.00	psi
-----------------	----------	-----

Figure 12.42 Steel Reinforcement Details and Material Properties for Blast-Loaded Panel of Example RC Tower

As shown in Figure 12.43, the explosive threat is defined as 1,000-lbs of ammonium nitrate and fuel oil (ANFO) deployed as a cylindrical charge having a length-to-diameter ratio of unity. The charge is placed essentially on the bridge deck, centered with the right-front RC tower panel (the hatched panel in Figure 12.43), and oriented such that its longitudinal axis is perpendicular to the plane of the bridge deck. The charge standoff is set at approximately 60-in. from the exterior face of the targeted RC tower panel. Plan and elevation views of the threat scenario are illustrated in the ATP-Bridge 3-dimensional graphics window in Figure 12.44.

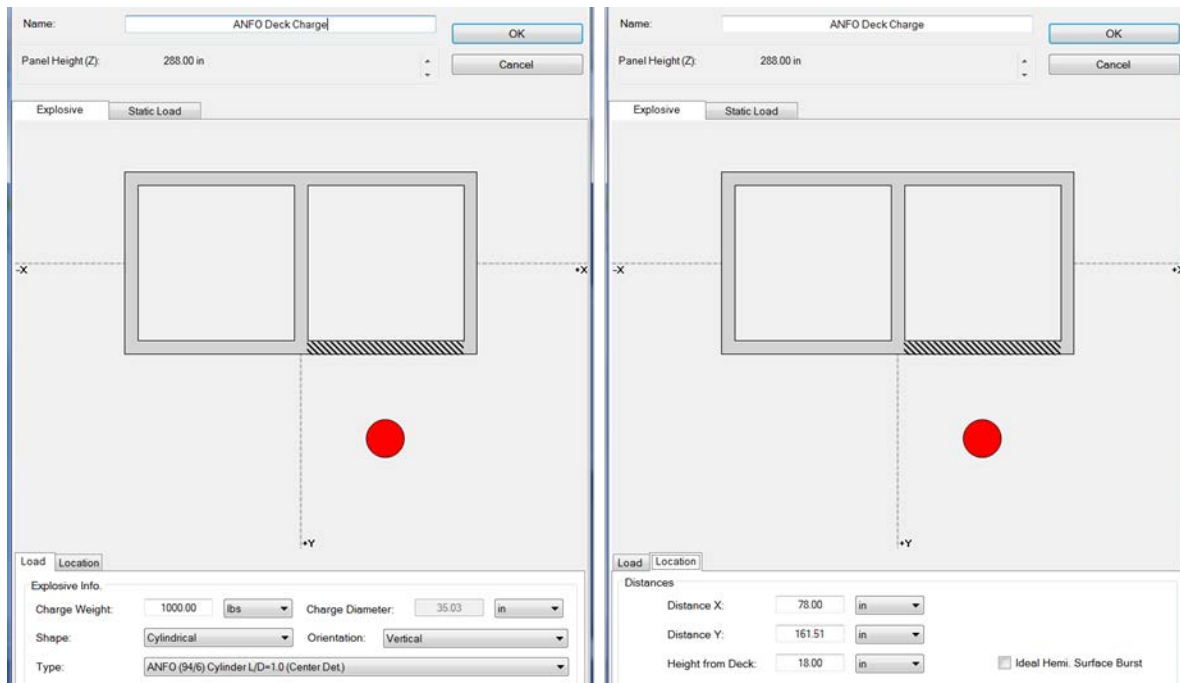


Figure 12.43 Explosive Threat Definition for Example RC Tower

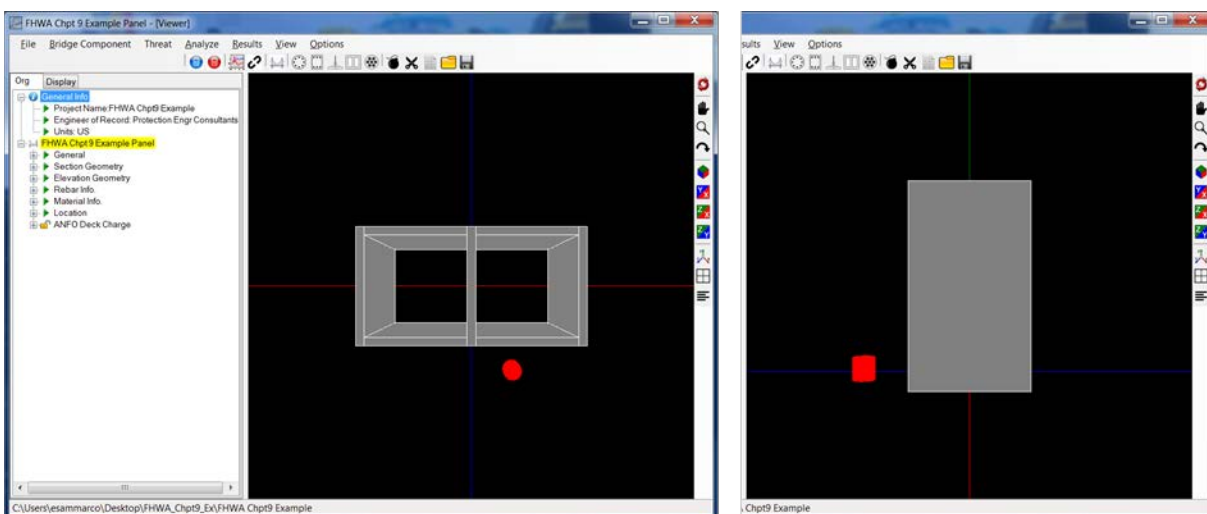


Figure 12.44 ATP-Bridge 3-Dimensional Graphics Display of Example RC Tower

Once the RC tower panel and explosive threat are defined, ATP-Bridge is used to perform an analysis to assess local spall and breach damage and predict peak component-level blast response. The results of the baseline analysis are presented in Figure 12.45. For this particular baseline example, ATP-Bridge predicts local breach damage in the form of a 43.5-in. diameter breach hole near the bridge deck. The ATP-Bridge local damage results also provide a spall threshold thickness of 62.60-in. and a breach threshold thickness of 28.36-in. These threshold thicknesses are interpreted as the RC panel thickness below which the stated material-level damage state will occur. For instance, to prevent breach damage for the given explosive threat and RC tower panel properties, the RC tower panel thickness would need to increase to 28.36-in. It should also be noted that, because local breach damage was predicted, the ATP-Bridge response algorithm terminated prior to assessing the blast-loaded RC panel's component-level response. This early termination occurs when local breach damage is predicted because (a) it should be taken as an undesirable limit state warranting a design change and (b) because the component-level part of the response algorithm was not developed to account for the effect of early-time breach damage on component-level response.

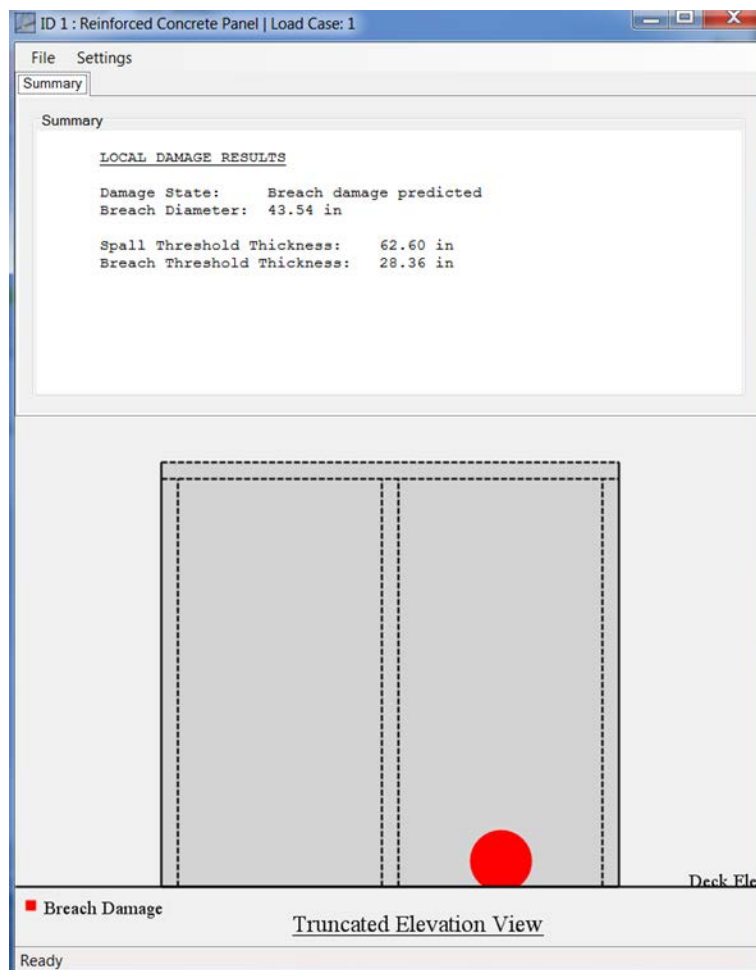


Figure 12.45 Material-Level Spall and Breach Damage of Baseline RC Tower Panel Design

From the baseline RC tower panel definition, two modifications are now made to illustrate their effect on material-level breach damage. First, the transverse reinforcing bar size in the targeted RC panel is increased to #6 bars. Local damage results for this modification are shown in the left image of Figure 12.46, where it can be seen that the breach diameter decreased from 43.54-in. to 41.96-in. with no change to the predicted damage threshold thicknesses. The second modification involves an increase in the static unconfined concrete compressive strength from 4,000-psi to 6,000-psi. Local damage results for this modification are shown in the right image of Figure 12.46, where it can be seen that (a) the predicted breach diameter increased from 43.54-in. to 46.37-in. and (b) the spall and breach threshold thicknesses both decreased from 62.60-in. and 28.36-in. to 58.90-in. and 26.68-in., respectively.

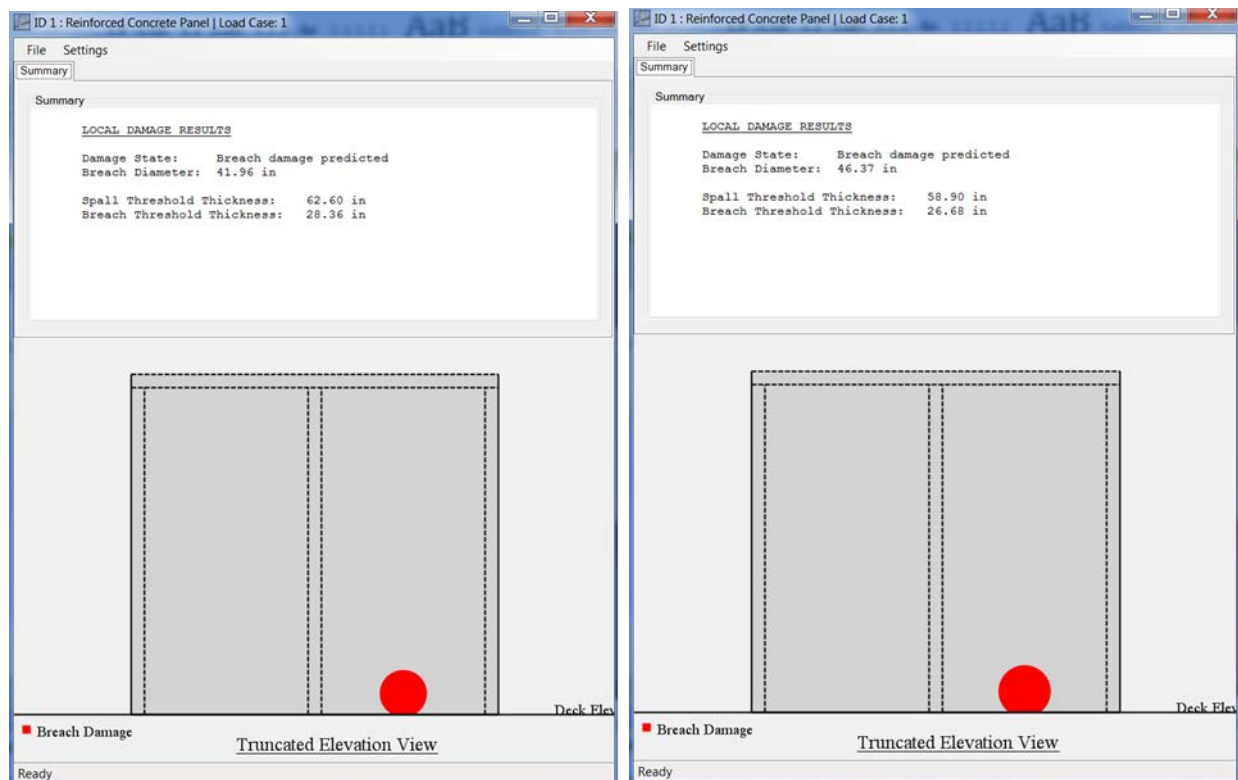


Figure 12.46 Effect of (left) Increasing Transverse Reinforcing Bar Size and (right) Increasing Concrete Strength on Material-Level Damage

In addition to investigating modifications to the RC tower panel section properties, the effect of having sustained axial compressive stress present in the targeted RC tower panel on material-level breach damage is investigated. Specifically, an axial compressive stress of 2,400-psi is introduced, as shown in the left image of Figure 12.47. Local damage results for this modification are shown in the right image of Figure 12.47, where it can be seen that the axial compressive load (which adds 1-dimensional confining stress to the concrete) acts to reduce the extent of breach damage from a diameter of 43.54-in. to 40.07-in. with no change to the predicted damage threshold thicknesses.

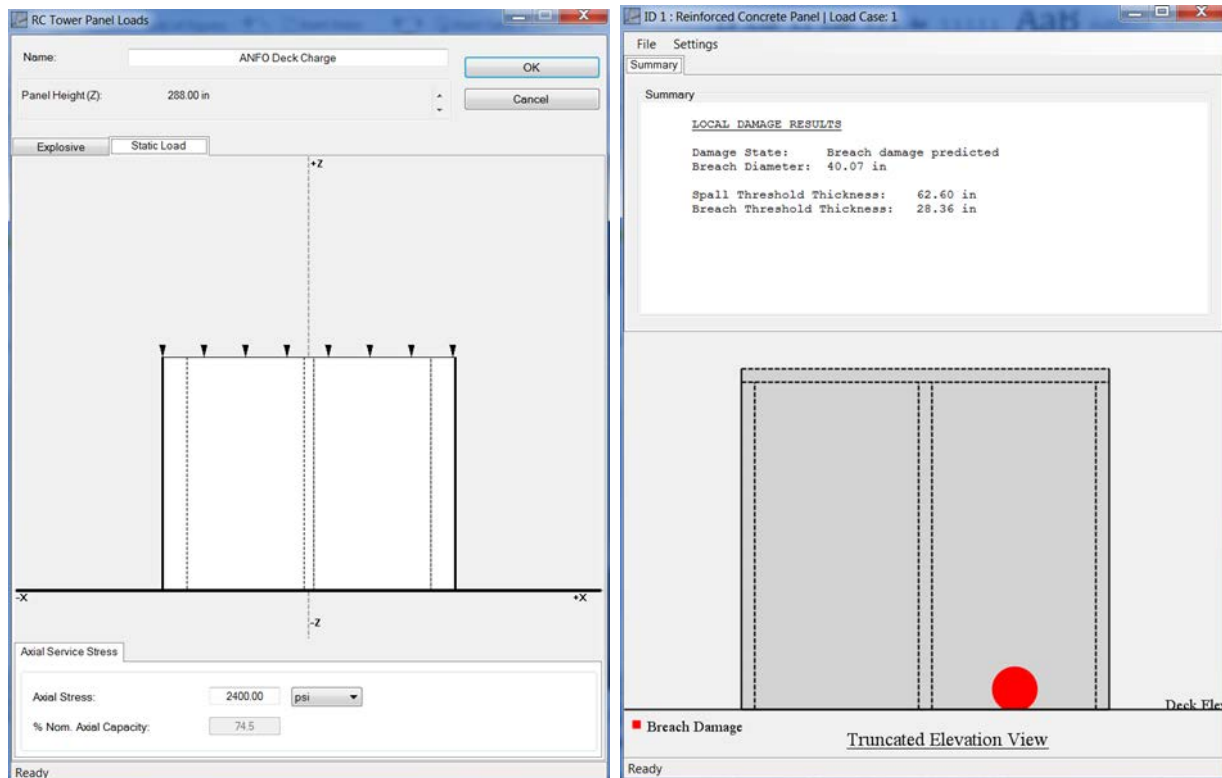


Figure 12.47 Effect of Increasing Sustained Axial Compressive Stress on Material-Level Damage

The last modification to investigate is the effect of increasing the targeted RC tower panel thickness to 30-in., which is above the reported breach threshold thickness. The thicker RC tower panel is then subjected to the same explosive threat (note, adjust explosive location to maintain standoff distance), and the results of the analysis are shown in Figure 12.48. The thicker RC tower panel did not suffer material-level breach damage; however, extensive spall damage (spall diameter of 78-in.) was predicted. Because breach damage was not predicted in this scenario, ATP-Bridge also performed a component-level dynamic analysis. In Figure 12.48, it can be seen that a peak dynamic displacement of 3.75-in. and a peak dynamic edge rotation of 3-deg were predicted. While component-level blast response limits for building structures are not entirely applicable for bridges (see Chapter 6 for more discussion on bridge-specific performance criteria), the U.S. Army's recommended single-degree-of-freedom response limits for blast-loaded RC panels [74] are provided in ATP-Bridge simply for comparison. The bottom portion of the ATP-Bridge form in Figure 12.48 presents a table of these response limits, and the blast-loaded RC tower panel is classified according to these response limits in the "Summary" box of the ATP-Bridge form shown in Figure 12.48. For instance, based on the component-level response prediction for this particular example, the blast-loaded RC tower panel was classified as a heavily damaged component corresponding to a very low level of protection. Predicted component damage for this classification includes significant, unreparable permanent deflections with component failure not likely.

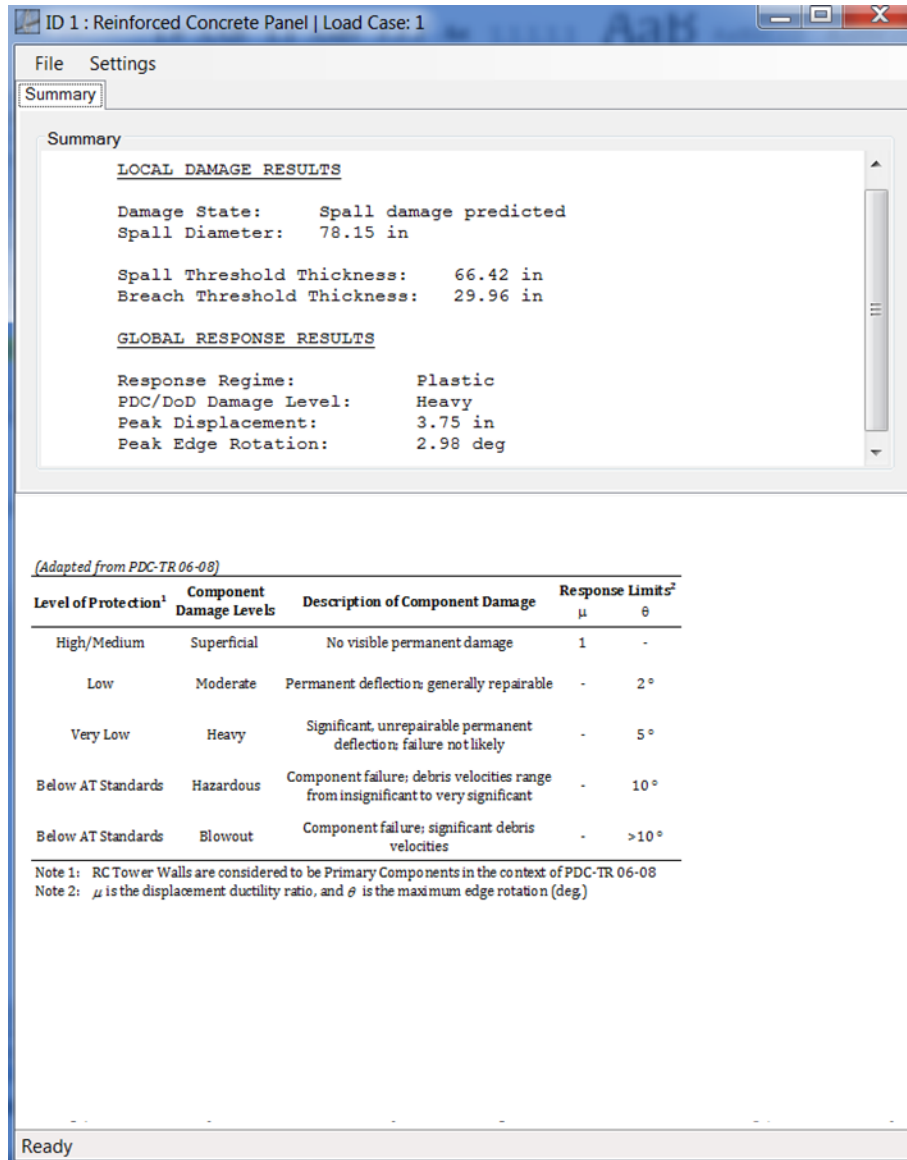


Figure 12.48 ATP-Bridge Analysis Results for RC Tower Panel having Increased Section Thickness

In addition to quantitative results, the ATP-Bridge 3-dimensional graphics utility in the Main Form can be used to qualitatively review dynamic response results. For instance, Figure 12.49 illustrates the 78-in. diameter extent of spall damage that was predicted for the blast-loaded 30-in. thick RC tower panel. In Figure 12.49, an isometric view of the two-cell RC tower leg is shown in the ATP-Bridge 3-dimensional graphics window with spall damage denoted by the yellow contour on the RC tower panel and the ANFO charge denoted by the red cylinder. In addition, Figure 12.50 qualitatively illustrates the predicted peak component-level dynamic response of the blast-loaded RC tower panel.

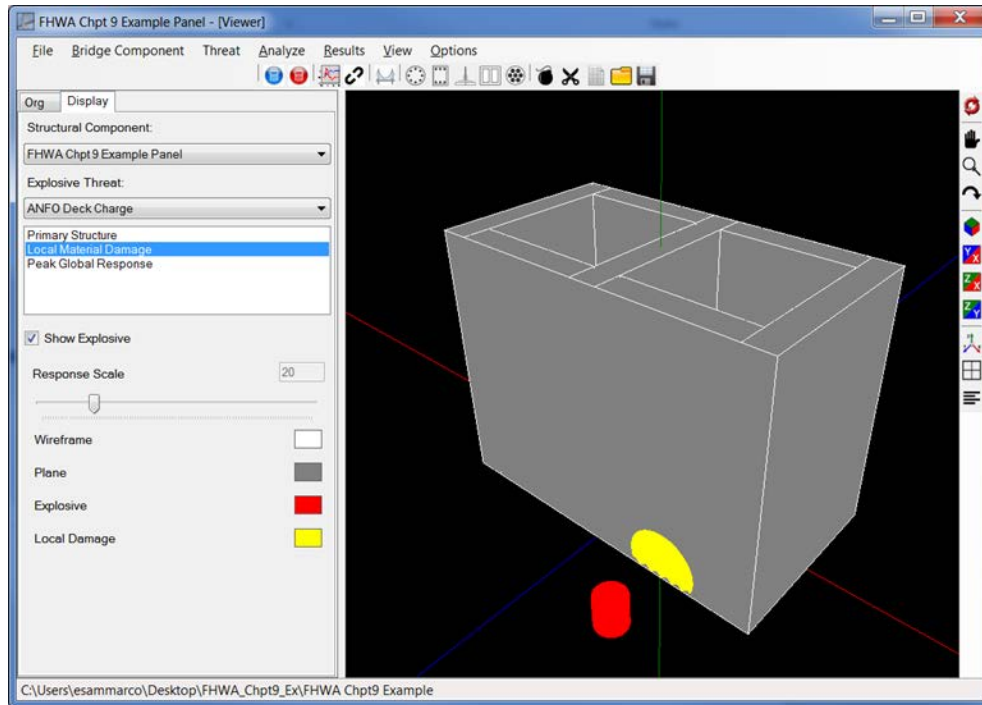


Figure 12.49 Illustrating Material-Level Spall Damage in ATP-Bridge 3-Dimensional Graphics Window

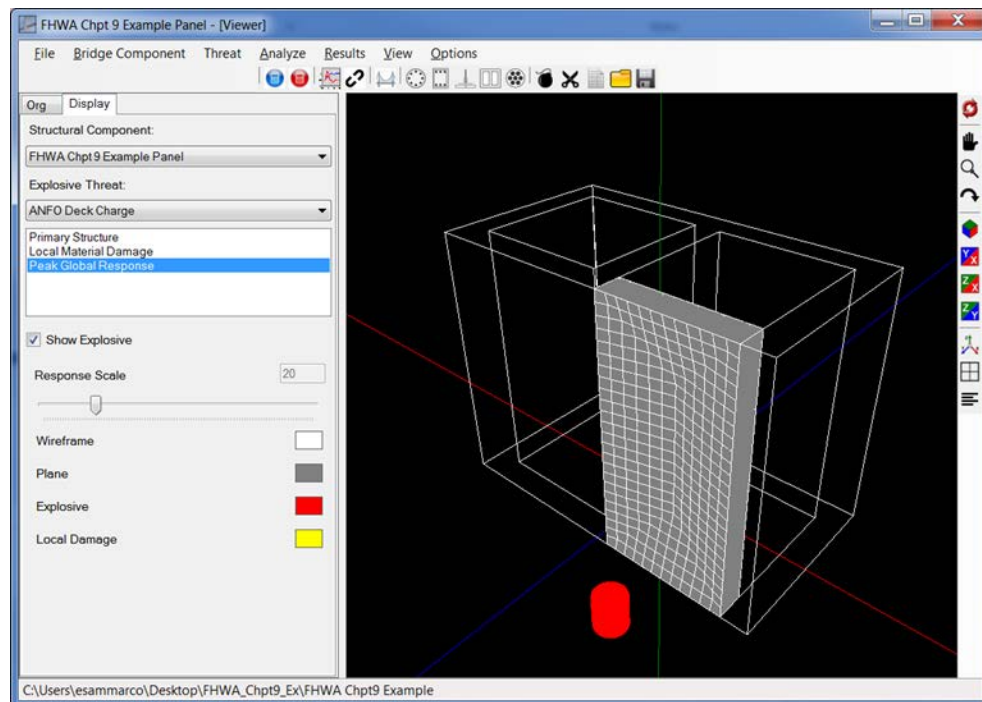


Figure 12.50 Illustrating Component-Level Peak Dynamic Response in ATP-Bridge 3-Dimensional Graphics Window

12.4.4 High-Strength Steel Cables

As was described in Chapter 10 of this manual, the design of a bridge to withstand a terrorist attack is a three step process. In the first step, the damage or failure of the individual cables or cable components would be assessed, with ATP-Bridge or with a detailed numerical simulation. In the second step, the damaged/failed components would be mapped into a numerical model of the overall bridge to create a new post-attack model; a representative example of a numerical model of an undamaged bridge is shown in Figure 12.51. In the third step, the post-attack bridge model would be subjected to the service loads that exist at the time of attack and the results of the analysis would be used to assess the probability that the damage will grow and the bridge will collapse.

Examples of the first step of the process are presented here, using ATP-Bridge to determine the level of damage and failure.

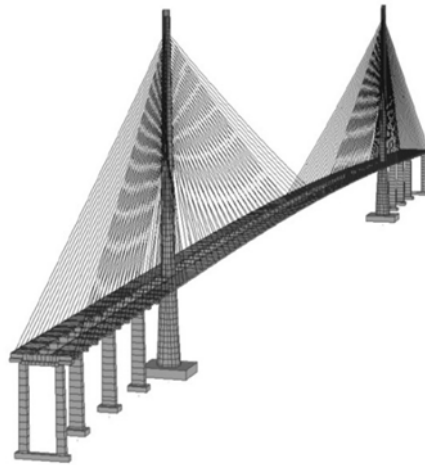


Figure 12.51 Example of Numerical Model of Undamaged Cable-Stayed Bridge [153]

Linear Shaped Charge against Stay Cable

In this example, the design basis threat for a cable-stayed bridge includes 200-gr/ft flexible linear shaped charges that will wrap around the circumference of a 13-strand stay cable.

After starting the ATP-Bridge software, a new project is created and a steel cable is defined as shown in Figure 12.52. The outer diameter of the environmental cover is chosen to be 3-in. The flexible linear shaped charge threat is defined as shown in Figure 12.52. The results of the analysis show that the cable is not severed; see the left side of Figure 12.53.

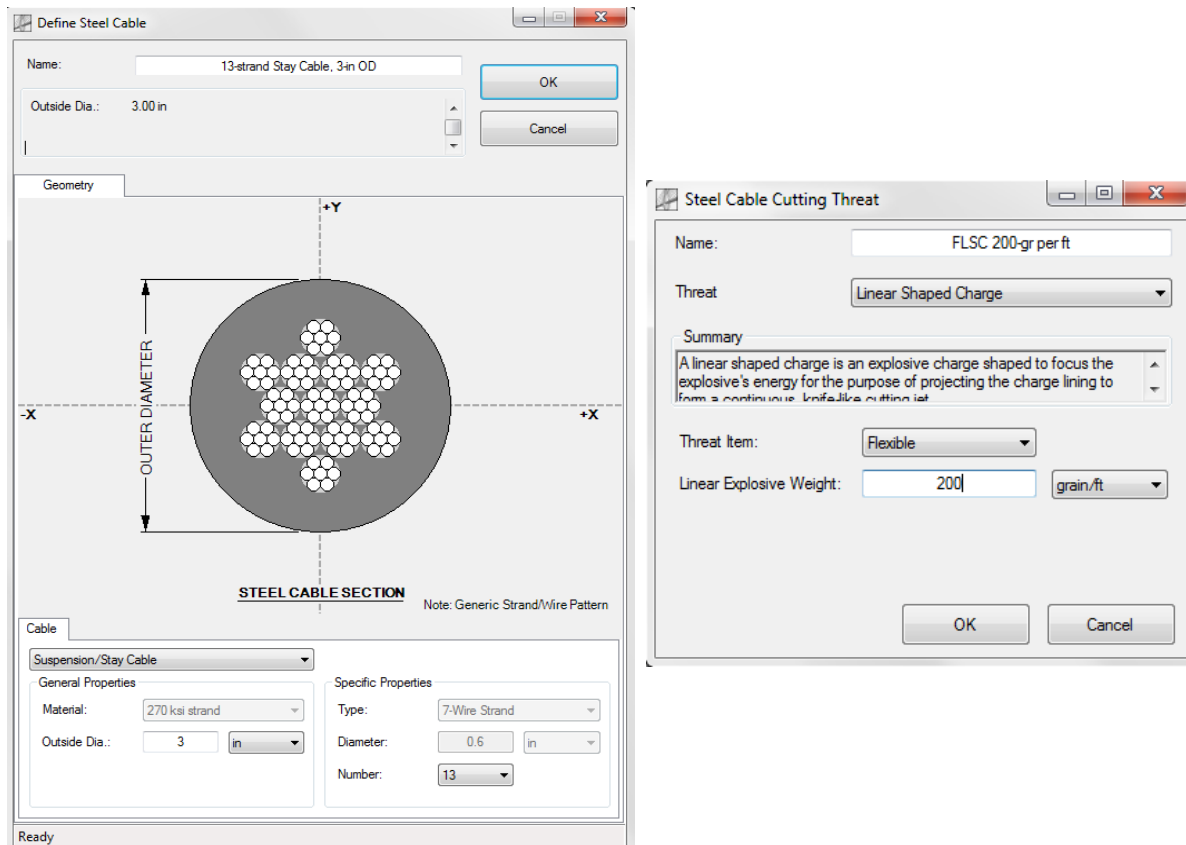


Figure 12.52 Cable and Flexible Linear Shaped Charge Input Screens

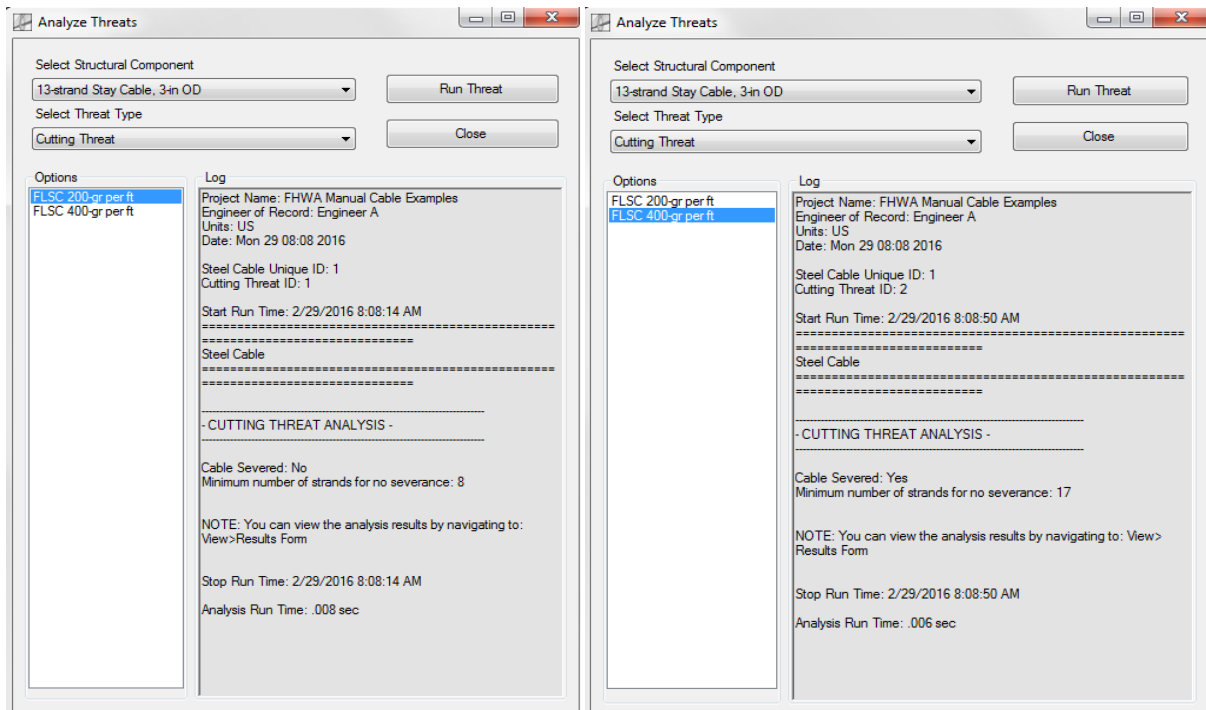


Figure 12.53 Analysis Results for 13-Strand Stay Cable Subjected to 200-gr/ft (left) and 400-gr/ft (right) Flexible Linear Shaped Charges

If the flexible linear shaped charge is increased to 400-gr/ft, the cable is severed, as shown in the right side of Figure 12.53.

Currently, ATP-Bridge only defines severed or non-severed as the final state. In reality, the 200-gr/ft charge will damage the cable to some extent and there will be a reduced capacity; however, current research and available data do not allow the definition of this reduced capacity.

Block Charge against Steel Cable

In this example, the design basis threat for a cable-stayed bridge includes a block of 20-lb TNT placed next to a 31-strand stay cable with a 4-in outer diameter for the environmental cover. The steel cable and the block charge are defined as shown in Figure 12.54. The results of the analysis show that 20 strands of the cable are severed and 11 intact strands remain; see left side of Figure 12.55.

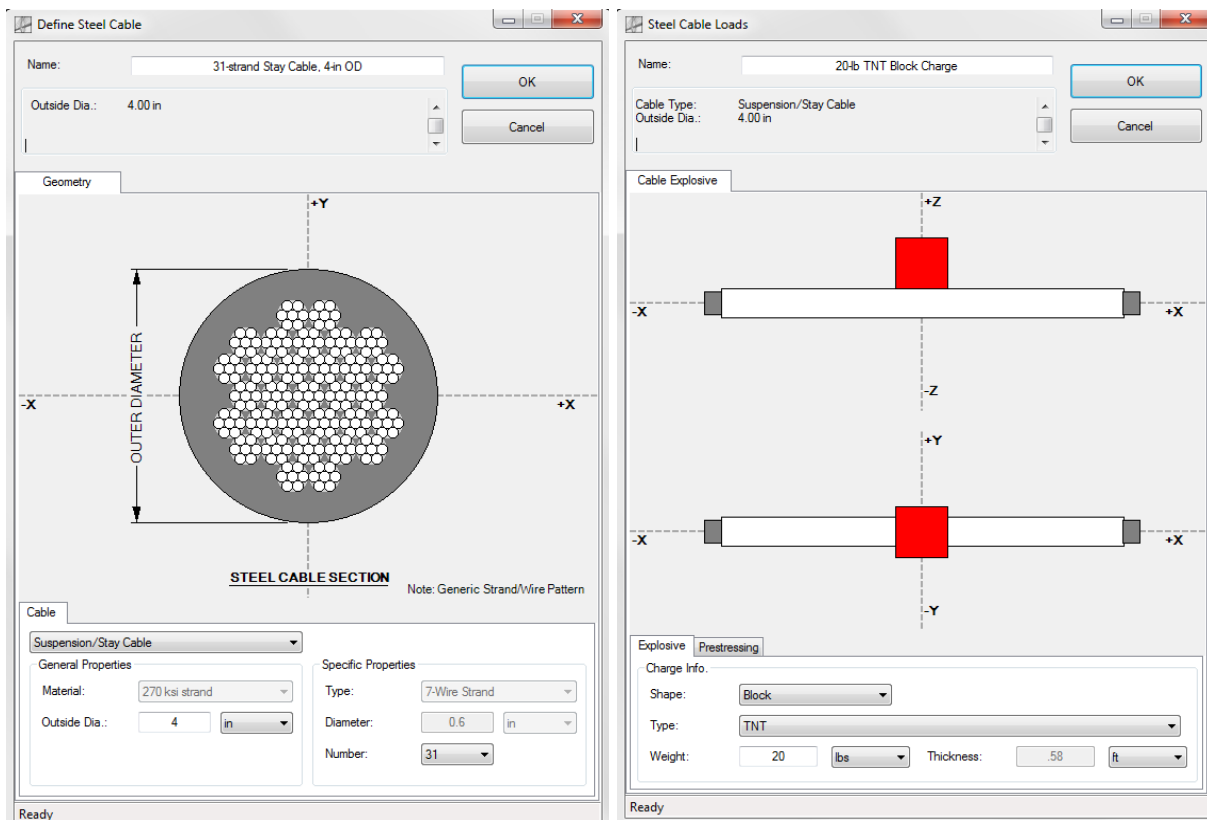


Figure 12.54 Cable and 20-lb TNT Block Charge Input Screens

If the standoff to the 20-lb charge is increased by 2-in. to 4-in (i.e., outer diameter of the environmental cover is increased to 8-in), the number of intact strands increases to 25, as shown in the right side of Figure 12.55.

As mentioned earlier, the engineer would multiply the number of intact strands by the cross-sectional area of each strand and use that to define the cross-sectional area for that cable in the numerical model of the entire (damaged) bridge.

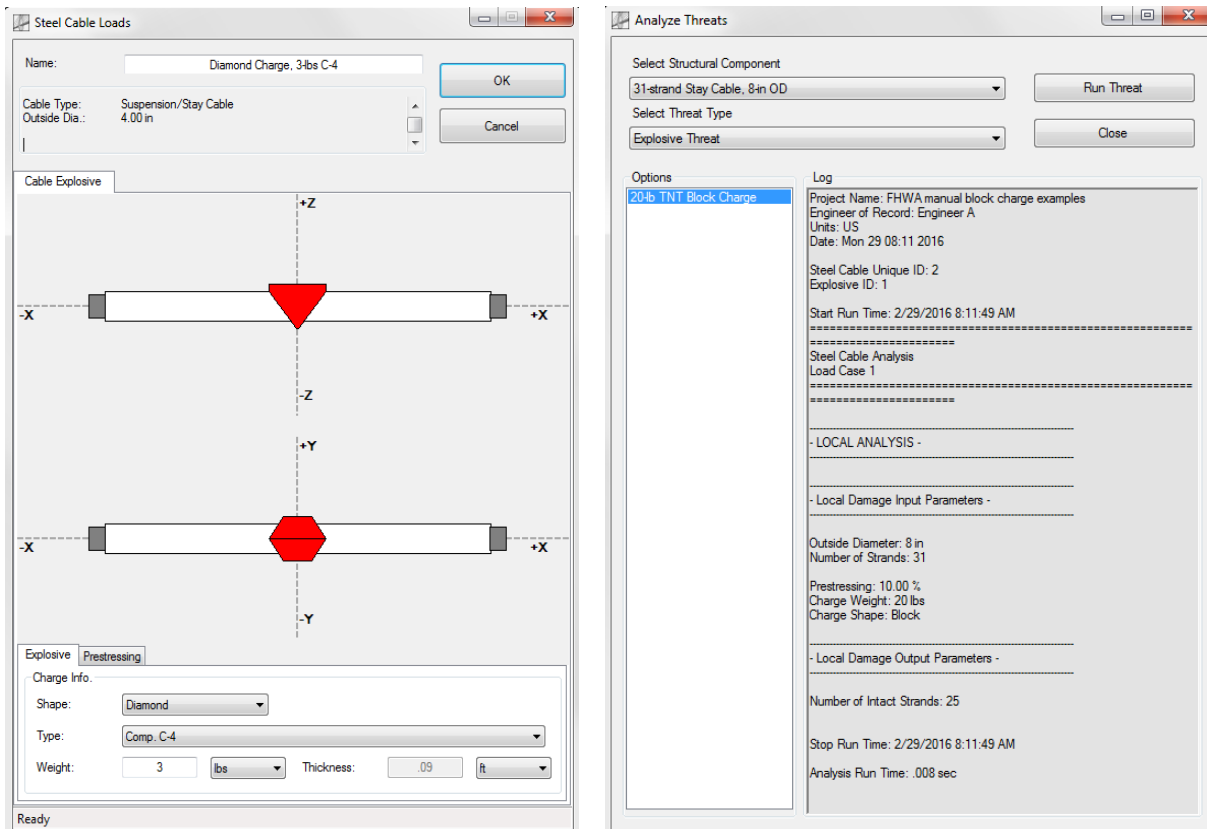


Figure 12.55 Analysis Results for 31-Strand Stay Cable Subjected to 20-lb TNT Block Charge with 4-in. OD (left) and 8-in. OD (right)

Diamond Charge against Steel Cable

In this example, the design basis threat for a cable-stayed bridge includes a 3-lb C-4 diamond charge placed on a 19-strand stay cable with a 4-in outer diameter for the environmental cover. The steel cable and the diamond charge are defined as shown in Figure 12.56. The results of the analysis show that 12 strands of the cable are severed and 7 intact strands remain; see left side of Figure 12.57.

If the number of strands is increased to 31 and the outer diameter is increased by 4-in to 8-in, no strand failure occurs, as shown in the right side of Figure 12.57.

As mentioned earlier, the engineer would multiply the number of intact strands by the cross-sectional area of each strand and use that to define the cross-sectional area for that cable in the numerical model of the entire (damaged) bridge.

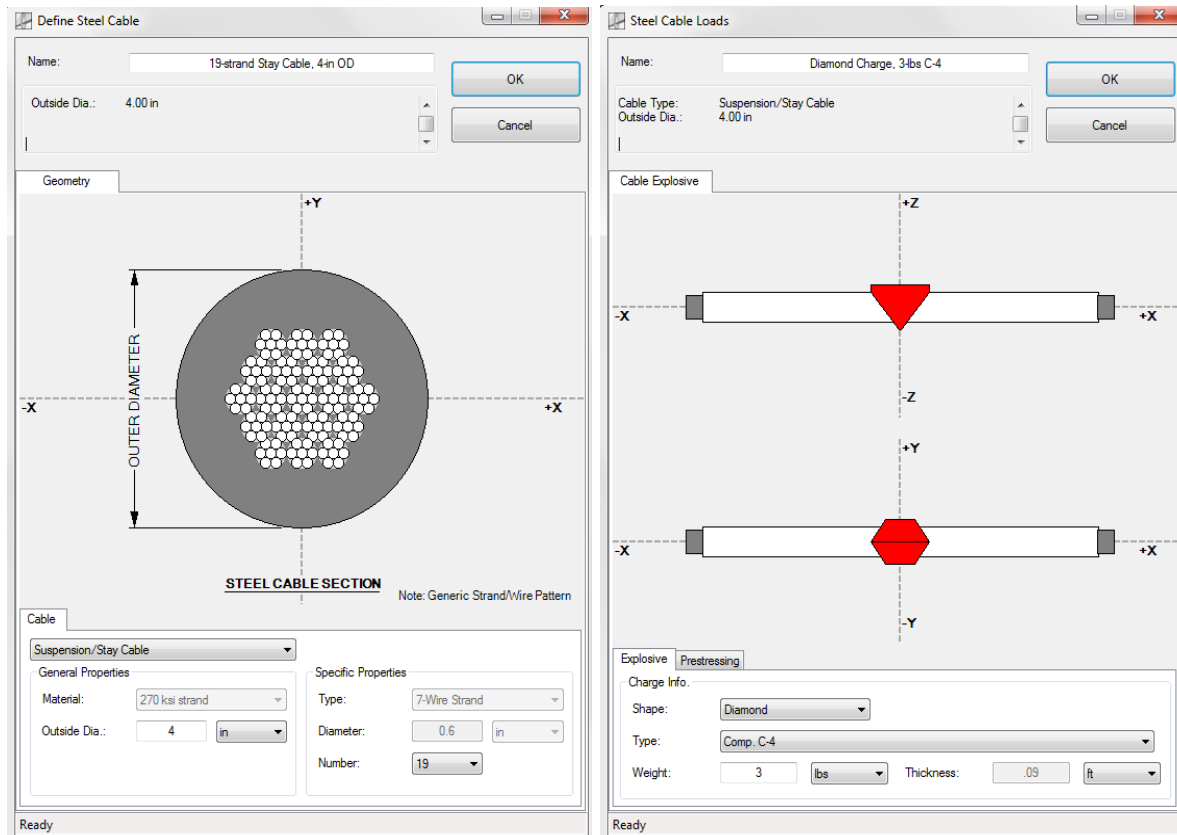


Figure 12.56 Cable and 3-lb Diamond Charge Input Screens

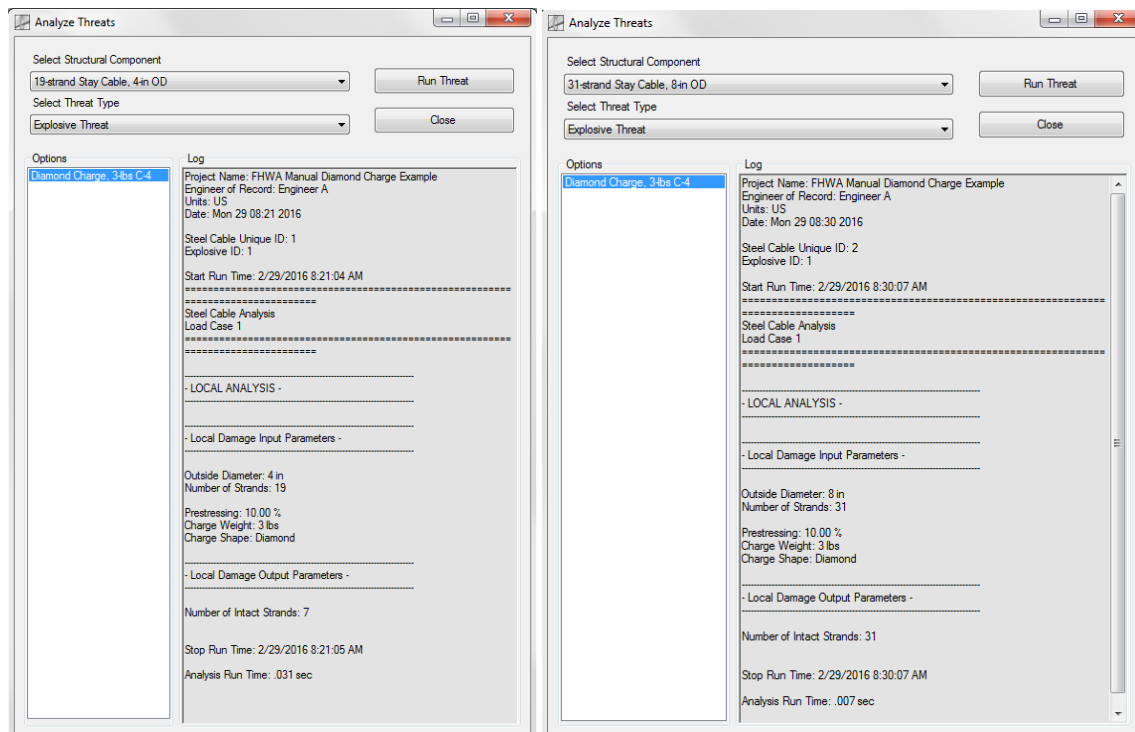


Figure 12.57 Analysis Results for 19-Strand Stay Cable with 4-in. OD (left) and 31-Strand Stay Cable with 8-in. OD (right) Subjected to 3-lb C-4 Diamond Charge

12.5 Chapter Summary

This chapter presented the ATP-Bridge software. Although prior chapters used this software to analyze specific examples, this chapter provided detailed background information on how the software works and the assumptions implicit within each of the analysis algorithms. Examples for each component type were also provided.

REFERENCES

- [1] U.S. Department of Transportation, "The Changing Face of Transportation, Report BTS00-007," Washington, D.C., 2000.
- [2] Wikipedia, "I-35W Mississippi River Bridge," 26 February 2009. [Online]. Available: http://en.wikipedia.org/wiki/I-35W_Mississippi_River_bridge. [Accessed 30 November 2015].
- [3] D. L. Cormany, "Small Retailers Struggle to Survive Bridge Collapse," Minnesota Post, [Online]. Available: <http://www.minnpost.com/politics-policy/2008/01/small-retailers-struggle-survive-bridge-collapse>. [Accessed 30 November 2015].
- [4] National Transportation Safety Board, "U.S. Towboat Robert Y. Love Allision with Interstate 40 Highway Bridge Near Webbers Falls, Oklahoma, May 26, 2002; Highway/Marine Accident Report NTSB/HAR-04/05," Washington, D.C., 2004.
- [5] Associated Press, "Queen Isabella Causeway Reconstruction Beginning," Amarillo Globe-News, [Online]. Available: http://amarillo.com/stories/092701/tex_queen.shtml. [Accessed 30 November 2015].
- [6] A. Boyd and J. P. Sullivan, "Emergency Preparedness for Transit Terrorism," *Transportation Research News*, vol. 208, no. May-June, pp. 12-17, 2000.
- [7] J. J. Green, "Washington's Top News: Growing Pool of Terrorists Overwhelms Tracking Capabilities," 19 February 2016. [Online]. Available: <http://wtop.com/national-security/2016/02/terrorist-overwhelming-tracking-capabilities/>. [Accessed 19 February 2016].
- [8] National Consortium for the Study of Terrorism and Responses to Terrorism, "Global Terrorism Database (GTD)," University of Maryland, 2016.
- [9] B. M. Jenkins, "Protecting Surface Transportation Systems and Patrons from Terrorist Activities: Case Studies of Best Security Practices and a Chronology of Attacks; MTI Report 97-04," Mineta Transportation Institute (MTI), San Jose, CA, 1997.
- [10] The Blue Ribbon Panel on Bridge and Tunnel Security, "Recommendations for Bridge and Tunnel Security," Special report prepared for FHWA and AASHTO, Washington, D.C., 2003.
- [11] J. J. Carafano, "U.S. Thwarts 19 Terrorist Attacks against America Since 9/11," The Heritage Foundation, 2007. [Online]. Available: <http://www.wokay.com/news/latest-news/bomb-threat-shuts-down-brooklyn-bridge-41041.html>. [Accessed 30 November 2015].
- [12] W. McPhee, J. G. Meek and S. Browne, "Brooklyn Bridge Plot Al Qaeda, Ohio Trucker Sought to Destroy Span," New York Daily News, 2003. [Online]. Available: http://www.nydailynews.com/archives/news/2003/06/20/2003-06-20_brooklyn_bridge_plot_al_qae.html. [Accessed 30 November 2015].

- [13] National Response Center, "National Response Team Incident Summaries (NRTIS) [Electronic Database]," 2004. [Online]. Available: <http://www.nrc.uscg.mil/insum2004/bombthreat.html>. [Accessed 30 November 2015].
- [14] Charles, "Bomb Threat Shuts Down Brooklyn Bridge," Wokay News and Magazine, 2010. [Online]. Available: <http://www.wokay.com/news/latest-news/bomb-threat-shuts-down-brooklyn-bridge-41041.html>. [Accessed 30 November 2015].
- [15] J. Winslow, "Bomb Scare on Coronado Island Ends with I-5 Reopening," 2011. [Online]. Available: <http://news.gather.com/viewArticle.action?articleID=281474979284435>. [Accessed 30 November 2015].
- [16] M. Muskal and A. Sweeney, "3 Men Get Prison in Failed Ohio Bomb Plot," Chicago Tribune, 2012. [Online]. Available: http://articles.chicagotribune.com/2012-11-20/news/chi-ohio-bridge-bomb-plot-20121120_1_ohio-bomb-plot-anthony-hayne-plastic-explosives-and-authorities. [Accessed 30 November 2015].
- [17] B. M. Jenkins and L. N. Gersten, "Protecting Public Surface Transportation against Terrorism and Serious Crime: Continuing Research on Best Security Practices, MTI Report 01-07," Mineta Transportation Institute (MTI), San Jose, CA, 2001.
- [18] E. L. Sammarco, "Development of Simplified Dynamic Response Models for Blast-Loaded Bridge Components.," Doctoral Dissertation, University of Texas at Austin, Austin, TX, 2014.
- [19] B. Kritzberg and S. Kritzberg, "Iraq Photo Gallery," 2003. [Online]. Available: http://www.kritzberg.com/Albums/Iraq_Sectors/Sectors.html. [Accessed 13 October 2013].
- [20] Federal Highway Administration, "Blast Design and Analysis of Highway Structures, FOCUS: Accelerating Infrastructure Innovations, Publication No. FHWA-HRT-06-028," August 2006. [Online]. Available: <http://www.fhwa.dot.gov/publications/focus/06aug/02.cfm>. [Accessed 13 October 2013].
- [21] E. L. Sammarco, E. B. Williamson and C. E. Davis, "Enhancing the Security of U.S. Highway Bridges: Developing Protective Design Guidance, Tools, and Techniques," *TR-News Magazine*, vol. 275, no. July-August, pp. 12-18, 2011.
- [22] J. C. Ray, "Risk-Based Prioritization of Terrorist Threat Mitigation Measures on Bridges," *Journal of Bridge Engineering*, vol. 12, no. 2, pp. 140-146, 2007.
- [23] Science Applications International Corporation, "A Guide to Highway Vulnerability Assessment for Critical Asset Identification and Protection," American Association of State Highway and Transportation Officials, Washington, D.C., 2002.
- [24] E. B. Williamson, O. Bayrak, G. D. Williams, C. E. Davis, K. A. Marchand, A. E. McKay, J. Kulicki and W. Wassef, "Blast-Resistant Highway Bridges: Design and Detailing Guidelines; Technical Report 645," National Cooperative Highway Research Program (NCHRP), Washington, D.C., 2010.

- [25] S. Fujikura and M. Bruneau, "Experimental Investigation of Seismically Resistant Bridge Piers Under Blast Loading," *Journal of Bridge Engineering*, vol. 16, no. 1, pp. 63-71, 2011.
- [26] S. Fujikura, M. Bruneau and D. Garcia, "Experimental Investigation of Multihazard Resistant Bridge Piers Having Concrete-Filled Steel Tube under Blast Loading," *Journal of Bridge Engineering*, vol. 13, no. 6, pp. 586-594, 1 November 2008.
- [27] W. F. Cofer, D. S. Matthews and D. I. McLean, "Effects of Blast Loading on Prestressed Girder Bridges," *Shock and Vibration*, vol. 19, no. 1, pp. 1-18, 2012.
- [28] J. C. Ray and B. E. Walker, "Validation of Numerical Modeling and Analysis of Steel Bridge Towers Subjected to Blast Loadings: Executive Summary; Technical Report ERDC/GSL TR-10-X," U.S. Army Engineer Research and Development Center (ERDC), Vicksburg, MS, 2010.
- [29] J. C. Ray, "Validation of Numerical Modeling and Analysis of Steel Bridge Towers Subjected to Blast Loadings," *Proceedings from the ASCE/SEI Structures Congress; St. Louis, MO*, 2006.
- [30] V. P. Chiarito, J. K. Minor, R. E. Walker, J. C. Ray, D. C. Guynes and S. A. Kiger, "Vulnerability of Reinforced Concrete Cable-Stayed Bridge Tower Walls to Vehicle-Borne Improvised Explosive Devices: Test Series 1, Baseline Vulnerability Tests; Technical Report ERDC/GSL TR-11-X," U.S. Army Engineer Research and Development Center (ERDC), Vicksburg, MS, 2011.
- [31] V. P. Chiarito, J. C. Ray, P. Papados, C. P. Rabalais, T. G. Coleman, P. J. O'Connor and E. M. Weinstein, "Assessment of the Vulnerability of Cable Bundles of Cable-Stayed Bridges to Explosive Threats; Technical Report ERDC/GSL TR-11-40," U.S. Army Engineer Research and Development Center (ERDC), Vicksburg, MS, 2011.
- [32] J. C. Ray, B. J. Armstrong and T. R. Slawson, "Airblast Environment beneath a Bridge Overpass," *Journal of the Transportation Research Board*, no. 1827, pp. 63-68, 2003.
- [33] G. D. Williams, "Analysis and Response Mechanisms of Blast-Loaded Reinforced Concrete Columns," Doctoral Dissertation, The University of Texas at Austin, Austin, TX, 2009.
- [34] G. J. Ballantyne, A. S. Whittaker, G. F. Dargush and A. J. Aref, "Air-Blast Effects on Structural Shapes of Finite Width," *Journal of Structural Engineering*, vol. 136, no. 2, pp. 152-159, 2010.
- [35] J. Son and A. Astaneh-Asl, "Blast Protection of Cable-Stayed and Suspension Bridges," in *Lifeline and Earthquake Engineering in a Multihazard Environment*, Oakland, CA, 2009.
- [36] American Association of State Highway and Transportation Officials, "Bridge Security Guidelines," AASHTO, Washington, D.C., 2011.
- [37] U.S. Department of Homeland Security, "Transportation Security Administration: Transportation Security Template and Assessment Toolkit (T-START)," [Online]. Available: <https://www.tsa.gov/for-industry/surface-transportation>.

- [38] E. B. Williamson and D. G. Winget, "Risk Management and Design of Critical Bridges for Terrorist Attacks," *Journal of Bridge Engineering*, vol. 10, no. 1, pp. 96-106, 2005.
- [39] U.S. Department of Homeland Security, "Transportation Security Administration Guidance on Sensitive Security Information (SSI)," [Online]. Available: <https://www.tsa.gov/for-industry/sensitive-security-information>.
- [40] B. M. Jenkins, "Protecting Public Surface Transportation against Terrorism and Serious Crime: An Executive Overview, MTI Report No. 01-14," Mineta Transportation Institute (MTI), San Jose, CA, 2001.
- [41] H. N. Abramson et. al., "Improving Surface Transportation Security: A Research and Development Strategy," Committee on R&D Strategies to Improve Surface Transportation Security, National Research Council, National Academy Press, Washington, D.C., 1999.
- [42] U.S. Department of Homeland Security, "FEMA 426, Risk Management Series: Reference Manual to Mitigate Potential Terrorist Attacks against Buildings," Federal Emergency Management Agency, Washington, D.C., 2003.
- [43] U.S. Department of Homeland Security, "FEMA 452, Risk Management Series: Risk Assessment, A How-To Guide to Mitigate Potential Terrorist Attacks against Buildings," Federal Emergency Management Agency, Washington, D.C., 2005.
- [44] U.S. Department of Defense, "Unified Facilities Criteria UFC 4-020-01, DoD Security Engineering Facilities Planning Manual," U.S. Department of Defense, Washington, D.C., 2008.
- [45] J. A. Zukas and W. P. Walters, *Explosive Effects and Applications*, Springer-Verlag, 1998.
- [46] T. Krauthammer, *Modern Protective Structures*, Boca Raton, FL, Florida: CRC Press, 2008.
- [47] A. Longinow, "Blast Basics," *Steel Building Symposium: Blast and Progressive Collapse Resistance*, pp. 13-19, 2003.
- [48] U.S. Department of Defense, "Unified Facilities Criteria UFC 3-340-01, Design and Analysis of Hardened Structures to Conventional Weapons Effects (FOUO)," U.S. Department of Defense, Washington, D.C., 2002.
- [49] E. J. Conrath, T. Krauthammer, K. A. Marchand and P. F. Mlakar, *Structural Design for Physical Security: State of Practice*, Structural Engineering Institute of ASCE, 1999.
- [50] U.S. Department of Defense, "Unified Facilities Criteria (UFC) 3-340-02 Change 2, Structures to Resist the Effects of Accidental Explosions," U.S. Department of Defense, Washington, D.C., 2014.
- [51] U.S. Department of Energy, "A Manual for the Prediction of Blast and Fragment Loadings on Structures, Revision 1," Technical Report DOE/TIC-11268, Albuquerque Operations Office, Albuquerque, NM, 1992.
- [52] U.S. Department of Defense, "Technical Manual TM 9-1300-214, Military Explosives," U.S. Department of Defense, Washington, D.C., 1984.

- [53] D. O. Dusenberry, Handbook for Blast-Resistant Design of Buildings, Hoboken, NJ: John Wiley & Sons, 2010.
- [54] J. W. Tedesco, W. G. McDougal and C. A. Ross, Structural Dynamics: Theory and Application, Menlo Park, CA: Addison Wesley Longman, 1999.
- [55] L. J. Malvar, "Review of Static and Dynamic Properties of Steel Reinforcing Bars," *ACI Materials Journal*, vol. 95, no. 5, pp. 606-616, 1998.
- [56] L. E. Schwer, "Strain Rate Induced Strength Enhancement in Concrete: Much ado about Nothing?," *Proceedings from the 7th European LS-DYNA Conference*, 2009.
- [57] L. J. Malvar and C. A. Ross, "Review of Strain Rate Effects for Concrete in Tension," *ACI Materials Journal*, vol. 95, no. 6, pp. 735-739, 1998.
- [58] Comité Euro-International du Béton, "CEB-FIP Model Code," Redwood Books, Trowbridge, Wiltshire, UK, 1993.
- [59] J. K. Wight and J. G. MacGregor, Reinforced Concrete Mechanics and Design, 5th Edition, Pearson Prentice Hall, 2009.
- [60] G. Thiagarajan, "Size and Strain Rate Effect Comparison of Three Concrete Material Models in LS-DYNA," *Presentation during the Blast and Impact Loading Response of Concrete Structures Session, ACI Fall Convention*, 2010.
- [61] Y. Wang, I. Burgess, F. Wald and M. Gillie, Performance-Based Fire Engineering of Structures, Boca Raton, FL: Taylor & Francis Group, 2013.
- [62] European Standard EN 1992-1-2, "Eurocode 2: Design of Concrete Structures - Part 1-2: General rules - Structural Fire Design," December 2004.
- [63] European Standard EN 1994-1-2, "Eurocode 4: Design of Composite Steel and Concrete Structures - Part 1-2: General Rules - Structural Fire Design," August 2005.
- [64] A. H. Buchanan, Structural Design for Fire Safety, West Sussex, England: John Wiley & Sons Ltd, 2002.
- [65] C. G. Salmon and J. E. Johnson, Steel Structures: Design and Behavior, 4th Edition, Upper Saddle River, NJ: Prentice-Hall, Inc., 1996.
- [66] G. R. Johnson and W. H. Cook, "A Constitutive Model and Data for Metals Subjected to Large Strains, High Strain Rates, and High Temperatures," *Proceedings from the 7th International Symposium on Ballistics*, 1983.
- [67] G. R. Cowper and P. S. Symonds, "Strain Hardening and Strain Rate Effects in the Impact Loading of Cantilever Beams," Applied Mathematics Report, Brown University, Providence, RI, 1958.
- [68] J. K. Paik and A. K. Thayamballi, Ship-Shaped Offshore Installations: Design, Building, and Operation, 2011.
- [69] B. Liu, "Experimental and Numerical Study on the Impact Strength of Beams and Plates," Master's Thesis, Technical University of Lisbon, Lisbon, Portugal, 2011.
- [70] European Standard EN 1993-1-2, "Eurocode 3: Design of Steel Structures - Part 1-2: General Rules - Structural Fire Design," April 2005.

- [71] W. D. Kennedy, "Effects of Impact and Explosion Vol. 1, Chapter 2: Explosions and Explosives in Air," Summary Technical Report of Division 2, National Defense Research Committee (NDRC), Washington, D.C., 1946.
- [72] W. E. Baker, *Explosions in Air*, Austin, TX: University of Texas Press, 1973.
- [73] G. C. Mays and P. D. Smith, *Blast Effects on Buildings*, London: Thomas Telford Publications, 1995.
- [74] U.S. Army Corps of Engineers, Technical Report PDC-TR 06-08 Rev 1, Single Degree of Freedom Structural Response Limits for Antiterrorism Design, Omaha, NE: Protective Design Center, 2008.
- [75] American Society of Civil Engineers, *Design of Blast-Resistant Buildings in Petrochemical Facilities*, 2nd Ed., Reston, VA: Task Committee on Blast Resistant Design, 2010.
- [76] J. R. Britt, B. K. Conklin, S. M. Frank, B. C. Smith and A. P. Ohrt, "Modeling Improvements in the Airblast Deffraction and Clearing Models in BlastX," in *Proceedings of the 79th SAVIAC Conference*, Orlando, FL, 2010.
- [77] B. Hopkinson, British Ordnance Board Minutes 13565, 1915.
- [78] C. Cranz, *Lehrbuch Der Ballistik*, Berlin: Springer-Verlag, 1926.
- [79] C. N. Kingery and G. Bulmash, *Airblast Parameters from TNT Spherical Air Burst and Hemispherical Surface Burst*, Aberdeen Proving Ground, MD: Technical Report ARBRL-TR-02555, U.S. Army Armament Research and Development Center, Ballistic Research Laboratory (FOUO), 1984.
- [80] C. E. Needham, *Shock Wave and High Pressure Phenomena: Blast Waves*, New York City, NY: Springer Heidelberg Dordrecht, 2010.
- [81] J. R. Britt and G. W. McMahon, "Tabular Explosive Source Models Used in BlastX," in *Proceedings from the 20th International Symposium on Military Aspects of Blast and Shock*, Oslo, Norway, 2008.
- [82] J. R. Britt, D. E. Ranta and C. E. Joachim, "BlastX Code, Version 4.2, User's Manual," Report ERDC/GSL TR-01-2, U.S. Army Engineer Research and Development Center (ERDC), Vicksburg, MS, 2001.
- [83] O. C. Zienkiewicz and R. L. Taylor, *The Finite Element Method 5th Edition, Volume 3: Fluid Dynamics*, Woburn, MA: Butterworth Heinemann, 2000.
- [84] J. C. Ray, "Airblast Environment Beneath a Bridge Overpass," *Journal of the Transportation Research Board*, vol. 1827, pp. 63-68, 2003.
- [85] K. A. Marchand and B. T. Plenge, "Concrete Hard Target Spall and Breach Model, Technical Report AFRL-MN-EG-TR-1998-7032," Air Force Research Laboratory, Munitions Directorate, Lethality and Vulnerability Branch, Eglin AFB, FL, 1998.
- [86] U.S. Army Corps of Engineers, "Technical Report PDC-TR 06-01 Rev 2, Methodology Manual for the Single-Degree-of-Freedom Blast Effects Design Spreadsheet (SBEDS)," Protective Design Center, Omaha, NE, 2012.

- [87] American Concrete Institute, "Report on High-Strength Concrete," ACI Report 363R-10, Farmington Hills, MI, 2010.
- [88] E. G. Nawy, Fundamentals of High-Performance Concrete, 2nd Edition, New York, NY: John Wiley & Sons, Inc., 2001.
- [89] A. B. Groeneveld and C. K. Crane, "Material Specifications for Attack Countermeasures on Bridges: Advanced Cementitious Materials for Blast Protection," U.S. Army Engineer Research and Development Center (ERDC), Vicksburg, MS, 2014.
- [90] American Concrete Institute, "Guide for Specifying, Proportioning, Mixing, Placing and Finishing Steel Fiber Reinforced Concrete," ACI Report 544.3R-93, Farmington Hills, MI, 1993.
- [91] T. D. Hrynyk and F. J. Vecchio, "Behavior of Steel Fiber-Reinforced Concrete Slabs under Impact Load," *ACI Structural Journal*, Vols. September-October, pp. 1213-1224, 2014.
- [92] C. Wu, D. J. Oehlers, M. Rebertus, J. Leach and A. S. Whittaker, "Blast Testing of Ultra-High Performance Fibre and FRP-Retrofitted Concrete Slabs," *Journal of Engineering Structures*, vol. 31, pp. 2060-2069, 2009.
- [93] J. M. Puryear, D. J. Stevens, K. A. Marchand, E. B. Williamson, E. L. Sammarco and R. W. Hendryx, "Breach Algorithm for Steel Plates: A Module for Anti-Terrorism Planner for Bridges (ATP-B), Technical Report ERDC/GSL TR-13-X," US Army Engineer Research and Development Center, Vicksburg, MS, 2013.
- [94] J. M. Biggs, Introduction to Structural Dynamics, New York, NY: McGraw-Hill, 1964.
- [95] Building Seismic Safety Council, "FEMA P-750, NEHRP Recommended Seismic Provisions for New Buildings and Other Structures," Federal Emergency Management Agency (FEMA), 2009.
- [96] U.S. Army Corps of Engineers, *Single-Degree-of-Freedom Blast Effects Design Spreadsheet (SBEDS), Version 5.1*, Omaha, NE: Protective Design Center, 2014.
- [97] U.S. Army Corps of Engineers, *ConWep v2.1.0.8*, Vicksburg, MS: Engineer Research and Development Center, 1997.
- [98] A. K. Chopra, Dynamics of Structures: Theory and Applications to Earthquake Engineering, 3rd ed., Upper Saddle River, NJ: Pearson Education, 2007.
- [99] R. W. Clough and J. Penzien, Dynamics of Structures, 2nd ed., New York, NY: McGraw-Hill, 1993.
- [100] U.S. Army Corps of Engineers, "Bridge Explosive Loading (BEL), Version 1.1.0.3," Engineer Research and Development Center, Vicksburg, MS, 2004.
- [101] H. A. Salim, R. Dinan, S. A. Kiger, P. T. Townsend and J. Shull, "Blast-Retrofit Wall Systems using Cold-Formed Steel Studs," in *16th Engineering Mechanics Conference*, Seattle, WA, 2003.

- [102] J. M. Magallanes, J. E. Crawford, S. Fu, J. Abraham, K. B. Morrill and J. Malvar, "Column Blast Analysis and Retrofit Design," in *ASCE/SEI Structures Congress*, Chicago, 2012.
- [103] J. A. Zukas, *Introduction to Hydrocodes*, Studies in Applied Mechanics 49, New York, New York: Elsevier Ltd, 2004.
- [104] D. G. Winget, K. A. Marchand and E. B. Williamson, "Analysis and Design of Critical Bridges Subjected to Blast Loads," *Journal of Structural Engineering*, vol. 131, no. 8, pp. 1243-1255, 2005.
- [105] Y. Shi, H. Hao and Z. X. Li, "Numerical Simulation of Blast Wave Interaction with Structure Columns," *Shock Waves*, vol. 17, pp. 113-133, 2007.
- [106] U.S. Army Corps of Engineers, *BlastX v8.0*, Vicksburg, MS: Engineer Research and Development Center, 2013.
- [107] S. Akers, D. Rickman, J. Ehrigott Jr. and T. Shelton, "Explosive Breaching of Reinforced Concrete Walls: Experimental Efforts and Numerical Simulations," in *ACI Symposium SP 281, Behavior of Concrete Structures Subjected to Blast and Impact Loadings*, 2011.
- [108] C. E. Holland, "Blast-Resistant Highway Bridge Columns," The University of Texas at Austin, Austin, TX, 2008.
- [109] J. E. Crawford, L. J. Malvar, K. B. Morrill and J. M. Ferritto, "Composite Retrofits to Increase the Blast Resistance of Reinforced Concrete Buildings," in *10th International Symposium on Interaction of the Effects of Munitions with Structures*, 2001.
- [110] J. E. Crawford, L. J. Malvar, J. W. Wesevich, J. Valancius and A. D. Reynolds, "Retrofit of Reinforced Concrete Structures to Resist Blast Effects," *ACI Structural Journal*, vol. 94, no. 4, pp. 371-377, 1 July 1997.
- [111] "Hardwire Armor Systems," 2015. [Online]. Available: <http://www.hardwirellc.com/solutions/hardwire/index.htm>. [Accessed 3 March 2015].
- [112] P. Fouche, M. Bruneau, V. Chiarito and J. Manor, "Blast and Earthquake Resistant Bridge Pier Concept: Retrofit and Alternative Design Options," in *ASCE/SEI Structures Congress*, Pittsburgh, PA, 2013.
- [113] R. E. Walker, J. C. Ray, L. A. Walker and J. K. Minor, "Validation of Numerical Modeling and Analysis of Steel Bridge Towers Subjected to Blast Loadings: Executive Summary," U.S. Army Engineer Research and Development Center (ERDC), Technical Report ERDC/GSL TR-11-11, Vicksburg, MS, 2011.
- [114] R. E. Walker, J. C. Ray, L. A. Walker and J. K. Minor, "Validation of Numerical Modeling and Analysis of Steel Bridge Towers Subjected to Blast Loadings: Series 1 Report," U.S. Army Engineer Research and Development Center (ERDC), Technical Report ERDC/GSL TR-11-11 Rept. 1, Vicksburg, MS, 2011.
- [115] R. E. Walker, J. C. Ray, L. A. Walker and J. K. Minor, "Validation of Numerical Modeling and Analysis of Steel Bridge Towers Subjected to Blast Loadings: Series 2

- Report," U.S. Army Engineer Research and Development Center (ERDC), Technical Report ERDC/GSL TR-11-11 Rept. 2, Vicksburg, MS, 2011.
- [116] R. E. Walker, J. C. Ray, L. A. Walker and J. K. Minor, "Validation of Numerical Modeling and Analysis of Steel Bridge Towers Subjected to Blast Loadings: Series 3 Report," U.S. Army Engineer Research and Development Center (ERDC), Technical Report ERDC/GSL TR-11-11 Rept. 3, Vicksburg, MS, 2011.
 - [117] R. E. Walker, J. C. Ray, L. A. Walker and J. K. Minor, "Validation of Numerical Modeling and Analysis of Steel Bridge Towers Subjected to Blast Loadings: Series 4 Report," U.S. Army Engineer Research and Development Center (ERDC), Technical Report ERDC/GSL TR-11-11 Rept. 4, Vicksburg, MS, 2011.
 - [118] M. Cabanatuan and J. Berton, "Bay Bridge Closed After Repair Falls Apart," 28 October 2009. [Online]. Available: <http://www.sfgate.com/bayarea/article/Bay-Bridge-closed-after-repair-falls-apart-3211953.php>. [Accessed 24 February 2016].
 - [119] W. Kane, E. Huet and K. Fagan, "Golden Gate Bridge Climber in Custody," 4 August 2012. [Online]. Available: <http://www.sfgate.com/bayarea/article/Golden-Gate-bridge-climber-in-custody-3760235.php>. [Accessed 23 February 2016].
 - [120] A. M. Kersul, "Devine Buffalo 6 Symposium Report," Defense Threat Reduction Agency (DTRA), Project Officers Report POR 7640, Dulles, VA, 2000.
 - [121] Wikipedia, "List of Longest Suspension Bridge Spans," [Online]. Available: https://en.wikipedia.org/wiki/List_of_longest_suspension_bridge_spans. [Accessed 21 February 2016].
 - [122] N. Jones, "Plastic Failure of Ductile Beams Loaded Dynamically," *Journal of Engineering for Industry*, pp. 131-136, 1976.
 - [123] M. Yashinsky, "Pitt River Bridge," [Online]. Available: http://www.bphod.com/2010/06/cable-stayed-bridges-pitt-river-bridge_22.html. [Accessed 8 March 2014].
 - [124] Geocaching, "Kaoping River Cable-Stayed Bridge," [Online]. Available: http://www.geocaching.com/geocache/GC1AAD6_kaoping-river-cable-stayed-bridge?guid=fa0b653a-fc50-4ef6-887e-b34c93b9317f. [Accessed 8 March 2014].
 - [125] The Happy Pontist, "A Blog from the UK about Bridges and Bridge Design," 16 October 2011. [Online]. Available: <http://happyontist.blogspot.com/2011/10/merseyside-bridges-2-marine-way-bridge.html>. [Accessed 1 March 2016].
 - [126] Post-Tensioning Institute, "Recommendations for Stay-Cable Design, Testing, and Installation, Guidance Document PTI DC45.1-12," Post-Tensioning Institute, Farmington Hills, MI, 2012.
 - [127] V. P. Chiarito, J. K. Minor, R. E. Walker, J. C. Ray, D. C. Guynes and S. A. Kiger, "Vulnerability of Reinforced Concrete Cable-Stayed Bridge Tower Walls to Vehicle-Borne Improvised Explosive Devices, Test Series 1: Baseline Vulnerability Tests," U.S. Army Engineer Research and Development Center (ERDC) Report ERDC/GSL TR-11-X, Vicksburg, MS, 2011.

- [128] J. C. Ray, B. E. Walker, V. P. Chiarito, J. K. Minor, D. C. Guynes and L. Walker, "Analysis of Reinforced Concrete Bridge Tower Walls Subjected to Blast Loadings: Series II Data Report," U.S. Army Engineer Research and Development Center (ERDC) Report ERDC/LAB TR-08-X, Vicksburg, MS, 2011.
- [129] H. Hao and E. K. C. Tang, "Numerical Simulation of a Cable-Stayed Bridge Response to Blast Loads, Part II: Damage Prediction and FRP Strengthening," *Journal of Engineering Structures*, vol. 32, pp. 3193-3205, 2010.
- [130] E. K. C. Tang and H. Hao, "Numerical Simulation of a Cable-Stayed Bridge Response to Blast Loads, Part I: Model Development and Response Calculations," *Journal of Engineering Structures*, vol. 32, pp. 3180-3192, 2010.
- [131] J. P. Moehle, T. Ghodsi, J. D. Hooper, D. C. Fields and R. Gedhada, "Seismic Design of Cast-in-Place Concrete Special Structural Walls and Coupling Beams: A Guide for Practicing Engineers," National Institute of Standards and Technology (NIST), Report NIST GCR 11-917-11 Revision 1, Gaithersburg, MD, 2012.
- [132] J. W. Wallace, "Behavior, Design, and Modeling of Structural Walls and Coupling Beams - Lessons from Recent Laboratory Tests and Earthquakes," *International Journal of Concrete Structures and Materials*, vol. 6, no. 1, pp. 3-18, 2012.
- [133] "Visual Dictionary Cable-Stayed Bridges," [Online]. Available: www.visualdictionaryonline.com.
- [134] FHWA, "Primer for the Inspection and Strength Evaluation of Suspension Bridge Cables, FHWA-IF-11-045," FHWA, 2012.
- [135] V. P. Chiarito, J. C. Ray, P. Papados, C. P. Rabalais, T. G. Coleman, P. J. O'Connor and E. M. Weinstein, "Assessment of the Vulnerability of Cable Bundles of Cable-Stayed Bridges to Explosive Threats, ERDC/GSL TR-11-40," US Army ERDC, Vicksburg, Mississippi, 2011.
- [136] Wikipedia, "Eastern span replacement of the San Francisco–Oakland Bay Bridge," [Online]. Available: https://en.wikipedia.org/wiki/Eastern_span_replacement_of_the_San_Francisco%E2%80%93Oakland_Bay_Bridge. [Accessed 25 February 2017].
- [137] Wikipedia, "Golden Gate Bridge," [Online]. Available: en.wikipedia.org/wiki/Golden_Gate_Bridge.
- [138] S. Strunsky, "George Washington Bridge," [Online]. Available: www.nj.com/news/index.ssf/2014/04/museum_ties_george_washington_bridge_to_its_steely_past.html.
- [139] Bridon, "Bridon," [Online]. Available: www.bridon.com.
- [140] VSL, "VSL," [Online]. Available: www.vsl.com.
- [141] M. A. Barsotti, J. M. H. Puryear, D. J. Stevens, E. B. Williamson and E. L. Sammarco, "Development of Damage Algorithm for Bridge Cables Subjected to Explosive Threats, ERDC/GSL TR-13-X," U.S. Army Engineer Research and Development Center, Vicksburg, MS, 2013.

- [142] N. T. Museum, "Norfolk Tank Museum," [Online]. Available: norfolktankmuseum.co.uk. [Accessed 22 February 2016].
- [143] DE Technologies, "DE Technologies," [Online]. Available: www.detek.com.
- [144] A. Wendt GmbH, "A. Wendt GmbH," [Online]. Available: http://www.ziehfix.com/shop/contents/en-us/d80_Thermo-Lanze_und_Zubehoer.html.
- [145] Bronco Rankin, "Broco® Industrial Cutting," [Online]. Available: <http://www.broco-rankin.com/industrial/>. [Accessed 25 February 2017].
- [146] U. Diltthey, "Welding Technology 1 - Welding and Cutting Technologies Lecture Notes," Welding Institute, RWTH -Aachen University, Germany, [Online]. Available: <http://www.scribd.com/doc/86474616/Welding-Technology-I-Script>.
- [147] Ensign-Bickford Aerospace and Defense, "Ensign-Bickford Aerospace and Defense," [Online]. Available: <http://www.eba-d.com/products/metal-clad-linear-shaped-charge/>.
- [148] Security Systems Technology, "Security Systems Technology," [Online]. Available: <http://www.securitysystems-tech.com/articles/sabrex-cuts-through-competition>.
- [149] "Semtex® Razor Mondial Defence Systems," [Online]. Available: <http://www.mondial-defence.com/default.htm>. [Accessed 25 January 2013].
- [150] E. L. Sammarco, J. Q. Bui, E. B. Williamson, J. Puryear, D. Stevens and C. K. Crane, "From Research to Practice: A Novel Vulnerability Assessment Software for Blast-Loaded Bridge Components," *Symposium on Interaction of the Effects of Munitions with Structures*, 2013.
- [151] J. M. H. Puryear, D. J. Stevens, B. T. Bewick, E. B. Williamson and E. L. Sammarco, "Cutting Algorithms - Thermal, Linear Shaped Charge and Mechanical, ERDC/GSL TR-13-X," US Army Engineering Research and Development Center, Vicksburg, MS, 2013.
- [152] J. C. Ray, V. P. Chiarito and S. L. Kinnebrew, "Mitigation of Hand-Emplaced Threats to Steel Cables and Structural Steel Members, ERDC/GSL TR-12-2," USACE Engineer Research and Development Center Geotechnical and Structures Laboratory, Vicksburg, MS, January 2012.
- [153] TDV Consulting GmbH, "TDV Consulting GmbH," [Online]. Available: www.tdv.at/reflist.php?pid=stonecutters.
- [154] P. S. Bulson, *Explosive Loading of Engineering Structures - A History of Research and a Review of Recent Developments*, E & FN Spon., 1997.
- [155] U.S. Department of Defense, "Unified Facilities Criteria UFC 4-023-03 Change 2, Design of Buildings to Resist Progressive Collapse," U.S. Department of Defense, Washington, D.C., 2013.
- [156] W. D. Liu, A. Neuenhoffer, M. Ghosn and F. Moses, "Redundancy in Highway Bridge Substructures," National Cooperative Highway Research Program (NCHRP), Report 458, Washington, D.C., 2001.

- [157] A. Noriega and C. K. Crane, "Impulse Load Response of Lattice Steel Columns," U.S. Army Engineer Research and Development Center, Report ERDC/GSL TR-13-X, Vicksburg, MS, 2013.
- [158] W. F. Chen and L. Duan, Bridge Engineering Handbook, 2nd Edition: Seismic Design, Boca Raton, FL: CRC Press, 2014.
- [159] A. Echevarria, A. E. Zaghi, V. Chiarito and R. Christenson, "Performance Evaluation of Reinforced Concrete Bridge Columns through Experimental Blast Testing," in *ASCE Structures Congress*, DOI: 10.1061/9780784413357.042, Portland, OR, 2014.
- [160] J. Q. Bui, "Development of Software Architecture to Investigate Bridge Security," Master's Thesis, The University of Texas at Austin, Austin, TX, 2012.
- [161] J. Shin, A. S. Whittaker and D. Cormie, "Incident and Normally Reflected Overpressure and Impulse for Detonations of Spherical High Explosives in Free Air," *Journal of Structural Engineering*, no. 13, pp. 1-13, 2015.
- [162] R. N. Murtha and T. J. Holland, "Analyses of WES FY82 Dynamic Shear Test Structures," Technical Memorandum 51-83-02, Naval Civil Engineering Laboratory, Port Hueneme, CA, 1982.
- [163] J. M. H. Puryear, D. J. Stevens and K. A. Marchand, "Anti-Terrorist Planner for Bridges: Local Damage Algorithms for Steel Plates and Reinforced Concrete Bridge Piers," Protection Engineering Consultants, Austin, TX, 2012.
- [164] J. M. H. Puryear, D. J. Stevens, K. A. Marchand, E. B. Williamson and E. L. Sammarco, "Spall and Breach Algorithms for Reinforced Concrete Tower Wall: A Module for Anti-Terrorist Planner for Bridges, Technical Report ERDC/GSL TR-13-X," U.S. Army Engineer Research and Development Center, Vicksburg, MS, 2013.
- [165] M. A. Barsotti, J. M. H. Puryear and D. J. Stevens, "Development of Damage Algorithm for Bridge Cables Subjected to Explosive Threats," Protection Engineering Consultants Technical Report Prepared for The University of Texas at Austin, Austin, TX, 2013.